Proceeding

CONFERENCE & EXHIBITION ON

CARBON NEUTRALITY IN CEMENT AND CONCRETE

Towards a Sustainable & Net Zero Future



19–20 NOVEMBER 2026

Centenary Convention Centre, Engineering Staff College of India, Gachibowli, Hyderabad – 500 032, Telangana, India

National Council for Cement and Building Materials

https://conference.ncbindia.com/

Message from Secretary, DPIIT

अमरदीप सिंह भाटिया, भा.प्र.से.
सचिव
Amardeep S. Bhatia, I.A.S.
SECRETARY

सत्यमेव जयते

भारत सरकार
वाणिज्य एवं उद्योग मंत्रालय
उद्योग संवर्धन और आंतरिक व्यापार विभाग
GOVERNMENT OF INDIA
MINISTRY OF COMMERCE & INDUSTRY
DEPTT. FOR PROMOTION OF INDUSTRY
AND INTERNAL TRADE



MESSAGE

Driven by the Government's sustained focus on infrastructure, housing and urban development, demand for cement in India continues to grow strongly. The Indian cement sector is one of the eight core industries. It makes a significant contribution to the nation's economic growth, employment and infrastructure creation. As we move towards Viksit Bharat @2047, it is expected that cement production will reach 1900 million tonnes and the sector must meet rising demand while also cutting its carbon footprint, in line with India's commitment to achieve Net Zero by 2070.

I am happy to know that the National Council for Cement and Building Materials (NCB) is organizing a **Conference & Exhibition on Carbon Neutrality in Cement and Concrete** on 19–20 November 2026. NCB is an autonomous R&D organization under the Department for Promotion of Industry and Internal Trade, Ministry of Commerce and Industry. The conference will be held at the Centenary Convention Centre, Engineering Staff College of India (ESCI), Gachibowli, Hyderabad. The theme is timely, because decarbonization is now central to the long-term competitiveness of the cement and concrete industry.

The programme covers the key pathways to carbon neutrality like blended and low-clinker cements, alternative fuels and raw materials, energy efficiency, renewable energy and green hydrogen, carbon capture, utilization and storage (CCUS) and circular economy.

In addition to the plenary and keynote addresses by eminent speakers, the programme includes panel discussions with policymakers, industry and academia, and technical presentations. Leading equipment manufacturers, technology providers and service providers will showcase their latest technologies, products and services at a Technical Exhibition of 35 stalls held alongside the conference.

I am confident that the deliberations will give participants a valuable platform to share knowledge and best practices. This includes the cement and concrete industry, policy planners, equipment and machinery manufacturers, researchers and academicians.

The conference should help them shape strategies for a sustainable, low-carbon future for the sector. I convey my best wishes to NCB for the success of the conference and exhibition.

12/XI/26

(Amardeep S. Bhatia)

Room No. 223, Vanijya Bhawan, Akbar Road, New Delhi-110 001, Tel.: 23038850, 23038851, E-mail : secy-ipp@nic.in

Message from Economic Adviser - DPIIT

उर्मिला, भा.आ.से.
आर्थिक सलाहकार
URMILA, IES
ECONOMIC ADVISER

सत्यमेव जयते

भारत सरकार
वाणिज्य एवं उद्योग मंत्रालय
उद्योग संवर्धन एवं आंतरिक व्यापार विभाग
GOVERNMENT OF INDIA
MINISTRY OF COMMERCE & INDUSTRY
DEPARTMENT FOR PROMOTION OF INDUSTRY
AND INTERNAL TRADE



MESSAGE

I commend National Council for Cement and Building Materials (NCB) for organizing the **Conference & Exhibition on Carbon Neutrality in Cement and Concrete** on 19–20 November 2026.

Cement is the backbone of infrastructure and housing, and India is the second largest producer of cement in the world. Cement production also accounts for about 7% of anthropogenic CO_2 emissions globally. India has committed to achieving Net Zero by 2070, and the cement and concrete sector will have a key role in getting there. The Indian cement industry has already become one of the most energy-efficient in the world. It has also made steady progress in blended cements, alternative fuels and raw materials, waste heat recovery and renewable energy.

Reaching carbon neutrality will take focused research and innovation to find the next generation solutions. These include low-clinker and novel cements, green hydrogen, electrification, carbon capture, utilization and storage (CCUS), and circular-economy approaches that use industrial by-products. This conference brings together policymakers, industry leaders, researchers, technology providers and international experts. They will share experience, discuss enabling policies and chart a practical roadmap for decarbonizing the sector. The exhibition held alongside it will showcase technologies, equipment and services that can speed up this transition.

For over six decades, NCB has served the cement and construction industries through research and development, technology transfer, testing and calibration, and consultancy. It has supported the industry in improving quality and productivity and in becoming more sustainable. Platforms such as this conference strengthen NCB's role as a knowledge partner to the Government and the industry on the path towards a low-carbon economy.

I congratulate the NCB team on organizing this conference and exhibition. I wish the deliberations every success, and I look forward to active participation from the cement and concrete fraternity.

(URMILA)

Room No. 221, Vanijya Bhawan, Akbar Road, New Delhi-110001, Tel. : 2303 8882, E-mail : ea-dpiit@gov.in

Message from Chairman, NCB



It gives me immense pleasure to extend a warm welcome to all delegates, speakers, researchers, industry representatives and exhibitors participating in the Conference & Exhibition on Carbon Neutrality in Cement and Concrete, organised by NCB, being held on 19–20 November 2026 at the Centenary Convention Centre, ESCI, Gachibowli, Hyderabad.

The theme of the conference, "Towards a Sustainable & Net Zero Future," reflects the growing importance of accelerating the transition towards a low-carbon and resource-efficient cement and concrete sector.

As one of the world's largest producers and consumers of cement, India has a significant responsibility as well as an opportunity to lead the transformation of this vital industry towards sustainability while continuing to support the country's ambitious infrastructure and development aspirations. The development and deployment of innovative and commercially viable technologies will be central for reduction of the cement industry's carbon footprint and advancing its Net Zero ambitions.

I am confident that this conference will provide an important platform to exchange knowledge, share experiences and deliberate on emerging technologies and practical solutions for decarbonisation. The accompanying exhibition will further provide an opportunity to showcase technological advancements, innovative products and solutions that can contribute to the sustainable transformation of the cement and concrete industry.

I would like to express my sincere appreciation to all the speakers, authors, sponsors, exhibitors and delegates for their valuable participation and support. I also compliment the organising team and all those associated with the conference for their efforts in bringing together stakeholders on this important subject.

I am confident that the deliberations over these two days will generate meaningful insights, encourage new partnerships and help accelerate the adoption of sustainable technologies and practices across the cement and concrete value chain.

I wish the conference great success and all the participants an engaging, productive and enriching experience.

Parth Jindal
Chairman-NCB

Message from Director General, NCB



Dear Delegates

It gives me immense pleasure to welcome you all to the Conference & Exhibition on Carbon Neutrality in Cement and Concrete Sector, being held during 19–20 November 2026 at the Centenary Convention Centre, Engineering Staff College of India, Gachibowli, Hyderabad.

India is the world's second-largest producer of cement and the sector will remain central to the nation's growth towards Viksit Bharat @2047. At the same time, cement and concrete have to support India's commitment to Net Zero by 2070. With Greenhouse Gas Emission Intensity targets now notified for the cement sector under the Carbon Credit Trading Scheme, carbon neutrality is no longer a distant goal. It is a measurable requirement that will shape investment, technology choices and competitiveness over the coming decade.

The objective of this Conference is to bring together the captains of the cement and concrete industry, policymakers, academicians, technology providers, engineers and scientists on a common platform. Together they will discuss practical pathways to carbon neutrality, efficient and responsible use of resources, and the circular economy, to make the sector sustainable in the long term.

The technical deliberations will include plenary talk, 13 keynote addresses and over 49 technical presentations. These cover low-carbon cementitious materials, energy-efficient cement manufacturing; alternative fuels and raw materials; carbon capture and utilisation, IS 456:2025 Draft, including mineral carbonation in concrete; ultra-high-performance and 3D printable concrete; and digital innovation and process automation. will be the highlights of this Conference.

About 34 leading equipment manufacturers, technology suppliers and service providers are showcasing their technologies, products and solutions for low-carbon cement and concrete in a concurrently held Technical Exhibition of 47 stalls.

On behalf of the Organizing Committee, I extend my sincere thanks to the key officials of the Government of Telangana, Keynote Speakers, Panellists, authors of technical papers, sponsors, exhibitors, media partners, dignitaries and all delegates.

I take this opportunity to express my sincere gratitude to the Department for Promotion of Industry and Internal Trade (DPIIT), Ministry of Commerce and Industry, Government of India, for its continued support and encouragement.

I am confident that the deliberations will produce actionable outcomes for a carbon-neutral cement and concrete sector. I wish the Conference all success and hope it will be a rewarding experience for all.

Dr L P Singh
Director General-NCB &
Chairman-Organizing Committee,
Conference & Exhibition on Carbon Neutrality in Cement and Concrete Sector

Message from Organising Secretary



It gives me immense pleasure and pride to welcome all delegates, distinguished speakers, exhibitors and guests to the Conference & Exhibition on "Carbon Neutrality in Cement and Concrete", being organised by the National Council for Cement and Building Materials (NCB) on 19–20 November 2026 at the Centenary Convention Centre, Engineering Staff College of India, Gachibowli, Hyderabad.

The conference provides an important platform for bringing together leaders from the cement and concrete industry, policymakers, researchers, academicians, equipment manufacturers, consultants and start-ups to deliberate on the challenges, opportunities and emerging solutions for achieving carbon neutrality in the cement and concrete sector.

The technical programme encompasses five key focus areas: Low-Carbon Cementitious Systems and Materials; Decarbonisation of Cement Manufacturing; Process Optimisation and Plant Engineering; Durable and Sustainable Concrete for Net Zero Construction; and Advanced Concrete Composites.

The conference features about 50 technical papers, selected through a rigorous peer-review process for oral presentation, along with plenary sessions and 13 keynote addresses by distinguished experts. A concurrent technical exhibition, featuring 34 exhibitors across 47 stalls, will showcase the latest technologies, innovative products, equipment and services contributing to the transformation of the cement and concrete sector.

Hosting this conference in Hyderabad, which is home to NCB's Hyderabad unit, holds special significance for us. The event also marks an important milestone in our journey towards the 17th International Congress on the Chemistry of Cement (ICCC 2027), which NCB will host in New Delhi in October 2027.

I also extend my heartfelt appreciation to our sponsors and partners: Chief Patron - JSW Cement Ltd.; Platinum Sponsors - UltraTech Cement Ltd., Sagar Cement Ltd., Fuller Technologies, KHD Humboldt Wedag India Pvt. Ltd. and TKIL; Gold Sponsors - My Home India Pvt. Ltd. and NTPC; Kit Bag Sponsor - NMDC; Silver Sponsors -Thermax, Vishnu Chemicals and Techcons Consulting; and Bronze Sponsor – SRM University-AP. My sincere thanks are also due to all exhibitors, Supporting Organisations - DPIIT, GCCA India and SICMA, Media Partners - Indian Cement Review and Cement and its Applications, as well as the authors, reviewers and delegates whose valuable contributions have made this event possible. I particularly acknowledge the dedication and tireless efforts of my colleagues at NCB in organising this conference.

I am confident that the deliberations, knowledge-sharing and interactions over these two days will help identify practical and implementable pathways for accelerating the decarbonisation of the cement and concrete sector while ensuring its competitiveness, resilience and sustainable growth.

I wish all participants an intellectually enriching, productive and memorable experience.

Dr. B. Pandu Ranga Rao
Joint Director & Organising Secretary
Conference & Exhibition on Carbon Neutrality in Cement and Concrete
National Council for Cement and Building Materials



Contents

Technical Session-1	1
Structural, Mechanical and Electrical Properties OF PSC/PPC-EG Composites	2
Influence of Activation Parameters on The Rheology of High-Volume Copper Mine Tailings-Based Alkali-Activated Binders and Their Application Potential	8
Synergistic Utilization of Fly Ash, GGBS and Limestone for Sustainable Multi-Blended Cement Development	19
Performance-Based Binder Optimization for Lower-Clinker Concrete: Strength Comparison of OPC–GGBS And Portland Slag Cement Systems	30
Adaptation of Different Methodologies for Estimation of Kaolinite Phase During Quality Assessment of Different Types of Clay for The Production of Low Carbon LC3 Cement	35
Technical Session -IIB	50
Advancing Large-Capacity Cement Production HWI Experience in Technology and Plant Performance	51
Energy-Efficient Coldgrinding In Mvr Vertical Roller Mills	60
Sustainable Cement Manufacturing Through Energy Efficient Raw Material Grinding with Polycom (High Pressure Grinding Roll) A Case Study	64
Sustainable Explosion Protection Concepts for Explosive Bulk Solids by Means of Explosion Venting	70
Advancement in Cement Manufacturing Process Automation Including AI/ML and Industry 4.0 Application	74
Process Audit–Driven Optimization of Vertical Roller Mills in Cement Manufacturing: Evidence from Four RawaAnd Slag Grinding Case Studies	88
Technical Session -IIIA	100
Decarbonisation of Cement Manufacturing at Scale: The Maha Cement (MHIPL) Integrated Model	101
Limestone Calcined Clay Cement (LC^3): Clay Activation Chemistry and Flash Calciner Process Technology	114
Evaluation of Waste-Derived Fuel Utilisation In an Indian Cement Plant	125



Carbon Mineralization of Steel Slag: A Pathway for CO2 Capture, Utilization, And Circular Raw Material Generation	136
Technical Session-IIIB	148
Comparison of Physics Informed Empirical Equation with Machine Learning Models For Concrete Compressive Strength Prediction Under Distribution Shift	149
Methodological Framework for Cradle-To-Gate Life Cycle Assessment of Precast Metro Bridge Girder	160
Mechanical Properties of Recycled Aggregate Concrete Made Using PSC As Binder	167
Development and Experimental Validation of A Mix Design For Ambient-Cured Geopolymer Concrete	174
Performance as The Criterion for Durability in Concrete Mix Proportioning	181
Technical Session-IVA	195
Technical Session-IVB	196
A Sustainable Route for Producing Highly Reactive SCM From Basic Oxygen Furnace Slag with Concurrent Iron Recovery	197
High Litre Weight Clinker Under Partial and Full Kiln Loading Conditions: Distinguishing Mineralogical Inefficiency from Burnability Limitation for Carbon-Neutral Cement Manufacturing	202
Waste Glass Powder as A Low-Carbon Supplementary Cementitious Material: A Comparative Study with Fly Ash-Based Blended Cements	209
Calcium Sulfoaluminate Cement Systems: A Critical Review of Hydration, Performance, Sustainability and Future Perspectives	2019
Oxyfuel Technology for CO2 Capture in Cement Industry	228
Technical Session -IVA(Contd.)	233
Efficacy of Bipolar Corrosion Inhibitor Admixtures in Reinforced Concrete	234
Technical Session -IVC	243
Efficient & Greener Raw Material Grinding Plants with Roller Press in Finish Mode: Case Studies From Telangana, India	244
Data-Driven Clinker Cooler Services: Integrating A Comprehensive Framework for Service Support, Condition Monitoring, And Inventory Optimization Through the Customer Care Service Program (CCSP)	256



Prepol Step Combustor: A Unique Solution to Combust Most Flexible Alternate Fuels	270
"Process Optimization and Plant Engineering" Cost Reduction, Dust-Free Operation and Power Saving in Cement Mill Bag Houses Through Floating Shoe Rotary Airlock Valves	277
Pioneering Technology: Polysius – Clinker Cooler with Remarkable Efficiency Polytrack® Eco – Clinker Cooler with Outstanding Operating Characteristics	284
Sustainable and Innovative Refractory Solutions for Enhanced AFR Utilization in Cement Manufacturing	292
Technical Session-VA	298
Reducing Cement Consumption and Embodied Carbon Through RCC-to-Structural Steel System Optimization A Case Study of an Hvdc Valve Hall	299
Comparative Bond Behaviour of Steel and GFRP Reinforcement in Geopolymer and OPC Concrete	308
Embodied Carbon Assessment of Expanded Polystyrene (EPS) Lightweight Concrete: Trade-Offs Between Density Reduction and Carbon Neutrality	319
Experimental Investigation on The Mechanical and Durability Performance of Graphene Oxide-Modified Concrete	327
Carbonation Resistance of Concrete Incorporating Fly Ash and Ground Granulated Blast Furnace Slag Under Accelerated Exposure	335
Technical Session-VB	347
Importance of Feasibility Study for an Alternate Fuel Feeding System	348
Ceramic Vortex Finder: A Durable Alternative to Increase Lifetime of Dip Tubes at The Preheater Lower Stages When Utilizing Alternative Fuels	353
Impact of Usage of High Ash Coal (Indian Coal) In Cement Industry	365
Mineralogy–Psd Decoupling in OPC 53 Cement: Explaining yhe Weak Correlation Between Cement Alite Content And 28-Day Strength Through Industrial Xrd And Particle Size Distribution Analysis	370



Technical Session-1

STRUCTURAL, MECHANICAL AND ELECTRICAL PROPERTIES OF PSC/PPC-EG COMPOSITES

*Mohammad Irshad Ansari *, Ashutosh Kumar, and Rajiv Prakash Department of Materials Science and Metallurgical Engineering, Indian Institute of Technology Bhilai, Durg-491002, Chhattisgarh India*

* Email: irshad@iitbhilai.ac.in

Abstract: Sustainable cements are attracting increasing attention as low-carbon construction materials with improved durability, performance, and environmental compatibility and with technological advancement the development of sustainable cement with sensitivity is solicited. In the present study, expandable graphite (EG) was incorporated as a functional additive into Portland slag cement (PSC) and Portland Pozzolana Cement (PPC) to investigate its effect on structural, mechanical and electrical properties. PSC/PPC-EG composites were mixed by ball milling, and their phase composition and microstructural characterization were examined using X-ray diffraction and field emission scanning electron microscopy respectively. Standard cement parameters viz. Insoluble residue, normal consistency, setting time, specific surface area were evaluated and found in line with the Indian standard code (ISC). The compressive strength for the composite has been seen to change as per the type of cement and the concentration of EG in the composite. At higher EG concentration (~2.5wt%), PSC based composite showed reduced strength while PPC based composite was in line with ISC. The electrical resistivity was found to vary with EG concentration in both the composites, depicting that EG imparts sensitivity to the sustainable cements. The results obtained in the present study indicate that the addition of EG is leading to sensitive sustainable cement for better strength and sensitivity.

Keywords: Portland Slag Cement, Compressive Strength, Sustainability, Sensitivity

1. *Introduction*

Sustainable or green cement is made using non-hazardous, eco-friendly industrial waste, partially replacing clinker. [1] Its production aims to cut CO_2 emissions, which account for about 7–8% of global emissions[2]. Materials like fly ash (waste product from power plants) and slag (waste product from steel industries) are used to lower emissions. Fly ash also improves water demand, workability, setting time, and durability. The rapid growth of smart construction requirements has increased interest in multifunctional or smart cement for structural health monitoring (SHM)[3].

Materials like carbon fiber, expandable graphite, carbon nanotubes, graphene, and steel slag are added to enhance strength and sensing abilities [3], [4], [5], [6]. Adding 15% steel slag boosts compressive strength by 15.85% and piezo resistivity by 64%.[7] The use of expandable graphite and carbon fiber also show excellent mechanical and sensing performance [3]

Most existing research focuses on Ordinary Portland Cement (OPC) as the primary binder, with conductive fillers added by partially replacing sand or fine aggregates. These studies primarily aim to enhance mechanical and sensing properties using traditional cement compositions. However, there is limited investigation into the performance of alternative, sustainable binders—specifically those based on fly ash and slag—as the primary cementing material in smart or sensing concrete applications[6], [8].

Given the urgent need for eco-friendly construction materials and the growing interest in smart infrastructure capable of real-time structural health monitoring, this study aims to develop sustainable cement with good mechanical strength and sensing properties. The primary objective is to explore and characterize an ultra-sensitive, sustainable cement composite using fly ash and slag as partial clinker replacements. Further by integrating expandable graphite fillers into this

green cement matrix, the study seeks to improve both the mechanical strength and sensing capabilities of the material. This approach not only contributes to sustainable development goals by reducing CO_2 emissions but also promotes innovation in multifunctional construction materials.

2. *Materials and Method*

2.1 Materials and Development of Materials-Process

Portland Slag Cement (PSC) and Portland Pozzolana Cement (PPC) were directly sourced from ACC Limited, Bhilai (Adani Cement). Standard sand (Grades 1, 2, and 3) and expandable graphite (EG, Sigma Aldrich) were commercially procured. Mortar was prepared using a standard cement-to-sand ratio of 1:3, as specified in IS 650 (1991)[9]. Expandable graphite, up to 1 wt.%, was added to both PPC and PSC. The resulting mixtures were designated as EP1 (PPC + EG) and ES1 (PSC + EG), respectively. The stoichiometric amounts of cement and EG were blended using a ball milling setup at 30 rpm for 10 minutes. These mixtures were then combined with varying amounts of water to perform several physical tests, including consistency, initial and final setting times, expansion, and compressive strength.

3.1 Characterization

The structural characterization of the PPC/PSC-EG mixture was performed using an X-ray diffractometer (Bruker D8 advance A25). The surface morphology and chemical compositions were studied using Field Emission Scanning Electron Microscope (FE-SEM, make: Carl ZEISS, Gemini SEM 500) and Energy dispersive X-ray spectroscopy (EDS) respectively. The elemental compositions present in the mixture was evaluated using handheld X-ray fluorescence (XRF, ARL 9900 Series).

Specific surface area (SSA) of PSC, ES1, PPC and EP1 was calculated with Blaine Apparatus. Fineness and residue were calculated by 90 micron and 45-micron Indian standard Sieve (IS sieve) respectively. Vicat Apparatus was used to calculate consistency limit, initial setting time and final setting time of blended cement. Expansion of cement was carried out with the Le-Chatelier apparatus. 70.6 mm cube was casted for blended cement, and performed compressive strength test after up to 3 days in Compression testing machine (CTM, ACTM -1000KN).

3. *Results and Discussion*

3.1 FE-SEM of Expandable graphite, Portland pozzolana cement and Expandable Portland pozzolana cement.

The surface morphology obtained from FESEM for EG, PPC and EP1 (Fig.1). Expandable graphite appears in a flaky structure, can be used as a filler and as an additive material in cementitious or composite matrices (Fig.1a). EG expands significantly when heated, altering from small particles to long, worm-like structure (Fig.3b, c). It is observed that below 200ºC very less expansion takes place and weight of EG reduces continuously, after increasing the temperature (Fig.2 a, b).

The center rounded particles indicate the fly ash and angular particles are clinker phase or un hydrated cement particles (Fig.3d, e).

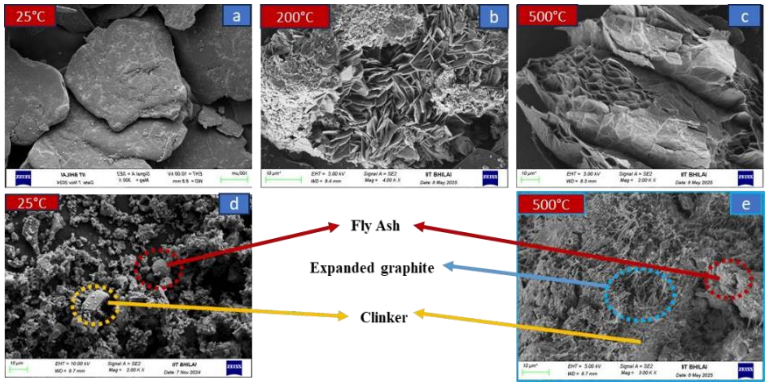


Fig.1: FESEM images of expandable graphite at different temperatures (a-c), and PPC-Expandable graphite composite at different temperatures (d, e).

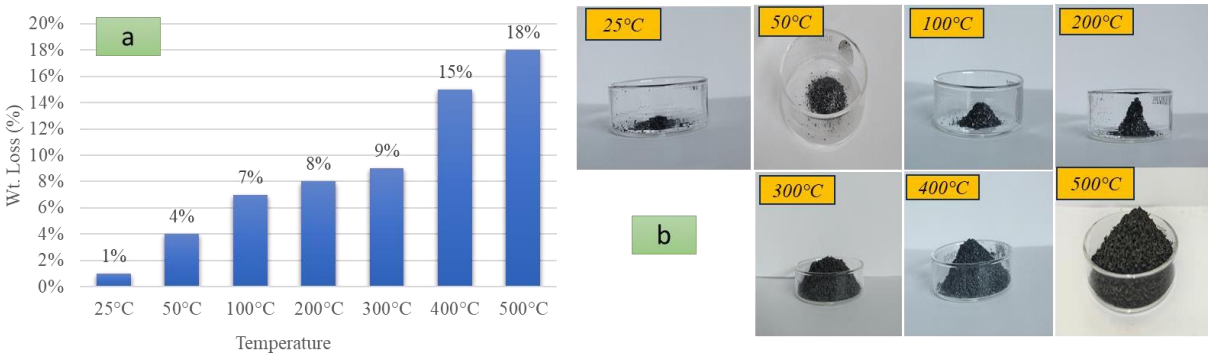


Fig. 2: (a) Weight loss during temperature of expandable graphite, (b) Expansion of expandable graphite.

3.2 X-ray Diffractometer (XRD) of Expandable graphite, Portland pozzolana cement and expandable Portland pozzolana cement.

The phase analysis of EG, PPC and EP1 are shown in Fig.4. It is observed that the peak of EG is between 26-27 degree. During the heat treatment peak shift towards the higher side. After adding the EG in PPC the peak is increased.

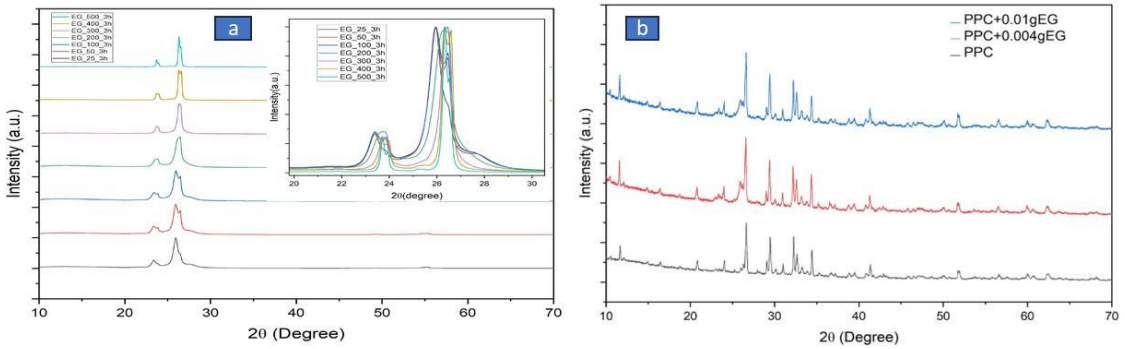


Fig. 4: XRD plot for: (a) Expandable graphite 25ºC - 500ºC, (b) PPC and EP1

3.3 X-ray fluorescence (XRF) of PSC, ES1, PPC and EP1

The elemental composition of PSC, ES1, PPC and EP1 are found by using XRF (Table 1). The major ingredients CaO, SiO2, Al2O3, Fe2O3, MgO and SO3 are present in the Compounds. They are

responsible for strength, setting time, workability and durability in cement.

Table 1: Chemical composition (%) of PSC, ES1, PPC and EP1

Cement	Chemical Composition									
	CaO	SiO2	SO3	Al2O3	Fe2O3	Na2O	MgO	K2O	Mn2O3	Gypsum
PSC	42.38	21.76	2.11	17.48	1.83	0.17	5.72	0.81	-	5.0
ES1	39.7	20.25	2.53	19.53	4.71	0.18	3.5	1.1	0.03	5.0
PPC	39.59	33.54	1.66	15.75	4.14	0.64	2	1.26	0.1	5.0
EP1	42.89	32.36	3.53	12.58	1.03	1.17	4.46	1.17	0.1	5.0

3.4 Mechanical Property: Specific surface area, Fineness, Expansion, Consistency, Compressive strength of PSC, EPSC, PPC and EPPC.

Specific surface area (SSA) is higher for EPSC and EPCC as compared to PSC and PPC. (Table 2). Due to higher SSA, leading to improved strength and durability. Fineness of composite found as per IS code [10], [11]. More fine cement provides larger surface area for hydration and leads to faster compressive strength gain and also increases the heat of hydration. Expansion is also reduced after adding the EG in PSC and PPC. Finer cement can experience greater drying shrinkage as it hydrates faster and is responsible for denser structure. The consistency of PSC and EPSC is achieved at 118 ml of water as well as for PPC and EPPC is achieved at 120 ml and 118 ml resp. initial setting time and final setting time is shown in table.2.

The result of compressive strength is illustrated in Table 2. It is noticed that adding 1% of EG in PSC, the compressive strength of Expandable graphite Portland slag cement (ES1) increased 7.7 MPa to 8.2 MPa at the curing age of 1 day. Although the addition of 1% of EG in PPC, the compressive strength of Expandable graphite pozzolana Portland cement (EP1) increased 15 MPa to 15.7 MPa at the curing age of 3 days.

Table 2: Physical property of Sustainable cement

SN	Physical test	PSC	ES1	PPC	EP1	Ref. IS Code PSC/(PPC)
1	Blaine value (m^2/kg)	309.02	319.10	388.85	398.05	IS 4031(part-2):1988 [9], [10]
2	Residue/fineness	19.1%	17.1%	8%	8.1%	IS 4031(part-2):1988 [9], [10]
3	Expansion	9 mm	8.5 mm	6.5 mm	5.2 mm	IS 4031(part-3):1988 [9], [10]
4	Consistency test	118 ml	118 ml	120 ml	118 ml	
	Initial setting time	180 minutes	180 minutes	242 minutes	223 minutes	IS 4031 (part-5):1998 [9],

	Final setting time	272 minutes	272 minutes	372 minutes	355 minutes	[10]
5	Compressive strength, 1day	7.7 MPa	8.2 MPa	-	-	IS 4031(part-6):1988 [9], [10]
3 days		-	-	15 MPa	15.7 MPa	

4. *Conclusion*

The Ultra-sensitive sustainable cement consists of slag, fly ash and expandable graphite was synthesized using a ball mill. The structural and microstructural studies of USSC were performed using XRD and Fe-SEM. The specific surface area is recorded as 319.10 m^2/kg and 398 m^2/kg for ES1 and EP1 respectively. The fineness of the composite is calculated 17.1% and 8.1% respectively. the addition of expandable graphite results in an enhancement value of compressive strength. It was calculated that the compressive strength of ES1 increased 7.7 MPa to 8.2 MPa at the curing age of 1 day and for EP1 compressive strength increased 15 MPa to 15.7 MPa at the curing age of 3 days. The preliminary results obtained in the present study indicates that the addition of EG in PSC and PPC may lead to USSC for better strength and sensitivity.

5. *Acknowledgment*

The authors would like to thank the Ministry of Human Resources and Development (MHRD) India for the PhD fellowship and also thank to Adani Cement work Bhilai (CG) for providing lab facilities.

1.1 References

[1] M. C. Bignozzi, "Sustainable cements for green buildings construction," in *Procedia Engineering*, Elsevier Ltd, 2011, pp. 915–921. doi: 10.1016/j.proeng.2011.11.2094.

[2] K. S. Thwe, J. Ayawanna, L. Z. Mase, and S. Chaiyaput, "Utilization of ladle furnace slag and fly ash as partially replacement of cement," *Clean Eng Technol*, vol. 25, p. 100910, Mar. 2025, doi: 10.1016/J.CLET.2025.100910.

[3] H. Wu *et al.*, "Smart cement for fire alarms and indoor climate control," *Chemical Engineering Journal*, vol. 482, p. 148298, Feb. 2024, doi: 10.1016/J.CEJ.2023.148298.

[4] W. Pichór and M. Frac, "Multifunctional cement composites with expanded graphite for temperature monitoring of buildings," *Advances in Cement Research*, vol. 32, no. 9, pp. 413–420, Mar. 2019, doi: 10.1680/JADCR.18.00034.

[5] Z. Wang *et al.*, "Principles, properties and applications of smart conductive cement-based composites: A state-of-the-art review," *Constr Build Mater*, vol. 408, p. 133569, Dec. 2023, doi: 10.1016/J.CONBUILDMAT.2023.133569.

[6] S. M. Ahmed and I. Kamal, "Electrical resistivity and compressive strength of cement mortar based on green magnetite nanoparticles and wastes from steel industry," *Case Studies in Construction Materials*, vol. 17, Dec. 2022, doi: 10.1016/j.cscm.2022.e01712.

[7] N. S. Piro, A. S. Mohammed, and S. M. Hamad, "Compressive strength and piezoresistivity of smart cement paste modified with waste steel slag," *Journal of Building Engineering*, vol. 70, p. 106393, Jul. 2023, doi: 10.1016/J.JOBE.2023.106393.

[8] V. C. Li, "High-Performance and Multifunctional Cement-Based Composite Material," *Engineering*, vol. 5, no. 2, pp. 250–260, Apr. 2019, doi: 10.1016/j.eng.2018.11.031.



[9] B. of Indian Standards, "IS 650 (1991): Specification for Standard Sand for Testing of Cement."

[10] B. of Indian Standards, "IS 455 (1989): Portland Slag Cement - Specification."

[11] B. of Indian Standards, "IS 1489-1 (1991): Specification for Portland pozzolana cement, Part 1: Flyash based."

CONFERENCE & EXHIBITION ON
CARBON NEUTRALITY IN CEMENT AND CONCRETE
"Towards a Sustainable & Net Zero Future"
19-20 NOVEMBER 2026
Centenary Convention Centre, Hyderabad



INFLUENCE OF ACTIVATION PARAMETERS ON THE RHEOLOGY OF HIGH-VOLUME COPPER MINE TAILINGS-BASED ALKALI-ACTIVATED BINDERS AND THEIR APPLICATION POTENTIAL

Sahil Surehali[1*], Rijul Kanth Ramasamy Jeyaprakash[1], Narayanan Neithalath[1]

[1]*School of Sustainable Engineering and the Built Environment, Arizona State University, Tempe, AZ 85287, USA;* [*]*ssurehal@asu.edu*

ABSTRACT

Low-carbon binders generally gain the trust of practitioners and industry only after they have been characterized comprehensively, from their fresh-state behavior to their hardened properties. Billions of tonnes of copper mine tailings (MT) are generated annually and largely disposed of in landfills. While our previous work established their reactivity and strength in zero-cement alkali-activated binders, their rheology, which governs mixing, pumping, and placement, remains largely uncharacterized. This study evaluates the rheology of binders containing primarily copper mine tailings (70-80% by mass) and slag (20 or 30% by mass) as the minor constituent. These dry mixtures were activated using sodium silicate solutions, with Na_2O-to-binder ratios (n) of 0.050–0.100 and silica moduli (M_s) of 1.0 and 1.5. Doubling n increases the Bingham yield stress of the MT–slag (MT–S) pastes by ~1.5-2.7 times and their plastic viscosity by ~5-9 times, attributable predominantly to the more viscous silicate-rich activator, while increasing M_s from 1.0 to 1.5 increases the yield stress by ~10-70%. Oscillatory rheology shows that the plateau storage modulus does not increase with n, indicating that the rise in yield stress reflects the liquid phase rather than a stronger particle network. Mapping the rheological signatures against the strength-based application classes, as established earlier, shows that mixtures within the same strength class can differ by ~8-fold in their rheological parameters, thereby informing mixing and placement guidelines for grouts, precast elements, and masonry applications that are recommended on a strength basis alone. Overall, this study completes the characterization of these binders from the fresh to the hardened state, supporting their use in precast and grouting applications.

Key Words: Mine tailings; Alkali-activated binders; Zero-cement binders; Rheology; Yield stress; Activation parameters.

1.0 Introduction

Concrete is the most widely used manufactured material, and the production of Portland cement clinker, which binds it, accounts for a substantial share of global anthropogenic CO_2 emissions [1]. Reducing the clinker content of binders is therefore central to the cement sector's net-zero roadmaps. The use of supplementary cementitious materials (SCMs) and alternative binders to replace ordinary Portland cement is considered the most vital strategy for developing low-carbon cementitious systems [2,3]. However, conventional SCMs such as fly ash and ground granulated blast-furnace slag (GGBFS) are finite and regionally constrained, and their supply is unlikely to keep pace with demand. This has prompted a search for alternative aluminosilicate precursors that are available in large quantities, and alkali activation as a vital route for converting such precursors into binders [4,5].

Several families of low-carbon binders are now at different stages of this transition. Blended cements containing fly ash or slag are codified (e.g., IS 1489 (Part 1) and IS 455 in India). They are in routine use, while limestone calcined clay cements (LC3) have progressed from laboratory studies to industrial production trials, supported by an extensive body of work on their hydration, strength, durability, and processing [6,7]. Alkali-activated materials (AAMs) based on slag and fly ash have been deployed in

several commercial projects [4,8]. In each case, the confidence of practitioners and industry, and the specifications and construction practices that followed, have rested on a comprehensive characterization of the binder, from its fresh-state behavior and reactivity through strength, durability, and environmental performance [4,6–8]. For AAMs, the limited availability of standards, the variability of precursors, and the sensitivity of both fresh and hardened properties to the activator remain the principal barriers to wider field use [4,8]. Any new precursor must meet the same bar of complete characterization before it can be trusted in the field.

Mine tailings (MT), which are the residue materials discharged after separating valuable ores in mining operations, are among the largest industrial waste streams, with an estimated 5-7 billion tonnes generated globally [9,10]. Most MT are impounded, occupying large land areas and posing risks of heavy metal leaching, acid mine drainage, and dam failure [11–13]. The silica- and alumina-rich composition of many tailings, including the copper tailings used here, makes them a plausible precursor for AAMs [13,14], offering twin benefits: diverting high volumes of hazardous waste to beneficial use, and producing a clinker-free binder. However, the principal impediment is the low reactivity of MT; binders based solely on activated MT generally attain 28-day compressive strengths of ≤5 MPa) [15–17]. Our earlier work has shown that incorporating GGBFS (slag) or ordinary Portland cement (OPC) as a minor reactive constituent (20-30% by mass) enables binders containing ≥70% MT to attain 28-day strengths of up to 40 MPa under ambient curing, with the slag-containing (MT–S) blends substantially outperforming the cement-containing (MT–C) ones [18]. For MT-based binders, however, the fresh-state behavior was characterized only through setting times and mini-slump spreads. While these provide basic metrics, a comprehensive rheological analysis is necessary to determine how the material will actually mix, pump, cast, and flow in practice.

The activator chemistry governs the rheology of AAMs to a much larger extent than that of OPC systems, and conventional superplasticizers are often ineffective in the highly alkaline pore solution [19,20]; studies on alkali-activated slag and fly ash-slag pastes report a strong dependence of yield stress and viscosity on the activator type, concentration, and silicate content [20–22]. The available studies on MT-based binders, including our own, focus on reactivity, strength, and microstructure [18,23–25], and their mixtures are consequently screened for setting time and assigned to applications based on strength alone [18]. A practitioner, therefore, cannot tell whether a mixture that meets a strength target can be pumped, grouted, or cast, or whether it will remain stable after placement. This is the critical gap between the laboratory development of MT-based binders and their field use.

This paper addresses this gap by evaluating the rheology of alkali-activated binders containing 70-80% copper MT by mass, with slag as the minor constituent, as a function of the slag content and the two principal activation parameters, viz., the Na_2O-to-binder ratio (n) and the activator silica modulus (M_s). Steady-shear flow curves are used to determine the yield stress, plastic viscosity, and apparent viscosity, and small-amplitude oscillatory shear is used to evaluate the viscoelastic response. The rheological signatures are then mapped against the strength-based application classes established earlier [18] to provide mixing and placement guidelines for each application. Since the setting, early-age reactivity, strength, reaction products, and leaching of the same binders have been characterized in our earlier work [18,23–25], this paper completes their characterization from the fresh to the hardened state. This is particularly relevant for the MT–S binders, which contain no Portland cement and can therefore be classified as zero-cement binders.

2.0 Experimental work

2.1 Materials

Mine tailings from a copper mine, supplied by Freeport-McMoRan Inc. (FMI) in slurry form, were dewatered, oven-dried at 80 ºC for 24 h, and crushed to a fine powder. GGBFS conforming to ASTM C989 was used as the minor reactive constituent. The chemical compositions (from X-ray fluorescence)

and physical properties of the binder constituents, also reported in [18], are listed in Table 1. The MT contains no detectable CaO; therefore, calcium in the binder is supplied only by the minor constituent. The median particle sizes (d_{50}, from laser diffraction) of MT and slag are 38.6 µm and 12.3 µm, respectively. Specific gravities were determined using a gas pycnometer, and fineness using Blaine's air permeability apparatus. A sodium silicate solution (waterglass) with a SiO_2-to-Na_2O mass ratio of 1.59 was used as the activator, and NaOH was added to it to lower the silica modulus to the desired values of 1.0 and 1.5 (to enable efficient activation), in line with previously reported work on alkali-activated binders [26,27].

Table 1: Chemical composition and physical properties of the binder ingredients.

Binder ingredients	Chemical composition									Physical properties	
Mine tailings #	SiO_2 (%)	Al_2O_3 (%)	SO_3 (%)	Fe_2O_3 (%)	Sn (%)	Mn (%)	Ti (%)	Sb (%)	P (%)	Sp. gravity	Blaine's Fineness (cm^2/g)
	64.2	19.95	1.94	8.26	1.35	0.81	0.48	2.49	0.15	2.76	898
					MgO (%)	Na_2O (%)	K_2O (%)	CaO (%)	LOI * (%)		
GGBFS	39.4	8.49	2.83	0.37	12.05	0.27	0.80	35.53	1.31	2.92	3950
*Loss on Ignition # - Heavy elements such as As, Ba, Cd, Cr, Pb, Se, and Ag were also detected in trace quantities in the mine tailings.											

2.2 Mixture Proportions

Slag replaced 20% or 30% of MT by mass, yielding binders designated 80MT-20S and 70MT-30S, respectively. The activator was proportioned using two parameters: n, the Na_2O-to-binder (MT + slag) mass ratio, and M_s, the SiO_2-to-Na_2O mass ratio of the activator. For the MT-S pastes, n values of 0.050, 0.075, and 0.100 and M_s values of 1.0 and 1.5 were used, at a water-to-binder ratio (w/b) of 0.35. Note that the water includes both the water from the activating solution and the externally added water. The mixture matrix is summarized in Table 2. The activator was prepared by adding NaOH to the waterglass and allowing the solution to cool to ambient temperature before mixing; the proportioning procedure is detailed in [18].

Table 2: Binder compositions and activation parameters of the pastes.

Binder system	Binder designation	Slag (% by mass)	n	M_s	w/b
Mine tailings (MT) – slag (S)	80MT–20S	20	0.050, 0.075, 0.100	1.0, 1.5	0.35
	70MT–30S	30	0.050, 0.075, 0.100	1.0, 1.5	0.35

2.3 Rheological Measurements

Rheological measurements were carried out using a TA Instruments AR 2000EX rotational rheometer

with a vane-in-cup geometry, which minimizes wall slip in cementitious suspensions [28]. The temperature was maintained at 25 ± 0.1 °C, and approximately 40 mL of paste was placed in the cup using a syringe. Three replicates were tested for each mixture, and the average values are reported. Steady-shear flow curves were obtained using a strain-controlled protocol adopted in our earlier work [29,30]: a stepped pre-shear from 10 to 100 s^{-1} over ~75 s to homogenize the paste, followed by a stepped ramp-down to 0.005 s^{-1}, a ramp-up to 100 s^{-1}, and a final ramp-down to 0.005 s^{-1}. At each step, data were acquired every second until three consecutive torque readings were within 8% of one another, after which the test proceeded to the next shear rate. The yield stress and plastic viscosity were obtained by fitting the Bingham model (Eq. 1) to the linear portion of the ramp-down flow curve; the yield stress thus obtained is the dynamic yield stress, extrapolated from the flowing state:

$$\tau = \mu_p \dot{\gamma} + \tau_y \quad (1)$$

where τ = shear stress (Pa); μ_p = plastic viscosity (Pa.s); $\dot{\gamma}$ = shear rate (s^{-1}); τ_y = yield stress (Pa). The apparent viscosity, $\eta = \tau/\dot{\gamma}$, was computed at each shear rate. Second, a small amplitude oscillatory shear study (stress-controlled) was used to determine the storage and loss moduli of MT-S pastes. An oscillatory stress was applied from 0.005 Pa to 10 Pa at a frequency of 1 Hz. This stress range was found to capture the linear viscoelastic regime in the MT-S pastes. The experimental duration was minimized to limit the effects of hydration.

3.0 Results and Discussions

3.1 Yield stress and plastic viscosity of MT-S pastes

Fig. 1 presents the yield stress and plastic viscosity of the MT–S pastes as a function of *n* for both M_s values. Both parameters increase with *n* for all the pastes. Doubling *n* from 0.050 to 0.100 increases the yield stress by ~1.5-2.7 times (from ~1.5-3.4 Pa to ~2.8-4.9 Pa) and the plastic viscosity by ~5-9 times (from ~0.8 Pa.s to ~3.8-6.9 Pa.s). The larger increase in plastic viscosity indicates that the effect of *n* is predominantly manifested in the liquid phase. At a constant M_s, a higher *n* requires a proportionally greater amount of sodium silicate, and the resulting activator is both denser and more viscous [31,32]. Since the Bingham yield stress is extrapolated from the flowing state, it is also influenced by the viscosity of the suspending liquid; as shown in Sections 3.2 and 3.3, the at-rest particle network does not strengthen in proportion to it. Similar increases in shear stress with Na_2O content have been reported for alkali-activated slag pastes [20].

Increasing M_s from 1.0 to 1.5 increases the yield stress by ~10-70%, depending on *n* and the slag content. Its influence on plastic viscosity, however, is marginal at *n* = 0.050 and 0.075, but pronounced at *n* = 0.100, where the plastic viscosity is ~60-65% higher at M_s = 1.5 than at M_s = 1.0. This dependence is expected, since the SiO_2 supplied by the activator scales with the product of *n* and M_s: at *n* = 0.050, raising M_s from 1.0 to 1.5 adds only 2.5 g of SiO_2 per 100 g of binder, whereas at *n* = 0.100 it adds 5 g. It is worth noting that a higher M_s has been shown to prolong the setting time of MT–S binders [23]. The higher yield stress and viscosity at M_s = 1.5 are therefore unlikely to arise from accelerated product formation. They are more plausibly attributable to the higher viscosity of the silicate-rich pore solution and the interaction of silicate species with the particle surfaces [19,33].

In general, the yield stress of the 70MT-30S pastes is ~20-45% lower than that of the corresponding 80MT-20S pastes (except *n* = 0.100 and M_s = 1.5, where the two are similar), while the plastic viscosity is only marginally affected. This is noteworthy since slag is ~3 times finer than MT, and replacing coarser particles with finer ones typically increases the yield stress of cementitious suspensions. Note that the difference in specific gravity between slag and MT (Table 1) alters the solid volume fraction by <0.5% at a constant *w/b*, and cannot explain the observed reduction. Two mechanisms are plausible: (i) since the van der Waals attraction between two particles scales with their size, replacing a part of the coarser MT with finer slag reduces the average interparticle attraction; and (ii) the Ca-rich slag surfaces

adsorb silicate species from the activator, increasing their negative surface charge and the electrostatic repulsion between particles [33].

Across all MT–S pastes, the yield stress and plastic viscosity increase together, though not strictly proportionally, and the activation parameters exert a stronger influence on rheology than the slag content within the range considered here. Furthermore, since lower M_s and higher n values have been shown to yield higher strengths in MT–S blends [18], selecting M_s = 1.0 over 1.5 at a high n offers a twin benefit: it favors strength development while reducing the plastic viscosity by ~35-40% at n = 0.100, thereby easing pumping and placement.

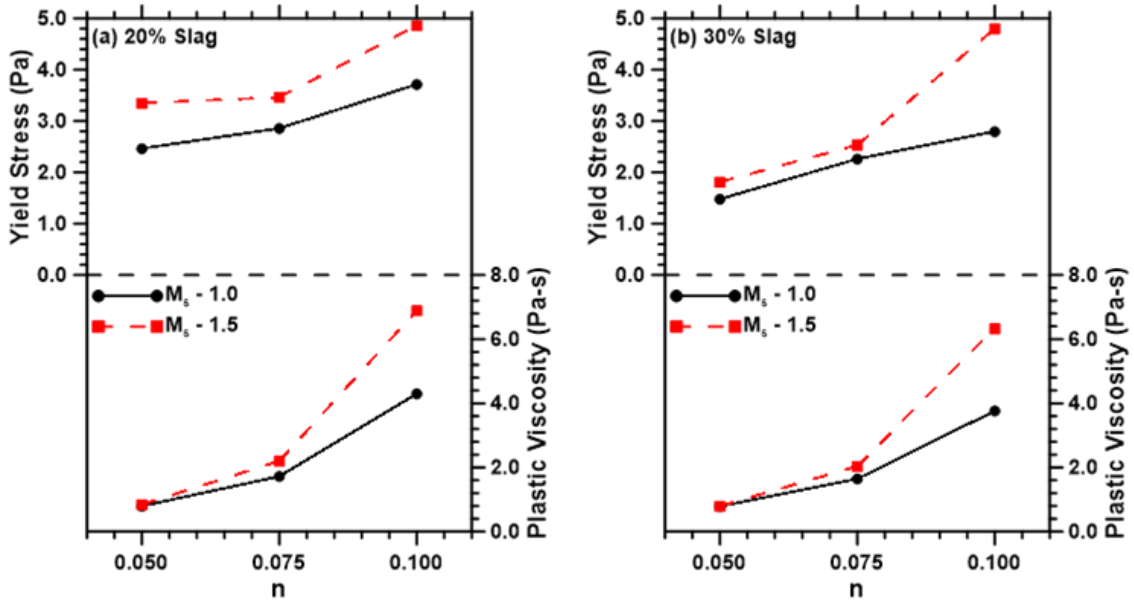


Figure 1: Yield stress and plastic viscosity for: mine tailings (MT) – slag (S) pastes with - (a) 20% slag content and (b) 30% slag content as a function of n, for Ms values of 1.0 and 1.5.

3.2 Apparent Viscosity

Fig. 2 shows the apparent viscosity of the MT–S pastes as a function of shear rate. All the pastes are shear-thinning, with the apparent viscosity decreasing by a factor of ~5 to >100 between 0.005 s^{-1} and 100 s^{-1}. At low shear rates, the flocculated particle network, held together by colloidal attractive forces, resists deformation; as the shear rate increases, this network is progressively broken down, and the viscous contribution of the suspending liquid begins to dominate [30]. Consequently, the apparent viscosities of all the pastes converge to ≲15 Pa.s above ~1 s^{-1}, and at these shear rates the pastes with n = 0.100 exhibit the highest apparent viscosity, in line with their higher plastic viscosity (Fig. 2).

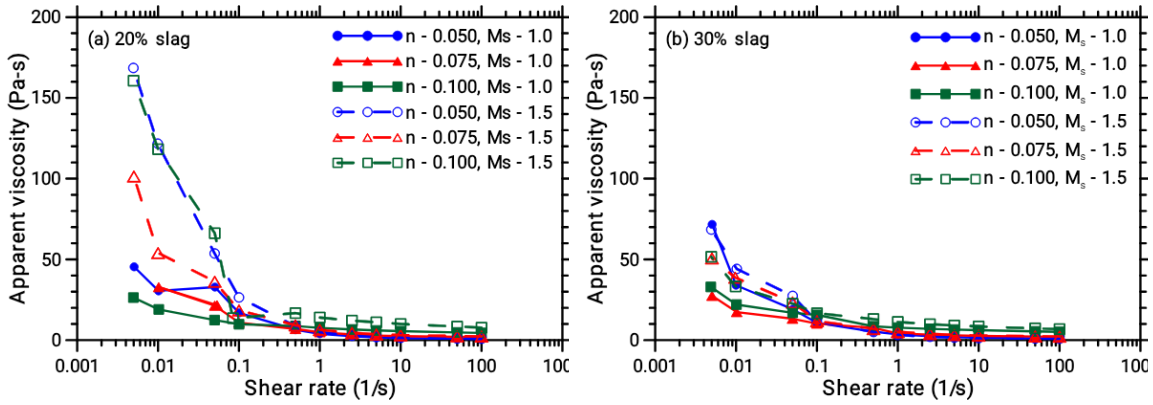


Figure 2: Apparent viscosity as a function of shear rate for MT–S pastes with (a) 20% slag and (b) 30% slag.

In contrast, at the lowest shear rates, the apparent viscosity is governed by the at-rest structure and does not follow the trends in plastic viscosity. For the 80MT-20S pastes, the apparent viscosity at 0.005 s^{-1} is ~100-170 Pa.s at M_s = 1.5, as compared to ~25-45 Pa.s at M_s = 1.0. Note that at M_s = 1.0, the 80MT–20S paste with n = 0.100 exhibits the lowest apparent viscosity at 0.005 s^{-1} (~25 Pa.s) despite having the highest Bingham yield stress (Fig. 1), which is corroborated by the oscillatory response in Section 3.3. For the 70MT-30S pastes, the values lie within a narrower band of ~25-70 Pa.s, once again reflecting the weaker interparticle attraction at the higher slag content (Section 3.1). The practical implication is that the differences among the activation parameters are most consequential at rest and at low shear rates, i.e., for stability against segregation and bleeding, and for the stress required to restart flow, while under the high shear rates encountered during mixing and pumping, the pastes behave rather similarly.

3.3 Viscoelastic Response from Oscillatory Rheology

Fig. 3 shows the storage and loss moduli of the 80MT–20S pastes as a function of the applied oscillatory stress. All the pastes exhibit the typical response of a structured suspension: a plateau at low stresses (the LVER), followed by a decrease in the moduli as the particle network breaks down beyond critical stress, and a low-modulus region at higher stresses [34]. Since the structure is probed without disruption within the LVER, these tests characterize the at-rest structure that steady-shear measurements cannot resolve.

At n = 0.050 and 0.075, G' (~30-50 Pa in the plateau) exceeds G", indicating a predominantly solid-like response. At n = 0.100, G″ exceeds G′ at both M_s values, i.e., the response becomes viscous dominated. Note that the plateau G′ does not increase with n: it remains at ~30-50 Pa at M_s = 1.5 and drops to ~5-10 Pa at n = 0.100 for M_s = 1.0. This corroborates the low-shear apparent viscosities (Section 3.2) and shows that the higher Bingham yield stress at higher n (Fig. 1) reflects the more viscous liquid phase rather than a stronger particle network. The larger dissipative contribution of the concentrated silicate solution raises G". In contrast, silicate species adsorbed on the particle surfaces plausibly increase interparticle repulsion [17,33], thereby limiting the build-up of the elastic network. The M_s value mainly influences the stability of the structure: at M_s = 1.5, the critical stress at which G′ begins to decrease shifts from ~0.1-0.2 Pa at n = 0.050 to ~0.5-1 Pa at n = 0.100, while G″ in the plateau increases from ~15 Pa to ~70 Pa, indicating a more viscous yet more stress-resistant structure at higher silicate contents. The pastes with 30% slag show similar trends, with generally lower moduli, consistent with their lower yield stresses.

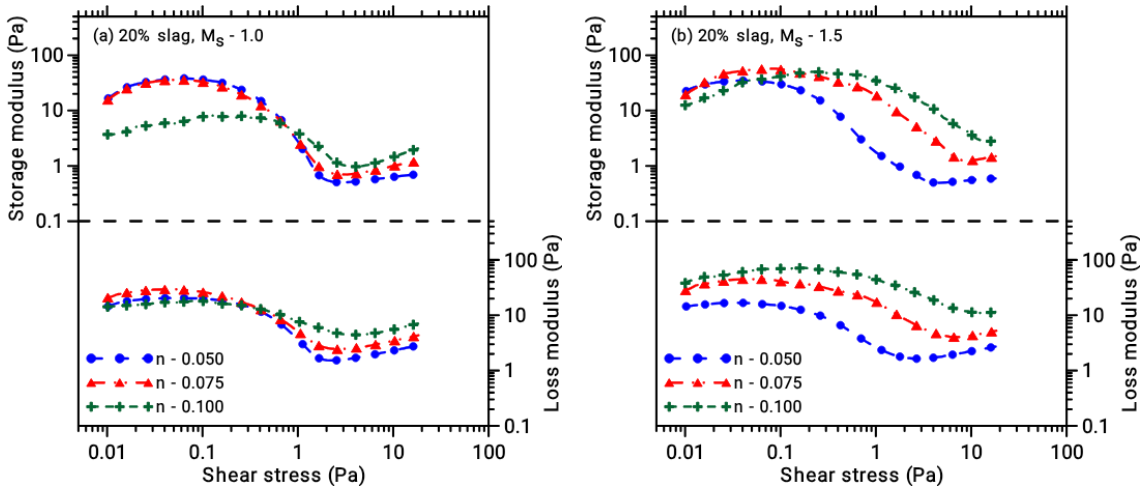


Figure 3: Storage modulus (upper) and loss modulus (lower) as a function of oscillatory shear stress for 80MT–20S pastes with M_s of (a) 1.0 and (b) 1.5.

3.4 Rheology-based selection of MT–S binders for end applications

In our earlier work [18], the MT-based were classified into end-application categories solely based on their 28-day compressive strengths. As noted in [18], this classification was intended to be augmented with information on flow and early-age behavior, as strength alone cannot be the criterion for selecting a mixture, since the mixture must first be mixed, transported, and placed. Ultimately, it is the setting and early-age flow behavior, in conjunction with hardened strength, that dictate whether this can be done and establish the decision guidelines for practical end-applications. Table 3, therefore, maps the same MT–S mixtures, with the strength-based application classes assigned to them in [18], against their rheological signature from this study, so that mixing and placement guidelines can be stated in terms of rheological properties for each application.

Table 3: Strength-based application classes of the MT–S mixtures [18] mapped against their rheological parameters (Fig. 1) and the resulting placement guidelines.

Binder	M_s	n	Application class based on 28-day strength [10]	τ_y (Pa)	μ_p (Pa·s)	Rheology-based placement guideline
80MT–20S	1.0	0.050	Grout for masonry (14–25 MPa)	2.5	0.8	Highly fluid (G1)
		0.075		2.9	1.7	Fluid (G2)
		0.100		3.7	4.3	Viscous (G3)
	1.5	0.050		3.3	0.8	Highly fluid (G1)
		0.075		3.5	2.2	Fluid (G2)
		0.100		4.9	6.9	Viscous (G3)
70MT–30S	1.0	0.050	High-strength grout and precast load-bearing (>25 MPa)	1.5	0.8	Highly fluid (G1)
		0.075		2.3	1.6	Fluid (G2)
		0.100		2.8	3.8	Viscous (G3)
	1.5	0.050		1.8	0.8	Highly fluid (G1)
		0.075		2.5	2.0	Fluid (G2)
		0.100		4.8	6.3	Viscous (G3)

G1: highly fluid (μ_p < 1 Pa·s); suited to pumped grouts and self-leveling fills, with stability against bleeding to be ensured. G2: fluid (μ_p ~1.5–2.5 Pa·s); suited to pumping and casting. G3: viscous (μ_p > 3.5 Pa·s); suited to casting, with higher pumping pressures required.

Two observations stand out from Table 3. First, mixtures that belong to the same strength class can differ substantially in their rheology: all the 70MT-30S mixtures qualify as high-strength grouts or precast load-bearing binders [18], yet their plastic viscosities span from 0.8 to 6.3 Pa.s, i.e., by a factor of ~8. The mini-slump spreads of these mixtures (~99-115 mm [18]) are rather invariant, showing that a simple flow test cannot discriminate among them, while the rheological parameters can. Second, within a given strength class, the rheology provides the basis for the final selection: for pumped high-strength grouts, n = 0.050-0.075 with M_s = 1.0 offers the lowest plastic viscosity (~0.8-1.6 Pa.s), albeit with the fastest setting among the MT–S blends at n = 0.05 [18], whereas n = 0.10 with M_s = 1.5 yields the most viscous paste and requires higher pumping pressures.

These guidelines also serve the sustainability objective of the binders. Every tonne of MT-S binder diverts 0.7-0.8 t of tailings from impoundment, uses slag (an industrial by-product) as the only other solid constituent, and contains no Portland cement. In AAMs, the activator, particularly sodium silicate, typically contributes the largest share of the embodied CO_2 [12]; the lowest n and M_s that satisfy the performance requirement therefore minimize activator-related emissions, and Table 3 enables this choice without compromising placement. The applications identified for these binders, such as precast masonry units, non-load bearing and load-bearing panels, and grouts [18], are those in which the handling of alkaline activators can be controlled in a factory or confined to small volumes. With the rheology reported here, the MT-S binders are now characterized from setting and flow through reactivity, strength, reaction products, and leaching [18,23–25], which is the same body of evidence on which the acceptance of several low-carbon cementitious systems is based, and which producers and specifiers require before applying a new binder in the field. Durability under field exposure and a system-specific life-cycle assessment are the remaining steps toward specifications for these binders.

4.0 Conclusions

This study evaluated the rheology of alkali-activated binders containing 70-80% copper mine tailings by mass, with slag as the remaining minor constituent. These dry materials were activated using sodium silicate solutions with n = 0.050-0.100 and M_s = 1.0-1.5. The objective was to determine how the activation parameters and the amount of the minor constituent influence the fresh-state behavior of these binders, and to relate this to the strength-based application classes established earlier. The conclusions drawn from this work are succinctly enumerated below.

1. Doubling n from 0.050 to 0.100 increased the yield stress of the MT–S pastes by ~1.5-2.7 times and their plastic viscosity by ~5-9 times, attributable predominantly to the more viscous silicate-rich activator. Increasing M_s from 1.0 to 1.5 increased the yield stress by ~30-70%, and the plastic viscosity by ~60-70% at n = 0.10.
2. Increasing the slag content from 20% to 30% generally reduced the yield stress by ~20-45%, despite the finer slag size, attributed to weaker van der Waals attraction and the adsorption of silicate species on the slag surfaces.
3. The at-rest response of the 80MT-20S pastes was solid-like ($G' > G''$) at $n \leq 0.075$ and viscous-dominated at n = 0.100; the plateau storage modulus did not increase with n, showing that the higher Bingham yield stress at higher n reflects the liquid phase rather than a stronger particle network.
4. Mixtures within the same strength-based application class differ substantially in rheology: the 70MT-30S mixtures, all classified for high-strength grouts or precast load-bearing use, span ~0.8-6.3 Pa.s in plastic viscosity with nearly identical mini-slump spreads. Rheological parameters,

therefore, provide the mixing and placement guidelines that strength and simple flow tests cannot, with M_s = 1.0 preferable for both workability and strength.

5. With their rheology established, the zero-cement MT–S binders containing 70-80% tailings are now characterized from setting and flow through reactivity, strength, reaction products, and leaching, providing the basis needed for their adoption in precast and grouting applications.

5.0 Acknowledgement

The authors sincerely acknowledge Freeport McMoRan Inc. for supplying the mine tailings and for financial support of this work through the NSF Engineering Research Center on Bio-Mediated and Bio-Inspired Geotechnics (CBBG) at ASU. The cement and slag used in this work were supplied by Salt River Materials Group (Phoenix Cement) and Cemex, respectively, and PQ Corp supplied the sodium silicate. Their contributions are also acknowledged.

References

[1] M. Schneider, The cement industry on the way to a low-carbon future, Cement and Concrete Research 124 (2019) 105792. https://doi.org/10.1016/j.cemconres.2019.105792.

[2] K.A. Knight, P.R. Cunningham, S.A. Miller, Optimizing supplementary cementitious material replacement to minimize the environmental impacts of concrete, Cement and Concrete Composites 139 (2023) 105049. https://doi.org/10.1016/j.cemconcomp.2023.105049.

[3] F. Althoey, W.S. Ansari, M. Sufian, A.F. Deifalla, Advancements in low-carbon concrete as a construction material for the sustainable built environment, Developments in the Built Environment 16 (2023) 100284. https://doi.org/10.1016/j.dibe.2023.100284.

[4] J.L. Provis, Alkali-activated materials, Cement and Concrete Research 114 (2018) 40–48. https://doi.org/10.1016/j.cemconres.2017.02.009.

[5] P. Duxson, A. Fernández-Jiménez, J.L. Provis, G.C. Lukey, A. Palomo, J.S.J. van Deventer, Geopolymer technology: the current state of the art, J Mater Sci 42 (2007) 2917–2933. https://doi.org/10.1007/s10853-006-0637-z.

[6] K.L. Scrivener, V.M. John, E.M. Gartner, Eco-efficient cements: Potential economically viable solutions for a low-CO2 cement-based materials industry, Cement and Concrete Research 114 (2018) 2–26. https://doi.org/10.1016/j.cemconres.2018.03.015.

[7] K. Scrivener, F. Martirena, S. Bishnoi, S. Maity, Calcined clay limestone cements (LC3), Cement and Concrete Research 114 (2018) 49–56. https://doi.org/10.1016/j.cemconres.2017.08.017.

[8] I. Pol Segura, N. Ranjbar, A. Juul Damø, L. Skaarup Jensen, M. Canut, P. Arendt Jensen, A review: Alkali-activated cement and concrete production technologies available in the industry, Heliyon 9 (2023) e15718. https://doi.org/10.1016/j.heliyon.2023.e15718.

[9] R.S. Krishna, F. Shaikh, J. Mishra, G. Lazorenko, A. Kasprzhitskii, Mine tailings-based geopolymers: Properties, applications and industrial prospects, Ceramics International 47 (2021) 17826–17843. https://doi.org/10.1016/j.ceramint.2021.03.180.

[10] S.M.A. Qaidi, B.A. Tayeh, A.M. Zeyad, A.R.G. de Azevedo, H.U. Ahmed, W. Emad, Recycling of mine tailings for the geopolymers production: A systematic review, Case Studies in Construction Materials 16 (2022) e00933. https://doi.org/10.1016/j.cscm.2022.e00933.

[11] A. Jamshidi-Zanjani, M. Saeedi, Metal pollution assessment and multivariate analysis in sediment of Anzali international wetland, Environ Earth Sci 70 (2013) 1791–1808. https://doi.org/10.1007/s12665-013-2267-5.

[12] J.L. Provis, Alkali-activated materials, Cement and Concrete Research 114 (2018) 40–48.



https://doi.org/10.1016/j.cemconres.2017.02.009.

[13] B.A. Akinyemi, P.A. Alaba, A. Rashedi, Selected performance of alkali-activated mine tailings as cementitious composites: A review, Journal of Building Engineering 50 (2022) 104154. https://doi.org/10.1016/j.jobe.2022.104154.

[14] Z. Xiaolong, Z. Shiyu, L. Hui, Z. Yingliang, Disposal of mine tailings via geopolymerization, Journal of Cleaner Production 284 (2021) 124756. https://doi.org/10.1016/j.jclepro.2020.124756.

[15] N. Ouffa, R. Trauchessec, M. Benzaazoua, A. Lecomte, T. Belem, A methodological approach applied to elaborate alkali-activated binders for mine paste backfills, Cement and Concrete Composites 127 (2022) 104381. https://doi.org/10.1016/j.cemconcomp.2021.104381.

[16] P. Perumal, H. Niu, J. Kiventerä, P. Kinnunen, M. Illikainen, Upcycling of mechanically treated silicate mine tailings as alkali activated binders, Minerals Engineering 158 (2020) 106587. https://doi.org/10.1016/j.mineng.2020.106587.

[17] B. Koohestani, P. Mokhtari, E. Yilmaz, F. Mahdipour, A.K. Darban, Geopolymerization mechanism of binder-free mine tailings by sodium silicate, Construction and Building Materials 268 (2021) 121217. https://doi.org/10.1016/j.conbuildmat.2020.121217.

[18] R.K.R. Jeyaprakash, S. Surehali, A. Simon, T. Han, A. Kumar, N. Neithalath, Early-age reactivity and strength development in high volume mine tailings-based alkali activated binders and their application potential, Minerals Engineering 213 (2024) 108759.

[19] K. Vance, A. Dakhane, G. Sant, N. Neithalath, Observations on the rheological response of alkali activated fly ash suspensions: the role of activator type and concentration, Rheol Acta 53 (2014) 843–855. https://doi.org/10.1007/s00397-014-0793-z.

[20] F. Puertas, C. Varga, M.M. Alonso, Rheology of alkali-activated slag pastes. Effect of the nature and concentration of the activating solution, Cement and Concrete Composites 53 (2014) 279–288. https://doi.org/10.1016/j.cemconcomp.2014.07.012.

[21] X. Dai, S. Aydin, M.Y. Yardimci, G. De Schutter, Rheology and structural build-up of sodium silicate- and sodium hydroxide-activated GGBFS mixtures, Cement and Concrete Composites 131 (2022) 104570. https://doi.org/10.1016/j.cemconcomp.2022.104570.

[22] M.F. Alnahhal, T. Kim, A. Hajimohammadi, Distinctive rheological and temporal viscoelastic behaviour of alkali-activated fly ash/slag pastes: A comparative study with cement paste, Cement and Concrete Research 144 (2021) 106441. https://doi.org/10.1016/j.cemconres.2021.106441.

[23] S. Surehali, A. Simon, R.K. Ramasamy, N. Neithalath, A Comparison of the Effect of Activator Cations (Sodium and Potassium) on the Fresh and Hardened Properties of Mine Tailing-Slag Binders, Construction Materials 3 (2023) 389–404. https://doi.org/10.3390/constrmater3040025.

[24] S. Surehali, T. Han, J. Huang, A. Kumar, N. Neithalath, On the use of machine learning and data-transformation methods to predict hydration kinetics and strength of alkali-activated mine tailings-based binders, Construction and Building Materials 419 (2024) 135523. https://doi.org/10.1016/j.conbuildmat.2024.135523.

[25] A. Simon, S. Surehali, N. Neithalath, Reaction Products, Microstructure, and Leaching Potential of Alkali-Activated Mine Tailings–Slag Binders, Journal of Materials in Civil Engineering 38 (2026) 04025503. https://doi.org/10.1061/JMCEE7.MTENG-20621.

[26] A. Dakhane, S. Das, S. Kailas, N. Neithalath, Elucidating the Crack Resistance of Alkali-Activated Slag Mortars Using Coupled Fracture Tests and Image Correlation, Journal of the American Ceramic Society 99 (2016) 273–280. https://doi.org/10.1111/jace.13960.



[27] K. Vance, M. Aguayo, A. Dakhane, D. Ravikumar, J. Jain, N. Neithalath, Microstructural, Mechanical, and Durability Related Similarities in Concretes Based on OPC and Alkali-Activated Slag Binders, Int J Concr Struct Mater 8 (2014) 289–299. https://doi.org/10.1007/s40069-014-0082-3.

[28] A. Arora, M. Aguayo, H. Hansen, C. Castro, E. Federspiel, B. Mobasher, N. Neithalath, Microstructural packing- and rheology-based binder selection and characterization for Ultra-high Performance Concrete (UHPC), Cement and Concrete Research 103 (2018) 179–190. https://doi.org/10.1016/j.cemconres.2017.10.013.

[29] S. Surehali, C. Gustafson, S.S. Volaity, R. Divigalpitiya, A. Kumar, N. Neithalath, Rheology and early-age structure development in binary and ternary blends modified with novel graphene types, Cement and Concrete Composites 156 (2025) 105869. https://doi.org/10.1016/j.cemconcomp.2024.105869.

[30] S. Surehali, A. Venkatachalam, R. Divigalpitiya, A. Kumar, N. Neithalath, Ultra-low dosages of novel graphene types enhance the rheological properties and buildability of 3D printed binders, Next Materials 8 (2025) 100811. https://doi.org/10.1016/j.nxmate.2025.100811.

[31] X. Dai, S. Aydin, M.Y. Yardimci, G. De Schutter, Rheology and structural build-up of sodium silicate- and sodium hydroxide-activated GGBFS mixtures, Cement and Concrete Composites 131 (2022) 104570. https://doi.org/10.1016/j.cemconcomp.2022.104570.

[32] M.F. Alnahhal, T. Kim, A. Hajimohammadi, Distinctive rheological and temporal viscoelastic behaviour of alkali-activated fly ash/slag pastes: A comparative study with cement paste, Cement and Concrete Research 144 (2021) 106441. https://doi.org/10.1016/j.cemconres.2021.106441.

[33] A. Kashani, J.L. Provis, G.G. Qiao, J.S.J. van Deventer, The interrelationship between surface chemistry and rheology in alkali activated slag paste, Construction and Building Materials 65 (2014) 583–591. https://doi.org/10.1016/j.conbuildmat.2014.04.127.

[34] J.E. Wallevik, Rheological properties of cement paste: Thixotropic behavior and structural breakdown, Cement and Concrete Research 39 (2009) 14–29. https://doi.org/10.1016/j.cemconres.2008.10.001.

SYNERGISTIC UTILIZATION OF FLY ASH, GGBS AND LIMESTONE FOR SUSTAINABLE MULTI-BLENDED CEMENT DEVELOPMENT

Manish Kuchya, Bhavik Patel, K Suresh, Awadhesh Singh & Satyabrata Sharma

Central R&D, UltraTech Cement Limited, Mumbai

Abstract

The development of low-carbon cementitious materials is critical for reducing the environmental footprint of the construction industry. Multi-blended cements incorporating supplementary cementitious materials (SCMs) such as fly ash, ground granulated blast furnace slag (GGBS), and limestone offer significant opportunities for clinker reduction while maintaining performance. This study investigates the synergistic utilization of fly ash, GGBS, and limestone for the development of sustainable multi-blended cements.

A comprehensive experimental program was undertaken involving characterization of constituent materials through chemical, physical, and mineralogical analyses, followed by the design of cement blends with varying replacement levels of fly ash, GGBS, and limestone. Hydration behavior was evaluated using isothermal conduction calorimetry to understand the influence of individual and combined SCMs on hydration kinetics. The performance of the developed blends was assessed through setting characteristics and compressive strength development at different curing ages.

The results demonstrate that the combined use of fly ash, GGBS, and limestone produces synergistic effects that enhance hydration, optimize particle packing, and improve strength development compared to conventional binary blended systems. The incorporation of limestone was found to accelerate early-age hydration, while fly ash and GGBS contributed to continued strength gain through pozzolanic and latent hydraulic reactions. The optimized multi-blended formulations achieved substantial clinker reduction without compromising performance.

The study highlights the potential of fly ash-GGBS-limestone multi-blended cements as sustainable low-carbon alternatives to conventional Portland cement, supporting circular economy principles and decarbonization objectives within the cement industry.

Keywords: Multi-blended cement, Fly ash, GGBS, Limestone, Low-carbon cement, Conduction calorimetry, Sustainable construction, Clinker reduction.

1. Introduction

Cement and concrete are indispensable to modern infrastructure; however, the manufacture of Portland cement clinker is associated with substantial carbon dioxide emissions arising from limestone calcination and high-temperature fuel combustion. With continued growth in global construction demand, reduction of the clinker factor has become one of the most technically mature and economically feasible pathways for lowering the embodied carbon of cementitious materials. Increased use of supplementary cementitious materials (SCMs), together with more efficient utilization of Portland cement clinker, has therefore been identified as a central strategy for the near- and medium-term decarbonisation of the cement and concrete industry [1,2].

Conventional blended cements generally incorporate a single SCM, most commonly fly ash or ground granulated blast-furnace slag (GGBS). Fly ash contributes to later-age performance through pozzolanic reactions involving its reactive aluminosilicate glass and the calcium hydroxide generated during clinker hydration. These reactions produce additional calcium silicate hydrate and calcium aluminosilicate hydrate phases, which can progressively refine the pore structure and improve long-term performance. GGBS, by contrast, is a latent hydraulic material with comparatively higher calcium

content and can contribute more significantly to intermediate- and later-age hydration when adequately activated by the alkaline and sulphate-bearing environment of hydrating Portland cement [2,3]. The extent of reaction of both SCMs is strongly governed by their glass content, chemical composition, fineness, curing temperature and the availability of water and reactive space [2,3].

Although clinker substitution with fly ash or GGBS can substantially reduce the environmental burden of cement, high replacement levels may result in slower early-age hydration, delayed setting and reduced early strength, particularly under ambient or low-temperature curing. These performance limitations arise partly from the dilution of rapidly reacting clinker phases and partly from the slower intrinsic reaction kinetics of the SCMs. Consequently, simply increasing the replacement level of an individual SCM does not necessarily result in an optimum balance among clinker reduction, hydration rate and mechanical performance. Multicomponent binder design offers an alternative approach in which materials with complementary physical and chemical characteristics are combined to compensate for their individual limitations [1–3].

Limestone is particularly attractive for multi-blended cement because it is widely available, requires substantially less processing energy than clinker, and can influence hydration through both physical and chemical mechanisms. Fine limestone particles improve particle-size distribution and provide additional surfaces for the nucleation and growth of hydration products, thereby accelerating the early hydration of clinker phases. Limestone also increases the effective water-to-reactive-solid ratio and provides additional space for hydrate precipitation when it partly replaces clinker or another SCM [4–6]. Experimental investigations of slag-limestone systems have shown that limestone can enhance both clinker and slag hydration through the combined effects of nucleation, increased hydrate-growth space and changes in pore-solution chemistry [5].

Limestone is therefore not necessarily an inert diluent in blended cement. Calcite can react with dissolved aluminate species released from clinker, fly ash and GGBS to form hemicarboaluminate and monocarboaluminate phases. This carbonate-aluminate interaction can stabilize ettringite, modify the AFt-AFm phase assemblage and increase the solid volume of hydration products [4–7]. The resulting changes in phase assemblage may contribute to pore refinement and strength development, provided that the limestone content, aluminate availability, sulphate balance and curing conditions are appropriately controlled. In ternary slag-limestone cement, the ability of limestone to enhance clinker and slag hydration and alter the distribution of aluminate-bearing hydrates has been demonstrated using isothermal calorimetry, quantitative X-ray diffraction, thermogravimetry, microscopy and pore-solution analysis [5].

Similar synergistic interactions have been reported in Portland cement-fly ash-limestone systems. Fine limestone can partly compensate for the lower early reactivity of fly ash through filler and nucleation effects, while the alumina released during fly ash reaction supports the formation of carbonate-bearing AFm phases. De Weerdt et al. reported that replacing a portion of fly ash with fine limestone in high-volume fly ash cement produced a measurable improvement in 28-day strength, indicating that the response could not be explained solely by dilution or particle packing [6,7]. Such observations demonstrate that the performance of multi-blended cement depends not only on the individual reactivity of its components but also on interactions among clinker hydration, SCM dissolution, carbonate-aluminate reactions and microstructural development.

The simultaneous incorporation of fly ash and GGBS offers further potential for complementary hydration. GGBS supplies relatively reactive calcium, silica and alumina and can support intermediate-age strength development, whereas fly ash generally contributes more gradually through pozzolanic transformation and continued refinement of the hydrate assemblage. Limestone may bridge the early-age performance gap by accelerating clinker hydration and providing nucleation sites, while its reaction with aluminate species derived from both GGBS and fly ash can increase the efficiency with which these constituents are utilized. Recent calorimetric studies of multicomponent cements continue to



demonstrate that the proportions of fly ash and GGBS markedly influence heat-flow characteristics, reaction kinetics and the timing and intensity of the principal hydration peaks [8].

Nevertheless, the behaviour of a fly ash-GGBS-limestone system cannot be predicted by simply superimposing the performance of corresponding binary cements. Increasing the total SCM content reduces the amount of clinker available to generate calcium hydroxide, sulphates and alkalis required for SCM activation. At the same time, competition may occur among silicate, aluminate, sulphate and carbonate reactions. The magnitude of synergy is therefore sensitive to constituent proportions, fineness, glass content, limestone purity, clinker mineralogy, sulphate balance, water-to-binder ratio and curing age [2,5,9]. Optimization is consequently necessary to identify formulations in which the clinker content is substantially reduced without causing unacceptable retardation, excessive dilution or loss of early and later-age strength.

Despite extensive research on binary Portland cement-fly ash and Portland cement-GGBS systems, and growing knowledge of fly ash-limestone and slag-limestone ternary cements, comparatively limited systematic information is available on Portland cement binders containing fly ash, GGBS and limestone simultaneously. Much of the available work has focused either on binary combinations, individual ternary systems, concrete-level performance, or alkali-activated and geopolymer binders rather than conventionally hydrated Portland multi-blended cement [5–10]. A 2024 investigation of fly ash, blast-furnace slag and limestone powder, for example, examined their combined use in alkali-activated geopolymer mortars, highlighting the continued research interest in optimising these three materials but also illustrating the need for corresponding understanding in Portland cement-based systems [10].

A further knowledge gap concerns the direct relationship between constituent proportions, early hydration kinetics, setting behaviour and strength development in four-component Portland cement-fly ash-GGBS-limestone binders. Isothermal conduction calorimetry is especially valuable in this context because changes in the induction period, main silicate peak, aluminate-related shoulder and cumulative heat release can reveal whether a particular blend primarily produces dilution, acceleration or genuine interaction among its constituents. Combining calorimetric measurements with physical, chemical and mineralogical characterization and age-wise compressive-strength evaluation provides a rational basis for distinguishing early filler and nucleation effects from the subsequent pozzolanic and latent hydraulic contributions of fly ash and GGBS.

Accordingly, the present study investigates the synergistic utilization of fly ash, GGBS and limestone for the development of sustainable multi-blended cement with a reduced clinker factor. A systematic series of formulations containing different proportions of the three supplementary constituents was prepared and evaluated. The constituent materials were characterized for their chemical, physical and mineralogical properties, while the hydration kinetics of the developed blends were studied using isothermal conduction calorimetry. Setting characteristics and compressive strength development at different curing ages were subsequently assessed to establish relationships among blend composition, hydration behaviour and engineering performance. The study aims to identify an optimized compositional window in which limestone-induced early hydration enhancement complements the pozzolanic reaction of fly ash and the latent hydraulic reaction of GGBS, thereby enabling substantial clinker reduction without compromising cement performance.

The findings are expected to support the scientific design of multicomponent cements rather than SCM substitution based solely on fixed replacement levels. From an industrial perspective, such an approach can improve the utilization of locally available fly ash, granulated blast-furnace slag and limestone; reduce dependence on clinker; and facilitate the transition towards resource-efficient, lower-carbon cement manufacture in accordance with circular-economy and sectoral decarbonisation objectives.

2. Materials and Methods

2.1 Materials

Ordinary Portland Cement (OPC) 53 Grade was used as the control cement in this research work. The cement was procured from the local market in India and manufactured at one of the production units of the country's largest cement producer. Class F fly ash (FA) was sourced from a thermal power plant in Nashik, GGBS slag was obtained from one of the Iron & Steel plant supplying slag to our units and High grade limestone was sourced from a local mineral supplier. Mineral gypsum was incorporated to achieve the target SO_3 content in the various cement blends. Both Fly ash and GGBS slag were ground to a fineness of 330±10 m2/kg and 370±10 m2/kg. Furthermore, the lime reactivity and cement reactivity of FA and Slag activity index of GGBS were evaluated in accordance with the procedures specified in IS 1727 & IS 16714 respectively

2.2 Preparation of the cement blends

The cement blends containing different proportions of Limestone LS, FA and GGBS were weighed according to the mix compositions presented in Table 1, with a total batch size of 5 kg. To ensure a consistent sulphate balance, the blends were formulated to achieve a target SO_3 content of 2.6 ± 0.1%. Subsequently, the materials were interground in a laboratory ball mill for 15 min to obtain a homogeneous cementitious blend.

Table 1. Mixture proportions of OPC and different Cement blends

	OPC	GYP	LS	FA	GGBS
OPC	100	0	0		0
MBC-01	46.5	3.5	5	10	35
MBC-02	46.5	3.5	5	15	30
MBC -03	46.5	3.5	5	20	25
MBC-04	46.5	3.5	5	25	20
MBC-05	41.2	3.8	10	15	30
MBC-06	41.2	3.8	10	20	25
MBC-07	41.2	3.8	10	25	20
MBC-08	35.8	4.2	10	15	35
MBC-09	35.8	4.2	10	20	30
MBC-10	35.8	4.2	10	25	25

2.3 Test Methods

2.3.1 Characterization of materials

Table 2 presents the chemical composition of the materials used in this research work. The chemical compositions were determined using an X-ray fluorescence (XRF) spectrometer (Axios, PANalytical), while the mineralogical compositions were characterized using X-ray diffraction (XRD) analysis (Bruker D8 Advance). The XRD diffractograms shown in Figure 1 indicate that GGBS is predominantly amorphous, with only minor quantities of crystalline quartz, whereas fly ash (FA) contains both crystalline and amorphous phases. The particle size distribution (PSD) characteristics of LS, FA and GGBS are presented in Table 3. The results reveal that GGBS is finer than FA, which may enhance its particle packing ability and reactivity in blended cement systems.

Table 2. Chemical composition of different materials

Materials	LOI	SiO_2	Al_2O_3	Fe_2O_3	CaO	MgO	SO_3	Na_2O	K_2O	Cl	TiO_2
OPC	1.35	20.68	5.23	3.82	62.81	0.92	2.50	0.12	0.38	0.032	0.49
LS	41.47	3.89	0.05	2.93	0.26	0.16	53.80	0.20	0.02	0.06	0.05
FA	1.25	63.78	22.90	3.20	1.86	0.65	0.17	0.37	2.08	0.003	1.04

GYP	20.55	1.05	0.17	0.10	32.18	0.95	43.67	0.02	0.06	0.005	0.03
GGBS	0.48	36.10	15.68	0.46	37.65	7.50	0.05	0.18	0.52	0.010	0.62

Table 3. Critical Particle Size Distribution Parameters of LS, FA and GGBS

	d10, µm	d50, µm	d90, µm	Mean Dia., µm	R+45µm, %
LS	2.14	12.99	25.37	13.52	4.05
FA	2.91	17.41	58.62	25.19	20.44
GGBS	3.33	15.58	35.87	18.05	3.35

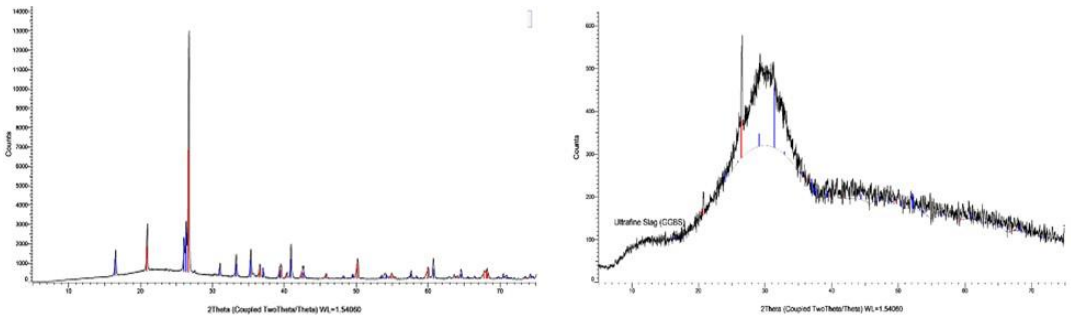


Fig.1 XRD of (a) FA indicating the main minerals -Quartz (Red Stick) & Mullite (Blue stick) along with the amorphous content and (b) GGBS indicating almost amorphous material with minor amounts of Quartz (Red stick) and Gehlenite (Blue stick)

2.3.2 Lime reactivity and Cement Reactivity: Pozzolanic activity

Lime reactivity and Cement Reactivity of the FA were determined in accordance with the method specified in IS 1727. The results obtained indicated in Table 3 shows that it has good reactivity and is suitable for cement manufacturing

Table 4. Lime Reactivity and Cement Reactivity of FA

	Lime Reactivity, MPa	Cement Reactivity, %	
		28 days	90 days
FA	4.9	81.0	86.0

2.3.3 Slag activity index:

The GGBS Slag Activity Index (SAI) is a key performance indicator that measures the reactivity of GGBS when used as a partial replacement for Portland cement in concrete or mortar. It reflects the pozzolanic activity and helps determine how well GGBS contributes to the strength of concrete compared to a control mix with 100% Ordinary Portland cement (OPC). Thus, the GGBS slag was subjected to Slag activity index and the result obtained as indicated in Table 5 clearly shows good SAI.

Table 5: SAI of GGBS slag

S No.	Particulars	Cement (OPC 43Gr), %	GGBS %	NC, %	Compressive Strength, MPa			
					7D, MPa	%	28D, MPa	%

1	Control	100	0	27.5	42.4	100	56.9	100
2	With GGBS	50	50	26.5	26.3	**62.0**	48.3	**84.9**

2.3.4 Standard consistency and Setting times

Method for determination of standard consistency for the performance evaluation of cement blends were as per IS 4031 (Part 4): 1988. Initial and final setting times of the various cement blends paste has been tested using the Vicat apparatus in accordance with the method mentioned in Bureau of Indian Standards IS:4031 (Part 5): 1988.

2.3.5 Compressive Strength

The compressive strength at different ages viz., 1, 3, 7, 28 days and 90 days have been determined for each cement blend using the Automatic compressive strength testing machine, CTM-314E of AIMIL India, in accordance with the method mentioned in Bureau of Indian Standards IS 4031(Part 6): 1988. The compressive strength has been tested on respective cement mortar cubes at the desired ages, prepared using the standard Ennore sand (Grade I, Grade II & Grade III) with the respective cement and the amount of water needed for making the cement mortars is calculated in accordance with the method mentioned in Bureau of Indian Standards IS 4031(Part 4): 1988.

2.3.6 Heat evolution studies

Isothermal conduction calorimetry (ICC) studies were carried out using TAM AIR isothermal calorimeter supplied by TA instruments, having air-based thermostat and easily interchangeable 8-channel standard volume offering high sensitivity and long-term temperature stability for detecting and characterizing heat flow for the different cement blends for a period of 72 hours at a water to cement ratio of 0.40 at 27^0C. Admix ampoule with 20 ml disposable glass ampoules system was used to study the hydration process to generate information related to very early hydration reactions right after water is added to the cement sample.

3.0 Results and Discussions

3.1 Performance evaluation of cement blends

The test results for the various physical properties of the cement such as Blaine, Standard consistency, Setting times and Compressive strength at 1Day, 3 Days, 7 Days, 28 Days & 90 days are indicated in Table 6. The results demonstrate the expected trade-off between early-age strength and clinker reduction, while importantly showing substantial continued strength development between 28 and 90 days. This later-age gain confirms that the supplementary constituents remained reactive beyond 28 days and that the MBC systems cannot be assessed solely on the basis of early-age strength.

Table 6. Physical Properties of different cement blends

Parameters	**OPC**	**MBC-01**	**MBC-02**	**MBC-03**	**MBC-04**	**MBC-05**	**MBC-06**	**MBC-07**	**MBC-08**	**MBC-09**	**MBC-10**
Blaine, m2/kg	320	345	350	356	360	368	362	370	374	366	362
IST, mins	125	190	180	170	165	210	195	175	240	225	215
FST, mins	175	260	245	235	225	300	280	265	350	330	320
NC, %	27.0	31.0	30.5	30.0	30.0	32.0	31.0	31.0	33.0	32.5	31.5
1D, MPa	21.2	14.5	14.0	13.4	12.1	13.1	11.9	10.8	12.4	11.7	10.4
3D, MPa	33.5	24.4	23.7	22.8	21.8	23.2	22.3	20.8	21.2	19.5	18.2

7D, MPa	47.2	34.8	33.7	32.6	30.9	31.9	30.3	28.4	28.4	27.6	26.1
28D, MPa	60.4	49.8	48.2	47.5	46.1	48.2	46.8	45.3	47.2	46.0	44.8
90D, MPa	66.8	59.8	57.8	55.8	52.3	56.5	53.9	51.2	55.2	53.3	50.5

3.2 Blaine, Standard consistency and Setting times

The Blaine fineness of the MBC formulations varied from 345 to 374 m²/kg, compared with 320 m²/kg for OPC. The higher fineness of the multi-blended cements is beneficial because the increased surface area can partially compensate for clinker dilution by improving particle packing and providing additional nucleation sites for hydration products. In limestone-containing composite cements, fine limestone particles accelerate early clinker hydration primarily through filler and heterogeneous nucleation effects, whereas the finer fractions of FA and GGBS provide greater reactive surface area for their subsequent pozzolanic and latent hydraulic reactions [1–3]. Limestone can also increase the effective space available for hydrate precipitation, thereby promoting the hydration of clinker and GGBS [5].

The standard consistency increased from 27.0% for OPC to 30.0–33.0% for the MBC formulations. This increase may be attributed to the higher overall fineness and greater specific surface area of the composite binders, as well as differences in the morphology and water demand of the FA, GGBS, LS and GYP particles. The highest consistency was recorded for MBC-08 at 33.0%, followed by MBC-09 at 32.5% and MBC-05 at 32.0%. The results indicate that water demand was influenced not only by clinker replacement but also by the relative proportions and particle characteristics of the individual constituents.

The incorporation of FA, GGBS and LS increased both the initial and final setting times compared with OPC. The initial setting time increased from 125 min for OPC to 165–240 min for the MBC formulations, while the final setting time increased from 175 min to 225–350 min. The progressive extension of setting time is consistent with the lower clinker content and the slower initial reaction of FA and GGBS relative to Portland cement clinker.

Among the MBC formulations, MBC-04 exhibited the shortest initial and final setting times of 165 and 225 min, respectively, while MBC-08 showed the longest setting times of 240 and 350 min. Although limestone can accelerate clinker hydration through nucleation, the net setting response in a multicomponent binder also depends on clinker dilution, SCM reactivity, sulphate availability, aluminate dissolution and the fineness of the individual materials. At higher clinker-replacement levels, the reduced concentration of rapidly hydrating clinker phases can dominate the acceleration effect of limestone and lead to extended setting [2,5].

The presence of high-purity mineral gypsum is important in these systems because the sulphate requirement of multi-blended cement may differ from that of OPC. Reactive alumina supplied by clinker, GGBS and FA can modify sulphate consumption and AFt/AFm phase development. Therefore, the observed setting behaviour should be interpreted as the combined outcome of clinker dilution, SCM reaction kinetics, limestone-aluminate interaction and sulphate balance rather than as an effect of limestone or an individual SCM alone.

3.3 Compressive strengths: Early and later ages up to 90 days

The early compressive strengths of all MBC blends were lower than those of OPC. At 1 day, the MBC strengths ranged from 10.4 to 14.5 MPa, compared with 21.2 MPa for OPC. At 3 days, the values ranged from 18.2 to 24.4 MPa, compared with 33.5 MPa for OPC; at 7 days, they ranged from 26.1 to 34.8 MPa, compared with 47.2 MPa for OPC.

The lower early-age strength is principally associated with the reduction in clinker content. As the proportion of OPC decreases, the amount of rapidly hydrating alite and aluminate phases is reduced, while FA and GGBS initially react more slowly. Fly ash, in particular, generally contributes

progressively after sufficient calcium hydroxide and alkaline activation have developed within the hydrating system. GGBS is more reactive than conventional siliceous fly ash but still requires activation by the alkaline and sulphate-bearing pore solution generated during clinker hydration [2,3].

Despite the high clinker replacement, the blends developed meaningful early strength. MBC-01 showed the highest 1, 3 and 7 day strengths among the multi-blended formulations, reaching 14.5, 24.4 and 34.8 MPa, respectively. MBC-02 and MBC-03 followed closely. This performance suggests that an appropriate combination of SCM proportions, fineness, limestone content and gypsum addition can partially compensate for clinker dilution. Fine LS can promote early hydration by providing nucleation sites, while the physical packing of FA, GGBS and LS can improve the distribution of solids and reduce inefficient void space [5–7]

At 28 days, the compressive strength of the MBC blends varied between 44.8 and 49.8 MPa. The strongest formulation was MBC-01 at 49.8 MPa, followed by MBC-02 and MBC-05, both at 48.2 MPa, and MBC-03 at 47.5 MPa. Although these values remained below the OPC strength of 60.4 MPa, all the blends developed substantial intermediate-age strength despite their markedly reduced OPC content. The relatively greater proportional increase observed in some of the higher-replacement blends indicates that the contribution of FA and GGBS became progressively more significant after the initial clinker-dominated hydration period. The GGBS contributes through latent hydraulic reactions that produce additional C-(A)-S-H-type hydrates, while the pozzolanic reaction of FA consumes calcium hydroxide and forms additional calcium silicate and calcium aluminosilicate hydrates. The combined reactions refine the hydrate assemblage and progressively densify the microstructure [2,3]

The most important feature of the results is the continued strength development of the multi-blended cements after 28 days. OPC increased from 60.4 MPa at 28 days to 66.8 MPa at 90 days, corresponding to an increase of only 6.4 MPa or 10.6%. In comparison, most MBC formulations exhibited substantially greater proportional strength gains over the same period.MBC-01 recorded the highest absolute and proportional later-age gain, increasing by 10.0 MPa, or 20.1%, between 28 and 90 days. MBC-02 showed a similarly high increase of 9.6 MPa, or 19.9%. MBC-03, MBC-05 and MBC-08 also recorded significant gains of 17.5%, 17.2% and 16.9%, respectively. Thus, the strength increase of the better-performing MBC blends was approximately 1.6–1.9 times the proportional increase observed for OPC.

This pronounced later-age development is consistent with the progressive activation and reaction of FA and GGBS. During the early hydration period, strength is controlled largely by the clinker fraction. At later ages, dissolution of the glassy phases of GGBS and FA contributes additional C-(A)-S-H-type products. These reactions increase the volume of binding hydrates, reduce capillary porosity and improve the continuity of the solid microstructure. Previous investigations of high-volume FA- and slag-containing systems have similarly shown slower initial strength development but continued strength gain at 90 days and beyond, with high-replacement blends approaching the strength of the OPC control at later ages [11].

The high-purity limestone is also likely to have contributed to the later-age performance through synergistic reactions with alumina released from FA and GGBS. Calcite can react with dissolved aluminate species to form hemicarboaluminate and monocarboaluminate phases, while stabilizing ettringite and increasing the solid volume of hydration products. These reactions can reduce porosity and improve strength relative to a system in which limestone acts purely as an inert replacement [5–7].

De Weerdt et al. demonstrated that the combination of fly ash and limestone can generate greater strength than expected from simple additive or dilution effects because alumina released during fly ash reaction participates in carboaluminate formation [6,7]. Similarly, Adu-Amankwah et al. reported that limestone enhanced both clinker and slag hydration through nucleation, increased hydrate-growth space and changes in pore-solution chemistry [5]. The simultaneous presence of FA, GGBS and LS in the

present MBC blends therefore provides several complementary mechanisms:

- Early physical acceleration, through limestone-assisted nucleation and finer particle packing.
- Intermediate-age latent hydraulic reaction, primarily from GGBS.
- Continued pozzolanic reaction, primarily from fly ash.
- Carbonate-aluminate interaction, involving limestone and reactive alumina from clinker, GGBS and FA.
- Pore refinement, resulting from continued formation of C-(A)-S-H and aluminate-bearing hydration products.

The results therefore indicate that limestone did not function solely as a diluent. Instead, LS participated indirectly and chemically in the multicomponent hydration process, improving the efficiency with which the aluminate-bearing SCMs were utilized.

3.4 Heat evolution studies

The normalized heat flow curves are shown in Fig.2, Fig.3 & Fig. 4 for the various multi-blends. The multi-blended cements exhibited the characteristic hydration stages of an initial dissolution peak, induction period, main silicate-hydration peak and a later aluminate-related peak. Compared with OPC, all MBC blends showed lower principal peak intensities because of their reduced clinker content; however, the main peaks remained well defined at approximately 8–10 h. This confirms effective hydration of the remaining clinker, assisted by the higher binder fineness and the nucleation effect of limestone. Fine limestone can accelerate clinker hydration by providing additional nucleation surfaces and space for hydrate growth, while GGBS contributes progressively following activation by the alkaline and sulphate-bearing pore solution [2,5-13].

A distinct secondary peak occurred between approximately 34 and 47 h in the MBC blends. This feature is attributed predominantly to renewed aluminate reaction following changes in sulphate availability, with overlapping contributions from GGBS activation and limestone–aluminate interactions. The dissolved aluminates supplied by clinker, GGBS and FA can react with sulphate to form ettringite and with calcite to form hemi- and monocarboaluminate phases. The timing and magnitude of this peak therefore depend on gypsum dosage, SCM reactivity and the FA-to-GGBS ratio [14–16].

Within each composition group, increasing FA and correspondingly reducing GGBS progressively delayed and broadened the secondary peak, most clearly in MBC-04, MBC-07 and MBC-10. This indicates slower alumina release and SCM activation in the FA-rich blends, consistent with their longer setting times and lower strengths. Conversely, GGBS-rich blends such as MBC-01, MBC-05 and MBC-08 exhibited earlier, more pronounced secondary peaks and higher compressive strengths. The sustained heat evolution beyond the main peak supports the continued latent hydraulic and pozzolanic reactions responsible for the substantial 28 to 90 days strength gain of the MBC blends.

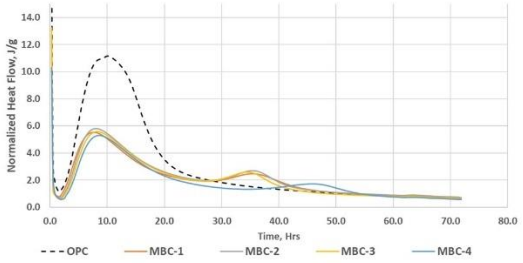


Fig.2 Normalized Heat Flow curves for MBC-01 to MBC-04 blends

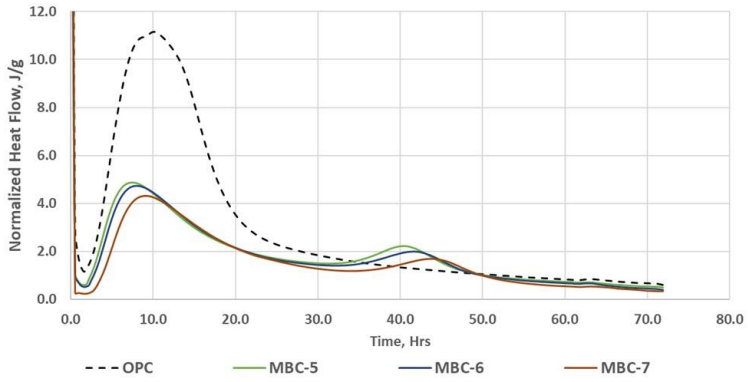


Fig.3 Normalized Heat Flow curves for MBC-05 to MBC-07 blends

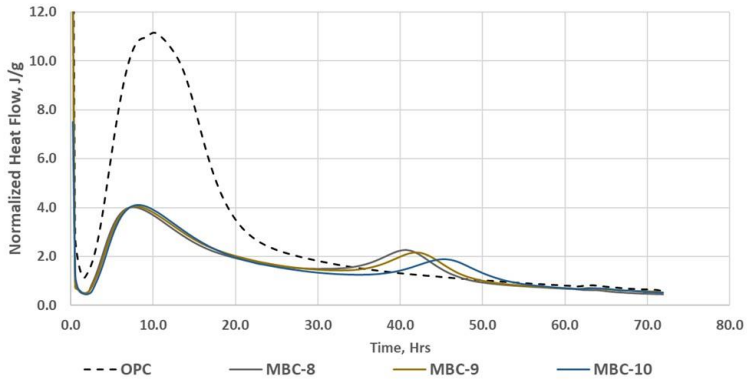


Fig.4 Normalized Heat Flow curves for MBC-08 to MBC-10 blends

4. Conclusions

The developed multi-blended cements demonstrate that fly ash, GGBS and limestone can be synergistically utilized to achieve considerable clinker reduction while retaining satisfactory mechanical performance. Although clinker dilution resulted in lower early-age strength and extended setting, the blends exhibited substantial later-age strength development. MBC-01 achieved the highest 90-day strength of 59.8 MPa, while MBC-08 attained 55.2 MPa despite containing only 35.8% OPC. Calorimetry showed well-defined silicate-hydration peaks and secondary aluminate-related peaks, confirming sustained reactions involving GGBS activation, fly ash pozzolanicity, sulphate-controlled hydration and limestone–aluminate interactions. Overall, blends containing 10–15% fly ash and 30–35% GGBS provided the most favourable balance between hydration kinetics and strength.

From a sustainability perspective, the high replacement of OPC with industrial by-products and minimally processed limestone offers the potential to reduce clinker consumption, associated CO_2 emissions, energy demand and dependence on virgin raw materials. The proposed approach also supports circular utilization of fly ash and GGBS and enables more resource-efficient cement production. However, the present study was limited to laboratory-scale preparation, one source of each constituent, strength testing up to 90 days and calorimetric evaluation up to 72 h. Environmental performance and durability were not quantified directly.

Future work should therefore assess long-term durability, dimensional stability, microstructural and phase evolution, admixture compatibility and concrete-scale performance under different curing and exposure conditions. Life-cycle assessment, embodied-carbon quantification, sulphate optimization and pilot-scale manufacturing trials are also required to confirm the environmental benefits, composition robustness and commercial scalability of the optimized multi-blended cements.

References

1. Scrivener, K.L., John, V.M. and Gartner, E.M. (2018). Eco-efficient cements: Potential economically viable solutions for a low-CO_2 cement-based materials industry. Cement and Concrete Research, 114, 2–26.
2. Lothenbach, B., Scrivener, K. and Hooton, R.D. (2011). Supplementary cementitious materials. Cement and Concrete Research, 41(3), 217–229.
3. Juenger, M.C.G., Snellings, R. and Bernal, S.A. (2019). Supplementary cementitious materials: New sources, characterization and performance insights. Cement and Concrete Research, 122, 257–273.
4. Matschei, T., Lothenbach, B. and Glasser, F.P. (2007). The role of calcium carbonate in cement hydration. Cement and Concrete Research, 37(4), 551–558.
5. Adu-Amankwah, S., Zajac, M., Stabler, C., Lothenbach, B. and Black, L. (2017). Influence of limestone on the hydration of ternary slag cements. Cement and Concrete Research, 100, 96–109.
6. De Weerdt, K., Kjellsen, K.O., Sellevold, E. and Justnes, H. (2011). Synergy between fly ash and limestone powder in ternary cements. Cement and Concrete Composites, 33(1), 30–38. .
7. De Weerdt, K., Ben Haha, M., Le Saout, G., Kjellsen, K.O., Justnes, H. and Lothenbach, B. (2011). Hydration mechanisms of ternary Portland cements containing limestone powder and fly ash. Cement and Concrete Research, 41(3), 279–291.
8. Influence of granulated blast furnace slag and silica fly ash on the hydration kinetics of multi-component cements (2026). Journal of Thermal Analysis and Calorimetry. Online publication, 24 September 2026.
9. De Weerdt, K., Sellevold, E.J., Kjellsen, K.O. and Justnes, H. (2011). Fly ash-limestone ternary cements: Effect of component fineness. Advances in Cement Research, 23(4), 203–214.
10. Aslan, S. and Erkan, İ.H. (2024). The effects of fly ash, blast furnace slag, and limestone powder on the physical and mechanical properties of geopolymer mortar. Applied Sciences, 14(2), 553.
11. Dhandapani, Y. and Santhanam, M. (2020). Assessment of pore structure evolution in the limestone-calcined clay cementitious system and its implications for performance. Cement and Concrete Composites.
12. Narmluk, M. and Nawa, T. (2014). Effect of fly ash on the kinetics of Portland cement hydration at different curing temperatures. Cement and Concrete Research, 61–62, 48–58
13. Bullard, J.W. et al. (2011). Mechanisms of cement hydration. Cement and Concrete Research, 41, 1208–1223.
14. Quennoz, A. and Scrivener, K.L. (2013). Interactions between alite and C_3A–gypsum hydrations in model cements. Cement and Concrete Research, 44, 46–54.
15. Parashar, A. and Bishnoi, S. (2021). Hydration behaviour of limestone–calcined clay and limestone–slag blends in ternary cement. RILEM Technical Letters, 6, 17–24.
16. Adu-Amankwah, S. et al. (2018). Effect of sulfate additions on hydration and performance of ternary slag–limestone composite cements. Construction and Building Materials, 164, 451–462.

PERFORMANCE-BASED BINDER OPTIMIZATION FOR LOWER-CLINKER CONCRETE: STRENGTH COMPARISON OF OPC–GGBS AND PORTLAND SLAG CEMENT SYSTEMS

Pawar Prashant S[1] and Dr. Purnanand P. Savoikar[2]

[1]Research Scholar; [2]Professor in Civil Engineering, Goa College of Engineering, Farmagudi, Goa, India (affiliated to Goa University)

psavoikar@gmail.com

ABSTRACT

Concrete producers increasingly seek binder combinations that meet specified strength with lower consumption of clinker-bearing cement. This paper examines 68 trial mixes containing separately batched Ordinary Portland Cement (OPC) and ground granulated blast-furnace slag (GGBS), alongside 11 mixes produced using Portland Slag Cement (PSC). The OPC–GGBS series contains

42.5–63.3% GGBS and achieved recorded 28-day compressive strengths of 27.26–51.07 MPa. At common total cementitious contents of 300, 320, 350 and 370 kg/m³, the mean strengths of OPC–GGBS mixes were 31.56, 37.83, 38.48 and 43.24 MPa, compared with 24.44, 27.30, 26.58 and

34.10 MPa for PSC. The data suggest a practical advantage for the separately proportioned mixes within the examined programme, but do not establish an intrinsic advantage of one cement manufacturing route: the mixtures were not fully matched for water–binder ratio, aggregate composition or other variables. The discussion considers the value of independent OPC and GGBS dosing, the importance of particle fineness and the need to verify strength and durability at minimum practical binder demand. Graphs of common binder dosages, individual trials and GGBS replacement bands are used to communicate the findings.

Keywords: low-carbon concrete; OPC–GGBS; Portland Slag Cement; binder optimisation; supplementary cementitious materials; compressive strength.

1.0 INTRODUCTION

Concrete strength is governed by the proportioned mixture and its production and curing conditions. Cement strength classification should not be confused with concrete grade: the water–binder ratio, aggregate grading, admixture compatibility and curing conditions all affect the final result [1,2]. This distinction is important when assessing blended cementitious systems intended to reduce the demand for clinker-bearing cement.

Slag can be introduced either through factory-manufactured PSC or as separately supplied GGBS added with OPC during concrete batching. Both approaches are technically established, but they offer different degrees of direct control over the separately added constituents. A ready-mixed concrete producer can measure and vary OPC and GGBS dosages independently when the materials are batched separately. With PSC, the producer normally works with the finished cement as supplied; the actual slag fraction and particle-size characteristics must be obtained from the manufacturer or verified by appropriate testing rather than inferred from the cement designation.

2.0 *EXPERIMENTAL RECORDS AND METHOD*

Two sets of mix-design and strength records were examined: 68 trials of OPC–GGBS and 11 PSC trials. Total cementitious content means OPC + GGBS for the separately batched mixes and PSC dosage for the PSC mixes. GGBS replacement is calculated as 100 × GGBS/(OPC + GGBS). The primary response is recorded 28-day compressive strength. The observations are trial-level results; they are not assumed to be independent specimen replicates.

The main comparison uses the four binder dosages appearing in both datasets: 300, 320, 350 and 370 kg/m³. Results at each dosage are shown as arithmetic means, with trial counts disclosed. The individual observations are also retained in a separate bar chart. To communicate replacement-level effects without a crowded scatter plot, the 68 OPC–GGBS mixes are grouped into five GGBS-percentage bands.

3.0 RESULTS AND DISCUSSION

3.1 Comparison at common binder dosages

Figure 1 and table 1 presents the comparison of 28-days compressive strength of cubes cast using commercial blended cements and using laboratory mix of cement + GGBS at various binder contents. At each common binder dosage, the mean strength recorded for separately batched OPC–GGBS is higher than that of the PSC series. At 300 kg/m³, for example, the corresponding averages are 31.56 and 24.44 MPa. This difference is relevant to practical mixture selection, but binder mass alone does not make the trials otherwise equivalent. The PSC and OPC–GGBS mixtures differ in their mix-design conditions; the observed difference therefore cannot be attributed solely to the method of blending or grinding.

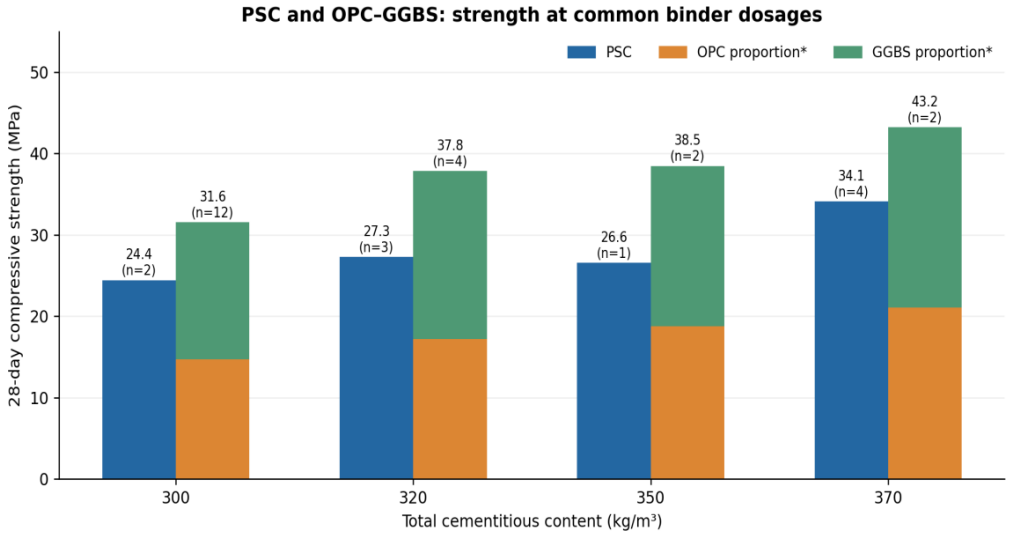


Figure 1. Mean 28-day compressive strength of PSC and OPC–GGBS mixes at common total binder contents. The orange and green portions represent the average OPC and GGBS mass fractions; they are not separate strength contributions.

Binder (kg/m³)	PSC (MPa)	PSC n	OPC–GGBS (MPa)	OPC–GGBS n
300	24.44	2	31.56	12
320	27.30	3	37.83	4
350	26.58	1	38.48	2
370	34.10	4	43.24	2

3.2 Results of individual trials

Figure 2 shows the individual results rather than replacing them with a single value per binder dosage. The number of available observations is uneven: for example, 12 OPC–GGBS mixes and two PSC mixes are reported at 300 kg/m³. The bar-chart format makes the spread of strengths visible and avoids implying a continuous strength relationship between distinct trial formulations.

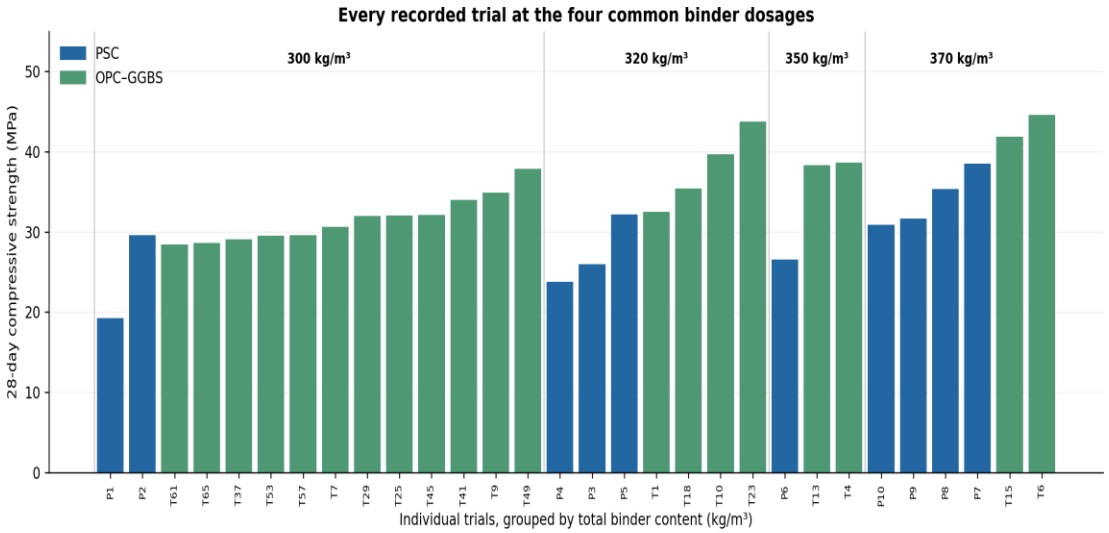


Figure 2. Individual 28-day strengths at 300, 320, 350 and 370 kg/m³ total cementitious content. Blue columns indicate PSC trials; green columns indicate separately batched OPC–GGBS trials.

3.3 Effect of GGBS replacement level

GGBS accounts for 42.5–63.3% of the separately batched binder. Figure 3 summarizes the strength results by replacement range, rather than displaying a dense set of individual points. The means do not change monotonically with replacement percentage. This is expected in a dataset where OPC dosage, total binder, water–binder ratio and other variables vary together. Accordingly, the figure should not be interpreted as identifying a universal optimum GGBS percentage.

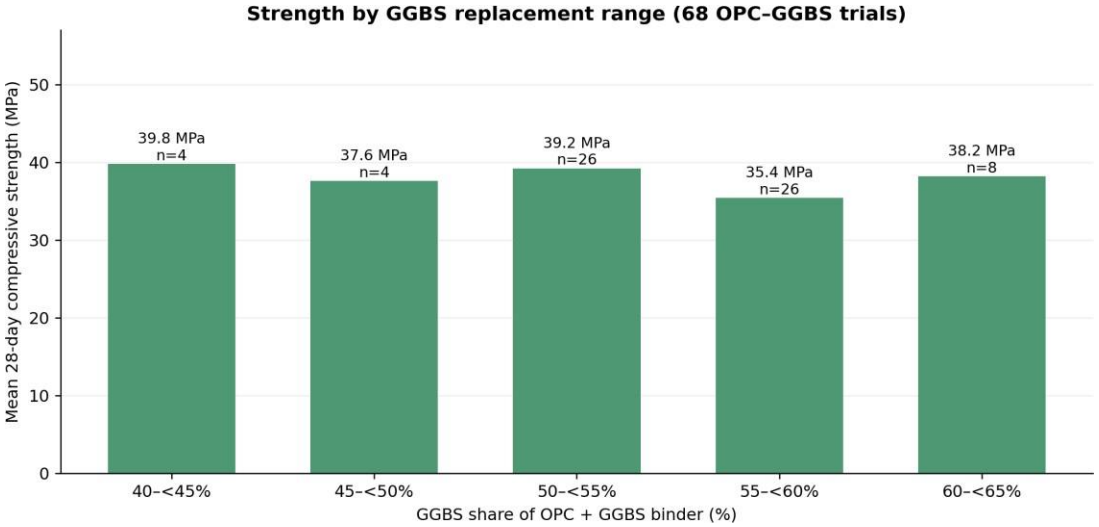


Figure 3. Mean 28-day strength of OPC–GGBS mixes grouped by GGBS replacement percentage. The number of trials in each band is given above the column.

3.4 Practical considerations: separate batching and factory-blended PSC

One practical attraction of separate OPC and GGBS batching is the ability of the concrete producer to specify, measure and adjust the two binder components independently. This can be particularly useful in ready-mixed concrete plants and dedicated project batching facilities, where strengthdevelopment, workability, temperature sensitivity and other performance requirements may vary from project to project. Separate batching also makes the externally added slag percentage



explicit in the mix-design records, whereas the exact slag fraction in a supplied PSC product may not be available to the concrete producer unless declared by the manufacturer.

Grinding behaviour is another consideration. Portland clinker and granulated blast-furnace slag have different grindabilities and may develop different particle-size distributions during intergrinding. Depending on the raw materials and mill operating conditions, preferential grinding can occur; therefore, the fineness and reactivity of the slag fraction in an interground cement cannot be assumed to be identical to those of independently ground GGBS. Separate grinding allows the fineness of OPC and GGBS to be specified and controlled individually. However, it would be incorrect to conclude from the present strength records that the PSC slag fraction was necessarily coarser, or that clinker was invariably finer: no constituent-specific particle-size distribution, Blaine fineness, slag activity index or cement microstructure measurements were supplied. Modern PSC may also be produced through separate grinding and blending, depending on the manufacturing process.

The present results are consistent with the usefulness of mix-specific binder control, but they do not establish that separately batched systems always outperform PSC. Proper comparison would require matched water–binder ratio, aggregates, admixtures, curing and measured cement/slag properties. Similarly, good 28-day strength alone does not establish improved durability; permeability, chloride ingress, carbonation and other exposure-related properties should be tested where relevant [2–5].

4.0 *IMPLICATIONS FOR LOWER-CARBON CONCRETE*

A lower-carbon binder strategy should consider the absolute consumption of clinker-bearing cement, the total binder required to achieve a specified concrete performance and the service-life requirements of the structure. High GGBS replacement may be advant ageous, but replacement percentage alone is not a carbon metric. For separately batched OPC–GGBS, the OPC and GGBS quantities are known; for PSC, the internal clinker/slag fractions must be obtained before meaningful clinker-consumption or embodied-carbon comparisons can be made. Verified environmental product data and a consistent assessment boundary are needed for any quantified CO_2-reduction claim.

5.0 *LIMITATIONS AND FURTHER INVESTIGATION*

This is a comparative examination of available mix-design trials, not a controlled factorial study. Binder dosages can be matched, but constituent characteristics and full mix-design conditions were not held constant. Neither the actual PSC slag fraction n or constituent-specific fineness and reactivity were measured. The study also does not compare nominal OPC 33-, 43- and 53-grade cements directly. Future work should include matched OPC–GGBS and PSC mixes, particle-size distribution and Blaine measurements, slag activity testing, strength development beyond 28 days, relevant durability tests and verified embodied-carbon factors.

6.0 *CONCLUSIONS*

Following important conclusions were drawn from the present study:

- Within the supplied trials, separately batched OPC–GGBS mixes recorded higher mean 28-day strengths than PSC at each of the four common total-binder dosages (300, 320, 350 and 370 kg/m^3).
- Separate OPC and GGBS batching gives the concrete producer direct control over constituent dosages and provides an opportunity to specify the fineness of independently supplied materials.
- Differences in grindability and particle-size distribution provide a technically plausible reason to investigate separately ground and interground slag systems, but the present data do not establish the fineness or reactivity of the slag fraction in the tested PSC.



- Concrete strength and lower-clinker design should be evaluated on the basis of the complete mix, with durability and environmental performance verified independently; a higher GGBS percentage alone does not establish a lower-carbon outcome.

REFERENCES

[1] IS 10262:2019, Concrete Mix Proportioning—Guidelines. Bureau of Indian Standards.

[2] IS 456:2000, Plain and Reinforced Concrete—Code of Practice. Bureau of Indian Standards.

[3] IS 455, Portland Slag Cement—Specification. Bureau of Indian Standards (applicable edition to be confirmed).

[4] IS 16714:2018, Ground Granulated Blast Furnace Slag for Use in Cement, Mortar and Concrete—Specification. Bureau of Indian Standards.

[5] A. Oner and S. Akyuz, "An experimental study on optimum usage of GGBS for the compressive strength of concrete," Cement and Concrete Composites, 29 (2007), 505–514.

[6] H. F. W. Taylor, Cement Chemistry, 2nd ed., Thomas Telford, 1997.

[7] K. L. Scrivener and A. Nonat, "Hydration of cementitious materials, present and future," Cement and Concrete Research, 41 (2011), 651–665.

ADAPTATION OF DIFFERENT METHODOLOGIES FOR ESTIMATION OF KAOLINITE PHASE DURING QUALITY ASSESSMENT OF DIFFERENT TYPES OF CLAY FOR THE PRODUCTION OF LOW CARBON LC3 CEMENT

Giasuddin Ahamed, G Jayachandra Naidu, Sanjeev Kumar Chaturvedi, Lok Pratap Singh

National Council for Cement and Building Materials

Corresponding Author: Giasuddin Ahamed, Email: ahamed.gias111@gmail.com

Abstract:

The idea of low carbon blended cement with a higher percentage of supplementary cementitious materials (SCMs), such as fly ash, granulated blast furnace slag (gbfs), calcined clay or metakaolin are being recognised by the cement research community to reduces the environmental carbon footprint by minimising the clinker factor. However, due to limited availability of fly ash and gbfs in different regions of the world, Portland Limestone Calcined Clay Cement also known as LC3 cement prepared with calcined natural pozzolanic clay and limestone has turned up as a top contender. The quality of clay varies greatly and the key mineral phase which determined the reactivity of calcined clay in the clay sample is mainly kaolinite. It was found that clays of the 1:1 type, which usually contain at least 40% "kaolinite" mineral, were appropriate for making LC3 cement. Thus, characterization of kaolinite content properly becomes crucial for the quality assessment of different types of clay to anticipate the pozzolanic reactivity of calcined clay for the production of low carbon LC3 cement.

In the present study five different types of clay samples having different chemistry and mineralogy were collected for the quality assessment in terms of kaolinite content using different methodologies. Chemical analysis of these clay samples was carried out by wet method as per Indian standard, whereas mineralogical and thermal characterisations were carried out by using X ray dffractometer (XRD) and thermal analayser (TG-DTA) respectively. The kaolinite phase was estimated according to loss of ignition (LOI) method as per the procedure described in Indian standard IS 18189:2023, clause 4.1 annex B along with the instrumentals techniques XRD and thermogravimetric analyzer (TG) respectively. It was observed that estimated kaolinite phase content found to be almost similar in the case of LOI method in between temperature 300°C to 750°C and TG-DTA respectively in non-calcareous kaolinitic type clay samples. Whereas clay sample having presence of impurities such as carbonates compounds interfere in the mass loss due to dehydroxylation and decarbonation at the same temperature range and produce misleading data in comparison to TG-DTA analysis. In the case of XRD analysis all (1:1) type of clay mineral polymorphs such as kaolinite, nacrite and dickite need to be considered for the estimation of the total kaolinite phase. The present study showed that the estimation of clay mineral phases mainly kaolinite content by thermogravimetric (TG) analysis method is straightforward and easy whereas quantative analysis by X-Ray Diffraction (XRD) with Rietveld refinement provides detail and precise mineral phase information for complex clay minerals but analysis is challenging and need high expertise.

Keywords: Low Carbon Cement, Limestone Calcined Clay Cement (LC3), Clay, Kaolinite, Thermal analayser (TG-DTA), X ray dffractometer (XRD)

1.0 *INTRODUCTION:*

The lasting importance of Portland cement (PC) in worldwide construction, known for its strong performance in various infrastructure and construction developments is increasingly being surpassed by the substantial environmental impact linked to its manufacturing. According to the World Cement Association report, worldwide cement production is expected to increase by 8.2 billion tonnes by 2030[2,3]. Considering the Indian scenario, India is the second largest producer and consumer of Portland cement in the world after China, with a current annual cement production of approximately 490 million tonnes, and is expected to increase by 700 million tonnes by 2032. The cement sector contributes significantly to global greenhouse gas emissions, accounting for about 7–8% of total CO2 emissions and approximately 50–60 % of these emissions result from limestone calcination into clinker and fossil-fuel combustion during the production process [4-12] Therefore, a crucial tactic in reducing the environmental impact of building is lowering the clinker component in the low carbon cement [13]

Therefore, research should be furnished on new types of materials that can potentially without compromising on the essential performance. A new motivating approach, receiving more and more recognition within the cement research fraternity, is the idea of low carbon blended cement by employing various supplementary cementitious materials (SCMs) such as fly ash, granulated blast furnace slag (gbfs) and calcined clay or metakoline results in reduced CO_2 footprint by minimizing the clinker factor in the cement sample [14-19]. Traditional fly ash based Portland pozzolana cement (PPC) and granulated blast furnace slag (gbfs) based Portland slag cement (PSC) are well established as low carbon cement in the market. However, due to limited availability of fly ash and gbfs in different regions of the world, Portland Limestone Calcined Clay Cement also known as LC3 ternary blend prepared with calcined natural pozzolanic clay and limestone has turned up as a top contender due to its ability to replace up to 50% of clinker without noticeable loss in mechanical performance to meet stringent low carbon sustainability targets. [20-24]

Clay samples are natural earthy materials with a great diversity in terms of their quality and widely present as fine-grained minerals (<2 μm) around the earth's surface which exhibits plasticity at an appropriate water content and hardens upon drying. The estimated kaolinite (white china clay) reserves in India are of the order of 2.4 billion tones [25]. The quality of clay varies greatly and in terms of structural variations based on the integration of a sheet of corner-linked tetrahedral silicate sheets and a sheet of edge-linked octahedral aluminate sheet, clay is categorized 1:1 type such as kaolinite, nacrite, and dickite or 2:1 types, such as smectite and vermiculite or 2:1:1 types such as chlorite [26,27]. Naturally occurring clays typically contain clay minerals and other non-clay minerals. The clays represent typical clay deposits in India and can be assigned to the different groups of "kaolinitic clays", "montmorillonite clays", "illitic clays" and "chloritic clays" depending on their mineralogy.

Generally, kaolinite is completely transformed into metakaolinite at around 450ºC-550ºC in clays. Metakaolinite is a result of removing the hydroxyl groups above 400°C, as shown in equation (1) and is well known as a highly disordered phase [39-40]. Because of this disorder it could not be identified by XRD.

$$Al_2O_3{\cdot}2SiO_2{\cdot}2H_2O \longrightarrow Al_2O_3{\cdot}2SiO_2 + H_2O \quad \text{(eq. 1)}$$

kaolinite metakaolinite

Past investigation reported that the optimum calcination temperature for kaolinitic clays, which are

common in the production of metakaolin, typically ranges between 600◦C and 850◦C [13,24.31,40]. Clays maintain their amorphous structure and achieve peak reactivity within this temperature range. Attaining the perfect calcination temperature is crucial for enhancing pozzolanic activity and improving the interaction between calcined clays and cement materials. Over-calcination (above~900 ◦C) leads to production of non-reactive phases such as mullite and spinel, which reduce or diminish pozzolanic reactivity [8,10,11,31,40]. On the

other hand, insufficient calcination (<700◦C) results in leftover kaolinite, reducing reactivity and effectiveness. [8,10,11]. In addition to this, the reactions that occur during calcination of the clays vary with types of clay and depends upon its chemical, physical and mineralogical properties.

Most of investigations on calcined clays in literature work is on kaolinitic clays and it was reported that clays of the 1:1 type, which usually contain at least 40% "kaolinite" mineral, were appropriate for making LC3 cement and demonstrate excellent pozzolanic and mechanical properties similar to ordinary Portland cement [28-32]. The degree of crystallinity, specific surface area, particle dimensions and structure of the clay minerals can affect the reactivity of the calcined clay. [33-40]. Certain studies related to clay science indicate that calcined disordered kaolinite may exhibit greater reactivity than well-structured kaolinite after the calcination. [33,37]. Therefore, a holistic knowledge of the chemical, mineralogical and thermal properties of raw clays is essential to properly assess its pozzolanic reactivity in the LC3 cement.

Therefore, it is important optimized appropriate methodologies for the estimation of kaolinite content in different types of clays as it helps to evaluate the performance of calcined clay as SCM in low carbon LC3 cement production. Also, the determination of kaolinite content is beneficial for quality assessment and identification of suitable type of clay. The objective of the present study is to adopt a suitable methodology or techniques for the quality control of the different types of clay in terms of estimation of kaolinite content using chemical (LOI), mineralogical (XRD) and thermal techniques (TG-DTA).

2.0 *MATERIALS AND EXPERIMENTAL SECTION:*

2.1 Raw Materials:

Five different types of clay samples named as Clay-A, Clay-B, Clay-C, Clay-D and Clay-E respectively were collected from different regions of the country for this research work. These samples were further processed for chemical, mineralogical, and thermal investigations.

2.2 Chemical Characterization:

The laboratory samples were prepared by drawing ~ 2 kg by coning & quartering procedure and ground to pass through a 90-micron sieve. It was further reduced to ~ 200 gms by coning and quartering procedure later subjected to chemical characterization. Chemical analysis of these homogenized clay materials was carried out as per Indian Standard IS: 1727 – 1967 [41] and shown in Table 1. Loss of ignition (LOI) of these clay samples were also estimated at temperatures 300°C and 750°C respectively as per the procedure described in Indian standard IS 18189:2023, clause 4.1 annex B[42].

2.3 Thermal Characterization by Simultaneous Thermal Analyzer (TG-DTA):

The thermal characterization of these powdered clay samples passed through 90µm were carried out using a Simultaneous Thermal Analyzer (TG-DTA) instrument to make Setaram, model-Themys one. Approximately 20-30 mg of clay samples were thermally analyzed in TG-DTA instrument by heating

from ambient to 1100□C temperature with a heating rate of 10□C per minute in a nitrogen atmosphere. The total weight loss as well as specific weight losses corresponding to various chemical transformations in the clay samples were recorded by the thermogravimetric (TG) and differential thermal analysis (DTA) curve and shown in **Fig. 1-5**.

2.4 Mineralogical Characterization by X-ray Diffractometer (XRD):

Mineralogical analysis of these powdered kaolinitic clay samples 100% passing through 90µm were carried out using an X-ray diffractometer, model-SmartLab SE 2, Rigaku Corporation, Japan, D-Max 2200V/PC using Cu-Kα radiation which is equipped with a copper anticathode (CuK α = 1.5418 Å), at a scanning speed of 1.0°/min, covering a range from 5° to 80°. and diffractograms are shown in **Fig. 5-8**. The

qualitative and quantitate mineralogical phases of clay samples were analyzed using ICDD Powder Diffraction File (PDF-4) data base and JADE softwares.

3.0 *RESULT AND DISCUSSION:*

3.1 Chemical Compositions:

Chemical analysis of these of the five different types of clay samples were investigated in this study as per Indian Standard IS 1727 and shown in Table 1. Clay samples are mainly comprised of high amount of SiO_2 and Al_2O_3. Chemical analysis results showed that the most dominant oxide SiO_2 percentage in these clay samples named Clay-A, Clay-B, Clay-C, Clay-D and Clay E were found to be 55.35, 52.67, 49.88, 48.81 and 52.41 respectively whereas Al_2O_3 present were estimated to be 29.90, 31.29, 29.86, 18.22 and 18.24% respectively. Fe_2O_3 content was observed to be in the range of 1.68–1.95% in the samples Clay-A, Clay-B, Clay-C, and Clay-D, however sample Clay E found to have substantially higher percentage of iron content of 9.59%. Chemical analysis results also indicated presence higher percentage of CaO of 4.04% and 13.98

% in the Clay-C and Clay D samples respectively. Trace amounts of K_2O, MgO, and Na_2O, are present as minor elements in the clay samples. The Al_2O_3/SiO_2 ratio was estimated to be in the range of 0.35-0.60 for all these clay samples.

Table 1. Chemical Composition of Clay Samples

Sample	**Chemical Composition**								
	LOI	SiO_2	Al_2O_3	Fe_2O_3	CaO	MgO	Na_2O	K_2O	Al_2O_3/SiO_2
Clay-A	8.16	55.35	29.90	1.87	1.57	0.58	0.19	0.88	0.54
Clay-B	10.76	52.67	31.29	1.95	0.81	0.51	0.19	0.19	0.59
Clay-C	11.41	49.88	29.86	1.68	4.04	0.48	0.21	0.46	0.60
Clay-D	13.62	48.81	18.22	1.76	13.98	1.28	0.28	0.38	0.37
Clay-E	8.87	52.41	18.24	9.59	2.79	1.62	1.7	2.22	0.35

3.2 Estimation of Loss of Mass on Ignition (LOI) and Determination of Kaolinite content:

The loss of mass on ignition (LOI) analysis was performed at different temperatures of 300°C and

750°C in a laboratory muffle furnace following the procedure mentioned in the Indian standard 18189:2023, annex B clause 4.1. The mass loss on ignition (LOI) in between the temperature range 300°C to 750°C were calculated as shown in the Table 2 for the estimation of kaolinite content in the clay samples. The kaolinite content (K, %) in the sample as per the LOI method was estimated using the below mentioned formula;

$$K = \frac{LoI\ 750°C - LoI\ 300°C}{0.14} * 100 \qquad \textbf{(1)}$$

Table:2 Estimation of Kaolinite Content in Clay Samples on the basis of LOI as per IS 18189:2023 annex B, clause 4.1

Sample Code	Loss of mass on ignition (LOI)			% Kaolinite as per Indian standard 18189:2023, annex B, clause 4.1
	300°C	750°C	300°C to 750°C	
Clay-A	0.79	9.39	8.60	61.43
Clay-B	0.41	10.49	10.08	72.00
Clay-C	0.38	11.29	10.91	72.93
Clay-D	0.43	13.15	12.72	90.85
Clay E	2.63	8.48	5.85	41.78

The results showed that LOI in temperature range 300°C to 750°C for samples Clay-A, Clay-B, Clay-C, Clay-D and Clay E were estimated to be 8.60%, 10.08%, 10.91%, 12.72% and 5.85% respectively, subsequently kaolinite content were estimated to be 61.43%,72.0%, 72.93%,90.85% and 41.78% correspondingly.

3.3 Thermal (TG-DTA) Analysis of Clay Sample

To illustrate the property of these clay samples concisely, thermal analysis of five different types of clay samples were investigated by TG-DTA and thermograms are shown in Fig. 1-5. DTA analysis revealed that the major endothermic peak that appeared in the range of 300-750°C or in some cases upto 300-650° were attributed to the dehydroxylation of crystal water from the kaolinite mineral phase present in all these clay samples and the concurrent formation of the reactive metakaolin phases. But in case of samples Clay-C and Clay-D, another endothermic peak in the temperature range of 650-800 °C at the expense of kaolinite dihydroxylation peak was also observed which due to the dissociation of calcite phase present in the clay samples as evident in the XRD results [43]. Thermogravimetric (TG) analysis of the sample Clay-A and Clay-B showed sharp one step weight loss in the temperature range 300-750°C which confirms its kaolinite purity, however TG analysis of Clay-C and Clay-D showed two step weight loss in the same temperature range due presence of calcite mineral as impurity. The DTA profiles of the first four clay samples showed an another sharp exothermic peak at >950°C, which is due to the crystallization of metakaolin phase into spinel or mullite phase formation for the respective clay samples [43-45]. However, it was observed that the TG-DTA graph of the Clay E sample is different from the other clay samples. DTA analysis of the Clay E showed several other endothermic peaks at

temperature 226°C, 308°C and 860°C respectively apart from the major peak at the temperature range of 350-750°C corresponding with multi steps weight loss in the TG analysis. These multi steps dihydroxylation at different temperatures confirms presence of illite as major phase along with other impurities. In case of TG-DTA methods, the mass loss that appeared (ΔG%) in TG analysis of the sample corresponds to the tangent of DTA peak at around 550°C related to the kaolinite dihydroxylation and formation of metakaoline was utilized for the calculation of the kaolinite content using the formula mentioned below;

Kaolinite content (K%) = 7.17 * ΔG (%)….(2)

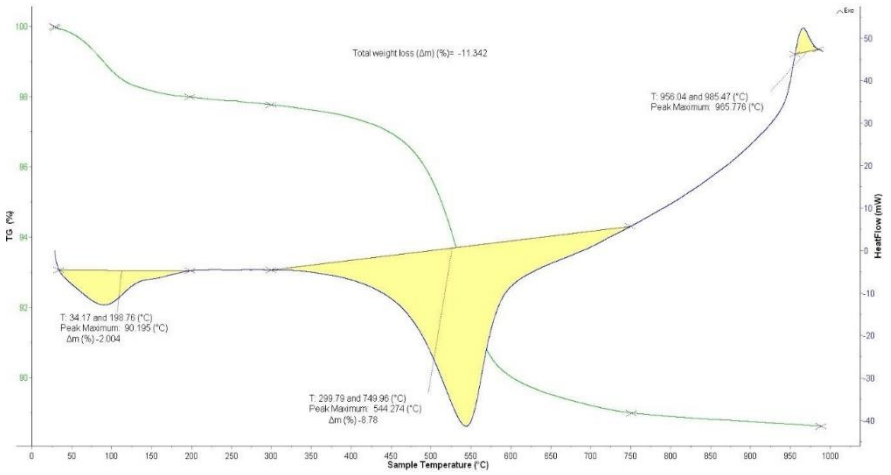


Fig.1: TG-DTA Thermograms of Clay-A

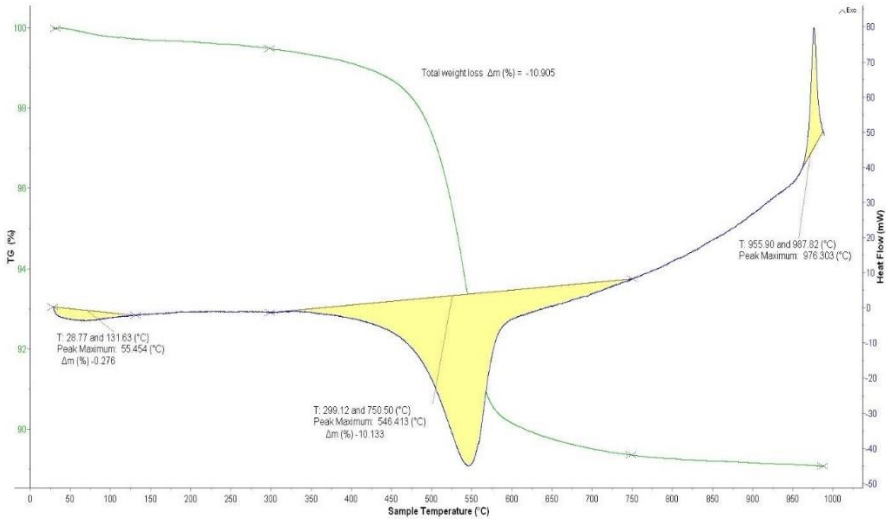


Fig.2 TG-DTA Thermograms of Clay-B

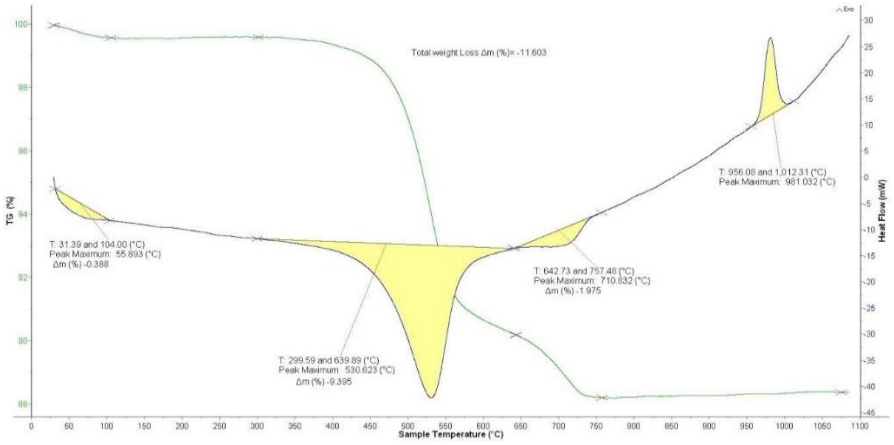


Fig.3: TG-DTA Thermograms of Clay-C

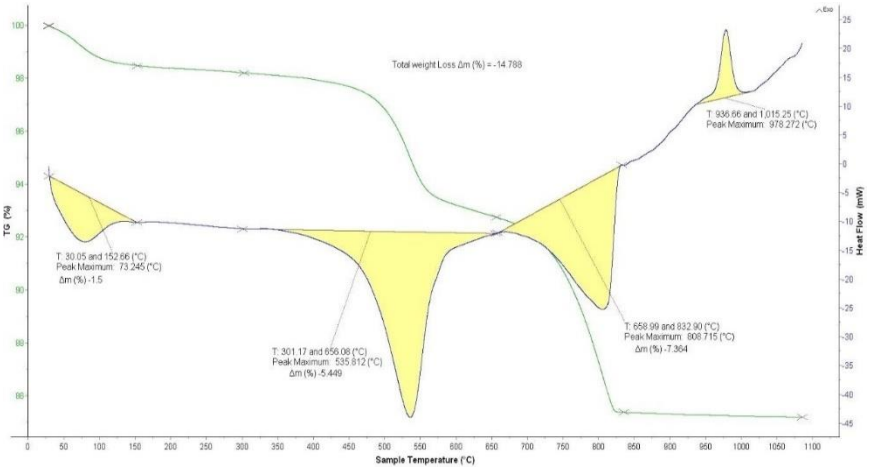


Fig.4: TG-DTA Thermograms of Clay-D

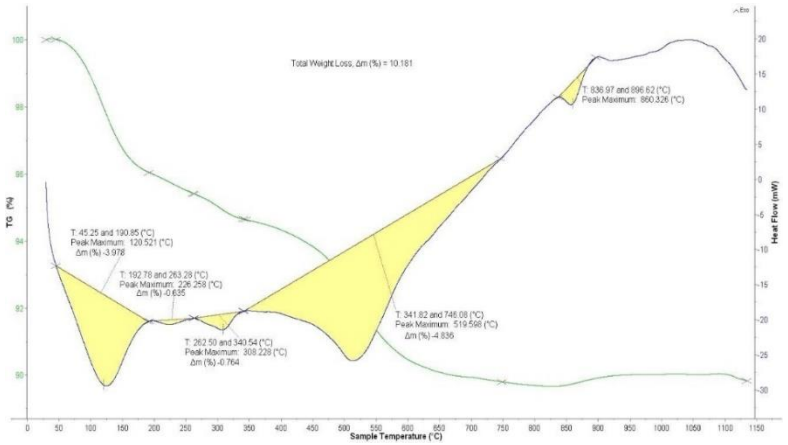


Fig.5: TG-DTA thermograms of Clay-E

The mass or weight loss corresponding to the kaolinite dihydroxylation for samples Clay-A, Clay-B, Clay-C, Clay-D and Clay E as per the thermogravimetric (TG) analysis were estimated to be 8.76%, 10.13%, 9.39%, and 5.44% respectively and kaolinite phase were calculated to be 62.80, 72.63%,67.35%, 39.00% and 34.63% respectively.

3.4 X-Ray Diffraction (XRD) Analysis of Clay Samples:

The brief qualitative and quantitative mineralogical analysis along with kaolinite phase content were carried out through XRD analysis and shown in the **Fig. 6-10**. XRD results indicated that kaolinite and quartz was the major dominant phase in the Clay-A samples whereas Clay B having nacrite and dickite as major mineral along with the kaolinite. Apart from major mineral kaolinite and quartz, presence of substantial amount calcite phase was also observed in the of Clay-C and Clay-D samples and the same was evident in the TG-DTA results. Other minor phases such as muscovite also found to be present as a minor percentage in some these clay samples. XRD analysis of Clay E samples revealed that the illite and quartz were the major phase along with minor amount of goethite, kaolinite and muscovite phases. The peaks of nacrite and dickite phase which are polymorphs of kaolinite minerals having same chemical formula obtained almost similar position so precise distinguish of these minerals is difficult. It was observed that identification of different clay minerals through XRD data analysis is complex and challenging. Hence high expertise of the operator is required. In the present study the during the calculation of the total kaolinite phase by XRD, nacrite and dickite phase were also included. Based on the X-ray diffractogram and Rietveld refinement the total kaolinite proportion was found to be 62%, 88%, 82, and 54 % in Clay-A, Clay-B, Clay-C, and Clay-D samples respectively. Whereas illite and kaolinite mineral percentage in the Clay E sample were estimated to be 70% and 5% respectively.

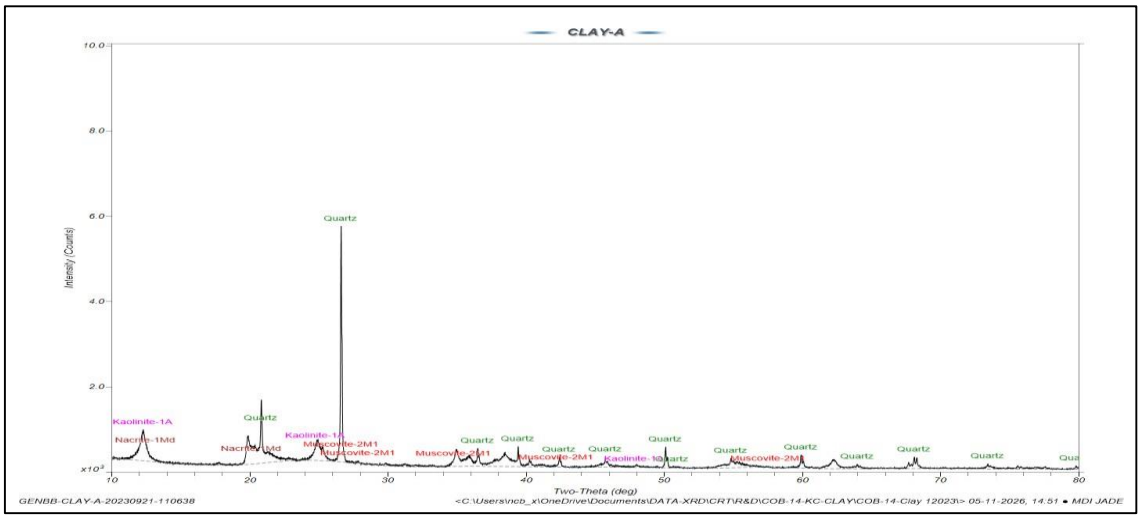


Fig.6: X-ray diffractogramme of Clay-A

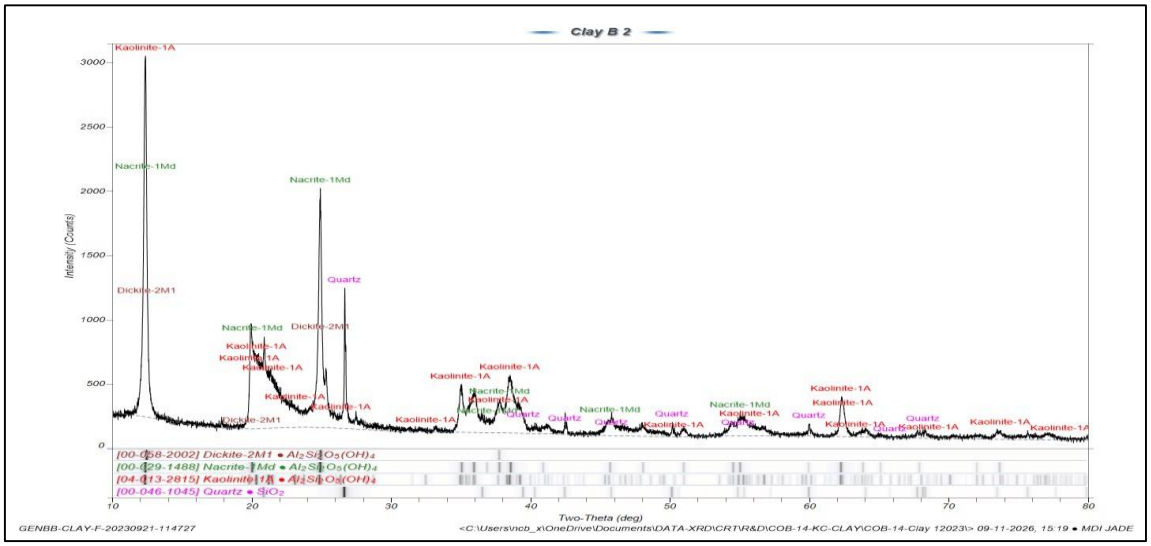


Fig.7: X-ray diffractogramme of Clay-B

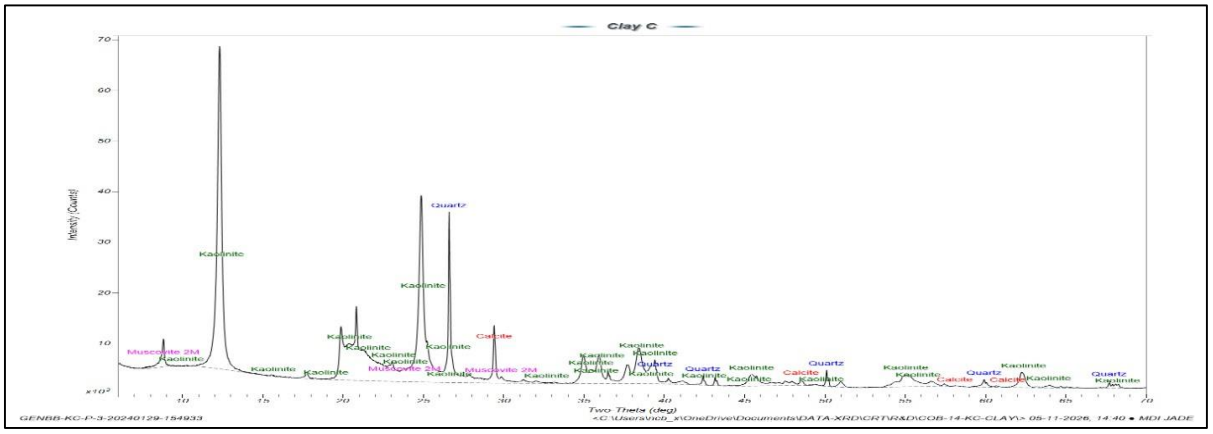


Fig.8: X-ray diffractogramme of Clay-C

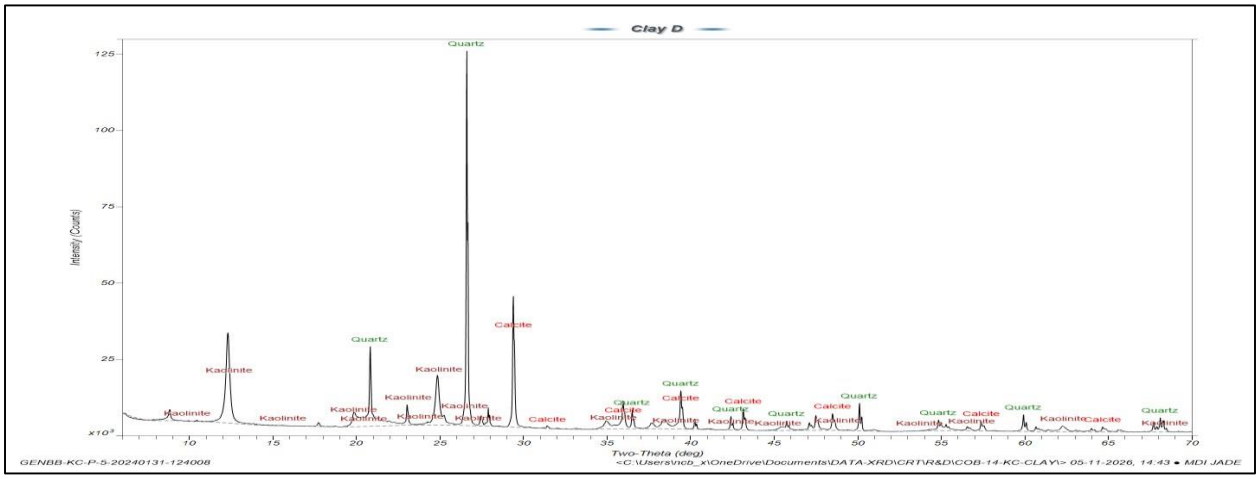


Fig.9: X-ray diffractogramme of Clay-D

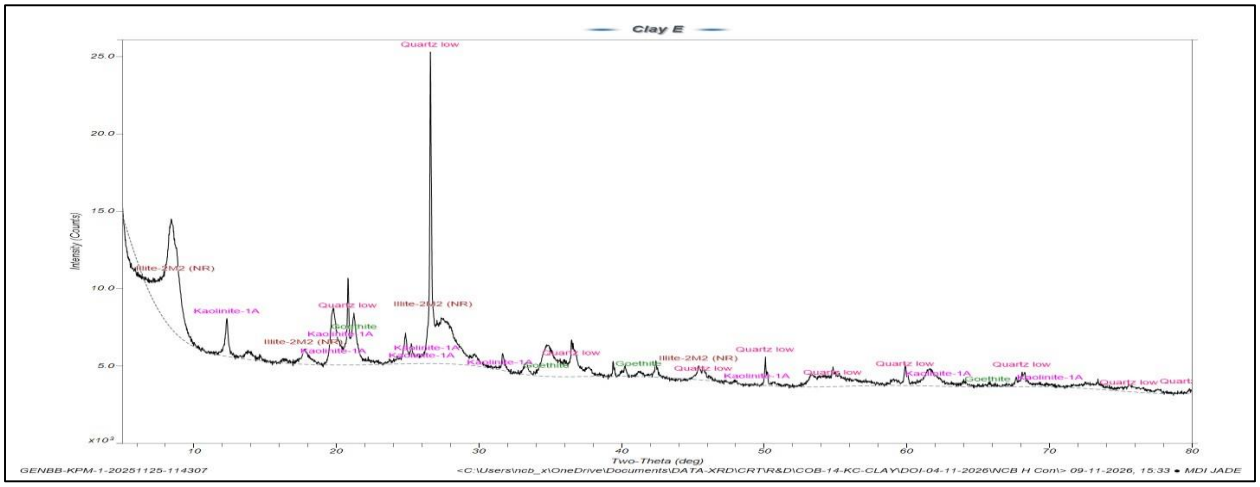


Fig.10: X-ray diffractogramme of Clay-E

3.5 Comparison of Different Methodologies for the Estimation of Kaolinite Percentage:

Series of experimental methodologies or techniques such as LOI method using laboratory muffle furnace as per the procedure IS 18189:2023, clause 4.1 annex B, thermogravimetric analysis (TG) using TG-DTA and mineralogical analysis by XRD has been performed to estimate the kaolinite content present in these clay samples and the detailed comparison data has been tabulated in Table 3.

It was evident that kaolinite content as estimated by different methodologies such as LOI in the temperature range of 300°C to 750°C and TG-DTA and XRD shown almost similar results for purer kaolinitic type clay or say non calcareous kaolinite type of clay samples that is Clay-A and Clay-B respectively. However, in case of clay samples, Clay-C and Clay-D having presence of calcite mineral or calcareous compound the obtained kaolinite content by LOI and TG-DTA as well XRD were found to be different from each other. Clay sample having presence of impurities such as carbonates compounds interfere in the mass loss (LOI) process due to dehydroxylation and decarbonation at the same temperature range and produce misleading data in comparison to TG-DTA analysis. These two step weight loss along with two different peaks due to the thermal events dehydroxylation of kaolinite and decarbonation of calcite minerals respectively are distinctly observed in the TG-DTA analysis in the sample Clay-C and Clay-D. The present study revealed that XRD analysis is required for the brief and precise phase analysis of the different types of complex clay

minerals. The results of the XRD analysis showed phases such as nacrite and dickite which are polymorphs of kaolinite phase having same chemical formula present in the sample Clay-B, along with the other major and minor minerals such as quartz, muscovite, calcite, goethite etc. present as impurity in the other different types of clay samples only be distinctly identified by XRD methodology. However precise distinguish and quantification of polymorphs of kaolinite phases like nacrite and dickite by XRD is difficult due to almost nearer peak position.

In case of non kaolinitic clay sample such as Clay E having illite as the dominant phase as per XRD analysis, showed estimation of kaolinite content as per the different methodologies of LOI and TG-DTA are very misleading due to multi steps dihydroxylation at different temperatures of the illite mineral and no correlation can be drawn from each other techniques. So mineralogical analysis by XRD analysis prove to be favorable techniques for either kaolinite or non kaolinitic clay such as illite type of

clay samples. Though XRD analysis provided brief and precise mineralogical information for the complex clay samples but the sample preparation is meticulous, and analysis is challenging as well required high expertise of the operator in comparison to the other methodologies. On the other hand, TG-DTA analysis can be performed rapidly on raw clay samples. Therefore, TG-DTA analysis found to be less complicated and may be adopted for purer type of kaolinite clay samples, however precise quantification of different types of clay minerals is limited.

Table 3. Kaolinite Percentage in Clay Samples Estimated using Different Methodologies

Sample	% Kaolinite by LOI (300°C-750°C) method as per Indian standard 18189:2023,	% Kaolinite By TG-DTA	% Kaolinite By XRD
Clay-A	61.43	62.8	63
Clay-B	72.00	72.63	78
Clay-C	72.93	67.35	60
Clay-D	90.85	39.00	54
Clay E	41.78	34.63	5.0

4.0 *CONCLUSIONS:*

- In present study quality of five different types of clay samples were assessed in terms of kaolinite content using different methodologies and techniques such as loss of ignition (LOI), X ray dffractometer (XRD) and thermal analayser (TG-DTA) respectively and comparison among each technique were drawn. Results indicated most of the clay samples Clay-A, Clay-B, Clay-C, Clay-D found to have high kaolinite content except the illite type Clay E sample.
- It was observed that estimated kaolinite percentage found to be almost similar in the case of LOI method in between temperature 300°C to 750°C and TG-DTA as well as XRD respectively in non-calcareous and purer type of kaolinitic clay samples. Whereas clay sample having presence of impurities such as calcite or carbonates compounds interfere in the mass loss (LOI) process due to the chemical events dehydroxylation and decarbonation respectively at the same temperature range and produce misleading data in comparison to each other techniques.
- The study showed that XRD analysis is required for the brief and precise phase analysis of the different types of clay minerals along with identification of polymorphs of kaolinite phase such as nacrite and dickite and these polymorphs are need to be considered during total kaolinite estimation.
- This investigation revealed that the estimation of clay mineral phases mainly kaolinite content by thermogravimetric (TG) analysis method is straightforward and easy for purer kaolinitic (1:1) type clay whereas quantative analysis by X-Ray Diffraction (XRD) with Rietveld refinement provides detail and precise mineral phase information for complex clay minerals but analysis is quite challenging and need high expertise.

5.0 ACKNOWLEDGEMENT:

Authors wish to acknowledge DPIIT, Ministry of Commerce and Industry, Govt. of India for financial support through R&D project funding COB-14 of 2023. The subject and the contents reported in this paper are based on the R& D work carried out in the Cement Research and Independent Testing Laboratory at the National Council for Cement and Building Materials (NCB), Ballabgarh, and being published with the kind permission of the competent authority.

6.0 DECLARATION OF COMPETING INTEREST:

The authors declare that they have no known competing financial interests or personal relationships that could have appeared to influence the work reported in this paper.

7.0 REFERENCES:

1. M. Sharma, S. Bishnoi, F. Martirena, K. Scrivener, Limestone calcined clay cement and concrete: a state-of-the-art review, Cem. Concr. Res. 149 (2021) 106564, https://doi.org/10.1016/j.cemconres.2021.106564.)

2. R. M. Andrew, Global CO_2 emissions from cement production. *Earth Syst. Sci. Data* 10, **2018**,195–217

3. N. Tkachenko, K. Tang, M. McCarten, et al., Global database of cement production assets and upstream suppliers. *Sci. Data* 10, **2023**, 696.

4. H.A. Kindi, H.A. Abdel-Gawwad, M.S. Meddah, K.A. Jabri, Y. Mohamedzein, An overview of the critical influential parameters on the performance of limestone calcined clay cement paste, mortar, and concrete, Constr. Build. Mater. 444 (2024) 137615, https://doi.org/10.1016/j.conbuildmat.2024.137615.

5. S. Barbhuiya, J. Nepal, B.B. Das, Properties, compatibility, environmental benefits and future directions of limestone calcined clay cement (LC3) concrete: a review, Journal of Building Engineering 79 (2023) 107794, https://doi.org/ 1016/j.jobe.2023.107794.

6. S. Overmann, A. Vollpracht, T. Matschei, Reactivity of calcined clays as SCM—A review, Materials. (Basel) 17 (2) (2023) 312, https://doi.org/10.3390/

7. A.A. Diaz, R.S. Reyes, T. Hanein, E.F. Irassar, Snellings, Properties and occurrence of clay resources for use as supplementary cementitious materials: a paper of RILEM TC 282-CCL, Mater. Struct. 55 (2022) 139

8. B.S. Abay, L. Tanacan, in: A review on Limestone Calcined Clay Cement (LC3) as an alternative. 2nd International Conference on Innovative Academic Studies, Konya, Turkey, 2023.

9. Gorry, S. Bishnoi, K. A. Riding, Fresh properties of concrete containing calcined clays: a review by RILEM TC-282 CCL, Mater. Struct. 55 (6) (2022) 151, https://doi.org/10.1617/ s11527-022-01971-3.

10. T. Hanein, K.-C. Thienel, F. Zunino, A.T.M. Marsh, M. Maier, B. Wang …, F. Martirena-Hern´andez, Clay calcination technology: state-of-the-art review by the RILEM TC 282-CCL, Mater. Struct. 55 (1) (2021) 3, https://doi.org/10.1617/ s11527-021-01807-6.

11. S. Joseph, Y. Dhandapani, D.A. Geddes, Z. Zhao, S. Bishnoi, M. Vieira …, K. A. Riding, Mechanical properties of concrete made with calcined clay: a review by RILEM TC-282 CCL, Mater. Struct. 56 (4) (2023) 84, https://doi.org/10.1617/ s11527-023-02118-8.



12. O.C YES¸ ˙ILYURT, Calcination and characterization of clays obtained from cement plants of Turkiye, A Thesis Submitted to the Graduate School of Natural and Applied Sciences of Middle East Technical University (2023).

13. Mariam Farouk Ghazy, El Said A. Maaty, Metwally Abd Elaty, Ala' A. Alrwashdeh- A comprehensive review of limestone calcined clay cement (LC3): Environmental and properties benefits, challenges, opportunities, and future directions: Results in Engineering 28 (2025) 108319

14. M. Hanifa, R. Agarwal, U. Sharma, P. Thapliyal, L. Singh, A review on CO2 capture and sequestration in the construction industry: emerging approaches and commercialised technologies, J. CO2 Util. 67 (2023) 102292, https://doi.org/10.1016/j.jcou.2022.102292.

15. J-H. Wee, A review on carbon dioxide capture and storage technology using coal fly ash. *Appl. Energy*,**2013**, 106, 143–51.

16. D. Suresh and K. Nagaraju, Ground granulated blast slag (GGBS) in concrete–a review. *IOSR J Mech Civ Eng.*,**2015**, 12, 76–82.

17. J. Alexandre, G.C. Xavier, A.R.G. Azevedo, S.N. Monteiro, C.M.F. Vieira, Determination of temperature and time calcination of clays for production of metakaolin based on Pozzolanic activity, Characterization of Minerals, Metals, and Materials 2014 (2014) 25–32.

18. M. Atasever, S.T. Erdo˘gan, Effects of clay type and component fineness on the hydration and properties of limestone calcined clay cement, Mater. Struct. 57 (8) (2024) 183, https://doi.org/10.1617/s11527-024-02461-4.

19. J. Ma˜nosa, A. Calder´on, R. Salgado-Pizarro, A. Maldonado-Alameda, J. M. Chimenos, Research evolution of limestone calcined clay cement (LC3): a comprehensive overview, Heliyon. 10 (3) (2024), https://doi.org/10.1016/j. heliyon.2024.e25117.

20. B. Kanagaraj, N. Anand, U.J. Alengaram, R.S. Raj, S. Karthick, Limestone calcined clay cement (LC3): a sustainable solution for mitigating environmental impact in the construction sector, Resources, Conservation & Recycling Advances 21 (2024) 200197, https://doi.org/10.1016/j.rcradv.2023.200197.

21. D. Zhang, B. Jaworska, H. Zhu, K. Dahlquist, V.C. Li, Engineered Cementitious Composites (ECC) with limestone calcined clay cement (LC3), Cement Concr. Compos. 114 (2020) 103766, https://doi.org/10.1016/j.cemconcomp.2020.103766.

22. N. Ijaz, W.-M. Ye, Z. ur Rehman, Z. Ijaz, M.F. Junaid, Global insights into micro-macro mechanisms and environmental implications of limestone calcined clay cement (LC3) for sustainable construction applications, Sci. Total Environ. 907 (2024) 167794, https://doi.org/10.1016/j.scitotenv.2023.167794.

23. G. Huang, Y. Liu, T. Benn, L. Luo, T. Xie, Y. Zhuge, A comprehensive framework for the design and optimisation of limestone-calcined clay cement: integrating mechanical, environmental, and financial performance, Journal of Composites Science 8 (12) (2024) 524, https://doi.org/10.3390/jcs8120524.

24. Kamal Hosen, Bing Chen: Limestone calcined clay cement (LC3): A review of materials, properties, production and environmental impact: Journal of Building Engineering 112 (2025)



113672

25. IBM (Indian Bureau of Mines) (2017) Indian Minerals Yearbook 2015(Part III Mineral Reviews): Kaolin, Ball Clay, Other Clays and Shale, Indian Bureau of Mines, Nagpur, India.
26. R.E. Grim, Clay Mineralogy, Science (1979) 135 (1962) 890–898. https://doi.org/10.1126/SCIENCE.135.3507.890.
27. M.H. Zhang, V.M. Malhotra, Characteristics of a thermally activated alumino-silicate pozzolanic material and its use in concrete, Cem Concr Res 25 (1995) 1713–1725. https://doi.org/10.1016/0008-8846(95)00167-0.
28. K. Scrivener, F. Martirena, S. Bishnoi, S. Maity, Calcined clay limestone cements (LC3), Cem. Concr. Res. 114 (2018) 49–56.https://doi.org/10.1016/J.CEMCONRES.2017.08.017.
29. V. Shah, A. Parashar, G. Mishra, S. Medepalli, S. Krishnan, S. Bishnoi, Influence of cement replacement by limestone calcined clay pozzolan on the engineering properties of mortar and concrete, Advances in Cement Research 32 (2020) 101–111. https://doi.org/10.1680/JADCR.18.00073
30. A.A. Díaz, R.S.A. Reyes, F.A. Carratalá, L.A.P. García, C.A.L. Rodríguez, J.F.M. Hernández, The Experience of Cuba TRC on the Survey of Kaolinitic Clay Deposits as Source of SCMs—Main Outcomes and Learned Lessons, RILEM Bookseries 25 (2020) 1–8. https://doi.org/10.1007/978-981-15-2806-4_1.
31. Avet, K. Scrivener, Investigation of the calcined kaolinite content on the hydration of Limestone Calcined Clay Cement (LC3), Cem Concr Res 107 (2018) 124–135. https://doi.org/10.1016/j.cemconres.2018.02.016.
32. Alujas, R. Fernández, R. Quintana, K.L. Scrivener, F. 890 Martirena, Pozzolanic reactivity of low grade kaolinitic clays: Influence of calcination temperature and impact of calcination products on OPC hydration, Appl Clay Sci 108 (2015) 94–101. https://doi.org/10.1016/J.CLAY.2015.01.028.
33. M.E. Awad, A. López-Galindo, R. Sánchez-Espejo, C.I. Sainz-Díaz, M.M. El-Rahmany, C. Viseras, Crystallite size as a function of kaolinite structural order-disorder and kaolin chemical variability: Sedimentological implication, Appl Clay Sci 162 (2018) 261–267. https://doi.org/10.1016/j.clay.2018.06.027
34. S. Ferreiro, M.M.C. Canut, J. Lund, D. Herfort, Influence of fineness of raw clay and calcination temperature on the performance of calcined clay-limestone blended cements, Appl Clay Sci 169 (2019) 81–90. https://doi.org/10.1016/j.clay.2018.12.021.
35. C. Bich, J. Ambroise, J. Péra, Influence of degree of dehydroxylation on the pozzolanic activity of metakaolin, Appl Clay Sci 44 (2009) 194. https://doi.org/10.1016/j.clay.2009.01.014
36. M.M. Mestdagh, L. Vielvoye, A.J. Herbillon, Iron in kaolinite: II. The relationship between kaolinite crystallinity and iron content, Clay Miner 15 (1980) 1–13. https://doi.org/10.1180/CLAYMIN.1980.015.1.01.
37. A. Shvarzman, K. Kovler, G.S. Grader, G.E. Shter, The effect of dihydroxylation /amorphization degree on pozzolanic activity of kaolinite, Cem Concr Res 33 (2003) 405–416. https://doi.org/10.1016/S0008-8846(02)00975-4.



38. S. Mohammed, Processing, effect and reactivity assessment of artificial pozzolans obtained from clays and clay wastes: a review. *Construct. Build. Mater.*,**2017**, 140, 10–9

39. G. Kakali, T. Perraki, S. Tsivilis, E. Badogiannis, Thermal treatment of kaolin: The effect of mineralogy on the pozzolanic activity, Appl Clay Sci 20 (2001) 73–80. https://doi.org/10.1016/S0169-1317(01)00040-0

40. Rodrigo Fernandez, Fernando Martirena, Karen L. Scrivener: The origin of the pozzolanic activity of calcined clay minerals: A comparison between kaolinite, illite and montmorillonite, Cement and Concrete Research Volume 41, Issue 1 (113-122) 2011.

41. Indian standard, IS 1727:1967- Methods of test for pozzolanic materials.

42. Indian standard, IS 18189:2023- Portland Calcined Clay Limestone Cement — Specification.

43. Chakraborty, A.K., 2014. Phase Transformation of Kaolinite Clay. Springer.

44. Characterization of Spinel Phase Formed in Kaolin-Mullite Thermal Sequence: Journal of the American Ceramic Society March 2005, 69(10):C-251 - C-253

45. Mullite formation in clays and clay-derived vitreous ceramics Journal of the European Ceramic Society; 2008, Pages: 465-471, Volume: Volume 28, Issue 2



Technical Session -IIB

Advancing Large-Capacity Cement Production HWI Experience in Technology and Plant Performance

Ashok Kumar Dembla & Deepti Varshney

Humboldt Wedag India

Preface - Evolution of Cement Plant Capacities in India

The Indian cement industry has undergone a remarkable transformation since the establishment of its early cement manufacturing units. In the initial stages, the industry developed around relatively small-capacity cement plants, with production systems sized to meet the regional demand and infrastructure requirements of that period. With the rapid expansion of India's economy, urbanisation and infrastructure development, cement demand increased steadily, leading to a gradual shift towards larger and more integrated manufacturing facilities.

India's cement industry has expanded substantially in both capacity and consumption over the past decade. As per the industry projections, installed cement capacity increased from 496 million tonnes in 2020 to 636.6 million tonnes in 2025, and is projected to reach 866.5 million tonnes by 2030. Cement consumption increased from 289 million tonnes in 2020 to 470.6 million tonnes in 2025, with consumption projected to reach 665.6 million tonnes by 2030. During the same period, per-capita cement consumption is projected to increase from 321.5 kg in 2025 to 436 kg by 2030, reflecting the continuing growth potential of the Indian cement market.

This growth over the past 5 years has also been accompanied by a continuous increase in the scale of individual production facilities. The industry has progressively moved from smaller kiln systems towards large single-line clinker production lines, driven by the need for economies of scale, improved resource utilisation, higher productivity and greater operational reliability. The projected increase in capacity indicates that large-scale capacity additions will remain an important part of the industry's expansion.

Technology Evolution Enabling Large-Capacity Cement Plants

The transition towards larger cement plants has been supported by advances in process technology. Increasing capacity is not simply a matter of scaling up individual equipment; it requires efficient and well-integrated systems capable of handling higher material and gas volumes while maintaining process stability, clinker quality and energy efficiency. Advances in preheating, calcination, firing, grinding, cooling and process control have progressively enabled larger single-line plants.

A key development has been KHD HE cyclone technology, which uses optimised inlet geometry and immersion tubes to achieve high separation efficiency with low pressure drop. Improved gas-solid separation reduces dust carryover and system resistance, contributing to lower fan power consumption and stable gas flow through the pyroprocessing system.KHD's Pyroclon Low NOx-AF calciner has similarly supported higher-capacity operation while addressing environmental requirements. It combines efficient calcination with reduced NOx formation and the flexibility to co-process higher quantities of alternative fuels. This provides greater fuel flexibility and supports higher Thermal Substitution Rate (TSR).The PYRO-JET® firing technology complements this system through controlled combustion with low primary-air consumption. High-momentum firing, flame shaping and improved fuel-air mixing support stable combustion and effective heat distribution. Its ability to handle conventional and alternative fuels further enhances operating flexibility while reducing fan loading.

In grinding, KHD Roller Press technology combined with efficient classification provides high-throughput grinding with low specific power consumption. The elimination of water injection also



avoids the associated thermal penalty. This enables the grinding system to support higher clinker production without a disproportionate increase in energy consumption.

The clinker cooler has also become an important part of the plant's energy balance. Efficient cooling recovers sensible heat from hot clinker for reuse in the pyroprocess. KHD's latest-generation PFC2cooler provides efficient and reliable cooling, while integration with Waste Heat Recovery Systems allows otherwise unused heat to be converted into captive electrical power.Another important development is the integration of alternative fuels and circular-economy principles into the basic plant design. Modern calciner and firing systems can accommodate higher TSR and different solid and liquid alternative fuels, helping reduce fossil-fuel consumption and CO_2 emissions while improving fuel flexibility. Provision for further TSR increases also allows plants to adapt as fuel availability and preparation infrastructure develop.

With increasing plant size, automation, process control and integrated material handling have become equally important. Higher material flows and greater interaction between process sections require closer monitoring and control. Advanced automation provides better process visibility and optimisation, while integrated handling systems ensure reliable movement of raw materials, fuels and clinker.

Together, these developments have changed the economics and practicality of large-capacity plants. Higher production from a single line can provide economies of scale, better infrastructure utilisation, lower operating cost per tonne and improved manpower and maintenance efficiency. At the same time, advances in process efficiency, automation, energy recovery and equipment reliability help manage the technical challenges associated with larger plants.For cement manufacturers, therefore, the move towards larger plants is not about capacity alone. It is about achieving higher productivity, lower specific energy consumption, lower production cost and better utilisation of capital, while maintaining the flexibility to adopt alternative fuels, waste heat recovery, low-NOx combustion and improved emission control.The evolution can therefore be seen as a continuous relationship between plant scale and technology: increasing capacity creates the need for better technology, while advances in technology make larger single-line plants increasingly practical and efficient.

Large-Capacity Cement Plants — KHD/HWI Technology in Application

The increasing capacity of cement plants has been accompanied by a corresponding increase in the size and capacity of the major process equipment. The projects presented in this paper illustrate the application of KHD technology across large-capacity raw grinding and pyroprocessing systems, with equipment sized to handle the higher material and gas flows associated with single-line clinker production. The following section summarise the major equipment configurations and their principal specifications, including raw grinding systems, preheaters, calciners, rotary kilns, clinker coolers and firing systems. The corresponding performance data, including production rate, specific heat and power consumption, pressure drop and grinding performance, are also presented to demonstrate the operating efficiency achieved with these large-capacity installations.

Dalmia Cement, Umrangsho - 9,500 TPD Low-Carbon Clinker Line

Project Green is a 9,500 TPD clinker production line at Umranghsu, Assam, developed by Dalmia Cement (Bharat) Limited .The main contract was awarded in June 2023, civil construction commenced in September 2023, and the plant was commissioned in October 2025, approximately 24 months after commencement of civil construction. The plant has also been designed for substantial alternative fuel utilization, with a 35% Thermal Substitution Rate (TSR) potential.

Raw Material Grinding System

System Configuration

Parameter	Specification
System Capacity	2 × 350 TPH
Product Fineness	15% residue on 90 µ
Roller Press	2 × RP16-170/180 , 2 × 1600 kW
Static Separator	Type: Static VS 96/20
Dynamic Separator	SKS LC 3750 @625000m3/hr fan volume

Operational Performance at glance:

Parameter	**Operational data**	
	Guarantee (Revised)	Achieved
Average production rate (tph)	2 x 330	2 x 330
Average Product Residue on 90 µ	15.0	15
Specific power consumption (kWh/t)	14.5	14.3

Pyro processing System

System Configuration

Parameter	Specification
Clinker Capacity	9,500 TPD
Preheater	6-stage, Double String (90 HE 75) with Pyroclon Low NOx-AF calciner
Rotary Kiln	Ø 5.2 m × 82 m, 1 x 1520kw
Burner	PyroJet Low NOx (522KO)

Operational Performance at glance:

Parameter	Operational data	
	Guarantee	Achieved
Production rate dry basis (tpd)	9500	9700-9800
Specific fuel consumption (kcal/kg-cli)	677	675-685
Specific power consumption (kWh/t)	13.5	12.5

JK Cement Panna — 10,000 TPD State-of-the-Art Pyro Process Line

The JK Cement Panna project comprises a 10,000 TPD clinker production line at Panna, Madhya Pradesh, developed as a major brownfield expansion

The project was executed on an accelerated schedule, with the plant commissioned approximately 19 months after commencement of civil works. HWI's scope included the complete pyroprocessing system along with raw material grinding and blending facilities. Currently the plant is operational and under stabilisation.

Raw Material Grinding System

System Configuration

Parameter	Specification
Roller Press	RP 20-220/180 with motor 2 x 2000 kW
Capacity	440 TPH, 1.50 % residue on 212 µ
V-Separator	Type: Static, Size: VS 96/22
Dynamic Separator	SKS-LC-4250 @ 8,30,000 m3/hr fan volume

Operational Performance at a Glance

Parameter	**Operational data**	
	Guarantee	Achieved
Average production rate (tph)	440	435-440
Average Product Residue on 212 µ	1.5	1.5-1.7
Specific power consumption (kWh/t)	14.3	13.5

Pyro processing System

System Configuration

Parameter	Specification
Preheater	95 HE 81 6 Stage, Double String Preheater with Low NOx-AF Calciner
Kiln	5.6 m dia. X 85 m @ 2 x 910 KW
Burner	PYROJET Low Nox (519 KO)

Operational Performance at a Glance

Parameter	Operational data	
	Guarantee	Achieved
Production rate dry basis (tpd)	11000	11900
Specific fuel consumption (kcal/kg-cli)	689	691
Specific power consumption (kWh/t)	13.10	11.6

UTCL, Nathdwara — 10,000 TPD Highly Efficient Pyro Process Line

UltraTech Cement Limited (UltraTech), a flagship company of the Aditya Birla Group, is a major player in the Indian cement industry, with a current total capacity of 200+ MTPA has became the world largest cement manufacturer outside China. The group has achieved rapid expansion through a combination of aggressive organic growth and strategic acquisitions. These efforts have made UltraTech, India's leading cement manufacturer, with a clear target of reaching 240 MTPA. The growth plan was undertaken in 4 phases and latest is the operation of Line III at Nathdwara.

Pyro processing System

System Configuration

Parameter	Specification
Preheater	95 HE 81 – 6 Stage Double String with LowNox-AF calciner
Kiln	5.6 m dia. X 85 m length, Motor – 2 x 910 kW
Burner	Pyrojet Low NOx Burner HPJ 481 KO

Operational Performance at a Glance

Parameter	Operational data	
	Guarantee	Achieved
Production rate dry basis (tpd)	10000	11750
Specific fuel consumption (kcal/kg-cli)	683	679
Specific power consumption (kWh/t)	12.5	11.5

My Home Cement Line IV- A transcript of cutting-edge Technology

My Home Industries has successfully commissioned its fourth production line (Line-4), with Humboldt Wedag India as the leading technology partner. This new line further secures MHIPL's position as a leading producer in South India and leverages modern process technology and energy-efficient equipment to set new standards for combining growth with sustainability in the industry. This plant features supplies starting from crushing to Packing in collaboration with other partners. In addition, Line IV includes a 13.3 MW WHR power plant, enhancing the facility's energy efficiency and sustainability outlook even further

Raw Material Grinding System:

System Configuration

Parameter	Specification
Roller Press	RP 20-220/180 with motor 2 x 2400 kW
Capacity	700 TPH, 15.0 % residue on 90 µ
V-Separator	Type: Static, Size: VS 112/26

Operational Performance at a Glance

Parameter	Operational data	
	Guarantee	Achieved
Average production rate (tph)	700	740
Average Product Residue on 90 µ	<15.0	14-15
Specific power consumption (kWh/t)	9.00	9.02

Pyro Process System

System Configuration

Equipment	Description
Preheater	90 HE 75 6 Stage Double String Preheater with Low NOx-AF Calciner
Kiln	5.2 m dia. X 82 m length with installed motor 1 x1520 KW
Cooler (Pyro Step2)	PSC² 4-203.18T, Grate Area 203 m² with hydraulic drive
Clinker Crusher	Roll Crusher PRC 540-5
Kiln Pyrojet Burner for Kiln	HPJ 502 KO

Operational Performance at a Glance

Parameter	Operational data	
	Guarantee	Achieved
Production rate dry basis (tpd)	8400	9500
Specific fuel consumption (kcal/kg-cli)	685.0	715 with 20 % TSR
Clinker Temperature (deg.C)	105	120 with 20 % TSR & WHRS ON

Cement Grinding System

System Configuration

Equipment	Description
Roller Press	RP 20-220/180 with motor 2 x 2400 kW
Capacity	235 TPH PPC 3600 Blaine
V-Separator	Type: Static, Size: VS 96/26
Dynamic Separator	SKS-LC-3750 with fan volume 5,00,000 m3/hr

Operational Performance at a Glance

Parameter	Operational data	
	Guarantee	Achieved
Average production rate (tph)	235 PPC	245 PPC
Blaine (m2/kg)	360	362
Average Product Residue on 45 Mic	NA	12.77
Specific power consumption (kWh/t)	21.6	18.63

Marwar Cement-9000 tpd State of Art Technology plant

Marwar Cement, Rajasthan, which has recently become part of the Adani Group through its Ambuja Cements business commissioned its Line 1 in Rajasthan.

The plant represents another step towards large-scale, integrated cement manufacturing in India, with a guaranteed clinker production capacity of 9,000 TPD. HWI is supplying the core process packages covering raw material grinding, pyroprocessing and cement grinding. The integration of these three major process sections provides a complete KHD-HWI technology chain from raw material preparation through clinker production to finished cement. For coal Mill VRM is provided in collaboration with another subsupplier.

Raw Material Grinding System

System Configuration

Parameter	Description
Roller Press	RP 18-200/180 with motor 2 x 1800 kW
Capacity	400 TPH, 15 % residue on 90 µ
V-Separator	Type: Static, Size: VS 96/22

Dynamic Separator	SKS-LC-3750 with fan volume 6,25,000 m3/hr

Operational Performance at a Glance

Parameter	Operational data	
	Guarantee	Achieved
Average production rate (tph)	400	406
Average Product Residue on 90 µ	15	8
Specific power consumption (kWh/t) for the equipments within battery limits	11.8	10.8

Pyro processing System

System Configuration

Parameter	Description
Preheater	95 HE 81 5 Stage Double String Preheater with Low NOx-AF Calciner
Kiln	5.6 m dia. X 82 m length with installed motor 2 x 870 KW
Burner	PYROJET Low NOX Burner HPJ 570 KO

Operational Performance at a Glance

Parameter	Operational data	
	Guarantee	Achieved
Production rate dry basis (tpd)	9000	9233
Specific fuel consumption (kcal/kg-cli) with 5 stage preheater	725.7@420HOR	723.9
Specific power consumption (kWh/t)	13	12.57

Cement Grinding System

System Configuration

Parameter	Description
Roller Press	RP 18-210/180 with motor 2 x 1800 kW, CHF Surface,
Capacity	290 TPH, 3200 Blaine
V-Separator	Type: Static, Size: VS 96/22
Dynamic Separator	SKS-VC-3750 with fan volume 6,25,000 m3/hr
Ball Mill	4.6 x 12.50, 2 x 2050kw

The cement grinding system is under commissioning stage.

Cross-Plant Analysis

The projects presented in this paper cover a range of large-capacity clinker production lines of approximately 9,000–12,000 TPD. Despite differences in plant configuration, site conditions and customer requirements, a common trend is evident across these installations: increasing production capacity has been achieved through a combination of higher-capacity equipment, improved process efficiency and integration of technologies across the complete production system. Increasing plant size is therefore not simply a matter of scaling individual equipment; it also requires stable process operation while handling substantially higher material and gas flows. The reported installations demonstrate this approach across raw material grinding, pyroprocessing, clinker cooling, alternative fuel utilisation, waste heat recovery and process control.

A significant feature across the projects is the evolution of pyroprocessing towards large single-line configurations. The equipment configurations indicate that these capacities are being achieved with large-diameter rotary kilns, six-stage twin-string preheaters and high-capacity calciners. The documented projects predominantly employ HE cyclone technology together with Pyroclon Low NOx-AF calciners, providing efficient gas-solid separation, low pressure drop and controlled calcination at high material throughput. At these capacities, effective gas-flow management and heat transfer become increasingly important to maintain thermal performance as production rates increase.

The performance data also indicate that increasing plant capacity does not necessarily result in a proportional increase in specific energy consumption. For example, the reported specific heat consumption of the large-capacity pyro lines is generally in the range of approximately 675–680 kcal/kg clinker, depending on plant configuration and operating conditions. These figures demonstrate that high clinker production rates can be combined with controlled thermal performance when the preheater, calciner, kiln and cooler are considered as an integrated system.

Raw material grinding has evolved in parallel with the increase in pyroprocessing capacity. The projects use KHD Roller Press systems, mainly RP16, RP18 and RP20, with capacities varying according to the grindability basis and product fineness. These installations demonstrate how Roller Press technology has been scaled to meet the higher material requirements of large-capacity clinker lines. At the same time, the reported specific power consumption shows that the focus is not only on achieving higher throughput, but also on maintaining low electrical energy consumption at the required product fineness.

Another common feature across the projects is the use of technologies aimed at reducing process resistance while maintaining high throughput. The HE cyclone design, with optimised inlet geometry and immersion tube configuration, provides efficient dust separation with low pressure drop. This becomes increasingly important at large plant capacities, where the volumetric gas flow through the preheater and associated gas-handling equipment increases substantially. Lower system resistance reduces the demand on the induced-draft system and helps control specific fan power. The benefit therefore extends beyond the cyclone itself and contributes to the overall electrical efficiency of the pyroprocessing system. The reported pressure-drop performance of Project Green, for example, highlights the importance of maintaining low resistance across the preheater system.

Alternative fuel utilisation is another area where the large-capacity plants demonstrate a change in process philosophy. At higher production rates, the ability to utilise solid and liquid alternative fuels provides not only a route towards lower fossil-fuel consumption and CO_2 emissions, but also greater flexibility in fuel selection. However, achieving high TSR at this scale requires stable calcination, appropriate combustion technology, reliable fuel feeding and effective control of combustion conditions. The experience across these projects indicates that alternative fuel capability needs to be considered as an integral part of the basic process design rather than added as a separate downstream modification.

Waste heat recovery has also become an integral element of large-capacity plant design. The projects considered include WHRS capacities of approximately 13.3 MW at My Home Cement, 20 MW at JSW

Nagaur and 23 MW at JK Cement Panna. The increasing incorporation of WHRS into large-capacity projects from the initial design stage demonstrates a shift from focusing on individual equipment efficiency towards optimisation of the overall energy balance of the manufacturing system.

The clinker cooler is similarly important to the overall thermal performance of the plant. At higher clinker production rates, maintaining clinker temperature and recovering a high proportion of the available heat become increasingly important, since even relatively small heat losses, when multiplied by the larger production rate, can translate into significant energy losses. The cooler therefore forms an important part of the overall thermal efficiency of the large-capacity line rather than functioning only as a clinker cooling device.

The experience across these projects also demonstrates that increasing capacity changes the nature of process risk. A larger production line offers economies of scale through reduced duplication of major equipment, more efficient utilisation of infrastructure and potentially lower operating cost per tonne. At the same time, the consequence of instability or equipment failure becomes greater because a larger proportion of the plant's production capacity is concentrated in a single production line. Consequently, the reliability of major equipment, low-pressure-drop process design, stable combustion, efficient cooling, automation and fuel flexibility become increasingly important as capacity increases. The objective of technology selection is therefore not simply to achieve the required nominal capacity, but to achieve it consistently with predictable energy and operating performance.

Conclusion

The cross-plant analysis ultimately indicates that the progression towards larger cement plants is being driven by a combination of capacity, efficiency and reliability. Higher production capacity provides the opportunity for improved economies of scale, while advances in process technology reduce the technical and operational barriers associated with handling larger material and gas flows. The experience from the plants discussed in this paper suggests that the next stage of capacity development will continue to depend on this interaction between equipment scale and process technology, with energy efficiency, alternative fuel utilisation, waste heat recovery, emissions control and automation becoming increasingly integral to the design of large-capacity cement production lines. KHD's technology portfolio has evolved in line with this progression and is now capable of supporting cement plant solutions with capacities exceeding 15,000 TPD, providing the equipment and process technologies required for reliable and energy-efficient operation at this scale.

ENERGY-EFFICIENT COLDGRINDING IN MVR VERTICAL ROLLER MILLS

Dr. Caroline Woywadt, Gurserjan Singh***

**Gebr. Pfeiffer SE, Kaiserslautern, Germany; **Gebr. Pfeiffer Private Ltd., Noida, India*

SUMMARY

Vertical roller mills combine grinding, drying and classification in a single machine, utilizing gas flow to affect the material transport. With the flexible layout and versatility, the performance of the vertical modular roller mill can be adjusted to meet not only product requirements but also energy-efficiency and sustainability. A VRM can process many different feed materials; SCMs or clinker replacement materials influence grindability, operational behavior, and reactivity. Reactivity indices of SCMs are very different and properties such as feed moisture and granulometry occur in a wide range. Therefore, a fine adjustment of the feed material properties and the target fineness of the finished product needs to be done.

If the moisture of the feed material is getting above a certain limit, the water needs to be evaporated. The thermal energy needed for this is provided by hot gases. Hot gases are available in cement plants from cooler exhaust gases or similar, in standalone grinding terminals a hot gas generator is needed. In a VRM the grinding bed needs to be stable for low-vibration operation. Often water injection into the grinding zone is used to stabilize the grinding bed or to cool hot clinker down. In some regions water resources are scarce and the use is limited as well. Excessive use of additional water to stabilize the grinding bed should be avoided in regard to cement quality and waste of thermal energy.

1.0 *Introduction*

As cement is the most widely consumed building product in the world, a huge volume is produced. Cement production is responsible for about 8% of man-made CO_2-emissions [1]. The International Energy Agency (IEA) has highlighted four principal CO_2 reduction levers. Key strategies to cut carbon emissions in cement production include improving energy efficiency, switching to lower-carbon fuels, promoting material efficiency (to reduce the clinker-to-cement ratio and total demand) and advancing process and technology innovations such as CCS [2]. Reducing the clinker proportion in cement is said to be by far the most effective measure. The use of Supplementary Cementitious Materials (SCMs) to replace clinker in cement is only part of the picture but gives a good indication to evaluate the effectiveness of composite cements regarding their carbon footprint.

Not only use of SCMs is an effective measure to reduce the carbon footprint, improving energy efficiency is also a key factor for grinding plants. In cement production more than 60% of electricity is used for grinding of raw material and cement. With this huge amount it seems mandatorily that energy efficient technologies should be used. The performance of MPS and MVR mills is defined by a required throughput at a required fineness paired with a low specific thermal and electrical energy consumption.

2.0 *Composite Cements - SCMs*

Supplementary Cementitious Materials (SCMs) are used since many decades. The amount of composite cements is still increasing considerably. SCMs can be artificial or natural. Artificial SCMs are for example fly ash, pond ash, granulated blast furnace slag (GBFS), silica fume. Natural SCMs

are e.g. limestone, pozzolana. The hydraulic reactivity is increasing with increasing CaO-content. Hydraulic Properties of pozzolana can be changed resp. increased by thermal treatment.

Artificial SCMs often in use are fly ash and GBFS. The utilization of fly ash in concrete or as an additive in cement introduces many benefits from economical, technical and environmental points of view.

Depending on the burning temperature, coal type and some other factors, fly ashes show different properties in different size fractions. The level of performance of fly ash depends on e.g. the lime reactivity, the carbon content and the fineness.

The engineering properties of GBFS, including its dewatering and transport characteristics, its tendency to consolidation, its grindability and, naturally, its reactivity are determined by its physical and chemical properties. The reaction potential is determined by many factors and parameters where the optimization depends on metallurgical and economic factors.

Pozzolanic materials do not harden on their own when mixed with water but, when finely ground and in the presence of water, they react at normal ambient temperature with dissolved calcium hydroxide (Ca (OH)2) to form strength developing calcium silicate and calcium aluminate compounds. These compounds are similar to those which are formed in the hardening of hydraulic materials. Pozzolanas consist essentially of reactive silicon dioxide (SiO2) and aluminium oxide (Al2O3). The remainder contains iron oxide (Fe2O3) and other oxides. The proportion of reactive calcium oxide for hardening is negligible.

In many countries the most available material as supplement is limestone. Limestone dilutes the clinker content of the cement and impacts the strength development.



Fig- 1: MVR 6000 C-6 installed in India

3.0 Water in the system

Essential for a smoothly running mill is a stable grinding bed. The bed formation is impacted by feed uniformity and feed PSD. Metal detection and extraction gives also success to avoid disturbance and damages in the mill internals. Water in the system is not only introduced by water injection onto the grinding table, moisture of feed materials, evaporated water during gypsum dehydration and grinding aids also provide a certain amount of moisture to the mill circuit. By the amount resp. ratio of exhaust gas and recirculation gas the proportion of water can be controlled as well.

Water injection has positive and negative impact on the grinding process and the product. Comminution depends on pressure and shear stress on the particle bed. The surface contact between the particles distributes the stress in the grinding bed. If the stress is sufficient, micro cracks are generated. These actions can only take place when a compressive strength of grinding bed is provided. In a dry grinding bed adhesive forces and electrostatic forces occur. For a better formation of the grinding bed liquid bridges are advantageous. The surface tension and capillary pressure in the liquid results in additional adhesive forces. Depending on this the compressive strength is increased and flowability is decreased.

The pros and cons of water addition resp. injection onto the grinding bed are given in Table 1. The effect on specific power consumption has to be highlighted due to the fact that a small amount of water reduces the specific power consumption in the range between 5 to 20 %.

1.2 Table 1: Pros and Cons of water injection / water in the mill system

Grinding Bed: adhesive forces, liquid bridge	Pro
Cooling of Clinker	Pro
Grinding Heat, especially for high fineness	Pro
Prehydration of Clinker	Con
Prehydration of Gypsum	Con
Disturbing the Grinding Bed	Con
Dam Ring Clogging	Con
Water consumption / Cost	Con
Impact on specific power consumption	Pro

4.0 *Cold-Grinding*

Grinding in the vertical roller mill is also described as cold-grinding because no external heat is used for the process. This type of grinding is a matter of the heat balance. Main factors impacting the possibility of cold-grinding are:

- Clinker temperature
- Moisture of additives
- Water spray into the grinding zone
- Fineness of the product resulting in specific energy consumption of the mill drive in kWh/t
- False air getting into the vertical roller mill circuit

1.3 Table 2: Examples for cold-grinding with MVR and MPS mills

Plant	A	B	B	C	D	E	F
Mill Size	MVR 6000 C-6	MVR 6000 C-6	MVR 6000 C-6	MVR 5600 C-4	MPS 5300 BC	MPS 4750 BC	MPS 4750 BC
Feed Mix	PPC 35%FA	OPC 6%Lst	PPC 35% FA	PPC 25% FA, 7% Pond	OPC	PLC 22% Lst	OPC
Feed Moisture	1.1%	0.6%	0.5%	2.5%	0.2%	0.15%	0.1%
Clinker Temperature	70°C	76°C	60°C	110°C	30°C	90°C	25°C
Water Injection	1.5%	1.0%	1.4%	Nil	1.5%	2.7%	1.4%
Temperature Mill Outlet	74°C	91°C	77°C	86°C	67°C	81°C	75°C
Capacity	382 tph	413 tph	409 tph	305 tph	215 tph	102 tph	90 tph
Fineness	4110 Blaine	3520 Blaine	3690 Blaine	3830 Blaine	3850 Blaine	4500 Blaine	5200 Blaine
SPC Mill	13.9 kWh/t	13.8 kWh/t	14.0 kWh/t	11.0 kWh/t	22.3 kWh/t	23.2 kWh/t	34.5 kWh/t

Table 2 shows examples of cold grinding with MVR and MPS mills installed in India, Tunisia,

Indonesia and France. The data sets for feed mixture, feed moisture and clinker temperature are given. Water injection and mill outlet temperatures in combination with capacity, product fineness and specific power consumption of the mill main drive are listed above. For all above examples no external heat was used. With a high clinker temperature, the feed moisture can be on a higher level to grind without external heat, water can also be injected to a certain degree to stabilize the grinding bed even more. For higher product fineness the specific power consumption of the mill main drive is also on a higher level, in this case it helps to get more water evaporated; therefore, a higher water injection can be accepted.

In the table above a PPC is produced in Plant C with a proportion of 7% Pond Ash in the feed mixture that results in a total feed moisture of 2.5%. In this plant the clinker temperature is quite high at about 110°C. No water is injected as the feed moisture already supports the grinding bed stabilization. The product fineness of 3830 Blaine is not giving a higher specific energy consumption of the mill main drive because the dry Fly Ash comes already with a high Blaine.

Plant F shows the production data for a very high strength OPC with a fineness of 5200 Blaine. This plant is getting imported clinker with ambient temperature. The required strength development can be achieved even with a water injection rate of 1.4% at a mill outlet temperature of 75°C.

The examples given in Table 2 are all re-calculated and evidenced in the heat-mass-balance program of Gebr. Pfeiffer. To get an operation without the use of external heat, several factors need to be in an equilibrium, that means the required heat needs to be on the same level as the available heat. The required heat is defined mainly through feed moisture, material temperature and false air intake into the mill system. The available heat is coming from the recirculation air, grinding heat of classifier drive and temperature increase of the main fan.

5.0 *Conclusions and Outlook*

Reducing the carbon footprint is a challenging situation for all industries. The performance of MPS and MVR mills is defined by a required throughput at a required fineness paired with a low specific thermal and electrical energy consumption. The combination of three process steps in one system – drying, grinding, separating – makes the vertical roller mill very versatile regarding handling dry and moist feed materials, and grinding these to very high fineness, creating the product properties required by the different market areas. SCMs are available from many sources and have a strong impact on improvement of cement properties and reduction of clinker factor.

Grinding without external heat – so called cold-grinding- is possible. The main impact parameters such as clinker temperature, feed material moisture, product fineness and specific energy consumption must be in the right combination to realize the heat mass balance without external heat input. Several examples given show the opportunities for cold-grinding for many different product types.

6.0 *References*

[1] Scrivener, K.; Dekeukelare, A., et al. (2024). "Financial Attractiveness of LC3". https://lc3.ch/financialattractiveness-of-lc3/

[2] IEA, Tracking Report Cement, November 2021, https://www.iea.org/reports/cement

SUSTAINABLE CEMENT MANUFACTURING THROUGH ENERGY EFFICIENT RAW MATERIAL GRINDING WITH POLYCOM (HIGH PRESSURE GRINDING ROLL) A CASE STUDY

Stefan Diedenhofen*, Vinod Wadile# and Prakash Wagh#

**thyssenkrupp Polysius Solutions GmbH, Beckum, Germany #TKIL Industries Private Ltd., Pune*

ABSTRACT

Grinding is one of the most energy-intensive operations in cement manufacturing, making the adoption of energy-efficient grinding technologies essential for reducing electrical energy consumption, improving plant performance, and lowering the carbon footprint of cement production. Vertical Roller Mills (VRMs) and High-Pressure Grinding Rolls (HPGRs) are established technologies in the cement industry, each offering distinct operational and energy-efficiency advantages. Under typical raw material grinding conditions, with a grindability of ~7 kWh/t at the VRM shaft, HPGR grinding systems can deliver power savings of ~3 kWh/t compared to a VRM system, with the savings increasing as material grindability increases. At UltraTech Cement Ltd.'s Tadipatri plant, the raw materials exhibit relatively high grindability requirements, with a typical grindability of 11–12 kWh/t at the VRM shaft at 15% residue on 90 µm. Following a comprehensive technical and economic evaluation, HPGR technology was selected for its potential to achieve substantial electrical energy savings and enhance Waste Heat Recovery System (WHRS) power generation, notwithstanding its higher initial capital investment compared with a single-VRM installation.

The polycom® HPGR, supplied by TKIL and operating in finish-grinding mode for raw material grinding, forms part of the 10,000 tpd Clinkerisation plant at Tadipatri. Commissioned in June 2024, the installation comprises of a polycom® 21/16-9 with an installed power of 2 x 1800 kW, integrated with a sepol PC Statosep 36/27-LMR 380 separator.

The installation has exceeded its guaranteed production capacity, achieving a throughput of 2 × 383 tph at 2–3% residue on 212 µm, against a guaranteed capacity of 2 x 362 tph at ≤2.5% residue on 212 µm. The measured specific power consumption of the complete grinding circuit is

~13.85 kWh/t, outperforming the warranted value of 14.9 kWh/t. This assessment includes the power consumption of HPGR, separator drive, recirculation bucket elevator, separator fan, raw mill/kiln baghouse fan, and associated auxiliaries, thereby providing a comprehensive measure of overall circuit energy performance.

A comparative evaluation of the HPGR finish-grinding circuit and a reference VRM circuit processing the same raw material and producing material of comparable fineness demonstrates the significant energy-saving potential of HPGR technology. The HPGR circuit achieves a specific power consumption of ~13.85 kWh/t, compared with 19.80 kWh/t for the VRM circuit, resulting in a saving of ~6.0 kWh/t, equivalent to a 30% reduction in specific electrical energy consumption.

In addition to direct electrical energy savings, the HPGR configuration eliminates the need for process water to establish the grinding bed, a requirement associated with the reference VRM under the reported operating conditions. The VRM consumes ~8,000–10,000 liters of water per hour for this purpose. Eliminating this requirement reduces process water demand and creates favorable conditions for enhanced heat recovery from the preheater. Consequently, the potential increase in WHRS power generation is estimated at ~1.2 MW compared to the reference VRM installation, further improving the overall energy-efficiency profile of the HPGR-based grinding system.

The operating performance at Tadipatri demonstrates the capability of polycom® HPGR finish-

grinding technology to achieve lower specific power consumption, reduced process water demand, and increased WHRS power generation potential. The combined benefits of direct electrical energy savings and additional waste heat recovery strengthen the case for HPGR technology, particularly in cement plants processing hard-to-grind raw materials. By improving energy efficiency and resource utilization, the installation offers a promising approach for reducing the carbon footprint of cement manufacturing and supporting the industry's transition towards carbon neutrality.

1.0 *Introduction*

Raw material grinding is one of the most energy-intensive operations in cement manufacturing, contributing significantly to the overall electrical energy consumption and associated CO_2 emissions. With increasing emphasis on energy efficiency and the cement industry's transition towards carbon neutrality, optimizing raw material grinding has become a key priority for reducing operating costs and improving the overall sustainability of cement production.

Although Vertical Roller Mill (VRM) technology is well established for energy-efficient raw material grinding, High-Pressure Grinding Roll (HPGR) technology in finish-grinding mode offers significant potential for reducing specific power consumption, minimizing process heat requirements and enhancing Waste Heat Recovery System (WHRS) potential. The combination of HPGR with a Stato-dynamic separator enables efficient grinding and classification, contributing to high throughput and consistent product fineness.

2.0 Features of polycom® (HPGR)

- ***Proven and reliable technology:***

  With more than 265 installations worldwide in cement industry of which ~85 are in India, thyssenkrupp Polysius is a pioneer in developing HPGR technology to suit requirement of cement industry.

- ***High specific grinding pressure:***

  Higher grinding pressure up to ~5500 kN/m^2 is beneficial in raw material grinding as it improves the grinding efficiency and reduces the specific power consumption.

- ***Large shaft diameter:***

  Large shaft diameter takes care of bending and torsional stresses. The optimum distance between bearings minimizes bending moments.

- ***Three types of roll tyres by TKIL / tk Polysius***

  Depending on the characteristics of the raw materials and the specific grinding application (Raw / Clinker / Slag), TKIL and thyssenkrupp Polysius offer three types of roll tyre wear protection concepts, as described below:

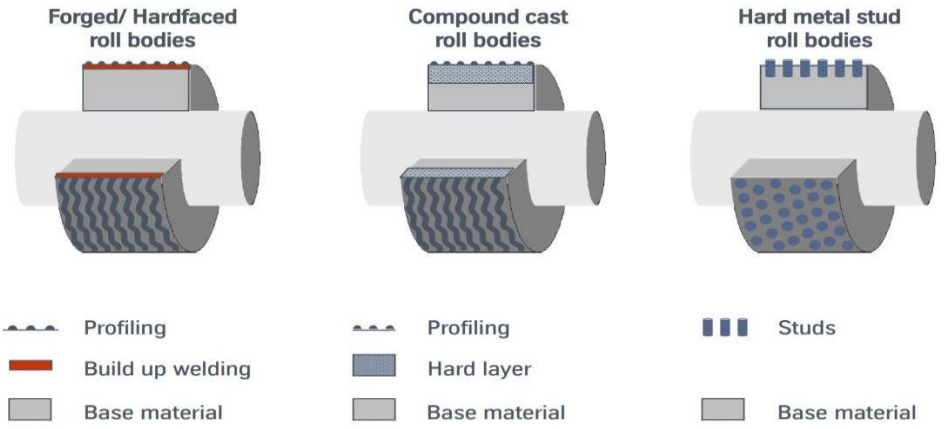


Figure 1: polycom® roll tyre wear protection concepts

3.0 Features of sepol® PC separator

- The sepol PC makes a convincing choice in a grinding circuit with a polycom HPGR.
- The sepol PC version is a combination of a compact static crossflow separator with a dynamic rotor separator.
- It is used effectively in finish-grinding and combi-grinding circuits.
- The fresh feed material and the compacted cakes from the polycom high-pressure grinding roll are deagglomerated and homogenized in the integrated feed system of the sepol PC.
- The compact design, particularly the static cross-flow separator, also reduces the construction volume of the grinding plant to a minimum.
- Drying by means of the connection of a separate hot gas generator is possible.
- The new separator is with curved guide vanes for better separation efficiency and swirl breakers for reducing pressure drop.

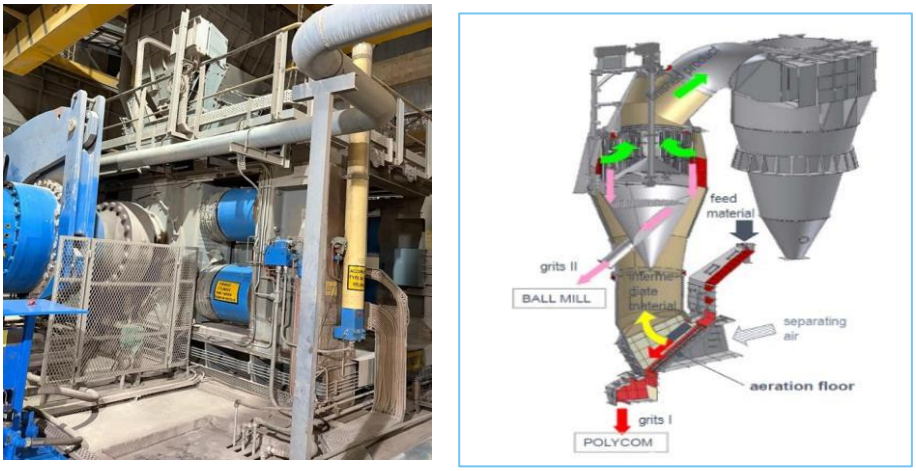


Figure 2: polycom® installation at UltraTech Cement Ltd., APCW-Tadipatri

4.0 *In house Machining & Assembly*

Quality plays an important role in manufacturing polycom roll shaft and body. TKIL Industries has their 'State of the Art', machine shop and excellent fabrication facilities at Pimpri, Pune aided by testing

equipment of international standards. The manufacturing facility follows highest standards of safety, productivity and quality.



Figure 3: polycom® assembly at TKIL Industries workshop, Pune

5.0 *Finish-grinding Circuit*

Raw material finish-grinding circuit consists of polycom (HPGR) and sepol PC (static and dynamic separator). Fresh feed and the recirculating cakes from polycom enter the static part of sepol PC via the feed chute (Figure 4). The feed material is then dispersed on an impact plate and slides downwards on the aerated floor made of wear resistant cast iron segments. Here the first separation takes place. The coarse material fraction is discharged directly into the polycom for further grinding.

The fines (with some amount of coarse fraction) are transported pneumatically to the subsequent dynamic part of the sepol PC. The dynamic stage of the sepol PC is of well-proven vertical cage rotor design. sepol PC is provided with the curved guide vanes, adjustable from outside the machine, impart the air swirl that is needed for the separation process. The cage rotor separates the finished material from the coarse fraction. The fines which are passing through the rotor are collected in cyclones or a bag house. The rotor grits are returned to polycom for further grinding.

The riser duct between the static and dynamic part of the separator is as short as possible to reduce building height. However, it can also be extended to facilitate drying of moist materials.

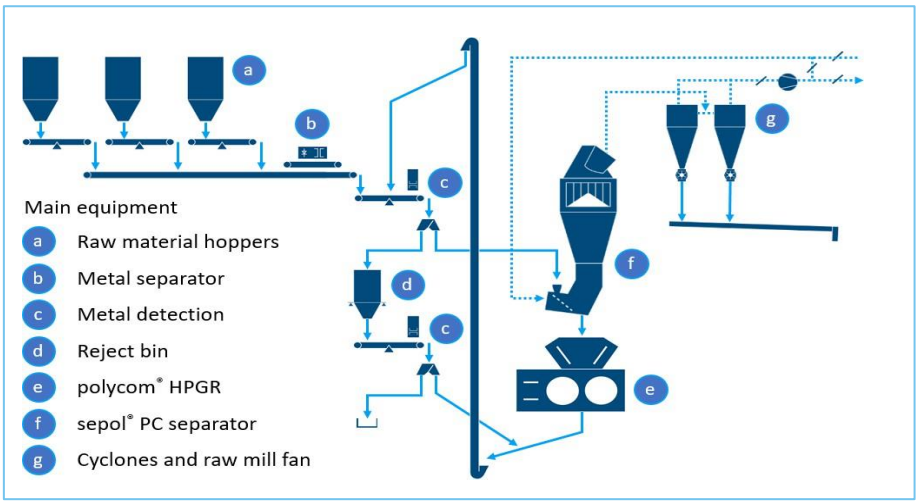


Figure 4: Conceptual flow sheet of the HPGR finish-grinding circuit with sepol® PC

6.0 *Operating Scenario at UltraTech Cement Limited, Tadipatri*

TKIL supplied 10,000 tpd Clinkerisation line to UltraTech Cement in Tadipatri, which was commissioned in June 2024.



Core Equipment	
polycom (HPGR) 21/16-9, 2 x 1800 kW **sepol PC** Statosep 36/27- LMR 380, Fan volume: 610,000 m3/hr	
Performance Warranted	**Achieved Performance**
2 x 362 tph at ≤ 2.5% R on 212 microns	2 x 383 tph at 2.6 % R on 212 microns
14.9 kWh/t Includes polycom, sepol drive, recirculation bucket elevator, separator fan, raw mill / kiln bag house fan and auxiliaries	~13.85 kWh/t Includes polycom, sepol drive, recirculation bucket elevator, separator fan, raw mill / kiln bag house fan andauxiliaries

Table 1. UltraTech Cement, Tadipatri - Warranted and achieved operating performance

This specific power consumption achieved is one of the lowest for raw material grinding circuits in this region.

7.0 *Finish grinding Circuit with sepol PC Compared with Vertical Roller Mill*

A comparative study between the two systems at UltraTech Cement-APCW Tadipatri where both "Finish grinding circuit with sepol PC" and "Vertical Roller Mill" are in operation, using the identical raw material source and having the similar product fineness, shows that there is not only a savings in the specific power consumption to the tune of ~6.0 kWh/t raw meal, but also provides additional benefits such as zero process water requirement, higher WHRS potential.

Parameter	HPGR in finish-grinding system	Vertical Roller Mill
Main Equipment	PC 21/16-9, 2 x 1800 kW	VRM with connected power 5300 kW
Product Fineness	2.6% R on 212 microns	2-3% R on 212 microns
Production capacity	2 x 383 tph	470-490 tph
Specific Power Consumption at meters	**~13.85 kWh/t** Includes polycom, sepol drive, recirculation bucket elevator, separator fan, raw mill / kiln bag house fan and auxiliaries	**~19.8 kWh/t** Includes VRM, mill fan, separator, recirculation BE, raw mill / kiln bag house fan and auxiliaries
Water Requirement	No	~8000-10000 lit/hr
Hot gas quantity and temperature required	466,000 Nm3/hr at 160 Deg.C	466,000 Nm3/hr at 185 Deg. C
WHR Potential from Pre-heater	WHRS potential will be higher by 1.2 MW	Reduced, since water is required for bed stability

8.0 *Conclusion*

"polycom / High Pressure Grinding Roll (HPGR)" technology is proven for raw material grinding application to provide higher benefits such as lower power consumption, better availability, zero process water, lower hot gas requirement and higher potential of a WHRS system for the pre-heater gases. With high efficiency separator sepol PC, the control on product fineness is much better and even the lower residues such as 1.5% R on 212 microns are no more a bottleneck for polycom in finish mode grinding. For dry, hard and abrasive materials, the savings achieved in polycom vis a vis VRM circuits are significantly higher.

In short, polycom is modern and user-friendly equipment for regulation, monitoring and control, combined with additional process gains, contributing to overall reduction of ~23,000 t in CO_2 emission per annum due to power saving and increased WHR potential which is a big step forward towards green cement

9.0 *Acknowledgements*

The authors would like to express their sincere gratitude to the UltraTech Cement project team, particularly Mr. Mahendra Kumar Mutyapwar and Mr. Sudhir Mohnot, for their valuable feedback, technical inputs, and guidance throughout the preparation of this paper.

The authors also extend their special thanks to the Tadipatri plant and site teams for their kind cooperation, support, and assistance in sharing the operational information and performance data essential to this case study.

10.0 *References*

1. Rahul Deshmukh and Prashant Garg (NCB-2019). "Operations and Maintenance of HPGR Rolls"
2. Stefan Diedenhofen, Vinod Wadile and Prakash Wagh (NCB-2024). "ROLLING OUT ELIABILITY SUCCESS OF POLYCOM (HIGH PRESSURE GRINDING ROLL) WITH STUDDED AND COMPOUND CAST ROLL TYRES"

SUSTAINABLE EXPLOSION PROTECTION CONCEPTS FOR EXPLOSIVE BULK SOLIDS BY MEANS OF EXPLOSION VENTING

Berthold Bussieweke Manoj Thakur***

** Thorwesten Vent GmbH, Beckum, Germany*

*** TECHCONS Consulting and Engineering Pvt. Ltd, Navi Mumbai, INDIA*

ABSTRACT

In the cement industry, coal has long served as a primary combustible fuel due to its high calorific value, powering approximately 90% of energy requirements. The grinding of coal in indirect firing systems generates finely ground particles essential for combustion, but also creates an explosive dust cloud under specific conditions: a critical concentration (approximately 60 g/m³), sufficient oxygen levels (approximately 12%), and an ignition source of adequate energy. As environmental regulations tighten globally, coal is increasingly being replaced by diverse alternative fuels. However, these alternative fuels also pose explosion risks during grinding and storage, mirroring the hazards associated with coal.

This paper explores sustainable explosion protection concepts for coal grinding plants and their adaptation to handle alternative fuels. It emphasizes the necessity of state-of-the-art explosion protection systems, focusing on self-reclosing explosion vents. These vents not only mitigate the ingress of oxygen and loss of inerting gases but also offer reusability and prevent direct contact between any internal fires and the external environment. Practical insights into the installation and advantages of these vents are discussed, highlighting their effectiveness in safeguarding against deflagrations and flame propagation within coal grinding and storage facilities.

Furthermore, the paper addresses compliance with essential safety directives such as the ATEX Directive 2014/34/EU and 1999/92/EC, crucial for ensuring workplace safety and equipment integrity in potentially explosive atmospheres. The application of DIN 14491 standards for designing explosion venting systems is also detailed, offering practical guidelines for calculating venting areas and optimizing vent placement.

By integrating self-reclosing explosion vents into coal grinding and storage systems, cement industry stakeholders can achieve enhanced safety and regulatory compliance while effectively managing the inherent explosion risks associated with both coal and alternative fuels.

1. Introduction

Various types of coals are forming the platform as major combustible fuel in the cement industry. As a result of the high calorific value, coal still provides around 90% of the energy. Corresponding burners require a specific fineness of the coal generated by coal grinding plants known as indirect firing systems. The specific fineness of the ground coal leads to the fact that an explosive atmosphere in the form of a dust cloud is produced. The simultaneous presence of such a dust cloud in the right concentration (approx. 60 g/m3), enough oxygen (approx. 12%) as well as an ignition source of sufficient energy an explosion will be triggered. Therefore such indirect firing systems in the form of a coal grinding plant need adequate state-of-the-art explosion protection. As a result of more stringent environmental rules and regulations in various countries, coal is substituted by various alternative fuels. The grinding process as well as the storage of alternative fuels should be taken very seriously as more than 50% of the alternative fuels are going to create explosive atmospheres as well.



Figure 1: Coal and Various Types of Alternative Fuels Used in the Cement Industry

Constructional explosion protection characterized by suitable self-re-closing explosion vents.



Figure 2: Bag Filter of an Indirect Coal Firing System Equipped with Rupture Panels Post Explosion

Above mentioned picture shows very significantly that the explosion has been vented accordingly but the presence of rupture panels and the corresponding ingress of oxygen tends to an uncontrolled fire respectively inefficient fire-fighting by the help of an emergency inerting system.

Therefore, the installation of self-reclosing explosion vents should be considered right from the beginning. The major advantages sounds as follows:

1) Avoidance of ingress of oxygen
2) Avoidance of loss of inerting gas
3) These vents are re-usable, no need to exchange them completely (e.g. rupture panels)
4) No direct contact between a possible fire in the system and the system's environment

Coal as basic burner fuel in cement industry

- to be ground in mills (vertical roller / horizontal ball mills)
- separated from air by dust collectors
- stored in pulverized fuel silos

b. Indirect firing system based on air-swept grinding plant



General risk of explosions / deflagrations!

A very significant issue for the proper explosion protection of coal grinding plants is the consideration of various design requirements.

1) ATEX Directive 2014/34/EU (Product / Equipment Directive)

2) ATEX Directive 1999/92/EC (User /Workplace Directive)

ATEX reflects the harmonization of the laws of the European Member States related to safety aspects with regard to the protection of the health of workers acting in potentially hazardous

areas as well as to equipment and protective systems intended for use in potentially explosive atmospheres.

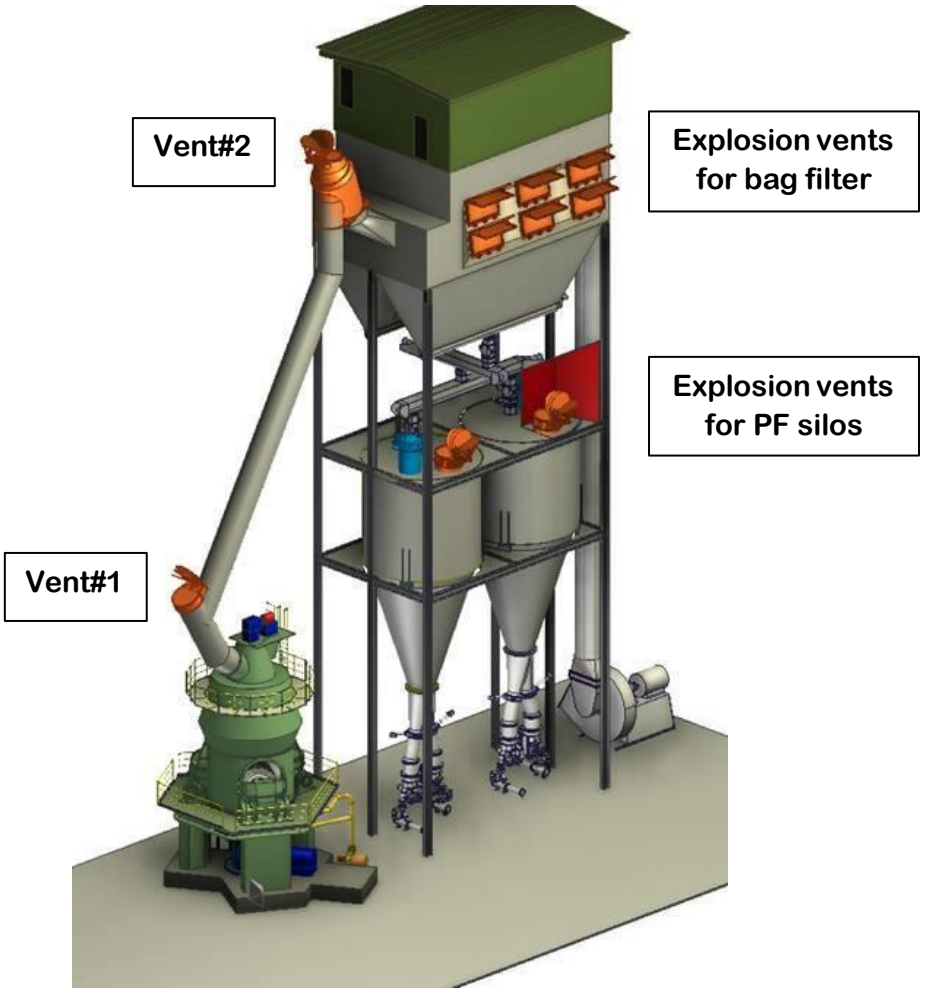
Manufacturers of ATEX relevant safety equipment have to undergo various verification and test procedures before the ATEX certificate is granted respectively the corresponding certificate of conformity is allowed to be issued by the manufacturer.

3) DIN 14491 Dust Explosion Venting Protective Systems

This rule states the design criteria for how the required venting area for a particular enclosure has to be calculated. In addition, various annexes provide fruitful information with regard to the positioning of explosion vents.

Intelligent protection of coal grinding plants by means of self re-closing explosion venting devices realizes the following aims:

- Effective mitigation of flame front propagation (Vent#1/Vent#2)
- Overall protection of bag house and pulverized fuel silo(s)


Vent#2
Explosion vents for bag filter
Explosion vents for PF silos
Vent#1

ADVANCEMENT IN CEMENT MANUFACTURING PROCESS AUTOMATION INCLUDING AI/ML AND INDUSTRY 4.0 APPLICATION

Author - Amit Kumar Kanojia Adani Cement

ABSTRACT

Cement manufacturing is moving from classical process automation toward a connected, data-driven and increasingly autonomous operating model. Distributed control systems, programmable logic controllers, online analyzers, robotic laboratories, and advanced process control have already improved stability, repeatability, and safety in modern cement plants. The next wave of performance improvement is being driven by artificial intelligence, machine learning, industrial Internet of Things, digital twins, computer vision, connected worker platforms and secure OT/IT integration. These technologies are relevant across the full cement value chain quarry planning and raw material management, crushing, blending, raw grinding, pyro processing, clinker cooling, cement grinding, quality control, packing, dispatch, and enterprise decision support.

The paper reviews current automation maturity, recent advances in model predictive control, AI/ML applications in process optimization and predictive maintenance, and Industry 4.0 enablers such as data lakes, cybersecure integration, industrial analytics, and digital twins. It also evaluates benefits in terms of productivity, fuel and power consumption, clinker and cement quality, equipment reliability, emissions reduction, and operational excellence. Evidence from industry publications and recent technical literature indicates that AI-enabled optimization can improve throughput and energy efficiency, Advance Process control (APC) can reduce specific energy and stabilize kiln and mill operations, and ML models can significantly improve real-time prediction of clinker phases compared with conventional steady-state calculations. However, sustainable impact requires more than software: high-integrity data, calibrated instrumentation, domain expertise, cybersecurity, organizational alignment, operator trust, and disciplined change management are decisive.

A practical roadmap is proposed for cement manufacturers: establish a robust automation and data foundation, prioritize high-value use cases, implement closed-loop optimization cautiously, institutionalize model governance, strengthen OT cybersecurity, build cross-functional digital capability, and scale through reference lines or reference plants. The paper concludes that AI/ML and Industry 4.0 should be treated not as isolated digital projects but as an integrated operating system for safer, more reliable, lower-carbon and more competitive cement manufacturing.

1.0 Introduction and industry context

The cement industry is at a critical point where productivity, quality, cost competitiveness and decarbonization must be improved simultaneously. Cement production remains difficult to decarbonize because it uses carbonate raw materials and high-temperature thermal processing. The International Energy Agency (IEA) identifies energy efficiency, material efficiency, and low-emissions fuels as important near-term measures, while deeper cuts require innovations such as alternative materials and carbon capture. In the IEA net-zero pathway, the clinker-to-cement ratio declines from 0.71 in 2022 to 0.65 by 2030 and 0.57 by 2050, while kiln thermal energy intensity declines from 3.6 GJ/t clinker in 2022 to 3.4 GJ/t by 2030 and 2.9 GJ/t by 2050 [1]. These milestones are not achievable through mechanical upgrades alone; they require consistent process control, online quality feedback, dynamic optimization, and data-driven decision support.

Process automation in cement has traditionally centered on programmable logic controllers (PLC), distributed control systems (DCS), supervisory control and data acquisition (SCADA), online analyzers, and operator control rooms. These systems remain the foundation of safe and reliable plant operation. However, the cement process is highly multivariable and nonlinear. Raw material chemistry, moisture, grindability, fuel calorific value, alternative fuel variability, burner flame behavior, preheater draft, cooler performance, kiln coating, circulating volatiles, mill ventilation and separator dynamics interact continuously. Conventional single-loop PID control and operator intuition can stabilize many variables, but they often cannot optimize across competing objectives such as throughput, specific heat consumption, alternative fuel substitution, clinker quality, emissions, and equipment protection.

The new automation frontier is therefore not simply more instruments or more dashboards. It is the integration of robust plant-floor automation with advanced process control, online analytics, AI/ML models, digital twins, connected maintenance systems and enterprise decision workflows. In this operating model, plant data are treated as a production asset. Algorithms support operators by predicting outcomes earlier, recommending setpoints, identifying anomalies, optimizing energy and quality, and improving maintenance planning. The most advanced systems can move from **advisory mode to supervised closed-loop operation**, while retaining engineering oversight and safety interlocks.

Core thesis

AI/ML and Industry 4.0 create value in cement manufacturing only when they are anchored in sound cement process knowledge, reliable instrumentation, stable automation, robust data governance, and disciplined change management. Digital tools amplify process capability; they do not replace cement chemistry, thermodynamics, mechanical reliability, or operator accountability.

Enterprise and cloud layer	**ERP, MES, CMMS, logistics platforms, sustainability dashboards, data lake, cloud analytics, portfolio benchmarking and management reporting.**
Digital twin and analytics layer	Physics-based and data-driven models for kiln, cooler, mills, emissions, energy, maintenance, quality and what-if simulations.
APC / MPC / AI control layer	Expert systems, model predictive control, reinforcement-learning-assisted setpoint optimization, inferential sensors and supervised closed-loop optimization.
Secure OT/IT gateway and edge layer	Industrial DMZ, edge computers, historians, protocol gateways, data buffering, contextualization, remote access control and cybersecurity monitoring.
DCS/PLC/SCADA and historian layer	Regulatory control, sequence control, interlocks, alarms, operator HMI, historian tags, event logs and production reporting.
Field instrumentation and analyzers	Temperature, pressure, flow, vibration, gas analyzers, kiln shell scanners, power meters, cameras, drones, XRF/XRD, PSD, Blaine, free lime and emission monitors.
Physical cement process	Quarry -> crusher -> raw mill -> blending -> preheater/precalciner -> kiln -> cooler -> clinker storage -> cement grinding -> packing -> dispatch.

Figure 1. Reference architecture for cement Industry 4.0

2.0 Cement manufacturing value chain and current automation state

A cement plant is a connected chain of unit operations. Improvements at one point can create constraints elsewhere; for example, a raw mill quality improvement can stabilize kiln operation, but only if blending, analyzer accuracy, and kiln feed transport delays are effectively managed. Therefore, digitalization should be mapped across the full value chain, not only around the kiln. Table 1 summarizes the current automation state and the next level of technology maturity by value-chain stage.

Table 1. Automation and Industry 4.0 opportunity map across the cement value chain

Value-chain stage	Typical current automation	Key pain points	Advanced / Industry 4.0 opportunity	Primary KPIs
Quarry and mines	GPS survey, mine planning tools, fleet tracking, crusher interlocks, and weighbridge integration.	Variable limestone quality, stockpile uncertainty, haul-route inefficiency, safety exposure.	Drones/LiDAR for volumetrics, online quality mapping, autonomous or assisted drilling, AI haul optimization, stockpile digital twin.	LSF variability, quarry cost/t, crusher utilization, inventory accuracy, safety.
Crushing and raw material handling	PLC/DCS interlocks, belt scales, stacker-reclaimer automation, material tracking.	Moisture and chemistry variation, feeder calibration drift, blending inefficiency.	Online analyzers, raw mix optimization, automated stockpile reconciliation, predictive belt and crusher maintenance.	Raw mix stability, feeder availability, power/t, dust and spillage.
Raw grinding and blending	DCS control, weigh feeders, mill DP control, separator speed control, silo blending, XRF lab feedback.	Grindability changes, mill vibration, unstable residue/Blaine, delayed lab results.	APC/MPC for mill optimization, soft sensors for fineness, AI energy optimizer, automated sampling and XRF/XRD feedback.	kWh/t raw meal, LSF/SM/AM variability, mill throughput, vibration.
Pyro processing: preheater, calciner, kiln and cooler	DCS/SCADA, PID loops, gas analyzers, kiln shell scanner, cooler grate control, interlocks, CEMS.	Nonlinear thermal dynamics, coating cycles, alternative fuel variability, NOx/SOx/CO control, kiln trips.	APC/MPC, AI kiln optimizer, digital twin, alternative fuel optimizer, predictive refractory and ring monitoring, combustion analytics.	kcal/kg clinker, t/h clinker, free lime, C3S, AF%, NOx/SOx/CO, kiln run factor.
Cement grinding	DCS control, separator controls, mill sound, vibration, PSD/Blaine lab feedback.	Overgrinding, variable clinker reactivity, additive moisture, separator inefficiency.	APC for VRM/ball mill/roller press, strength prediction, online PSD/Blaine, AI recipe optimization for blended cements.	kWh/t cement, Blaine/PSD, 1/3/7/28-day strength, throughput.
			Robotic labs,	

Automated quality control	XRF/XRD, sample prep, LIMS, manual/automatic samplers in mature plants.	Sampling bias, delay between process event and result, manual workload, traceability gaps.	pneumatic sampling, online XRF/XRD, AI-assisted XRD method selection, predictive quality analytics.	Cycle time, sample throughput, reproducibility, off-spec tonnage, clinker factor.
Packing, dispatch and logistics	Packing line automation, weighbridges, ERP dispatch, truck tracking in mature sites.	Truck queues, manual weighbridge errors, silo allocation mistakes, demurrage, customer visibility.	RFID/ANPR, unmanned weighbridge, connected ERP/OT dispatch, AI route planning, e-POD, dispatch command center.	Truck TAT, dispatch t/day, disputes, loading accuracy, on-time delivery.
Maintenance and reliability	CMMS, preventive maintenance, vibration rounds, shutdown plans.	Reactive work, poor failure prediction, expert knowledge loss, long MTTR.	Predictive maintenance, asset performance management, AR remote assist, mobile work instructions, automatic work order triggers.	MTBF, MTTR, availability, maintenance cost/t, shutdown adherence.

The key message from Table 1 is that the automation journey is uneven. Many plants have mature DCS and interlocking, but still rely on manual sampling, spreadsheet-based decision support, disconnected maintenance data, and human memory for abnormal situations. Industry 4.0 is a way to close these gaps by connecting plant-floor data with process models, reliability systems, quality systems, and business workflows. The Cement Manufacturers Association has similarly described digitalization opportunities in predictive maintenance, digital twins, predictive quality analytics, alternative fuel optimization, integrated control towers, and supply-chain digitalization in Indian cement operations.

3.0 Advances in process control: DCS, APC, MPC expert system, and autonomous operations

4.0 The first level of control in a cement plant is regulatory control: PID loops, cascade loops, ratio control, interlocks, alarms, and equipment sequences. These remain essential. The next level is supervisory optimization, where the controller coordinates multiple manipulated variables while respecting constraints. In cement, this level is commonly called advanced process control (APC).

APC may use rule-based expert systems, fuzzy logic, model predictive control (MPC), neural network models, inferential models, or a hybrid of these techniques.

MPC is particularly suitable for kiln and mill control because it can explicitly manage multivariable interactions, time delays, and operational constraints. A 2023 review in the Journal of Process Control notes that the cement kiln is a major energy-intensive process, that efficient controllers are required to minimize fuel consumption, enhance clinker production and improve cement quality, and that MPC is predominantly used to control burning zone temperature because it can accommodate practical constraints and provide optimal control actions

Table 2. Evolution of cement process control technologies

Control approach	Typical use in cement	Strengths	Limitations	Best-fit applications
PID / regulatory control	Loops for temperature, pressure, flow, draft, feeder rates, mill DP and level control.	Simple, robust, transparent, easy to maintain.	Single-loop focus; weak handling of nonlinear interactions and long delays.	Base layer for all automation.
Rule-based expert system	Operator-like rules for kiln, cooler, mill and blending.	Captures plant expertise; explainable; useful where models are difficult.	It can become complex; needs updating as plant behavior changes.	Kiln stability, start-up support, abnormal situation handling.
Fuzzy logic / hybrid APC	Soft rule systems for nonlinear behavior.	Manages qualitative rules and gradual transitions.	Tuning can be subjective; performance depends on rule quality.	Kiln burning zone, cooler and mill operation.
Model predictive control	Optimization over prediction horizon with constraints.	Manages multivariable constraints, delays, and trade-offs.	Needs model identification, tuning, maintenance, and operator trust.	Kiln, calciner, cooler, raw mill and cement mill optimization.
Inferential / soft sensor models	Predicts unavailable or delayed variables such as strength, free lime, fineness, or emissions risk.	Provides early quality and process signals before lab results.	Data drift and sensor bias can reduce reliability.	Quality prediction, emissions monitoring, energy optimization.
AI-enhanced adaptive APC	ML layer updates targets, predicts disturbances or adjusts APC setpoints.	Can adapt to changing fuel, raw mix and equipment conditions.	Requires strong data governance, validation, cybersecurity, and fallback logic.	Advanced kiln optimization, alternative fuel, quality-energy trade-off.
Autonomous operation	Closed-loop recommendations executed with limited human intervention under guardrails.	Highest consistency and response speed.	Must be carefully bound by safety, process and cybersecurity constraints.	Selected mature use cases after successful advisory and supervised pilots.

4.1 From control room automation to intelligent plant operation

The shift from classical automation to intelligent operation changes the role of the control room. Operators move from manually balancing dozens of loops to supervising a hierarchy of control and optimization layers. The operator still owns safety, production priorities, and abnormal situation response, but the system provides earlier warnings, more consistent setpoint recommendations and continuous KPI visibility. This makes human-machine interface design important: alarm rationalization, contextual displays, simplified graphics, role-based dashboards,

and clear explanation of AI recommendations are necessary for trust.

4.2 Advisory supervised and closed loop development.

- Advisory mode: the model predicts outcomes and recommends setpoints. Operators decide whether to implement. This is the safest starting point for most AI/ML deployments.
- Supervised closed-loop mode: the system writes setpoints within pre-approved limits while operators monitor performance and can intervene. This is appropriate after stable advisory performance is proven.
- Autonomous mode: the optimizer operates continuously with limited manual intervention under engineered constraints, fail-safe logic, cybersecurity controls, and model-performance monitoring. This should be limited to mature use cases and reviewed regularly.

4.0 AI/ML application across Cement Manufacturing

Artificial intelligence is broad term. In cement plants, the most useful applications are usually machine learning, anomaly detection, time-series forecasting, optimization, computer vision, natural-language interfaces for knowledge search, and hybrid physics-plus-data models. These systems learn patterns from historical and real-time data, but they must be constrained by process knowledge. A model that is statistically accurate but violates kiln chemistry, equipment limits or environmental constraints is not acceptable for plant operation.

Table 3. AI/ML use-case matrix for cement manufacturing

Use case	Data foundation	Model / method	Decision output	KPI impact	Maturity
Predictive maintenance	Vibration, temperature, oil, current, pressure, maintenance history, failure codes.	Anomaly detection, remaining useful life models, classification.	Failure risk, maintenance priority, spare planning.	Run factor, MTBF, MTTR, maintenance cost/t.	Proven
Kiln stability and fuel optimization	Kiln feed chemistry, fuel CV, feed rate, draft, O2/CO/NOx, BZT proxy, shell scan, cooler data.	MPC, neural networks, hybrid optimizer.	Fuel/air/feed/calciner targets and constraint alerts.	kcal/kg clinker, t/h clinker, free lime, emissions.	Proven to advanced
Alternative fuel management	AF composition, moisture, chlorine/sulfur, feed rates, combustion indicators.	Predictive models, constraint optimization.	AF substitution targets, blending and dosing strategy.	Thermal substitution rate, stability, emissions, cost.	Advanced
Raw mix and blending optimization	XRF data, quarry chemistry, feeder rates, silo levels, raw meal modules.	Optimization, MPC, soft sensors.	Feeder setpoints and module targets.	LSF/SM/AM variability, burnability, kiln stability.	Proven

Clinker phase prediction	XRD/XRF, kiln feed, hot meal, process parameters, residence-time aligned data.	NN, GPR, SVR, XGBoost and explainable ML.	Predicted alite/belite/ferrite and uncertainty.	Quality consistency, waste reduction, proactive correction.	Emerging with strong evidence
Cement strength prediction	Mill data, clinker quality, gypsum/additives, PSD/Blaine, curing/lab data.	Regression, gradient boosting, neural networks.	Predicted 1/3/7/28-day strength and recipe targets.	Spec compliance, additive cost, clinker factor.	Advanced
Grinding optimization	Mill load, power, separator speed, fan power, DP, vibration, PSD/Blaine.	MPC/APC and ML soft sensors.	Feed, pressure, separator and airflow targets.	kWh/t, throughput, fineness, vibration.	Proven
Emissions monitoring and control	CEMS, kiln/calciner gas, fuel, raw mix sulfur/chlorine, hydrate/lime dosing.	Forecasting, anomaly detection, APC.	Violation risk, reagent dosing, combustion correction.	NOx/SOx/CO compliance, reagent cost.	Advanced
Computer vision for safety and process	CCTV, thermal cameras, PPE images, flame/clinker images, belt cameras.	CNNs, object detection, segmentation.	Unsafe behavior alerts, flame/coating/clinker observations.	Safety, process visibility, response time.	Emerging to proven
Decision support and knowledge search	SOPs, manuals, shift logs, alarms, historian trends, maintenance records.	Generative AI with retrieval, summarization, root-cause assistants.	Guided troubleshooting, shift summary, technical search.	Faster decisions, knowledge retention.	Emerging

4.1 *Predictive maintenance and asset performance*

Predictive maintenance is often the first high-return AI/ML use case because cement plants contain large rotating assets whose failure causes immediate production loss: kiln drives, ID fans, preheater fans, baghouse fans, VRMs, roller presses, ball mills, bucket elevators, compressors, crushers, conveyors and packing machines. A predictive system does not simply replace preventive maintenance; it prioritizes maintenance based on condition, consequence, and production plan. The most valuable systems integrate sensor analytics with CMMS workflows so that alerts are converted into validated inspections, work orders, spare reservations, and shutdown actions.

4.2 *Process Optimization and kiln Stability*

Kiln optimization remains the highest-value process control application. Small improvements in specific heat consumption, alternative fuel substitution, feed rate, kiln stability, and clinker quality compound over large production volumes. AI/ML models can detect relationships that are difficult for operators to see, such as how raw meal chemistry, fuel variability, cooler efficiency,

and preheater drafts jointly affect free time, NOx and coating behavior. However, kiln optimization must be governed by explicit constraints: free lime and liter weight targets, coating health, refractory protection, emissions limits, kiln torque, cooler grate loading, ID fan margin and bypass limitations.

4.3 *Quality Prediction and automated laboratories*

Quality control is moving from delayed laboratory confirmation to near-real-time prediction and automated feedback. Robotic laboratories can standardize sample preparation, reduce manual handling, and improve traceability. Fuller Technologies states that QCX/RoboLab can automate sample preparation and analysis, coordinate samples from auto-sampling systems, support XRF/XRD and other tests, and provide a modular route from task automation to fully automated laboratories [10].

4.4 Computer vision and connected Woker application

Computer vision can support both safety and process monitoring. Examples include PPE detection, proximity monitoring, conveyor belt condition, truck loading verification, flame observation, clinker nodulization monitoring and raw material particle-size analysis. Connected workers and augmented reality solutions provide another Industry 4.0 layer. Some big companies connect case describes AR-based remote service in cement, including remote troubleshooting, support for commissioning, preventive maintenance guidance, alternative fuel and combustion optimization support, spare identification and knowledge capture through documented cases [1

5.0 Industry 4.0 technology stack and digital architecture

Industry 4.0 in cement manufacturing is an architecture, not a specific product. It links physical equipment, sensing, control systems, data infrastructure, analytics, people and business processes. It describes Industry 4.0 as integrating smart machinery, IoT, AI, ML and cloud computing, and emphasizes that real-time insights from analytical instruments can be fed back into process streams to improve efficiency and prevent downtime [14]. The practical architecture must support five requirements: high-quality data capture, secure connectivity, contextualization, model deployment and operational adoption.

Table 4. Industry 4.0 architecture layers for cement manufacturing.

Layer	Key components	Design priorities	Typical cement examples	Risks if weak
Field and instrumentation	Sensors, analyzers, cameras, scales, drives, lab instruments.	Calibration, sampling representativeness, reliability, maintenance.	XRF/XRD, gas analyzers, shell scanners, vibration sensors, belt scales.	Bad data, wrong model outputs, operator distrust.
Control and historian	PLC, DCS, SCADA, HMI, alarm system, historian, LIMS.	Stable tags, time synchronization, loop performance, alarm quality.	Kiln, mill, cooler, packing control rooms and quality lab.	Data silos, poor context, weak troubleshooting.
Edge and OT/IT integration	Edge servers, OPC UA, MQTT, gateways, industrial DMZ.	Latency, buffering, protocol security, data normalization.	Connecting DCS and lab data to analytics without exposing control network.	Cybersecurity and reliability exposure.

Data platform	Industrial data lake, asset hierarchy, event model, metadata, quality flags.	Single source of truth, lineage, access control, retention.	Plant-wide data model linking equipment, batch, sample, shift and KPI.	Unusable historical data and high model rework.
Analytics and AI/ML	Soft sensors, predictive models, anomaly detection, optimization engines.	Validation, explainability, drift monitoring, fallback logic.	Free lime prediction, fan failure warning, mill energy optimizer.	False alerts, unsafe recommendations, model decay.
Application workflow	CMMS, MES, ERP, mobile apps, dashboards, operator advisory.	Actionability, owner assignment, workflow integration.	Automatic work order, shift handover, dispatch dashboard.	Insights do not become operational value.
Governance and cybersecurity	Policies, roles, risk assessment, access, audit, backups, incident response.	IEC 62443/NIST alignment, segmentation, least privilege, recovery.	OT zones, DMZ, vendor remote access, patch and backup strategy.	Plant downtime, data loss, safety and compliance risk.

5.1 Computer vision and connected Woker application

Data governance is the difference between a pilot and a scalable digital capability. Cement plants often have multiple historians, DCS tag naming conventions, lab systems, maintenance databases and spreadsheets. AI models require consistent asset hierarchy, units of measure, timestamps, material flow alignment, sensor calibration records, shutdown flags and quality labels. Model governance should define who owns each model, what data it uses, how performance is measured, how drift is detected, when retraining is allowed, how changes are approved and what fallback logic applies.

5.2 Cybersecurity and resilience

Greater connectivity increases the importance of OT cybersecurity. NIST SP 800-82 provides guidance for securing industrial control systems including SCADA, DCS and PLC configurations while addressing unique performance, reliability and safety requirements [15]. ISA/IEC 62443 defines requirements and processes for implementing and maintaining secure industrial automation and control systems, with a holistic approach bridging operations and information technology as well as process safety and cybersecurity. NIST CSF 2.0 provides a broader framework for managing cybersecurity risks through governance, identification, protection, detection, response and recovery outcomes

6.0 Benefits and impact assessment

The impact of automation and AI/ML must be assessed against measurable operational KPIs. The most credible business cases connect technology to specific constraints: kiln heat consumption, mill kWh/t, run factor, refractory life, clinker free lime variability, cement strength margin, packing throughput, truck turnaround time, or maintenance backlog. Table 5 summarizes benefits and the type of evidence available from the reviewed sources.

Table 5. Benefit mechanisms and evidence assessment.

Impact area	Mechanism	Evidence / indication from sources	Typical KPIs	Confidence
Energy efficiency	APC/AI stabilizes kiln and mill operation, reduces overcorrection and improves constraint operation.	IEA identifies thermal intensity reduction as a net-zero pathway milestone; McKinsey reported up to 10% throughput and energy-efficiency improvement in one AI autonomous-mode cement kiln/mill case [1,3].	kcal/kg clinker, kWh/t cement, fan power, mill power.	High for APC; case-dependent for AI.
Throughput and productivity	Optimized feed, mill loading, separator settings, cooler control and dispatch flow.	ABB describes APC applications in kiln, mill, blending and AF management; Mastek reports 24x7 automated dispatch and one truck processed every 3 minutes in Yanbu Cement case [6,20].	t/h clinker, t/h mill, dispatch t/day, truck TAT.	Medium to high.
Clinker and cement quality	Predictive quality models and automated labs reduce delays and variability.	Fayaz et al. reported ML clinker phase prediction outperforming Bogue equations on industrial data [5].	Free lime, C3S/C2S/C4AF, LSF/SM/AM, Blaine/PSD, 28-day strength.	High for prediction; implementation-dependent for closed-loop.
Reliability	Predictive maintenance detects degradation earlier and links to CMMS.	CMA identifies predictive maintenance as useful for gearboxes, mills and kiln installations [13].	Run factor, MTBF, MTTR, maintenance cost/t.	High when data are reliable.
Emissions and sustainability	Fuel efficiency, AF optimization, reagent control and clinker-factor reduction.	ABB/Carbon Re state Expert Optimizer typically reduces specific energy 1-5% and can increase alternative fuel	CO2/t cement, NOx, SOx, AF substitution, clinker factor.	Medium to high; must verify locally.

		usage up to 50%, while the AI layer could further reduce specific energy up to 5% [7].		
Safety and skills	Computer vision, AR remote support, digital workflows and reduced manual sampling.	thyssenkrupp describes AR remote service, structured knowledge capture and reduced downtime potential in cement service [18].	Incidents, exposure hours, first-time fix, training time.	Medium.
Operational excellence	Standardized dashboards, benchmarking and decision support across plants.	CMA describes integrated control towers and digital value-chain visibility for Indian cement operations [13].	OEE, shift variance, KPI adherence, action closure.	Medium; depends on management system.

A disciplined benefit model should separate hard savings from enabling benefits. Hard savings include reduced fuel, power, maintenance cost, refractory cost, demurrage and off-spec material. Enabling benefits include improved operator decision quality, faster troubleshooting, higher auditability, stronger data availability and better customer service. Both matter, but only hard savings should be used for conservative payback calculations unless enabling benefits are quantified through agreed KPIs.

7.0 Implementation challenges and risk control

The cement industry has many examples of successful automation, but also many digital pilots that do not scale. The reasons are usually not algorithmic alone. They include weak data quality, lack of process context, unclear ownership, poor integration with workflows, cybersecurity concerns, insufficient operator involvement and unrealistic ROI expectations. Fuller Technologies notes that Industry 4.0 adoption depends on a solid automation foundation, usable high-resolution data with metadata, cybersecurity readiness, organizational KPI alignment and business models that support continuous software improvement [9].

Table 6. Implementation challenges and risk controls.

Challenge	Why it matters in cement	Risk control	Owner
Data quality and time alignment	Material residence times and lab delays can create false correlations.	Data audit, historian cleanup, residence-time mapping, shutdown flagging, calibration records.	Process + quality + automation.
Sensor reliability	Dust, heat, vibration and poor calibration degrade model accuracy.	Critical-instrument health monitoring, preventive calibration, redundancy for key variables.	Instrumentation + process.

Model drift	Raw materials, fuels, equipment condition and product mix change over time.	Drift dashboards, periodic validation, retraining policy, uncertainty bands.	Data science + process owner.
Operator trust	If recommendations are unexplained or unstable, operators bypass the system.	Advisory pilots, explainable KPIs, operator training, feedback loops, HMI clarity.	Operations.
Cybersecurity	Cloud, remote access and OT/IT integration increase attack surface.	IEC 62443 zones/conduits, DMZ, least privilege, monitored remote access, tested backups.	OT security + IT + automation.
KPI conflicts	Different departments may optimize different objectives.	Plant-level optimization hierarchy and governance board.	Plant management.
Vendor lock-in and integration	Closed systems limit scale and future innovation.	Open standards, data ownership clauses, API requirements, architecture review.	Management + procurement + automation.
Skill gaps	Digital systems need process-data translators and model-aware engineers.	Training, cross-functional squads, digital champions, documentation and knowledge base.	HR + plant leadership.
Pilot trap	Successful demo may fail at scale without lifecycle support.	Reference line, scale criteria, support model, ROI tracking and change management.	Digital steering committee.

8.0 Emerging trends and outlook

The next decade of cement automation will be shaped by five trends.

First, AI will move from isolated advisory tools to adaptive APC layers that continuously update targets within safe constraints.

Second, digital twins will expand from equipment monitoring to process-wide simulation, integrating raw mix chemistry, fuel variability, kiln thermodynamics, cooler performance, quality prediction and emissions.

Third, generative AI will become a knowledge interface for operators, maintenance teams and engineers, helping search SOPs, summarize shifts, analyze alarms and support troubleshooting.

Fourth, robotic and automated quality systems will become more important as blended cements, alternative fuels and supplementary cementitious materials increase quality-control complexity.

Fifth, cybersecurity and resilience will become non-negotiable because connected plants cannot risk uncontrolled remote access, ransomware or compromised setpoints.

9.0 Conclusions

Advances in cement manufacturing automation are entering a new phase. Classical DCS/PLC/SCADA systems remain essential, but competitive advantage now comes from integrating them with APC, MPC, AI/ML, automated laboratories, digital twins, IIoT, connected worker tools and secure enterprise workflows. The strongest applications are those tied directly to cement plant KPIs: kiln stability, heat consumption, mill power, clinker quality, cement strength, alternative fuel use, emissions compliance, equipment availability and dispatch efficiency.

The evidence reviewed in this paper supports four conclusions. First, APC and MPC are mature and highly relevant for cement kilns, coolers and grinding systems. Second, AI/ML can add value where nonlinear relationships, delayed measurements and multivariable trade-offs limit conventional control. Third, quality-control automation and ML-based prediction can materially improve the speed and consistency of clinker and cement quality decisions. Fourth, implementation success depends on data quality, domain expertise, cybersecurity, operator adoption and governance at least as much as model selection.

Acknowledgement

I would like to express his sincere gratitude to Dr. Abhishek Rai, Country Quality Head, for his visionary leadership, technical guidance, and continuous encouragement toward innovation, digital transformation, and excellence in cement quality management. His strategic insights and commitment to leveraging advanced technologies in cement manufacturing have been a constant source of inspiration in developing the concepts presented in this paper.

I also extend heartfelt thanks to the Plant Head and leadership team for fostering a culture of operational excellence, continuous improvement, and technology adoption. Their unwavering support in pursuing process optimization, automation, and sustainable manufacturing practices.

Special appreciation is extended to my colleagues and team members across Quality, Process, Operations, Maintenance, Automation, and Manufacturing Excellence functions, particularly those who have continuously shared their practical experiences, technical knowledge, and valuable perspectives on process control, data analytics, quality assurance, and operational optimization.

Finally, I acknowledge the contributions of researchers, industry experts, technology providers, and professional institutions whose published work on Advanced Process Control (APC), Artificial Intelligence (AI), Machine Learning (ML), Industry 4.0, and digital transformation in cement manufacturing has served as an important reference for this paper. This work reflects the author's professional experience and understanding of the subject and is based on publicly available information and industry knowledge. No confidential or proprietary information has been disclosed.

References

1. International Energy Agency (IEA). Cement - Analysis, Net Zero Emissions Guide, 2023 update. Published 26 September 2023. https://www.iea.org/reports/cement-3
2. National Council for Cement and Building Materials (NCB). Conference & Exhibition on Carbon Neutrality in Cement and Concrete - Technical Paper themes, 2026. https://conference.ncbindia.com/
3. Feldmann, R. Artificial intelligence helps cut emissions and costs in cement plants. McKinsey & Company, December 2019.
4. Ramasamy, V.; Kannan, R.; Muralidharan, G.; Sidharthan, R.K.; Veerasamy, G.; Venkatesh, S.; Amirtharajan,



5. R. A comprehensive review on Advanced Process Control of cement kiln process with the focus on MPC tuning strategies. Journal of Process Control, 121, 85-102, 2023. DOI: 10.1016/j.jprocont.2022.12.002.

6. Fayaz, S.J.; Montiel-Bohorquez, N.; Bishnoi, S.; Romano, M.; Gatti, M.; Krishnan, N.M.A. Industrial-scale prediction of cement clinker phases using machine learning. Communications Engineering, 4, Article 94, 2025.

7. ABB. Building an intelligent cement plant - Advanced Process Control (APC) for cement process optimization. ABB cement systems and solutions.

8. Dam, A.N. A Risky Road? Only if You are Not Prepared. Fuller Technologies / World Cement reprint Fuller Technologies. QCX/RoboLab Systems - cement laboratory automation.

9. Cement Manufacturers Association (CMA), India. Digitalisation in Cement Industry. 12 November 2021. NIST. Guide to Industrial Control Systems (ICS) Security. Special Publication 800-82 Rev. 2, 2015.

10. International Society of Automation (ISA). ISA/IEC 62443 Series of Standards - industrial automation and control systems cybersecurity.

11. NIST. The NIST Cybersecurity Framework (CSF) 2.0. NIST CSWP 29, 26 February 2024. PTC. Augmented Reality in Maintenance - Vuforia solutions for service and maintenance.

PROCESS AUDIT–DRIVEN OPTIMIZATION OF VERTICAL ROLLER MILLS IN CEMENT MANUFACTURING: EVIDENCE FROM FOUR RAW AND SLAG GRINDING CASE STUDIES

Anil Kumar Popuri, Saurabh Bhatnagar and K P K Reddy

National Council for Cement and Building Materials

ABSTRACT

Vertical Roller Mills (VRMs) combine grinding, drying, transportation and classification and are widely used for grinding multiple raw materials in a cement plant. Their performance depends on coupled mechanical, air flow, material and control variables, so an audit is necessary to evaluate energy, throughput, product quality and operational stability together. This paper presents four plant case studies: two implemented audits (*one raw mill and one slag mill*) and operating trials on two raw mills of different design. The audit method combined CCR review, field measurement of gas flow, temperature, pressure and oxygen profile, mill internal inspection and operating trials. The audits identified feed-size and feed-control problems, false-air ingress, nozzle-ring velocity and classifier size constraints, dam-ring height, grinding-pressure control and water-spray system. Reported specific-power reductions were 1.3 kWh/t (*9.3%*) and 4.1 kWh/t (*10.1%*) for Cases 1 and 2, with throughput gains of 15 and 16 tph; trials in Cases 3 and 4 increased output by 25 and 30 tph, respectively, with mill-cum-fan specific-power reductions of 1.06 and 0.23 kWh/t respectively. These values are case-specific as the energy limits differ between the implemented audits and the trials, and reporting matched product-quality data, repeated trials or long-term verification is out of purview of this paper. The results therefore show measurement-based troubleshooting as a promising low-capital intervention, but not a benchmarking savings estimate.

Key Words: Vertical Roller Mill, Process Optimization, Specific Power Consumption, Nozzle Ring Velocity, False Air, Cement Grinding & Energy Efficiency.

1.0 Introduction

Cement manufacture is energy intensive, and grinding performance affects electrical cost, plant throughput and product quality. Vertical Roller Mills (VRMs) are widely used for grinding raw meal, slag and cement because a single circuit can integrate grinding, drying, transportation and classification. Their performance still is sensitive to feed physical and chemical properties, grinding pressure, bed height, airflow and separator operation and efficiency; literature emphasizes that practical improvement requires stabilizing the entire grinding process rather than changing a single setpoint in isolation [1].

A VRM grinds material in a bed between a rotating table and hydraulically loaded rollers. Gas flow transports material to a classifier, which returns coarse particles and allows the product fraction to leave the circuit. This means that mill power, fan power, internal circulation, drying and product fineness must be interpreted together; an energy reduction is not an improvement if it is obtained by relaxing product-quality or throughput requirements [2, 3 and 4].

Performance evaluation is therefore central to control and improvement. This paper reports four industrial case studies drawn from process-optimization audits on raw-meal and slag grinding mills. Its useful contribution is the integration of field measurements, internal inspection and operating trials across several plants. To make the evidence more technically interpretable, the following literature review places the cases alongside experimental, CFD and control studies; later sections distinguish measured outcomes from proposed mechanisms and identify boundaries on causal results and comparative case analysis.

2.0 Literature Review

Research on VRM optimization has developed along three connected lines: (i) experimental characterization of grinding and classification variables, (ii) fluid/particle-flow and design optimization, and (iii) plant-data modelling and control. Earlier review work identifies pressure, feed, bed, gas flow, separator and maintenance as interacting performance levers, but does not make one operating range transferable to mills with different geometry, materials and product targets [1]. This distinction matters for the present audit: field ranges are useful diagnostic references, not universal reference values.

The trade-offs are better understood through experimental studies. Liu et al. used laboratory VRM experiments and response-surface methodology to relate loading pressure, table speed and moisture to energy consumption and grinding efficiency [3]., Ghalandari et al. reported that increasing classifier speed from 53 to 65 rpm reduced P90 residue from 18.2% to 10.8% while specific energy increased from 19.7 to 22.3 kWh/t in an industrial raw-mill case [4]. The findings from these two studies suggest a constrained, multi-objective strategy where the focus is on minimizing circuit specific energy while maintaining required fineness, throughput, moisture and stability, instead of optimizing energy consumption.

Ali et al. applied CFD to detect bottom air ingress in a new VRM, linked it to powder recirculation, and then verified design changes on a pilot scale [5]. Huang et al. utilized CFD–discrete-particle modelling with a Kriging surrogate and NSGA-II optimization; their reported model case showed an increase in yield by 5.34% and a specific surface area by 9.07%, with a maximum reported relative error of 2.02% [6]. According to a separate CFD/DPM nozzle-ring analysis, adding splitters led to lower peak gas velocity and turbulence, but it emphasized the need for validation on an industrial scale [7]. In a 2026 conference study, researchers similarly examined ways to reduce pressure drop by modifying the hot-gas-duct, classifier, and nozzle-ring-cover [8]. These results emphasize the importance of measuring false air across the system, velocity, and pressure drop; however, simulated or pilot results cannot be claimed as proven savings for the plant.

Explanatory models and closed-loop control are becoming the focus of plant-data research. Fatahi et al. applied SHAP with XGBoost to an industrial cement VRM dataset, identifying working pressure and input-gas rate as key factors influencing power and outlet temperature; the abstract reports a test-set R^2 above 0.80, which suggests a predictive association, not a guarantee that modifying either variable will reduce energy [9]. Zhu et al. described a data-driven decision framework for cement plants that provides operating recommendations based on stable-state patterns and noted a reduction in vibration during continuous operation [10]. Vijayabhaskar and Jayalalitha compared a dual adaptive model-predictive controller with PI/MPC by using plant data for identification and reported simulation tracking tests, yet their control result does not equate to a long-duration plant energy trial [11].

Yao et al. employed DEM, response-surface modelling, and multi-objective search to study the design variables and wear of rollers/tables [12]; Woywadt et al. reported AI-derived setpoints in two modular pozzolan/GGBFS applications with savings of 7–12% in mill-and-fan specific power [13]; and Wan et al. reported the results of XGBoost prediction plus Q-learning control on a single large VRM, which was deployed for two weeks [14]. While studies point to a trend from single parameter tuning to data-driven optimization, evidence's reliability varies significantly. Laboratory experiments, simulations, case reports from conferences and individual plant applications cannot be generalized to predict a uniform level of savings. Therefore, this paper's contribution is its process-audit framework, which would be further strengthened by including matched product-quality measurements, definitive energy boundaries, similar experiments and post-implementation data.

3.0 VRM Operating Fundamentals

VRM reviews and experimental studies highlight that the main variables are coupled, and their impacts are influenced by the material and the mill design [1] – [4]. Table 1 contains audit-reported comparison

values, which differ from universal OEM limits.

- **Grinding pressure.** The process needs to be adjusted for the feed and target fineness for optimal results. While excess pressure can increase vibration or affect bed stability, the pressure values on the hydraulic bar are not directly comparable to specific grinding pressure (kN/m²) unless cylinder area, lever geometry, and force distribution are considered.
- **Grinding bed, dam and support ring.** The bed height must correspond to the grinding pressure. It is primarily regulated by adjusting the dam-ring and support ring height, based on material, feed moisture, and product fineness.
- **Gas flow and nozzle-ring velocity.** Airflow, nozzle geometry and classifier settings together affect entrainment, pressure drop, transport and coarse-particle return. Each mill has a unique response; neither a higher nor lower velocity is universally optimal. CFD analyses point out that leakage and duct/nozzle geometry are material factors [5] – [8].
- **Recirculation and classification.** The recirculating load and the output a mill can provide for a power, is determined by the number of recirculation cycles of coarse material through the separator.

There is an interaction among the above variables. Changes to pressure, dam-ring height, spray or fan speed can influence bed stability, motor load, fan load, rejects and product fineness simultaneously. While fan affinity laws suggest a cubic power-speed relation for similar fan/system conditions, a VRM circuit's varying density, leakage, pressure drop and operating point necessitate measuring fan power instead of inferring it from speed alone. The optimization target should be lowest measured circuit SEC that satisfies product quality, throughput and stability [3], [4], [8].

Table 1

Audit-reported operating bands (*mill-specific; not universal*)

Parameter	Raw mill	Cement / slag mill
Grinding pressure (*kN/m²*)	600–800	1600–2000
Nozzle-ring velocity (*m/s*)	50–55 (35–45) *	40–45
False air (*%*)	< 15	< 15
Separator rotor loading (*tph/m²*)	10–12	10–12
Separator outlet dust loading (*g/m³*)	< 650	< 650

** These are reported audit values, not benchmark. Manuscript gives different raw-mill velocity ranges (50–55 and 35–45 m/s); confirm the applicable OEM design, gas reference state, leakage and material conditions before changing nozzle area.*

4.0 Audit Methodology

In each scenario, the same step-by-step method was utilized (see Figure 1). Initially, a multi-disciplinary team of process engineers reviewed the operating history with plant personnel and compiled central-control-room data such as production figures, specific power consumption, setpoints, actual measurements, and, if available, monthly averages. The audit included all stages from material receipt and storage to crushing, reclaiming, and extending downstream of the mill.

Measurements were conducted using portable instruments: pitot tubes, digital temperature and manometer systems, gas analysers and an anemometer. From these data, false-air ingress was determined from the circuit's oxygen increase; nozzle-ring velocity from gas flow, referenced to the nozzle plane and effective ring area; separator rotor loading as tonnes/hr./m^2 of rotor reference area; separator outlet dust loading (*g/m^3 of gas*); and circulation-fan efficiency. The original method uses fan-

inlet gas flow to estimate nozzle velocity, but this input must be corrected for leakage and gas-state changes before being treated as nozzle-plane flow. The mill was then opened and inspected, including rollers, bowl and table, grit cone, feed chute, nozzle ring, dam ring, spray nozzles and the separator. Finally, controlled trials were carried out from the CCR, with one or more setpoints varied while monitoring throughput, power, and stability.

4.1 Performance indices

The derived indices utilize the standard relations listed below, where the measured quantities are specified below:

Nozzle-ring Velocity: $v = Q / (3600 \cdot A)$ [m/s] (1)

False Air: $FA = (O_{2,out} - O_{2,in}) / (21 - O_{2,out}) \times 100$ [%] (2)

Rotor loading: $L = m / (\pi \cdot D \cdot H)$ [tph/m²] (3)

Dust loading: $C = 10^6 \cdot m / Q$ [g/m³] (4)

Fan efficiency: $\eta = Qs \cdot \Delta p / P$ (5)

For dimensional consistency, Q in Equation (1) represents the actual volumetric gas flow at the nozzle-ring reference plane, with fan-inlet flow only serving as a proxy if adjustments for leakage, temperature and pressure are made. False-air relation in Equation (2) assumes that inlet and outlet O_2 are measured on the same dry basis and that 21% reference represents ambient air. Equation (3) uses πDH as a cylindrical lateral reference area, explicitly defining this as rotor-loading. Equation (4) has units of g/m³ only if m represents the solids mass flow rate actually suspended at sample plane; the current text defines m as product rate, which is not necessarily the same flow. For Equation (5) should use actual gas volume flow and total pressure rise, with shaft power as the denominator; if electrical input is used, mentioning the motor/VFD efficiency correction. Using the example values, Equation (2) gives 27.56% and Equation (3) results in 10.64 tph/m², in line with the reported rounded values. Figure 3 differentiates the Case 1 target from measured values.

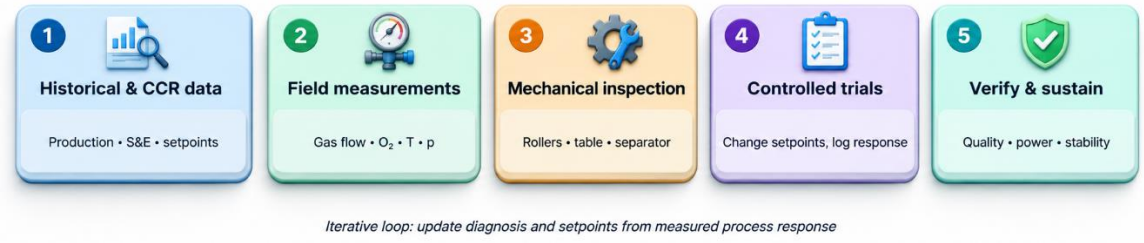


Figure 1. Measurement-based VRM audit and optimization workflow.

5.0 Case Studies

Four mills at three plants are reported. Case 1 is a Raw Mill of ~510 t/h, Case 2 a Slag Mill of ~154–170 t/h and Cases 3 and 4 are two Raw Mills of 350 t/h rated capacity at the same plant. Cases 1 and 2 are presented through the audit findings and the measured before/after performance, whereas Cases 3 and 4 include the full set of measured indices on-line trials. All specific-energy consumption figures are for the grinding circuit and, wherever stated, include main motor, circulation fan, separator and auxiliaries.

5.1 Case 1- Raw mill, 510 t/h

Plant A, operates a raw-meal VRM and has experienced high specific energy consumption, leading to increased production costs. The audit encompassed entire circuit from limestone mining and additive storage to the measurements in the mill. The principal findings and the corresponding actions were

detailed as:

- **Grit cone.** Gap between the end of grit cone and grinding table was 850 mm reduced to 750 mm to improve material distribution to the rollers.
- **Bed height and dam ring.** The mean operational bed height was ~75 mm and reached 100 mm, considered too high for raw grinding. With a 20 mm dam ring, low nozzle rejects and consistent feed moisture of 5–8 %, the dam ring was removed entirely to reduce main-motor load.
- **Grinding-pressure control.** The operating bandwidth between setpoint and actual hydraulic pressure ranged from −10 bar to +5 bar; the authors recommended reducing it to ±2 bar. Such a big band indicates poor pressure tracking and follows bed disturbance.

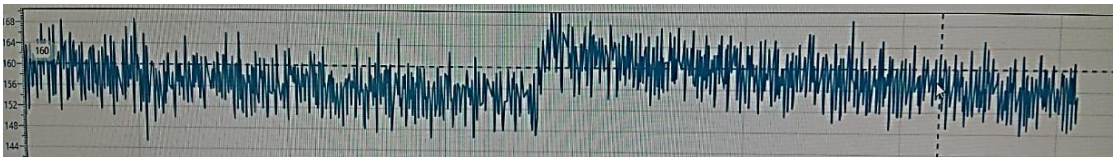


Fig-2: Hydraulic grinding-pressure trace before optimization, showing fluctuation of roughly ±8 bar about a 160 bar mean

- **Feed control.** Apron feeder and belt weigh feeder were not tuned together and no PID loop held the set point; the set-point-to-actual gap was 20–60 tph, forcing frequent operator intervention and reducing output.
- **Nozzle ring.** With an effective area of 4.8 m², the gas velocity was about 34 m/s, considered too low for raw mill operation. The plant operated at high gas flow and a high dam ring to limit rejects, which raised pressure drop. Therefore, eight nozzles behind the rollers were blocked, targeting 40 m/s in the first step and later 45 m/s.

Table 2 summarises the outcome. Total circuit specific power reduced from 14.0 to 12.7 kWh/t (*−1.3 kWh/t, 9.3 %*) while feed rate rose from 510 to 525 t/h. The main-motor power improved most (*5.9 → 5.0 kWh/t, −15 %*), followed by the mill fan (*5.4 → 4.9 kWh/t, −9 %*), consistent with a lower bed and lower gas flow. Auxiliary consumption rose marginally (*2.7 → 2.8 kWh/t*). Table rejects rose from 15 to 20 tph, which the more stable bed accepted.

Table 2: Case 1 - Before and After Implementation

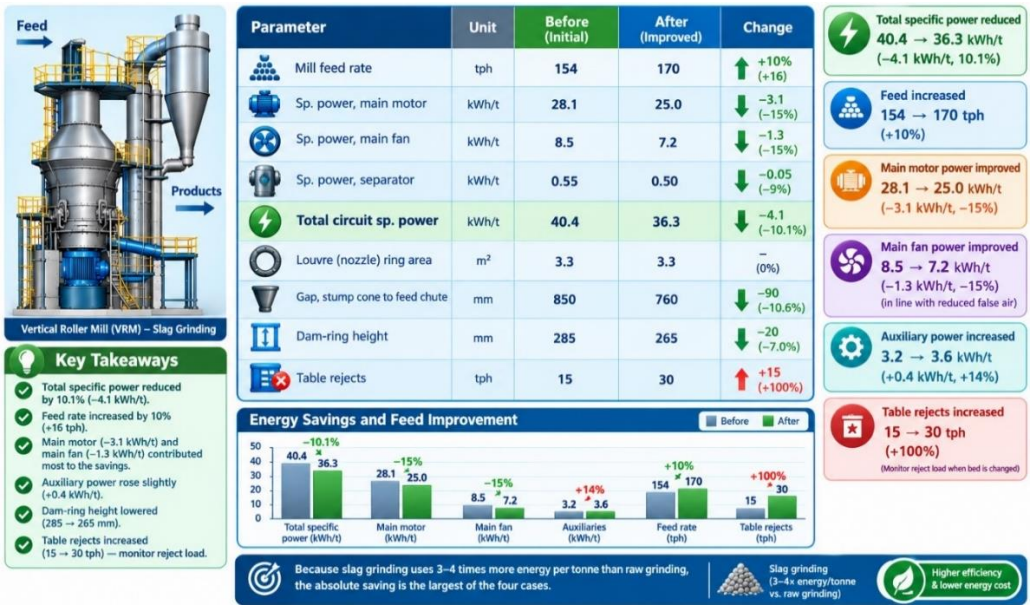


5.2 Case 2 — Slag mill (PSC/OPC grinding)

Plant B utilized a VRM to grind granulated slag for producing both blended and ordinary cement, resulting in high specific power. Starting from slag receipt and storage, the audit included raw-slag sampling and process measurements. Lumps in the slag feed, high false-air ingress across the circuit, high main-motor load, idle running of the circuit during feed cuts, stoppages caused by mill vibration and non-usage of support rollers that stabilize the grinding bed were discovered.

The implementation, as depicted in Table 3, reduced total specific power from 40.4 to 36.3 kWh/t (*−4.1 kWh/t, 10.1 %*) and increased feed from 154 to 170 tph (*+10 %*). In line with the reduction in false air, the main motor contributed −3.1 kWh/t and the main fan −1.3 kWh/t (*−15 %*), while auxiliary power saw an increase of 0.4 kWh/t. The height of the dam-ring was decreased from 285 to 265 mm. Table rejects rose from 15 to 30 t/h, a reminder that the reject load should be monitored during bed changes.

Table 3: Case 2 — Before and After Implementation



5.3 Cases 3 and 4 — Two raw mills at one plant

At Plant C, there are two raw-meal lines: Mill 3 has a three-roller, 4.5 m table and Mill 4, featuring four rollers and a 4.6 m table, both rated at 350 t/h with residues of 15 % and 28 % on a 90 µm respectively. The feed for both mills consist of roughly 98–99 % limestone with 1–2 % clay and a moisture content of about 2 %. Mill 3 produced an average of 345 t/h and 12.59 kWh/t over the last 12 months, and Mill 4 averaged about 420 t/h and 11.5 kWh/t. The Bond work index for limestone in two samples was 10.7 and 11.4 kWh/t, showing that the raw material itself was not the limiting factor.

Hydraulic systems, rollers, table, armour ring and nozzle rings were all found to be in good condition during internal inspection, with only minor wear on sinter-cast liners. Aerodynamic issues and feed preparation problems were identified: (i) the feed highest size was 100–120 mm (*Mill 3*) and up to 160 mm (*Mill 4*), not meeting the target of 100 % passing 75 mm and 90–95 % passing 50 mm; (ii) welded extensions on grit cone left only 380 mm (*Mill 3*) and 400 mm (*Mill 4*) clearance above the table, restricting material flow from the table centre to the rollers; (iii) Mill 3 had a pointed table-spray nozzle, and it was proposed to widen it to the roller width; and (iv) a table water spray of 13–13.5 m³/h in Mill 4 caused material to cake and harden on the table. The hydraulic pressure control in Mill 3 had a bandwidth of 6 bar. Table 4 compares the measured performance indices. False air was high in Mill 3 (*27.3 %*) and above acceptable value in Mill 4 (*17–19 %*) also. Nozzle velocity in Mill 3 was only about

30 m/s, causing high rejects and an unstable bed, while Mill 4 operated at about 45 m/s, nearing the top of the recommended 35–45 m/s band (*Figure 3*). Separator rotor loading was acceptable (*10.6 and 10.0 tph/m²*) but outlet dust loading exceeded the 650 g/m³ norm for both mills. Mill fan efficiency was acceptable at about 78 % and 77 % respectively.

Table 4: Measured Performance Indices (*Cases 3 and 4*)

Index	Audit reference	Mill 3	Mill 4
False air (*%*)	< 15	27.3	17–19
Nozzle velocity (*m/s*)	35–45	30	45
Separator rotor loading (*tph/m²*)	10–12	10.64	10.0
Outlet dust loading (*g/m³*)	< 650	726	803
Circulation-fan efficiency (*%*)	—	78.2	77.2
Grit-cone clearance (*mm*)	—	380	400

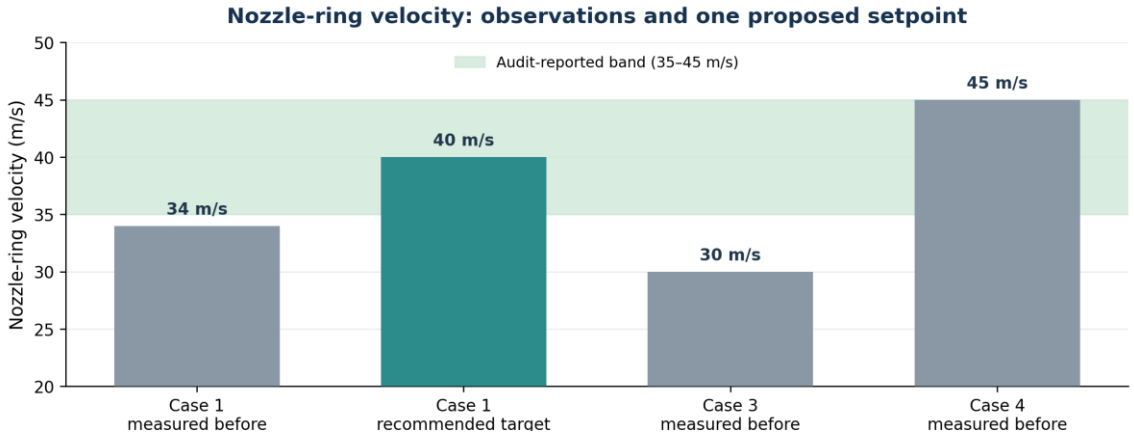


Figure 3. Nozzle-ring velocity observations and proposed Case 1 target.

On-line trials. Table 5 lists the CCR trials.

Throughput increased from 345 to 370 t/h in Mill 3. The water spray was reduced from 9.5 to 7.0 m³/h, the bed height was increased from 120 to 110 mm, the separator speed was increased from 1140 to 1193 rpm, the recirculation damper was opened from 83 to 95%, and the fan speed was increased from 890 to 935 rpm. Fan power increased by 203 kW while main-motor power decreased by 314 kW; the net specific power (*mill + fan*) decreased from 11.26 to 10.20 kWh/t (*−9.4%*).

With water spray decreased from 13 to 8.5 m³/h and bed height increased from 85 to 80 mm, Mill- 4 throughput increased from 420 to 450 t/h; specific power increased by a lesser 0.23 kWh/t (*−2.2%*) as the main motor drew 222 kW more to transmit the additional output. The mill could run continuously at about 450 tph, and water spray should be lowered to less than 5 m³/h.

Table 5: On-Line Optimization Trials (Cases 3 and 4)



Design comparison (Table 6): Because the stated rotor is smaller and runs at higher radial and circumferential velocities, Mill 3's lower claimed throughput compared to Mill 4 follows a separator-capacity constraint. Although the comparison does not identify separator size as the cause, the suggested mechanism—increased recirculation, particle interference and larger coarse carry-over—is logical. Additionally, the roller count, rated fineness, high feed size, false-air intrusion and nozzle velocity of the mills vary; the reported production of Mill 4 surpasses the nominal capacity of 350 t/h. Before the separator can be said as the principal causative constraint, a matched-quality, matched-feed comparison or a controlled separator refit is required.

Table 6: Design Comparison of Mill 3 and Mill 4

Item	Mill 3	Mill 4
Rollers	3	4
Table diameter (mm)	4500	4600
Classifier rotor diameter (mm)	3450	4400
Classifier rotor speed (rpm)	94	45
Radial air velocity (m/s)	15	9.4
Circumferential speed (m/s)	16.7	10.6
Nozzle velocity (m/s)	30	45
Bed height (mm)	110	80

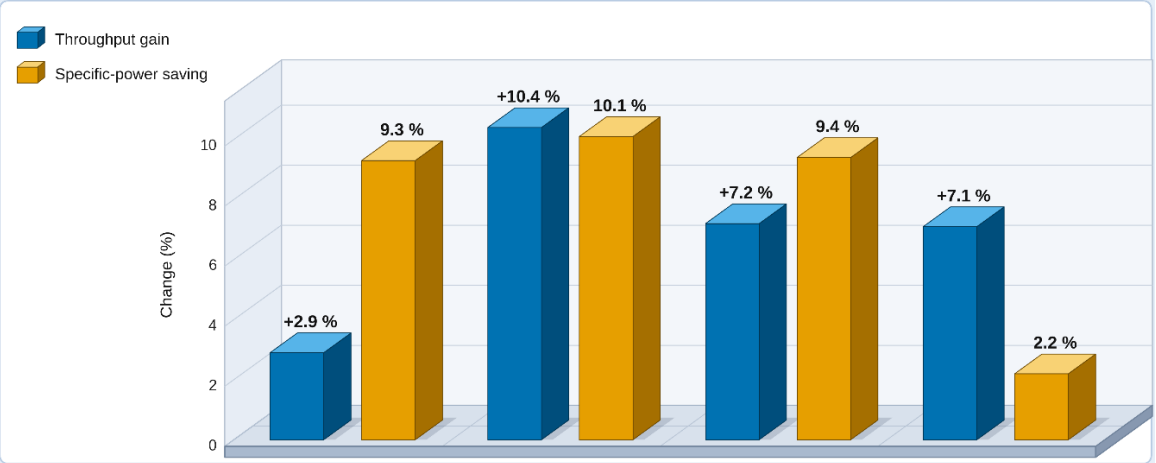
For Mill 3, two sets of actions were suggested. Controlling feed top size, altering the spray nozzle, testing a gradual increase in nozzle velocity from 30 to 40 m/s, and, if the design permits, tweaking separator guide vanes were all low-cost solutions. These actions are hypotheses to test, not guaranteed universal remedies. The authors report that a 30–40 rpm increase in fan speed raised output from 330 to 360 t/h, but the associated increase in fan power and product quality should be reported alongside output.

A larger separator is a higher capital option; and the projected output near 400 t/h using such an option requires a matched-quality acceptance test and equipment-margin verification.

6.0 Cross-Case Discussion

Table 7 places the four cases side by side.

Table 7: Comparative before-after statement of four case studies



Metric	Case 1	Case 2	Case 3	Case 4
Mill type	Raw	Slag	Raw	Raw
Throughput change (tph)	510→525	154→170	345→370	420→450
Throughput gain	**+2.9 %**	**+10.4 %**	**+7.2 %**	**+7.1 %**
Sp. power change (kWh/t)	14.0→12.7	40.4→36.3	11.26→10.20	10.53→10.30
Sp. power saving	**1.3 (9.3 %)**	**4.1 (10.1 %)**	**1.06 (9.4 %)**	**0.23 (2.2 %)**
Basis	Actual	Actual	Trial	Trial

Summary of Results

- **Aerodynamics set the stability.** Nozzle velocity was off-band in Cases 1 and 3, and false air was above 15 % in Cases 2, 3 and 4. Low velocity forces compensating actions (*high dam ring, high gas flow*) that waste fan and motor power; false air reduces fan capacity before gas reaches the nozzle ring. Reducing the false air in the circuit and modifying the nozzle area are first low-cost actions.
- **Bed management for the main motor.** Lower bed height, smaller or no dam ring, stable grinding pressure and less water spray were associated with the largest main-motor savings (*−15 % in Case 1, −11 % in Case 2*). Wet, caked beds (*Case 4*) and over-thick beds (*Case 3*) both reduce effective grinding.
- **Feed quality and feed control are upstream constraints.** Oversized feed, lumps in slag, and poorly tuned feeders (20–60 t/h swings), disturb the bed regardless of how well the mill itself is set.
- **Savings shift between power consumers.** In every case, the fan or auxiliary term partly offset gains in the main motor, so the evaluation must use total circuit specific power.
- **Structural limits need capital.** The audit shows a design bottleneck (*the separator in Case 3*), operating changes recover only part of the gap; the remainder needs a retrofit.

Important basis limitation: Cases 1 and 2 report total-circuit power, whereas Cases 3 and 4 report mill-plus-fan power only. Table 7 therefore supports within-case before/after comparisons, but not direct ranking of absolute SEC or percentage savings across all four cases.

6.1 Recommended audit checklist

These findings can be tabulated into a checklist (Table 8) for a plant to use for a detailed study. Each item pairs a symptom visible in the control room or at the mill with its probable cause and the corrective action that worked in the cases above.

Table 8: Symptom–Cause–Action Checklist

SYMPTOM	PROBABLE CAUSE	ACTION
High rejects, unstable bed	Nozzle velocity < 35 m/s AND high false air	Block selected nozzles; seal inlet ducts, joints
High main-motor power, thick bed	Dam ring too high AND bed 100+ mm	Lower/remove dam ring; reduce bed height
Vibration trips	Wide pressure band; wet or lumpy feed; no bed support	Narrow pressure deviation (±2–3 bar); control feed size; use support rollers
Cake on table	Excess water spray	Cut spray to < 5 m³/h; < 5 m³/h; widen spray to roller width
High rejects, unstable bed	Nozzle velocity < 35 m/s AND high false air	Block selected nozzles; Seal inlet ducts, joints
High main-motor power, thick bed	Dam ring too high; Bed 100+ mm	Lower/remove cam ring; Reduce bed height
Vibration trips	Wide pressure band; Wet/lumpy feed; No bed support	Narrow pressure deviation; Control feed size; Use support rollers
Cake on table	Excess water spray	Cut spray to < 5 m³/h; Set poin; Widen spray to roller width
Feed swings of 20–60 tph	Untuned feeders, no PID loop	Tune feeder loop and set point
Poor flow to rollers	Welded grit-cone extension; 380-400 mm	Remove extension to ≥= 580 mm clearance
Mill idles during feed cuts	No interlock or ramp-down logic	No interlock or ramp-down logic; Review stop/start logic; stop idle running
High dust loading, low output	Small separator, high radial velocity	Tune vane angle; Consider larger separator

The sequence in which actions are implemented is important. Feed-size control and false air reduction are inexpensive and enhance all other levers; nozzle-area adjustments should be made gradually (*for example, from 30 to 40 m/s and then toward 45 m/s*) while monitoring reject load and vibration; grinding-pressure and feeder control tuning should then be locked in before bed-height adjustments are attempted, so gains are attributable to the correct change.

6.2 Critical limitations of study

The case series has practical utility because it integrates process data, field measurements, inspections, and operational modifications in operational VRMs. Nevertheless, the interventions were combined as many setpoints and mechanical conditions were altered simultaneously and the study does not describe a randomized or repeated trial sequence, uncertainty intervals, matched control period, or full implementation duration. Therefore, while the before/after differences show improvement under the stated operating conditions, they do not guarantee continuity at various feed rates and material qualities or evaluate the independent causal effect of each measure.

Second, there are differences between the four case studies. Compared to Cases 3–4, which only include mill and fan power, Cases 1-2 reflect a wider energy circuit boundary. Also, energy savings cannot be verified at equal product specification since product fineness/quality is not consistently reported, especially for Cases 1-2.

Further, plants were advised that a multi-day, matched-feed and matched-quality trial with a uniform energy boundary is carried out with calibrated flow/pressure instruments, product fineness, vibration, rejections and assumptions to validate the results. These adjustments would establish the sustainability of savings and enable one to distinguish between actual efficiency benefits from operating-point shifts.

7.0 Conclusions

Across four audits and operating trials, the findings indicate that troubleshooting guided by measurement can increase production throughput while lowering the specific energy consumption values reported for the mills studied. The most pronounced reported benefits occur in two change categories: the total-circuit modifications implemented in Cases 1 and 2, and the combined mill-and-fan trial modifications implemented in Cases 3 and 4. Because these interventions were evaluated under different energy boundaries, the results cannot be compared directly.

Several diagnostic steps recur consistently throughout the cases which include managing airflow and leakage, maintaining feed and bed stability, ensuring reliable classifier performance, controlling grinding pressure and economising water spray. Taken together, the accumulated evidence supports treating these factors as optimization targets that are specific to the plant context, rather than as universal benchmarks or as isolated causal drivers.

A rigorous follow-up study should therefore go beyond reporting these changes and instead include matched product quality, use identical energy boundaries across comparisons, demonstrate repeatability, quantify uncertainty/assumptions and verify sustained operational performance after the changes are implemented.

8.0 Acknowledgement

The authors thank the plant managements for their cooperation and the project teams for the process audits on which these case studies are based.

9.0 References

[1] P. Pareek and V. S. Sankhla, "Review on vertical roller mill in cement industry & its performance parameters," Materials Today: Proceedings, 2021, doi: 10.1016/j.matpr.2020.10.916.

[2] D. Altun, H. Benzer, N. A. Aydoğan, and C. Gerold, "Operational parameters affecting the vertical roller mill performance," Minerals Engineering, 2016, doi: 10.1016/j.mineng.2016.08.015.

[3] C. Liu, Z. Chen, Y. Mao, Z. Yao, W. Zhang, W. Ye, Y. Duan, and Q. Xie, "Analysis and optimization of grinding performance of vertical roller mill based on experimental method," Minerals, vol. 12, no. 2, Art. no. 133, 2022, doi: 10.3390/min12020133.

[4] V. Ghalandari, M. Esmaeilpour, N. Payvar, and M. T. Reza, "A case study on energy and exergy analyses for an industrial-scale vertical roller mill assisted grinding in cement plant," Advanced Powder Technology, 2021, doi: 10.1016/j.apt.2020.12.027.

[5] M. Ali, A. López, M. Pasha, and M. Ghadiri, "Optimisation of the performance of a new vertical roller mill by computational fluid dynamics simulations," Powder Technology, 2023, doi: 10.1016/j.powtec.2023.119282.

[6] R. Huang, Y. Ma, H. Li, C. Sun, J. Liu, S. Zhang, H. Wang, and B. Hao, "Operation parameters multi-objective optimization method of large vertical mill based on CFD-DPM," Advanced Powder Technology, 2023, Art. no. 104014, doi: 10.1016/j.apt.2023.104014.

[7] G. B. Ardana, R. N. Athif, A. S. Pramanta, R. A. Pamungkas, A. D. Harahap, and H. Prasetiawan, "Optimizing vertical roller mill performance: CFD study on nozzle ring design with modular sickle-shaped splitters," Journal of Advanced Research in Technology and Innovation Management, 2025, doi: 10.37934/jartim.15.1.4352.

[8] C. Woywadt and M. Schiefer, "Fluid-dynamic optimization of vertical roller mills," in Proceedings of the 2026 IEEE-IAS/ACA Cement Industry Conference, 2026, doi: 10.1109/ias/aca70326.2026.11629777.



[9] R. Fatahi, H. Nasiri, E. Dadfar, and S. Chehreh Chelgani, "Modeling of energy consumption factors for an industrial cement vertical roller mill by SHAP-XGBoost: A 'conscious lab' approach," Scientific Reports, 2022, doi: 10.1038/s41598-022-11429-9.

[10] M. Zhu, Y. Ji, Z. Zhang, and Y. Sun, "A data-driven decision-making framework for online control of vertical roller mill," Computers & Industrial Engineering, 2020, doi: 10.1016/j.cie.2020.106441.

[11] B. Vijayabhaskar and S. Jayalalitha, "Dual adaptive model predictive controller application to vertical roller mill process used in the cement industry," IEEE Access, 2020, doi: 10.1109/ACCESS.2020.3045163.

[12] J. Yao, Y. Shi, A. Wan, and W. Lu, "Optimisation of the particle milling process in a vertical roller mill using response surface methodology," in Proceedings of the International Conference on Mechanical Engineering, Intelligent Manufacturing, and Mechatronics, 2025, doi: 10.1117/12.3078034.

[13] C. Woywadt, L. Schmitt, S. Rathgeber, and P. Marijan, "Optimization of vertical roller mill systems using AI (artificial intelligence)," in Proceedings of the 2025 IEEE-IAS/PCA Cement Industry Conference, 2025, doi: 10.1109/ias/pca63579.2025.11346748.

[14] A. Wan, Y. Gao, W. Liu, R. Yin, and K. Al-Bukhaiti, "Real-time optimization of vertical roller mills using XGBoost prediction and Q-learning control," Computers, Materials & Continua, 2026, doi: 10.32604/cmc.2026.081719.



Technical Session -IIIA

DECARBONISATION OF CEMENT MANUFACTURING AT SCALE: THE MAHA CEMENT (MHIPL) INTEGRATED MODEL

Sanjay K Singh

Chief Sustainability Officer & Corporate Head (Environment & Sustainability), My Home Industries Private Limited, Hyderabad, India

ABSTRACT

Purpose - Cement decarbonisation must address avoidable clinker, fuel and electricity emissions before sizing capture for residual calcination CO2. This paper develops and tests a boundary-consistent, source-first architecture using My Home Industries Private Limited's (MHIPL) existing 12.6 Mt/yr network as a heterogeneous multi-plant case; the separate 3.0 Mt/yr OGU under commissioning will raise capacity to 15.6 Mt/yr in FY 2026-27.

Method - Plant mass and energy balances, clinker-output-weighted thermal SEC, kiln-heat-weighted TSR, lifecycle avoidance, corporate inventory, verified product EPDs, CCTS trajectories, route-level freight MRV and emerging MHIPL-Captimise CCU/CCUS evidence are reconciled within one physical inventory. Six NCB levers are sequenced and screened through technical readiness, operability, avoided-CO2 and scale-up gates. Capture routes include MEA, promoted hot potassium carbonate and membranes; rail savings are conditional on a locked road counterfactual and complete-chain data.

Results - FY 2024-25 gross and net Scope 1+2 emissions were 4.4487 and 4.2406 MtCO2e after 0.2081 MtCO2e of stated avoidance, corresponding to 0.599 and 0.572 tCO2e/t. FY 2025-26 cement output was 8.773 Mt at a network electrical SEC of 63.84 kWh/t. Across 6.51 Mt integrated clinker, thermal SEC averaged 718.9 kcal/kg (3.01 GJ/t) and energy-weighted TSR averaged 12.18%, with line TSR varying from 3.32% to 17.51%. Installed WHR totals 35 MW. All OPC, PPC, PSC and composite cement products have verified EPDs. An illustrative test shows that reducing clinker factor, fossil-fuel share and kiln heat before capture lowers the 90% gross capture load from 0.498 to 0.405 tCO2/t cement, about 19%. The 14.19-percentage-point TSR spread proves that portfolio averages cannot prescribe line action. CONCOR rail logistics can reduce Scope 3 only after route-ledger assurance. The MHIPL-Captimise AB, Sweden, feasibility programme creates a pioneering India-Sweden decarbonisation platform to identify the most effective plant-integrated CCU/CCUS pathway, using site-specific flue-gas, utility, lifecycle and CO2-destination evidence to maximise credible emissions reduction and enable future scale-up.

Contribution - The paper converts a broad decarbonisation roadmap into three testable propositions and a reproducible decision system. It shows how plant, product, freight, CCTS and capture claims can reconcile without double counting, and how source reduction strengthens the effectiveness and economics of residual capture. The method is transferable to heterogeneous Indian cement portfolios.

Keywords: cement decarbonisation; alternative raw materials and fuels; energy efficiency; WHR; renewable energy; Scope 3 rail; CCUS; EPD; CCTS; MHIPL

1. Introduction

Cement generates about 7% of global energy-system CO2; roughly two-thirds of direct production emissions arise from calcination. Because process CO2 persists after heat and power decarbonise, cement requires a chemistry-led transition [1-5].

India must grow while pursuing net zero by 2070. CCTS creates plant-level intensity obligations, while the Union Budget 2026-27 allocates INR 20,000 crore over five years to cross-sector CCUS [9-12].

Research questions RQ1 - Which sequence minimises lifecycle CO2 and capture duty? RQ2 - How can kiln, corporate, EPD and route claims reconcile without double counting? RQ3 - Which measured gates can convert rail and CCU/CCUS opportunities into scalable abatement? MHIPL's varied lines, products and freight form the industrial test bed.

2. Carbon anatomy and accounting boundary

a. Unavoidable chemistry, avoidable intensity

Calcination (CaCO3 -> CaO + CO2) releases 0.44 tCO2/t pure CaCO3. IPCC Tier 2 uses clinker output, an emission factor and cement-kiln-dust correction; the default is about 0.507 tCO2/t clinker. Plant-specific carbonate and CKD data refine inventory and capture design [5].

$E_{process} = M_{clinker} \times EF_{clinker} \times CF_{CKD}$ *(1)*

Plant intensity combines process, fuel, power and other emissions. Consistent product, denominator, transfer and fuel rules expose clinker-factor leverage; integrated plants and grinding units must remain distinct before consolidation.

$GEI_{gross} = (E_{process} + E_{fuel} + E_{power} + E_{other}) / Q_{equivalent_product}$ *(2)*

$GEI_{net} = (E_{gross} - \text{eligible deductions} - \text{captured-and-verified } CO_2) / Q_{equivalent_product}$ *(3)*

Accounting caution A company-labelled operational 'net' intensity is not a net-zero claim. Report gross and net together and disclose credits, renewable attributes, capture energy, transport and permanence.

b. From captured CO2 to verified avoided CO2

Lifecycle accounting converts capture performance into credible climate benefit. Use a transparent counterfactual holding cement output and quality constant.

$CO_{2,avoided} = CO_{2,captured} - E_{capture_energy} - E_{conditioning} - E_{transport} - E_{use_or_storage_leakage}$ *(4)*

$\text{Avoidance ratio} = CO_{2,avoided} / CO_{2,captured}$ *(5)*

Durable storage and methanol displacement create climate value when permanence and fossil displacement are verified. Track capture efficiency, avoidance and permanence separately.

Figure 1. Sequenced abatement architecture for cement manufacturing



Source: Author's synthesis based on IEA, GCCA, IPCC and UNIDO pathways [1-6].

3. Methodology and decision tests

The case study combines peer-reviewed pathways, stoichiometric balances, MHIPL FY 2024-25/FY 2025-26 records, lifecycle accounting and emerging CCU/CCUS feasibility evidence. Levers are screened for avoidance, readiness, integration value and infrastructure dependency; measured, public and illustrative evidence remain distinct.

Marginal abatement cost (MAC) uses CO2 avoided and annualised capital, energy, reagents, maintenance, waste and logistics, net of verified savings and revenues.

MAC = (Annualised CAPEX + Delta OPEX - savings - verified revenues) / annual CO2_avoided *(6)*

MHIPL data retain stated boundaries. Electrical SEC is cement-output weighted; with clinker K, heat H and line TSR T, H-bar = sum(KH)/sum(K) and TSR-bar = sum(KHT)/sum(KH). Line values remain primary, and corporate intensity is not equated with CCTS GEI.

Testable propositions P1 - upstream abatement lowers residual capture duty; P2 - line heterogeneity changes the optimal portfolio; P3 - one inventory can reconcile corporate, EPD, freight and capture claims. Evidence failing boundary closure remains unclaimed.

LeadIT positions MHIPL-Captimise as a feasibility, pilot-design and e-methanol programme building evidence for technology selection and investment.

4. Integrated decarbonisation levers

a. Reduce the clinker burden before capturing it

Clinker substitution avoids calcination and kiln heat. Prioritise proven SCMs and qualified binders against strength, durability and standards. India's OPC, PPC, PSC and composite portfolio is the platform; OPC remains necessary for selected specifications. As fly ash and slag tighten, LC3 - typically 50% clinker, 30% calcined clay, 15% limestone and 5% gypsum - can cut binder CO2 about 40% versus high-clinker cement [7,8]. Verify clinker factor, energy and constituent transport.

Optimisation must test kaolinite, calcination, grinding, sulphate balance, reactivity, strength, admixture demand and exposure durability. Mine plans must prevent carbon reduction from transferring material or quality risk.

Alternative raw materials can displace virgin minerals only within chemistry, trace-element, chloride/alkali and leachability limits.

b. Thermal efficiency and stable pyroprocessing

Kiln stability underpins every later lever. False-air reduction, low-pressure-drop gas paths, cooler recuperation, burner/refractory control and calibrated advanced control reduce heat and variability. AI adds value only with reliable instruments, actuators and operator logic.

Excess air, bypass and unstable CO increase gas flow, fan power and solvent risk while reducing WHR. Close the heat/mass balance before capture design at a defensible operating percentile.

c. Alternative fuels: carbon benefit with process discipline

TSR must be energy-based: wet, low-calorific fuel can raise tonnage without substitution. Control calorific-value basis, moisture, ash, biomass fraction, chlorine, sulphur, alkalis, metals and size. Separate fossil, biogenic and non-renewable waste carbon; sustained feeding matters more than

peak TSR.

TSR (%) = 100 x Energy_from_alternative_fuels / Total_kiln_thermal_energy *(7)*

Co-processing displaces fossil fuel and recovers minerals, but benefits depend on carbon fractions and the counterfactual. Control chlorine cycles, CO, TOC, mercury, dioxins and furans [16]; pre-processing, sampling and rapid release are as critical as dosing hardware.

d. Electricity, grinding, WHR and renewable supply

Efficient grinding, separation, variable-speed drives and utility control reduce demand. WHR output depends on kiln uptime, gas condition, water, auxiliaries and extraction after process needs.

Shift residual demand to credible renewables and PPAs. Report location- and market-based Scope 2 separately

[17] and manage attributes, time matching, curtailment, wheeling, storage and minimum dispatch.

e. Scope 3 and product-side demand

Address purchased materials, freight, fuels, packaging, capital goods and downstream concrete. Low-carbon modes, circular packaging and performance-based concrete reduce Scope 3. ISO 14067-aligned EPDs must reconcile to corporate inventory and allocation [18,19,32].

f. CCUS: a strategic opportunity for residual process emissions

Residual calcination creates a strategic role for non-carbonate binders and carbon capture. The IEA 2030 pathway combines lower clinker, 30% low-emission kiln fuels and 170 MtCO2/yr cement capture [1]. Norway's 0.4 MtCO2/yr Brevik facility demonstrates industrial viability and the value of integrated utilities, transport and storage [13].

Table 1. Capture routes relevant to cement flue gas

Route	Where it fits	Principal advantage	Critical engineering gate
Amine absorption	Cleaned flue gas	Mature; high capture	Steam/cooling; corrosion
Promoted HPC	CO2-rich gas	Low volatility	Kinetics; heat duty
Membranes	Hybrid train	Compact; solvent-free	Compression; recovery/purity
Calcium looping	Calciner	High-temperature synergy	Oxygen, heat; sorbent decay
Oxyfuel/direct separation	New kiln/retrofit	Concentrated CO2	Air separation; sealing

Chemical absorption offers the most mature near-term platform, while pilots and demonstrations are expanding the CCUS innovation pipeline [6,14,15].

g. CO2 utilisation, hydrogen and durable climate value

CO2 utilisation can create climate value through durable incorporation or verified fossil displacement after lifecycle accounting. E-methanol requires 0.136 tH2 and yields 0.727 t methanol per tonne CO2; at 50-55 kWh/kg H2, electrolysis uses 6.8-7.5 MWh/tCO2. Thus, 10 tCO2/day needs 1.36 tH2/day, yields 7.27 t methanol/day and requires 68-75 MWh/day before purification, compression and synthesis. Low-carbon H2 and confirmed fossil displacement strengthen the opportunity.

5. MHIPL multi-plant case study

a. Portfolio and reporting context

MHIPL's existing 12.6 Mt/yr capacity comprises MCW, YCW and VGU. The separate 3.0 Mt/yr Odisha Grinding Unit (OGU) project is under commissioning and is excluded from 12.6 Mt/yr; commissioning during FY 2026-27 will raise total capacity to 15.6 Mt/yr. OPC, PPC, PSC and composite cements all have verified EPDs [23]. Legacy/new integrated lines and stand-alone grinding enable product, renewable, AFR and CCU/CCUS engineering without portfolio-average distortion or high-carbon lock-in.

For FY 2024-25, MHIPL reported 4,448,665.7 tCO2e gross Scope 1+2, 208,088.0 tCO2e stated avoided and 4,240,577.7 tCO2e net. Gross and net intensities were 0.599 and 0.572 tCO2e/t. Report both because deductions do not change the physical gross inventory.

Figure 2. Graphical abstract: MHIPL's integrated decarbonisation pathway anchored at MCW



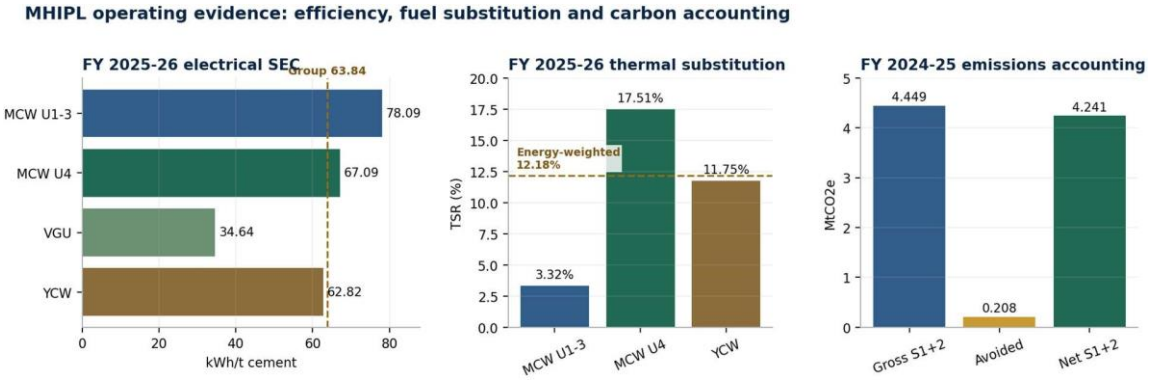
Plant photograph: Maha Cement. Technical overlay: author's synthesis.

Table 2. MHIPL FY 2025-26 operating indicators

Reporting unit	Configuration	Cement output (Mt)	Electrical SEC (kWh/t cement)	Thermal SEC (kcal/kg clinker)	TSR (%)
MCW Units 1-3	Integrated	2.080	78.09	712.0	3.32
MCW Unit 4	Integrated; 9,500 t/day kiln	2.916	67.09	719.5	17.51
VGU	Grinding unit	1.251	34.64	N/A	N/A
YCW	Integrated	2.525	62.82	724.0	11.75
Total / weighted*	Mixed boundary	8.773	63.84	718.9	12.18

Source: MHIPL records. Electrical SEC is cement-output weighted across all units. Integrated-kiln metrics use 6.51 Mt clinker: thermal SEC is clinker-output weighted (718.9 kcal/kg; 3.01 GJ/t), and TSR is total-kiln-energy weighted (12.18%). VGU is excluded from thermal metrics.

Figure 3. Selected MHIPL efficiency, TSR and emissions indicators



Source: MHIPL records. Avoided emissions are shown positively and subtracted from gross emissions.

b. Quantified results and implementation evidence

Across 6.51 Mt clinker, thermal SEC was 718.9 kcal/kg and energy-weighted TSR 12.18%. Unit 4 reached 17.51% TSR versus 3.32% for Units 1-3. Network electrical SEC was 63.84 kWh/t, or 68.70 kWh/t at integrated sites. The 14.19-point TSR spread supports P2: line constraints must set fuel strategy.

Installed WHR totals 35 MW: 14 MW at MCW Units 1-3, 14 MW at Unit 4 and 7 MW at YCW. Track net generation, availability, displaced power and capture-heat interaction. MHIPL targets RE50/RE100 by 2030/2050 and TSR 25%/50%/100% by 2030/2050/2070; each kiln needs a bankable fuel, quality and capex plan.

MCW co-processed 27,050 t of pharmaceutical liquid waste in FY 2021-22, with an estimated 10,080 tCO2 reduction [21]. Scale-up requires a diversified, assured and continuously controlled portfolio with fossil/biogenic analysis, stable feed and emissions safeguards.

PPC, PSC and composite cement lower clinker intensity while OPC serves selected applications; verified EPDs enable performance-equivalent comparison [18,19,23]. Match each requirement to the lowest verified lifecycle footprint. Initial Scope 3 screening (about 0.07 tCO2e/t) remains provisional pending coverage and assurance; water-positive status is not counted as carbon abatement.

c. Scope 3 reduction through CONCOR rail logistics

MHIPL's CONCOR MoU supports bulk-cement tank-container movement from MCW to ICD Bengaluru, a receiving silo at DRT Dronagiri and a Railway Board rake configuration involving 50 MHIPL containers [26-28]. Closed bulk rail can reduce road tonne-kilometres, bags and losses while extending the reach of lower-carbon dispatch.

MCW's rail siding was commissioned in 2012. A historical report recorded over 99% of clinker and about 40-45% of cement dispatch and coal receipts by rail [29]. This proves capability, not today's modal split, which requires current ERP, rail and terminal records.

Freight falls in Scope 3 Category 4 or 9 depending on procurement [32]. Calculate avoidance for each origin-destination pair against a locked road counterfactual, including actual rail and first-/last-mile distances, terminal/silo energy, empty returns and losses. Record factor geography, energy basis, year and well-to-wheel boundary:

Delta E_logistics = M x [(D_road x EF_road) - (D_rail x EF_rail + D_first_last x EF_road)] -

E_terminal - E_empty_return *(8)*

Claim discipline Quantify CO2 only after assuring the route ledger, road baseline and complete chain; reconcile with corporate and EPD boundaries.

Table 3. Minimum MRV dataset for MHIPL-CONCOR rail logistics

Data stream	Unit	Control	Carbon use
Dispatch mass by route	t	Reconcile ERP, loading and rail receipt	Activity data
Rail and road-leg distance	km	Controlled route/terminal master	Mode t-km
Mode-specific factors	kgCO2e/t-km	Record source, geography, year and basis	Route emissions
Empty return; terminal/silo energy	t-km; kWh	Allocate per loaded tonne	Chain adjustment
Packaging and loss change	bags/t; %	Verified baseline	Material co-benefit
Avoided-emission allocation	tCO2e	Lock baseline; prevent duplication	Scope 3 KPI

Adapted from GHG Protocol Scope 3 guidance [32].

Count packaging and spillage only when bag mass, recycled content, loss and end-of-life baselines are measured; count terminal electricity and product loss separately. Reconcile both with the product EPD.

Once assured, the route ledger can guide dispatch planning, customer disclosure and expansion of bulk terminals using marginal CO2 avoided alongside cost.

d. CCTS makes the trajectory measurable

CCTS creates a near-term signal. Yanakandla moves from a 0.7449 baseline to 0.7314 tCO2e/t equivalent product in 2026-27; Mellacheruvu moves from 0.8332 to 0.8100 [9,10]. Translate these methodology-specific targets into line actions without conflating CCTS GEI and corporate intensity.

Table 4. Notified MHIPL-linked CCTS greenhouse-gas intensity trajectory

Plant / obligated entity	2023-24 baseline	2025-26 target	2026-27 target	Reduction to 2026-27
Sree Jayajothi Cement, Yanakandla	0.7449	0.7412	0.7314	1.81%
My Home Industries Ltd., Mellacheruvu	0.8332	0.8267	0.8100	2.78%

Unit: tCO2e/t equivalent product. CCTS GEI is not directly comparable with corporate cementitious-product intensity.

e. A pioneering CCU/CCUS opportunity with Captimise AB, Sweden

MHIPL and Captimise AB, Sweden (ANDRITZ Group), are creating a pioneering CCU/CCUS pathway through LeadIT. Technology-neutral screening of MEA, promoted hot potassium carbonate (HPC) and membranes, coupled with pilot design and e-methanol assessment, preserves

optionality while plant evidence identifies the best route and scale [30,31]. Concepts compare about 2 and 5 tCO2/day; selection balances maturity, heat, kinetics, compression and recovery-purity.

MCW Unit 4's 0.95 million Nm3/h flue gas at 110-140 °C and 17-21% CO2 creates a strong plant-integrated capture platform. Post-dryer and bypass constituents (0.72 and 0.078 million Nm3/h) are not additive to the main stack. Representative gas campaigns, pretreatment, heat recovery, fan-margin and WHR integration will convert this advantage into a stable, lifecycle-positive pathway.

Table 5. MCW Unit 4 opportunity and capture-design envelope

Stream	Indicative flow (Nm3/h)	Temp. (°C)	CO2 (vol.%)	Design implication
Main stack	948,865	110-140	17-21	Absorber, duct and fan envelope
Post-dryer constituent	718,972	80-90	20-23	Confirm moisture and dust
Kiln-bypass constituent	77,723	120-130	20-27	Impurity and volatility-cycle risk

Source: emerging MHIPL-Captimise evidence, 2026; battery-limit confirmation supports pilot design.

Table 6. Evidence-led scale-up gates for the MHIPL-Captimise programme

Gate	Measured evidence	Selection criterion	Deliverable
Flue-gas boundary	Flow, composition, impurities, availability	Closed mass balance; design percentile	Validated basis
Technology screen	Recovery, purity, utilities, reagent/waste	CO2 and cost per tonne avoided	Ranked options
Plant integration	Steam, power, cooling, pressure drop, WHR	Acceptable kiln/fan/WHR penalty	Integration scheme
Pilot scale-up	Mass transfer, degradation, uptime, dynamics	Scalable 2 and 5 t/day correlations	Design/test package
CO2 destination	Specification, H2, offtake, permanence	Bankable lifecycle-positive pathway	Use/storage plan

Measured evidence converts capture performance into lifecycle CO2 avoided and investment-ready scale-up.

The pilot will generate commercial-scale evidence on mass transfer, degradation, impurities, heat/power, cooling, pressure drop, dynamics, CO2 purity, waste and analyser closure. Lifecycle CO2 and cost avoided at equal availability will identify the strongest scale-up route.

Pilot scale will follow learning objectives: smaller units resolve solvent kinetics and impurity response; larger units strengthen hydrodynamics, heat integration and operability. Design-of-experiments, analyser redundancy, mass/energy closure, availability criteria and scale-up correlations will create an investment-ready package linked to credible energy and a bankable CO2 product or destination.

6. Results: sequenced abatement and capture-duty test

For illustrative cement at 0.70 clinker factor, 0.507 tCO2/t clinker process factor, 3.0 GJ/t clinker, 94.6 kgCO2/GJ fuel, 64 kWh/t and 0.70 tCO2/MWh power, process, fuel and electricity equal 0.355, 0.199 and

0.045 tCO2/t, or 0.598 total. Its proximity to MHIPL's 0.599 is not an inventory reconstruction; deductions and allocation require audited data.

Table 7. Illustrative abatement arithmetic per tonne of cement

Action	Illustrative calculation	Gross saving before rebound / added energy
Reduce clinker factor 0.70 -> 0.60	0.10 x 0.507 process + 0.10 x 3.0 x 0.0946 fuel	About 79 kgCO2/t cement
Increase zero-fossil TSR by 10 percentage points	0.70 x 3.0 x 10% x 0.0946	About 20 kgCO2/t cement
Reduce heat by 30 kcal/kg clinker	0.70 x 0.1256 GJ/t x 0.0946	About 8 kgCO2/t cement
Replace 0.70 tCO2/MWh grid power	0.064 MWh/t x 0.70	About 45 kgCO2/t cement
Capture 90% of residual stack CO2	After upstream reductions; deduct capture-chain emissions	Large but project-specific

Levers are interactive: lower clinker factor reduces fuel and capture loads; benefits depend on the energy mix and counterfactual.

Applied sequentially, clinker factor 0.60, ten percentage points of zero-fossil TSR and a 30 kcal/kg heat reduction lower illustrative stack CO2 from 0.554 to about 0.450 t/t cement. A 90% gross capture load falls from 0.498 to 0.405 t/t - about 19% - before capture-chain energy. This supports P1 and prevents excess steam, cooling, fan and capital duty.

A decision model should vary clinker factor, grid factor, alternative-fuel fossil fraction, kiln output, capture energy and availability together. Report central, optimistic and conservative cases and identify the crossover where a lever stops reducing lifecycle emissions, preventing false precision from driving investment.

7. A staged MHIPL roadmap

Each investment should pass avoidance, operability and scalability gates. New capacity should be low-clinker, renewable-, AFR- and capture-ready by design, while brownfield lines require sequenced annual operating envelopes rather than portfolio averages.

Table 8. Decision-gated decarbonisation roadmap for MHIPL

Horizon	Operating objective	Priority actions	Decision gate / KPI
2026-2030: no-regret	Beat GEI targets; lower capture duty	Kiln stability; clinker reduction; AFR contracts; WHR; RE50; CONCOR route ledger and bulk scale-up; assured Scope 1-3/EPDs; 2-5 t/day pilot	Product tCO2e/t; sustained TSR/heat; rail CO2; pilot avoidance and uptime
2030-2040: transform	Low-carbon product, energy and logistics systems	Scale composite/calcined-clay products; renewable firming; higher TSR/rail share; capture demonstration with credible sink	Acceptance; modal CO2; MAC; CO2 specification and offtake

2040-2050: infrastructure	Remove controllable energy emissions	RE100; TSR50; fleet50; shared-hub CCUS; integrated digital MRV	Availability; annual CO2 avoided; assurance
2050-2070: residual	Net zero by 2070	Near-complete fossil displacement; residual capture; durable storage/removals; TSR100/fleet100 where sustainable	Near-zero product; residual and permanence evidence

MHIPL roadmap milestones; 'TSR100' means eliminating unabated fossil kiln fuel, subject to safety, supply and lifecycle tests.

8. MRV and digital control architecture

Financeable decarbonisation needs one controlled dataset linking mass flows, fuel/biomass, carbonate/CKD, power attributes, CEMS, capture utilities and CO2 destination. The same source data must serve heat balance, inventory, CCTS, EPDs and project claims. Each point needs unit, boundary, frequency, calibration, owner and approval trail.

- Use plant-specific carbonate/clinker data and one declared calorific-value basis for TSR; separate fossil, biogenic and non-renewable waste carbon.
- Report location- and market-based Scope 2, test contractual-attribute quality and prevent duplicate renewable claims.
- Reconcile product and route factors exactly to plant totals, including clinker transfers and grinding-unit allocation; meter capture utilities and calculate system-boundary CO2 avoided.
- Apply version control, calibration status, maker-checker approval, exception flags and ISO 14064-1/14067-aligned independent assurance [18,19].

9. Economics, policy and infrastructure

CCUS extends conventional abatement when paired with shared transport/storage, liability clarity and bankable demand. Brevik demonstrates technology readiness and the value of integrated infrastructure. India's INR 20,000-crore programme can catalyse repeatable capture-to-destination value chains [11,13].

First-of-a-kind capture can be accelerated through CCTS-linked incentives, grants, concessional finance, hubs, contracts for difference, near-zero demand and performance-based procurement. Reward verified lifecycle avoidance rather than plant-boundary capture tonnes.

Investment rule Use one marginal abatement curve while preserving capture tie-ins, plot space and renewable-ready systems that avoid retrofit lock-in.

10. Discussion, transferability and limitations

P1 and P2 are supported: source-first sequencing cuts the illustrative 90% capture load by 19%, and a 14.19-point TSR spread invalidates portfolio-average prescriptions. P3 remains conditional until current route and allocation data reconcile.

CONCOR shows that Scope 3 needs infrastructure and MRV. Close counterfactual, feeder legs, terminal energy, empty returns, losses and packaging route-by-route without duplicating EPD benefits.

At 712-724 kcal/kg clinker, heat gains still lower fuel and capture duty. MHIPL-Captimise can turn favourable site conditions into scalable decarbonisation through kiln stability, WHR integration, impurity control and a credible CO2 destination.

Transferability rests on common variables - clinker factor, heat, fossil fraction, power factor, route tonne-kilometres, capture utilities and CO2 destination - while plant limits remain explicit. Optimise quality, availability, cost and emissions as one constrained system.

Limitations: The feasibility phase is building FEED-ready evidence; the architecture supports decisions, not audited attribution.

11. Conclusions: answers to the research questions

1. RQ1 - Use a source-first sequence: measure; reduce clinker and demand; stabilise and minimise energy; substitute fossil fuel and power; capture residual process CO2; verify destination. In the illustrative test, upstream kiln levers reduce 90% gross capture load by about 19%.
2. RQ2 - Reconcile line balances, corporate gross/net totals, verified product EPDs, CCTS GEI, freight ledgers and capture utilities in one physical inventory; count no deduction twice.
3. RQ3 - Complete-chain route data can scale CONCOR rail; flue-gas, utility, operability, lifecycle and destination gates can progress Captimise from screening to pilot and scale-up.
4. MHIPL delivered 8.773 Mt cement at 63.84 kWh/t; integrated kilns produced 6.51 Mt clinker at 718.9 kcal/kg and 12.18% energy-weighted TSR, supported by 35 MW WHR. The 14.19-point TSR spread requires line-specific portfolios.
5. All OPC, PPC, PSC and composite products have verified EPDs. Report 0.599 gross and 0.572 net tCO2e/t together; deductions must not obscure physical emissions.
6. The transferable contribution is a falsifiable, decision-gated architecture for India's six NCB levers. CCTS and CCUS can accelerate deployment when combined with shared infrastructure, liability clarity and near-zero-cement demand.

Acknowledgements

The author acknowledges MHIPL's operating, process, energy, environment and sustainability teams; CONCOR; Captimise AB and LeadIT programme partners.

Data availability and declaration

Public sources are listed below. Internal operating and feasibility data require MHIPL technical and management approval before publication. Engineering ranges must be reconfirmed at the selected battery limit. No vendor or investment decision is implied; the author declares no financial conflict.

References

[1] International Energy Agency (IEA). Cement: Net Zero Emissions Guide. Paris, 2023. [Online]

[2] International Energy Agency (IEA). Cement - Energy System, latest findings updated June 2026. [Online]

[3] Global Cement and Concrete Association (GCCA). Concrete Future: 2050 Cement and Concrete Industry Roadmap for Net Zero Concrete. London, 2021. [Online]

[4] Global Cement and Concrete Association (GCCA). Cement and Concrete Industry Net Zero Action and Progress Report 2025/26. London, 2025. [Online]

[5] Intergovernmental Panel on Climate Change (IPCC). 2006 IPCC Guidelines for National Greenhouse Gas Inventories, Volume 3, Chapter 2: Mineral Industry Emissions. [Online]



[6] United Nations Industrial Development Organization (UNIDO). A Snapshot of Cement and Concrete Decarbonization Technologies. 2025. [Online]

[7] Scrivener, K.L., John, V.M. and Gartner, E.M. Eco-efficient cements: Potential economically viable solutions for a low-CO2 cement-based materials industry. Cement and Concrete Research 114 (2018), 2-26. [Online]

[8] LC3 Project / UNIDO. Limestone Calcined Clay Cement: clinker substitution for fast emission cuts. 2026. [Online]

[9] Bureau of Energy Efficiency. Indian Carbon Market and Carbon Credit Trading Scheme - compliance mechanism. Updated 2026. [Online]

[10] Government of India. Greenhouse Gases Emission Intensity Target Rules, 2025, Gazette notification G.S.R. 739(E), 8 October 2025. [Online]

[11] Government of India, Ministry of Finance. Union Budget 2026-27 Speech, paragraph 38: Carbon Capture Utilisation and Storage. 1 February 2026. [Online]

[12] Ministry of Environment, Forest and Climate Change. India's Long-Term Low-Carbon Development Strategy. 2022. [Online]

[13] Heidelberg Materials. World premiere: CCS cement facility opens in Norway. 18 June 2025. [Online]

[14] International Energy Agency. CCUS in Clean Energy Transitions: CCUS technology innovation. 2020. [Online]

[15] LEILAC. Technology for direct separation of cement and lime process CO2; project and technical updates. [Online]

[16] Global Cement and Concrete Association. Policy Document on Co-processing. 2024. [Online]

[17] Greenhouse Gas Protocol. Scope 2 Guidance: An amendment to the GHG Protocol Corporate Standard. [Online]

[18] ISO 14064-1:2018. Greenhouse gases - Part 1: Specification with guidance at the organization level for quantification and reporting. [Online]

[19] ISO 14067:2018. Greenhouse gases - Carbon footprint of products - Requirements and guidelines for quantification. [Online]

[20] Global Cement and Concrete Association. Definitions for Low-Carbon and Near-Zero Cement and Concrete, Version 1. 2024. [Online]

[21] National Council for Cement and Building Materials. 17th NCB International Conference Proceedings: Use of pharmaceutical liquid waste as an alternative fuel, N.S. Rao and Pankaj Kumar, My Home Industries Private Ltd. 2022. [Online]

[22] Bureau of Indian Standards. IS 16415:2015, Composite Cement - Specification. New Delhi, 2015. [Online]

[23] My Home Industries Private Limited. Sustainability, energy and operating performance records, FY 2024-25 and FY 2025-

[24] 26. Unpublished internal records.

[25] My Home Industries Private Limited and Captimise AB. Cement-kiln CCUS feasibility study and preliminary design basis. 2026. Unpublished work in progress.



[26] My Home Industries Private Limited. Mellacheruvu Cement Works: Factory and Machinery; official plant photographs and manufacturing profile. Accessed 19 August 2026. [Online]

[27] Railway Board, Government of India. Rake formed by a combination of tank containers loaded with bulk cement and normal containers loaded with bagged cement, circular dated 6 February 2025. [Online]

[28] India Shipping News. CONCOR introduces bulk cement movement in tank containers, boosting efficient and green logistics. [Online]

[29] Infrastructure Today. CONCOR plans entry into shipping pending approvals: interview with the Chairman and Managing Director. [Online]

[30] My Home Industries Private Limited. Environmental-clearance compliance report for expansion of Cement Plant Unit II, October 2016-March 2017; rail-siding and modal-movement status. [Online]

[31] Stockholm Environment Institute / LeadIT. India-Sweden projects pioneer a greener future for steel and cement in India. [Online]

[32] Leadership Group for Industry Transition. Advancing India's net-zero plans: new India-Sweden pioneering projects in steel and cement. [Online]

[33] Greenhouse Gas Protocol. Technical Guidance for Calculating Scope 3 Emissions, including Categories 4 and 9 transportation and distribution. [Online]

CONFERENCE & EXHIBITION ON
CARBON NEUTRALITY IN CEMENT AND CONCRETE
"Towards a Sustainable & Net Zero Future"
19-20 NOVEMBER 2026
Centenary Convention Centre, Hyderabad



LIMESTONE CALCINED CLAY CEMENT (LC³): CLAY ACTIVATION CHEMISTRY AND FLASH CALCINER PROCESS TECHNOLOGY

A Value-Creating Route to Lower-Carbon Cement Production

Ashok Kumar Dembla[1], Anurag Johari[1], Jens Briedenbach[2] Marc Feiss[2]

[1]Humboldt Wedag India Pvt. Ltd. · [2]KHD Humboldt Wedag GmbH, Cologne, Germany

ABSTRACT

Limestone calcined clay cement (LC³) has emerged as one of the most immediately deployable levers for reducing the carbon intensity of cement production. By substituting a significant fraction of clinker with thermally activated clay and ground limestone, producers can cut CO_2 emissions while drawing on raw materials that are abundant, low-cost, and widely distributed. This paper consolidates process engineering and technology-selection material developed for the calcination of clay as a supplementary cementitious material (SCM), covering the mineralogical basis of clay activation, the comparative merits of fluidised bed, rotary kiln, and flash calciner technologies, and the detailed process design of a flash calciner plant. Typical operating envelopes, fuel heat consumption, product colour control strategy, and indicative plant footprint are presented for production capacities from 250 to 2,000 t/d. The paper further reviews regulatory and market developments in India between 2023 and 2026 — including the introduction of IS 18189:2023 and the first commercial LC³ dispatches — before closing with a summary of the value proposition of calcined clay within a broader portfolio of decarbonisation technologies for the cement industry, in direct support of the sector's transition toward carbon neutrality.

Keywords: *LC³, limestone calcined clay cement, supplementary cementitious materials, clay calcination, flash calciner, kaolinite, clinker substitution, cement decarbonisation, net zero*

1. Introduction

Clinker production is the single largest source of process-related CO_2 emissions in the cement industry, arising both from the calcination of limestone and from the fuel required to reach clinkering temperatures. Reducing the clinker factor of cement — replacing part of the clinker with supplementary cementitious materials (SCMs) — is consequently one of the most direct and near-term routes to decarbonising cement production, and a central theme of the sector's net-zero transition.

Traditional SCMs such as blast furnace slag and fly ash are effective but geographically constrained: their availability is tied to steel and coal-fired power production, both of which are themselves in structural decline in many regions. Calcined clay, by contrast, can be produced from raw materials available in most parts of the world, including low-grade clays and quarry overburden that would otherwise be regarded as waste. This combination of wide availability, low sourcing cost, and low process CO_2 has made calcined clay — used in combination with limestone as LC³ — one of the most promising SCM routes for the next decade of cement decarbonisation.

This paper draws on two complementary bodies of engineering work: (i) the technology selection and detailed process design for clay calcination equipment, and (ii) the wider value proposition of LC³ within a portfolio of value-creating cement technologies. Together they provide both the technical basis and the strategic rationale for calcined clay adoption in support of a sustainable, net-zero cement industry.

2. LC³ in the Cement Decarbonisation Portfolio

Value in cement production is created through two related levers — reduction of production cost and reduction of CO_2 emissions — and the two are converging, as carbon cost increasingly drives production

economics. Within this context, several technology tracks are expected to contribute over different time horizons: maximising alternative fuel (AF) firing at low pre-processing cost is regarded as the first "low-hanging fruit"; composite cements incorporating calcined clay are expected to become dominant over the next three to ten years; smart-plant technologies using industrial IoT and AI are expected to leverage operational intelligence into cost reduction; and decarbonised kiln technologies (e.g. oxyfuel firing, hydrogen/oxygen burners) are expected to become essential from roughly five years onward.

Calcined clay sits firmly within the medium-term horizon of this roadmap. Because it is a pozzolanic material, calcined clay (metakaolin) can substitute for clinker in the same way as slag or fly ash, and because the calcination reaction itself does not release CO_2 (unlike limestone calcination in clinker production), the carbon intensity of calcined clay is substantially lower than that of clinker. Replacing up to 30% of clinker with calcined clay can correspondingly eliminate up to roughly 30% of cement-related CO_2 emissions, subject to site-specific factors governing the achievable substitution rate.

3. Mineralogical Basis of Clay Activation

3.1 Clay mineralogy

Clays are a group of hydrous aluminosilicate minerals, formed by the weathering of parent rock and available in most regions of the world. Of the clay minerals of major abundance — kaolinite, illite, and montmorillonite — kaolinite exhibits by far the highest potential for pozzolanic activity once thermally activated. Raw materials containing more than approximately 40% kaolinite are generally well suited to calcination for SCM production; deposits with lower kaolinite content than would be required for ceramic or paper-grade clay can still be suitable feedstock for cement-grade calcined clay, widening the pool of usable, previously unsourced clay pits.

3.2 Thermal activation (dehydroxylation)

Pozzolanic activity is realised through thermal activation of the clay, driving off structural water from the kaolinite lattice in the dehydroxylation reaction:

$$Al_2O_3{\cdot}2SiO_2{\cdot}2H_2O \text{ (kaolinite)} \rightarrow Al_2O_3{\cdot}2SiO_2 \text{ (metakaolinite)} + 2\ H_2O \text{ (evaporated)}$$

Reported optimum calcining temperatures span roughly 600–900 °C, with most process designs targeting 650–800 °C; the exact requirement depends on the mineralogical composition of the feed. Critically, dehydroxylation is a fast mineral transformation, complete in under one second, which permits compact, high-throughput calcination equipment such as flash calciners. The theoretical heat of formation for the reaction is, in turn, significantly lower than that required for clinker formation — typically under 100–200 kcal/kg versus several times that value for clinkerisation — which is the underlying reason calcined clay production is markedly less energy-intensive than clinker production.

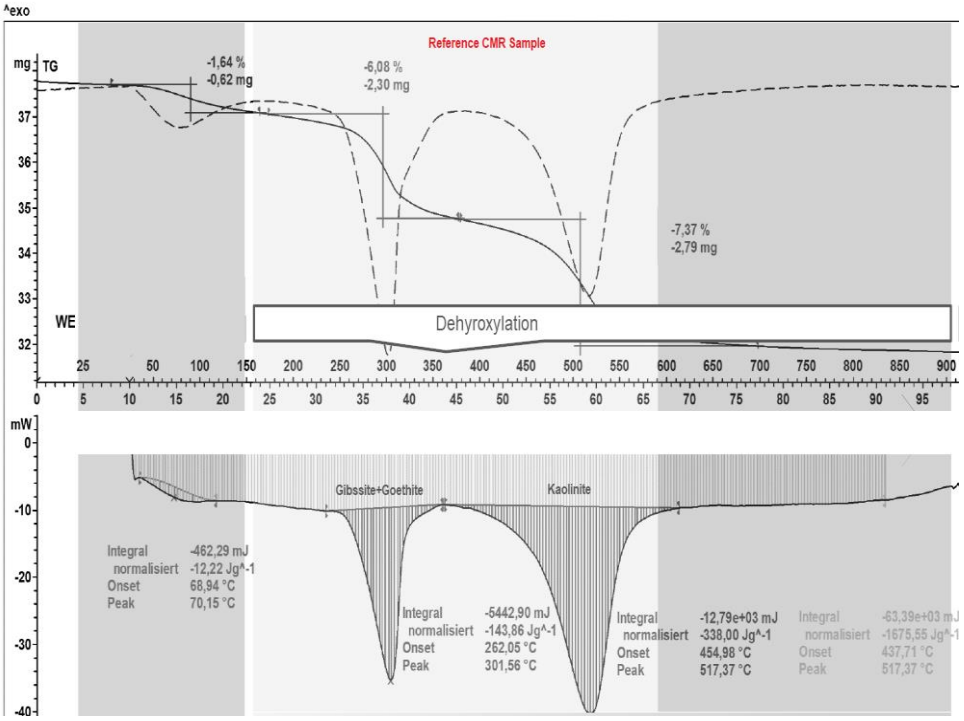


Figure 1. Example TGA/DSC characterisation of clay dehydroxylation, showing the enthalpy associated with the kaolinite-to-metakaolinite transformation (approximately 477 kJ/kg clay, or 565 kJ/kg on a calcined-clay basis, in the example data set).

3.3 Rationale for adoption

- Suitable clay is available in almost every region and can often be sourced from low-grade deposits or quarry overburden at low cost.
- Traditional SCMs (fly ash, slag) are of limited or no availability in many markets, whereas clay resources are comparatively ubiquitous.
- Specific thermal energy demand is less than half that required for clinker production.
- Calcined clay cement is a demonstrably "greener" product: the calcination reaction itself does not emit CO_2, and overall production is less energy-intensive.
- Incorporation of calcined clay can improve the workability and early strength of mortar and concrete relative to some alternative SCMs.

4. Calcination Technology Selection

Three calcination technologies are in industrial use for clay activation: fluidised bed calciners, rotary kilns, and flash (suspension) calciners. Each presents a distinct balance of thermal efficiency, product homogeneity, and operability.

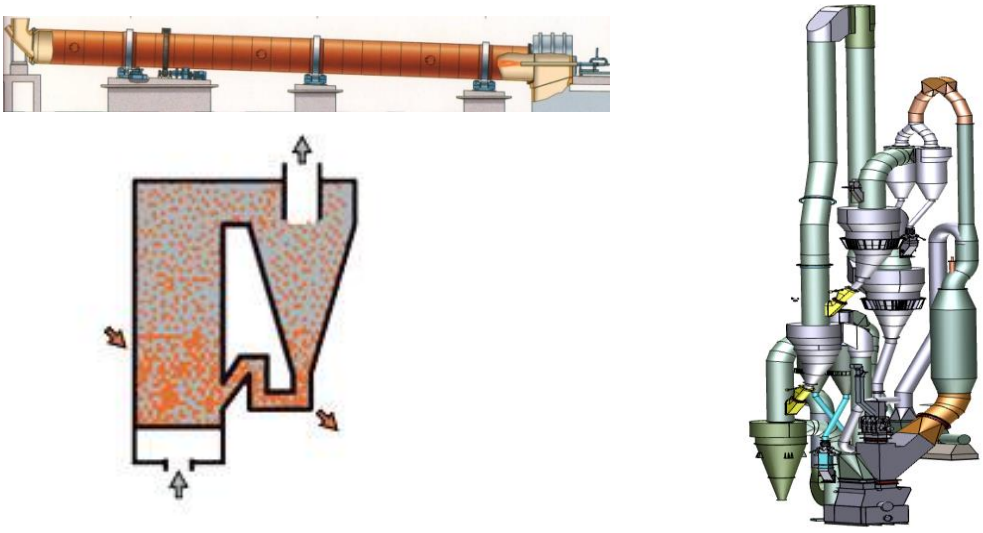


Figure 2. Schematic comparison of rotary kiln, fluidised bed and flash calciner configurations for clay calcination.

Table 1. Comparative characteristics of clay calcination technologies.

Technology	Thermal efficiency	Calcination homogeneity	Operability	Key limitation
Rotary kiln	Low	Inhomogeneous	Simple; existing units re-usable	Lower strength development limits clay addition rate
Fluidised bed	High	Homogeneous	Operationally sensitive	Problematic with decreasing feed particle size
Flash calciner	High	Homogeneous	Easy operation	Requires additional building height

Fluidised bed calciners achieve homogeneous calcination with high thermal efficiency, but operation becomes problematic as feed particle size decreases — a significant constraint given that fine grinding is often required to liberate kaolinite from the parent rock. Rotary kilns benefit from process familiarity (the equipment is closely related to clinkerisation kilns) and allow re-use of existing installations, which can lower capital cost for retrofit projects; however, the inherent temperature gradient along the kiln length produces inhomogeneous calcination, which in turn limits achievable strength development and constrains the permissible addition rate of calcined clay in the finished cement. Retrofitting an existing rotary kiln can nonetheless offer a lower-CAPEX option than new-build flash calcination where suitable idle kiln capacity exists; production capacities for rotary kiln routes typically span 250–2,000 t/d, at calcination temperatures of 650–900 °C and feed moisture up to 40 wt.%.

On the basis of this comparison, flash calciner technology has been selected as the preferred route for new clay calcination capacity, on account of its high energy efficiency, good and consistent quality control, low maintenance burden, easy operability, and reliance on proven components and unit operations already established across the wider cement equipment portfolio. Flash calcination is considered particularly well suited to greenfield projects, where the additional building height it requires

is not constrained by existing plant layout.

5. Flash Calciner Process Design

Flash calciner plant design draws on a long tradition of dry- and semi-wet-process clinkerisation plant engineering, including semi-wet clinkerisation units developed for raw materials of high moisture content. The clay calcination process is organised into three main sections: drying and comminution of the raw material, preheating and calcination, and recuperation and product cooling.

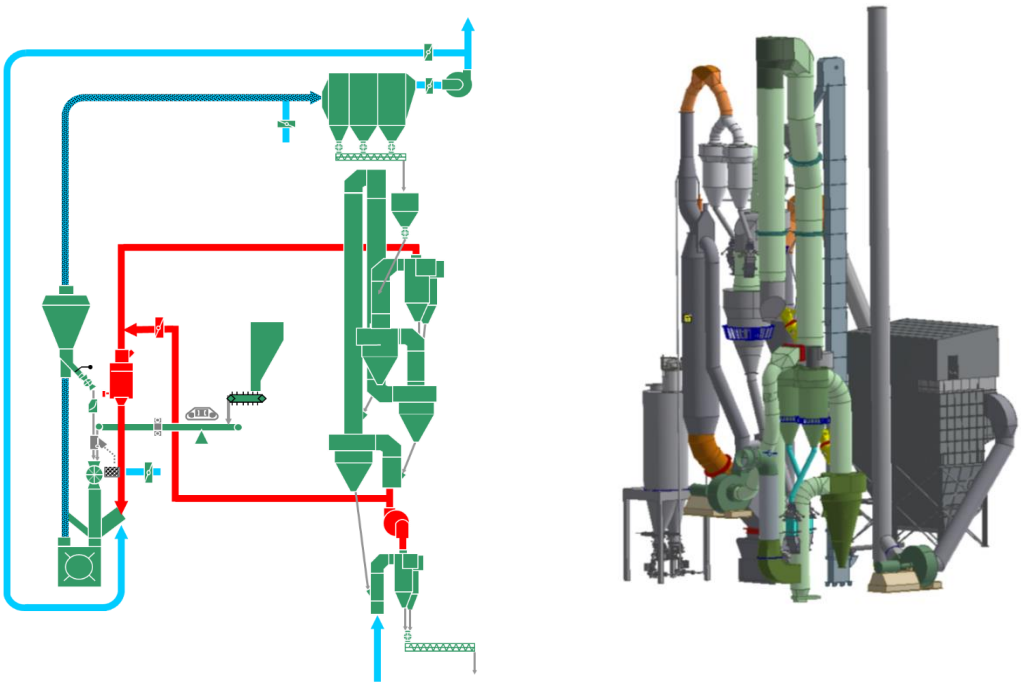


Figure 3. Process flow diagram of the flash calciner plant, showing the drying & comminution, preheating & calcination, and recuperation & product cooling sections.

5.1 Drying and comminution

Raw clay is fed to an impact hammer mill, where it is simultaneously comminuted to meal particle size and dried using hot gas recovered from the preheating and calcining section. A gas-suspension dryer reduces residual moisture to 1–3%, and a static separator (type LS) controls the fineness of the raw meal, typically targeting approximately 30% retained on a 90 µm sieve, via adjustable guide vanes and a two-stage classification path. Fines are routed to direct dedusting and transport to the feed bin. This arrangement is deliberately flexible with respect to feed moisture, and where raw material moisture exceeds roughly 20 wt.%, a dedicated clay dryer can be included ahead of the mill.

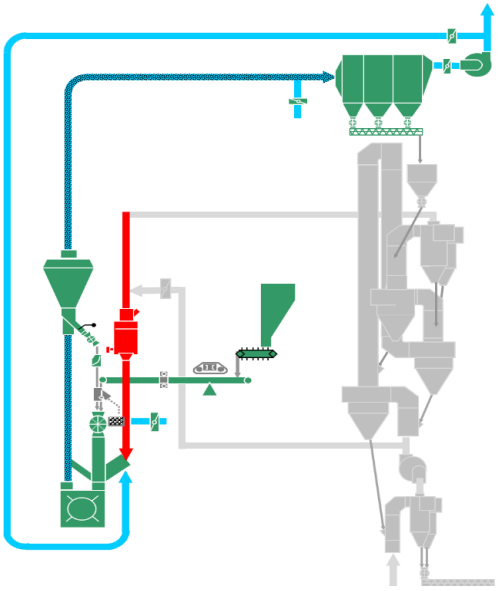
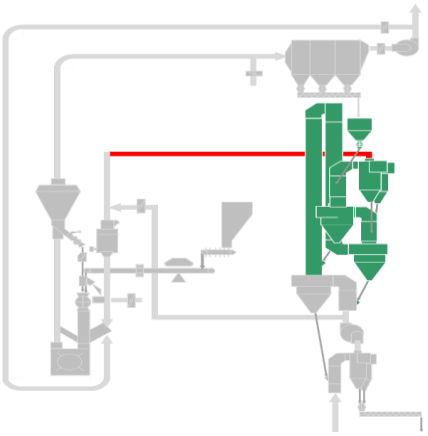


Figure 3a. Process flow diagram showing the drying & comminution

5.2 Preheating and calcination



Dried meal is dosed continuously from the feed bin into a multi-stage (typically three-stage) preheater. Residual moisture is removed in the top preheater stage, and the meal is progressively preheated by hot gas rising from the calcination section before being routed, from an intermediate cyclone stage, into the calciner itself. Fuel is combusted in preheated combustion air, and the clay is thermally activated at the required temperature — typically 650–900 °C — under low excess air. Calcination is deliberately carried out under a reducing atmosphere to control the colour of the finished product (see Section 5.4). Hot meal is separated from the combustion gas in the lowest cyclone stage before proceeding to cooling.

Figure 3b. Process flow diagram showing the preheating & calcination

5.3 Recuperation and product cooling

Activated product meal is routed to a combustion-air preheater (CA PH) and subsequently to a multi-stage product cooler. Combustion air is preheated in a riser duct feeding the CA PH cyclones and the cooling-air cyclone, recovering process heat that would otherwise be lost. Cooler waste gas is partially routed back to the impact hammer mill and CA PH, further improving overall thermal recuperation. The number of cooling cyclones can be adjusted to meet the required product handling temperature, allowing the cooling train to be tailored to downstream storage and transport requirements. Rapid quenching of the calcined material immediately following calcination also plays a role in stabilising product colour.

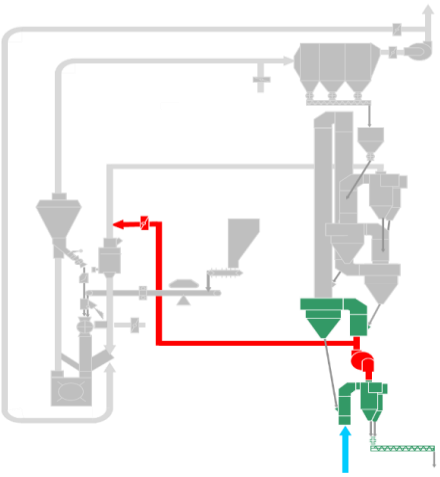


Figure 3b. Process flow diagram showing the recuperation & product cooling

5.4 Product colour control

Product colour is a critical quality attribute for calcined clay, since iron compounds present in the raw clay (principally hematite, Fe_2O_3, and goethite, FeO(OH)) can impart an undesirable reddish-brown colouration if oxidised during calcination. To prevent this, the calciner is operated with a low excess air amount, creating a reducing atmosphere above roughly 650 °C that converts iron oxides toward magnetite (Fe_3O_4) rather than hematite, giving the product a more neutral grey colour comparable to Portland cement clinker. The combustion atmosphere is readily controlled via the main dedusting fan, and no additional fuel injection is required specifically for colour control. Carbon monoxide generated under the reducing calcination conditions is subsequently post-combusted in a hot gas generator, upstream of the impact hammer mill, at close to 0% O_2, avoiding the emission of unburned CO while still preserving the reducing conditions at the point of calcination. Depending on the total iron content of the feed, a multi-stage calcination sequence may be required to fully stabilise product colour.



Figure 4. Effect of oxidising versus reducing burning conditions on iron-oxide speciation (hematite vs. magnetite) and resulting product colour.

5.5 Typical process and operating conditions

Parameter	Typical range
Production rate	250 – 2,000 t/d
Calcination temperature	600 – 900 °C (typ. 650 – 800 °C)
Feed moisture (raw clay)	up to 30 – 40 wt.%
Fuel heat consumption	390 – 670 kcal/kg calcined clay
Theoretical heat of formation	< 100 – 200 kcal/kg (vs. ~380–420 kcal/kg for clinker)
Dehydroxylation reaction time	< 1 s
Suitable fuels	Solid, liquid or gaseous

Table 2. Typical process and operating parameters for flash-calciner clay activation plants.

Fuel heat consumption depends strongly on raw material moisture and throughput. For an indicative 720 t/d case at 30% feed moisture, total fuel heat consumption of approximately 655–670 kcal/kg has been reported; for a smaller 260 t/d case at 12% feed moisture, consumption falls to approximately 390 kcal/kg, reflecting the reduced drying duty. In both cases, the great majority of fuel heat is consumed in drying and calcination, with a smaller share attributable to recuperation losses and radiation.

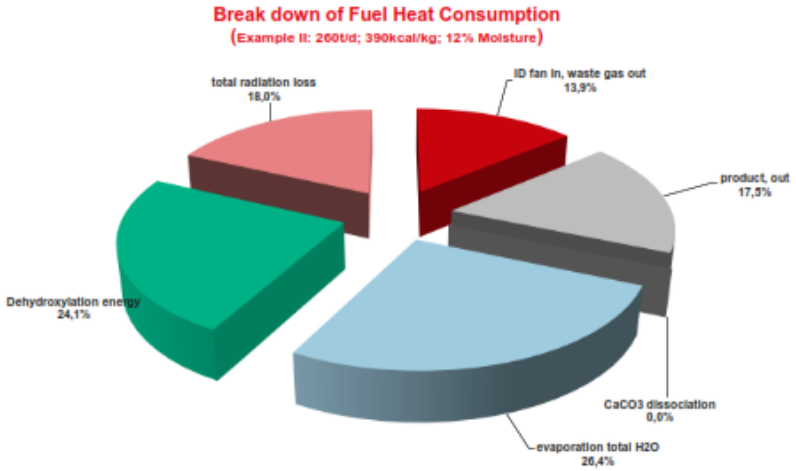


Figure 5. Indicative breakdown of fuel heat consumption for a flash calciner case (900 t/d, ~410 kcal/kg, 10% feed moisture).

5.6 Plant footprint

Because the flash calciner process relies on a vertical, multi-stage preheater and cooling train, plant footprint is compact relative to throughput, though building height is correspondingly greater than for a rotary-kiln retrofit. For a 900 t/d plant, the overall footprint is approximately 22 m by 15 m, with characteristic tower heights around 40 m for the principal process sections.

Table 3. Indicative plant footprint for a 900 t/d flash calciner installation.

Dimension	Example I: 900 t/d
Footprint (plan)	22 m × 15 m
Building height	≈ 40 m (plant)

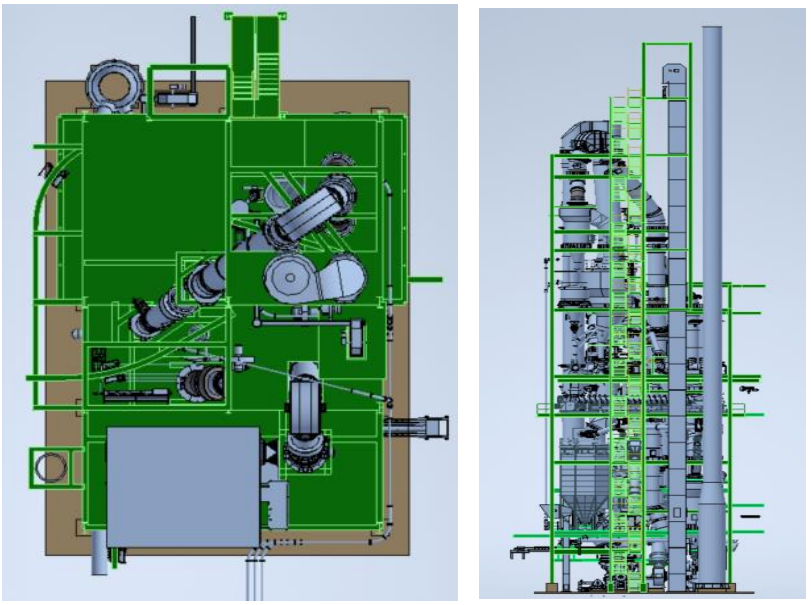


Figure 6. Indicative plant layout (plan, left) and elevation (right) for a 900 t/d flash calciner installation.



6. LC³ Cement: Standardisation and Benefits

The commercial adoption of LC³ has been supported by the progressive introduction of national and regional cement standards recognising limestone calcined clay cement as a distinct, standardised product — including, among others, Cuban standard NC 95:2011 and Indian standard IS 16415:2015 — which allow LC³ to be specified and used with the same regulatory confidence as conventional composite cements.

The benefits of clay calcination for cement production can be summarised as follows:

- Lower carbon emissions: the clay calcination reaction itself does not release CO_2, in contrast to the calcination of limestone in clinker production and can displace a substantial share of clinker in the finished cement.
- Lower fuel and heat consumption per tonne of SCM produced, relative to the specific energy required for clinker manufacture.
- A lower-cost, environmentally responsible replacement for clinker, drawing on raw materials that are widely available and inexpensive to source.
- Compatibility with proven, reliable plant components already established across the cement equipment portfolio, supporting straightforward integration into both greenfield and brownfield projects.

7. Regulatory and Market Developments (2023–2026)

IS 18189:2023. The Bureau of Indian Standards issued a dedicated Indian Standard for Portland Calcined Clay Limestone Cement, giving LC³ the same formal standing as OPC, PPC, and PSC and clearing the main regulatory hurdle to commercial sale and specification in public procurement and construction contracts.

First commercial production. A cement producer in the northern part of India has become one of the first companies in India — and reportedly in Asia — to commercially produce LC³ under IS 18189:2023, with an initial trial mix of roughly 50% clinker, 32% calcined clay, 12% non-commercial-grade limestone, and 6% gypsum at its plant in Rajasthan. A flagship application has been cement supply for the Airport project. Company-reported pilot data suggests CO_2 savings in the region of 35% relative to OPC for that project, alongside coal-usage reductions.

Wider industry uptake. By early 2026, at least two commercial cement producers in India have produced LC³, with early commercial volumes in the low thousands of tonnes — a signal of a technology moving from pilot to early commercial scale rather than one that has yet reached mass-market volumes.

Real-estate demand-side pull. Some of the real estate developers have also piloted LC³ in commercial construction in the western part of India through partnerships with research bodies, building a demand-side case study alongside the supply-side manufacturing developments.

Carbon policy. India's Greenhouse Gases Emission Intensity Target Rules 2025, notified under the Carbon Credit Trading Scheme (CCTS), set facility-level emission-intensity baselines and targets for 186 cement facilities for 2026 and 2027, with a credit-and-penalty mechanism. This creates a direct financial incentive for producers to lower clinker factors — precisely the lever LC³ pulls hardest. LC³'s reported inclusion in India's emerging carbon-credit and offset mechanisms for the construction sector further strengthens its investment case.

National roadmap. NITI Aayog's cement-sector decarbonisation roadmap and the GCCA India–TERI industry roadmap both frame clinker-factor reduction, alongside energy efficiency and grid decarbonisation, as the near-term levers for the sector's stated 2070 net-zero goal, with India's average

clinker factor (around 0.75 as of 2020) still notably above the global average of roughly 0.63.

8. Challenges to Scale-Up

Despite a favourable resource and policy backdrop, several constraints will govern the pace of LC³ adoption:

- *Raw material characterisation*. Systematic mapping of India's clay reserves by kaolinite content and reactivity is still incomplete; not all clays perform equally, and non-kaolinitic or multi-mineral clays require mix-design optimisation, an active area of ongoing research.
- *Capital investment in calcination*. While retrofits are comparatively modest next to a new clinker line, they still require dedicated calciner capacity, fuel supply, and quality-control systems that smaller and mid-sized producers may be slower to fund than large integrated players.
- *Admixture compatibility*. Chemical admixtures optimised for OPC and PPC do not always perform identically in LC³ systems; formulation of LC³-specific admixtures remains an active area of applied research.
- *Market and specifier familiarity*. Architects, structural consultants, and public-works departments have decades of experience specifying OPC, PPC, and PSC; building confidence and updating specification codes for a new standard cement type takes time, even where the underlying standard (IS 18189:2023) already exists.
- *Public procurement signal*. Because a large share of Indian cement demand flows through government infrastructure and housing programmes, explicit LC³ specification in public tenders would likely be the single fastest lever to shift volumes and remains a work in progress based on industry commentary.

9. Outlook

Three trends point toward calcined clay's expanding role over the remainder of the decade:

- *A widening resource gap*. As cement capacity climbs toward roughly 850 MTPA by 2030 while fly ash utilisation is already near saturation and slag output is capped by steel volumes, LC³'s largely unconstrained raw material base becomes progressively more valuable in absolute, not just relative, terms.
- *Tightening carbon economics*. The phased rollout of facility-level emission-intensity targets under the CCTS, alongside rising global and domestic scrutiny of embodied carbon in construction, raises the cost of staying clinker-intensive and improves the relative economics of ternary blends like LC³.
- *Proof points moving from pilot to commercial*. The shift from IIT Delhi–led pilot studies to IS-standard commercial dispatch by a listed cement major, paired with early real estate-sector demand pull, suggests the technology is crossing from demonstration into early commercial deployment, though volumes remain small relative to total blended-cement output as of 2026.

Calcined clay is unlikely to displace fly ash- and slag-based cements outright in the near term — both retain cost and performance advantages in the regions where their feedstocks are abundant. The more probable trajectory is a diversifying blended-cement portfolio, in which LC³ becomes the primary growth vector for further clinker-factor reduction precisely because it is the one major SCM whose supply the cement industry can expand on its own terms, supported by an increasingly mature global base of calcination technology suppliers.

10. Conclusions

Calcined clay, deployed as part of limestone calcined clay cement (LC³), offers a technically mature

and immediately deployable route to reducing the carbon intensity of cement production. The underlying mineralogy — dehydroxylation of kaolinite-bearing clays at 600–900 °C — is well understood, fast-reacting, and compatible with a range of calcination technologies. Among the available technologies, flash calcination offers the best overall combination of thermal efficiency, product quality, and operability for new capacity, while rotary kiln retrofits remain a valid lower-CAPEX option where suitable existing infrastructure is available. Careful control of the calcination atmosphere allows product colour to be managed without additional fuel input, and typical fuel heat consumption of 390–670 kcal/kg compares favourably with the energy demand of clinker production. As national standards for LC³ continue to be adopted and refined, calcined clay is positioned to become a dominant composite-cement route over the coming decade, complementing alternative-fuel firing, smart-plant optimisation, and, longer term, decarbonised kiln technologies in the broader transition toward a sustainable, net-zero cement industry.

References

[1] Bureau of Indian Standards, IS 18189:2023 — Portland Calcined Clay Limestone Cement.

[2] RMI / RMI India Foundation, "Unleashing the Potential of Limestone Calcined Clay Cement (LC3)."

[3] Lodha Group / Net Zero Urban Accelerator, "Creating and Sustaining Market for LC3 in India."

[4] International Climate Initiative (IKI), "Cementing the Future: Scaling Low-Carbon Cement in India."

[5] CemNet, "JK Lakshmi Cement prepares for calcined clay cement production."

[6] Outlook Business, "JK Lakshmi Cement Launches Eco-Friendly Limestone Calcined Clay Cement."

[7] Chemistry World, "Accelerating decarbonisation for India's cement industry."

[8] NBMCW, "From Grey to Green: The Journey Towards Decarbonizing India's Cement Industry."

[9] IBEF, "Indian Cement Industry Analysis."

[10] Cement Manufacturers' Association (CMA) India, "The Cement Industry: Largest Consumer of Fly Ash" and "Green Growth Initiatives."

[11] Arthur D. Little, "Green cement: Next frontier for Indian cement industry."

[12] Ministry of Railways / NTPC, National Conference on Fly Ash Utilisation (2025).

[13] NITI Aayog, "Roadmap for Cement Sector Decarbonisation" (2026).

[14] KHD Humboldt Wedag, "Clay Calcination" and "Cement beyond Carbon" (technology pages).

[15] KHD Humboldt Wedag, project announcement — clay calcination plant for Ciments de l'Afrique (CIMAF), Burkina Faso.

[16] Indian Cement Review, "JK Lakshmi Cement ties up with TARA to integrate calcined clay tech."

Note: This paper synthesises publicly reported industry, policy, and research developments as of July 2026. Figures such as capacity, production volumes, and commercial rollout status are evolving rapidly and should be verified against the latest company and government disclosures before use in investment or policy decisions.

EVALUATION OF WASTE-DERIVED FUEL UTILISATION IN AN INDIAN CEMENT PLANT

Kaustubh Phadke[1*], Luckman Muhmood[2]

[1]Research Scholar, Department of Mechanical Engineering, *K J Somaiya School of Engineering, Somaiya Vidyavihar University, Mumbai, Maharashtra 400077, India*

[2]Professor, Department of Mechanical Engineering, *K J Somaiya School of Engineering, Somaiya Vidyavihar University, Mumbai, Maharashtra 400077, India*

[*] kaustubh.Phadke@somaiya.edu

ABSTRACT

The Indian cement sector is the second-highest global producer and is expected to grow 2.5 to 5 times by 2050 from 453 million tons/year (2025). It is the most energy-efficient among other countries and is a progressive sector in finding ways to reduce its emission footprint. The calcination process in cement manufacturing generates CO_2 emissions and requires a substantial amount of fossil fuel (coal or pet coke) to heat limestone to 1,400 degrees Celsius, resulting in higher CO_2 emissions per ton of cement (Process and fuel emissions).

The fuel can be replaced with the Segregated Non-Recyclable Combustible Fraction of the Municipal Solid Waste as an alternative fuel, also known as Refuse Derived Fuel (RDF). The thermal Substitution Rate in the Indian cement industry is between 6% and 7%, and there is an enormous potential to harness alternative fuels, as other countries have achieved more than 50% thermal substitution.

This paper identifies the opportunities and barriers for scaling AFR in the Indian Cement Industry through a literature review. The study also evaluates the combustion characteristics of various waste fuel types to find the best fuel source to use as an alternative fuel. Through the study, it identifies that high CAPEX, weak policy incentives, Cost economics, and quality issues are the main barriers. At the plant, it was found that Britannia Plastic Waste had the highest calorific value, while the waste solid mix had the lowest calorific value. Britannia Plastic Waste and Carbon Powder are identified as the best fuel substitutes and are identified as the next steps for this study. The paper also highlights the next steps for the project.

Key Words: Refuse Derived Fuel (RDF), Municipal Solid Waste (MSW), Cement, net-zero, Circular Economy, CO_2

1.0 Introduction

Introduction to the Cement Industry

India is the world's second-largest manufacturer of cement. The installed capacity of the Indian cement industry is 700 million tonnes, whereas cement production was 453 million tonnes in 2024-25 (Cement Manufacturers Association, CMA Dashboard). There has been immense growth in the Indian cement sector as it is a primary building material. Meeting its energy needs is a significant concern because it is an energy-intensive sector (IBM Indian Minerals Book 2014). The energy consumed by the cement industry accounts for around 2% of global energy consumption (V. K. et al., Cleaner Production Journal, 2020), while the carbon dioxide (CO2) emissions from the calcination process account for 5% of global emissions (GCCA India Blended Cement Report 2022). The Cement & Concrete industry contributes to approximately 7% of global anthropogenic emissions.

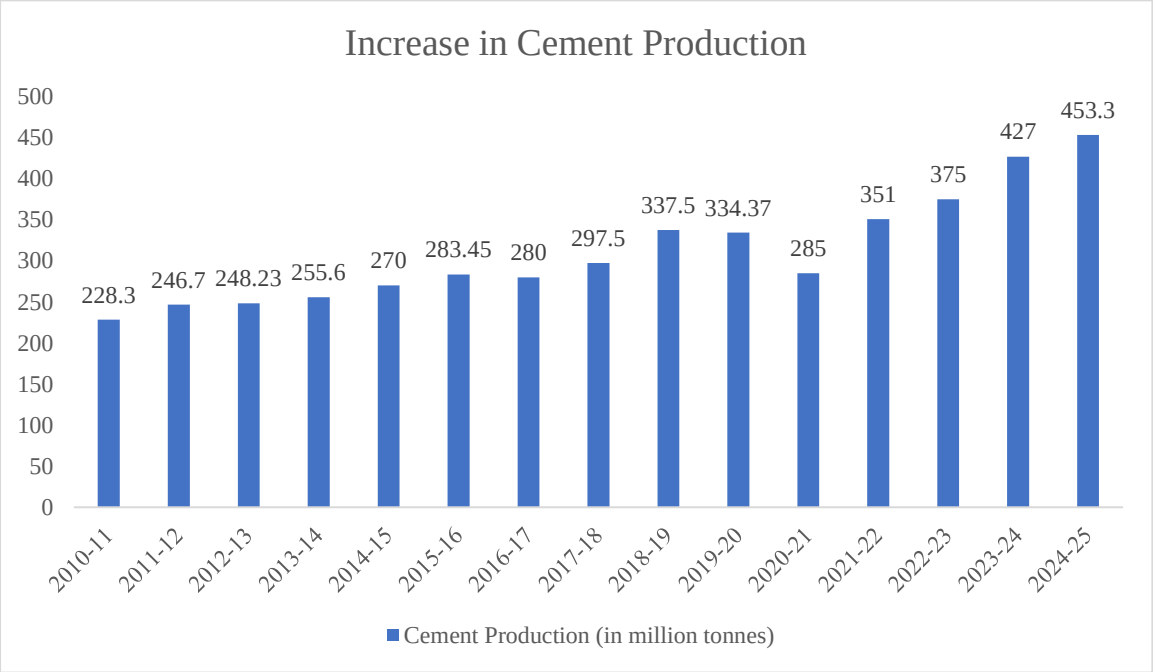


Figure 1: Cement Production in million tons/year in India

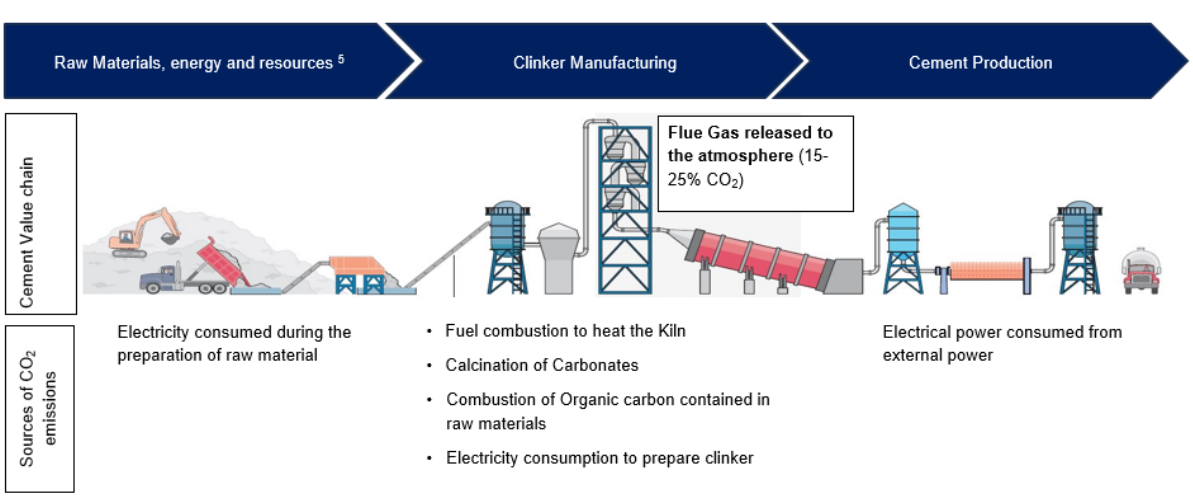


Figure 2: Cement manufacturing process

Current Energy Sources for Clinker Manufacturing

Clinker manufacturing is an energy-intensive process that primarily relies on thermal energy, traditionally derived from coal, pet coke, biomass and alternative fuels. In India, the cement sector consumes approximately 9.29 million tonnes of coal annually. Coal and pet coke currently supply over 94% of the thermal energy requirements in clinker manufacturing, contributing heavily to CO_2 emissions (GCCA India-TERI 2025). The fuel can be replaced with the Segregated Non-Recyclable Combustible Fraction of the Municipal Solid Waste as an alternative fuel, also known as Refuse Derived Fuel (RDF). Despite Indian cement industries' prominent improvements in energy efficiency, the lower percentage of alternative fuel use in cement manufacturing remains a major area of concern (International Cement Review, RDF utilisation in India, 2017).

Municipal Solid Waste Dynamics and RDF Potential

As in many other nations, effective Municipal Solid Waste (MSW) management and disposal have already become a major challenge. As India progresses in economic development, the quantum of MSW generation is expected to increase significantly from 62 million tons per annum to 165 million tons by 2031 (MoHUA, Guidelines for MSW, 2016) due to the country's fast urbanisation and rising per capita income.

Global solid waste production is anticipated to rise from 2.01 billion tons to 3.14 billion tons by 2050. In India, landfills are used to dispose of 91% of all waste.

Table 1: Generation and Disposal of MSW Generated in India

Annual MSW Generated in India	62 MT (2016)
Projected MSW generation in India	165 (2031)
Percentage of MSW collected in India	70%
Biologically or Thermally Processed in India	22-28%
Disposed in open dumps/landfills in India	More than 90% (required approx. 1240 acres of land)

Although the Government of India's Swachh Bharat Mission had set a target of scientific management of the entire MSW generated by 2nd October 2019, a high percentage of MSW, including the non-recyclable combustible fraction, ends up in landfills, making the goal unachievable. As per the Solid Waste Management (SWM) Rules 2016, industrial units are mandated to replace at least 5% of their fuel requirement with RDF. A few cement companies in India are already successfully using RDF as a substitute for fossil fuel. However, an enabling ecosystem needs to be built up to address the standardisation of RDF quality, appropriate price structure, higher transportation costs, and standard documents for enhanced use of RDF by industries.

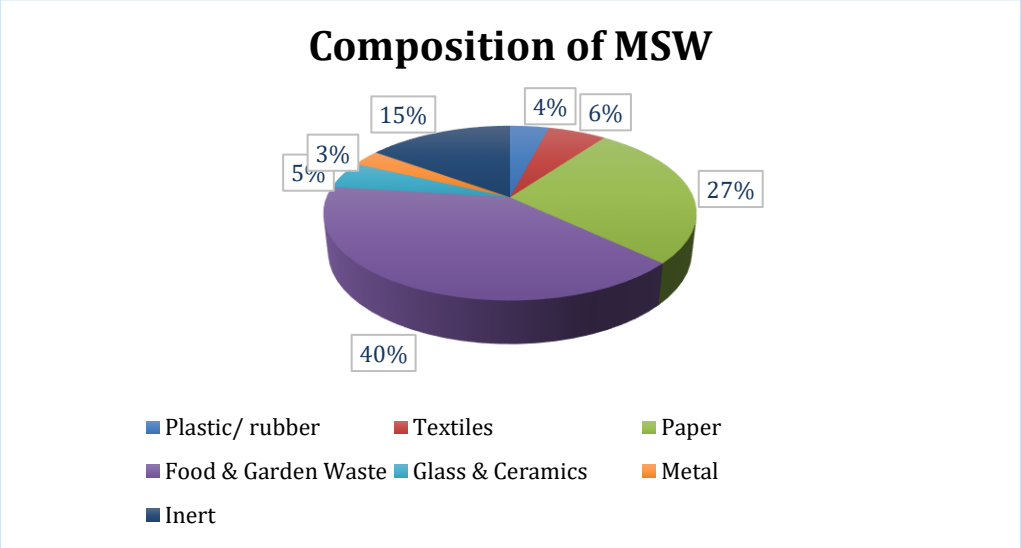


Figure 3: Composition of MSW (Yadav P, and Samaddar S, 2014)

MSW Composition in India

MSW comprises recyclable organics, inert materials, paper, plastics, leather, textiles, glass, household hazardous materials, and metals. Inert waste includes waste that is chemically and biologically unreactive. Examples of inert waste include concrete and sand waste, wood, bricks, etc. (Yadav P and Samaddar S, 2014).

RDF and its utilisation techniques

RDF comprises materials including rubber, leather, cloth, paper, and plastic. The basic idea of RDF production is to separate high-quality fuel fractions from trash, mainly by removing recyclable materials like glass and metal, transforming the raw waste into a more usable fuel with uniform particle size and a better calorific value than raw MSW. The fuel's intended use determines the necessary RDF quality. One of the processes of deriving RDF from MSW is described in Figure 4 (Salaripoor H et al. 2025).

Pre-processing & utilisation techniques

At the solid waste management facility, the following procedures produce RDF:

- **Screening and Separation**: Multi-deck vibrating screens are used on the site to treat old MSW that has been dumped. Mixed MSW is separated using an OREX (organic extrusion press), with the dry fraction going to the RDF line, which includes a magnetic separator, flip flow screen, and wind sifter, and the organic fraction going into the fermenter (composting drums).
- **Fractionation and use**: The -30mm portion is sent to make compost, while the +30mm fraction is used to produce RDF.
- **Sorting lines for shredding materials**: separation of recyclables, organic/inert fraction, and flammable fraction.
- **Mechanical biological treatment**: the creation of SRF/RDF linked to mechanisation or compost production. Drying (thermal or biological) is essential for producing alternative fuels that cement plants can use.
- **Supply to Cement Companies:** RDF is bagged and transferred to the cement mill with a size of less than 25mm (two dimensions). It is baled at the factory and transported mechanically or pneumatically before being burned in the calciner or burner.

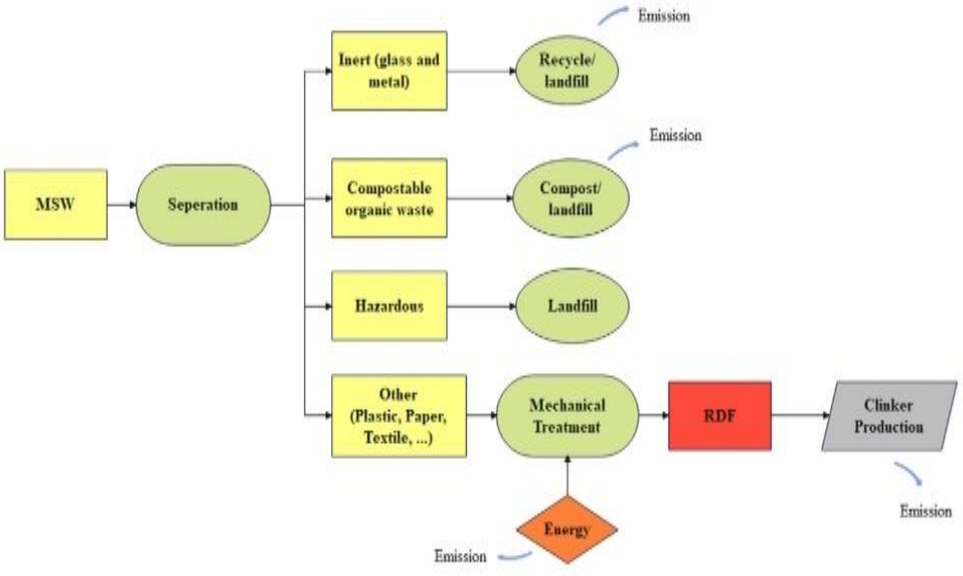


Figure 4: RDF Deriving Technologies

Depending on the kind of collection, pre-processing, and makeup of the waste source, a different amount of RDF can be produced per tonne of MSW. RDF yield from mixed MSW is typically in the 20–30% range, but if the material is correctly segregated, 80–90% yield can be attained.

It is further processed in the densification unit to create RDF pellets, depending on the end user's needs. Finding a long-term sustainable solution for efficiently managing municipal garbage, on the one hand, and minimising the use of coal in the production of cement, on the other, this option represents a win-win situation.

Characterisation of RDF

In Indian cement factories, RDF is used as an alternative fuel (AF) to fossil fuels like pet coke or coal and typically replaces up to 3%-5% of fossil fuels, whereas in Europe some plants exceed 80% or run entirely on RDF (International Cement Review, RDF utilisation in India, 2017). The reason is the quality of RDF; high levels of moisture, chloride/chlorine, and heavy metal content are unacceptable.

Moisture: Increases energy consumption and can limit the cement kiln's ability to produce clinker if the pre-heater fan capacity is restricted.

Chloride concentrations: Cause pre-heater buildup and clinker degradation, leading to production loss and kiln shutdowns unless mitigated by gas bypass systems

Heavy metal content: To protect clinker quality, high heavy metal content in RDF will limit its use to

Table 2: Raw MSW & RDF characteristics (MoHUA Guidelines 2016)

Parameter	Unit	Raw MSW	RDF
Yield of RDF	%	100	10-15
Calorific Value	Kcal/kg	1500-2000	3000
Moisture Content	%	40-45	<20
Chlorine Content	%	1-2	<0.7
Ash Content	%	20-40	<25
Bulk Density	t/m3	0.5	0.1-0.2
Particle Size	Mm	Up to 1000	2D <120 mm 3D< 70 mm

low TSR levels ().

Objective of the Study

To identify the opportunities and barriers for scaling AFR in the Indian Cement Industry through a literature review. The study also evaluates the combustion characteristics of various waste fuel types to find the best fuel source to use as an alternative fuel.

2.0 Experimental work

Potential and barriers to scaling TSR in Indian Cement Kilns

Barriers

High Capex and Weak Policy Incentives: The initial cost to set up the plant, along with the policy implications, is a significant obstacle in setting up the AFR plants. The lack of strict carbon emission rules and the lack of initiative taken by the waste producers to pay the gate fees are resulting in the potential utilisation of AFR being below.

Cost economics are not favourable for industries, as they need to add pre-processing facilities. Grants and initiatives from the Government can push the cement industries to install pre-processing facilities for processing the MSW into RDF pellets.

Quality issues: Inconsistent supply and quality lead to lower TSR in the cement kiln. If quality is maintained, a high level of TSR can be achieved.

Opportunity

Increased waste dumped at MSW landfill sites: The increase in MSW waste being dumped at the landfills can easily be tackled by transforming it into AFR technologies. Instead of landfill sites, these sites have become dumping grounds. The MSW can be segregated and sent to the processing facilities for ease of RDF generation.

Decarbonization of cement, a hard-to-abate sector: The cement industry is responsible for approximately 7% of the global anthropogenic CO_2 emissions. With the use of AFR technologies, emission levels can be reduced to a great extent. (GCCA India, Blended Cement report, 2022).

RDF is bagged and transferred to the cement mill with a size of less than 25mm (two dimensions). It is baled at the factory and transported mechanically or pneumatically before being burned in the calciner or burner. Depending on the quality of the RDF, reasonably high TSR percentages of AF can be used.

At the Cement plant

About the cement plant

The Cement plant 'A' is located in Tamil Nadu near Coimbatore. It is an integrated cement plant.

Currently, the plant operates with a dry process of cement manufacturing, with a capacity of 1.4 million tons of cement per year (0.5 million tons of clinker manufacturing capacity). The plant is currently running at 1600 TPD and exclusively manufactures Pozzolana Portland Cement (PPC).

The primary fuel used at the plant is pet coke and coal. The plant has excellent rail and road connectivity; the nearby towns are Salem and Erode. The primary raw material, Limestone, is sourced from the nearby open mines owned by Plant A. The limestone is transported by large-capacity trucks (> 20 Tons capacity) by road. The yellow limestone, which has a higher CaCO3 content, is also obtained from a nearby open mine.

The plant is spread over approx. 335 Acres of land, which consists of

- The main integrated cement production facilities
- Limestone storage and crushing units
- Clinker production and grinding sections
- Internal roads and green belt development
- Administrative buildings and housing colony

Cement manufacturing at the plant

The length of the Kiln is 47 meters, with a diameter at the inlet of 3.8 m and reducing to 3.2 m at a slope of 3.5%. This gradient ensures that kiln feed moves steadily from the inlet (pre-heater side) to the outlet (clinker cooler side). The kiln rotates at 2.5 to 4 RPM. The slow rotation allows the raw meal to stay longer in the kiln for complete chemical transformation into clinker. The highest temperature attained in the kiln is 1400 0C. The outlet is connected to the Electrostatic Precipitator (ESP).

The entire cement manufacturing facility, including the AF feed mechanism, cement ball mills, cement bag packaging, etc., was visited with cement plant officials.

The process flow diagram of Cement manufacturing is given in the following Figure 5.

The Plant Head provided complete support to conduct the plant visit, provided the necessary information and coordinated the visit.

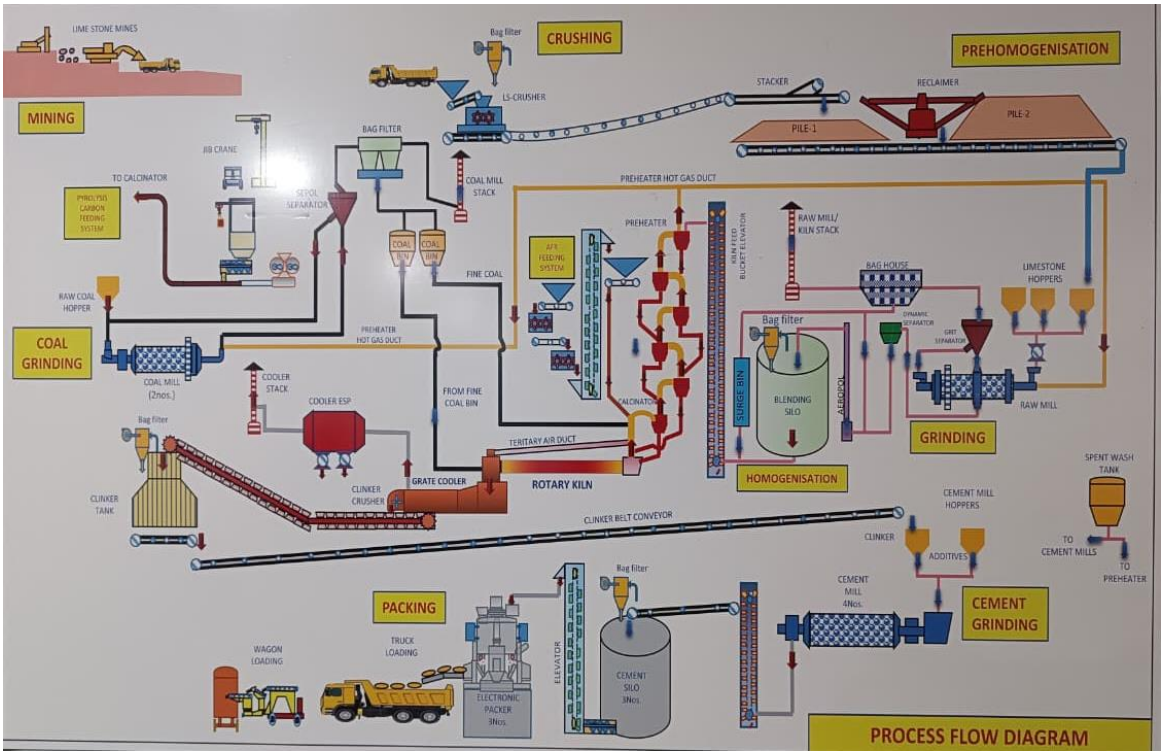


Figure 5: Plant A- Flow Diagram

Alternative Fuel (AF) utilisation at the plant

- The plant is currently using alternative fuel, substituting more than 16% of primary fuel (pet coke)
- The AF used are wooden chips, black carbon (tyre industry waste), RDF component of Municipal Solid Waste (MSW), industrial waste (having calorific value more than 2500 Kcal/kg), bio sludge, lime sludge from the nearby paper industry, and spent wash from the distillery.
- For use as an AF, the minimum Gross Calorific Value of waste required by the plant is 2500 Kcal/kg
- The pet coke consumption is approximately 120 tons/day, whose GCV is 8300 Kcal/kg
- The current alternative fuel consumption is approximately 50 tons/day, whose GCV is 3500 Kcal/kg with a moisture content of 20%. The chloride and heavy metal concentrations are currently not measured.
- Feeding AF:
    - The AFR feeding process is semi-automatic. There are two shredders for the MSW and other solid materials. The first shredder reduces the AF size to 80 to 90 mm, followed by the second shredder, which reduces the AF size to 25 to 30 mm.
    - The shredded material is fed at the pre-calciner level and mixes with the cooler exhaust gases, along with the pet coke and the black carbon.



- Based on the supply of spent wash, it is also fed before the AF in the pre-calciner
- The waste provides heat and then moves from one to six-stage pre-heaters where it is mixed with the raw meal at 150 ^{0}C.
- The temperature at the six stages increases gradually

- Stage 1: 100 ^{0}C – 150 ^{0}C (Raw meal is introduced)
- Stage 2: 200 ^{0}C – 250 ^{0}C
- Stage 3: 350 ^{0}C – 500 ^{0}C
- Stage 4: 650 ^{0}C – 700 ^{0}C
- Stage 5: 800 ^{0}C – 850 ^{0}C
- Stage 6: 950 ^{0}C – 1000 ^{0}C
  - The exhaust of the ID fan is supplied to the coal mill (grinding) and the raw meal grinding
- The laboratory conducts basic tests like calorific value and the moisture content, but the chloride and the heavy metal concentrations are not calculated for the AF
- The industrial waste (such as bio-sludge and lime sludge) is mixed with the raw limestone at the crusher before it is transported by stacker into different piles and later reclaimed and fed to limestone hoppers
- The plant is operated from the Central Control Room (CCR) around the clock, and the cement manufacturing process, including AFR feed, is monitored and controlled by the process engineers.
- Adequate supply of RDF sourced from the MSW can be obtained from the nearby towns. In fact, the municipal councils are supplying the RDF to the plant free of cost.
- The plant has a plan to increase the AFR utilisation to 30% and has made a capex of INR 1.2 for the AFR facility augmentation

3.0. Results and Discussions

The following table shows the different types of RDFs used at Plant 'A' and a comparison of their characteristics (Gross Calorific Value, Ash Content and heavy Metal Risk)

Table 3: Waste Characterisation of different Alternative Fuels used at Cement Plant

Sl	Waste Stream	Gross CV (kcal/kg)	Ash Content (%)	Heavy Metal Risk	Remark
1	Britannia Plastic Waste (Unshrouded)	6845	1.70	Low (limited data, Cl 0.53%)	Highest energy, very low ash, excellent fuel substitute
2	Carbon Powder – 1	6154	18.15	Medium (ZnO 26.92%, As 0.19 mg/kg)	Very high CV, but moderate ash and Zn presence
3	Tape Roll	5170	4.55	Low (Cl 0.36%)	Good CV, low ash, safer chlorine levels
4	PET Bottle Waste	4196	8.47	Low–Medium (Cl 0.63%)	Decent CV, moderate ash, chlorine needs

Sl	Waste Stream	Gross CV (kcal/kg)	Ash Content (%)	Heavy Metal Risk	Remark
	(Shredded)				monitoring
5	Package Waste (Shredded)	3598	10.30	Low	Balanced CV, moderate ash, high CaO beneficial for kiln
6	Oil-Soaked Cotton Waste	3616	17.65	Medium (Zn 5.76 mg/kg, V 0.92 mg/kg)	Good CV, but higher ash and trace metals
7	Municipal Waste (Shredded)	3426	4.97	Low (Cl 0.51%)	High carbon (63.96%), low moisture, but variable composition
8	Dolochar	2742	43.67	High (Pb 36 mg/kg, Cd 8.23 mg/kg, Zn 36 mg/kg)	Moderate CV, very high ash, significant heavy metals
9	Woodchips	2715	5.93	Low	Renewable source, but lower CV compared to plastics
10	Waste Solid Mix	2040	48.65	Medium (Pb 2.38 mg/kg, Zn 3.96 mg/kg)	Lowest CV, very high ash, limited fuel potential

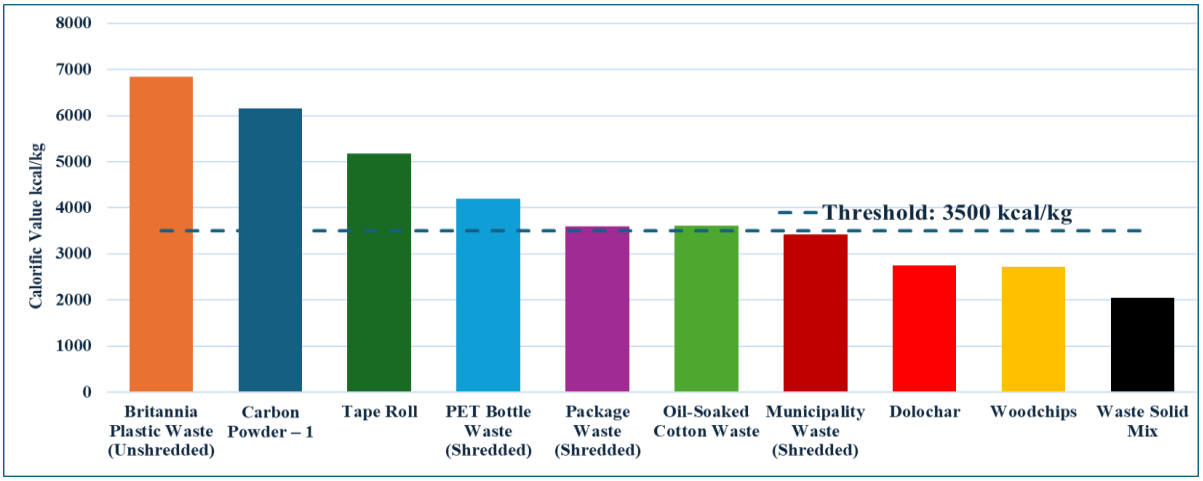


Figure 6 Comparison of the calorific value of different waste streams

The comparative analysis provides the following results. (Refer figure 6)

- Highest Energy Value: Britannia Plastic Waste (6845 kcal/kg).
- Lowest Energy Value: Waste Solid Mix (2040 kcal/kg).
- Lowest Moisture: PET Bottle Waste (0.89%).
- Highest Ash Content: Waste Solid Mix (48.65%) and Dolochar (43.67%).
- Best Fuel Substitute Potential: Britannia Plastic Waste and Carbon Powder (high CV, high carbon, low ash).

- Environmental Risk: Dolochar shows elevated heavy metals (Pb, Cd, Zn).
- Best Fuel Substitutes: Britannia Plastic Waste and Carbon Powder (high CV, low ash).
- Moderate Options: Tape Roll, PET Bottle Waste, Package Waste, Oil-Soaked Cotton Waste.
- Least Suitable: Waste Solid Mix and Dolochar (high ash, heavy metals).
- Environmental Risk: Dolochar is the most problematic due to elevated Pb, Cd, and Zn.

The following figure shows a comparison of the calorific value of different wastes with respect to the threshold value of 3500 kcal/kg of Gross Calorific Value (MoHUA, Guidelines for usage of RDF 2018)

4.0 Conclusions

This study demonstrates that alternative fuels and raw materials (AFR), particularly refuse-derived fuel (RDF), have significant potential to reduce fossil-fuel consumption and support the decarbonisation of the Indian cement industry. Co-processing RDF in cement kilns also offers a sustainable pathway for diverting non-recyclable combustible waste from landfills and advancing circular-economy objectives. However, wider adoption is constrained by high capital requirements, unfavourable cost economics, weak policy incentives, inconsistent RDF quality and inadequate monitoring of parameters such as moisture, chlorine and heavy-metal content.

The assessment at Plant A confirms the technical feasibility of increasing the thermal substitution rate (TSR). The plant currently substitutes more than 16% of its primary fuel with alternative fuels and plans to increase this share to 30%. Among the waste streams evaluated, Britannia Plastic Waste exhibited the highest gross calorific value and lowest ash content, making it the most suitable fuel substitute. Carbon Powder and Tape Roll also showed strong energy potential, although their ash, zinc and other trace-element concentrations require monitoring. In contrast, Waste Solid Mix and Dolochar were the least suitable because of their low calorific values, high ash content and, particularly for Dolochar, elevated heavy-metal concentrations.

The findings indicate that alternative fuels should not be selected solely on the basis of calorific value. A systematic evaluation of moisture, ash, chlorine, heavy metals, particle size, supply consistency and effects on clinker quality is essential before increasing substitution rates. Scaling AFR utilisation will therefore require improved waste segregation and pre-processing, standardised RDF specifications, stronger laboratory-testing protocols, reliable supply chains and supportive policy and financial mechanisms. With these measures, Indian cement plants can progressively increase TSR while maintaining kiln performance and product quality, reducing dependence on coal and pet coke, and contributing to national waste-management and net-zero objectives.

The following next steps are proposed as the next part of the study.

- Replacing Pet coke/coal with RDF and carrying out tests and Material Evaluation: Conduct a detailed assessment of input-quality variation by evaluating different waste mixes to understand physical, chemical, and thermal characteristics, along with their availability year-round

- Laboratory Testing: Utilise the plant laboratory to evaluate specific materials, including wood chips, plastic waste, and municipal solid waste (MSW), to establish a baseline for quality and conduct solid and gas analysis
- Benchmarking Visits: Plan visits to high-performing plants, specifically those achieving higher TSR
- Analysis of clinker and final product through scientific process alignment: Define a methodology to align raw mix and fuel mix designs to ensure clinker quality remains consistent regardless of the AFR percentage used

5.0 Acknowledgement

The authors acknowledge that this study is supported by the Cement Plant Head and his team.

6.0 References

1. Cement Manufacturers Association (CMA-Dashboard)
2. Central Pollution Control Board (CPCB) https://cpcb.nic.in/zobengaluru/MSW_Perspectives%20.pdf
3. Central Pollution Control Board - Guidelines for Pre-processing and Co-processing of Hazardous and Other Wastes in Cement Plants as per H&OW(M&TBM) Rules 2016
4. Global Cement and Concrete Association (GCCA) India, "Blended Cement- Green, Durable and Sustainable," GCCA India, 2022.
5. GCCA India-TERI. (2025). Decarbonization Roadmap for the Indian Cement Sector: Net-zero CO2 by 2070.
6. ICR (International Cement Review), RDF production and utilisation in India (2017); https://optoce.no/wp-content/uploads/2019/03/RDF-India_ICR_Dec-2017.pdf
7. Indian Bureau of Mines, "Indian Minerals Yearbook 2014,"
8. McKinsey, Article, Laying the Foundation for Zero Carbon Cement, 2020 https://www.mckinsey.com/industries/chemicals/our-insights/laying-the-foundation-for-zero-carbon-cement
9. MoHUA (Ministry of Housing and Urban Affairs) Guidelines for Municipal Waste Management (2016), https://mohua.gov.in/upload/uploadfiles/files/Part2.pdf
10. McKinsey, Article, Laying the Foundation for Zero Carbon Cement, https://www.mckinsey.com/industries/chemicals/our-insights/laying-the-foundation-for-zero-carbon-cement
11. The Ministry of Housing and Urban Affairs (India) Guidelines on the usage of Refuse-Derived Fuel in Various Industries 2018
12. V. K. e. al., "The feasibility analysis of cement kiln as an MSW treatment infrastructure: From a life cycle environmental impact perspective," Journal of Cleaner Production, vol. 267, 2020

CARBON MINERALIZATION OF STEEL SLAG: A PATHWAY FOR CO_2 CAPTURE, UTILIZATION, AND CIRCULAR RAW MATERIAL GENERATION

Mahima Srivastava[1]*, Priyapratim Patra[1], Pratik Goyal[1], J. Suresh[1], Amol Satpute[1], Dilip Makhija[1], Jagabandhu Kole[1] , Manoj Kumar Rustagi[1]

[1]*Research and Development, JSW Cement Ltd, Vijayanagar, Bellary, Karnataka-583275*

[2]*Department of Civil Engineering, Indian Institute of Technology, Kanpur, Uttar Pradesh 208016*

**E Mail: mahima.shrivastava@jsw.in*

ABSTRACT

Steel slag is a by-product generated during the steelmaking process that contains a significant amount of free calcium oxide (CaO), free magnesium oxide (MgO), heavy metals, and low cementitious properties compared to ground granulated blast furnace slag (GGBS). Due to these characteristics, a substantial amount of steel slag remains unused and is often disposed of in landfills, creating environmental and land-use concerns. The cement and concrete industry could be a favorable pathway for the utilization of steel slag; however, the direct incorporation of untreated steel slag into cement-based systems (CBS) can adversely affect durability and performance because of the volumetric instability caused by free CaO and MgO. Therefore, suitable treatment methods are required to enhance the stability of steel slag. Carbonation of steel slag can be one possible approach that converts free CaO and MgO into stable carbonate phases while simultaneously enabling CO_2 sequestration. In this study, an Integrated Carbon Capture and Mineralization (ICCM) process was employed to simulate CO_2 capture from a simulted flue gas stream and utilize the captured CO2 for steel slag carbonation and mineralization. Two steel slag types, namely Argon Oxygen Decarburization (AOD) slag and Electric Arc Furnace (EAF) slag, were treated using a proprietary mineralization solution, and at the end of the process, carbonated steel slag and a silica-rich precipitate were recovered. The recovered materials were characterized using X-ray diffraction (XRD), Fourier transform infrared spectroscopy (FTIR), and thermogravimetric analysis (TGA) to evaluate mineralogical and chemical transformations. The results indicated the carbonation of AOD slag through the formation of calcite ($CaCO_3$), whereas EAF slag exhibited limited carbonation, likely due to the presence of relatively stable calcium silicate phases that restricted carbonation. Carbonated AOD slag showed a CO_2 uptake of 33.02 kg CO_2 per tonne of slag and produced 17.63 kg of silica-rich precipitate per tonne of slag, establishing the potential of the process for both carbon sequestration and resource recovery. The carbonated AOD slag was further used in a Portland slag-based system as a partial replacement for GGBS. It was observed that a 10% replacement level resulted in compressive strengths comparable to the control mixture, whereas higher replacement levels resulted in reduced strength due to the dilution of reactive cementitious phases. Overall, the ICCM process represents a sustainable pathway for steel slag valorization by combining CO_2 capture, mineralization, and the production of value-added materials for applications in the cement and concrete industry.

Key words: Steel slag, Carbon Capture, Carbon utilisation Mineralisation Carbonated Steel Slag, Reactive Silica Recovery

INTRODUCTION

Steel slag is a by-product generated when impurities present in raw materials react with oxidants and fluxes during the steelmaking process. Currently, India generates approximately 19 million tonnes of steel slag annually from its integrated steel plants as a solid industrial waste. Amid ongoing growth of the steel industry, 300 million tonnes of steel production is anticipated by FY2030, resulting in an increase in steel slag generation to nearly 60 million tonnes per year [1]. At present, only 15–20% of the steel slag is utilised, and the remaining goes either into landfills or remains as stockpiles in open yards, creating significant environmental and land-use concerns [2]. These disposal practices cause air, soil and water contamination because of the presence of toxic heavy metal such as lead (Pb), cadmium (Cd), mercury (Hg), chromium (Cr), and arsenic (As) [3,4]. To reduce the potential risk to the environment, stringent environmental regulations and sustainability requirements are being developed to effectively reuse steel slag, transforming it from a hazardous waste into an environmentally beneficial resource.

The steel slag moslty consumed in different areas such as agricultural (acidic soil conditioner), wastewaster treatment (heavy metal ion adsorption), marine (algae growth), construction material (concrete and road), and CO_2 sequestration (carbonation and mineralisation) [5]. Utilisation of steel slag as a construction material represents a most promising pathway, which supports both resource conservation and sustainable construction practices. However, its utilisation as a construction material comes with several challenges, such as poor grindability [6]; irregularity in chemical and mineralogical composition due to the generation route of the steel slag [7,8]; volume instability resulting from free calcium oxide (f-CaO) and magnesium oxide (f-MgO) [9,10]; and high specific gravity and angular particle morphology, which increase overall water demand and affect the workability of fresh concrete [11]. Predominantly, the low hydraulic reactivity of C_2S, even after fine grinding, makes it inadequate as a supplementary cementitious material (SCM) [11]. These factors comprehensively obstruct the vast implementation of steel slag in cementitious systems. Mineralisation of steel slag is one of the solutions to the challenges associated with steel slag and has become popular, as this technique can also permanently sequester CO_2. In this process, captured CO_2 from flue gas can be used to convert f-CaO and f-MgO into thermodynamically stable solid carbonates, $CaCO_3$ and $MgCO_3$, respectively [13]. A study also reported that CO_2 mineralisation refines the particle size and enhances the material properties [14]. Moreover, the carbonation of steel slag results in the generation of silica gels and calcium carbonates that enhance the overall properties of steel slag [15,16]. It was reported that the use of silica gel in the cement-based system (CBS) improves the pozzolanic reactivity, and the use of carbonated steel slag as a cement replacement also enhances the reactivity of the CBS as compared to raw and fine-ground steel slag by influencing the hydration of cement and strength development [15-18].

In this study, the carbonation behavior of Argon Oxygen Decarburization (AOD) and Electric Arc Furnace (EAF) slags was investigated using an Integrated Carbon Capture and Mineralization (ICCM) process employing a proprietary carbonated NaOH solution. This approach attempted to simultaneously capture CO_2, recover silica-rich precipitates, and produce carbonated steel slag. The recovered products were characterized using X-ray diffraction (XRD), Fourier transform infrared spectroscopy (FTIR), and thermogravimetric analysis (TGA) to evaluate carbonation efficiency and product characteristics. Furthermore, the potential application of carbonated steel slag as a partial replacement for ground granulated blast furnace slag (GGBS) in Portland Slag Cement (PSC) mortar was assessed through

compressive strength testing. The findings provide insights into the feasibility of integrating CO_2 sequestration, resource recovery, and sustainable construction material development through the valorization of steel slags.

MATERIAL AND METHODS

Raw Material

Steel slags used in this study, namely AOD and EAF slag, were obtained from JSW Steel, Vijayanagar, India. The received slag samples consisted of particles smaller than 2 mm and were utilized for the recovery of carbonated slag residue, and silica. Carbonation was carried out using a proprietary 2 M carbonated aqueous NaOH solution. In addition, the potential use of carbonated steel slag as a partial replacement of GGBS was investigated. Furthermore, Ordinary Portland Cement (OPC) conforming to IS 269 [19] and GGBS conforming to IS 16714 [20] were obtained from JSW Cement, Vijayanagar, and used as cementitious materials. The specific surface areas for both OPC and GGBS were 325 m²/kg. The chemical compositions of AOD slag, EAF slag, OPC, and GGBS are presented in **Table 1**. Manufactured sand (M-sand), conforming to IS 383 and having a specific gravity of 2.7, was used as the fine aggregate in this study [21].

TABLE 1. CHEMICAL COMPOSITION OF THE RAW MATERIAL

Material	Oxide Composition (%)									
	CaO	MgO	SiO_2	Fe_2O_3	Al_2O_3	P_2O_5	TiO_2	MnO	Na_2O	K_2O
AOD	62.39	10.87	12.57	2.19	4.02	0.02	0.99	1.38	0.18	0.11
EOF	45.37	5.36	12.68	24.95	6.44	0.66	0.89	1.63	0.22	0.53
OPC	60.45	2.51	21.4	4.42	5.95	-	-	-	-	-
GGBS	36.04	7.82	33.06	0.89	20.12	-	-	0.12	-	-

Carbonation of Steel Slag and recovery of silicates

The ICCM experimental setup used in this study was a semi-continuous carbonation unit located at IIT Kanpur, The ICCM setup functioned as an integrated carbon capture unit that also facilitated mineralisation, wherein CO_2 was captured using a proprietary solvent while simultaneously producing calcium carbonate and silica-rich products with potential applications as raw materials for cement manufacturing. Two experimental runs were conducted for each slag sample. In the first run, a freshly prepared proprietary carbonated NaOH solution was used as the solvent. Steel slag carbonation was performed at a liquid-to-solid ratio of 5 L/kg using a 2 M carbonated NaOH solution. After the addition of the steel slag sample, the suspension was continuously stirred for 2 hours at room temperature. Subsequently, the slurry was allowed to settle for 1 hour to facilitate the separation of carbonated slag particles. During the carbonation process, a series of dissolution and precipitation reactions occurred, resulting in the dissolution of reactive phases from the steel slag. Following the settling period, the carbonated slag residue was collected, oven-dried, and weighed. The supernatant solution was then passed through a series of filters to remove suspended particles. The resulting filtrate, expected to

contain dissolved silica primarily in the form of sodium silicate and related species, was transferred to a second reactor. In this reactor, CO_2 was continuously introduced at a pressure for 2 hours while the suspension was stirred continously. During this stage, the precipitation of dissolved silicate takes place. The resulting suspension was filtered and precipitates were collected. The recovered product, appearing as a white gelatinous precipitate, was subsequently dried in a hot-air oven at 100 °C. After drying, the mass of the recovered reactive silica precipitate was recorded. In the second experimental run, the solvent recovered from the first run was reused after the addition of the required make-up solvent. At the end of the experiment, the volumes of spent solvent, make-up solvent, and process holdup were measured to estimate solvent losses. The dry masses of the carbonated slag residue and the recovered reactive silica precipitate were also determined. **Figure 1** shows the recovered carbonated steel slag and precipitated mass from the steel slag after carbonation.



a. Carbonated steel slag b. Recovered precipitates

Figure 1. Carbonated Slag and precipitate

Characterization study of the carbonated steel slag and silicates and aluminates

The carbonation efficiency and the effectiveness of silicate phase extraction from steel slag were evaluated using various characterization techniques. Following the carbonation process, the $CaCO_3$ phases present in the carbonated steel slag were identified using a PANalytical Aeris XRD. In addition, TGA using F5 Jupiter, Make: Netzsch, Germany was performed to determine the CO_2 uptake of the carbonated steel slag by measuring weight loss over the temperature range of 0-1000 °C, which helped provide insights into the formation of $CaCO_3$. Moreover, FTIR of the carbonated steel slag and recovered silica gel were carried out using a Agilent Carry 630 over a wavenumber range of 600-1600 cm^{-1}.

Preparation of carbonated steel slag blended system

The effect of carbonated steel slag on the performance of CBS was evaluated in this study. The carbonated slag was ground to a particle size of approximately 300 µm and used as a partial replacement for GGBS at replacement levels of 5%, 10%, 15%, and 20% by weight in PSC. The water-to-binder ratio (w/b) was maintained at 0.41 by weight, based on the average normal consistency of all mixtures. The sand-to-cement ratio was maintained at 3:1 by weight for all mixtures. The mix proportions used in the study are presented in **Table 2**. The compressive strength of the CBS was determined in accordance with IS 4031 (Part 6) [22]. The average compressive strength of the carbonated slag blended mortar was evaluated at curing ages of 1, 3, 7, and 28 days.

TABLE 2. MIXTURE PROPORTION FOR THE PSC

S. No.	Mix Id	GGBS Composition (%)		PSC Composition (%)		
		GGBS	Carbonated slag	OPC	GGBS	Carbonated slag
1	PSC-BLANK	100	0	40	60	0
2	PSC_CS_5	95	5	40	57	3
3	PSC_CS_10	90	10	40	54	6
4	PSC_CS_15	85	15	40	51	9
5	PSC_CS_20	80	20	40	48	12

RESULTS AND DISCUSSION

Carbonation of steel slag and recovery of silicates

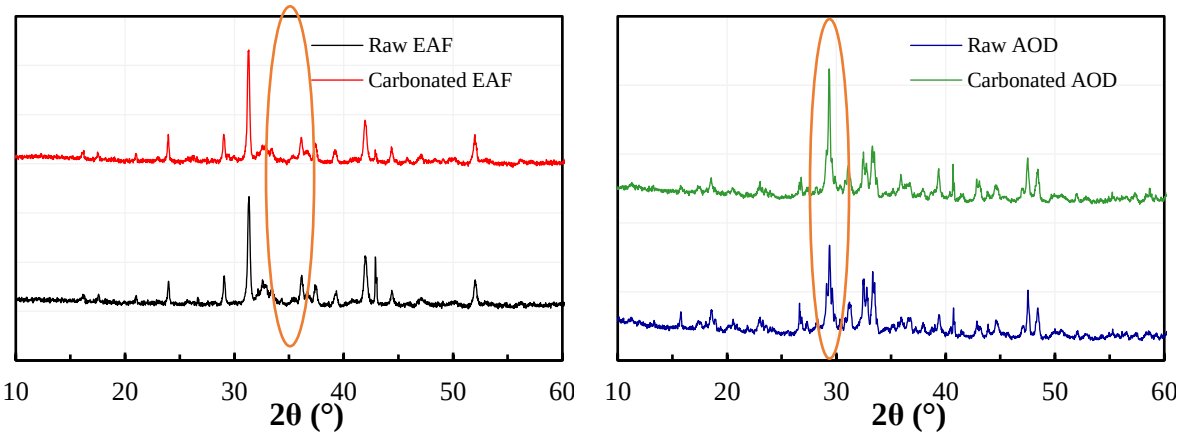
It was observed that, following the initial mixing of steel slag with the carbonated NaOH solution, the combined yield of the carbonated steel slag was comparable to the mass of the original steel slag feed. It was initially hypothesized that the interaction of steel slag with the carbonated NaOH solution would result in the dissolution of silicate phases into the solution. However, the negligible difference between the initial and final masses suggests that the dissolution of these phases was compensated by the formation of carbonate phases within the slag matrix, resulting in an overall mass balance close to that of the original feed. Furthermore, carbonation of the supernatant solution in the second reactor under pressurized CO_2 resulted in the precipitation of white gelatinous product expected to be rich in silica. The yield of the recovered silica-rich precipitate was approximately 17.63 kg per tonne of slag for AOD slag carbonation. In contrast, no precipitate was recovered following the carbonation of EAF slag, indicating limited dissolution and carbonation of reactive phases. Previous studies have reported that the major phases present in EAF slag are calcium silicates, calcium ferroaluminates, and the RO phase. As calcium in EAF slag predominantly exists within calcium silicate phases, it is chemically bound in relatively stable mineral structures that limit the further dissolution and carbonation reactions [23]. Unlike AOD slag, which contains significant amounts of free and highly reactive CaO, EAF slag primarily consists of calcium silicates, requiring greater energy for bond breakdown and subsequent reaction with CO_2 [24]. In addition, the overall solvent losses for the complete process were found to be less than 5%, indicating that the ICCM setup is an efficient semi-continuous process with minimal solvent consumption while simultaneously producing carbonated slag and silica-rich precipitates. The characterization study on the recovered products were performed using various analytical techniques, and the results are discussed in the following sections.

XRD

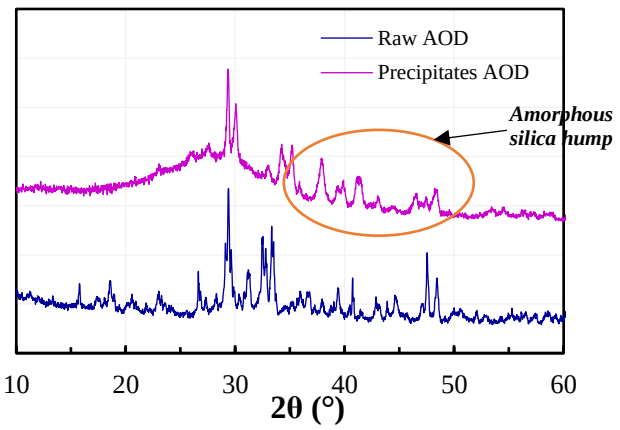
Figure 2 illustrates the XRD patterns of raw and carbonated steel slags, along with the precipitate recovered from AOD slag. According to the previous studies, the characteristic diffraction peak of calcite ($CaCO_3$) occurs at approximately 29.4° (2θ) and was used in this study to assess carbonate

formation following carbonation [25,26]. As shown in **Figure 2(a)**, the characteristic calcite peak was absent in both the raw and carbonated EAF slag samples, indicating limited or negligible carbonation of the EAF slag. In contrast, **Figure 2(b)** shows a significant increase in the intensity of the calcite peak at 29.4° after carbonation of the AOD slag. This observation indicates that the free CaO present in the AOD slag reacted with CO_2 in the proprietary carbonated NaOH solution, resulting in the formation of $CaCO_3$. The increased intensity of the calcite peak confirms the successful carbonation of AOD slag and suggests a higher degree of carbonation compared to EAF slag.

Furthermore, **Figure 2(c)** demonstrate the XRD pattern of the precipitated product recovered from the supernatant solution in comparison with the raw AOD slag. The recovered precipitate exhibited a broad hump in the diffraction pattern, indicating the presence of a predominantly amorphous phase. This amorphous material is expected to be rich in silica, which precipitated from the dissolved silicate species during the secondary carbonation stage. This demonstrating the potential for simultaneous recovery of reactive silica during the carbonation process.



a. EAF *b. AOD*



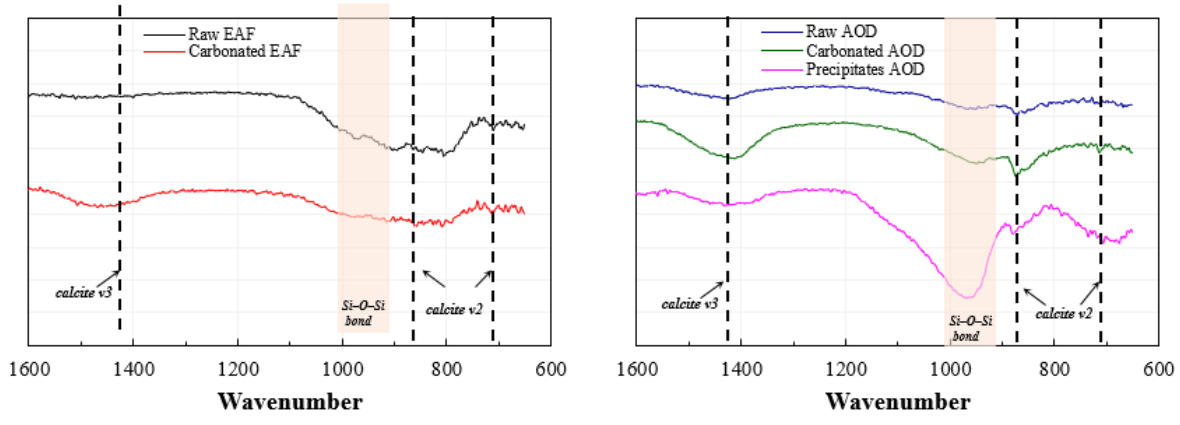
c. Precipitated from AOD

Figure 2 XRD pattern of raw and carbonated steel slags

FTIR

Figure 3 shows the FTIR spectra of the raw and carbonated steel slags. FTIR analysis was performed to identify the structural changes associated with the formation of $CaCO_3$ and silica gel during the carbonation of steel slag. As shown in Figure 5, characteristic absorption bands were observed at approximately 1414 cm^{-1}, 870 cm^{-1}, 712 cm^{-1}, and 919-1010 cm^{-1}. The band at 1414 cm^{-1} corresponds to the asymmetric stretching vibration (ν_3) of the carbonate group, while the bands at 870 cm^{-1} and 712 cm^{-1} are associated with the out-of-plane and in-plane bending vibrations of the C-O bond in calcite, respectively [17,27]. An increase in the intensity of these bands after carbonation indicates the formation of carbonate phases within the slag matrix.

As shown in **Figure 3(a)**, carbonation of EAF slag resulted in only a slight increase in the absorption band at 1414 cm^{-1}, indicating limited carbonation. This behaviour may be attributed to the stable calcium silicate phases present in EAF slag, in which calcium is chemically bound and therefore less available for reaction with CO_2 [23,24]. Furthermore, no precipitated silica-rich product was recovered from EAF slag carbonation; hence, the FTIR spectrum of a precipitated product is not available. **Figure 3(b)** illustrate the FTIR spectra of raw AOD slag, carbonated AOD slag, and the precipitated product recovered after carbonation. A noticeable increase in the intensity of the characteristic carbonate bands at 1414 cm^{-1}, 870 cm^{-1}, and 712 cm^{-1} was observed after carbonation, confirming the effective formation of $CaCO_3$. In addition, evidence of silica gel formation was observed through changes in the Si-O absorption band, which shifted from approximately 919 cm^{-1} in the raw slag to around 1010 cm^{-1} after carbonation. The absorption band near 1010 cm^{-1} corresponds to the asymmetric stretching vibration of the Si-O-Si bond and is attributed to the formation of highly polymerized silica gel [17,28,29]. These observations suggest that a significant portion of the silica released during slag dissolution initially formed silica gel, which subsequently dissolved under the highly alkaline Na_2CO_3-rich solution conditions. This interpretation is consistent with the XRD results, which indicated the presence of an amorphous silica-rich precipitate recovered during the secondary carbonation stage. Based on the XRD and FTIR findings, EAF slag exhibited limited carbonation and did not produce a recoverable silica-rich precipitate. Therefore, EAF slag was not considered for further evaluation of CO_2 uptake or for assessing the performance of carbonated steel slag as a partial replacement for GGBS in PSC.



a. EAF *b. AOD*

Figure 3 FTIR of raw and carbonated steel slags

TGA

Based on the previous results, it was evident that EAF slag did not undergo carbonation efficiently. Therefore, TGA was performed on the raw and carbonated AOD slag to quantify CO_2 uptake. **Figure 4** presents the mass loss as a function of temperature for the raw and carbonated AOD slag samples. The CO_2 uptake was determined from the mass loss associated with the decomposition of $CaCO_3$ within the temperature range of 520 °C to 800 °C [17]. Based on the TGA results, the total CO_2 storage capacity of the carbonated AOD slag was calculated to be 33.02 kg CO_2 per tonne of slag, while the total $CaCO_3$ content was found to be 14.75 wt.%. These results confirm that the operating conditions employed in the present study are favorable for the ICCM process and enable the formation of carbonate phases within the slag matrix. The observed carbonation demonstrates the potential of the process for simultaneous CO_2 sequestration and the production of value-added carbonated products. However, the current level of CO_2 uptake remains moderate and could be further enhanced through optimization of the process parameters, such as solvent composition, liquid-to-solid ratio, reaction time, CO_2 partial pressure, and mixing conditions.

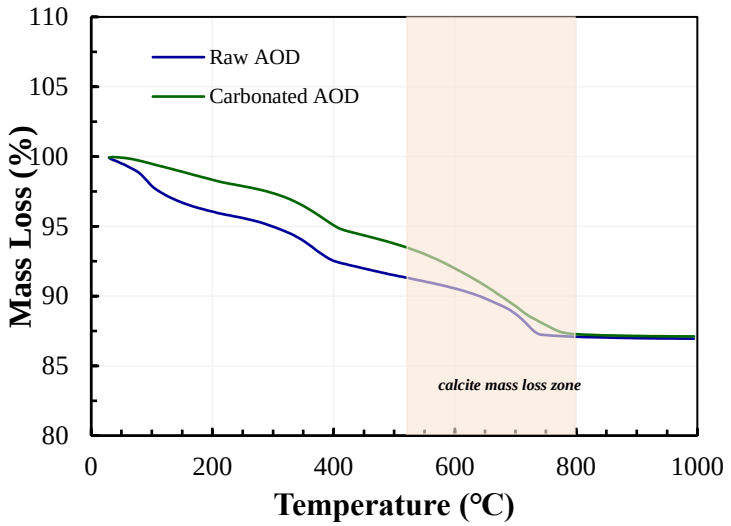


Figure 4 TGA of raw and carbonated steel slags

Effect of carbonated AOD steel slag on the performance of the PSC cement

Figure 5 shows the compressive strength development of carbonated AOD steel slag-blended PSC mortar. For all mixtures, compressive strength increased with curing age, indicating the continued progress of cement hydration. At 1 day, the incorporation of carbonated AOD steel slag resulted in a slight improvement in compressive strength, with an increase of approximately 7-9% observed as the replacement level increased. This enhancement may be attributed to the filler effect of the fine carbonated particles and the presence of calcium carbonate, which can promote early-age hydration.

However, at 3 and 7 days, the compressive strength of mixtures containing 20% carbonated AOD steel slag was significantly lower than that of the control specimen. This reduction may be attributed to the dilution effect caused by the replacement of GGBS with carbonated slag [30,31]. Higher levels of carbonated steel slag reduced the amount of reactive cementitious phases available for hydration,

thereby decreasing the formation of hydration products and hindering the development of mechanical strength. Furthermore, reactive silica was extracted separately during the carbonation process, while calcium carbonate remained in the solid residue. As a result, the carbonated slag contained limited pozzolanic or latent hydraulic phases, leading to weaker bonding between slag particles and the hydrated cement matrix [17,32]. In addition, the contribution of $CaCO_3$ to strength development is inadequate due to the limited availability of reactive aluminosilicate phases as compred to the uncarbonated slag system [33].

A similar trend was observed at 28 days, where replacement levels of 15% and 20% resulted in a significant reduction in compressive strength compared to the control mix. In contrast, mixtures containing 5% and 10% carbonated AOD steel slag exhibited compressive strengths comparable to that of the control specimen. This behavior may be attributed to two primary factors. First, the precipitated $CaCO_3$ particles can act as microfillers, occupying voids within the cement matrix, reducing porosity, and promoting a denser microstructure [17]. Second, the alkaline nature of the carbonated AOD steel slag may increase the alkalinity of the pore solution, facilitating the dissolution of the amorphous phases present in GGBS. This enhanced dissolution can accelerate hydration reactions by promoting the release of reactive silica and alumina, thereby contributing to strength development. Consequently, at lower replacement levels, the beneficial filler and hydration-promoting effects of the carbonated slag can compensate for the dilution effect, resulting in compressive strengths comparable to those of the control mixture.

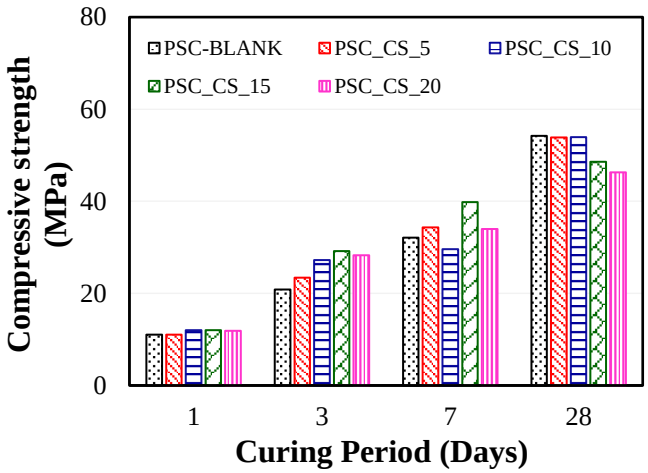


Figure 5 Influence of carbonated AOD steel slag on PSC

CONCLUSION

Based on the findings of the present study, the following conclusions can be drawn:

1. AOD slag exhibited significantly higher carbonation reactivity than EAF slag, leading to substantial $CaCO_3$ formation, while EAF slag showed limited carbonation due to the presence of stable calcium silicate phases.
2. The ICCM process enabled the simultaneous recovery of carbonated slag and silica-rich precipitate, with a silica yield of approximately 17.63 kg per tonne of AOD slag.

3. Characterization by XRD, FTIR, and TGA confirmed the formation of calcite and the successful carbonation of AOD slag.
4. The carbonated AOD slag achieved a CO_2 storage capacity of 33.02 kg CO_2/t slag with a corresponding $CaCO_3$ content of 14.75 wt.%.
5. Incorporation of carbonated AOD slag as a partial replacement for GGBS showed that 5-10% replacement levels achieved compressive strengths comparable to the control mix.
6. Higher replacement levels (15-20%) resulted in reduced strength due to the dilution of reactive cementitious phases and the limited hydraulic activity of the carbonated residue.

ACKNOWLEDGEMENT

The authors acknowledge the support of Indian Institute of Technology Kanpur (Dr. Raghavendra Ragipani, Dr. Soumyabrata Roy, Ms. Samsrutha Karnati, Dr. Pankaj Kumar, and Mr. Adarsh Jain) for conducting the experimental testing and characterization studies associated with this research.

REFERENCES

1. https://www.csir.res.in/en/csir-success-stories/steel-slag-road-sustainable-valorization-steel-slag-road-making-aggregates- accessed 26-8-2026
2. Tiwari, M.K., Bajpai, S. and Dewangan, U.K. (2016) 'Steel slag utilization — overview in Indian perspective', International Journal of Advanced Research (IJAR), 4(8), pp. 2232–2246. doi: 10.21474/IJAR01/1442.
3. Zhou, X., Xiang, X. and Li, C. (2014) 'Ecological security analysis and advances in innocent treatment of steel slag' (in Chinese), Multipurpose Utilization of Mineral Resources, 3, pp. 8–11.
4. Song, Q., Guo, M.-Z., Wang, L. and Ling, T.-C. (2021) 'Use of steel slag as sustainable construction materials: A review of accelerated carbonation treatment', Resources, Conservation and Recycling, 173, 105740. doi:10.1016/j.resconrec.2021.105740.
5. Gao, W., Zhou, W., Lyu, X., Liu, X., Su, H., Li, C. and Wang, H. (2023) 'Comprehensive utilization of steel slag: A review', Powder Technology, 422, 118449. doi: 10.1016/j.powtec.2023.118449.
6. Moura, C., Nascimento, L., Loureiro, C., Rodrigues, M., Oliveira, J. and Silva, H. (2022) 'Viability of using high amounts of steel slag aggregates to improve the circularity and performance of asphalt mixtures', Applied Sciences, 12, 490. doi:10.3390/app12010490
7. Kumar, P. and Shukla, S. (2023) 'Utilization of steel slag waste as construction material: a review', Materials Today: Proceedings, 78, pp. 145–152. doi:10.1016/j.matpr.2023.01.015.
8. Moura, C., Nascimento, L., Loureiro, C., Rodrigues, M., Oliveira, J. and Silva, H. (2022) 'Viability of using high amounts of steel slag aggregates to improve the circularity and performance of asphalt mixtures', Applied Sciences, 12, 490. doi:10.3390/app12010490
9. Gonzalez, P.L.L., Novais, R.M., Labrincha, J.A., Blanpain, B. and Pontikes, Y. (2019) 'Modifications of BOF slag microstructure and their effect on alkali-activated binders', Cement and Concrete Composites, 97, pp. 143–153. doi: 10.1016/j.cemconcomp.2018.12.013.



10. Iluțiu-Varvara, D.A., Tintelecan, M., Aciu, C. and Sas-Boca, I.-M. (2020) 'Reuse of the steel mill scale for sustainable industrial applications', Proceedings, 63(1), p. 14. doi: 10.3390/proceedings2020063014.

11. Kumar, P. and Shukla, S. (2023) 'Utilization of steel slag waste as construction material: a review', Materials Today: Proceedings, 78, pp. 145–152. doi:10.1016/j.matpr.2023.01.015.

12. Su, B., Sun, Y., Jiang, P., Zhang, C., Cui, K., Zheng, Y., Qiu, J. and Zhao, Y. (2025) 'Valorization of steel slag through CO_2 mineralization toward improved reactivity and cementitious performance', Journal of Environmental Chemical Engineering. doi:10.1016/j.jece.2025.119757.

13. Liu, G., Tang, Y. and Wang, J. (2023) 'Effects of carbonation degree of semi-dry carbonated converter steel slag on the performance of blended cement mortar – reactivity, hydration, and strength', Journal of Building Engineering, 63, 105529. doi:10.1016/j.jobe.2022.105529.

14. Qiu, Q. (2020) 'Carbonation in cementitious materials: mechanisms and implications', Construction and Building Materials, 247, 118503. doi:10.1016/j.conbuildmat.2020.118503.

15. Moon, S., Kim, E., Noh, S., Triwigati, P.T., Choi, S. and Par, Y. (2024) 'Carbon mineralization of steel and iron-making slag: Paving the way for a sustainable and carbon-neutral future', Journal of Environmental Chemical Engineering. doi:10.1016/j.jece.2024.112448.

16. Peng, L., Jiang, Y., Ban, J., Shen, Y., Ma, Z., Zhao, Y., Shen, P. and Poon, C.-S. (2023) 'Mechanism underlying early hydration kinetics of carbonated recycled concrete fines–ordinary Portland cement (CRCF–OPC) paste', Cement and Concrete Composites. doi:10.1016/j.cemconcomp.2023.105275.

17. Zhang, Z., Zheng, K., Xu, M., Chen, L., Yuan, Q. and Cao, Q. (2025) 'Aqueous carbonation of steel slag with Na_2CO_3 solution: Synthesis of amorphous silica gel and performance enhancement of carbonated steel slag blended cement paste', Sustainable Materials and Technologies. doi:10.1016/j.susmat.2025.e01659.

18. Zhao, Y., Zheng, Y., Cui, K., Shen, P., Poon, C.-S., Peng, G. et al. (2025) 'Development of ultrafine and highly reactive SCMs via combined CO_2 and mechanical activation of steel slag', Chemical Engineering Journal, 516, 163999. doi:10.1016/j.cej.2025.163999.

19. Bureau of Indian Standards (2015) Ordinary Portland cement — Specification: IS 269:2015. New Delhi: Bureau of Indian Standards.

20. Bureau of Indian Standards (2018) Ground granulated blast furnace slag for use in cement, mortar and concrete — Specification: IS 16714:2018. New Delhi: Bureau of Indian Standards.

21. Bureau of Indian Standards (2016) Coarse and fine aggregate for concrete — Specification: IS 383:2016. New Delhi: Bureau of Indian Standards.

22. Bureau of Indian Standards (1988) Methods of physical tests for hydraulic cement: Part 6 Determination of compressive strength: IS 4031 (Part 6):1988. New Delhi: Bureau of Indian Standards.

23. Tong, Z., Ma, G., Zhang, X. and Cai, Y. (2017) 'Microwave-supported leaching of electric arc furnace (EAF) slag by ammonium salts', Minerals, 7, p. 119.



24. Tong, Z., Ma, G., Zhou, D., Yang, G. and Peng, C. (2019) 'The indirect mineral carbonation of electric arc furnace slag under microwave irradiation', Scientific Reports, 9, p. 7676. doi:10.1038/s41598-019-44162-x

25. Kontoyannis, C.G. and Vagenas, N.V. (2000) 'Calcium carbonate phase analysis using XRD and FT-Raman spectroscopy', Analyst, 125(2), pp. 251–255. doi:10.1039/A908609I.

26. Hossain, M.S. and Ahmed, S. (2023) 'Crystallographic characterization of naturally occurring aragonite and calcite phase: Rietveld refinement', Journal of the Saudi Chemical Society, 27, 101649. doi:10.1016/j.jscs.2023.101649.

27. Khan, R.I., Ashraf, W. and Olek, J. (2021) 'Amino acids as performance-controlling additives in carbonation-activated cementitious materials', Cement and Concrete Research, 147, 106501. doi:10.1016/j.cemconres.2021.106501.

28. Liu, X., Feng, P., Cai, Y., Yu, X. and Liu, Q. (2022) 'Carbonation behaviors of calcium silicate hydrate (C-S-H): effects of aluminum', Construction and Building Materials, 325, 126825. doi:10.1016/j.conbuildmat.2022.126825.

29. Ma, Z., Liao, H., Pan, Z. and Cheng, F. (2022) 'Insights into coproduction of silica gel via desulfurization of steel slag and silica gel adsorption performance', ACS Omega, 7, pp. 21062–21074. doi:10.1021/acsomega.2c01857.

30. Lim, J.S., Cheah, C.B. and Ramli, M.B. (2019) 'The setting behavior, mechanical properties and drying shrinkage of ternary blended concrete containing granite quarry dust and processed steel slag aggregate', Construction and Building Materials, 215, pp. 447–461.

31. Ma, M., Mehdizadeh, H., Guo, M.-Z. and Ling, T.-C. (2021) 'Effect of direct carbonation routes of basic oxygen furnace slag (BOFS) on strength and hydration of blended cement paste', Construction and Building Materials, 296, 124628. doi:10.1016/j.conbuildmat.2021.124628.

32. Liu, G., Tang, Y. and Wang, J. (2022) 'Effects of carbonation degree of semi-dry carbonated converter steel slag on the performance of blended cement mortar – Reactivity, hydration, and strength', Journal of Building Engineering, 52, 105529. doi:10.1016/j.jobe.2022.105529.

33. Scrivener, K., Martirena, F., Bishnoi, S. and Maity, S. (2018) 'Calcined clay limestone cements (LC3)', Cement and Concrete Research, 114, pp. 49–56. doi:10.1016/j.cemconres.2017.08.017.



Technical Session-IIIB

CONFERENCE & EXHIBITION ON
CARBON NEUTRALITY IN CEMENT AND CONCRETE
"Towards a Sustainable & Net Zero Future"
19-20 NOVEMBER 2026
Centenary Convention Centre, Hyderabad

COMPARISON OF PHYSICS INFORMED EMPIRICAL EQUATION WITH MACHINE LEARNING MODELS FOR CONCRETE COMPRESSIVE STRENGTH PREDICTION UNDER DISTRIBUTION SHIFT

Singh, Dharmendra Kumar[a,b]

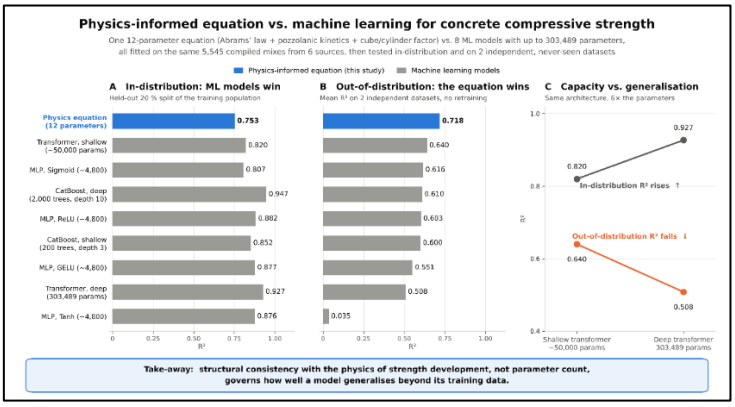
[a]*CC-EOC, NTPC Bhawan, Besides Sattva Necklace Mall, Kavadiguda Road, Secunderabad, Hyderabad-500080 (Telangana), INDIA*

[b]*NTPC School of Business, Plot No. 5-14, Sector 16-A, NOIDA- 201301 (U.P.), INDIA*

Email: dksingh05@ntpc.co.in[a], *x22dharmendraks@nsb.ac.in*[b];

Abstract

Machine learning models for concrete compressive strength prediction routinely report strong in sample accuracy, yet the conditions under which these models are trained rarely match the full range of mix designs, aggregate sources and testing conventions encountered in practice. This study compiles a cleaned dataset of 5,545 concrete mixes drawn from six independent sources, develops a twelve parameter physics informed empirical formula grounded in Abrams' law, pozzolanic reaction kinetics, cube to cylinder conversion factors and compares it against eight machine learning models, including shallow and deep gradient boosted trees, multilayer perceptron with four different activation functions and transformer architectures of two different depths. All machine learning models achieve better accuracy than the formula on held out data drawn from the same compiled population. However, on two independently published, out of distribution datasets that were never used for fitting or training, the formula outperforms every machine learning model tested, achieving a mean R squared of 0.718 against a best competing result of 0.640. Large ML models reach highest in sample accuracy but their out of distribution performance falls even below the accuracy of smaller models trained with less capacity. The results support a specific, testable explanation that a model's structural correctness with respect to the physical process it describes, rather than its parameter count, may govern how well it generalizes beyond its training distribution.



Keywords

Concrete compressive strength, Physics informed empirical equation, Machine learning, Out of distribution generalization, Deep learning, Transformer neural networks, Model interpretability, Inductive bias

1. Introduction

Concrete compressive strength is a very important property in structural design and predicting it accurately from mix proportions before a structure is built has been a central problem in civil engineering for over a century. Abrams' original water to cement ratio law, published in 1918 [1], remains the conceptual starting point for nearly every model developed since, and decades of research have added terms for supplementary cementitious materials like fly ash, slag and silica fume [2, 3], for admixtures such as superplasticizers and for the difference between strength measured on cube and cylinder specimens. In parallel, the last decade has seen a large body of work applying machine learning (ML), from simple regression trees to deep neural networks and transformers, to the same prediction problem, generally reporting accuracy that exceeds classical empirical formulas by a wide margin.

That comparison is generally made on data drawn from a single laboratory's mix designs, a single compiled dataset or a random split of one. A model evaluated this way is being asked to interpolate within a distribution shape it has already seen. Concrete cubes cast at construction sites rarely offer that luxury. A predictive model of concrete strength is useful when it is applied to a new project, a new set of local aggregates, a different cement source, a mix design outside the range represented in the dataset on which the model was trained or a different testing convention like cube or cylinder, that differs from the training population's own convention. In this real world situation the model is being asked to extrapolate, not interpolate, and the two tasks place very different demands on a model. A model that fits its training data closely by learning incidental correlations, rather than the underlying physical relationships, can fail silently the moment it is applied outside that data's boundaries, a failure mode that may be dangerous in a structural engineering context where the consequence of an overconfident, wrong prediction is not a small loss in accuracy but a genuine safety risk.

This study addresses that gap directly. A physics informed empirical formula and eight machine learning models, spanning gradient boosted trees [4], multilayer perceptron (MLP) with four different activation functions and transformer architectures [5] at two depths are all trained and validated on the same compiled, cleaned dataset, then evaluated without any modification on two independently published datasets that were never used during fitting or training. The formula's structure is kept deliberately close to established concrete science, an Abrams' law power term [1], saturating kinetics for pozzolanic reactions [2, 3], a logarithmic maturity function for age and a cube to cylinder correction consistent with published conversion factors [6, 7]. The central finding is that this structural discipline is what allows the formula to generalize where the machine learning models, including ones with tens of thousands of times more parameters, do not. Further experiments, deliberately increasing gradient boosted trees and transformer's depth and capacity, show that additional capacity can improve in-distribution (ID) performance while worsening out of distribution (OOD) performance. This demonstrates that ID and OOD accuracy are not simply two views of the same underlying model quality and can move in opposite directions.

2. Literature Review

Prediction of concrete compressive strength from mix proportions has evolved from empirical relationships to increasingly sophisticated ML models. Abrams' water cement ratio law [1] established the fundamental relationship between water content and strength and subsequent empirical models incorporated curing age, aggregate proportions and supplementary cementitious materials (SCMs) such as fly ash, blast furnace slag and silica fume [2, 3]. These models possess an important advantage i.e. their functional forms are grounded in established concrete science and therefore tend to behave in physically meaningful ways beyond their calibration range. However, their accuracy can be limited for the increasingly diverse concrete mixtures encountered in modern practice.

The introduction of ML, particularly following Yeh's widely used 1,030 record high-performance concrete dataset [8], substantially improved reported prediction accuracy. Support vector regression, random forests, gradient boosting, artificial neural networks and other approaches have subsequently achieved high coefficients of determination (R^2), commonly above 0.85–0.95. Critical reviews have generally concluded that ML models provide greater predictive accuracy and flexibility than conventional empirical equations. However, most studies evaluate performance using random train test splits or cross validation (CV) within the same dataset used for model development. Such evaluation primarily measures interpolation within the training distribution, rather than the ability to predict genuinely new concrete populations. Notably, Yeh's original study also cautioned that the ML model was not intended for extrapolation beyond the domain represented by the accumulated data [8].

More recent studies have attempted to improve robustness by compiling multiple published datasets [9] and by adopting ensemble methods, interpretable model trees and newer architectures such as TabPFN [10]. Studies on SCM based concrete [11], high volume slag concrete [3], silica fume concrete [2] and self-compacting concrete [12] have demonstrated that model performance and even model rankings can vary substantially with the dataset considered. Dataset compilation therefore increases the coverage of the mix-design space, but it does not by itself establish whether a trained model can generalize to an independent population.

A parallel development in the broader ML literature is physics-informed learning, in which established physical relationships are incorporated into model structure rather than left entirely for the algorithm to discover from data. Such approaches have been shown in several engineering fields to improve robustness and generalization under conditions outside the training distribution. In concrete strength prediction, however, physical knowledge has generally been used only for feature selection such as including water cement ratio or age rather than to constrain the functional form of the prediction model itself.

This leads to an important unresolved issue. High ID accuracy does not necessarily imply reliable OOD prediction. Flexible ML models can exploit statistical correlations specific to the training population, which may not represent transferable relationships between concrete constituents and strength. Consequently, a model that performs exceptionally well on a random split may fail when applied to a new cement source, aggregate, SCM combination, mix-design range or testing convention.

The literature reviewed reveals a specific gap i.e. few studies have evaluated concrete strength models against genuinely independent datasets that were completely excluded from model development. No study identified in this review simultaneously examines OOD performance while systematically varying model capacity. The present study addresses this gap by comparing a physics informed empirical equation with eight ML models including gradient boosted trees, multilayer perceptron and transformers of different capacities using a common training population and two independently published OOD datasets under an identical evaluation protocol.

3. Materials and Methods

3.1 Dataset compilation and cleaning

The training dataset compiles 5,545 concrete mix records from six independently published sources, listed in Table 1, spanning ordinary Portland cement mixes and blends incorporating fly ash, blast furnace slag, and silica fume, tested at ages from one to 365 days. Compiling data from independent sources of this kind is expected to introduce duplication because several source studies are themselves compilations that draw on earlier published datasets. A two-stage cleaning procedure was therefore applied. First, the nine mix-design variables and compressive strength were rounded to six decimal places to eliminate insignificant floating-point differences, and exact duplicates were identified using composition and strength while intentionally ignoring specimen type. This removed 91 duplicate records. Second, composition-matched cube/cylinder pairs with different strengths were examined for

repeated strength ratios. Ratios repeating at least three times within a tolerance of 0.001 were treated as evidence of a likely fixed arithmetic cube-to-cylinder conversion rather than independent measurements. Two such conversion ratios, approximately 1.059 and 1.176, occurred 14 and 13 times, respectively, and 27 corresponding cube-side records were removed. The raw compiled dataset of 5,663 records was thereby reduced by 118 records to a final cleaned dataset of 5,545 records. This cleaning procedure was intended to prevent duplicated or mechanically converted records from artificially inflating in-distribution model performance and from contaminating subsequent out-of-distribution comparisons.

Table 1. Sources contributing to the compiled training dataset after cleaning.

Source	Rows contributed	Specimen type	Remarks
Yeh, I. C. (1998) [8]	1,005	Cylinder	Widely used benchmark dataset
Shah, H. A. (2022) [2]	782	Cube	Silica-fume concrete; M5P model-tree study
Liu W. (2026) [11]	1,448	Cylinder	SCM-based concrete compilation; overlaps with three other sources, duplicates removed
Guangxi University (2024) [13]	1,580	Cube	Independent dataset; verified against GB/T 50081
Ciclab Ntust (2022) [14]	578	Cube	Published cube-strength dataset included in the multi-source compilation
Rathakrishnan V. (2022) [3]	152	Cube	High-volume GGBS concrete; boosting ML study
Total after cleaning=	**5,545**	**3,092 Cube / 2,453 Cylinder**	**Six independent published sources after duplicate removal**

3.2 The Physics Informed Empirical Equation

A physics informed empirical equation was developed on the cleaned 5,545 row dataset to predict cylinder strength as a sum of physically motivated terms, then applies a single multiplicative correction for cube specimens. The base term follows a power law form of Abrams' law in cement to water ratio, multiplied by a logarithmic age maturity function. Fly ash and silica fume contributions follow saturating exponential kinetics, reflecting the well established observation that pozzolanic reactions proceed toward a plateau rather than continuing linearly with age. Silica fume additionally carries a quadratic diminishing returns term, reflecting reduced marginal benefit at high dosages. Slag contributes through a logarithmic function of age, consistent with its slower, more sustained reaction relative to silica fume. Superplasticizer contributes through a bounded exponential form in cement content. Aggregate content enters through the water to total aggregate and coarse to total aggregate ratios.

$$f_{cy} = K\left(\frac{C}{W}\right)^{\alpha}[\ln(1+t)]^{\beta} + a_{FA}F_A(1-e^{-K_{FA}t}) + (a_{SF}S_F + b_{SF}\frac{S_F^2}{100})(1-e^{-K_{SF}t}) + a_{BFS}B_{FS}\ln(1+t) + a_{SP}S_P e^{b_{SP}C} + a_{Ag}[\frac{W}{C_{Ag}+F_{Ag}}] + b_{Ag}\left[\frac{C_{Ag}}{C_{Ag}+F_{Ag}}\right] \quad \text{--- (1)}$$

$$f_{cu} = f_{cy}R_{Cu} \;\; if\ Cube, \qquad f_{cu} = fcy \;\; if\ Cylinder$$

Here C=Cement, W=Water, F_A=Fly Ash, S_F=Silica Fume, B_{FS}=Blast Furnace Slag, S_P=Super plasticizer, C_{Ag}=Coarse Aggregate, F_{Ag}=Fine Aggregate (All concrete constituent quantities are in kg/m^3 for 1 m^3 of Concrete), t=curing time in days, f_{cy}= Cylinder compressive strength in MPa, f_{cu} = Cube compressive strength in MPa.

The fitted parameters, obtained by nonlinear least squares on the full 5,545 row dataset, are detailed in Table-2, together with coefficient of variation from 40 bootstrap resamples. All 12 fitted parameters are sign stable and fall under 20 percent coefficient of variation, with the cube to cylinder multiplier the most stable of all, at 0.8 percent.

Two reaction rate constants, governing the fly ash and silica fume kinetics, were held fixed rather than freely fit, at K_{FA}=0.02613 and K_{SF}=0.036253 respectively. Both were found to destabilize badly under bootstrap resampling when left free, correlating with and destabilizing the associated coefficient terms, indicating the compiled dataset alone cannot reliably identify them. This is a genuine limitation rather than an appeal to an external standard, since pozzolanic reaction kinetics are known to vary by material source and batch in the literature and no single universal rate constant exists to substitute in their place. Every other parameter, including the cube to cylinder multiplier, is fit freely from the data, allowing the formula to continue rederiving this value independently on every refit.

Table 2. Fitted formula parameters and bootstrap stability.

Parameter	Description	Fitted value	Bootstrap CV	Remarks
K	Strength scaling constant for cement to water power law term	18.878	4.6%	No direct equivalent; this constant is specific to this study's power law parameterization rather than a universally reported figure
α	Exponent of cement to water ratio (generalized form of Abrams' original water to cement law)	0.787	2.8%	Varies by dataset and study in the wider literature; no single agreed value, since it depends on the specific functional form chosen
β	Exponent of logarithmic age maturity term (controls how strength gain varies with time)	0.315	3.9%	Age-strength curves are commonly reported as showing rapid early strength gain followed by progressively slower development, consistent with this term's shape; exact exponent values are dataset specific
a_{FA}	Fly ash contribution coefficient	0.0885	6.8%	No single fixed literature value; pozzolanic reaction rates for fly ash are known to vary by material source and fineness
a_{SF}	Silica fume contribution coefficient	0.5215	4.8%	No single fixed literature value, for the same reason as fly ash, though silica fume is consistently reported as contributing a larger, faster acting benefit than fly ash, reflected here in a noticeably larger coefficient
b_{SF}	Silica fume diminishing returns coefficient (penalty term reducing the marginal benefit of silica fume at high dosages)	−0.2077	14.2%	Consistent with the well documented observation that Silica fume may show diminishing marginal benefit at higher dosages; no single universal coefficient is reported.
a_{SP}	Superplasticizer contribution coefficient	0.5575	19.8%	No fixed literature constant; superplasticizer performance is well known to be product and chemistry specific

b_{SP}	Superplasticizer to cement interaction rate	−0.004165	10.4%	No fixed literature constant
a_{BFS}	Blast furnace slag contribution coefficient	0.03282	2.0%	No fixed literature constant, though the logarithmic, slow and sustained shape is consistent with slag's well documented slower reaction rate relative to silica fume
a_{Ag}	Water dilution coefficient in the aggregate term	−73.05	7.9%	No directly comparable published constant; specific to this study's aggregate parameterization
b_{Ag}	Aggregate packing coefficient	−9.808	13.4%	No directly comparable published constant; specific to this study's aggregate parameterization
R_{Cu}	Cube to cylinder strength conversion factor	1.135	0.8%	EN 206-1: 1.15 to 1.25 [7]. CEB-FIP Model Code: 1.22 [6]. This study's fitted value sits at the lower edge of, but within, the published range

3.3 Machine learning models

Eight machine learning models were trained on the same compiled dataset and feature set (cement, slag, fly ash, silica fume, water, superplasticizer, coarse aggregate, fine aggregate, age and a binary cube or cylinder indicator). Two gradient boosted tree models were trained using CatBoost [4], a shallow configuration with 200 trees at depth three, and a deep configuration with 2,000 trees at depth ten. Four multilayer perceptrons, each with two hidden layers of 64 units, were trained with ReLU, Tanh, Sigmoid, and GELU activation functions respectively, isolating the effect of activation choice while holding architecture constant. Two transformer models, following a feature tokenizer architecture [5, 15] in which every input feature is projected into its own embedding, were trained at two depths, a shallow version with three encoder layers and an embedding width of 48, and a substantially deeper version with six encoder layers, an embedding width of 64 and roughly six times as many parameters overall, i.e., 303,489 versus approximately 50,000.

3.4 Out of distribution validation datasets

Two independently published datasets, never used during fitting or training of any model, were used for out of distribution evaluation. The first, referred to as OOD1, comprises 1,062 fly ash concrete records from Zhao et al. (2026) [10], itself compiling an earlier dataset reported by a separate research group. The second, referred to as OOD2, comprises self compacting concrete records from Inqiad et al. (2023) [12], drawing on thirteen underlying source studies. Both datasets were independently verified for duplicate overlap with the training compilation. Three rows in OOD2 were found to be exact, high precision matches to rows already present in the training data via the Yeh (1998) source, and were removed before evaluation, leaving 228 of the original 231 rows.

3.5 Evaluation protocol

In-distribution performance is reported using held-out R^2 and root mean squared error (RMSE) from an 80:20 train-test split. The same fixed 80:20 split was used for all nine models. For the empirical formula, 100-iteration Monte Carlo cross-validation was additionally performed. Out of distribution performance is reported as R^2 on the two independent datasets described above, with no retraining, recalibration, or parameter adjustment of any kind performed on either dataset.

4. Results

4.1 In distribution performance

Table-3 reports held out accuracy for all nine models. Every machine learning model outperforms the physics formula on this measure, with the deep CatBoost model reaching the highest held out R^2 of any model tested, 0.947, and the deep transformer close behind at 0.927. The formula's held out R^2, 0.753, is the lowest of the nine. This ordering, with models having substantially greater flexibility fitting the training population's held-out split more closely, is exactly what would be expected and is not in itself informative about which model has learned relationships that generalize beyond in-sample population.

Table 3. In distribution held out performance, all models.

Model	Parameters	Held out R^2	Held out RMSE (MPa)
Physics Informed Equation (this study Eq.1)	12 fitted parameters	0.753	10.34
CatBoost, shallow [4]	~200 trees, depth 3	0.852	8.40
CatBoost, deep [4]	~2,000 trees, depth 10	0.947	5.01
MLP, ReLU [16, 17]	~4,800	0.882	7.50
MLP, Tanh [16]	~4,800	0.876	7.68
MLP, Sigmoid [16]	~4,800	0.807	9.59
MLP, GELU [16, 18]	~4,800	0.877	7.66
Transformer, shallow [5, 15]	~50,000	0.820	9.25
Transformer, deep [5, 15]	303,489	0.927	5.63

4.2 Out of distribution performance

The picture changes substantially once the same models are evaluated on the two independent, out of distribution datasets, reported in Table-4 and ranked by mean R squared across both. The physics formula achieves the highest mean out of distribution R squared of any model tested, 0.718, ahead of the next best result, the shallow transformer at 0.640, by a margin of 0.078. The formula is the only model to exceed 0.69 on both datasets individually. The Tanh-activated MLP shows the most severe OOD degradation of any model, with a negative R^2 of −0.442 on OOD2, indicating performance worse than simply predicting the mean of that dataset.

Table 4. Out of distribution performance on two independent datasets, ranked by mean R^2

Model	OOD1 R^2	OOD2 R^2	Mean OOD R^2
Physics formula (this study Eq.1)	0.693	0.743	0.718
Transformer, shallow [5, 15]	0.638	0.643	0.640
MLP, Sigmoid [16]	0.686	0.546	0.616
CatBoost, deep [4]	0.638	0.582	0.610
MLP, ReLU [16, 17]	0.583	0.624	0.603
CatBoost, shallow [4]	0.610	0.589	0.600
MLP, GELU [16, 18]	0.607	0.495	0.551
Transformer, deep [5, 15]	0.604	0.411	0.508
MLP, Tanh [16]	0.513	-0.442	0.035

4.3 The relationship between model capacity and out of distribution generalization

The two transformer models, identical in architecture except for depth and width, provide a direct, controlled test of whether additional capacity helps or hurts generalization once a model is pushed outside its training distribution. Table-5 places their in distribution and out of distribution results side by side. Increasing the transformer's parameter count roughly sixfold, from approximately 50,000 to 303,489, increased held out R^2 from 0.820 to 0.927, a substantial improvement in in-sample performance, while decreasing mean out of distribution R squared from 0.640 to 0.508, with the second out of distribution dataset falling most sharply, from 0.643 to 0.411.

Table 5. Transformer capacity against in distribution and out of distribution performance.

Transformer version	Parameters	Held out R^2	OOD1 R^2	OOD2 R^2
Shallow	~50,000	0.820	0.638	0.643
Deep	303,489	0.927	0.604	0.411

This result is important because it isolates capacity as the variable of interest, holding architecture family, training data, and evaluation protocol fixed. The larger model exploited its additional capacity to achieve a better fit to the training population but this improvement came at the expense of performance on data drawn from different populations.

4.4 Feature importance

SHAP [19] feature importance shown in Figure-1 was computed for all nine models using a shared background and explanation sample drawn from the training population, with the physics formula treated identically to the learned models through a model agnostic Kernel SHAP explainer. Cement is identified as the most important feature by every model without exception, followed by age and either water or slag depending on the model. The physics formula's top three features, cement, age, and slag, are consistent with the other models' rankings, indicating that despite its very different functional form and far smaller parameter count, the formula distributes importance across features in a manner broadly consistent with what the flexible ML models independently learn from the data.

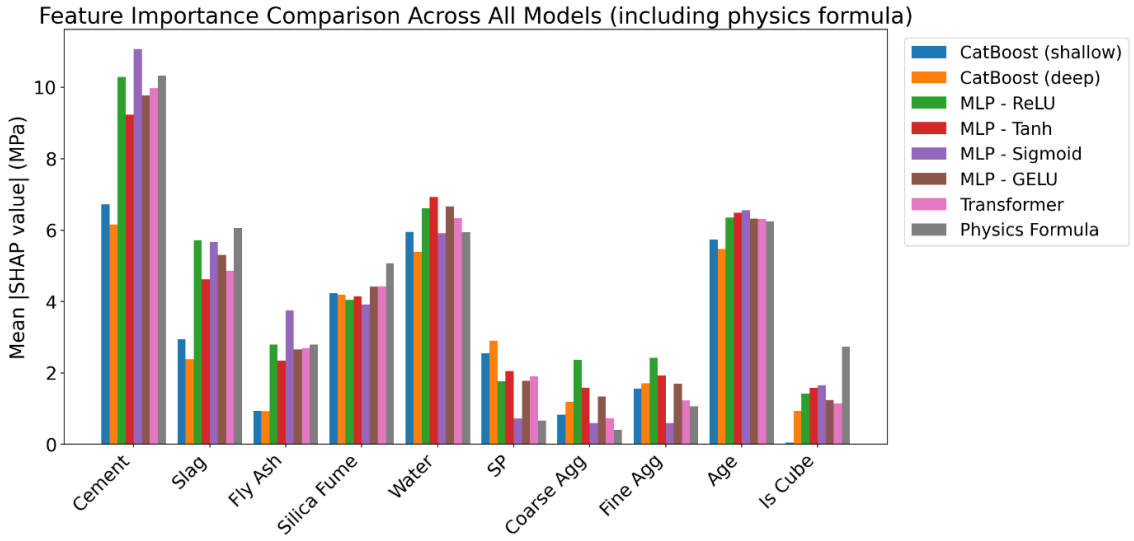


Figure 1: Feature importance comparison across all eight predictive approaches

5. Discussion

A 12 fitted parameter equation and a 300,000 parameter transformer differ in more than size, they differ in what functions they are structurally capable of representing. The formula's terms, an Abrams' law power relationship [1], saturating pozzolanic kinetics [2, 3], a logarithmic age maturity function, a cube to cylinder multiplier independently corroborated by published conversion factors [6, 7], encode constraints derived from established concrete chemistry before any data is seen. The formula cannot represent a relationship in which, for example, fly ash content correlates with strength for a reason specific to which laboratory measured a given batch, because no term in its structure has the freedom to express that kind of relationship. A flexible neural network can represent exactly that kind of spurious correlation and with sufficient capacity, the results here indicate that it can learn such correlations.

The practical implication for engineering applications of machine learning is that in sample accuracy, the number most commonly reported in the literature, is not a reliable proxy for the property that actually matters in practice, trustworthy behaviour on a new project, a new material source, or a testing convention the model has not encountered before. A model selection process that optimizes purely for held out accuracy within a single compiled dataset may favour models that perform well on the training population but generalize poorly to the independent datasets examined here. Where a credible physical model of the underlying process exists, as it does for concrete strength, this study's results suggest that structural discipline, encoding known relationships directly into a model's functional form even at real cost to in sample fit, is a defensible and in this case demonstrably superior choice for applications where the model will be asked to extrapolate, which is particularly relevant when models are deployed on projects, materials or testing conditions not represented in the training population.

6. Limitations

- The formula's scope is bounded to ordinary and high strength concrete. It does not apply to ultra high performance concrete, and this study offers no claim about its behaviour in other specialized regimes, such as lightweight or fibre reinforced concrete, that were not tested.
- The two fixed reaction rate constants governing fly ash and silica fume kinetics are set based on this dataset's own identifiability limits rather than an external, universally agreed standard, since pozzolanic reaction kinetics are known in the wider literature to vary by material source and batch.
- The out of distribution datasets, while independently published and never used in training, are themselves compilations drawing on other underlying sources. Therefore, the possibility of some undetected overlap cannot be ruled out completely, although overlap was actively checked for.

7. Conclusion

A 12 parameter, physics informed empirical formula for concrete compressive strength was compared against eight machine learning models spanning two gradient-boosted tree models, four multilayer perceptrons with different activation functions and two transformers of different depths, all trained on the same 5,545 row compiled and cleaned dataset. Every machine learning model outperformed the formula on data drawn from the same population as its training data, as expected given their far greater flexibility. On two independently published, out of distribution datasets never used in training, the formula outperformed every machine learning model tested, and a deliberate capacity increase in the best performing architecture improved in sample fit while measurably worsening out of distribution generalization, a direct demonstration that the two properties can move in opposite directions rather than tracking each other. For engineering applications in which a model is applied beyond the exact population on which it was trained, these results suggest that structural consistency with established physical relationships should be considered alongside flexibility and in-sample accuracy when selecting models for deployment beyond the training population.

Acknowledgement

I extend my heartfelt gratitude to NTPC Limited for the opportunity to pursue this study. This research paper, "Comparison of physics informed empirical equation with machine learning models for concrete compressive strength prediction under distribution shift" was made possible by the collaborative support of academic and industrial experts.

Special thanks are due to my HOD, Sh. Sudhakar Panjala and Group Head, Sh. Debasis Mandal for their unwavering guidance and my NTPC colleagues for their invaluable contributions and inputs.

References



1. Abrams, D.A., 1918. *Design of concrete mixtures* (Vol. 1). Structural Materials Research Laboratory, Lewis Institute.
2. Shah, H.A., Nehdi, M.L., Khan, M.I., Akmal, U., Alabduljabbar, H., Mohamed, A. and Sheraz, M., 2022. Predicting compressive and splitting tensile strengths of silica fume concrete using M5P model tree algorithm. *Materials*, *15*(15), p.5436.
3. Rathakrishnan, V., Bt. Beddu, S. and Ahmed, A.N., 2022. Predicting compressive strength of high-performance concrete with high volume ground granulated blast-furnace slag replacement using boosting machine learning algorithms. *Scientific Reports*, *12*(1), p.9539.
4. Prokhorenkova, L., Gusev, G., Vorobev, A., Dorogush, A.V. and Gulin, A., 2018. CatBoost: unbiased boosting with categorical features. *Advances in neural information processing systems*, *31*.
5. Vaswani, A., Shazeer, N., Parmar, N., Uszkoreit, J., Jones, L., Gomez, A.N., Kaiser, Ł. and Polosukhin, I., 2017. Attention is all you need. *Advances in neural information processing systems*, *30*.
6. Euro-International Committee for Concrete and de la Précontrainte, F.I., 1993. *CEB-FIP model code 1990: Design code*. Telford.
7. British Standards Institution, 2021. BS EN 206:2013+A2:2021. Concrete: specification, performance, production and conformity. London: BSI Standards Limited.
8. Yeh, I.C., 1998. Modeling of strength of high-performance concrete using artificial neural networks. *Cement and Concrete Research*, *28*(12), pp.1797-1808.
9. Mandal, A., 2025. Predicting compressive strength of concrete using advanced machine learning techniques: a combined dataset approach. *Asian Journal of Civil Engineering*, *26*(3), pp.1225-1241.
10. Zhao, Z., Wang, J., Ma, G. and Han, M., 2026. TabPFN-Based Prediction of Concrete Compressive Strength. *Buildings*, *16*(14), p.2781.
11. Liu, W., Mo, H. and Lee, C.K., 2026. Compressive strength prediction for SCM-based concretes using a multiple machine learning models and datasets approach. *Results in Engineering*, p.110262.
12. Inqiad, W.B., Siddique, M.S., Alarifi, S.S., Butt, M.J., Najeh, T. and Gamil, Y., 2023. Comparative analysis of various machine learning algorithms to predict 28-day compressive strength of Self-compacting concrete. *Heliyon*, *9*(11).
13. Ke, L. and Qiu, M., 2024. Dataset of compressive strength and slump of normal concrete. Mendeley Data, V1. doi:10.17632/zrsbhndz9f.1.
14. Cheng, M.Y., Cao, M.T. and Dao-Thi, N.M., 2023. A novel artificial intelligence-aided system to mine historical high-performance concrete data for optimizing mixture design. *Expert Systems with Applications*, *212*, p.118605.
15. Gorishniy, Y., Rubachev, I., Khrulkov, V. and Babenko, A., 2021. Revisiting deep learning models for tabular data. *Advances in neural information processing systems*, *34*, pp.18932-18943.
16. Rumelhart, D.E., Hinton, G.E. and Williams, R.J., 1986. Learning representations by back-propagating errors. *Nature*, *323*(6088), pp.533-536.
17. Nair, V. and Hinton, G.E., 2010. Rectified linear units improve restricted Boltzmann machines. In Proceedings of the 27th International Conference on Machine Learning (ICML), pp.807–814.



18. Hendrycks, D. and Gimpel, K., 2016. Gaussian Error Linear Units (GELUs). arXiv preprint arXiv:1606.08415.

19. Lundberg, S.M. and Lee, S.I., 2017. A unified approach to interpreting model predictions. *Advances in neural information processing systems*, *30*.

METHODOLOGICAL FRAMEWORK FOR CRADLE-TO-GATE LIFE CYCLE ASSESSMENT OF PRECAST METRO BRIDGE GIRDER

Dr. Sakthivel T., and Mr. Prasad Selvam S. R.*

L&T Construction, Heavy Civil Infrastructure (IC), Chennai, INDIA

**Corresponding author: sakthivel.t@lntecc.com*

ABSTRACT

The rapid expansion of metro rail networks has increased the demand for precast concrete construction, necessitating evaluation of their environmental impacts. This study presents a cradle-to-gate Life Cycle Assessment (LCA) of a 25 m precast U-girder used in the Chennai Metro Rail Limited (CMRL) Phase II project. The assessment considered raw material, material production, transportation and precast manufacturing processes. Primary inventory data were obtained from the casting yard, while emission factors were taken for Indian databases. Global Warming Potential (GWP) was used as the primary impact indicator. Results showed that the cradle-to-gate carbon footprint of one U-girder was 41.52 t CO_2-eq. Reinforcing steel production was the largest contributor (58.67%), followed by cement production (36.35%), together accounting for approximately 95% of total emissions. Transportation, prestressing strands, aggregates, silica fume, and admixtures contributed less than 5%. Sensitivity analysis indicated that replacing 30% of ordinary Portland cement with supplementary cementitious materials (SCMs) could reduce GWP by 10.9%. The findings highlight the significance of low-carbon steel and clinker reduction strategies in minimizing embodied carbon and provide a benchmark for sustainable metro infrastructure development.

Keywords: Life Cycle Assessment, Precast U-Girder, Metro Viaduct, Embodied Carbon, Global Warming Potential, Cradle-to-Gate, Supplementary Cementitious Materials**.**

2.0 Introduction

Metro rail has become an important part of urban transportation since it holds larger passengers, improve connectivity and reduce the dependency on road transport [1,2]. In densely developed urban territories, elevated metro offers a rational solution for constructing new transit corridors although curtailing interfering with existing land uses. Nevertheless, the extensive civil infrastructure required for metro development involves considerable consumption of concrete, steel, fuel and electricity. The environmental consequences of this resource-intensive construction therefore need to be considered together with conventional project requirements such as durability, cost, safety and schedule [3, 5]. Among the materials used in construction, cement concrete is particularly relevant to embodied-carbon reduction because of their very high global consumption and the emissions [1-4]. Energy used during production, transit of materials and elements, operation, electricity and the waste generation can also contribute to the overall burden. A meaningful carbon-reduction strategy must therefore consider the interaction of these activities throughout the construction process rather than optimizing an individual material. Life Cycle Assessment (LCA) provides a structured methodology for examining these interactions and quantifying environmental impacts associated with the systems. The consistency of a comparative LCA depends on how the assessment boundary, functional unit, inventory data, allocation procedures and relevant life-cycle stages are established [5,6]. Recent research has also highlighted the importance of considering the functional performance of structural systems when comparing their environmental impacts [6,7]. For instance, two concrete alternatives cannot certainly be considered environmentally equivalent just because they occupy the same volume if their strength and service life differs. Recent LCA studies on metro infrastructure have demonstrated that environmental impacts are

distributed across several components, including viaducts, stations, tunnels, track systems and power-related infrastructure [7,8]. Studies have further demonstrated the usefulness of LCA in identifying the components and activities that contribute significantly to the environmental burden of metro systems [9-11]. Despite the increasing application of LCA to transportation infrastructure, a specific research gap remains in relation to the environmental performance of precast girders used in elevated metros. Previous studies also provided valuable methodological insights, but their findings cannot necessarily be transferred directly to metro girders because the dimensions, structural requirements, transportation characteristics and erection methods of metro components can be substantially different. [9,10]. Evaluating these factors using the project data can thus provide a more representative understanding of the environmental performance of the system and identify the processes responsible for the largest carbon contributions.

3.0 Overview of Chennai Metro Rail Limited Phase II Project

Chennai Metro Rail Limited (CMRL) Phase II is a major urban transit designed to expand the mobility and increase the connectivity within the city. Corridor 5 extends approximately 47 km from Madhavaram to Sholinganallur, linking residential and commercial hubs. The C5-ECV-02 package comprises approximately 12.431 km of elevated viaduct from Koyamabedu to Puzhuthivakkam. The alignment passes through urban and business corridor, like Mugalivakkam, DLF IT SEZ, Chennai Trade Centre etc. The construction in a densely developed urban background exhibits a significant case for investigating material consumption, construction efficiency, and embodied carbon emissions associated with large-scale transportation infrastructure.

4.0 Methodological Framework

The present study adopts a cradle to gate methodology as provided in Figure 1 to evaluate the environmental impacts associated with the production of precast concrete U-girders employed in metro viaduct construction. It provides a systematic approach to quantify the environmental burdens arising from material, manufacturing, transportation, and precast activities prior to the delivery. Considering the substantial quantity of cement, steel, aggregates, admixtures, energy and transportation resources involved in the segment production a comprehensive assessment is essential for identifying major emission hotspots and for environmental improvement. The assessment was conducted in accordance with the principles and framework outlined in ISO 14040 and 14044 standards. The study focuses only on the quantification of impacts generated during the production stage of the U-girder and excludes impacts associated with the operational and end-of-life phases. The environmental evaluation aims to identify the contribution of each constituent material and manufacturing activity toward the overall carbon footprint and energy demand of the girder. The functional unit serves as the reference basis for all inventory calculations and environmental impact assessments conducted. It ensures consistency and comparability of results across all life cycle stages and impact categories.

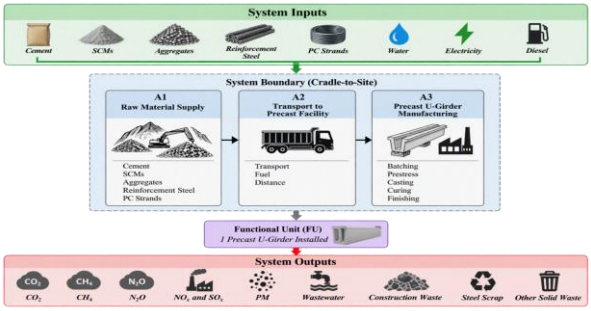


Figure 1 Cradle-to-site LCA system boundary for a precast U-girder in elevated metro viaduct construction, including modules A1-A3 from raw material supply to exit gate for installation.

The functional unit selected for the present investigation is one precast U-girder of length 25 m manufactured in a casting yard. All material quantities (see table 1), energy inputs, transportation distances, emissions, and environmental impacts are normalized with respect to this single U-girder. The selection of an individual girder as the functional unit enables a direct quantification of environmental impacts associated with the structural element commonly used in elevated metro viaduct systems. Primary inventory data were collected directly from the casting yard involved in the production. Secondary data comprising embodied energy values, emission factors and environmental impact coefficients were obtained from recognized databases and published literature relevant to Indian construction practices. The collected inventory data were subsequently converted into environmental impact indicators through characterization factors corresponding to each material and process.

The Life Cycle Impact Assessment (LCIA) phase converts the inventory flows identified in the LCI stage into measurable environmental impacts. Characterization factors are applied to inventory emissions and resource consumption data to quantify environmental impacts across multiple categories. The assessment includes Global Warming Potential (GWP) and Cumulative Energy Demand (CED). These indicators collectively provide a comprehensive evaluation of the environmental performance of precast bridge girder production. The environmental impact for each category is calculated using: $I_j = \sum(Q_i \times CF_{ij})$ where $I_j$is the impact score for category j, $Q_i$represents the quantity of emission i, and $CF_{ij}$is the characterization factor that converts the emission into the selected impact category. For Global Warming Potential, greenhouse gas emissions are expressed as carbon dioxide equivalents:$GWP = \sum(GHG_i \times GWP_i)$ where $GHG_i$is the quantity of greenhouse gas emitted and $GWP_i$is its global warming characterization factor. The resulting impact values provide a quantitative representation of the environmental consequences associated with material production, transportation and manufacturing processes within the cradle-to-gate boundary. Following impact assessment, contribution analysis is performed to identify environmental hotspots. The contribution of each process to a particular environmental impact category is calculated as: $Contribution(\%) = \frac{I_{process}}{I_{total}} \times 100$ where $I_{process}$is the environmental impact associated with an individual process and $I_{total}$is the overall impact for the selected category. This analysis assists in identifying the dominant sources of emissions and resource consumption. For example, cement production frequently accounts for the largest share of GWP due to the energy-intensive clinker manufacturing process and process-related CO_2 emissions. Quantifying the percentage contribution of each life cycle stage enables the prioritization of environmental improvement strategies and supports the development of low-carbon precast girder designs. The interpretation phase represents the final stage of the LCA study and involves evaluating the significance the impact assessment. The quantified environmental impacts and contribution analysis results are examined to identify key environmental hotspots within the cradle-to-gate production system. Emphasis is placed on materials and processes with the highest environmental burdens, such as cement production and steel manufacturing. The findings provide guidance for reducing embodied carbon, improving resource efficiency, and developing sustainable girders through optimized material selection, reduced transportation impacts, energy-efficient manufacturing processes, and increased utilization of supplementary cementitious materials.

Table 1. Material inventory for one functional unit of prestressed U-girder.

Material	Unit	Quantity per Girder
Concrete	m^3	54.00
OPC	kg	23,220
Silica Fume	kg	1,350
Fine Aggregate	kg	39,852
Coarse Aggregate	kg	27,216
Water	kg	7,125

Superplasticizer	kg	As per design
Reinforcing Steel	kg	12,000
Prestressing Strand	kg	299
Electricity Consumption	kWh	Measured value
Diesel Consumption	L	Measured value

5.0 Data Analysis and Interpretation

The calculated environmental impacts were analysed through contribution analysis and hotspot identification. Individual impacts of materials, transportation, energy consumption, and casting operations were assessed. The contribution analysis presented in Figure 2 exhibit that the reinforcing steel production is the major contributor to the cradle-to-gate GWP accounting for approximately 58.67% of the total carbon footprint. Cement production represents the second-largest contributor 36.35% of the total emissions. In contrast, transportation, prestressing strands, aggregates, silica fume and admixtures collectively account for less than 5% of the total environmental load. The high contribution of reinforcing steel is primarily attributed to the energy-intensive nature of steel manufacturing, while the significant impact of cement production is associated with clinker manufacturing and process-related carbon dioxide emissions during calcination.

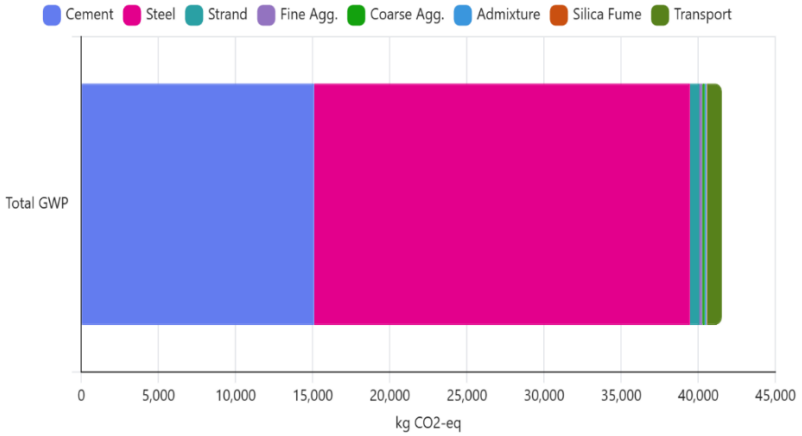


Figure 2 Contribution Analysis of GWP

Figure 2 confirms the dominance of steel and cement in influencing the environmental hotspot. It displays that the first two contributors jointly account for approximately 95% of the total GWP. Strategies such as the use of low-carbon steel, recycled steel content, clinker reduction, and alternative cementitious materials are expected to produce substantially benefits.

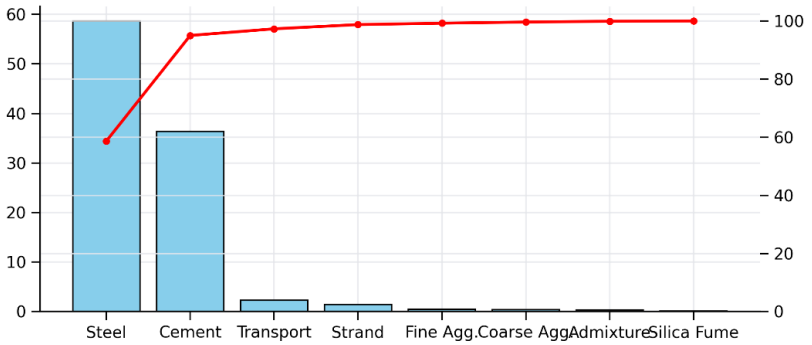


Figure 2 Environmental Hotspot Pareto Chart

The sensitivity analysis for supplementary cementitious material (SCM) replacement shown in Figure 3 demonstrates a nearly linear reduction in GWP with increasing cement replacement levels. The baseline scenario produced a carbon footprint of 41.52 t CO_2-eq per girder, while replacing 30% of the cement with SCMs reduced emissions to approximately 37.0 t CO_2-eq, corresponding to a reduction of nearly 11%. This finding confirms that cement substitution is one of the most effective mitigation strategies available for precast concrete structures. The reduction occurs because SCMs generally possess significantly lower embodied carbon than conventional Portland cement and often utilize industrial by-products that would otherwise require disposal. The results indicate that adopting SCMs can simultaneously improve sustainability and reduce environmental impacts without major modifications to existing manufacturing processes.

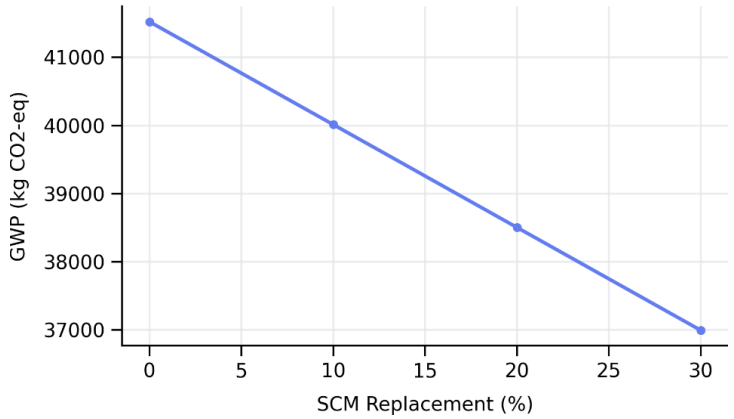


Figure 3 SCM Replacement Sensitivity

As provided in Table 2, the environmental hotspot analysis shows that reinforcing steel production is the foremost contributor accounting for 58.67% of the total environmental impact, followed by cement production at 36.35%, indicating that these two materials are responsible for over 95% of the U-girder embodied impact. Transportation and prestressing strand production contribute relatively minor shares of 2.28% and 1.46%, respectively. The impacts from aggregates, admixtures, and silica fume are negligible (<1% each).

Table 7. Environmental Hotspot Ranking

Process	**Contribution (%)**
Reinforcing Steel Production	58.67
Cement Production	36.35
Transportation	2.28
Prestressing Strand Production	1.46
Fine Aggregate Production	0.48
Coarse Aggregate Production	0.39
Admixture Production	0.28
Silica Fume Production	0.09

6.0 Conclusions

Based on the present study the following conclusion has been conclude.

- The cradle-to-gate Life Cycle Assessment (LCA) of a precast prestressed metro U-girder estimated a total carbon footprint of 41.52 t CO_2-eq per girder.

- Reinforcing steel production (58.67%) was identified as the largest contributor to environmental impacts, followed by cement manufacturing (36.35%).
- Reinforcing steel and cement collectively accounted for approximately 95% of the total Global Warming Potential (GWP), making them the primary environmental hotspots.
- Sensitivity analysis revealed that replacing 30% of cement with supplementary cementitious materials (SCMs) can reduce greenhouse gas emissions by approximately 10.9%.
- Variations in transportation distance had a limited effect on overall environmental performance compared to material-related emissions.
- The findings demonstrate that material optimization, particularly through reducing cement consumption and adopting lower-carbon steel production pathways, offers the greatest potential for environmental improvement. The study provides a useful benchmark for the environmental assessment of precast metro bridge components and supports the integration of sustainable material strategies in future urban rail infrastructure projects.

7.0 Acknowledgement

The authors sincerely thank Ms. Nandita S.K. Chakraborti, Snr. DGM & Mr. Johnson, Assistant Manager, L&T Construction, Heavy Civil Infrastructure, for their support in providing and collecting project-related data for this study.

8.0 References

1. S. Chen, Y. Teng, Y. Zhang, C. K. Y. Leung, and W. Pan, "Reducing embodied carbon in concrete materials: A state-of-the-art review," Resources, Conservation and Recycling, vol. 188, Art. no. 106653, 2023, doi: 10.1016/j.resconrec.2022.106653.
2. F. Althoey, W. S. Ansari, M. Sufian, and A. F. Deifalla, "Advancements in low-carbon concrete as a construction material for the sustainable built environment," Developments in the Built Environment, vol. 16, Art. no. 100284, 2023, doi: 10.1016/j.dibe.2023.100284.
3. J. Thorne, D. V. Bompa, M. F. Funari, and N. Garcia-Troncoso, "Environmental impact evaluation of low-carbon concrete incorporating fly ash and limestone," Cleaner Materials, vol. 12, Art. no. 100242, 2024, doi: 10.1016/j.clema.2024.100242.
4. Witte and N. Garg, "Quantifying the global warming potential of low carbon concrete mixes: Comparison of existing life cycle analysis tools," Case Studies in Construction Materials, vol. 20, Art. no. e02832, 2024, doi: 10.1016/j.cscm.2023.e02832.
5. J. A. Olsson, S. A. Miller, and J. D. Kneifel, "A review of current practice for life cycle assessment of cement and concrete," Resources, Conservation and Recycling, vol. 206, Art. no. 107619, 2024, doi: 10.1016/j.resconrec.2024.107619.
6. Haji Hossein, H. AzariJafari, and R. Khoshnazar, "The role of performance metrics in comparative LCA of concrete mixtures incorporating solid wastes: A critical review and guideline proposal," Waste Management, vol. 140, pp. 40–54, 2022, doi: 10.1016/j.wasman.2022.01.010.
7. V. Tavares, N. Soares, N. Raposo, P. Marques, and F. Freire, "Prefabricated versus conventional construction: Comparing life cycle impacts of alternative structural materials," Journal of Building Engineering, vol. 41, Art. no. 102705, 2021, doi: 10.1016/j.jobe.2021.102705.
8. J. Jayawardana, M. Sandanayake, J. A. S. C. Jayasinghe, A. K. Kulatunga, and G. Zhang, "A comparative life cycle assessment of prefabricated and traditional construction—A case of a



developing country," Journal of Building Engineering, vol. 68, Art. no. 106550, 2023, doi: 10.1016/j.jobe.2023.106550.

9. H. Kim, S. Roh, and J. Kim, "Embodied carbon of BIM bridge models according to the application of off-site prefabrication: Precast concrete applied to superstructure and substructure," Developments in the Built Environment, vol. 20, Art. no. 100550, 2024, doi: 10.1016/j.dibe.2024.100550.

10. Y. Aryan, A. K. Dikshit, and A. M. Shinde, "Life cycle environmental assessment of elevated metro rail system: Insights from the Mumbai Metropolitan Region for sustainable urban mobility," Innovative Infrastructure Solutions, vol. 10, no. 1, Art. no. 31, 2025, doi: 10.1007/s41062-024-01852-4.

11. Y. Aryan, A. K. Dikshit, and A. M. Shinde, "Environmental life cycle assessment of underground metro rail: A case study in Mumbai Metropolitan Region, India," Environmental Impact Assessment Review, vol. 106, Art. no. 107501, 2024, doi: 10.1016/j.eiar.2024.107501.

MECHANICAL PROPERTIES OF RECYCLED AGGREGATE CONCRETE MADE USING PSC AS BINDER

Bhashya V., and Bhaskar S[#].*

*Scientist-E, CSIR – Structural Engineering Research Centre, India**

Scientist-G, CSIR – Structural Engineering Research Centre, India[#]

ABSTRACT

In the present study, Experimental studies are carried out on recycled aggregate concrete (RAC). Recycled aggregate (RA) are obtained from a C&D waste processing plant located in Chennai. Physical and mechanical properties of RA and mechanical properties of concrete made by using RA have been studied. Portland slag cement (PSC) is used as binder in recycled aggregate concrete. The w/c ratio used for the conventional and RAC mixes is 0.45. Different percentage replacements of conventional aggregate (0%,50% and 100%) with recycled aggregate (both fine and coarse) are studied. It is found that concrete made using recycled aggregate showed lower compressive strength and split tensile strength when compared with natural aggregate concrete. This could be due to the presence of adhered mortar, brick waste, tiles waste, etc in the recycled aggregates. Nevertheless, concretes up to 30MPa can be made by using RA with 100% replacement of natural aggregate. Hence, by proper selection and characterization, recycled aggregate can be used in the concrete construction.

Key Words: Recycled aggregate, brick waste, tiles waste, recycled aggregate concrete, compressive strength, split tensile strength, water absorption.

1.0 Introduction

The recent surge in construction and demolition (C&D) waste production is due to rapid expansion of infrastructure, redevelopment of urban dwelling, structural renovations, and demolitions of constructed facilities. Major Indian municipalities estimate an annual C&D waste generation of approximately 150-500 million tonnes, contributing 35% to 40% of the global C&D waste each year, creating a significant challenge due to the scarcity of large landfill sites, especially in urban areas [1]. Consequently, there is a need for eco-friendly disposal methods for C&D waste. The conventional production of natural aggregates through quarrying not only impacts land stability but also disrupts local ecosystems, leading to air, water, and noise pollution. In view of economic growth of developing country like India, the development of infrastructure is pivotal. Therefore, utilizing recycled aggregate concrete could offer a single step solution to the problems of C&D waste disposal, preventing the depletion of natural resources and promoting sustainability in the future.

Ram et al. [2] reported a case of Chennai, where the existing dumpsites had been overflowing with C&D wastes necessitating the need for newer dumpsites to meet the city's disposal requirements. Kumar and Deoliya [3] focused on the application recycled concrete fine aggregate. Prajapati et al. [4] made an effort to optimize the thermos-mechanical beneficiation for the RCA. Bhashya and Bharat kumar [5] carried out experimental studies on the applicability of recycled concrete coarse aggregate (RCA).

The present study focused on concrete made using recycled aggregates (RA). These aggregates were obtained from C&D waste processing plant located in Chennai. RA is produced from C&D waste that have undergone industrial treatment processes involving sorting, crushing, and screening. The RA was a mixture of waste concrete, brick waste, tiles, glass, and a small amount of metals. Figure 1 and Figure 2 shows the composition of recycled aggregates of nominal size 10mm and 20mm.

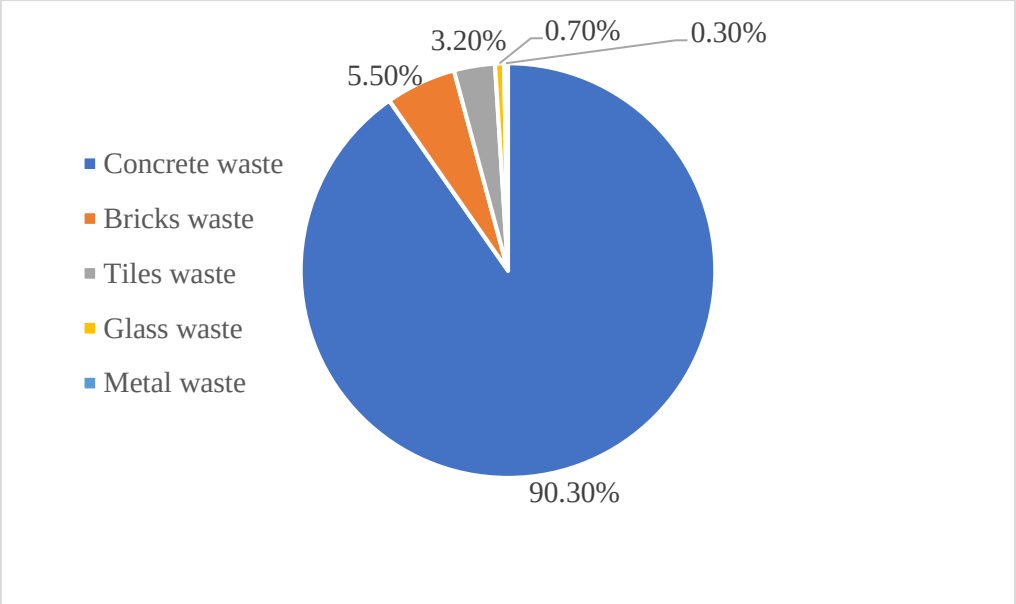


Fig-1: Composition of RA of nominal size 10 mm

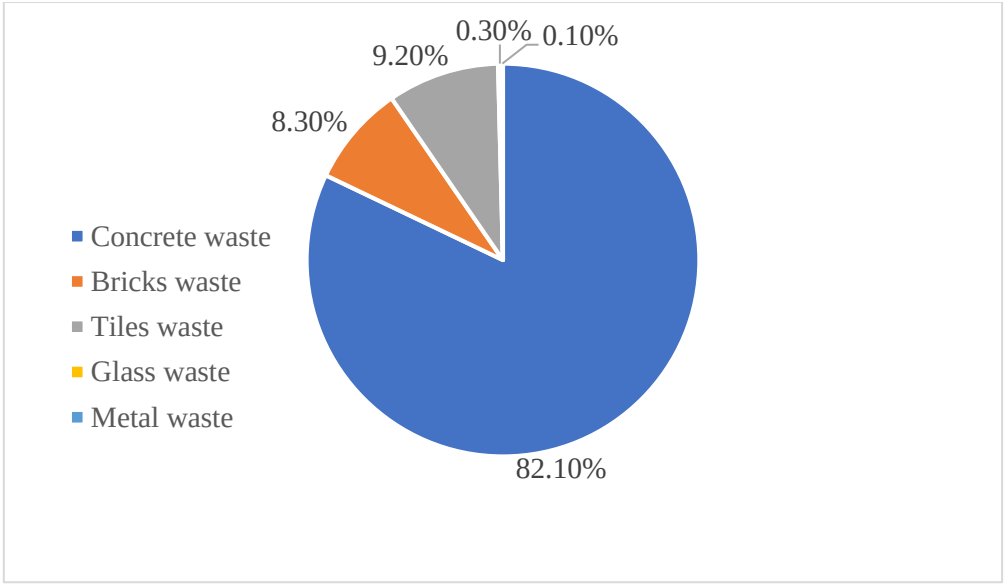


Fig-2: Composition of RA of nominal size 20 mm

2.0 Experimental work

2.1 Physical properties of RA

Physical and mechanical properties of recycled aggregate are given in Table-1. Recycled aggregate (RA) of nominal size 10mm and 20mm had very high percentages of water absorption. The influence of porous materials leads to a higher water absorption. Hence, RA with old cement paste and brick waste tends to absorb more water. The water absorption of recycled aggregate of size 10mm and 20mm are 6.42 times and 7.96 times more when compared with natural aggregate, respectively.

Recycled aggregates have lower specific gravity when compared to natural aggregates. This was due to the presence of adhered mortar, brick waste, etc in the recycled aggregates. Specific gravity of recycled aggregates of nominal size 10mm and 20mm are 11.26% and 17.72% less when compared to natural aggregates, respectively.

The crushing value of RA was found to be 32.80%, which is 56% higher than that of natural aggregate (21.02%). Similarly, the impact value of RA was found to be 34.79%, which is 46% higher than that of natural aggregate (23.84%). The resistance against crushing of RA are relatively lower than natural aggregate due to the separation and crushing of porous mortar, bricks, tiles, etc.

Table 1

Physical and mechanical properties of different aggregates

Property	**River sand**	**FRA**	**M-sand**	**NA**		**RA**	
				10mm	20mm	10mm	20mm
Specific gravity	2.59	2.40	2.39	2.71	2.74	2.41	2.25
Water absorption (%)	1.41	4.46	4.24	0.56	0.53	3.40	4.38
Crushing value (10mm-12.5mm, %)	-			21.02		32.80	
Ten percent fines value (10mm-12.5mm, kN)	-			-		70.46 (Percentage fines 8.64)	
Aggregate impact value (10mm-12.5mm, %)	-			23.84		34.79	
Fineness Modulus	2.2	3.75	2.69	6.4	7.2	5.8	6.9
Grading Zone	Zone III	Zone I	Zone II	-	-	-	-

Figure 3 shows the PSD of natural and recycled coarse aggregates. From the results it is observed that the fineness modulus of fine recycled aggregate (FRA), M-sand and river sand are 3.75, 2.69 and 2.2, respectively. Results indicate that the FRA are coarser when compared to river sand.

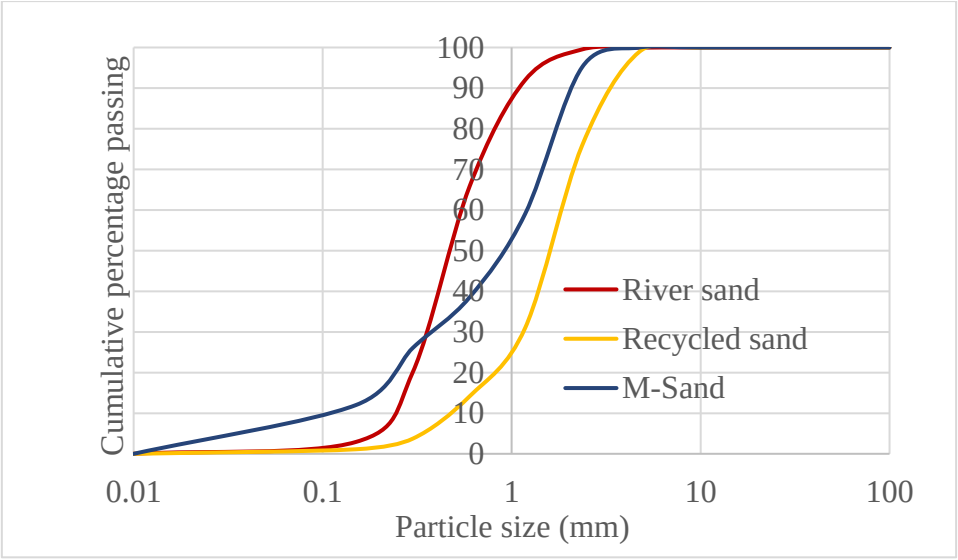


Fig-3: PSD for fine aggregates

2.2 Casting of test specimens

Experimental investigations are proposed on concrete by replacing the natural aggregates with recycled aggregates. Recycled coarse aggregate (CRA) of size 20mm and 10 mm was used in the ratio of 60:40. Portland slag cement conforming to IS 455-2015 was used [6]. Locally available M-sand (MS) passing through a 4.75-mm sieve was used as natural fine aggregate and recycled sand passing through a 4.75-mm sieve was used as fine recycled aggregate (FRA). These recycled aggregates were obtained from C&D waste processing plant located in Chennai. Blue granite crushed stone aggregate of size 20mm and 10 mm was used as same ratio of 60:40 by volume as natural aggregate (NA).

The concrete mix proportions were designed in accordance with IS 10262-2019 [7], with a common target slump of 70 ± 10 mm. A superplasticizer made of sulphonated naphthalene formaldehyde was used. The content was 0.3 to 0.5 % by weight of the binder. The w/c ratio of 0.45 is used for both conventional and recycled aggregate concrete. The mixes are designated as MS-100-NA-100, MS-100-CRA-100, FRA-100-NA-100, FRA-100-CRA-50 and FRA-100-CRA-100. The first alphabets represent fine aggregates (MS: m-sand, FRA: fine recycled aggregate), 2nd numeric digit represents the percentage replacements of fine aggregates, third alphabets represent coarse aggregates (NA: natural aggregate, CRA: coarse recycled aggregate) and 4th numeric digit represents the percentage replacement of coarse aggregates, respectively. Mix details of conventional and recycled aggregate concrete are shown in Table-2.

Table 2

Mix details of conventional and recycled aggregate concrete

Mix details of conventional and RAC (Kg/m3)						
Mix ID	Cement	M- sand	Recycled sand	NA	CRA	Water
MS-100-NA-100	413	626	-	1132	-	186
MS-100-CRA-100	413	626	-	-	960	186
FRA-100-NA-100	413	-	582	1168	-	186
FRA-100-CRA-50	413	-	582	584	503	186
FRA-100-CRA-100	413	-	582	-	1006	186

2.3 Testing of the specimens

2.3.1 Compression and splitting tensile test

Cubes of size 100mm were tested for compressive strength and the cylinders of size 100mm diameter 200mm length were tested for splitting tensile strength. Compression test was carried out at the age of 28, 56 and 90 days, split tensile strength test at the age of 28 days using compression testing machine of 1000kN capacity. The compression test and splitting tensile strength tests have been carried out as per IS 516-2021 [8].

2.3.2 Water absorption test

Water absorption in hardened concrete are determined using ASTM C 642 [9]. Concrete samples of size 50 mm thick were cut from the concrete cylinder having 100mm diameter and 200mm height. The specimens are dried in an oven at a temperature of 100^{o} C for 24 hours determined the weight (A). After final drying, cooling the specimens were immersed in water for 24 h. Determined the saturated surface dry weight of the specimen (B). The following equation is used to calculate the water absorption of concrete.

Water absorption, % = [(B – A)/A] x 100

3.0. Results and Discussions

Table-3 shows the comparison of compressive strength of natural and recycled aggregate concrete with different percentage replacement of NA at the age of 28,56 and 90 days. At 28 days, the results show that the addition of recycled aggregate resulted in 23.07%, 2.56%, 28.21% and 33.33% reduction in concrete compressive strength for MS-100-CRA-100, FRA-100-NA-100, FRA-100-CRA-50 and FRA-100-CRA-100, respectively, when compared with the control concrete (MS-100-NA-100). At 56 days and 90 days, the results show that the addition of recycled aggregate resulted in 21.73%, 4.34%, 21.73%, 34.78% and 29.09%, 16.36%, 32.72% and 41.81% reduction in concrete compressive strength for MS-100-CRA-100, FRA-100-NA-100, FRA-100-CRA-50 and FRA-100-CRA-100, respectively, when compared with the control concrete (MS-100-NA-100). This reduction can be attributed to the lower crushing value (resulted from brick aggregates, tiles, etc) of recycled aggregates compared to that of conventional aggregates. It was also contributed by the porous structure of the attached mortar of the recycled aggregates, leading to a more porous concrete matrix of recycled aggregate concrete than that of NACs. However, compressive strength of recycled aggregate concrete increased with the age and concrete made using replacement of both fine and coarse recycled aggregate achieved a compressive strength of 30MPa in 56 days.

Table 3

Compressive strength of RAC with different percentage replacement of NA

Mix ID	Average Compressive strength (MPa)		
	(28 days)	(56 days)	(90 days)
MS-100-NA-100	39	46	55
MS-100-CRA-100	30	36	39
FRA-100-NA-100	38	44	46
FRA-100-CRA-50	28	36	37
FRA-100-CRA-100	26	30	32

Table-4 shows the results of splitting tensile strength for conventional and recycled aggregate concrete. For recycled aggregate concrete, the results show that the splitting tensile strength of recycled aggregate concrete were lower when compared with conventional concrete in a similar manner to that observed in the compressive strength tests. The reduction in splitting tensile strength for RAC were 16.83%, 2.02%, 5.72% and 23.91% for MS-100-CRA-100, FRA-100-NA-100, FRA-100-CRA-50 and FRA-100-CRA-100, respectively, when compared with the control concrete (MS-100-NA-100). Reduction in splitting tensile strength of RAC when compared with NAC were due to the adhered old cement mortar, brick waste, tiles waste, etc. in the recycled aggregate and the weaker interfacial zone between new cement mortar and recycled aggregate.

Table 4

Split tensile strength for recycled aggregate concrete

Mix ID	Average splitting tensile strength (MPa) (28 days)
MS-100-NA-100	2.97
MS-100-CRA-100	2.47
FRA-100-NA-100	2.91

FRA-100-CRA-50	2.80
FRA-100-CRA-100	2.26

Figure 4 shows the results of water absorption for conventional and recycled aggregate concrete. The results show that the water absorption of recycled aggregate concrete was higher when compared with conventional concrete. The water absorption for MS-100-CRA-100, FRA-100-NA-100, FRA-100-CRA-50 and FRA-100-CRA-100 were 1.55, 1.06, 1.22 and 1.63 times of the control concrete (MS-100-NA-100), respectively. The increase in water absorption of RAC when compared with NAC were due to the adhered old cement mortar, brick waste, tiles waste, etc. in the recycled aggregate.

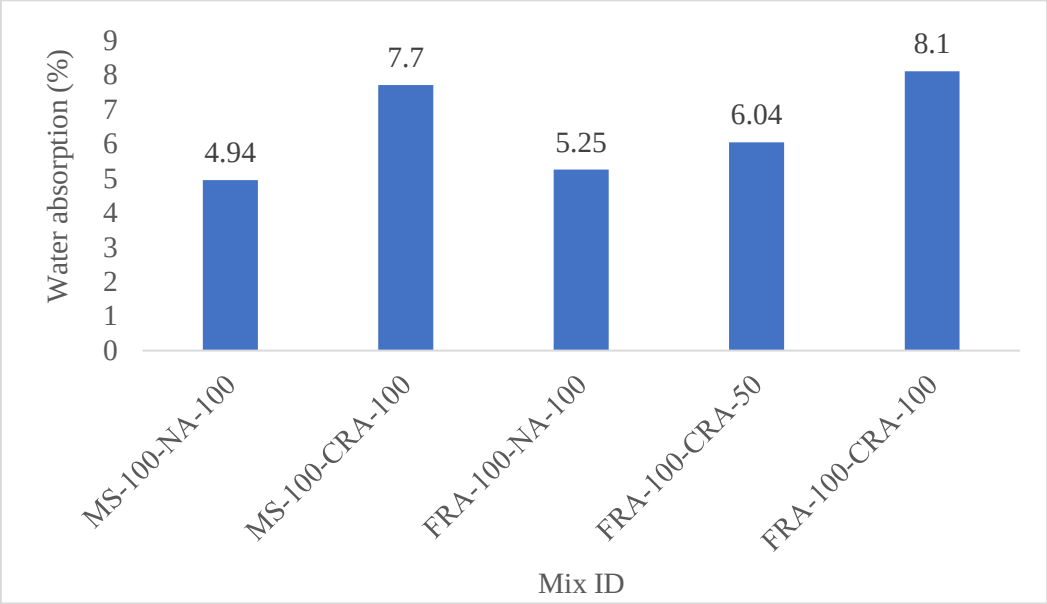


Fig-4: Water absorption of RAC with different % replacement of NA with RA

4.0 Conclusions

In this study, experimental investigations were carried out on concrete made using recycled aggregate (RA) which are obtained from a C&D waste processing plant located in Chennai. Physical and mechanical properties of RA and also mechanical properties of concrete made by using RA are studied. The experimental studies are carried out using PSC as binder. Recycled aggregate concrete made using replacement of both fine and coarse aggregates with natural aggregate are studied in detail. Results show that the water absorption of recycled aggregate are 6 to 8 times more when compared with natural aggregate, however, within the limits asper IS 383-2016 [10]. Specific gravity of recycled aggregates are 11 to 17 times less when compared to natural aggregates. The replacement of NA with 100% recycled aggregates resulted in a significant reduction (up to 33%) in concrete compressive strength compared with the control concrete at the curing age of 28 days. The water absorption of concrete made using recycled aggregates is below 10%. The splitting tensile strength of recycled aggregate concrete were lower when compared with conventional concrete in a similar manner to that observed in the compressive strength tests. This could be due to the presence of adhered mortar, brick waste, tiles waste, glass waste, etc in the recycled aggregates. However, concrete made using recycled aggregate (both fine and coarse aggregates) achieved an average compressive strength of 30MPa at the curing age of 56 days. Hence, recycled aggregate can be used in the concrete construction.

5.0 Acknowledgement

This paper is being published with kind permission of the Director, CSIR-Structural Engineering

Research Centre (SERC) Chennai. Authors gratefully acknowledge the support of project team and technical staff at Advanced Materials Laboratory (AML), SERC, Chennai during the experimental work. This paper has been assigned the registration number CSIR-SERC-11/2026 and the research is funded by generous grant from CSIR, New Delhi.

6.0 References

1. https://www.pib.gov.in/PressReleaseDetail.aspx?PRID=2007106&reg=3&lang=1, Ministry of Housing & Urban Affairs, 19 FEB 2024, PIB Delhi.
2. Ram, V.G., Kishore, K.C. and Kalidindi, S.N. (2020) "Environmental benefits of construction and demolition debris recycling: Evidence from an Indian case study using life cycle assessment", Journal of Cleaner Production, 255:120258.
3. Kumar, G.S. and Deoliya, R. (2022) "Recycled cement and recycled fine aggregates as alternative resources of raw materials for sustainable cellular light weight flowable material", Construction and Building Materials, 326:126878.
4. Prajapati, R., Gettu, R. and Singh, S. (2021) "Thermomechanical beneficiation of recycled concrete aggregates (RCA)", Construction and building materials, 310:125200.
5. Bhashya, V. and Bharatkumar, B.H. (2018) "Mechanical and durability properties of concrete produced with treated recycled concrete aggregate'' ACI Materials Journal, 115 (2):209-217.
6. Bureau of Indian Standards (BIS), "Portland slag cement-Specification", IS: 455-2015, BIS, New Delhi, India.
7. Bureau of Indian Standards (BIS), "Concrete mix proportioning-Guidelines", IS: 10262-2019, BIS, New Delhi, India.
8. Bureau of Indian Standards (BIS), "Hardened concrete- Methods of test", IS: 516 (Part 1/Sec 1)-2021, BIS, New Delhi, India.
9. ASTM C 642-21. Standard test method for density, absorption and voids in hardened concrete. American Society for Testing and Materials Standard Practice, Philadelphia, Pennsylvania.
10. Bureau of Indian Standards (BIS), "Coarse and fine aggregate for concrete specification", IS: 383-2016, BIS, New Delhi, India.

DEVELOPMENT AND EXPERIMENTAL VALIDATION OF A MIX DESIGN FOR AMBIENT-CURED GEOPOLYMER CONCRETE

*S Jagandas, Prabha Mohandoss**

Ph.D. Scholar, Department of Civil Engineering, National Institute of Technology Tiruchirappalli, Trichy, Tamil Nadu, India

Assistant Professor, Department of Civil Engineering, National Institute of Technology Tiruchirappalli, Trichy, Tamil Nadu, India

**Corresponding Author: prabham@*nitt.edu

Abstract

The decarbonization of the construction industry requires sustainable alternatives to ordinary Portland cement (OPC) concrete with reduced environmental impacts and practical field applicability. This study presents a novel mix design procedure for ambient-cured geopolymer concrete (GPC) incorporating fly ash (FA) and ground granulated blast furnace slag (GGBS), activated using a single alkaline solution, Neutral Grade Sodium Silicate (NGSS), with silica moduli (Ms = SiO_2/Na_2O) of 2.92 and 3.5. The proposed GPC mix design integrates the absolute volume method of IS 10262:2019 with DIN EN 206:2021 aggregate grading, considering NGSS-to-binder (NGSS/B) ratios of 0.4–0.8 to achieve improved material utilization and mechanical performance. The influence of binder composition, activator chemistry, and mix proportions on compressive strength. The 100% GGBS mortar achieved 28-day compressive strengths of 52.13 MPa and 62.39 MPa at Ms values of 2.92 and 3.5, respectively. Microstructural observations revealed a denser reaction matrix with increasing GGBS content, at lower NGSS/B ratios. The proposed methodology eliminates the need for separate NaOH preparation and external heat curing, offering a simplified approach for developing sustainable, high-performance GPC. The findings demonstrate the potential of NGSS-based geopolymer technology to support resource efficiency industrial by-product utilization, and low-carbon construction practices.

Keywords: Ambient-cured geopolymer concrete; Neutral Grade Sodium Silicate; Sustainable mix design; Carbon reduction; Microstructural characterization.

Introduction

The increasing demand for sustainable construction materials has encouraged the development of alternative binders to reduce the environmental impacts associated with ordinary Portland cement (OPC) production. Geopolymer concrete (GPC), produced through the alkaline activation of aluminosilicate-rich industrial by-products, has emerged as a promising alternative owing to its potential for reduced carbon emissions and satisfactory mechanical performance [1-2]. Fly ash (FA) and ground granulated blast furnace slag (GGBS) are widely investigated precursors because of their availability and complementary chemical characteristics. However, FA-based GPC often require elevated-temperature curing to achieve adequate early-age strength, whereas GGBS incorporation promotes strength development under ambient conditions through the formation of N-A-S-H gels. But the variations in precursor composition, activator chemistry, and curing conditions significantly influence compressive strength performance [3-5].

Despite considerable advancements, the absence of a universally accepted mix design methodology remains a major challenge for the practical implementation of GPC. Unlike OPC concrete, GPC mix proportioning involves several interdependent parameters, including precursor composition, alkaline activator concentration, silica modulus, solution/binder ratio [5-7]. Similarly, proposed an ambient-cured GPC mix design incorporating the absolute volume method, combined aggregate grading, and a solution/binder to strength relationship [2]. Although these approaches established systematic

proportioning procedures, their applicability was evaluated using specific alkaline activator compositions, particularly combined sodium hydroxide (NaOH) and sodium silicate solutions, limiting their direct application to alternative single-solution activators [1-7].

The proposed a comprehensive mix design methodology for FA-based geopolymer mortar based on target compressive strength and workability [3]. However, the procedure required separate NaOH and sodium silicate solutions and elevated-temperature curing. Onoue et al. (2019, 2022) employed the Taguchi method to optimize activator composition, mixing conditions, and curing parameters, demonstrating the complexity of geopolymer manufacturing. The utilized response surface methodology to optimize ambient-cured FA/GGBS GPC, achieving a compressive strength of 80.46 MPa [8-12]. Nevertheless, these approaches primarily relied on dual alkaline activators and empirical optimization rather than establishing a simplified, code-based concrete mix design methodology. More recently, developed a mix design procedure for one-part FA/GGBS GPC using solid alkaline activators; however, its applicability to liquid sodium silicate-activated concrete remains unexplored[13-15].

Conventional GPC production commonly involves separate NaOH and sodium silicate solutions, requiring careful control of NaOH molarity, solution proportions, and preparation procedures [16-17]. Furthermore, elevated-temperature curing increases processing requirements and restricts field applicability [18-20]. Neutral Grade Sodium Silicate (NGSS), a commercially available liquid alkaline activator, offers an alternative by supplying soluble silica, alkali, and water through a single solution, eliminating separate NaOH preparation. However, the silica modulus (Ms = SiO_2/Na_2O) and NGSS-to-binder (NGSS/B) ratio govern the availability of reactive species, dissolution kinetics, gel formation, and resulting mechanical properties. Despite their significance, the combined effects of NGSS chemistry, FA/GGBS composition, and activator dosage have received limited attention within existing code-based GPC mix design methodologies.

Furthermore, conventional concrete mix design standards, including IS 10262:2019, provide systematic volumetric proportioning principles but do not explicitly account for alkaline activator chemistry and geopolymerization reactions. Although previous studies have incorporated absolute volume calculations and aggregate grading, a validated framework integrating these principles with single-solution NGSS activation at different Ms remains limited in the reviewed literature.

To address these research gaps, the present study proposes a systematic mix design procedure for ambient-cured FA/GGBS GPC by integrating the absolute volume method of IS 10262:2019 with DIN-based combined aggregate grading. The methodology considers NGSS silica moduli of 2.92 and 3.5 and NGSS/B ratios ranging from 0.4 to 0.8. The influence of binder composition and activator chemistry on compressive strength and microstructural development is evaluated using experimental testing and scanning electron microscopy (SEM). The proposed approach eliminates separate NaOH preparation and external heat curing, providing a simplified mix proportioning framework for developing sustainable GPC with improved practical applicability.

Experimental work

Materials

The primary materials used in this study were fly ash (FA), ground granulated blast furnace slag (GGBS), Neutral Grade Sodium Silicate (NGSS), fine aggregate, and coarse aggregate. FA and GGBS were employed as aluminosilicate-rich precursors for producing ambient-cured GPC. The FA contained predominantly SiO_2 (60.11%) and Al_2O_3 (26.54%), whereas GGBS consisted mainly of CaO (32.65%), SiO_2 (34.07%), and Al_2O_3 (20.05%). Commercially available liquid NGSS was used as the sole alkaline activator, eliminating the need for separate sodium hydroxide (NaOH) preparation. Two NGSS solutions with silica moduli (Ms = SiO_2/Na_2O) of 2.92 and 3.5 were investigated. The corresponding SiO_2, Na_2O, and H_2O contents were 28.98%, 9.92%, and 61.10% for Ms = 2.92 and 31.12%, 8.89%, and 60.00% for Ms = 3.5, respectively. Coarse and fine aggregates were proportioned using a combined

grading approach, with fine aggregate, 6–12 mm coarse aggregate, and 12–20 mm coarse aggregate constituting 40%, 43%, and 17% of the total aggregate mass, respectively. All mixtures were prepared and cured under ambient conditions without external heat treatment.

Proposed mix design procedure

The proposed mix design procedure adapts the concrete proportioning principles of IS 10262:2019. The absolute volume method is used for constituent calculations, while DIN-based combined aggregate grading is used to select aggregate fractions. The method is adapted to FA/GGBS GPC activated by a NGSS solution under ambient curing.

Step 1. Determination of target mean compressive strength

The specified characteristic compressive strength (fck) was selected, and a coefficient of variation (CoV) of 5% was assumed for preliminary laboratory proportioning. The standard deviation and target mean strength were calculated as follows. The assumed CoV is a study assumption, not a prescribed value of IS 10262:2019.

$S = 0.05 \times fck$

$f'ck = fck + 1.65S$

Step 2. Selection of NGSS content

NGSS dosage was maintained at 186 kg/m³ for all mixtures from IS 10262:2019, based on preliminary trials targeting approximately 50–100 mm slump and a nominal maximum aggregate size of 20 mm.

Step 3. Selection of NGSS/binder

The conventional strength-based W/c ratio selection concept was adapted by treating NGSS/B as the principal proportioning variable. Ratios of 0.4, 0.5, 0.6, 0.7, and 0.8 were investigated, and their 28-day compressive strengths were established experimentally. IS 10262:2019 does not specify NGSS/B–strength relationships.

Step 4. Selection of combined aggregate grading

A DIN-based combined aggregate grading concept was adopted to obtain a suitable particle-size distribution. The selected blend comprised 40% fine aggregate passing 4.75 mm, 43% coarse aggregate in the 6–12 mm fraction, and 17% coarse aggregate in the 12–20 mm fraction, expressed by mass.

Step 5. Calculation of total binder content

With NGSS fixed at 186 kg/m³, total binder content was calculated from the selected NGSS/B ratio.

$$Binder\ content\ (B) = \left(\frac{NGSS}{\left(\frac{NGSS}{B}\right)}\right)$$

Step 6. Calculation of aggregate volume

The absolute volume method was adapted to calculate the aggregate volume after subtracting the volumes of FA, GGBS, NGSS, and entrapped air from 1 m³ of concrete. An entrapped air fraction of 2% was assumed for this study; it should not be presented as the IS 10262:2019 tabulated value for 20 mm aggregate.

$$VA = 0.98 - \left\{\left(\frac{W_{FA}}{SG_{FA}} + \left(\frac{W_{GGBS}}{SG_{GGBS}}\right)\right\} + \left\{\left(\frac{W_{NGSS}}{SG_{NGSS}}\right)\right\} \times \left(\frac{1}{1000}\right)\right\}$$

Step 7. Calculation of individual aggregate quantities

For aggregate proportions defined on a mass basis, total aggregate mass was determined from the combined absolute volume and individual specific gravities. The selected mass fractions were then applied to calculate the constituent aggregate masses.

Weight of aggregate = a% $\times V_A \times SG \times 1000$

Step 8. Experimental validation (IS 10262:2019)

The proposed mixtures were evaluated through 7- and 28-day compressive strength tests under ambient curing. Relationships between NGSS/B and 28-day strength were established separately for both Ms. The trial-mix verification concept of IS 10262:2019 was adopted, while the geopolymer-specific strength relationships were experimentally derived.

Results to validate mix design

TABLE 3. COMPRESSIVE STRENGTH OF AMBIENT-CURED GEOPOLYMER CONCRETE AT DIFFERENT NGSS/B RATIOS, SILICA MODULI, AND CURING AGES.

NGSS/B Ratio	7-day Compressive Strength (MPa)		28-day Compressive Strength (MPa)		56-day Compressive Strength (MPa)	
	Ms = 2.92	Ms = 3.5	Ms = 2.92	Ms = 3.5	Ms = 2.92	Ms = 3.5
0.4	35.18	37.84	52.13	54.51	55.81	62.39
0.5	27.52	30.23	46.47	48.45	49.84	50.25
0.6	18.51	19.81	31.63	35.22	37.75	40.51
0.7	17.23	18.22	29.55	31.10	36.73	38.18
0.8	13.18	13.85	24.13	28.18	29.70	31.00

Influence of NGSS/B ratio on compressive strength

A systematic inverse relationship was observed between the NGSS/B ratio and compressive strength at all curing ages shown in Figure 1. At 28 days, increasing NGSS/B from 0.4 to 0.8 decreased strength from 52.13 to 24.13 MPa (53.71%) for Ms = 2.92 and from 54.51 to 28.18 MPa (48.30%) for Ms = 3.5. The corresponding 7-day decreases were 62.54% and 63.40% shown in Table 3. Because NGSS dosage was fixed at 186 kg/m³, increasing NGSS/B simultaneously reduced binder content from 500 to 250 kg/m³. Lower binder availability may limit reaction-product formation and matrix densification; confirmation of this mechanism requires microstructural evidence.

Influence of silica modulus and curing age

The higher Ms = 3.5 produced greater compressive strength than Ms = 2.92 at every tested ratio and age. At 28 days, the relative gain ranged from 4.26% (NGSS/B = 0.5) to 16.78% (NGSS/B = 0.8). At NGSS/B = 0.4, 56-day strength increased from 55.81 to 62.39 MPa, an 11.79% improvement trend shown in Figure 1. The effect associated with differences in available silica and alkali, although the solutions differ in both constituents. All mixtures gained strength between 7 and 56 days, consistent with continuing reactions under ambient curing.

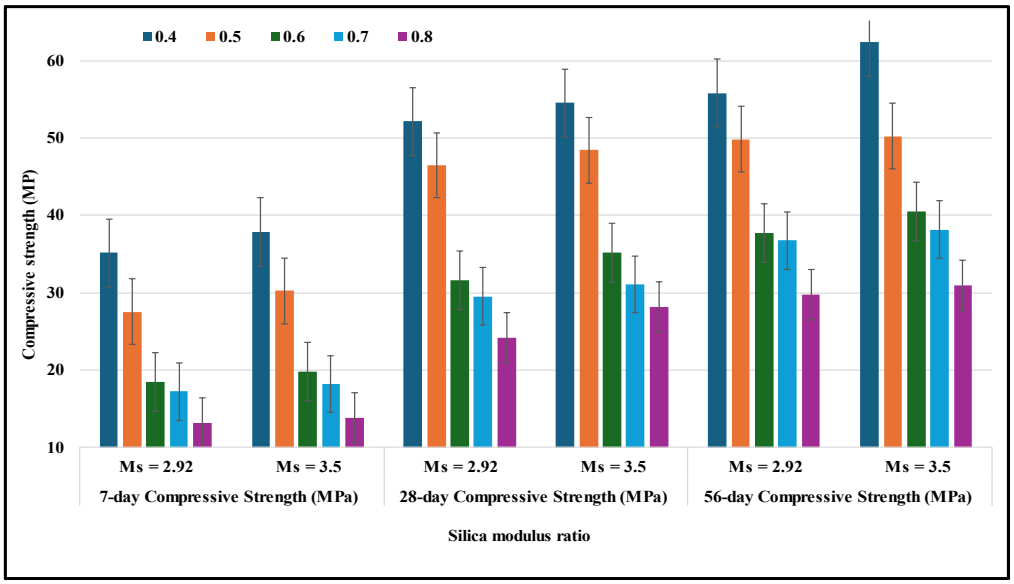


Figure 1. Effect of NGSS/B ratio and silica modulus on the compressive strength of ambient-cured geopolymer concrete at different curing ages.

Standard deviation and coefficient of variation

TABLE 4. STATISTICAL ANALYSIS OF COMPRESSIVE STRENGTH AT DIFFERENT CURING AGES

Age	Ms	Mean (MPa)	Sample SD (MPa)	CoV (%)	Linear R^2
7	2.92	22.32	8.89	39.84	0.932
	3.5	23.99	9.80	40.86	0.936
28	2.92	36.78	11.92	32.41	0.936
	3.5	39.49	11.43	28.94	0.938
56	2.92	41.97	10.60	25.25	0.950
	3.5	44.47	12.16	27.34	0.948

As shown in Table 4 Across the five mix ratios, the 28-day mean strengths were 36.78 MPa (Ms = 2.92) and 39.49 MPa (Ms = 3.5), with sample SDs of 11.92 and 11.43 MPa and CoVs of 32.41% and 28.94%, respectively. These values quantify intentional differences between mixture proportions. They must not be compared with the assumed 5% laboratory CoV as if they represented specimen-level variability. Replicate cube or cylinder strengths for each mix and age are needed to determine experimental SD, CoV, and uncertainty.

Assessment of the proposed mix design methodology

The strength results provide preliminary support for the proposed mix proportioning framework, which adapts the absolute volume principle of IS 10262:2019 and uses DIN-based aggregate grading alongside a single NGSS activator. At NGSS/B = 0.4, 28-day compressive strengths reached 52.13 MPa (Ms = 2.92) and 54.51 MPa (Ms = 3.5), demonstrating the feasibility of relatively high-strength ambient-cured mixtures. The monotonic strength trend and the 28-day linear fits ($R^2 \approx 0.94$) support NGSS/B as an empirical proportioning parameter within this experimental domain. However, compliance with a specified characteristic strength, the assumed 5% CoV, and true predictive validation cannot be established from mix means alone. Independent confirmation mixtures and replicate specimen data are required.

Limitations and requirements for full validation

Report individual replicate compressive strengths for each NGSS/B ratio, silica modulus, and curing age to calculate within-mixture SD and CoV. Compare experimentally observed mean and characteristic strengths with the target strengths used in the proposed design. Use independent trial mixes to quantify prediction errors of the empirical 28-day strength equations. Clarify the exact DIN grading standard and the mass-versus-volume basis of the aggregate proportions. Describe IS 10262:2019 as an adapted absolute volume framework, not as a code prescribing NGSS/B ratios.

Conclusions

- The proposed mix design methodology, developed by adapting the absolute volume principles of IS 10262:2019 and incorporating DIN-based aggregate grading, demonstrated the feasibility of proportioning ambient-cured geopolymer concrete using a single NGSS solution without additional NaOH or external heat curing.
- The NGSS/B ratio significantly influenced compressive strength. Increasing the ratio from 0.4 to 0.8 reduced the 28-day strength by 53.71% (52.13 to 24.13 MPa) for Ms = 2.92 and 48.30% (54.51 to 28.18 MPa) for Ms = 3.5, primarily associated with the reduction in binder content from 500 to 250 kg/m³.
- Increasing the silica modulus from 2.92 to 3.5 consistently improved compressive strength. At NGSS/B = 0.4, the 56-day strength increased from 55.81 to 62.39 MPa, representing an 11.79% improvement, indicating the beneficial influence of the higher-modulus NGSS solution within the investigated range.
- The highest 28-day compressive strengths of 52.13 MPa and 54.51 MPa were achieved at NGSS/B = 0.4 for Ms = 2.92 and 3.5, respectively. The corresponding 56-day strengths reached 55.81 and 62.39 MPa, confirming continued strength development under ambient curing conditions.
- Linear regression analysis established strong inverse relationships between NGSS/B ratio and 28-day compressive strength, with coefficients of determination of R^2 = 0.936 and 0.938 for Ms = 2.92 and 3.5, respectively. These relationships provide a preliminary basis for strength-oriented mix proportioning within the investigated range.
- The experimental results support the feasibility of the proposed NGSS-based mix design framework. However, independent trial mixtures and specimen-level statistical analysis are required to confirm characteristic-strength compliance, experimental variability, and the broader predictive reliability of the methodology.

References

1. Rafeet, a., vinai, r., soutsos, m. and sha, w. (2017). guidelines for mix proportioning of fly ash/ggbs based alkali activated concretes. construction and building materials, 147, 130–142.
2. Reddy, m. s., dinakar, p. and rao, b. h. (2018). mix design development of fly ash and ground granulated blast furnace slag based geopolymer concrete. journal of building engineering, 20, 712–722.
3. Naghizadeh, a. and ekolu, s. o. (2019). method for comprehensive mix design of fly ash geopolymer mortars. construction and building materials.
4. Shi, x., zhang, c., wang, x., zhang, t. and wang, q. (2022). response surface methodology for multi-objective optimization of fly ash-ggbs based geopolymer mortar. construction and building materials, 315, 125644.



5. Onoue, k., sagawa, y., atarashi, d. and takayama, y. (2022). optimization of mix proportions and manufacturing conditions of fly ash-based geopolymer mortar by parameters design with dynamic characteristics. cement and concrete composites, 133, 104645.

6. Naghizadeh, a. and ekolu, s. o. (2020). effects of compositional and physico-chemical mix design parameters on properties of fly ash geopolymer mortars.

7. Ge, x., hu, x. and shi, c. (2022). the effect of different types of class f fly ashes on the mechanical properties of geopolymers cured at ambient environment. cement and concrete composites, 130, 104528.

8. Hardjito, d., wallah, s. e., sumajouw, d. m. j. and rangan, b. v. (2004). on the development of fly ash-based geopolymer concrete. aci materials journal, 101(6), 467–472.

9. Lloyd, n. a. and rangan, b. v. (2010). geopolymer concrete with fly ash. second international conference on sustainable construction materials and technologies.

10. Deb, p. s., nath, p. and sarker, p. k. (2014). the effects of ground granulated blast-furnace slag blending with fly ash and activator content on the workability and strength properties of geopolymer concrete cured at ambient temperature. materials & design, 62, 32–39.

11. Nath, p. and sarker, p. k. (2014). effect of ggbfs on setting, workability and early strength properties of fly ash geopolymer concrete cured in ambient condition. construction and building materials, 66, 163–171.

12. provis, j. l. and van deventer, j. s. j. (2009). geopolymers: structures, processing, properties and industrial applications. woodhead publishing.

13. Provis, j. l. (2018). alkali-activated materials. cement and concrete research, 114, 40–48.

14. Ismail, i., bernal, s. a., provis, j. l., san nicolas, r., brice, d. g., kilcullen, a. r., hamdan, s. and van deventer, j. s. j. (2013). influence of fly ash on the water and chloride permeability of alkali-activated slag mortars and concretes. construction and building materials, 48, 1187–1201.

15. García-lodeiro, i., palomo, a., fernández-jiménez, a. and macphee, d. e. (2011). compatibility studies between n-a-s-h and c-a-s-h gels. study in the ternary diagram na_2o–cao–al_2o_3–sio_2–h_2o. cement and concrete research, 41(9), 923–931.

16. Yip, c. k., lukey, g. c. and van deventer, j. s. j. (2005). the coexistence of geopolymeric gel and calcium silicate hydrate at the early stage of alkaline activation. cement and concrete research, 35(9), 1688–1697.

17. Duxson, p., fernández-jiménez, a., provis, j. l., lukey, g. c., palomo, a. and van deventer, j. s. j. (2007). geopolymer technology: the current state of the art. journal of materials science, 42, 2917–2933.

18. Turner, l. k. and collins, f. g. (2013). carbon dioxide equivalent (co_2-e) emissions: a comparison between geopolymer and opc cement concrete. construction and building materials, 43, 125–130.

19. Bureau of indian standards (2019). is 10262:2019, concrete mix proportioning—guidelines. bureau of indian standards, new delhi, india.

20. Deutsches institut für normung (2021). din en 206:2021, concrete—specification, performance, production and conformity. din, germany.

PERFORMANCE AS THE CRITERION FOR DURABILITY IN CONCRETE MIX PROPORTIONING

B. Kameswara Rao (ORCID ID: 0000-0002-6161-2575),

Civil Engineering Department, KL (deemed to be) University, Vaddeswaram, AP, India.

bkrao1@kluniversity.in

Abstract:

Usually, a concrete mix is proportioned to satisfy the three criteria: strength, workability, and Durability. Durability is met by prescribing certain minimum cement content, minimum compressive strength, maximum water-binder ratio, and more parameters suited to concrete exposure conditions. These criteria often yield unsatisfactory results and underestimate the potential of supplementary cementitious materials. It is generally accepted that concrete's resistance to the penetration of aggressive media reflects an accurate picture of Durability.

Given this, some experimental studies have been conducted to express durability in terms of coulombs (charge passed from one end to the other) due to chloride ion penetration. This charge is linked to different water-binder ratios and percentages of supplementary cementitious materials (SCMs) over varying curing days. This data will help the mix designer proportion the concrete by expressing durability in terms of Chloride Ion Permeability.

Keywords: Performance, Chloride Ion Permeability, Durability, Coulombs, Supplementary Cementitious Materials.

1 Introduction

Construction requires large amounts of concrete, making it the second-most consumed material (only water consumes more). This chapter discusses the sustainability of concrete and assesses its carbon footprint from life cycle and environmental-impact perspectives, emphasizing cement and cement-substitute materials used in construction. The life-cycle evaluation of concrete includes data on raw material production, concrete manufacture, and the use of additional materials such as fly ash and metakaolin, silica fume, ground-granulated blast-furnace slag, chemical admixtures, and concrete recycling. It describes reducing concrete's environmental impact by partially replacing cement, improving cement manufacturing, developing alternative binders, reusing waste by-products, and improving Durability. This chapter discusses substituting cement with fly ash, GGBS, and silica fume; it uses the Rapid chloride penetration test to assess the Durability of concrete with different replacement binders and water-binder ratios. Corrosion of reinforcing steel caused by chloride intrusion is generally a prevailing environmental attack that causes concrete structures to deteriorate. Bridge deck overlays, parking garages, marine buildings, industrial structures, etc., are being damaged by poor concrete quality, which causes corrosion and incurs repair costs in the millions of dollars annually. Because of recurring repair costs, the durability issue has received more attention in recent years.

Chlorides enter crack-free concrete through several mechanisms, including capillary absorption, hydrostatic pressure, diffusion, and evaporative movement. Diffusion is the most common. Diffusion happens when chloride absorption on the external surface of a concrete member is larger than the concentration on the internal surface. As a result, chloride ions pass through the concrete to the reinforcement steel level. Alternating wetting and drying cycles in oxygen favor reinforcement corrosion. The pore Structure inside the concrete mainly determines the rate of chloride ion infiltration. Factors influencing pore Structure include mix design, degree of hydration, curing conditions, usage of extra cementitious ingredients, and building procedures. As a result, if chloride-induced corrosion is possible, the concrete must be tested for chloride permeability. We want a quick, easy check for project

conditions and quality control. The rapid chloride permeability test meets these objectives. Whiting invented the RCPT in 1981, and its results closely match the traditional 90-day salt ponding test. AASHTO T 277 or ASTM C 1202 have standardized testing protocols.

2 Literature Survey

In an experimental study on chloride penetration in Class F fly ash concrete, the authors stated that chloride penetration decreases as fly ash content increases [1]. The authors compared the compressive strength, diffusion, resistivity, chloride permeability, and accelerated corrosion of ordinary Portland cement and pozzolana Portland cement mixes [2]. From the RCPT test, the authors stated that PPC concrete has 24% less chloride penetration than OPC concrete. Studies on compressive strength, diffusion, resistivity, chloride permeability, and accelerated corrosion of fly ash concrete indicate that partial fly ash replacement enhances concrete durability [3]. The compressive strength and RCPT tests were conducted on the high-volume fly ash (HVFA) concrete and compared with plain concrete. The RCPT test revealed that HVFA had greater resistance than plain concrete [4]. Two tests were conducted on concrete partially replaced with GGBS: the conventional RCPT test and the chloride ion penetration test using silver nitrate. They performed these tests in both normal and marine environments. The authors also stated that concrete in the marine environment acts similarly to normal concrete when GGBS is replaced at 30–50% [5]. RCPT tests compared nanomaterial concrete with plain or normal cement concrete. They found that substituting cement with nanomaterials decreased chloride ion penetration [6]. The authors conducted compressive strength testing, water penetration depth testing, and chloride permeability testing on plain concrete, fly ash-based concrete, and silica fume-based concrete. The authors developed a high-quality concrete mix with crushed limestone aggregate with the above testing data [7]. The authors compared strength and durability tests for fly ash and silica fume specimens with plain concrete. They also correlated compressive strength and durability with different replacements [8]. The durability assessment is chloride ion penetration in the concrete after substituting cement with Class F fly ash. The authors stated that the major point is that the RCPT value decreased with higher amounts of Class F fly ash compared to non-fly ash concrete [9]. RCPT tests were conducted on ordinary Portland cement-based carbonated concrete and pozzolana Portland cement-based carbonated concrete using three w/c ratios (0.40, 0.45, and 0.55). These samples were preserved in the accelerated carbonation chamber for 150 days at a constant 10% carbon dioxide (CO_2). The low w/c of PPC-based concrete shows strong resistance in carbonation and RCPT tests [10]. The mechanical and Durability properties of LC^3 concrete were studied and compared with all OPC concrete values and fly ash-based modified cement. The resistivity of LC^3 concrete was greater than that of OPC and fly ash-based concrete [11]. The concrete's compressive strength and durability properties. The alternate cementitious materials used in this experiment are Alcofine and GGBS. Nine different mixes were cast in this experiment. They stated that using both cementitious materials enhanced the concrete's durability [12]. The sulfate attack and RCPT, Durability of concrete investigated the high volume of slag cement with a cement ratio: GGBFS is 50:50, having the w/b ratio from 0.55 to 0.27, and tested for different ages of curing. The results showed very low chloride penetration at later concrete ages [13]. The strength and chloride penetration of the concrete with different percentages of cement with GGBFS. The specimens were cast for different curing ages. It was concluded that at 50% replacement of GGBS, it had got better strength and chloride penetration than the other mixes cast and tested [14]. A popular technique in non-destructive testing is RCPT, but it has limitations in the field. So, they adopted the electrical resistivity technique. This compared the results between both techniques. From the results obtained, it was found that those with less chloride permeability have larger resistivity. Hence, electrical resistivity directly influences chloride penetration [15]. In the experimental study on concrete's strength and durability properties. They have done this test on high-strength concrete with a 50% concrete substitution. This 50% substitution outperformed the control mix regarding chloride penetration [16]. The chloride penetration per ASTM C 1202 with concrete was replaced with silica fume at different percentages. This test showed reduced chloride penetration when the cement was substituted with silica

fume [17]. The investigation used concrete with silica fume and rice husk ash as a substitute for slag cement. The Durability of the concrete replaced with RHA follows the same trend as that of silica-fume concrete. In rice-producing countries, RHA can substitute for cement as well as silica fume [18]. In the tests on high-performance concrete with the substitution of silica fume in cement. The substitution percentages were 5%, 7.5%, 10%, and 12.5%. Chloride penetration decreases as the substitution of cement with silica fume increases [19]. A few tests were performed on fly ash and silica fume-modified concrete for different curing conditions. The testing evaluated RCPT, RCMT, and electrical resistance in fly ash- and silica fume-based concrete. Chloride ion penetration resistance decreases as the percentage of both cementitious materials increases [20]. An article [21] titled "A review on performance-based specifications toward concrete durability" mentioned that an obvious shift is detected globally from "prescriptive" to "performance-oriented specifications, particularly in the large infrastructure construction sector. The main objective of this research is to evaluate the "prescriptive approach" as well as the "performance-based approach". The boundaries of the "prescriptive approach" are emphasised and the successful application of the "performance-based approach". It was observed that "performance-based specifications" can assure the accomplishment of essential quality and longstanding Durability.

3 Materials

In this experimental investigation, OPC 53 grade is used. Fly ash and GGBS are employed as mineral admixtures. Fine and coarse aggregates are obtained from a local quarry. The fine aggregate is confined to zone II; the coarse aggregate used is 12mm and 20 mm. We carried out tests such as specific gravity and sieve analysis on all materials used in the experiment. The following tables discuss OPC's physical properties, chemical composition, cementitious materials, and superplasticizers. Aggregates were tested as per I.S.: 383-2016, and fly ash values as per ASTM C618. Cement was tested per I.S.: 269-2015 and I.S.: 4031-1988.

Table 1. Physical Properties of Cement

Property	**Value**
Specific gravity	3.15
Bulk density (kg/m^3)	1440
Specific surface area (cm^2/gm)	2960
Standard consistency (%)	28
Initial Setting Time (min.)	135
Final Setting Time (min.)	240
3D Strength (MPa)	37.8
7D Strength (MPa)	48.0
28D Strength (MPa)	61.0

Table 2. Chemical Composition of cement

Chemicals	Value
Lime Saturation Factor	0.85
Insoluble residue	3.26
Magnesium Oxide (MgO)	0.99
Sulphur trioxide (SO3)	2.26
Chloride	0.02
Loss of Ignition (LOI)	3.38
Alumina Ratio = (Al2O3/Fe2O3)	1.20

Table 3. Physical properties of Aggregates

Material	Fine Aggregate	Coarse aggregate
Specific Gravity	2.65	2.64
Bulk density (kg/m^3)	1700	1550

Table 4. Physical Properties of Cementitious Materials

Materials	Fly ash	GGBS
Specific Gravity	2.25	2.91
Specific Surface Area (cm2/gm)	3980	4000

Table 5. Chemical Composition of Fly ash

Oxides	Percentages
SiO2+Al2O3+Fe2O3	89.98
Calcium Oxide (CaO)	2.02
Magnesium Oxide (MgO)	1.89
Sulphur trioxide (SO3)	0.15
Potassium Oxide (K2O)	3.09
Titanium Oxide (TiO2)	1.11
Sodium Trioxide (Na2O3)	0.28
Loss of Ignition	0.295

Table 6. Chemical Composition of GGBS

Oxides	Percentages
Silicon Dioxide (SiO2)	34.92
Aluminium Oxide (Al2O3)	19.29
Ferric Oxide (Fe2O3)	0.8
Calcium Oxide (CaO)	34.22
Magnesium Oxide (MgO)	8.97
Others	3.41

4 Mix Proportions:

This research considered three binder-content categories (533.33 kg/m3, 400 kg/m^3, and 320 kg/m^3), and used water-binder ratios of 0.3, 0.4, and 0.5 to make concrete for testing. All fly ash and GGBS mixtures have a water content of 160 kg/m^3. The mix was designed on a volumetric basis; the binder content was fixed initially, and later the water-binder ratio was set based on it. The residual volume is balanced among fine and coarse aggregate in an inexact ratio of 34:66. Furthermore, the coarse aggregate was 12-mm aggregate and 20-mm aggregate in a 40:60 ratio. The binder content of the PCE-based superplasticizer (SP) addition was also adjusted to achieve a target slump of 80–120 mm. The concretes were uniformly mixed in a pan mixer at 25 rpm and 27 °C. Table 8 shows the compressive strength values.

5 Experimental Program

D. Whiting of the Federal State Highway Authority created this method between 1981 and 1988. The American Association of State and Highway Transportation Officials (AASHTO) accepted it in the early 1990s, and ASTM accepted it in the late 1990s. It covers diffusion, migration, capillary suction, adsorption, and desorption. This test is simpler and faster. It is a widely used test procedure worldwide.

This test establishes concrete's resistance to chloride ions. The laboratory test evaluates concrete's resistance to rapid chloride ion penetration. This test mainly evaluates the materials and proportions used in the actual design. The specimen's age is a critical factor governing the results. Initially, this method was used to evaluate alternative materials, but it has also been useful for quality control and acceptance testing over time. The apparatus is known as the Rapid Chloride Permeability Tester and tests according to ASTM C 1202. Electrical indication of concrete's capacity to resist chloride ion penetration.

Although the Rapid Chloride Ion Permeability Test (RCPT) has many advantages, it also has criticisms and limitations. They are:

i. The specimen gets heated up due to high voltage, and the test may not represent the ambient condition.
ii. The other negatively charged ions may also get transported in the given electrical field.
iii. This may not be suitable for concretes with larger-sized aggregates.
iv. Chloride Ions may get transported to weak interfaces and micro-cracks.

Despite these limitations, the RCPT is the best method for evaluating concrete durability. The instrument has four cells, connecting cables, temperature sensors, desiccators, vacuum pumps, and Software. The Rapid Chloride Permeability Tester has four channels, and it can test four concrete specimens at a time by applying an electrical potential across each specimen. When the RCPT tester starts, the instrument automatically selects 60 V DC. It displays actual voltage, current, and temperature throughout the test. It also logs the data required by the standard. A user can change test parameters before starting the test. Finally, the collected Software data can be saved, representing the total charge or Coulombs passed across the specimens. This test has some demerits, as the sample is heated by the high voltage. The test may not accurately depict the environment. Other negatively charged ions may be carried in the given electrical field. This may not be suitable for concrete with larger aggregates. Chloride ions may transfer across weak surfaces and microcracks.

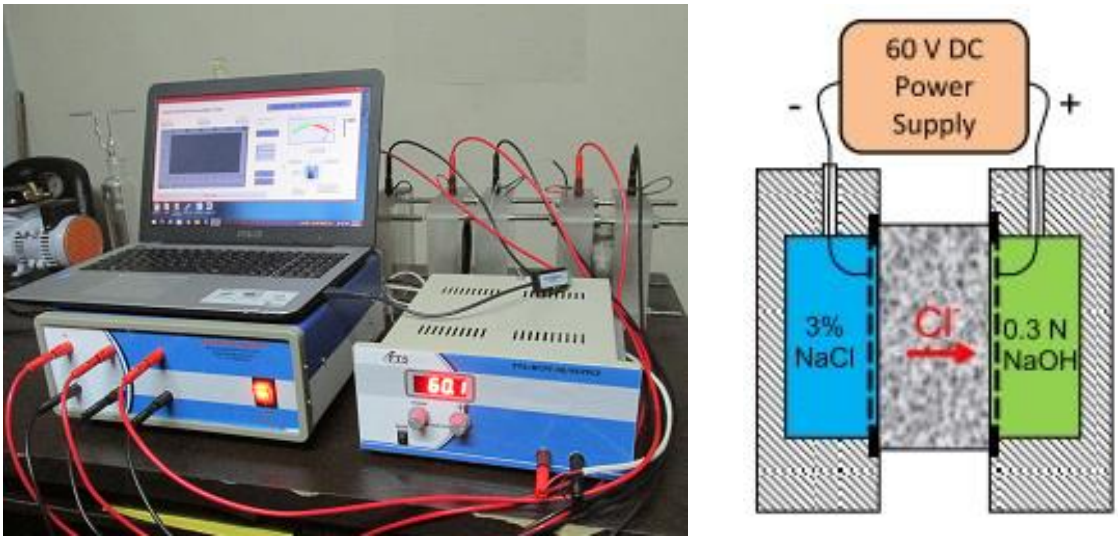


Fig 1. Chloride Ion Penetration Apparatus

Table 8: Compressive Strength

Fly Ash	w/b	28D	56D	90D
0	0.3	55.56	59.11	63.11
20	0.3	54.67	60.44	66.67
30	0.3	52.89	63.56	69.33
40	0.3	51.11	60.44	65.78
50	0.3	45.78	54.22	60.89
60	0.3	40.00	51.56	58.67
70	0.3	36.89	49.78	56.00
0	0.4	46.22	50.67	55.11
20	0.4	44.00	54.22	58.22
30	0.4	43.11	55.11	59.56
40	0.4	40.89	52.44	56.89
50	0.4	38.22	48.44	53.33
60	0.4	33.78	44.89	50.22
70	0.4	30.67	41.33	48.44
0	0.5	38.67	41.78	44.44
20	0.5	36.00	42.67	46.67
30	0.5	33.33	44.89	47.56
40	0.5	30.67	41.78	45.78
50	0.5	28.89	36.00	40.44
60	0.5	25.33	32.00	37.33
70	0.5	23.11	29.33	34.67

GGBS	w/b	28D	56D	90D
0	0.3	55.56	59.11	63.11
20	0.3	56.89	66.67	71.11
30	0.3	54.67	67.56	72.89
40	0.3	53.33	64.44	69.78
50	0.3	48.00	57.78	62.67
60	0.3	38.22	53.33	58.67
70	0.3	32.89	49.78	55.56
0	0.4	46.22	50.67	55.11
20	0.4	47.11	54.67	60.44
30	0.4	44.89	57.33	63.11
40	0.4	43.56	53.33	60.00
50	0.4	38.67	50.67	56.89
60	0.4	34.67	44.89	51.56
70	0.4	32.00	41.33	48.44
0	0.5	38.67	41.78	44.44
20	0.5	40.00	44.89	55.56
30	0.5	36.00	46.67	58.22
40	0.5	34.22	44.00	54.22
50	0.5	32.00	40.44	50.67
60	0.5	28.89	38.22	47.11
70	0.5	28.00	35.56	43.56

Table 9. Coulombs passed through specimens.

Charge Passed in Coulombs	**Chloride Ion Penetability**
More than 4000	High
From 2000 to 4000	Moderate
From 1000 to 2000	Low
From 100 to 1000	Very Low
Less than 100	Negligible

6 Results and Discussion

Table 10. Charge passed in Coulombs through 0.3 water/binder ratio specimens with fly ash.

		RCPT (Charge Passed in Coulombs)		
w/b ratio	Fly ash-%	28-Days	56-Days	90-Days
0.3	0	1617	1141	846
0.3	20	1162	655	435
0.3	30	1044	552	357
0.3	40	951	422	289
0.3	50	846	396	221
0.3	60	740	326	207
0.3	70	635	300	195

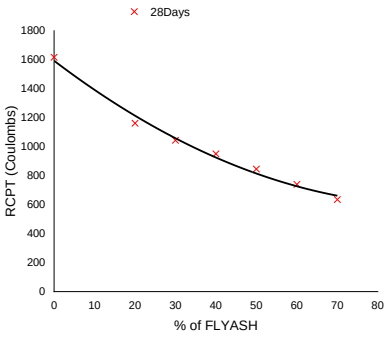


Fig: 2. w/b – 0.3 – Fly ash – 28 Days

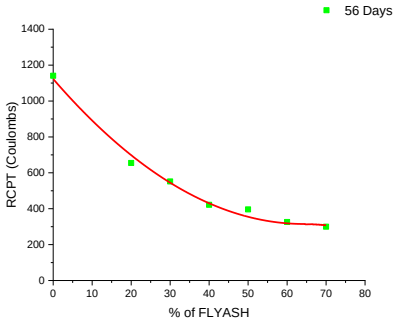


Fig: 3. w/b – 0.3 – Fly ash – 56 Days

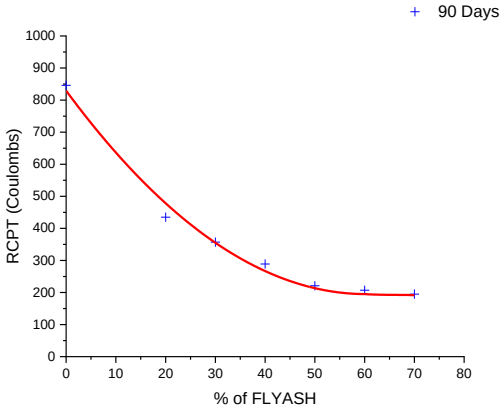


Fig: 4. w/b – 0.3 – Fly ash – 90 Days

Table 10 and Figs. 2 to 4 give the charge values passed through fly ash-based concrete specimens with a water-binder ratio of 0.3. The different ages (28, 56, and 90 days) used in the experiment were for water curing. The values for 0%, 20%, 30%, 40%, 50%, 60%, and 70% have decreased by 47.68%, 62.57%, 65.81%, 69.62%, 73.88%, 72.03%, and 68.3%, respectively, from 28 days to 90 days of water curing. The lowest chloride ion permeability is obtained at 70% fly ash replacement, with charges passed of 635, 300, and 195 coulombs at the ages mentioned above.

Table 11. Charge passed in Coulombs through 0.4 water/binder ratio specimens with fly ash.

		RCPT (Charge Passed in Coulombs)		
w/b ratio	Fly ash-%	28-Days	56-Days	90-Days
0.4	0	1820	1526	1398
0.4	20	1214	839	493
0.4	30	1113	587	403
0.4	40	1038	528	346
0.4	50	941	456	282
0.4	60	866	400	275
0.4	70	725	375	215

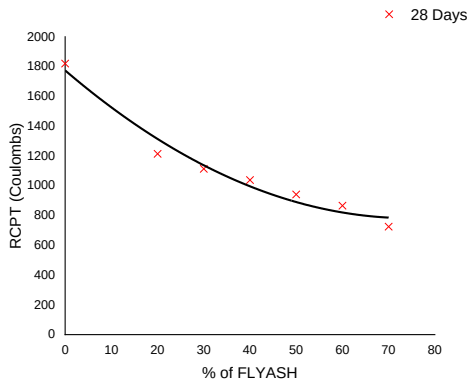


Fig: 5. w/b – 0.4 – Fly ash – 28 Days

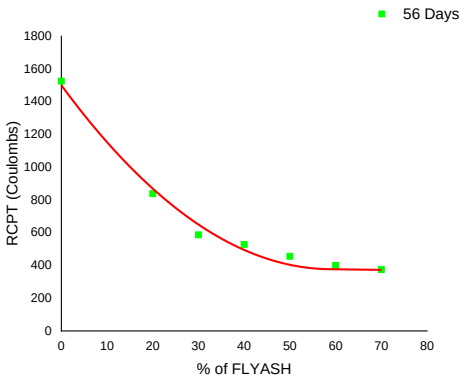


Fig: 6. w/b – 0.4 – Fly ash – 56 Days

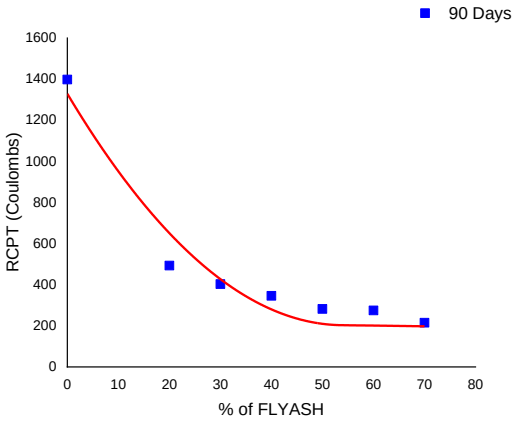


Fig: 7. w/b – 0.4 – Fly ash – 90 Days

Table 11 and Figs. 5 to 7 give the charge values passed through fly ash-based concrete specimens with a water-binder ratio of 0.4. The different ages (28, 56, and 90 days) used in the experiment were for water curing. The values for 0%, 20%, 30%, 40%, 50%, 60%, and 70% have decreased by 21.68%, 59.39%, 63.79%, 66.67%, 70.03%, 68.24%, and 70.34%, respectively, from 28 days to 90 days of water curing. The lowest chloride ion permeability is obtained at 70% fly ash replacement. The charge passed was 725, 375, and 215 coulombs when tested at the ages of concrete mentioned above.

Table 12. The charge passed in Coulombs through 0.5 water/binder ratio specimens with fly ash.

		RCPT (Charge Passed in Coulombs)		
w/b ratio	Fly ash-%	28-Days	56-Days	90-Days
0.5	0	2075	1741	1675
0.5	20	1395	946	783
0.5	30	1194	637	472
0.5	40	1150	552	393
0.5	50	1055	477	374
0.5	60	995	434	327
0.5	70	825	395	295

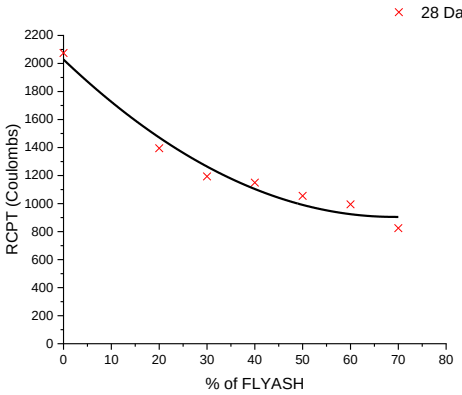


Fig: 8. w/b – 0.5 – Fly ash – 28 Days

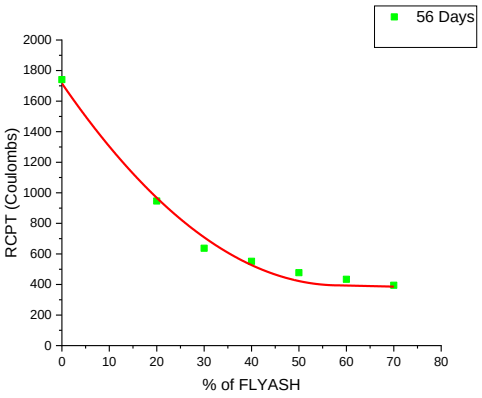


Fig: 9. w/b – 0.5 – Fly ash – 56 Days

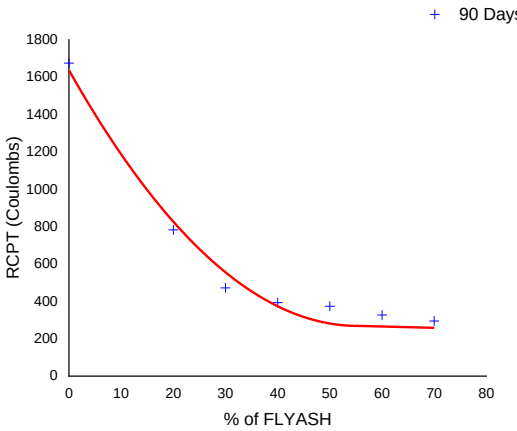


Fig: 10. w/b – 0.5 – Fly ash – 90 Days

Table 12 and Figs. 8 to 10 show the charge values passed through fly ash-based concrete specimens with a water-binder ratio of 0.5. The values for 0%, 20%, 30%, 40%, 50%, 60%, and 70% have decreased by 19.28%, 43.87%, 60.47%, 65.83%, 64.549%, 67.14%, and 64.24%, respectively, from 28 days to 90 days of water curing. The lowest chloride ion permeability is obtained at 70% replacement of fly ash with cement, and the charges passed through it are 825, 395, and 295 coulombs when tested at the ages of concrete mentioned above, respectively.

Table 13. Charge passed in Coulombs through 0.3 water/binder ratio specimens with GGBS.

		RCPT (Charge Passed in Coulombs)		
w/b ratio	GGBS-%	28-Days	56-Days	90-Days
0.3	0	1617	1141	846
0.3	20	1240	944	578
0.3	30	1055	876	516
0.3	40	900	734	427
0.3	50	774	559	347
0.3	60	587	385	201
0.3	70	465	285	177

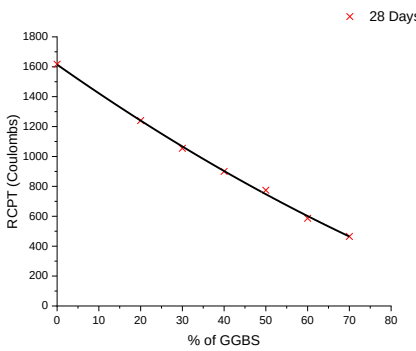


Fig: 11. w/b – 0.3 – GGBS – 28 Days

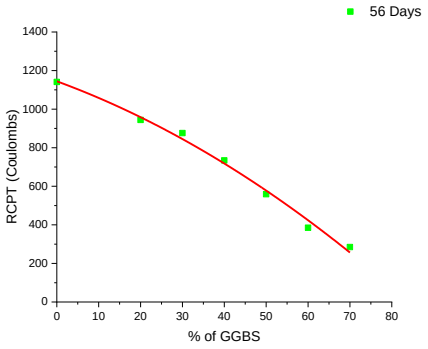


Fig: 12. w/b – 0.3 – GGBS – 56 Days

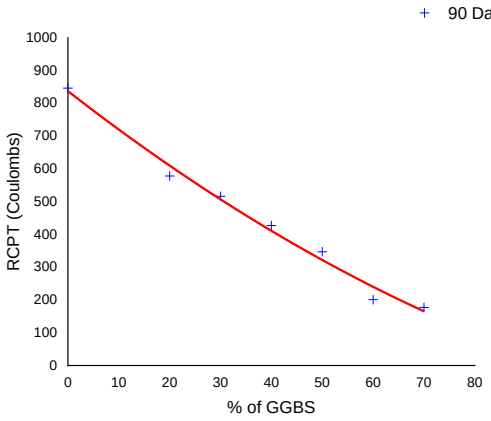


Fig: 13. w/b – 0.3 – GGBS – 90 Days

Table 13 and Figs. 11 to 13 give the charge values passed through GGBS-based concrete specimens with a water-binder ratio of 0.3. The different ages (28, 56, and 90 days) used in the experiment were for water curing. The values for 0%, 20%, 30%, 40%, 50%, 60%, and 70% have decreased by 47.68%, 53.39%, 51.09%, 56.69%, 55.17%, 65.75%, and 61.93%, respectively, from 28 days to 90 days of water curing. The least chloride ion permeability is obtained at 70% replacement of GGBS with cement. The charges passed through it are 465, 285, and 177 coulombs when tested at the ages of concrete mentioned above, respectively.

Table 14. Charge passed in coulombs through 0.4 w/b ratio specimens with GGBS

		RCPT (Charge Passed in Coulombs)		
w/b ratio	GGBS-%	28-Days	56-Days	90-Days
0.4	0	1820	1526	1398
0.4	20	1785	969	689
0.4	30	1614	899	575
0.4	40	1486	774	456
0.4	50	1357	666	368
0.4	60	1228	413	281
0.4	70	1185	350	185

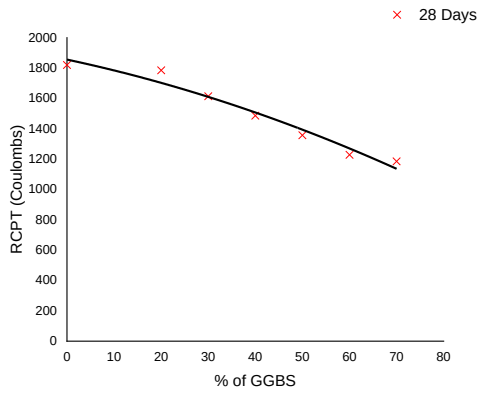


Fig: 14. w/b – 0.4 – GGBS – 28 Days

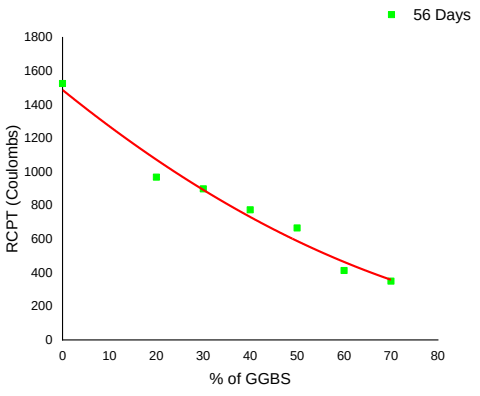


Fig: 15. w/b – 0.4 – GGBS – 56 Days

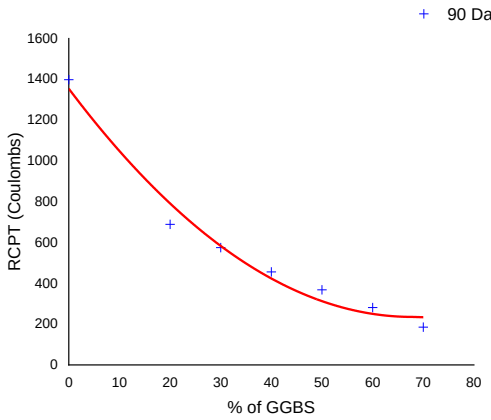


Fig: 16. w/b – 0.4 – GGBS – 90 Days

Table 14 and Figs. 14 to 16 show the charge values passed through GGBS-based concrete specimens with a water-binder ratio of 0.4. The different ages (28, 56, and 90 days) used in the experiment were for water curing. The values for 0%, 20%, 30%, 40%, 50%, 60%, and 70% have decreased by 21.68%, 62.14%, 64.37%, 69.31%, 72.88%, 77.11%, and 84.38%, respectively, from 28 days to 90 days of water curing. The lowest chloride ion permeability is obtained at 70% replacement of GGBS with cement. The charges passed through it are 1185, 350, and 185 coulombs when tested at the ages of concrete mentioned above, respectively.

Table 15. Charge passed (Coulombs) through 0.5 water/binder ratio specimens with GGBS.

w/b ratio	GGBS-%	Charge Passed in Coulombs		
		28-Days	56-Days	90-Days
0.5	0	2075	1741	1675
0.5	20	1855	1068	1058
0.5	30	1746	1018	776
0.5	40	1546	821	471
0.5	50	1445	734	395
0.5	60	1341	531	308
0.5	70	1265	485	275

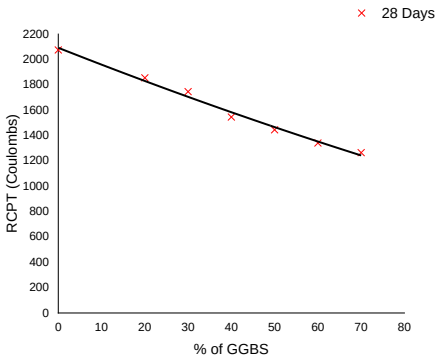


Fig: 17. w/b – 0.5 – GGBS – 28 Days

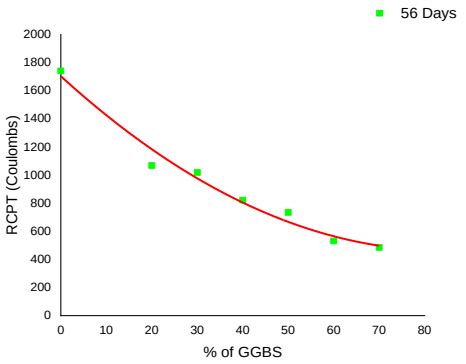


Fig: 18. w/b – 0.5 – GGBS – 56 Days

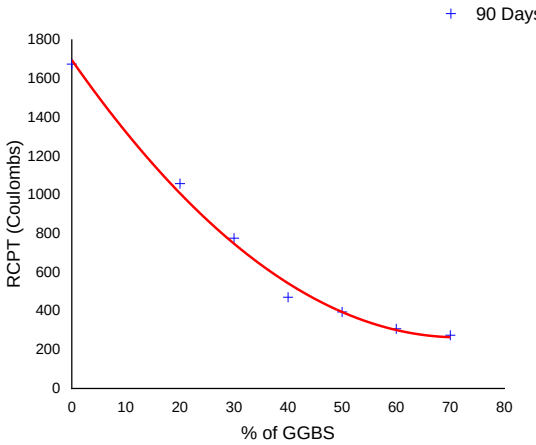


Fig: 19. w/b – 0.5 – GGBS – 90 Days

Table 15 and Fig: 17 to 19 given the charge values passed through specimens of GGBS-based concrete with a water-binder ratio of 0.5. The different ages (28, 56, and 90 days) was adopted in experimentation is for of water curing. The values for 0%, 20%, 30%, 40%, 50%, 60%, and 70% have decreased by 19.28%, 42.96%, 55.56%, 69.53%, 72.67%, 77.03%, and 78.26%, respectively, from 28 days to 90 days of water curing. The lowest chloride ion permeability is obtained at 70% replacement of GGBS with cement, with charges passed of 1265, 485, and 275 coulombs when tested after 28, 56, and 90 days of curing, respectively.

Conclusions

i. There is an increase in the permeability of chloride ions (number of coulombs) with the increase in the water-binder ratio.

ii. There is a decrease in permeability with the increase in the percentage of supplementary cementitious material (Fly Ash and GGBS), which indicates an increase in terms of Durability due to the reduction in chloride ion permeability (number of coulombs).

iii. The permeability is reduced in all the mixes with the increase in age. This reduction is due to pore refinement in concrete from the formation of secondary CSH gel due to the pozzolanic reaction.

iv. The above-published data will be helpful to the concrete mix designer to consider RCPT as the criterion for Durability at the time of concrete mix proportioning.

References

1. Madhavi T, Martin S, Luther, Senthil Velan, Prabhath Kumar, Swamy Raju, Deepak Mathur (2015) Chloride penetration in fly ash concrete. International Journal of Research in Engineering and Technology 4(1):2321-7308.
2. Prabakar J, P Devadas Manoharan, Neelamegam M (2011) Effect of fly ash on durability and performance of concrete. The Indian Concrete Journal 11:1-10.
3. Nath P, Sarker P (2011) Effect of fly ash on the durability properties of high strength concrete. Procedia Engineering 14:1149–1156.
4. KrishnaTeja K, B Kameswara Rao (2018) Strength and durability of high-volume fly ash concrete. International Journal of Civil Engineering and Technology 9(6):109-116.
5. Aneesh V Bhat, Sunil kumarTengli (2019) Behaviour of ground granulated blast furnace slag concrete in marine environment under chloride attack. International Journal of Innovative Technology and Exploring Engineering 9(1):278-302.
6. Jemimah Carmichael, Prince Arulraj M (2019) Rapid chloride permeability test on concrete with nanomaterials. International Journal of Engineering and Advanced Technology 8(3):249-258.
7. Shamsad Ahmad, Walid A Al-Kutti, Omar S Baghabra Al-Amoudi, Mohammad Maslehuddin (2008) Compliance criteria for quantity concrete. Construction and building materials. 22:1029-1036.
8. Omar S Baghabra Al-Amoudi, Walid A Al-Kutti, Shamsad Ahmad, Mohammed Maslehuddin (2009) Correlation between compressive strength and certain durability indices of plain and blended cement concrete. Cement and Concrete Composites 31:672-676.
9. Kanta Rao M, Naga Satish Kumar Ch (2019) Durability assessment of concrete with class-F fly ash by chloride ion permeability. International Journal of Recent Technology and Engineering 8(4):1-19.
10. Das BB, Singh DN, Pandey SP (2012) Rapid chloride ion permeability of OPC and PPC based carbonated concrete. Journal of Material in Civil Engineering 21:228-239.
11. Yuvaraj Dhandapani, Sakthivel T, Manu Santhanam, Ravindra Gettu, Radhakrishna G Pillai (2018) Mechanical properties and durability performance of concretes with limestone calcined clay cement (LC3). Cement and Concrete Research 107:136-151.
12. Balamuralikrishna R, Saravanam J (2019) Effect of alccofine and GGBS addition on the durability of concrete. Civil Engineering Journal 5(6):1-14.
13. Vijyagowri T, Sravana P, Srinivasa Rao P (2015) Rapid chloride permeability test on high volumes of slag concrete. Journal on Structural Engineering 4(1):1-17.
14. Rama Mohan Rao P, Himath Kumar Y (2014) The effect of GGBS on the strength and chloride penetration of concrete. International Journal of Chemical Science 12(3):957-964.



15. Abdullah Ahmed Lasker, Partha Ghosh (2019) Durability assessment of concrete by using electrical resistivity and rapid chloride permeability technique. International Journal of Engineering and Advanced Technology 9(1):249-261.

16. Raghavendra YB, Ramalinga Reddy Y, Nabil Hossiney, Dinesh HT (2021) Properties of high strength concrete with reduced amount of portland cement –a case study. Cogent Engineering. 8(1):256-272.

17. Juanlizarazo-Marriaga, Lucio Guillermo lopez Yepez, (2012) Effect of silica fumes addition on the chloride related transport properties of high-performance concrete. Medellin 21:105-110.

18. Smita Sahoo, Pravatkumar Parhi, Bikash Chandra (2012) Durability properties of concrete with silica fume and rice husk ash. Cleaner Engineering and Technology 11:1-14.

19. Krishna kumar S, Asif Abdul Vahab, Akhil Raj SR, Jayasree S, Job Thomas (2018) Effect of silica fumes on the resistance to chloride ion penetration in high-performance concrete. American Journal of Engineering Research 2: 01-05.

20. Alireza Bagheri, Hamed Zanganeh, Hadi Alizadeh, Mohammad Shakerinia, Mohammad Ali Seifi Marian (2013) Comparing the performance of fine fly ash and silica fume in enhancing the properties of concretes containing fly ash. Construction and Building Materials 47:1402-1408.

21. Bhaskar Sangoju, Ramesh Gopal, Bharatkumar Bhajantri H, (2020) A review on performance-based specifications toward concrete Durability, Structural Concrete.



Technical Session-IVA



Technical Session-IVB

A SUSTAINABLE ROUTE FOR PRODUCING HIGHLY REACTIVE SCM FROM BASIC OXYGEN FURNACE SLAG WITH CONCURRENT IRON RECOVERY

Priyapratim Patra*, Mahima Srivastava, Pratik Kumar Goyal, J. Suresh, Amol Satpute, Dilip Makhija, Manoj Kumar Rustagi, Jagabandhu Kole

Research and Development, JSW Cement Ltd., Vijayanagar, Bellary, Karnataka-583275

*E Mail: priyapratim.patra@jsw.in

Abstract

The cement industry is one of the largest contributors to anthropogenic CO_2 emissions, accounting for ~8% of global CO_2 emissions. Clinker, the primary constituent of conventional cement, possesses the highest carbon footprint among all cement components. Therefore, reducing the clinker factor is one of the most effective strategies for lowering the carbon footprint of cement. Supplementary Cementitious Materials (SCMs) play a crucial role in enabling this transition. In this study, Basic Oxygen Furnace (BOF) slag, an industrial by-product of the steel industry, was valorized to produce two value-added products: metallic iron and Granulated Modified BOF Slag (GMBOFS). The modification process involves remelting the BOF slag, followed by the reduction of iron oxide (FeO) to metallic iron through reactions with carbon and aluminum. Subsequently, silica was added to adjust the slag chemistry, reducing its basicity (CaO/SiO2 ratio) and bringing its composition closer to that of blast furnace slag. In the final stage, the molten slag was rapidly quenched through water granulation to obtain a highly glassy structure. The developed GMBOFS exhibited superior SCM characteristics, comparable to those of Ground Granulated Blast Furnace Slag (GGBS), demonstrating its potential as a sustainable alternative SCM for reducing clinker consumption and the associated carbon emissions of cement.

1. Introduction:

Conventional Ordinary Portland Cement (OPC) is composed of clinker (~95%) and gypsum (~5%) [1, 2]. Clinker is the main hydraulic component of OPC. This is produced by the pyro treatment of majorly calcium carbonate (like limestone) and alumino-silicate sources (like clay/shale) at the temperature of ~1450°C. This process involves with thermal decomposition of limestone (Calcium Carbonate) and combustion of fossil fuel, which causes huge CO_2 emission (~800 kg CO_2/ton of clinker). Hence, clinker becomes the most carbon intensive material. Therefore, reduction of clinker factor can directly reduce the carbon foot print of cement. Supplementary Cementitious Materials (SCMs) is a class of materials, having huge potential to reduce the clinker factor in cement [3]. Mostly these are certain types of industrial by-product (like fly ash, ground granulated

blast furnace(GGBS slag) etc.), which can directly be blended with conventional cement in a certain proportion to make different type of blended cements. In Indian market the available blended cements are like Portland Pozzolana Cement (PPC; 35% Fly Ash), Portland Slag Cement (PSC; 70% GGBS), Composite cement (Comp Cem; ~25% GGBS & ~25% fly ash), which utilizes a significant amount of SCMs and replaces clinker. So, SCM is a key enabler of carbon neutrality of cement sector.

Broadly, Iron and Steel sector generates two classes of slags as a byproduct. Firstly, Granulated Blast Furnace slag (GBFS) is the iron making slag that been generates from blast furnace process. And,

secondly the steel making slags, which are generated from multi-steps steel refining processes (like primary and secondary refining). Currently although GBFS is completely been consumed for cement making (PSC, Comp Cement etc.), steel making slags are still not have been explored from upcycling perspective. Basic Oxygen Furnace Slag (BOF Slag) is a primary steel making slag which is one of the major contributor in the class of steel slag. Almost 180 kg of BOF slag is being generated for every 1 ton of crude steel production. BOF Slag possess certain shortcomings, which restricts its utilization for cement making like highly crystalline structure that ensures less reactivity, presence of free lime (Calcium Oxide: CaO) that causes volume expansion during hydration, and content higher amount of iron oxide (FeO), which has no cementitious reactivity.

Herein this work has explored a modification path that involves high temperature melting of BOF slag followed by reduction of FeO to make metallic iron. Then the molten reduced slag is subjected to regulate the chemical composition by addition of silica to reduce the basicity (CaO/SiO_2 ratio), and finally the water granulation. This explored method has extracted metallic iron from BOF Slag and generated a granulated slag water quenching. That granulated slag has exhibited superior SCM reactivity to make blended cement like PSC.

2. Materials and Method:

2.1 Materials:

2.2 Developing PSC using Clinker (JSW Cement, Nandyal), mineral gypsum, GGBS (JSW Cement Ltd) and BOF Slag (JSW Steel Ltd). Methodology:

BOF Slag was taken in a carbon crucible (1 dm^3 volume) and allowed to melt in a Tammann furnace at the temperature of 1650 °C as shown in Fig. 1 (a). After melting carbon powder (2.5% of BOF Slag) and Aluminum metal beads (2.5% of Slag) was added to the crucible and allowed to react for 20 min. After that quartz silica powder (18% of BOF Slag) was added to the crucible and continue the reaction for next 15 min. Then the molten modified slag was quenched in a lab scale water granulation system as shown in Fig. 1 (b). Molten metallic iron formed by the reduction of FeO content from BOF slag was accumulated at the bottom of the carbon crucible was collected in a refractory crucible for properties evaluation. Granulated slag was collected, dried and used for further characterization and properties evaluation.

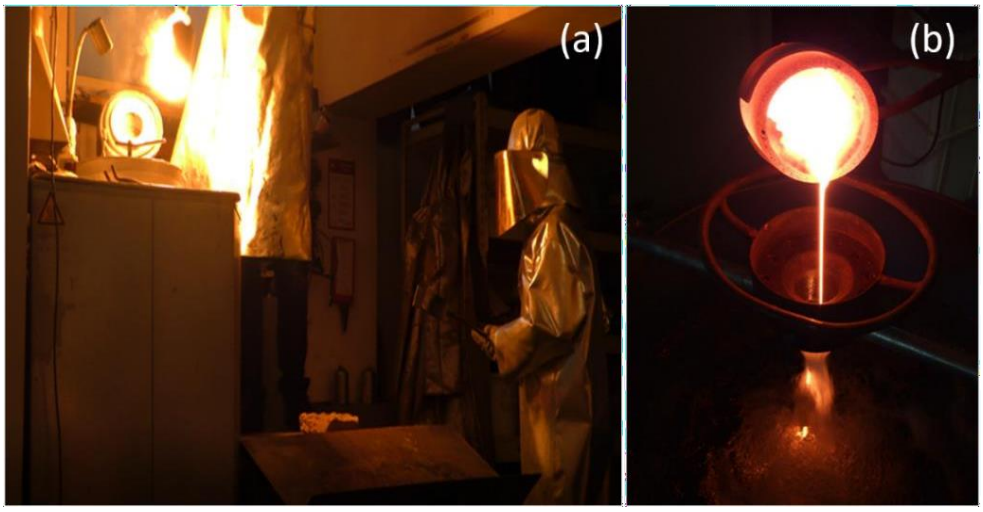


Fig 1. (a) Tammann furnace and Carbon crucible are being used for slag modification experiment, (b) Lab scale slag granulation process.

3. Results and Discussion:

3.1 Slag Modification

After melting of BOF Slag, the modification of chemistry is involved with two major chemical process like reduction of FeO to metallic iron and basicity reduction. The reduction of FeO happens following two different reactions as mentioned in following equations, where carbon powder and aluminum were used as reducing agents-

$FeO + C = Fe + CO$ ----------Eq. 1

$3FeO + 2Al = 3Fe + Al_2O_3$----------Eq. 2

Metal yield from the process is 16% (with respect to BOF Slag feed). After reduction, the reduced slag was undergone basicity (CaO/SiO2 ratio) reduction by addition of quartz powder. Additional silica reacts with molten slag and converted into different silicates, that leads to reduction of overall basicity of slag. Table 1 has demonstrated the Oxide chemical composition of BOF slag and modified BOF Slag. It has been found that Metallic Fe and iron oxides content (FeO and Fe2O3) almost eliminated in modified BOF slag. This confirms the reduction procedure. It has also been found that SiO2 content of BOF slag is increased in modified slag (31.5%) as compared to before modification (12.1 %). This modification has been reflected by the reduced basicity of modified slag (1.41) than that of before modification (3.48). This observation further confirms that addition of SiO_2 has been reacted with molten slag and contributed to regulate the chemical composition of slag.

Table 1: Chemical composition of BOF Slag and Modified BOF Slag.

Components (%)	**Material Name**	
	BOF Slag	**Modified BOF Slag**
Insoluble Residue	2.1	0.24
CaO	42.2	44.5
MgO	8.2	10.2
SiO2	12.1	31.5
Al2O3	4.1	9.37
TiO2	0.67	0.78
Fe (Metal)	1.85	0.0
FeO	11.9	0.0
Fe2O3	8.74	0.4
Basicity (CaO/SiO2)	3.48	1.41

3.2 Material Characterization

Optical Microscopy: Fig. 2 has demonstrated the digital image of BOF slag (Fig 2.a) and modified BOF Slag (Fig 2.b). The transformation of a non-glassy BOF slag to a glassy material is clearly visible. Microscopy of these two materials were performed using an optical polarized microscope (Model: DM4P, Leica) is transmittance mode. Fig 2. (c & d) have demonstrated the microscopic

images. BOF slag has demonstrated black and colourful particles under microscope, which indicates non-glassy and crystalline nature of the material. But, modified BOF slag has demonstrated transparent particles and that indicates the glassy nature of the material. Calculated glassy content is from the microscopy analysis of BOF slag is ~5%, where as, in modified BOF slag, it increases to 90%.

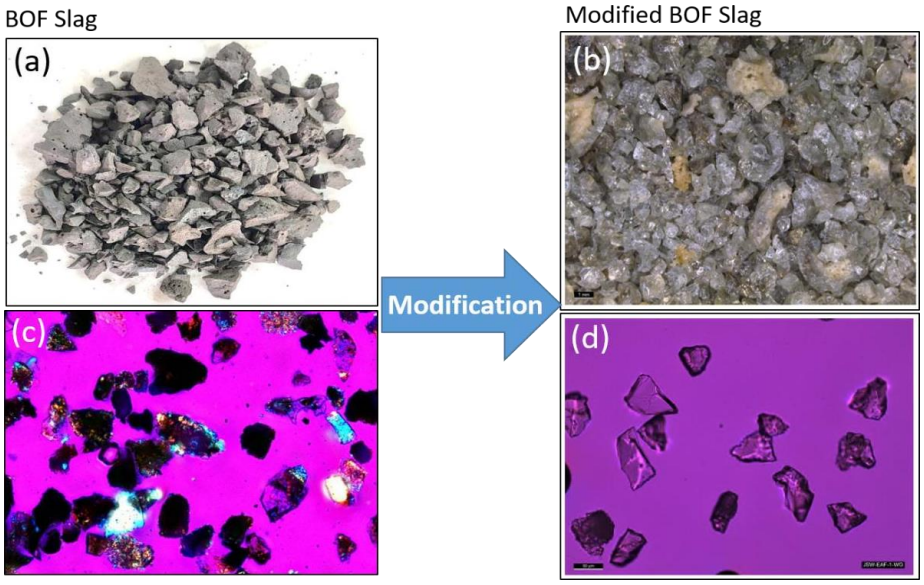


Fig. 2 (a) Digital image of BOF Slag; (b) Digital image of glassy modified BOF slag; (c) Microscopic image of BOF slag and (d) Microscopic image of modified BOF slag.

X-Ray Diffraction: Fig. 3 has demonstrated XRD diffractogram of BOF Slag (Fig. 3.a) and modified BOF slag (Fig. 3.b). Sharp signals of the diffractogram of BOF slag represents different crystalline phases and confirms the crystalline behavior of BOF slag. Whereas modified BOF slag has demonstrated a broad signal in diffractogram, which confirms the amorphous (glassy) nature of modified BOF slag.

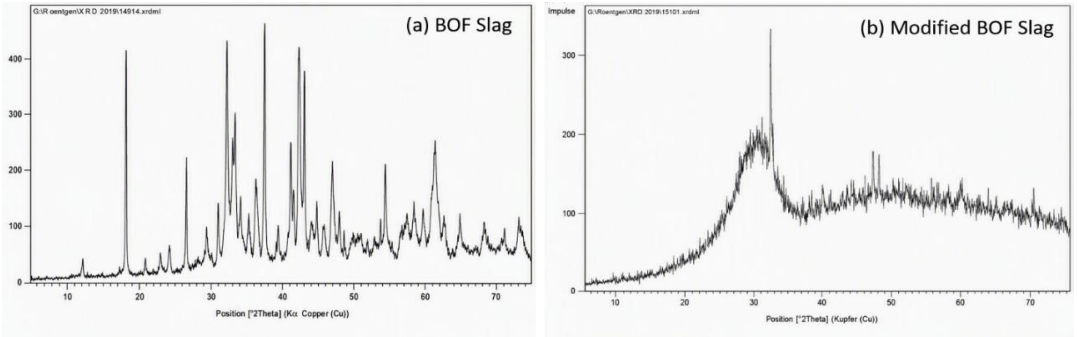


Fig. 3 XRD diffractogram of (a) BOF Slag and (b) modified BOF slag.

3.3 Performance of modified BOF Slag in PSC Cement:

To assess the performance of modified BOF slag, two different PSC cements were prepared. Composition of these cements were demonstrated in Table 2. A common OPC cement (specific surface area: 350 m^2/kg) was prepared by grinding 93% of clinker and 7% mineral gypsum, using ball mill. Then separately granulated BF slag and modified BOF Slag were ground with similar specific surface area (~350 m^2/kg). PSC Cements were prepared by blending 40% of OPC and 60% of prepared GGBS

and ground modified BOF slag (GMBOFS). Then mortar cubes were casted (complying IS 4031) to asses compressive strength (CS). CS data has been demonstrated in Table 2. It has been found that the CS of PSC_GMBOFS increases by 16.83%, 27.55%, 10.24%, and 8.52% from CS of PSC_GGBS after 1day, 3days, 7days, and 28 days of curing respectively, which further confirms the better reactivity of PSC_GMBOFS over PSC_BOFS. . Even the higher heat of hydration (HoH) of PSC_GMBOFS (7D HoH: 386 J/g) than PSC_GGBS (7D HoH: 360 J/g) supports the superior reactivity of GMBOFS as SCM. This confirms that the modification of BOF slag has led to a material that possess superior SCM behavior.

Table 2: Properties and performance parameters of GMBOFS for cement making.

Components	**PSC_GGBS**	**PSC_GMBOFS**
Composition		
OPC (93% Clinker + 7% Gyp**)**	40%	
GGBS/GMBOFS	60% GGBS	60% GMBOFS
Properties		
Specific Surface Area (m^2/kg)	348	345
N.C. (%)	29.5	29.25
Compressive Strength		
1 Day	10.1	11.8
3 Days	19.6	25.1
7 Days	33.2	36.6
28 Days	49.3	53.5
7 Day's Heat of Hydration (J/g)	260	286

4. Conclusion:

This experimental research work has explored a sustainable route to valorize BOF slag. That leads to metallic iron recovery as well as produces a slag which shows efficient SCM quality, which has superior reactivity like GGBS. Valorized BOF slag has an outstanding efficiency to reduce clinker factor in PSC, which leads to reduction of carbon footprint of cement. This approach has transformed an industrial waste (BOF Slag) to valuable materials and made it a zero waste process.

Acknowledgements:

Authors and JSW Cement R&D acknowledges FEhS, Germany for collaboration regarding this collaborative research work.

Reference:

1. Renewable Electrified Cement Production: Flexibility and Economic Competitiveness, Sebastian Andres, Quevedo Parra, Matteo C. Romano, ***Ind. Eng. Chem. Res.***, 2026, 65 (21), 10813–10839.
2. Carbon emissions reduction and financial effects of a cap and tax system on an operating supply chain in the cement sector, Nora Cadavid-Giraldo, Mario C. Velez-Gallego, Alexandre Restrepo-Boland, ***Journal of Cleaner Production***, 2020, 275, 122583.
3. Reactivity of supplementary cementitious materials (SCMs) in cement blends, Jørgen Skibsted, Ruben Snellings, ***Cement and Concrete Research***, 2019, 124, 105799.

High Litre Weight Clinker Under Partial and Full Kiln Loading Conditions: Distinguishing Mineralogical Inefficiency from Burnability Limitation for Carbon-Neutral Cement Manufacturing

Suresh Palla, Vipul Mishra, Lalit Patodi, Mukesh Kakde, Suresh K, Sandeep Deshmukh

Abstract

Carbon neutrality in cement manufacturing requires production of highly reactive clinker at the lowest possible thermal energy consumption and CO_2 intensity. Industrial observations frequently reveal clinker exhibiting high litre weight despite inferior mineralogical quality. Two distinct clinker phenomena are commonly encountered. The first occurs during partial kiln loading (60–80% of design throughput) where clinker exhibits high litre weight (1250–1350 g/L), low free lime (<1.6%), and reduced C_3S (38–42%). The second occurs during full kiln loading where clinker simultaneously exhibits high litre weight (>1200 g/L) and elevated free lime (1.6–1.8%). Although both conditions generate dense clinker, the underlying clinkerization mechanisms differ fundamentally. This paper reviews clinker reaction mechanisms, liquid-phase thermodynamics, alite nucleation and stabilization, burnability limitations, quartz dissolution kinetics, combustion efficiency, and implications for carbon-neutral cement manufacturing. The study demonstrates that high litre weight should not be interpreted as a standalone indicator of clinker quality and that proper diagnosis is essential for reducing thermal energy consumption and CO_2 emissions.

Keywords: Clinker Chemistry, Alite, Belite, Free Lime, Litre Weight, Carbon Neutrality, Burnability, XRD, Microscopy.

Introduction

The cement industry contributes approximately 7–8% of global anthropogenic CO2 emissions, making the optimization of parameters like clinker reactivity, specific heat consumption, clinker factor, kiln throughput, and combustion efficiency vital for future decarbonization strategies. Traditionally, assessing clinker quality has relied on evaluating key metrics such as free lime, litre weight, kiln inlet temperature, and visual appearance; however, industrial observations show that a high litre weight does not always signify superior clinker quality. This nuance is clearly illustrated by two frequently misunderstood clinker phenomena that both produce a dense clinker through entirely different reaction pathways: Case 1 occurs during partial kiln loading and results in a high litre weight paired with low free lime and low tricalcium silicate C3S, whereas Case 2 occurs under full kiln loading conditions, resulting in a high litre weight accompanied by high free lime. Understanding these differences is critical because incorrect diagnosis frequently leads to unnecessary fuel addition and increased CO_2 emissions.

Literature Review

According to Taylor, Lea, Perry, Hewlett, and Odler, clinker quality is controlled primarily by raw meal burnability, clinker melt characteristics, residence time, liquid phase quantity, diffusion kinetics and cooling rate. While most published literature discusses free lime reduction, burnability improvement, and clinker mineralogy, little attention has been given to differentiating between high LW + low FL + low C3S and high LW + high FL. This paper directly addresses that gap.

Materials and Methods

A generalized industrial approach is utilized for monitoring and evaluating typical kiln feed chemistry and overall operational quality. The baseline chemical parameters for the kiln feed are strictly defined by specific ranges, including Lime Saturation Factor (LSF) of 94–97, Silica Modulus (SM) of 2.2–2.8, and Alumina Modulus (AM) of 1.3–1.8. To ensure process stability and product integrity, comprehensive quality assessment parameters are monitored, encompassing chemical and structural indicators such as free lime, litre weight, XRD phase composition, and clinker microscopy. Additionally, operational variables like carbon monoxide (CO) concentration, secondary air temperature, and the kiln loading factor are tracked to optimize the efficiency of the industrial kiln system.

Case 1: Partial Kiln Loading (60–80%)

Table 1

Parameter	Value
Load	60-80%
LW	1250-1350
FL	0.8-1.6
C_3S	38-42
C_2S	High

Typical Characteristics

Reduced Throughput
↓
Increased Residence Time
↓
Longer Exposure in Liquid Phase
↓
(1250–1450°C)
↓
Crystal Coarsening
(Alite & Belite Grain Growth)
↓
(1350–1450°C)
↓
Reduced Effective Alite (C_3S)
Development
↓
Lower C_3S / Higher C_2S
↓
Higher Litre Weight
↓
Lower Early Strength

Figure 1: Clinkerization Mechanism Under Partial Kiln Loading

Excessive Liquid Phase Residence

When the kiln throughput decreases, the overall rate of raw material feeding into the system slows down. This reduction in material volume causes the material to remain longer within the critical liquid phase zone. Because less material passes through the kiln per unit of time, the total heat absorbed per tonne of material increases significantly, leading to an elevated residence time within this high-temperature zone.

Ostwald Ripening

Ostwald ripening during cement clinker production occurs when an extended residence time in the kiln causes smaller, less stable alite C_3S crystals to dissolve into the liquid phase and redeposit onto larger, more stable crystals. This thermodynamic process drives crystal coarsening, which leads to significantly larger alite grains and a reduction in active nucleation sites. As a direct consequence, the microstructural profile shifts: the overall alite crystal size increases, the total count of individual alite grains drops, and the amount of highly reactive C_3S decreases, potentially impacting the final strength and hydration performance of the cement.

Microscopy Expectations

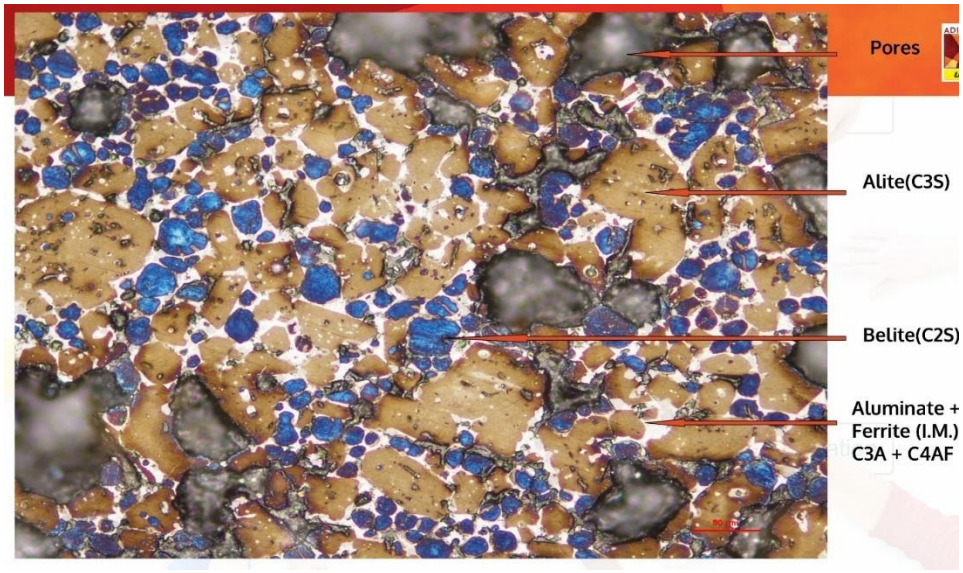
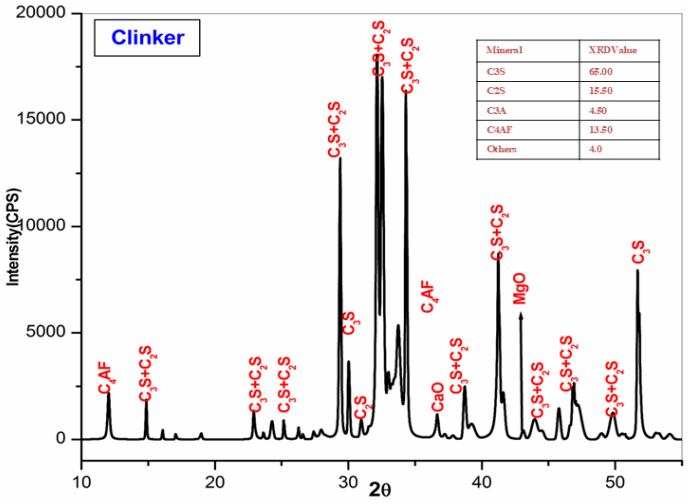


Figure 2: Typical Clinker Minerals distribution

Microscopy Comparison

Table 2

Parameter	Full Load	Partial Load
Alite size	Medium	Large
Alite Density	High	Lower
Belite Area	Normal	Higher
Porosity	Moderate	Lower
LW	Lower	Higher



XRD Expectations:

Table 3

Mineral	Full Load	Partial Load
C3S	46-50	38-42
C2S	20-25	28-35
Free Lime	Similar	Similar

Figure 3: X-ray diffractogram of clinker

Reduction in C_3S occurs primarily through a shift toward belite rather than increased free lime.

Case 2: Full Loading with High LW and High FL

Typical Characteristics

Table 4

Parameter	Value
Load	Full
LW	>1200
FL	1.6-1.8
Burnability	Poor

Quartz Dissolution Limitation

Quartz Dissolution Limitation occurs primarily when dealing with coarse quartz particles. Because of their large size, there is a slow dissolution rate, which significantly reduces the availability of silica within the reaction or melt mixture. The direct result of this reduced silica availability is an incomplete reaction with lime, leading to a noticeable increase in free lime remaining in the final product.

High Silica Modulus

A high Silica Modulus (SM) in cement production indicates a higher proportion of silica relative to alumina and iron oxide, which significantly impacts the clinkerization process. When the SM is high, it reduces the quantity of the liquid phase formed in the kiln and increases the viscosity of the melt. The main consequence of this stiffer, less abundant liquid phase is that the diffusion rate of ions decreases. Because diffusion is hindered, the chemical combination slows down, leading to a decrease in alite formation and potentially leaving more uncombined free lime remaining in the final product.

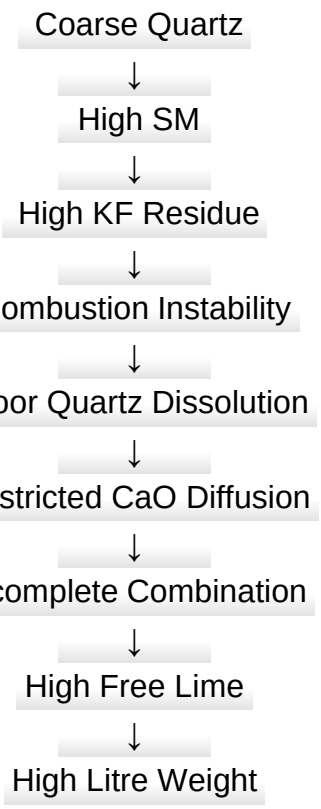


Figure 4: Schematic diagram of coarse quartz vs Litre weight & Free Lime

High Kiln Feed Residue and High CO Impact

High kiln feed residue and a high carbon monoxide (CO) impact significantly disrupt the clinkerization process in cement manufacturing by altering the kiln's internal atmosphere and chemical kinetics. When a high kiln feed residue is present, it creates a long diffusion path for the raw materials. This extended path slows down the process, directly resulting in a decreased reaction rate and an undesirable increase in free lime levels.

Simultaneously, a high CO impact creates an unfavorable reducing atmosphere within the kiln. Instead of achieving complete and optimal combustion via the standard reaction:

$$C + O_2 \rightarrow CO_2$$

the system experiences incomplete combustion, forming carbon monoxide according to the reaction:

$$2C + O_2 \rightarrow 2CO$$

The combined consequences of a long diffusion path and a reducing atmosphere lead to severely reduced combustion efficiency, poor clinkerization quality, and elevated amounts of high free lime in the final product.

Comparative Discussion

Table 5

Feature	Partial loading	Full Loading
LW	High	High
Free Lime	Low	High
C_3S	Low	Moderate
Root Cause	Residence time	Burnability
Main Mechanism	Crystal coarsening	Incomplete combination
Corrective action	Increase throughput	Improve burnability

Carbon Neutrality Implications

In cement manufacturing, addressing a decrease in alite content by simply increasing fuel addition is an incorrect practice that leads to higher Specific Heat Consumption (SHC), increased CO_2 emissions and minimal mineralogical improvement. To achieve carbon neutrality and improve clinker quality effectively, operators should implement targeted corrective strategy based on the specific root cause. For Case 1, increasing production throughput, improving the filling degree of the kiln, and reducing excessive material residence time to optimize thermal efficiency and mineral formation is necessary. Whereas Case 2, requires improving quartz fineness, reducing coarse residues, optimizing the Silica Modulus (SM), and ensuring a stabilized combustion process.

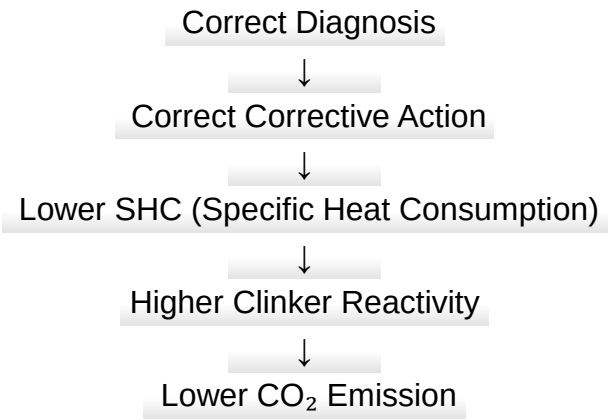


Figure 5: Flow of correlation

Conclusions

- High litre weight does not necessarily mean high clinker quality.
- Under partial loading, low C_3S is primarily caused by excessive liquid-phase residence and crystal coarsening.



- Under full loading, high free lime is primarily caused by burnability limitations.
- The two conditions require fundamentally different corrective actions.
- Misdiagnosis leads to unnecessary fuel consumption and increased CO_2 emissions.
- Proper distinction supports carbon-neutral cement manufacturing through improved clinker reactivity and lower specific heat consumption.

References

- H.F.W. Taylor, *Cement Chemistry*.
- Lea's *Chemistry of Cement and Concrete*.
- K.E. Peray, *The Rotary Cement Kiln*.
- P.C. Hewlett, *Lea's Chemistry of Cement and Concrete*.
- I. Odler, *Special Inorganic Cements*.
- Fundal, *Clinker Burning and Quality Control*.
- International Cement Review Technical Papers.
- World Cement Technical Publications.
- Cement and Concrete Research (CCR) publications on clinker mineralogy.
- AUCBM and NCB conference proceedings on clinker chemistry.

Novelty Statement

High litre weight clinker can arise from two fundamentally different mechanisms. Under partial kiln loading, high litre weight is associated with low C_3S despite acceptable free lime due to excessive liquid-phase residence and altered alite evolution. Under full kiln loading, high litre weight accompanied by elevated free lime is primarily associated with burnability limitations including coarse quartz, high residue, excessive silica modulus, and combustion inefficiencies. Failure to distinguish these mechanisms often leads to unnecessary fuel consumption and increased CO_2 emissions.

WASTE GLASS POWDER AS A LOW-CARBON SUPPLEMENTARY CEMENTITIOUS MATERIAL: A COMPARATIVE STUDY WITH FLY ASH-BASED BLENDED CEMENTS

Manish Kuchya, Ajay Mahadela, Jyoti Pansare, K Suresh, Awadhesh Singh & Satyabrata Sharma

Central R&D, UltraTech Cement Limited, Mumbai

Abstract

The cement industry is actively pursuing low-carbon alternatives to reduce clinker consumption and mitigate greenhouse gas emissions while promoting the utilization of industrial and municipal wastes. Waste glass powder (WGP), owing to its high amorphous silica content and widespread availability, has emerged as a promising supplementary cementitious material (SCM) capable of contributing to both sustainability and circular economy objectives. However, the variability in glass waste characteristics and limited understanding of its reactivity relative to established SCMs such as fly ash have constrained its broader adoption in cement manufacturing.

This study evaluates the potential of WGP as a low-carbon SCM through a comprehensive investigation encompassing material characterization, reactivity assessment, and cement performance evaluation. The waste glass powder was characterized using particle size distribution, chemical composition, mineralogical analysis, and morphological examination to establish its suitability as a reactive siliceous material. The pozzolanic potential of WGP was assessed through lime reactivity and cement reactivity studies and benchmarked against conventional fly ash. Subsequently, blended cement formulations incorporating WGP were developed and compared with cements containing 20% and 35% fly ash replacement levels. Fresh and hardened state properties, including water demand, setting behaviour, compressive strength development, and strength activity index, were evaluated to determine the effectiveness of WGP as a clinker replacement material. Similarly, WGP performance were evaluated with M30 Grade concrete mix by completely replacing 35% FA content with equivalent amount of WGP.

The results indicate that the predominantly amorphous nature and high silica content of WGP contribute to significant pozzolanic activity, leading to progressive strength development and improved utilization of calcium hydroxide during hydration. The performance of WGP-blended cements was found to be comparable to, and in selected formulations superior to, conventional fly ash-based blended cements. The findings demonstrate that appropriately processed waste glass powder can serve as an effective SCM, enabling clinker factor reduction while maintaining acceptable cement performance.

The study highlights the technical feasibility of incorporating waste glass powder in blended cement systems and provides a pathway for valorizing an underutilized waste stream into a high-value construction material. The adoption of WGP as a supplementary cementitious material can contribute to resource efficiency, waste diversion from landfills, and the development of sustainable low-carbon cements aligned with global decarbonization goals.

Keywords: Waste glass powder, supplementary cementitious material, low-carbon cement, pozzolanic reactivity, fly ash, blended cement, circular economy, clinker reduction.

1. Introduction

The cement industry is under increasing pressure to decarbonize while meeting the growing global demand for infrastructure and housing. Ordinary Portland cement (OPC) production contributes approximately 7–8% of global anthropogenic CO_2 emissions, primarily due to limestone calcination and the energy-intensive clinker manufacturing process [1–3]. Consequently, lowering the clinker



factor through the incorporation of supplementary cementitious materials (SCMs) is widely recognized as one of the most effective strategies for reducing the carbon footprint of cementitious materials [2,4]. Conventional SCMs such as fly ash and ground granulated blast furnace slag (GGBS) have significantly contributed to clinker reduction over the past decades; however, their long-term availability is expected to decline owing to the progressive phase-out of coal-fired power plants and changes in industrial production patterns [2,5]. This scenario has intensified research into alternative SCMs derived from industrial, municipal, and construction waste streams.

Among the emerging SCMs, waste glass powder (WGP) has gained considerable attention because of its high amorphous silica content, widespread availability, and potential to support circular economy objectives through the beneficial utilization of post-consumer and post-industrial glass waste [6–9]. Globally, millions of tonnes of waste glass are generated annually, a substantial fraction of which is disposed of in landfills because contamination, mixed colours, and economic limitations restrict conventional remelting and recycling routes [6,7]. The conversion of waste glass into finely ground powder for incorporation into cementitious systems presents an attractive opportunity to reduce landfill burden while simultaneously decreasing clinker consumption and associated CO_2 emissions [6,8].

The pozzolanic behavior of waste glass is primarily attributed to its high content of amorphous silica, which reacts with calcium hydroxide released during cement hydration to form additional calcium silicate hydrate (C-S-H) gel [10,11]. Previous studies have demonstrated that when ground to sufficiently fine particle sizes, typically below 75 μm, waste glass exhibits significant pozzolanic reactivity and can perform comparably to traditional SCMs such as fly ash [10–12]. In addition to the pozzolanic contribution, fine glass particles provide a micro-filler effect that enhances particle packing density, refines pore structure, and improves hydration efficiency [8,11,13]. These mechanisms often result in improved long-term strength development and enhanced durability characteristics.

Recent investigations have further demonstrated that WGP can positively influence the mechanical and durability performance of cement-based materials. Researchers have reported improvements in compressive strength, chloride penetration resistance, sulfate resistance, and pore structure refinement at optimized replacement levels [7,8,11,14]. Furthermore, finely ground waste glass has been shown to mitigate alkali-silica reaction (ASR), which has traditionally been a concern associated with glass-containing concrete, by consuming alkalis through pozzolanic reactions and reducing the availability of reactive silica in coarse glass particles [12,14].

From a sustainability perspective, waste glass powder offers significant environmental advantages. Life-cycle assessment studies indicate that clinker substitution with WGP can reduce embodied carbon, conserve natural resources, and divert substantial quantities of waste from landfills [6–8]. Recent reviews on emerging SCMs have identified waste glass powder as one of the promising alternative materials capable of supporting the development of next-generation low-carbon cements and climate-resilient binders while contributing to global decarbonization and circular economy targets [2,6].

Despite these advantages, the widespread industrial adoption of WGP remains limited due to variability in waste glass sources, differences in chemical composition and fineness, and incomplete understanding of its reactivity relative to established SCMs such as fly ash [2,6,8]. Therefore, systematic investigations integrating material characterization, reactivity assessment, and cement performance evaluation are necessary to establish the technical viability of WGP for clinker replacement applications.

Accordingly, the present study investigates the suitability of waste glass powder as a low-carbon supplementary cementitious material through comprehensive physicochemical characterization, pozzolanic reactivity assessment, performance evaluation in blended cement systems and concrete mixes with complete fly ash replacement. Particular emphasis is placed on benchmarking the behavior of WGP against conventional fly ash and assessing its potential to reduce clinker content while maintaining the fresh and hardened properties required for sustainable cement applications.

2. Materials and Methods

2.1 Materials

Ordinary Portland Cement (OPC) 53 Grade was used as the base cement in this study. The cement was procured from the local market in India and manufactured at one of the production units of the country's largest cement producer. Class F fly ash (FA) was sourced from a thermal power plant in Nashik, while waste glass powder (WGP) was obtained from a local commercial supplier. Mineral gypsum (GYP) was incorporated to achieve the target SO_3 content in the various cement blends. The particle size distribution (PSD) of FA and WGP was determined to characterize their particle size characteristics and fineness using CILAS analyzer. Furthermore, the lime reactivity and cement reactivity of FA and WGP were evaluated in accordance with the procedures specified in IS 1727 to assess their pozzolanic reactivity.

2.2 Preparation of the cement blends

The cement blends containing fly ash (FA) and waste glass powder (WGP) investigated in this study were prepared at two replacement levels, namely 20% and 35%, for each supplementary cementitious material. The constituent materials were proportioned according to the mix compositions presented in Table 1, with a total batch size of 5 kg. To ensure a consistent sulphate balance, the blends were formulated to achieve a target SO_3 content of 2.6 ± 0.1%. Subsequently, the materials were interground in a laboratory ball mill for 30 min to obtain a homogeneous cementitious blend.

Table 1. Mixture proportions of OPC and different Cement blends

	OPC	GYP	FA	WGP
OPC	100	0	0	0
CEM-FA20	78.80	1.20	20	0
CEM-FA35	62.90	2.10	35	0
CEM-WGP20	78.80	1.20	0	20
CEM-WGP35	62.90	2.10	0	35

2.3 Test Methods

2.3.1 Characterization of materials

Table 2 presents the chemical composition of the materials used in this research work. The chemical compositions were determined using an X-ray fluorescence (XRF) spectrometer (Axios, PANalytical), while the mineralogical compositions were characterized using X-ray diffraction (XRD) analysis (Bruker D8 Advance). The XRD diffractograms shown in Figure 1 indicate that WGP is predominantly amorphous, with only minor quantities of crystalline quartz, whereas fly ash (FA) contains both crystalline and amorphous phases. The particle size distribution (PSD) characteristics of FA and WGP are presented in Table 3. The results reveal that WGP is marginally finer than FA, which may enhance its particle packing ability and reactivity in blended cement systems.

Table 2. Chemical composition of different materials

Materials	LOI	SiO_2	Al_2O_3	Fe_2O_3	CaO	MgO	SO_3	Na_2O	K_2O	Cl	TiO_2
OPC	1.44	20.90	5.52	4.12	62.42	1.05	2.50	0.23	0.52	0.012	0.52
FA	1.25	63.78	22.90	3.20	1.86	0.65	0.17	0.37	2.08	0.003	1.04
WGP	0.70	73.10	1.12	0.12	8.53	3.42	0.33	12.18	0.25	0.004	0.03
GYP	20.55	1.05	0.17	0.10	32.18	0.95	43.67	0.02	0.06	0.005	0.03

Table 3. Critical Particle Size Distribution Parameters of FA and WGP

	d10, µm	d50, µm	d90, µm	Mean Dia., µm	R+45µm, %
FA	2.91	17.41	58.62	25.19	20.44
WGP	2.25	11.15	61.77	22.65	16.93

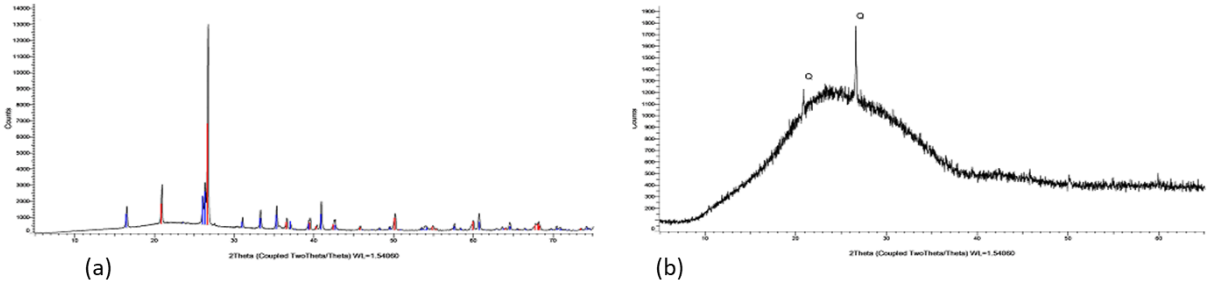


Fig.1 XRD of (a) FA indicating the main minerals -Quartz (Red Stick) & Mullite (Blue stick) along with the amorphous content and (b) WGP indicating almost amorphous material with minor amounts of Quartz

2.3.2 Lime reactivity and Cement Reactivity: Pozzolanic activity

Lime reactivity and Cement Reactivity of the FA and WGP were determined in accordance with the method specified in IS 1727. The results obtained for the two different materials are indicated in Table 4. Lime reactivity is found to be higher for FA compared to WGP. Comparatively the cement reactivity is found to be better for WGP.

Table 4. Lime Reactivity and Cement Reactivity of FA and WGP

	Lime Reactivity, MPa	Cement Reactivity, %	
		28 days	90 days
FA	4.9	81.0	86.0
WGP	4.3	89.7	92.0

2.3.3 Standard water requirement and Setting times

Method for determination of standard consistency for the performance evaluation of cement blends were as per IS 4031 (Part 4): 1988. Initial and final setting times of the various cement blends paste has been tested using the Vicat apparatus in accordance with the method mentioned in Bureau of Indian Standards IS:4031 (Part 5): 1988 considering the respective standard consistency.

2.3.4 Compressive Strength

The compressive strength at different ages viz., 1, 3, 7, and 28 days have been determined for each cement blend using the Automatic compressive strength testing machine, CTM-314E of AIMIL India, in accordance with the method mentioned in Bureau of Indian Standards IS 4031(Part 6): 1988. The compressive strength has been tested on respective cement mortar cubes at the desired ages, prepared using the standard Ennore sand (Grade I, Grade II & Grade III) with the respective cement and the amount of water needed for making the cement mortars is calculated in accordance with the method mentioned in Bureau of Indian Standards IS 4031(Part 4): 1988.

2.3.5 Heat evolution studies

Isothermal conduction calorimetry (ICC) studies were carried out using TAM AIR isothermal calorimeter supplied by TA instruments, having air-based thermostat and easily interchangeable 8-channel standard volume offering high sensitivity and long-term temperature stability for detecting and characterizing heat flow for the different cement blends for a period of 72 hours at a water to cement ratio of 0.40 at 27^0C. Admix ampoule with 20 ml disposable glass ampoules system was used to study the hydration process to generate information related to very early hydration reactions right after water is added to the cement sample.

2.3.6 SEM studies

Morphology & Microstructural features in the vacuum dried hydrated cement blends with highest substitution of FA and WGP hydrated for 28 days periods were determined using a ZEISS FESEM SIGMA equipped an energy dispersive X-ray analyser. Samples for the SEM analysis were gold coated for a duration of 120 secs using a sputter coater to prevent the charging of the samples prior to detailed SEM analysis.

2.3.7 Mix proportions of concrete

Concrete mixtures were designed for M30 grade concrete in accordance with the guidelines of IS 10262:2019. Normal concrete mix containing 35% FA and Concrete mix replacing the FA with equivalent amount of WGP were studied. The total binder content, comprising OPC, fly ash, and waste glass powder, was maintained at 415 kg/m³ across all mixtures, while the water-to-binder ratio was kept constant at 0.34. Locally available crushed stone sand conforming to Zone II was used as fine aggregate, while crushed coarse aggregates with a nominal maximum size of 20 mm were used. A polycarboxylate ether-based superplasticizer (Chryso 9421) was added to both the concrete mixes to maintain comparable workability. The water-to-binder ratio and aggregate proportions were kept constant across both the mixes to ensure that the observed changes in performance could be directly attributed to the binder composition. This approach helped in clearly understanding how the two supplementary cementitious materials influence the behavior of the respective concrete systems. The superplasticizer dosage was adjusted for the individual mixtures to achieve the required fresh-state properties.

3.0 Results and Discussions

3.1 Performance evaluation of cement blends

The test results for the various physical properties of the cement such as Blaine, Standard consistency, Setting times and Compressive strength at 1Day, 3 Days, 7 Days & 28 Days are indicated in Table 5. The superior performance of WGP-blended cements can be attributed to its higher amorphous silica content, finer particle size, and higher cement reactivity compared with FA. Although both materials exhibited similar lime reactivity, WGP showed significantly higher cement reactivity at 28 and 90 days than FA, indicating greater pozzolanic contribution to strength development [2,9-11].

At 20% replacement, CEM-WGP20 achieved higher compressive strengths at all ages, reaching 61.6 MPa at 28 days compared with 58.1 MPa for CEM-FA20. Similarly, at 35% replacement, CEM-WGP35 developed 56.7 MPa compared with 52.4 MPa for CEM-FA35. The enhanced strength of WGP blends is attributed to the combined filler effect of finer particles and the formation of additional secondary C-S-H through pozzolanic reactions, resulting in improved particle packing and matrix densification [10,11,13]. WGP blends also exhibited shorter setting times than corresponding FA blends, indicating lower retardation effects. Overall, the results demonstrate that finely ground waste glass powder can effectively replace clinker and deliver strength performance comparable to or superior to conventional fly ash-based cements, highlighting its potential as a sustainable low-carbon supplementary cementitious material [2,8,9].

Table 5. Physical Properties of different cement blends

Sample	Blaine, m2/kg	w/c	Setting times, mins		Compressive Strength, MPa			
			IST	FST	1D	3D	7D	28D
CEM-FA20	332	30.5	180	250	15.1	27.4	38.8	58.1
CEM-FA35	365	32.5	240	310	11.7	21.9	31.2	52.4
CEM-WGP20	380	32.0	175	235	17.0	30.9	44.3	61.6
CEM-WGP35	445	34.0	190	260	13.6	24.6	35.6	56.7

3.2 Heat evolution

The normalized heat flow curves are shown in Fig.2 for the various cement blends. The normalized heat flow curves of the FA- and WGP-blended cements exhibited similar hydration profiles, characterized by an induction period followed by the main hydration peak associated with C_3S hydration and C-S-H formation. However, at both 20% and 35% replacement levels, the WGP blends showed a slightly higher main hydration peak and higher heat evolution during the acceleration period compared to the corresponding FA blends. This behaviour can be attributed to the finer particle size and higher amorphous silica content of WGP, which enhance the filler and nucleation effects, thereby promoting early cement hydration [4,10,15].

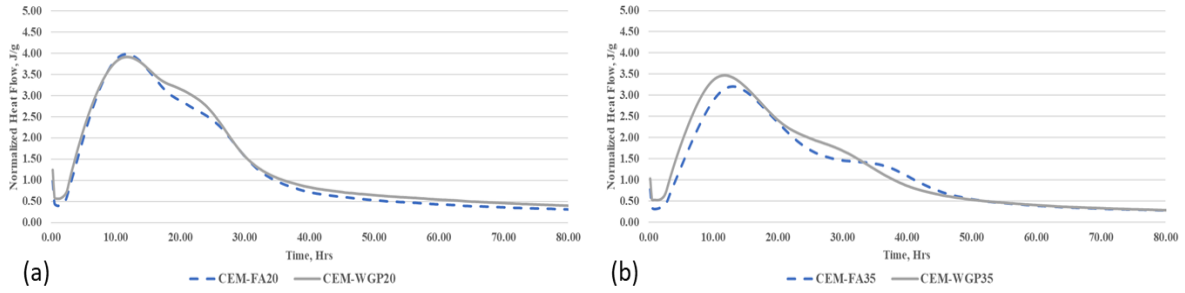


Fig.2 Normalized Heat Flow curves for (a) CEM-FA20 & CEM-WGP20 and (b) CEM-FA35 & CEM-WGP35

The effect was more pronounced in the 35% replacement system, where CEM-WGP35 exhibited a higher peak heat flow than CEM-FA35, indicating greater early-age reactivity. The enhanced hydration kinetics correlate well with the higher compressive strengths obtained for WGP-containing cements. At later ages, the heat flow curves gradually converged, reflecting the slower pozzolanic reactions of both SCMs. The results indicate that WGP provides more effective hydration acceleration than fly ash while maintaining the typical hydration behaviour of blended cement systems. Similar observations for finely ground glass powders have been reported in previous calorimetric and microstructural studies [9-11].

3.3 SEM studies – Hydrated pastes

Representative SEM micrographs of 28-day hydrated CEM-FA35 and CEM-WGP35 pastes are presented in Fig.3 and Fig.4. Both systems exhibited the presence of hydration products dominated by C-S-H gel; however, distinct differences in morphology and matrix densification were observed. The CEM-FA35 paste showed a relatively heterogeneous microstructure characterized by clusters of C-S-H intermixed with visible voids and partially reacted fly ash particles embedded within the hydration matrix. Some needle-like hydration products and porous regions remained evident, suggesting the slower pozzolanic reactivity typically associated with Class-F fly ash at 28 days [4,16].

In contrast, the CEM-WGP35 paste exhibited a noticeably denser and more compact microstructure with a greater extent of foil-like and fibrillar C-S-H gel formation and reduced visible porosity. Only a limited number of partially reacted glass particles were observed, indicating a higher degree of participation of WGP in hydration reactions. The denser matrix is attributed to the combined filler and

pozzolanic effects of finely ground waste glass powder, which accelerates nucleation of hydration products and promotes the formation of additional secondary C-S-H through reaction of amorphous silica with calcium hydroxide [4,9,11]. Similar microstructural refinement in glass powder blended cement systems has been reported by Mejdi et al. [11] and Omran et al. [9], who observed that the high amorphous silica content and finer particle size of WGP enhance hydration product development and reduce pore connectivity.

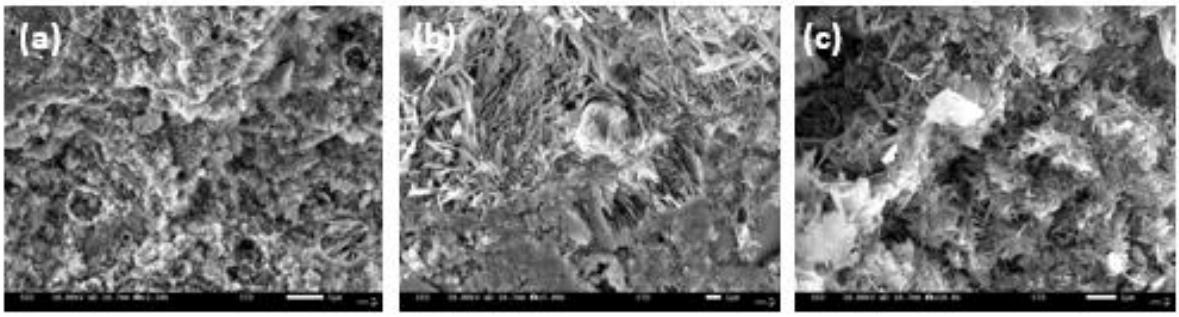


Fig.3 CEM-FA35 at different magnifications (a)2.5K (b)5.0K (c)10.0K showing major C-S-H formation and some unreacted FA particles

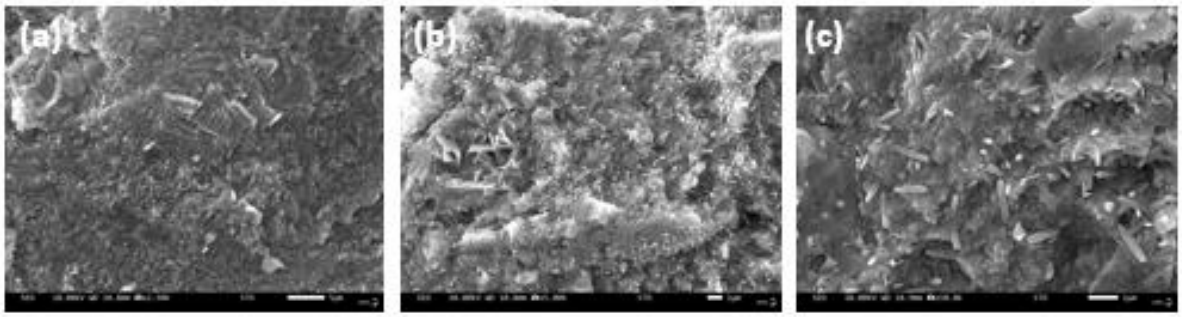


Fig.4 CEM-WGP35 at different magnifications (a)2.5K (b)5.0K (c)10.0K showing dense C-S-H formation with comparatively less porosity and some unreacted WGP particles

The observed microstructural differences are consistent with the higher cement reactivity, compressive strength, and durability performance of the WGP blends. The denser C-S-H matrix and reduced pore volume in CEM-WGP35 explain the superior 28-day strength, lower water permeability, and significantly reduced chloride ion penetrability observed in this study. These results confirm that waste glass powder can provide greater microstructural densification than fly ash at equivalent replacement levels, thereby contributing to improved mechanical and durability properties of low-carbon blended cement systems [9-12].

3.4 Performance of Concrete mixes

The concrete incorporating 100% replacement of FA with WGP exhibited significant improvements in both mechanical and durability performance compared with the control M30 concrete. At a constant binder content and water-to-cement ratio (w/c = 0.34), the WGP mix achieved higher compressive strengths at 1, 7, and 28 days, respectively, compared for the control mix with FA as indicated in the Table 6. The 28-day strength enhancement of approximately 31% can be attributed to the high amorphous silica content and finer particle size of glass powder, which promote both filler and pozzolanic effects. Finely ground glass particles improve particle packing, provide nucleation sites for hydration products, and react with calcium hydroxide to generate additional secondary C-S-H gel,

leading to a denser and stronger microstructure [1–4]. Similar improvements in compressive strength due to the incorporation of finely ground waste glass powder have been reported by Shi et al. [10], Du and Tan [13], and Mejdi et al. [11].

Table 6: Performance of Concrete mixes with FA and WGP

Parameters (kg/m^3)	Control M30 with FA	WGP Replacing FA 100%
OPC	270	270
Fly ash	145	0
Glass Powder	0	145
Coarse aggregate 20mm	609	625
Coarse aggregate 10mm	417	421
Fine aggregate	901	900
Chemical admixture	3.3	3.3
Water	140	140
Density	2487	2504
W/C	0.34	0.34
Comp. Strength, MPa		
1 Day	9.8	12.7
7 Day	31.9	39.4
28 Day	52.4	68.8
Water Permeability, mm	17.5	10.0
RCPT, coulomb	4022	1447

The durability performance showed even more pronounced improvements. Water permeability was reduced from 17.5 mm to 10.0 mm, representing a reduction of approximately 43%, while the Rapid Chloride Permeability Test (RCPT) value decreased from 4022 coulombs to 1447 coulombs, indicating a transition from moderate chloride ion penetrability to low penetrability as per ASTM C1202 classification. The substantial reduction in permeability and chloride ingress resistance can be attributed to pore refinement resulting from the pozzolanic consumption of calcium hydroxide and the formation of additional C-S-H, which reduces pore connectivity and densifies the interfacial transition zone (ITZ) [8-9,11-12]. Previous studies have similarly reported significant reductions in permeability, chloride penetration, and transport properties in concretes containing finely ground waste glass powder due to enhanced microstructural densification and reduced capillary porosity [6,12,13]. The results clearly demonstrate that complete replacement of fly ash with appropriately processed waste glass powder can not only maintain but significantly enhance both strength and durability performance, highlighting its potential as a sustainable supplementary cementitious material for low-carbon and high-performance concrete applications.

4. Conclusions

Waste glass powder (WGP) demonstrated significant potential as a low-carbon supplementary cementitious material and an effective alternative to fly ash in blended cement systems. Owing to its higher amorphous silica content, finer particle size, and superior cement reactivity, WGP-blended cements exhibited improved hydration kinetics, denser microstructure, and higher compressive strength than corresponding fly ash blends. Isothermal calorimetry revealed enhanced early hydration, while SEM observations confirmed the formation of a more compact C-S-H matrix with reduced porosity. These improvements translated into superior concrete performance, where complete replacement of fly ash by WGP increased 28-day compressive strength from 52.4 MPa to 68.8 MPa, reduced water permeability by 43%, and lowered RCPT values from 4022 to 1447 coulombs. Overall, the results



establish WGP as a technically viable SCM capable of simultaneously improving strength, durability, and sustainability while contributing to clinker reduction and circular utilization of waste glass.

The present study was conducted using a specific waste glass source and replacement levels under laboratory conditions. Long-term durability aspects such as carbonation, sulfate resistance, shrinkage, creep, and alkali-silica reaction mitigation were not evaluated. Future work should focus on long-term durability assessment, optimization of glass powder fineness and dosage, validation under field conditions, and advanced microstructural characterization. Life-cycle and techno-economic analyses are also recommended to establish the large-scale sustainability and commercial viability of waste glass powder in low-carbon cement and concrete applications.

References:

[1] International Energy Agency (IEA). Cement Technology Roadmap: Carbon Neutrality in the Cement Industry. IEA, Paris, 2023.

[2] Snellings, R.; Suraneni, P.; Skibsted, J. Future and emerging supplementary cementitious materials. Cement and Concrete Research, 2023, 171, 107199.

[3] Scrivener, K.L.; John, V.M.; Gartner, E.M. Eco-efficient cements: Potential economically viable solutions for a low-CO_2 cement-based materials industry. Cement and Concrete Research, 2018, 114, 2–26.

[4] Juenger, M.C.G.; Snellings, R.; Bernal, S.A. Supplementary cementitious materials: New sources, characterization, and performance insights. Cement and Concrete Research, 2019, 122, 257–273.

[5] Hewlett, P.C.; Liska, M. (Eds.). Lea's Chemistry of Cement and Concrete, 5th Edition, Butterworth-Heinemann, Oxford, 2019.

[6] Al-Hellali, N.; Bengtsson, M.; Nagy, A.; Sadagopan, M. Glass Waste as a Supplementary Cementitious Material in Climate Reduced Concrete: A Review. Nordic Concrete Research, 2025, 72(1), 167–181.

[7] Barbhuiya, S.; Kanavaris, F.; Ashish, D.K.; Tu, W.; Das, B.B.; Adak, D. Ground waste glass as a supplementary cementitious material for concrete: Sustainable utilization, material performance and environmental considerations. Journal of Sustainable Cement-Based Materials, 2025, 14(7), 1221–1249.

[8] Bameri, M.; Mohammadhasani, M.; Khaloo, A.; Ashour, A.; NikKhah, M. Influence of Waste Glass Powder as a Supplementary Cementitious Material on the Mechanical Properties, Expansion, Environmental Impact, and Microstructure of Cementitious Mortar. Engineering Reports, 2025, 7, e70238.

[9] Omran, A.; Soliman, N.; Zidol, A.; Tagnit-Hamou, A. Performance of ground-glass pozzolan as a cementitious material: A review. Advances in Civil Engineering Materials, 2018, 7(1), 237–270.

[10] Shi, C.; Wu, Y.; Riefler, C.; Wang, H. Characteristics and pozzolanic reactivity of glass powders. Cement and Concrete Research, 2005, 35(5), 987–993.

[11] Mejdi, M.; Wilson, W.; Saillio, M.; Chaussadent, T.; Divet, L.; Tagnit-Hamou, A. Hydration and microstructure of glass powder cement pastes: A multitechnique investigation. Cement and Concrete Research, 2022, 151, 106610.

[12] Zheng, K. Pozzolanic reaction of glass powder and its role in controlling alkali-silica reaction. Cement and Concrete Composites, 2016, 67, 30–38.

[13] Du, H.; Tan, K.H. Properties of high-volume glass powder concrete. Cement and Concrete Composites, 2017, 75, 22–29.

[14] Mehta, P.K.; Monteiro, P.J.M. Concrete: Microstructure, Properties and Materials, 4th Edition,



McGraw-Hill Education, New York, 2014.

[15] Snellings, R., Lothenbach, B., Scrivener, K., & Mertens, G. Early age hydration and pozzolanic reactivity of supplementary cementitious materials. Cement and Concrete Research, 2012.

[16] Lothenbach, B., Scrivener, K., Hooton, R.D. Supplementary Cementitious Materials. Cement and Concrete Research, 41(12), 1244-1256, 2011.



CALCIUM SULFOALUMINATE CEMENT SYSTEMS: A CRITICAL REVIEW OF HYDRATION, PERFORMANCE, SUSTAINABILITY AND FUTURE PERSPECTIVES

Dr.D. Praseeda[1], Ms. Priyanka Burra[1*], Mr. Suresh Vanguri[2], Mr. Srinivas[3]*

[1] Department of Civil Engineering, VNR VJIET, Hyderabad, India

[2] National Council for Cement and Building Materials, Hyderabad, India

[3]Ultratech Cement, Hyderabad, India

[*]Corresponding author: Dr.D. Praseeda Praseeda_d@vnrvjiet.in

ABSTRACT

The cement industry contributes about 7-8% of human-caused CO_2 emissions, highlighting the need for low-carbon alternatives. One promising option is calcium sulphoaluminate (CSA) cement, which produces 20-40% less CO_2 and uses less energy due to its lower clinkerization temperature (1200-1300°C) compared to traditional Ordinary Portland Cement (OPC) (1450-1500°C). This review covers recent advances in CSA cement from 2010 to 2025, including different types like conventional CSA, belite-CSA, alite-modified CSA, ye'elimite-rich CSA, and ternesite-containing CSA. Key topics include the chemistry of hydration, how the microstructure develops, mechanical strength, durability, and overall sustainability. The review pays special attention to how key components like ye'elimite and belite hydrate, the formation of ettringite and calcium silicate hydrate (C-S-H), and how these affect setting times, strength, and durability. It also looks at how factors like gypsum content, water-to-binder ratio, curing conditions, and supplementary materials influence performance. Advanced techniques like X-ray diffraction, electron microscopy, thermogravimetric analysis, infrared spectroscopy, and calorimetry help explain the changes in phases and structure during hydration. The review also explores how industrial wastes such as phosphogypsum, fly ash, steel slag, red mud, marble waste, and recycled concrete powder can be reused to reduce resource consumption and promote a circular economy. Studies show CSA cement sets quickly (15-45 minutes) and gains strong compressive strength—over 30 MPa in 24 hours and 50-80 MPa after 28 days—while significantly cutting environmental impact compared to OPC. However, challenges remain with long-term durability, raw material variability, controlling expansion, and scaling up production. This review critically assesses the current knowledge and points to future research directions to help CSA cement become widely accepted for sustainable building.

Keywords: CSA cement, Durability, Sustainable cement, ye'elimite, Recycled Material.

2. INTRODUCTION:

The primary sources of CO_2 emissions in the cement industry stem from the clinkerization of Ordinary Portland Cement (OPC) at temperatures between 1450-1500°C, and the calcination of limestone, which collectively account for approximately 7-8% of global human-induced CO_2 emissions. This considerable carbon footprint has sparked efforts to identify alternative binders that can maintain engineering performance while also reducing emissions and energy use during production. Calcium sulphoaluminate (CSA) cement is one of the low-carbon alternatives that has attracted increasing attention in recent years due to its manufacturing temperature range of 1200-1300 °C, as well as its potential to decrease the quantity of limestone required and lower CO_2 emissions by 20-40% compared to OPC. In addition to these advantages for the environment, it has been discovered that CSA cements have high early strength, good dimensional stability, and fast setting capabilities. These qualities are advantageous for applications such as expansive cements, precast components, and rapid repair materials [1, 6].

The performance of CSA cement is determined by the hydration characteristics of the main clinker phases. The initial strength and setting are caused by the interconnecting crystalline network that is created when the CaS combines with the ye'elimite [1, 11]. It has been discovered that belite hydrates more slowly, which leads to the development of calcium-silicate-hydrate (C–S–H) gel, a densification of the microstructure, and a later age strength gain [6, 7]. The relative levels of early reactivity, which will affect long-term performance, are determined by these phases in conjunction with sulfate availability, water-to-binder ratio, and curing conditions.

Recent research has also focused on compositional variations, such as ternesite–ye'elimite cements, ye'elimite rich systems, alite modified CSA, and belite rich CSA (BCSA), all of which seek to maximize different aspects of durability and strength development [4–12]. Concurrently, efforts have been made to reduce the use of natural resources and follow the circular economy principles by employing industrial wastes such as fly ash, phosphogypsum, steel slag, and marble waste as additional raw materials [8, 10, 14–18].Even though the body of research on the topic has grown since 2010, there are still certain gaps. The majority of the reviewed literature concentrates on particular aspects of CSA technology, such as waste utilization or hydration chemistry, while offering fragmented discussions of various cement variations without connecting the effects of cement mineralogy, reaction mechanisms, microstructure evolution, mechanical properties, and quantifiable sustainability metrics. Additionally, a large number of studies discuss the environmental concerns of CSA cement in qualitative terms, leaving out quantitative elements like embodied CO2, energy usage, and resource efficiency. Thus, there is currently no cohesive synthesis that takes these dimensions into account and clearly identifies the long-term behavior control and strength development elements.

This review's goal is to evaluate recent advancements in the field of CSA cements. A systematic search of peer-reviewed publications from 2010 to 2025 was used to find the literature, with an emphasis on those that included experimental data on clinker composition, hydration reactions, microstructural characterization (XRD, SEM, TGA, FTIR, and isothermal calorimetry), mechanical properties, and sustainability metrics. Particular focus is placed on the mechanisms of ettringite and C-S-H production, ye'elimite and belite hydration, and their impact on the setting behavior and strength progression.The review's primary objectives are to: (i) summarize current understanding of the chemistry and hydration mechanisms of the main families of CSA; (ii) assess the impact of sulfate balance, curing conditions, and supplemental materials on strength development and microstructure; (iii) evaluate the quantitative sustainability benefits of CSA cement compared to OPC, such as CO2 reduction and use of industrial by-products; and (iv) identify the remaining challenges for durability, raw-material variability, and industrial scale implementation. In addition to establishing the science supporting the use of CSA cement for sustainable construction, the review's goal is to pinpoint future research avenues.

2.1. Types and Properties of Calcium Sulphoaluminate Cement

2.1.1 Conventional Calcium Sulphoaluminate Cement

The main components of traditional calcium sulphoaluminate cement are ye'elimite (C4A3Ŝ),belite, calcium sulfate, and trace amounts of ferrite phases. This is because ye'elimite's high reactivity causes ettringite to develop early when calcium sulfate is present, controlling its mechanical, microstructural, and physical characteristics.

2.1.1.1 Physical properties

Conventional CSA cement typically has a quick setting time and a high early heat of setting due to the rapid breakdown of calcium sulfate and ye'elimite [1]. Setting behavior is significantly influenced by the sulfate to ye'elimite ratio, the water-to-cement ratio, and the curing temperature. Due to the development of ettringite, a quick reaction, and a lower ratio of Portland-type silicate phases, CSA cement often has better dimensional stability and less drying shrinkage than OPC cement [2]. However, early hydration may reduce workability, necessitating the use of appropriate superplasticizers or

retarders. Admixture compatibility, gypsum content, and clinker fineness are other process-related variables that influence the rheological characteristics.

2.1.1.2 Mechanical properties

The early precipitation of ettringite, which creates a linked crystalline framework that provides early rigidity and load bearing capability, is primarily responsible for the high early compressive strength of typical CSA cement [1]. A few hours or days after hydration, significant strength, good flexural strength, little shrinking, and sulfate resistance can be formed. The amount and activity of belite in the clinker have an impact on the strength development of later age. A significant amount of belite will contribute to gradual pore refinement and strength growth by forming more C-S-H gel throughout the delayed hydration process.

2.1.1.3 Microstructure

Early on in the hydration process, the microstructure is mostly composed of amorphous aluminum hydroxide gel and needle-shaped ettringite crystals that swiftly fill capillary pores and form a dense hydration network [1]. The material's quick rate of hardening and comparatively low early permeability are caused by the ettringite forming around partially hydrated clinker grains, forming an interlocking structure [2]. Later, at higher ages, belite hydration produces C-S-H gel in the spaces left between the ettringite crystals, improving the matrix's compactness. As a result, the microstructure that results is a mixture of gel-type silicate hydrates and crystalline ettringite [3].

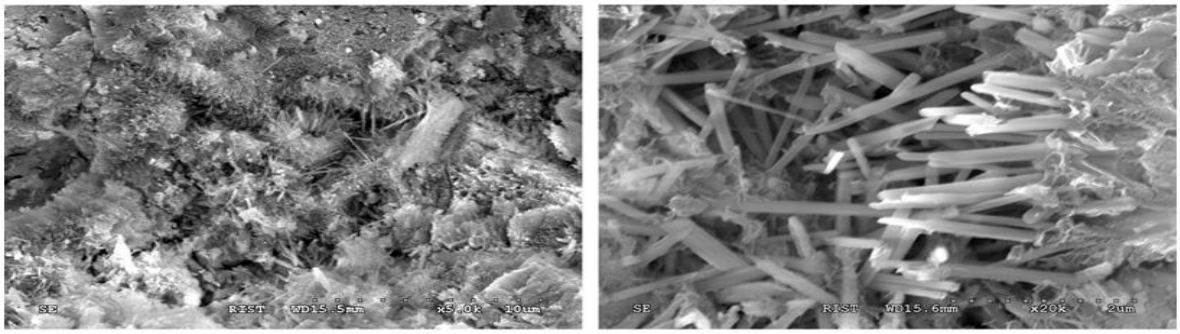


Figure 1. SEM images showing ettringite formation. Image courtesy of Cho,B.S.; Lee, H.H.; Choi, Y.C. Effects of aluminate rich slag on compressive strength, drying shrinkage and microstructure of blast furnace slag cement. Constr. Build. Mater. 2017, 140, 293–300 [3].

2.1.2 Alite-Based Calcium Sulphoaluminate Cement

Ye'elimite and a substantial amount of alite are found in calcium sulphoaluminate cement, which is alite-based. It was intended to hydrate more fast than typical early-hydrating cement and to gain strength more gradually than alite hydration.

2.1.2.1 Physical properties

Because the two phases would require distinct thermochemical conditions, it is challenging to stabilize alite and ye'elimite simultaneously in a single clinker [4]. It has been discovered that both phases coexist with the proper mineralizers in the regulated sulfur and oxygen atmospheres. Due to the increased reactivity of alite and ye'elimite, which speeds up early hydration and causes the production of a dense structure at early ages, sulfur-modified alite-CSA cement has a high early heat evolution and a short setting time [5].The composition of the clinker, the availability of sulfates, and the stability of the phases all have a significant impact on the physical behavior of the cement. If the raw material mix contains insufficient amounts of sulfates, the alite content may decrease or the ye'elimite content may be lost during the clinker-making process, which will negatively impact the cement's physical characteristics [4].

2.1.2.2 Mechanical properties

Both ye'elimite and alite participate in the hydration process in alite-based CSA cement, which results in strong early compressive strength. Alite produces calcium hydroxide and C–S–H gel, while ye'elimite aids in the catalysis of ettringite [5]. Since the ongoing alite hydration process helps to the development of strength after the first quick hardening period, alite can also help overcome some of the constraints of later age strength development that are occasionally observed in conventional CSA systems [4].When ettringite and C-S-H are formed together, the matrix becomes more compact and performs better mechanically over time. However, in order to avoid undesired heat evolution and dimensional instability, it is crucial to carefully regulate the clinker's composition and the sulfate balance [5].

2.1.2.3 Microstructure

Ettringite, C-S-H gel, hydrates including aluminum, calcium hydroxide, and unreacted clinker phases make up the hydrated microstructure of alite-CSA cement. Because it comprises both crystalline and gel-type hydration products, this cement differs from the traditional ye'elimite-dominated CSA systems [4]. Ettringite forms rapidly in the early eras, while the C-S-H progressively fills the capillary gaps in the later ages. The enhanced mechanical performance of the material is thought to be caused by the high density of ettringite and C-S-H composite structure [5].

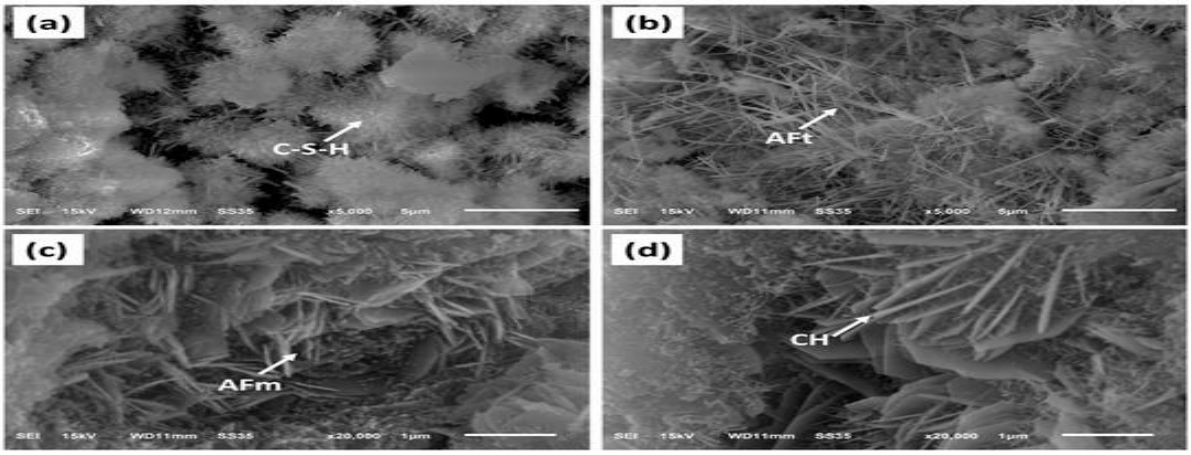


Figure 2. SEM images showing A-CSA formation. Image courtesy of X. Li, G. Kang, S. Dou, B. Ma, J. Tang, H. Zhou, H. Zhang, J. Wang, and X. Shen, "Preparation and properties of sulfur-modified alite calcium sulfoaluminate cement," Materials, vol. 17, no. 24, p. 6258, 2024 [5].

2.1.3 Belite-Calcium Sulphoaluminate Cement

The cement known as belite-calcium sulphoaluminate (BCSA) has a comparatively high belite and ye'elimite content. It uses belite hydration to age later and ye'elimite hydration to harden very early.

2.1.3.1 Physical properties

Compared to ordinary Portland cement, BCSA cement can be produced with a lower clinkerization temperature and less limestone, which reduces process CO2 emissions and thermal energy consumption [6]. However, because belite hydrates more slowly than highly reactive ye'elimite-rich systems, high-belite systems are often found to have higher dimensional stability and less early heat evolution [7]. Additionally, BCSA cement has been effectively produced using industrial waste materials by thermal and hydrothermal processing. The composition, hydration reactivity, and setting time of the clinker stages are all impacted by these kinds of waste-derived source materials [8].

2.1.3.2 Mechanical properties

There are two phases to the BCSA cement hydration process. The early strength is influenced by the quick formation of ettringite, and later age strength is influenced by the gradual formation of belite [6]. The benefit of this sequential mechanism is that it combines early strength with long-term performance. Concrete's compressive strength, crack resistance, and dimensional stability have all been observed to increase with the addition of belite hydration [7]. For example, the BCSA's compressive strength reached approximately 64 MPa in 28 days when phosphate-rock acid-insoluble residues were used. This is because the BCSA matrix contains both ettringite and C–S–H [9].

2.1.3.3 Microstructure

In the early phases of hydration, the BCSA cement features an ettringite, aluminum hydroxide gel, and unreacted belite microstructure [6]. Belite becomes C-S-H gel, which fills the spaces between the initial hydration products, as it continues to hydrate. The ettringite-rich structure gradually transforms into a denser composite matrix through the creation of C–S–H, allowing the structure to become stronger and more durable [7]. Both the method of heat treatment and the raw material composition have an impact on the form and dispersion of the hydration products. A compact microstructure resembling that of the native raw material BCSA can be obtained by appropriately processing the waste-derived BCSA clinker [8].

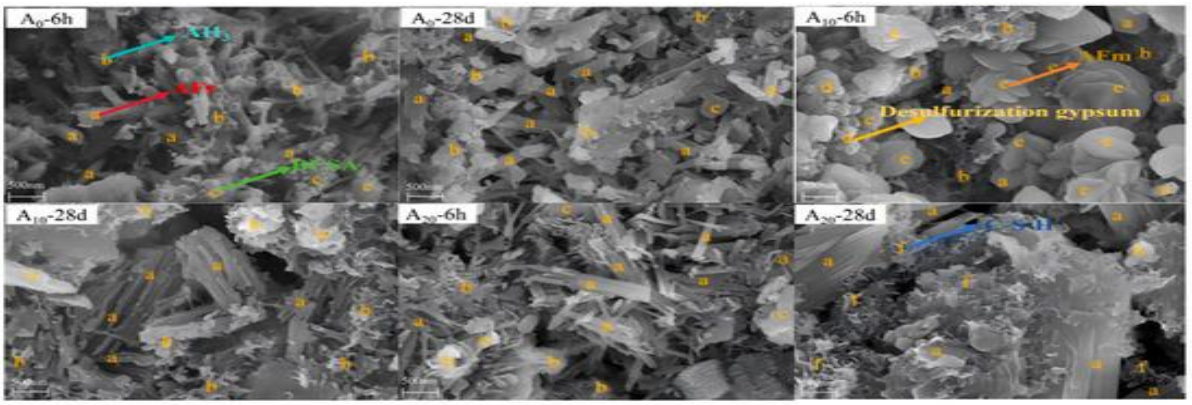


Figure 3. Microscopic morphology of hydrated samples. Image courtesy of H. Liu, C. Liu, J. Wu, Y. Gao, J. Shao, C. Wang, T. Su, F. Cao, W. Zhang, Q. Yang, et al., "Preparation of High-Belite Calcium Sulfoaluminate Cement and Calcium Sulfoaluminate Cement from Industrial Solid Waste: A Review," Sustainability, vol. 17, p. 4269, 2025, doi: 10.3390/su17104269 [7].

2.1.4 Ye'elimite-Rich Calcium Sulphoaluminate Cement

Ye'elimite-rich CSA cement is cement that contains ye'elimite and is primarily utilized when controlled expansion, high early strength, and quick setting are needed.

2.1.4.1 Physical properties

Ye'elimite can be produced from man-made wastes that contain calcium, aluminum, and sulfate. The type of phases that are created and the clinker's reactivity are greatly influenced by the raw material composition and the burning circumstances [10]. Alkali content and calcium sulfate availability have a significant impact on hydration and setting behavior. Alkalis have an impact on the pace at which ettringite precipitates and ye'elimite dissolves [11]. While high sulfate content can increase the capacity for expansion and lengthen the time needed for the development of ettringite, low sulfate content accelerates the formation of AFm. In order to regulate the cement's workability and dimensional stability, it is crucial to optimize the sulfate content.

2.1.4.2 Mechanical properties

The rapid early strength of ye'elimite-rich binders is caused by the early development of ettringite,

which is controlled by the quantity and rate of ettringite formation, hence regulating the binder's early load-bearing ability [11]. Phase purity, reactivity, and sulfate availability all affect the strength performance of synthetic ye'elimite-rich clinker. The hydration efficiency and compressive strength of the hardened cement may be reduced by unreacted or impurity-rich phases [10]. Sulfate depletion affects strength growth and dimensional stability as people age. Long-term mechanical behavior may be impacted by changes in the pore structure during the partial conversion of ettringite to monosulfate [11].

2.1.4.3 Microstructure

The early growth of ettringite, which is regulated by the quantity and rate of ettringite production and thus controls the binder's early load-bearing capabilities, is what causes the quick early strength of ye'elimite-rich binders [11]. The strength performance of synthetic ye'elimite-rich clinker is influenced by phase purity, reactivity, and sulfate availability. Unreacted or impurity-rich phases may lower the hardened cement's hydration efficiency and compressive strength [10]. As people age, sulfate depletion has an impact on dimensional stability and strength growth. Changes in the pore structure during the partial conversion of ettringite to monosulfate may have an effect on long-term mechanical behavior [11].

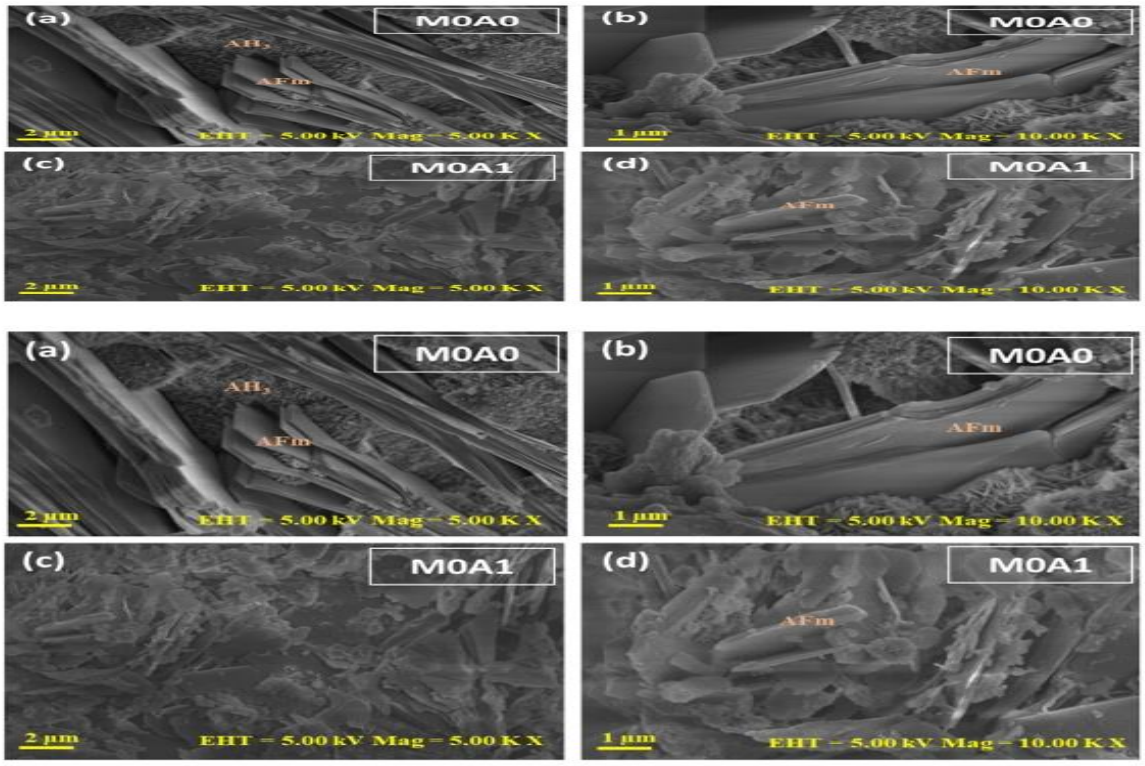


Figure 4. The microstructure captured in SE imaging in SEM for 3 day hydrated ye'elimite a–b without alkali and c–d with alkali (in the absence of gypsum) Image courtesy of B. Thaivalappil, V. K. Shenbagam, and P. Chaunsali, "Early-age hydration of ye'elimite (calcium sulfoaluminate phase) in presence of alkalis: role of calcium sulfate," Materials and Structures, vol. 57, p. 108, 2024, doi: 10.1617/s11527-024-02384-0 [11]

2.1.5 Ternesite–Ye'elimite Cement

Ternesite and ye'elimite cement are combined to create ternesite–ye'elimite cement. This binder is designed to use ye'elimite hydration for quick early hardening and ternesite for later age strength growth.

2.1.5.1 Physical properties

Ternesite is added to ye'elimite-based cement to change its hydration rate and heat-evolution behavior. In the later phases of hydration, ternesite is the primary contributor and is comparatively non-reactive at early ages [12]. Setting behavior is influenced by the ratio of ternesite to ye'elimite, the availability of sulfate, the curing temperature, and the fineness of the clinker. The reaction rate is lower at an early age and more favorable at a later age when the percentage of ternesite is larger.

2.1.5.2 Mechanical properties

The primary factor influencing early compressive strength is ye'elimite hydration, which is accompanied by the production of ettringite. Since ternesite supplies calcium, silica, and sulfate to take part in the extra hydration reactions, its contribution to later age strength is more noticeable [12]. The ideal ternesite composition can then enhance the cement's strength growth at later ages while preserving its early age strength features. Direct numerical comparisons of the traditional CSA or BCSA methods are few in the literature.

2.1.5.3 Microstructure

Ettringite and aluminum hydroxide gel make up the early microstructures. As ternesite ages, more silicate-containing hydration products are created, which tend to fill the remaining pores and increase the matrix's density [12]. Depending on the system's chemical makeup, ettringite, C-S-H, or C-A-S-H type gels may form the mature microstructure.

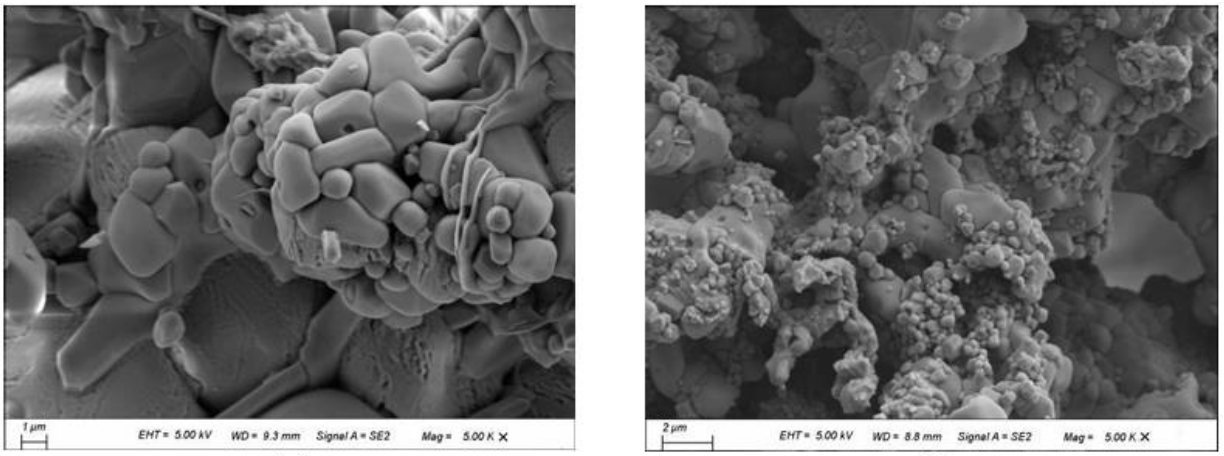


Figure 5. SEM micrographs of cement clinkers with 0.3% Na2O. (a) BCSA; (b) TCSA. Image courtesy of Y. Huang, W. Li, X. Zhang, et al., "Preparation and Performance of Ternesite–Ye'elimite Calcium Sulfoaluminate Cement," Materials, vol. 15, p. 4369, 2022, doi: 10.3390/ma15124369 [12].

3. FUTURE SCOPE:

There are still several issues that need to be addressed even if calcium sulphoaluminate cement has a lot of potential to replace OPC with low carbon. In order to improve long-term strength, durability, and dimensional stability without raising production costs or CO2 emissions, future research should concentrate on improving the clinker's composition. In order to reduce dependency on natural raw materials and accomplish particular objectives, more use of industrial by-products such as steel slag, fly ash, recycled concrete powder, and phosphogypsum should be explored.

Concurrently, more comprehensive life cycle analyzes and long-term durability testing are required to determine the true environmental benefits of these cements. For its practical application, compatibility tests with other cementitious materials and chemical admixtures will also be essential. Lastly, in order

to obtain CSA cement from bench scale research for usage on a broader scale for sustainable construction, manufacturing criteria and design concepts must be established.

4. CONCLUSION:

With its combination of lower clinkerization temperatures, less limestone usage, and quick strength development, calcium sulphoaluminate (CSA) cement presents a competitive low-carbon substitute for ordinary Portland cement. Sulfate balance and clinker mineralogy play a major role in determining its performance. Rapid ettringite production from ye'elimite drives early strength, whereas C–S–H creation from belite, alite, or ternesite contributes to later-age strength and microstructural densification.

Due to its lower clinkerization temperature (1200–1300 °C) and lower limestone use, CSA cement has been shown to have significant sustainability advantages over Ordinary Portland Cement, with reported CO2 emission reductions of 20–40% [10, 14]. By lowering dependency on virgin raw materials, the utilization of industrial by-products such steel slag, fly ash, and phosphogypsum further amplifies these advantages. It is usual to record compressive strengths greater than 60 MPa at 28 days. However, issues with long-term durability, raw material heterogeneity, and the absence of standardized production requirements continue to prevent widespread use. To fully realize the potential of CSA cement in sustainable construction, more research and industrial cooperation will ***be necessary.***

REFERENCES:

1. Winnefeld and B. Lothenbach, "Hydration of calcium sulfoaluminate cements—Experimental findings and thermodynamic modelling," *Cement and Concrete Research*, vol. 40, no. 8, pp. 1239–1247, 2010, doi: 10.1016/j.cemconres.2009.08.014.
2. K.L. Scrivener and A. Capmas, "Calcium sulfoaluminate cements," in *Lea's Chemistry of Cement and Concrete*, 4th ed., P.C. Hewlett, Ed. Oxford: Butterworth-Heinemann, 1998, pp. 713–782.
3. M.C.G. Juenger, F. Winnefeld, J.L. Provis and J.H. Ideker, "Advances in alternative cementitious binders," *Cement and Concrete Research*, vol. 41, no. 12, pp. 1232–1243, 2011, doi: 10.1016/j.cemconres.2010.11.012.
4. T. Hanein, T.Y. Duvallet, R.B. Jewell, A.E. Oberlink, T.L. Robl, Y. Zhou, F.P. Glasser and M.N. Bannerman, "Alite calcium sulfoaluminate cement: Chemistry and thermodynamics," *Advances in Cement Research*, vol. 31, no. 3, pp. 94–105, 2019, doi: 10.1680/jadcr.18.00118.
5. X. Li, G. Kang, S. Dou, B. Ma, J. Tang, H. Zhou, H. Zhang, J. Wang and X. Shen, "Preparation and properties of sulfur-modified alite calcium sulfoaluminate cement," *Materials*, vol. 17, no. 24, Art. no. 6258, 2024, doi: 10.3390/ma17246258.
6. K.L. Scrivener, A. Telesca and A. Gartner, "Development of calcium sulfoaluminate–belite cements," *Cement and Concrete Research*, vol. 41, no. 7, pp. 651–665, 2011.
7. H. Liu, Y. Gao, Z. Wu and J. Chen, "Preparation of high-belite calcium sulfoaluminate cement and calcium sulfoaluminate cement from industrial solid waste: A review," *Sustainability*, vol. 17, Art. no. 4269, 2025.
8. Rungchet, P. Chindaprasirt, S. Wansom and K. Pimraksa, "Hydrothermal synthesis of calcium sulfoaluminate-belite cement from industrial waste materials," *Journal of Cleaner Production*, vol. 115, pp. 273–283, 2016.
9. Y. Huang, J. Qian, X. Kang, J. Yu, Y. Fan, Y. Dang, W. Zhang and S. Wang, "Belite-calcium sulfoaluminate cement prepared with phosphogypsum: Influence of P_2O_5 and F on clinker formation and cement performance," *Construction and Building Materials*, vol. 203, pp. 432–442, 2019.
10. R. Kusiorowski, B. Lipowska and A. Gerle, "Synthesis of ye'elimite from anthropogenic waste," *Minerals*, vol. 13, no. 2, Art. no. 137, 2023.
11. B. Thaivalappil, V.K. Shenbagam and P. Chaunsali, "Early-age hydration of ye'elimite in the presence of alkalis: Role of calcium sulfate," *Materials and Structures*, vol. 57, Art. no. 108,



2024.
12. Y. Shen, X. Chen, W. Zhang, X.P. Li and J.S. Qian, "Influence of ternesite on the properties of calcium sulfoaluminate cements blended with fly ash," *Construction and Building Materials*, vol. 193, pp. 221–229, 2018.
13. Y. Shen, X. Chen, W. Zhang and X.P. Li, "Effect of ternesite on the hydration and properties of calcium sulfoaluminate cement," *Journal of Thermal Analysis and Calorimetry*, vol. 136, pp. 687–695, 2019.
14. P. Julphunthong and P. Joyklad, "Utilization of industrial wastes as raw materials for calcium sulfoaluminate cement," *Materials*, vol. 12, Art. no. 3929, 2019.
15. Y. Gan Yanze, A. Nana, P.N. Lemougna, R.C. Kaze, S. Tome, H. Rahier *et al.*, "Development of calcium sulfoaluminate cements from rich-alumina bauxite and marble wastes: Physicochemical and microstructural characterization," *International Journal of Ceramic Engineering & Science*, vol. 6, Art. no. e10216, 2024, doi: 10.1002/ces2.10216.
16. Rungchet, C.S. Poon, P. Chindaprasirt and K. Pimraksa, "Synthesis of low-temperature calcium sulfoaluminate-belite cements from industrial wastes and their hydration: Comparative studies between lignite fly ash and bottom ash," *Cement and Concrete Composites*, vol. 83, pp. 10–19, 2017.
17. Y. Shen, J. Qian, Y. Huang and D. Yang, "Synthesis of belite sulfoaluminate-ternesite cements with phosphogypsum," *Cement and Concrete Composites*, vol. 63, pp. 67–75, 2015.
18. Y. Shen, P. Wang, X. Chen, W. Zhang and J. Qian, "Synthesis, characterisation and hydration of ternesite," *Construction and Building Materials*, vol. 270, Art. no. 121392, 2020.
19. F. Winnefeld and S. Barlag, "Calorimetric and thermogravimetric study on the influence of calcium sulfate on the hydration of ye'elimite," *Journal of Thermal Analysis and Calorimetry*, vol. 101, pp. 949–957, 2010.
20. F. Song, Z. Yu, F. Yang, Y. Lu and Y. Liu, "Microstructure of amorphous aluminum hydroxide in belite-calcium sulfoaluminate cement," *Cement and Concrete Research*, vol. 71, pp. 1–6, 2015.

OXYFUEL TECHNOLOGY FOR CO_2 CAPTURE IN CEMENT INDUSTRY

Syed Rayees Ahmed, Anand Bohra and Anil Kumar Popuri

National Council for Cement and Building Materials

ABSTRACT

The cement industry contributes approximately 7% of global anthropogenic carbon dioxide (CO_2) emissions. Process emissions account for about 60% of this total and arise primarily from limestone calcination ($CaCO3 \rightarrow CaO + CO_2$). These emissions originate from the chemical decomposition of the raw materials. Energy-efficiency improvements, use of alternate raw materials and fuel switching alone cannot eliminate them completely. Carbon Capture, Utilization, and Storage (CCUS) is therefore a necessary component of pathways to net-zero emissions.

Oxyfuel combustion is one of the leading options among CCUS routes, which also include post-combustion amine scrubbing and calcium looping. The process of oxyfuel replaces ambient air with high-purity oxygen and recycled flue gas, producing an exhaust stream with a substantially elevated CO_2 concentration. This composition can reduce the complexity of downstream purification and compression. This paper examines the underlying process principles, international practices, pilot-scale and industrial deployments, technical and economic constraints, prospective developments, and the conditions governing adoption in the Indian cement industry.

In India, oxyfuel is best regarded as a strategic carbon-capture option for selected large cement plants, rather than as an immediate requirement for every kiln. A staged programme—beginning with laboratory and pilot validation, followed by a retrofit demonstration and integration with CO_2 transport and storage infrastructure—would enable scale-up against demonstrated performance criteria.

1. Introduction & Fundamental Principles of Oxyfuel Technology

1.1 The Operational Concept

In conventional cement plant kilns, fossil fuels and alternative fuels are combusted with ambient air, which contains approximately 79% nitrogen and 21% oxygen. Nitrogen entering with the combustion air forms a large proportion of the resulting flue gas and dilutes the CO_2 concentration to approximately 14–33% (dry basis). This dilution increases the energy demand and cost of subsequent CO_2 separation.

Oxyfuel technology changes the combustion environment through two principal measures:

- High-purity oxygen (≥ 95% O_2) is supplied to the main kiln burner and precalciner in place of ambient air.
- A controlled fraction of the CO_2-rich flue gas (RFG) is recycled. This stream moderates flame temperatures, maintains the gas mass flow required through the kiln system, and supports effective heat transfer.

1.2 Technology description and process configuration

A representative oxyfuel cement installation comprises the following interconnected process systems:

1. Air separation unit (ASU): Atmospheric air is separated into oxygen and nitrogen. Oxygen is delivered to the kiln and/or calciner at the desired purity and pressure specified by the selected process configuration.

2. Kiln and calciner combustion: Oxygen replaces the oxygen in conventional combustion air. Recycled CO_2-rich gas controls flame temperature while maintaining the gas flow and heat-transfer conditions required by the process.
3. Flue-gas recirculation: A regulated portion of the exhaust stream is routed back into the process. This recycle stream helps establish suitable combustion conditions and preserve kiln heat transfer.
4. Gas conditioning and purification: Dust, water vapour, oxygen and other impurities are controlled to satisfy the inlet requirements of the CO_2 purification unit and the specifications for subsequent transport or storage.
5. CO_2 compression and delivery: Following purification, CO_2 is compressed and transferred to a utilisation facility, a transport network, or a permanent geological storage site.

Oxyfuel capture requires an integrated process design. An ASU installation by itself, or the introduction of oxygen into an existing kiln without corresponding changes to gas recirculation and exhaust handling, does not constitute a complete oxyfuel carbon-capture installation.

1.3 Advantages over Post-Combustion Capture

- High CO_2 Purity: The exhaust stream consists predominantly of CO_2 and water vapor. Removing water by condensation produces a gas stream containing over 80–90% (and up to 99% with purification) CO_2.
- Footprint Efficiency: Oxyfuel equipment is integrated with the principal thermal units, including kilns and precalciners. This configuration can avoid the large absorption towers commonly required by post-combustion chemical-solvent systems.
- Cost Competitiveness: Oxyfuel eliminates the need for large solvent-regeneration circuits. On this basis, techno-economic assessments frequently identify it as one of the lower-cost options per tonne of avoided CO_2 for greenfield plants and kilns undergoing major retrofit.

2. International Best Practices & Technological Milestones

European research programmes, particularly the multi-phase work coordinated by the European Cement Research Academy (ECRA), have established much of the technical foundation for contemporary oxyfuel cement production. International development has focused on several principal design practices:

- Air-Oxygen Switchable Kiln Design: Kiln configurations are being developed to support conventional air-firing during start-up and transition, followed by operation in full oxyfuel mode. The changeover must preserve stable operation and consistent clinker quality.
- Advanced Burner and Cooler Modifications: Burners require adaptation for high-oxygen/high-CO2 atmospheres, which affect flame ignition speed, radiation characteristics, and temperature profiles. Clinker coolers must also be modified to limit nitrogen ingress and to maintain suitable secondary/tertiary air-equivalent gas circuits.
- Cryogenic Air Separation Unit (ASU) Integration: Cement plants can be integrated with cryogenic ASUs or pressure swing adsorption (PSA) units designed to provide a dependable supply of high-purity oxygen at an appropriate energy and operating cost.

3. Global Status: Pilot Plants and Full-Fledged Industrial Installations

During the past decade, oxyfuel development has advanced from theoretical modelling and laboratory-scale experiments to multi-megawatt pilot facilities and commercial projects designed for capture at the million-tonne-per-year scale.

Country/project	Technology or role	Published status as of 2026	Scale or milestone
Germany — catch4climate	Pure oxyfuel	Industrial-scale R&D facility operating in test campaigns	450 t/day clinker; first reported CO_2 capture in July 2026
Bulgaria — ANRAV	Oxyfuel CCS	Planned commercial-scale project	Approx. 0.8 $MtCO_2$/year; target around 2028
Germany — GeZero	Oxyfuel CCS	Planned commercial-scale project	Approx. 0.7 $MtCO_2$/year; target around 2029
China — Sinoma/CUCC-related development	Oxyfuel pilot and demonstration development	Published literature reports a pilot platform and associated demonstration	Reported 2,00,000 t/year project; exact integrated operating scope needs verification
Norway — Brevik CCS	Post-combustion capture	Industrial carbon-capture benchmark; not oxyfuel	Approx. 0.4 $MtCO_2$/year

The above project portfolio indicates that oxyfuel has progressed beyond conceptual development. Industrial research campaigns and planned commercial projects in Europe and Asia are now testing the technical and deployment requirements for large-scale application.

4. Key Technical and Economic Limitations

Oxyfuel can achieve high CO_2 capture rates, but its deployment remains subject to significant operational and economic constraints:

- High Energy Penalty (The "Oxygen Penalty"): Cryogenic ASUs consume substantial electrical power to produce high-purity oxygen. Their integration therefore increases the overall specific electricity consumption of the cement plant.
- Capital Expenditure (CapEx): The installation of ASUs, flue gas recirculation circuits, CO_2 purification units (CPU), and corrosion-resistant materials requires substantial initial investment.
- Refractory and Material Wear: At elevated temperatures, high concentrations of CO_2 and moisture can change the chemical conditions to which kiln refractory bricks are exposed. These conditions may accelerate or alter refractory attack and create a need for suitably engineered lining materials.
- CO_2 Transport and Storage Infrastructure: Capture alone does not complete the CCUS chain. In the absence of shared regional transport pipelines and qualified geological storage formations, captured CO_2 cannot be permanently stored or reliably supplied to utilisation markets.

5. Future Prospects and Technological Evolution

Research on Second-Generation Oxyfuel Systems, including work associated with the AC2OCem initiative, is directed towards reducing process energy demand and improving integration with cement-plant operations. Two areas of development are particularly relevant:

- Membrane-based Oxygen Separation: Ion transport membranes (ITM) and ceramic oxygen generator modules are being investigated as alternatives to energy-intensive cryogenic ASUs. Integration with waste heat recovery (WHR) streams could further improve overall process efficiency.



- Direct Integration with Alternative Fuels (AF): Oxyfuel combustion must be adapted to mixtures containing substantial proportions of biomass, refuse-derived fuels (RDF), and hazardous wastes. The objective is to maintain stable combustion while supporting the use of alternative fuels and associated circular-economy outcomes.

6. The Indian Cement Industry Context: Adoption Strategies, Constraints, and Limitations

India is the world's second-largest cement producer, with installed capacity exceeding 700 million tonnes per annum (MTPA). Decarbonisation of this sector is a national priority as the country pursues its 2070 net-zero target. The deployment of oxyfuel technology, however, must account for several technical, infrastructural, and economic conditions specific to India.

6.1 Specific Limitations & Challenges in India

1. Prohibitive Capital Intensity: Indian cement producers generally operate in markets characterised by narrow margins and sensitivity to changes in retail prices. The substantial CapEx required for ASUs and CPUs makes standalone oxyfuel retrofits financially challenging, particularly in the absence of effective carbon pricing, regulatory obligations, or targeted incentives.
2. Electrical Grid Carbon Intensity & Power Supply Stability: Oxyfuel installations require a large and reliable auxiliary electricity supply. Where oxygen separation is powered by a coal-intensive grid, indirect emissions can materially reduce the net lifecycle CO_2 benefit. Industrial electricity tariffs in India are also relatively high in comparison with raw fuel costs.
3. Lack of CO_2 Pipeline and Storage Ecosystem: In contrast to the US and Northwest Europe, India does not yet have mature regional CO_2 transport networks or well-characterized commercial offshore and onshore saline aquifer storage sites. The geographical availability of Enhanced Oil Recovery (EOR) opportunities is also limited.
4. Scale and Brownfield Constraints: A substantial proportion of India's cement capacity is distributed among small- and medium-sized kilns at geographically dispersed sites. Many existing plants have limited space for large cryogenic oxygen-production facilities and CO_2 compression equipment.

6.2 Pathways and Adaptation Strategies for India

- Phased Hybrid Adoption: Major Indian producers should first pursue energy efficiency, waste heat recovery (WHR), and clinker substitution using Calcined Clays (LC3) and fly ash. Partial oxy-fuel retrofits could then be evaluated on large greenfield production lines (>5,000 TPD), where plant layout and utilities can be incorporated into the original design.
- Policy and Carbon Market Integration: A functioning domestic compliance carbon-credit market, including India's Carbon Credit Trading Scheme - CCTS, would help assign economic value to verified emissions reductions. Such a mechanism could narrow the cost gap facing CCUS projects and improve their investment case.
- Industrial Clusters: Regional industrial clusters could allow several cement plants to share centralized oxygen production and a common CO2 trunk pipeline or utilisation hub. Potential outlets include green chemicals, urea manufacturing, and construction aggregate mineralization.

7 Conclusion & Strategic Roadmap

Oxyfuel technology offers a technically developed route for capturing process emissions from cement manufacture. Major projects in Europe and Asia provide commercial-scale demonstrations or proofs-of-concept. The principal barriers—capital requirements, electricity demand, and the absence of transport and storage infrastructure—remain significant worldwide and are particularly consequential in developing markets such as India.

Widespread conversion of the Indian cement sector to full oxyfuel operation is not presently a practical near-term option. A staged strategy is more appropriate: clinker substitution and energy-efficiency measures should take priority in the short term; partial oxyfuel operation should be assessed through pilot programmes at large, modern plants over the medium term; and shared CCUS infrastructure should be developed to support commercial-scale deployment towards 2040–2050.

Note: Project capacities and target dates are identified as reported plans where applicable. Cost figures are preliminary screening estimates; detailed engineering and independently verified operating data are required before investment decisions.

References

[1] CI4C / catch4climate — Official project information. Technology description, 450 t/day research facility and project partners.

[2] CI4C — First successful CO_2 capture, July 2026. Reported oxyfuel operation and initial CO_2 capture in the CPU.

[3] Heidelberg Materials — catch4climate inauguration, July 2026. Project investment, operating milestones and industrial-scale R&D scope.

[4] International Energy Agency — Innovation Gaps: Industry. Carbon capture technology principles and the case for capturing cement process emissions.

[5] NITI Aayog — Roadmap for Cement Sector Decarbonisation, January 2026. Indian sector priorities, CCUS pilots, policy support and infrastructure requirements.

[6] Press Information Bureau — CCU testbeds in the cement sector, July 2025. Government statement on proposed cement-sector testbeds and industry–academia collaboration.

[7] Global Cement — Carbon-capture project listings. Project-level information on oxyfuel and other cement-sector carbon-capture developments.

[8] Environmental Science & Technology — Carbon Capture in the Cement Industry: Technologies, Progress, and Retrofitting. Technical background on capture technologies, retrofit complexity and energy requirements.



Technical Session -IVA (Contd.)

EFFICACY OF BIPOLAR CORROSION INHIBITOR ADMIXTURES IN REINFORCED CONCRETE

Puneet Kaura, Dheerendra Singh, Brijesh Singh & Amit Trivedi

National Council for Cement & Building Materials, Ballabgarh, India

ABSTRACT

Corrosion of reinforcing steel is a major durability concern in reinforced concrete structures. The incorporation of corrosion-inhibiting admixtures into concrete offers a potential strategy for mitigating reinforcement corrosion; however, their effectiveness must be systematically evaluated through electrochemical, gravimetric, and chloride-transport assessments. The present study investigates the efficacy of a liquid-based bipolar corrosion-inhibiting admixture (BCIA)in reinforced concrete using a comprehensive experimental programme. The evaluation comprises a 720-hour immersion test based on reinforcement weight loss, Tafel polarization testing in a 3.5% NaCl solution over 20 days, chloride penetration assessment using ASTM C1202 and AASHTO T259, and long-term corrosion evaluation in accordance with ASTM G109. The immersion test provides a gravimetric assessment of corrosion-related metal loss, while Tafel polarization enables the evaluation of corrosion rate from the polarization curves. ASTM C1202 provides an electrical indication of concrete's resistance to chloride-ion penetration, whereas AASHTO T259 assesses chloride ingress under ponding conditions. ASTM G109 provides complementary information on macrocell corrosion behaviour in reinforced concrete specimens exposed to chloride environments. By integrating these testing methods, the study aims to establish a comprehensive assessment of the inhibitor's performance in terms of corrosion inhibiting efficiency

Key Words: Bipolar corrosion inhibitor; liquid-based admixture; reinforced concrete; chloride-induced corrosion; Tafel polarization; reinforcement weight loss; ASTM C1202; AASHTO T259; ASTM G109

1.0 Introduction

Reinforced concrete is one of the most widely used construction materials in civil engineering because of its high compressive strength, durability, versatility, and economic advantages. Under normal conditions, the highly alkaline environment of concrete, typically characterized by a pore-solution pH of approximately 12.5–13.5, promotes the formation of a passive oxide film on the surface of embedded reinforcing steel. This passive film protects the reinforcement against corrosion. However, the ingress of chloride ions and the penetration of atmospheric carbon dioxidecan compromise this protective condition [1-3] . Various strategies have been developed to mitigate reinforcement corrosion, including the use of low-permeability concrete, increased concrete cover, protective coatings, cathodic protection, corrosion-resistant reinforcement, and corrosion-inhibiting admixtures. Among these approaches, corrosion inhibitors offer a practical means of providing additional protection by modifying the electrochemical reactions responsible for steel corrosion. Their effectiveness depends on their chemical composition, dosage, transport characteristics, interaction with the steel–concrete interface, and exposure conditions. Based on their electrochemical mechanisms, corrosion inhibitors are commonly classified as anodic, cathodic, or mixed (bipolar) inhibitors [3,4].

Bipolar corrosion-inhibiting admixtures (BCIA)are of particular interest because they are designed to provide combined protection against the electrochemical processes responsible for reinforcement

corrosion. The evaluation of bipolar corrosion-inhibiting admixtures requires particular attention because different test methods measure different aspects of durability and corrosion performance. Short-term screening methods, including visual assessment of corrosion, steel-immersion tests, gravimetric measurements, and electrochemical polarization techniques, can provide information about corrosion initiation, metal loss, and corrosion kinetics under controlled conditions. Electrochemical techniques, such as Tafel polarization and linear polarization resistance, are especially useful for estimating corrosion current density and comparing the relative performance of inhibitor-treated and untreated specimens. However, results obtained using bare steel or simplified electrolytes may not fully represent the combined effects of the cementitious matrix, steel–concrete interface, moisture conditions, and inhibitor transport in actual reinforced concrete. Although several studies have investigated commercially available bipolar corrosion-inhibiting admixtures using short-term electrochemical tests and longer-term exposure of reinforced concrete specimens, the interpretation and comparison of results remain challenging because the methods differ in their underlying mechanisms, measurement parameters, and exposure conditions [2,4]. A systematic assessment is therefore necessary to determine the extent to which individual tests can reliably characterize the performance of bipolar corrosion inhibitors and to identify an appropriate combination of methods for performance evaluation, product qualification, and quality control.

Research Significance:

This paper addresses the comprehensive evaluation of a liquid-based bipolar corrosion-inhibiting admixture using gravimetric, electrochemical, chloride-penetration, and long-term corrosion assessment methods. The 720-hour immersion test, Tafel polarization in 3.5% NaCl over 20 days, ASTM C1202, AASHTO T259, and ASTM G109 collectively provide insights into reinforcement weight loss, electrochemical corrosion behaviour, chloride ingress, and macrocell corrosion respectively. This integrated approach enables a more reliable assessment of inhibitor efficacy than reliance on a single test method and helps distinguish improvements in corrosion resistance from changes in concrete's chloride-transport properties.

2.0 Experimental Methodology

The study was carried on different grades (M20, M30, M35, M40 & M50) of concrete as discussed in 2.3, comprising of various combination of cementitious materials as discussed below in section 2.1.

2.1 Materials

2.1.1 Concrete making Constituents

Ordinary Portland cement (OPC 43 grade), ground granulated blast-furnace slag (GGBFS), silica fume, coarse aggregates of 20 mm and 10 mm nominal maximum sizes, crushed fine aggregates, a locally available superplasticizer, and mixing water were used. All constituent materials were found to conform to the requirements of IS 269:2015, IS 16714:2018, IS 15388:2003, IS 383:2016, IS 9103:1999, and IS 456:2000 [5-11], as applicable.

2.1.2 Corrosion Inhibitors

Seven different brands of liquid-based bipolar corrosion-inhibiting admixtures (i.e. BP1, BP2, BP3, BP4, BP5, BP6, & BP7) were tested for pH, ash content, dry material content, and chloride ion content in accordance with the relevant test procedures specified in IS 9103:1999 [11]. The test results were

evaluated against the applicable requirements of RDSO Specification No. 6-68-0017 Rev.2 [2] Test results are presented below in table 1.

Table-1: Physical & chemical Characteristics of various Bipolar Corrosion Inhibitors

Sr. no.	Sample ID	BP1	BP2	BP3	BP4	BP5	BP6	BP7
1.	Specific gravity	1.09	1.07	1.05	1.05	1.05	1.05	0.99
2.	pH	10.14	13.50	9.90	10.45	11.14	9.85	11.01
3.	Ash content	0.08	9.00	5.57	4.11	0.04	0.30	0.06
4.	DMC	16.28	7.69	10.80	6.85	28.14	19.36	0.21
5.	Chloride content	0.002	0.383	0.003	0.004	0.006	0.010	0.018

2.1.3 Concrete Mix Proportions

In the present study, corrosion as well as durability properties of concrete were evaluated by comparing control sample with experimental sample to assess the efficacy of seven commercially available bipolar corrosion-inhibiting admixtures across different grades of concrete, as presented in Table-2. The control sample were prepared without the addition of a corrosion inhibitor, whereas the experimental sample incorporated the respective inhibitor at the dosage recommended by each manufacturer. All other constituent materials and mix proportions were kept identical between the corresponding control and experimental mixtures to ensure a consistent basis for comparison and to evaluate the influence of the corrosion-inhibiting admixtures on concrete performance. The concrete grades studied & dosage of bipolar corrosion-inhibiting admixtures (provided by the manufacturer recommendation) to be admixed in concrete are presented in Table-3

Table 2: Concrete mix proportion of different grades of concrete

Mix Constituents	M20	M30A1	M30A2	M35	M40	M50
	Quantity (kg/m^3)					
Cement (OPC 43 Grade)	280	356	214	229	400	375
GGBS	-	-	142	152	-	100
Silica fume	-	-	-	-	-	25
Total Cementitious content	280	356	356	381	400	500
Water	182	160	160	160	160	150
Fine Aggregate (crushed)	762	725	712	758	668	700
Coarse Aggregate -20-10mm	725	757	743	711	762	823
Coarse Aggregate -10-4.75mm	485	501	492	471	504	350
Chemical Admixture by wt. of cementitious content	-	2.67	2.85	2.670	4.0	2.25
Water – Cementitious Ratio	0.65	0.45	0.45	0.42	0.40	0.30

Table-3: Recommended dosages and concrete mix studied under specific BCIA

Bipolar Corrosion Inhibitor Admixture (BCIA) samples	Details of grade of concrete studied in different tests				Bipolar Corrosion Inhibiting admixture dosage (by weight of Concrete) (kg/m^3)
	Polarization Test by Tafel Polarization	RCPT as per ASTM C1202	Chloride ponding test as per AASTHO T259	Long Term Corrosion Test as per G-109	
BP1	M20	M40	M40	M40	2.42
BP2	M20	M35	M35	M35	1.91
BP3	M20	M30, M40, M50	M30, M50	M30, M40, M50	2.50
BP4	M20	M30, M40	-	M30, M40	2.00
BP5	M20	M30, M40	-	M30, M40	2.00
BP6	M20	M30, M40	-	M30, M40	3.00
BP7	M20	M30, M40	-	M30, M40	2.00

2.2 Test Conducted

To access the suitability & efficacy of bipolar corrosion inhibitors (BCIA) in concrete in the dosage recommended by the manufacturer, following test as defined in table 4 [13-15] have been studied with different grades of concrete:

Table- 4: Test

Sr. No.	Test	Brief
1	Modified Accelerated Corrosion Test (based on JIS Z 1535)	Steel specimens (16 mm diameter × 12 mm thick) were fitted into 1 L glass bottles using rubber stoppers. Control and BCIA-treated specimens were conditioned as per JIS Z 1535, and corrosion spots were visually observed at 27 ± 2°C.
2	Immersion Test (720 h) – Rebar Weight Loss Method	Three steel specimens each were immersed in raw water, with and without 1% (w/w) BCIA, for 720 h. Weight loss and corrosion rates (mpy) were determined as per ASTM G1.
3	Tafel Polarization Test (3.5% NaCl, 20 days)	M20 concrete slabs (350 × 250 × 100 mm), with and without BCIA, containing 12 mm diameter reinforcement, were cured for 28 days and exposed to 3.5% NaCl for 20 days. Electrochemical measurements followed ASTM G3 sign conventions.
4	Rapid Chloride Permeability Test (RCPT) (ASTM C1202)	Three 50 mm-thick slices from 100 × 200 mm concrete cylinders, with and without BCIA, were tested after 28 days of water curing. A 60 V DC potential was applied for 6 h, and charge passed was used to classify chloride-ion penetrability.
5	Chloride Ponding Test (AASHTO T259)	Concrete slabs (300 × 300 × 100 mm), with and without BCIA, were ponded with 3% NaCl for 90 days after conditioning. Cores were sliced into 10 mm discs up to 30 mm depth, and acid-soluble chloride content was determined as per IS 14959 (Part 2).
6	Long-Term Corrosion Test (ASTM G109)	Concrete specimens (280 × 150 × 115 mm), with and without BCIA, containing three 12 mm diameter reinforcing bars, were cured for 28 days and subjected to wetting–drying cycles with 3% NaCl. Voltage and current were measured, and cumulative macrocell charge was calculated using the trapezoidal rule.

3.0 Results and Discussion

3.1 Characterization of the bipolar corrosion inhibitor

The characterization tests were conducted to evaluate the physical and chemical properties of the seven bipolar corrosion inhibitors before assessing their corrosion-protection performance. The measured properties included specific gravity, pH, ash content, dry material content, chloride content, and visual appearance. The specific gravity values ranged from 0.99 for BP7 to 1.09 for BP1, with most products falling within the stated RDSO range of 1.0–1.1. The pH values ranged from 9.85 to 13.50. Although most products were within or close to the stated pH range of 9–12, BP2 had a notably higher pH of 13.50. These differences indicate that the products have different physical and chemical characteristics, which may influence their compatibility with concrete and their behaviour in a corrosive environment. Ash content and dry material content also varied considerably, suggesting differences in formulation and the proportion of non-volatile or solid constituents. Chloride content was low for most products, although BP2 had the highest reported value of 0.383. Since chloride ions can promote reinforcement corrosion, chloride content is an important consideration when selecting an inhibitor for reinforced concrete. However, these characterization results alone do not establish which product provides the best corrosion protection; that must be assessed using the subsequent performance tests.

3.2 Visual examination of bipolar corrosion inhibitor as per JIS Z1535 for corrosion spot identification

In the present study, JIS Z 1535 method was employed to visually examine the presence and extent of corrosion spots over the test specimen. The test specimen has been exposed to an environmental condition with and without corrosion inhibitor and comparison has been drawn. It is quite evident from the figure 1. that there has been considerable reduction in both the size and extent of corrosion spots on the bipolar corrosion inhibitor-treated specimens compared with the control specimens. These observations indicate that the bipolar corrosion inhibitor admixture effectively reduced the occurrence of visible corrosion.

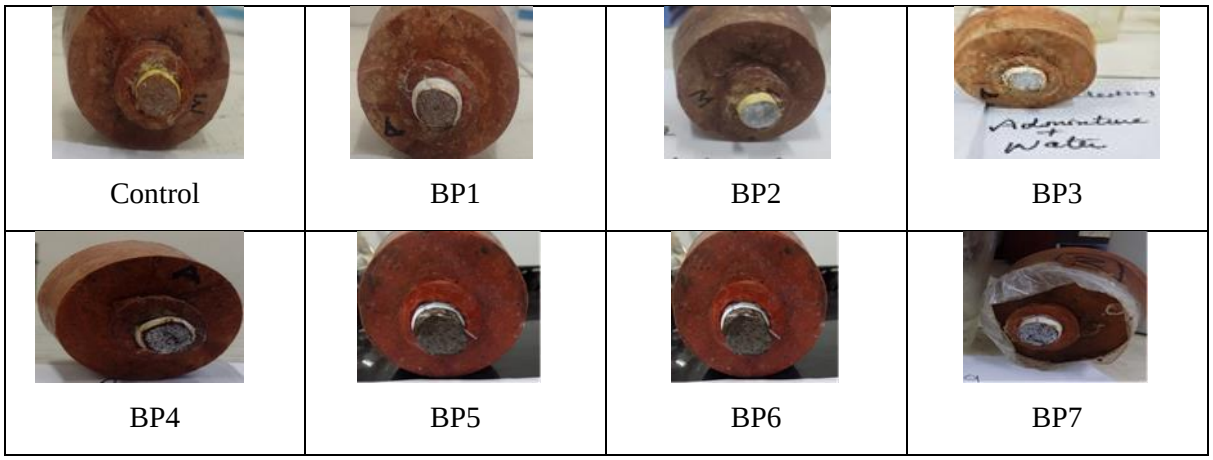


Fig1.Formation of Corrosion spots in control and sample with corrosion inhibitor

3.3 Efficiency of bipolar corrosion inhibitor in immersion test

The immersion test was conducted to evaluate the corrosion resistance of metal specimens treated with the bipolar corrosion inhibitors by measuring their corrosion rates during exposure to the test environment. The control specimen had a reported corrosion rate of 3.251 mils/year, while the inhibitor-treated specimens showed lower rates. BP5 exhibited the best performance, with a corrosion rate of 1.257 mils/year and an inhibition efficiency of 61.33%. BP1 followed with an efficiency of 50.88%, while BP4 achieved 48.45%. BP3, BP2, BP6, and BP7 showed efficiencies of 42.19%, 37.95%, 28.24%, and 26.04%, respectively. The lower corrosion rates indicate that the inhibitors reduced corrosion compared with the untreated control. One possible explanation is that inhibitor constituents adsorb onto the metal surface or otherwise reduce the metal's exposure to corrosive species.

3.4 Efficiency of bipolar corrosion inhibitor in Tafel Polarization test

The Tafel polarization test was used to evaluate the electrochemical corrosion behaviour of the specimens and estimate their corrosion rates. The reported corrosion rate of the control specimen was 0.3775 mm/year. All seven inhibitors produced lower reported corrosion rates, indicating reduced electrochemical corrosion relative to the control. BP1 demonstrated the highest inhibition efficiency at 79.73%, with a corrosion rate of 0.0765 mm/year. BP2 achieved 64.32%, followed by BP4 at 49.38%, BP5 at 34.57%, BP6 at 33.90%, BP7 at 32.51%, and BP3 at 26.42%. The high efficiency of BP1 suggests that it was particularly effective at reducing the measured electrochemical corrosion current under the test conditions. A possible reason is the formation of a protective surface layer or the inhibition of electrochemical reactions responsible for metal dissolution. However, the Tafel results do not independently confirm which mechanism was responsible. The contrast between BP1's strong Tafel performance and BP5's strong immersion performance also demonstrates that inhibitor rankings can change with the test method.

Table -5. Corrosion rate and corrosion inhibiting efficiency

Test	Immersion Test		Tafel Polarization test	
Sample ID	Corrosion rate with bipolar corrosion inhibitor (in mils/yr)	Corrosion Inhibiting Efficiency, %	Corrosion rate with bipolar corrosion inhibitor (in mm/yr)	Corrosion Inhibiting Efficiency, %
BP1	1.597	50.88	0.0765	79.73
BP2	2.017	37.95	0.1347	64.32
BP3	1.879	42.19	0.2778	26.42
BP4	1.676	48.45	0.1911	49.38
BP5	1.257	61.33	0.2470	34.57
BP6	2.333	28.24	0.2495	33.90
BP7	2.404	26.04	0.2548	32.51

3.5 Efficiency of bipolar corrosion inhibitor in Rapid Chloride Penetration Test

The Rapid Chloride Permeability Test (RCPT) was used to assess the electrical charge passed through concrete specimens, reported in coulombs, as an indicator of their resistance to ionic transport. In general, a lower charge indicates lower electrical conductivity and is often associated with reduced

chloride-ion transport, although the result is also affected by pore-solution chemistry, moisture condition, and other concrete properties. In the reported M40 concrete results, BP1 reduced the charge from 2015 coulombs for the control to 897.33 coulombs, corresponding to a reported efficiency of 55.46%, the highest among the listed M40 inhibitor results. BP5 achieved 30.35%, while BP7, BP6, BP4, and BP3 achieved 23.88%, 23.07%, 22.64%, and 15.82%, respectively. In the M30A2 specimens, BP7 showed the highest reported efficiency at 50.20%, reducing the charge from 3806 to 1895.33 coulombs. BP4 achieved 46.01%, BP5 achieved 34.08%, and BP6 achieved 16.91%. BP3 results were also reported for M30A1 and M50 concrete, with efficiencies of 8.44% and 21.61%, respectively. These findings suggest that the effect of an inhibitor on RCPT results depends on both the product and the concrete mix.

Table -6. Durability test value and corrosion inhibiting efficiency

Test	RCPT			Salt Ponding Test		Corrosion Current	
Sample ID	Grade of the Concrete	RCPT values in terms of coulombs	Corrosion-inhibiting efficiency, %	With bipolar corrosion inhibitor, % acid soluble chloride at 10 mm interval	Corrosion-inhibiting efficiency	With bipolar corrosion inhibitor, total charge (C) i.e. corrosion current at the end of 9 cycles	Corrosion-inhibiting efficiency at the end of 9 cycles, %
BP3	M30A1	476.91	8.44	0.257	29.97	0.254	56.63
BP4	M30A2	2055.00	46.01	-	-	0.3108	42.68
BP5	M30A2	2509.00	34.08	-	-	0.2190	59.61
BP6	M30A2	3162.57	16.91	-	-	0.3131	42.27
BP7	M30A2	1895.33	50.20	-	-	0.4009	26.07
BP2	M35	393.00	17.00	0.197	20.24	0.1482	68.94
BP1	M40	897.33	55.46	0.0983	31.26	0.1904	63.64
BP3	M40	1696.00	15.82	-	-	0.3401	45.19
BP4	M40	1558.67	22.64	-	-	0.2822	35.06
BP5	M40	1403.33	30.35	-	-	0.3558	46.12
BP6	M40	1549.99	23.07	-	-	0.3054	32.06
BP7	M40	1533.67	23.88	-	-	0.1904	41.68
BP3	M50	886.33	21.61	0.079	37.80	0.2308	36.58

3.6 Efficiency of bipolar corrosion inhibitor in salt ponding test as per ASTHO

The salt ponding test evaluates chloride content in concrete following 90 days exposure to a chloride-containing environment. The table 6. shows the test results of acid-soluble chloride content at a depth of 10 mm for four bipolar corrosion inhibitor. Lower chloride content than the corresponding control suggests reduced chloride accumulation at that depth for M30A1 concrete treated with BP3, chloride content decreased from 0.367% to 0.257%, giving a reported efficiency of 29.97%. For M35 concrete

treated with BP2, the value decreased from 0.247% to 0.197%, corresponding to 20.24%. BP1 in M40 concrete reduced chloride content from 0.143% to 0.0983%, with a reported efficiency of 31.26%. The highest reported efficiency was obtained by BP3 in M50 concrete, where chloride content decreased from 0.127% to 0.079%, corresponding to 37.80%. These reductions indicate that the treated specimens contained less acid-soluble chloride at the measured depth than the corresponding controls. Possible explanations include differences in chloride transport, concrete pore structure, or interactions between the inhibitor formulation and the concrete system. Nevertheless, the results do not establish that the inhibitors physically blocked chloride transport, because the measured chloride content may also be influenced by the concrete composition and experimental conditions. Since different concrete grades were used, comparisons between products should be made cautiously.

3.7 Efficiency of bipolar corrosion inhibitor in corrosion current at the end of 9 cycles

The ASTM G109 test was used to evaluate the corrosion performance of reinforced concrete specimens exposed to chloride-containing conditions over repeated test cycles. The paper reports the charge measured after nine cycles and compares inhibitor-treated specimens with their respective controls. For M35 concrete, BP2 achieved the highest reported efficiency of 68.94%, reducing the charge from 0.4756 C to 0.1482 C. BP1 in M40 concrete achieved 63.64%, with the charge decreasing from 0.5237 C to 0.1904 C. In M30A2 concrete, BP5 performed best among the listed products, achieving 59.61% efficiency by reducing the charge from 0.5423 C to 0.2190 C. BP4 and BP6 in M30A2 concrete achieved 42.68% and 42.27%, respectively, while BP7 achieved 26.07%. In M40 concrete, the reported efficiencies for BP3, BP4, BP5, and BP6 were 45.19%, 35.06%, 46.12%, and 32.06%, respectively. BP3 in M50 concrete achieved 36.58%. These results generally indicate reduced measured charge in inhibitor-treated specimens, suggesting improved performance under the test conditions. The reduction may be associated with inhibition of reinforcement corrosion or changes in ionic transport and electrochemical behaviour.

4.0 Conclusion

The results demonstrate that the seven bipolar corrosion inhibitor admixtures provided varying levels of corrosion mitigation relative to the corresponding control specimens. In the immersion test as per ASTM G 3, the reported corrosion inhibition efficiencies ranged from 26.04% to 61.33%, with BP5 showing the highest efficiency. In the Tafel polarization test, corrosion inhibiting efficiencies ranged from 26.42% to 79.73%, with BP1 exhibiting the strongest reported performance. These findings indicate that the effectiveness of the admixtures under direct corrosion-testing conditions differed considerably, potentially because of differences in their formulations and interactions with the test environment. The RCPT results further showed that the reduction in electrical charge passed depended on both the inhibitor and the concrete mix. BP7 showed the highest reported efficiency among the listed M30A2 combinations, while BP1 performed best in the reported M40 group. The salt ponding results showed reduced acid-soluble chloride content at 10 mm for all four reported combinations, with BP3 in M50 recording the highest reported efficiency. In ASTM G109, the highest reported efficiencies included BP2 in M35, BP1 in M40 and BP5 in M30A2. Visual examination also indicated a reduction in the size and extent of corrosion spots on treated specimens. The differences between test results may be associated with variations in exposure conditions, concrete composition, ionic transport and the electrochemical mechanisms affected by each inhibitor. The findings instead demonstrate that bipolar corrosion inhibitor performance should be evaluated using complementary methods and under concrete

and exposure conditions representative of the intended application.

5.0 References

1. Ojha, P. N., Kaura, P., Mittal, P., & Arora, V. V. (2020). *Performance evaluation of corrosion inhibitors and their corrosion inhibiting efficiency for RCC structures*. *Indian Concrete Journal.*
2. Ojha, P. (2026). Research contributions of National Council for Cement and Building Materials in the research-driven evolution of Indian Standards. *Indian Concrete Journal.*
3. Zomorodian, A., & Behnood, A. (2023). Review of corrosion inhibitors in reinforced concrete: Conventional and green materials. *Buildings, 13*(5), Article 1170.
4. Shrivastava, R., Maurya, R., & Katiyar, P. K. (2025). A review on bipolar electrochemistry for corrosion testing: Highlighting mechanisms, applications, and future prospects. *Journal of Solid State Electrochemistry, 29*(2), 471–511.
5. Bureau of Indian Standards. (2015). *IS 269:2015: Ordinary Portland cement—Specification* (Reaffirmed 2020). Bureau of Indian Standards.
6. Bureau of Indian Standards. (2018). *IS 16714:2018: Ground granulated blast furnace slag for use in cement, cement mortar and concrete—Specifications.* Bureau of Indian Standards.
7. Bureau of Indian Standards. (1967). *IS 1727:1967: Methods of test for pozzolanic materials* (Reaffirmed 2018). Bureau of Indian Standards.
8. Bureau of Indian Standards. (2013). *IS 3812 (Part 1):2013: Pulverized fuel ash—Specification—Part 1: For use as pozzolana in cement, cement mortar and concrete* (Reaffirmed 2022). Bureau of Indian Standards.
9. Bureau of Indian Standards. (2000). *IS 456:2000: Plain and reinforced concrete—Code of practice* (Reaffirmed 2021). Bureau of Indian Standards.
10. Bureau of Indian Standards. (2016). *IS 383:2016: Coarse and fine aggregates for concrete—Specifications.* Bureau of Indian Standards.
11. Bureau of Indian Standards. (1999). *IS 9103:1999: Concrete admixtures—Specifications* (Reaffirmed 2018). Bureau of Indian Standards.
12. Research Designs and Standards Organisation. (n.d.). *Specification No. 6-68-0017, Revision 2: Bipolar concrete penetrating corrosion inhibitor admixture.*
13. ASTM International. (2025). ASTM C1202-25: Standard test method for electrical indication of concrete's ability to resist chloride ion penetration. https://doi.org/10.1520/C1202-25
14. American Association of State Highway and Transportation Officials. (2025). AASHTO T 259-02 (2025): Resistance of concrete to chloride ion penetration.
15. ASTM International. (2023). ASTM G109-23: Standard test methods for determining effects of chemical admixtures on corrosion of embedded steel reinforcement in concrete exposed to chloride environments. https://doi.org/10.1520/G0109-23



Technical Session -IVC

EFFICIENT & GREENER RAW MATERIAL GRINDING PLANTS WITH ROLLER PRESS IN FINISH MODE: CASE STUDIES FROM TELANGANA, INDIA

Venkatesh Vanam, Atul Johri*, Alexander Knoch**, Kai Weider***

**Humboldt Wedag India Pvt. Ltd., India*

***Humboldt Wedag GmbH, Germany*

ABSTRACT

Energy saving is one of the major multinational targets of the 21st century. In a cement plant, grinding departments take more than two thirds of the electrical energy to produce one ton of cement. Therefore, it is an ecological and economical important process. By consuming the lowest specific energy per ton of any kind of target product, the combination of Roller Press and modern separator technology, known as KHD Comflex® Grinding System, has proven to be the most favorable grinding solution in the market.

KHD Humboldt Wedag can rely on the experience of more than 450 successful Roller Press grinding projects for all the applications be it raw material grinding, clinker grinding and slag grinding. New carbon footprint reduction policies are forcing cement manufacturers to opt for greener technologies for new plants. The first raw material grinding circuit in finish mode was installed in 1990s and since then this configuration has become the state-of-the-art technology. All the finish mode circuits are the most energy efficient grinding systems in operation. Finish grinding of raw materials, clinker and slag with Roller Press has been a well proven technology for many years. In view of the above, this paper presents an overview of the technology being offered for new raw material grinding plants with RP in finish mode and two successful case studies.

1.0 Introduction

A revolutionary idea of a different grinding technology was born in year 1977. Prof Klaus Schoenert invented and patented this grinding technology. In 1980s KHD Humboldt Wedag picked up this idea and pioneered this application with the first industrial Roller Press (High pressure grinding rolls) for the pre-grinding of slag. With the invention of V separator a few years later, KHD Humboldt Wedag cleared the way for worldwide expansion of Roller Press technology as a grinding unit. During the last decades the Roller Press became one of the major equipment in the cement world. Currently RP technology in finish mode provides energy savings of more than 50% when compared with traditional grinding systems such as ball mills and up to 20% when compared with vertical roller mills.

In the last two decades, it is clear that cement industry accepted and adopted Roller Press technology in finish mode in place of ball mill and VRM technologies for raw material grinding application due to lower power demand, high availability and lower maintenance. As there is a global pressure on cement industry to reduce the carbon emmisions and go greener, it is the right time to switch from other technologies to RP technology.

2.0 KHD Roller Press circuits: Proprietary equipment being offered

The most efficient grinding circuit today consists of a roller press, a static separator (V Separator) and

a dynamic separator (SK Separator) downstream for the final cut. It can be arranged as a single grinding stage, producing raw meal, slag meal or cement. The circuit can also handle all possible qualities and quantities of additives and substitute materials which might be difficult to grind. A variety of moisture contents, hard or soft feed, and even highly abrasive materials are best suited to be processed in a roller press grinding circuit from KHD.

The development of Comflex® ('com'minution with 'flex'ibility) led to a broad range of applications of roller press technology. Comflex® (Fig-1) enables KHD to design and use an identical grinding circuit for raw material, cement and slag grinding. At the same time Comflex® can handle any kind of moist material feed (with a moisture of up to 20 %) in the same grinding circuit layout and still offers the flexibility to be operated in finish and semi-finish grinding mode.

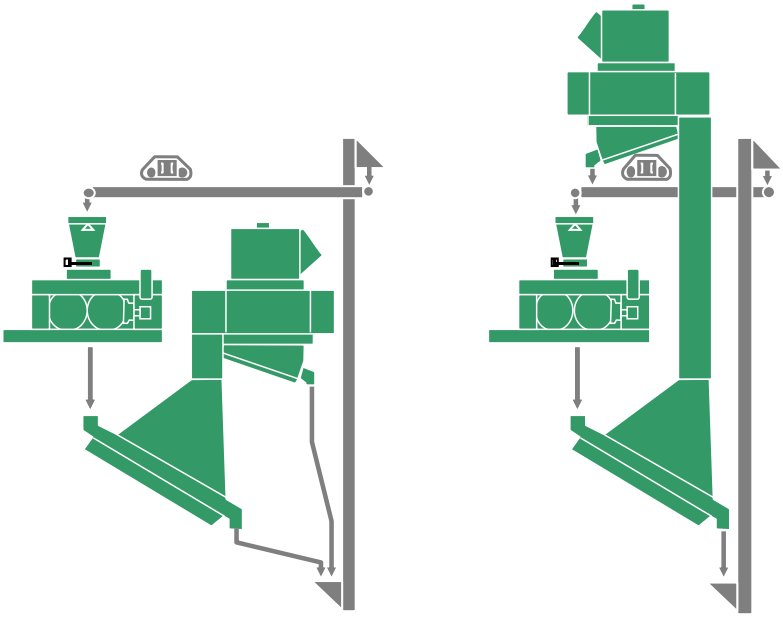


Fig-1: KHD Comflex® arrangement options

2.1 Roller Press

KHD Roller Presses (Fig-2) are available in seven sizes, ranging from 7 to 27 Mega-Newton grinding force. The roller diameter is standardized from 1.7 m to 2.5 m to handle material feed in sizes of up to 100 mm. The roller width is related to the grinding force and ranges from 0.9 m to 1.8 m.

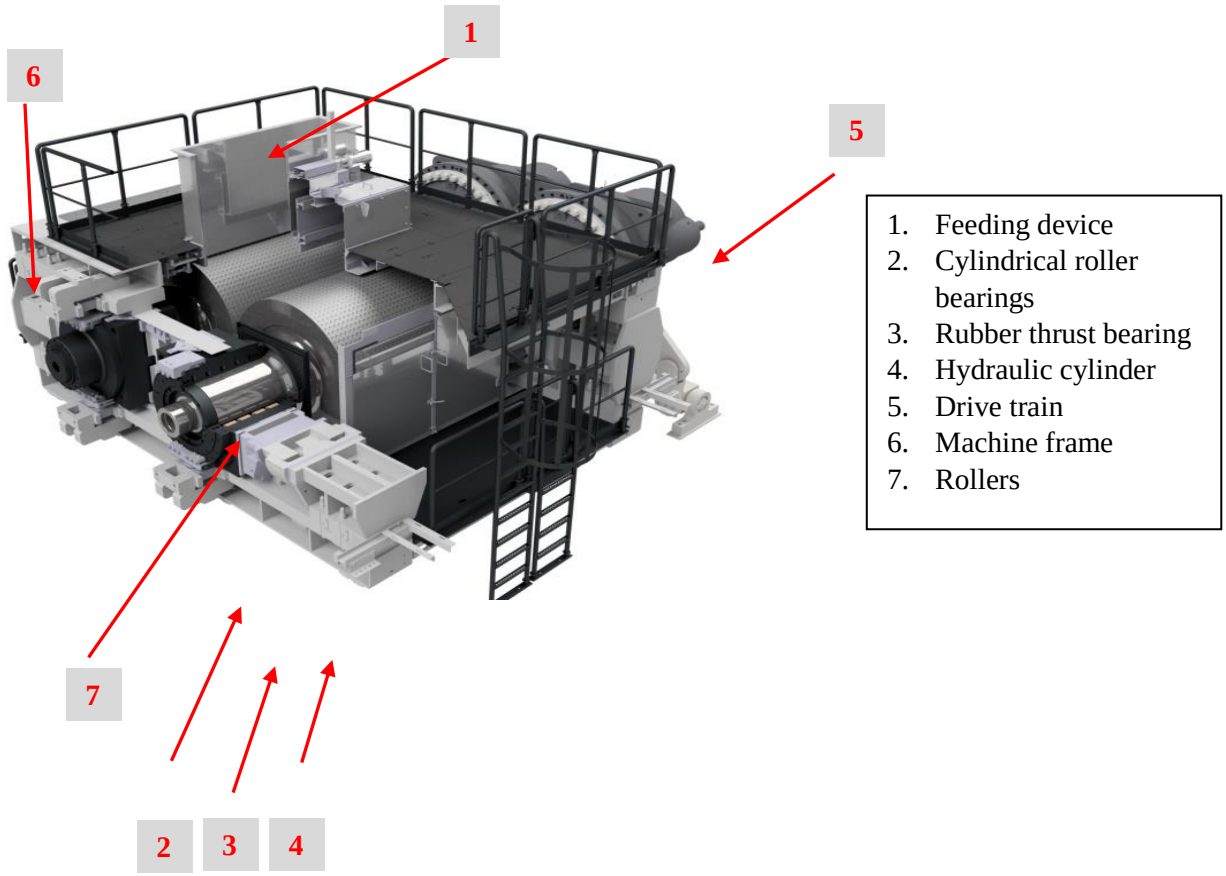


Fig-2: KHD Roller Press

KHD continuously improved its roller presses with the following mechanical features to enhance their reliability and performance:

- use of multi-row cylindrical roller bearings
- exterior roller guide to allow skewing without material stress
- roller surface design with welded or ground profiles, or advanced stud lining
- optimized hydraulic system
- simple but effective feeding device
- special frame structure
- intelligent machine design that ensures easy access and exchange of the rolls

Roller surfaces require continuous attention to ensure best grinding performance, wear life and nipping properties. As a result, the roller surface has received a variety of improvements and developments over the years. Today, KHD offers the following surface options:

- Complete hard facing
  "CHF" (Complete Hard Facing) has proven successful over decades and is widely used. This surface type offers the balance between low investment and wear life. Although the surface requires maintenance intervals for rewelding, this can be executed quickly during regular stoppages. CHF (Fig-3) combines a base material, different buffer layers and the multi-layered hard facing.

- Stud lining
  Stud lining (Fig-4) offers best-in-class wear protection and outstanding performance. Firstly, the used tungsten carbide studs are extremely wear-resistant thanks to a hardness of 65 to 67 Rockwell. Secondly, due to the stud arrangement, an additional wear protection layer is formed from ground material that remains between the studs during regular grinding. And thirdly, studs also offer superior nipping properties as well as the use of thicker slabs. This allows for an increased throughput rate.

- High-chrome
  KHD's newest surface option is a special compound casting bandage (HCB) with a wear-resistant top layer made of high-chrome (Fig-5). This surface combines robustness with ease of use because it does not need to be rewelded. In comparison to competitor solutions, KHD's profile application method is also advanced. Because we grind the profile into the surface instead of welding extra material on it, we prevent tiny surface cracks, that can lead to major follow-up problems during regular operation.



Fig-3: CHF surface



Fig-4: Stud lined surface



Fig-5: High Chrome surface

2.2 Static and dynamic separators

KHD V Separator (Fig-6 left) is multifunctional static equipment for de-agglomeration, separation and drying / cooling used in combination with Roller Press. Static LS Separator (Fig-6 right) is recommended for final separation in raw material grinding plants where the product is coarser compared to cement grinding.

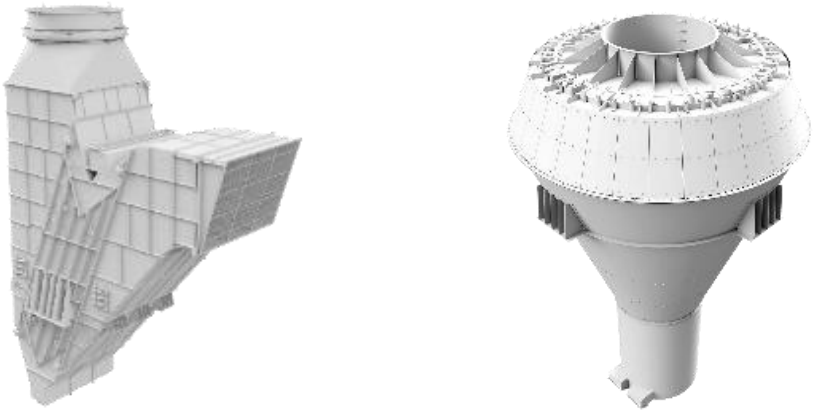


Fig-6: KHD Static separators, V Separator (left) and LS separator (right)

KHD dynamic separators (Fig-7) are designed with side entry of gases in SKS-Z/V and bottom entry of gases in SKS-LC. Later one is mainly used for raw material grinding plants.

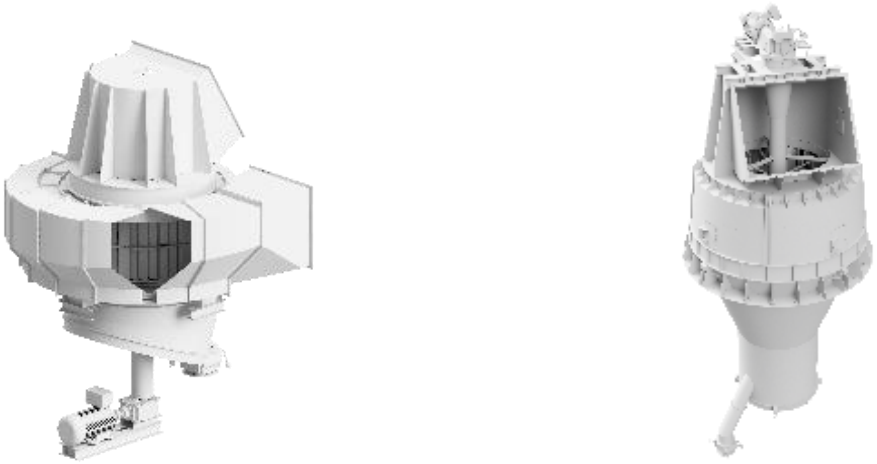


Fig-7: KHD dynamic separators, SKS-Z/V (left) and SKS-LC (right)

3.0. KHD Roller Press circuits in finish mode: Best solution for raw material grinding plants

In the beginning the RP was used only in pre-grinding mode or semi finish mode. The first raw material grinding circuit in finish mode was installed in 1990s and since then this configuration has become the state-of-the-art technology. All the finish mode circuits are the most energy efficient grinding systems in operation. Finish grinding of raw materials, clinker and slag with Roller Press has been a well proven technology for many years.

The operating costs of any grinding plant technical wise are mainly resulting from electrical consumption, heat demand and maintenance efforts. In all these three categories, modern KHD roller press circuits are superior to any VRM or ball mill solution:

- KHD roller press circuits are operated at lower spec. electric energy consumption than vertical mills and ball mills.
- Heat demand often is lower than in vertical roller mills as water spray typically is not used in KHD roller press. This also results in higher potential in creating electrical power in a WHRS.
- With HCB / STUD lining the lifetime of the roller surface of KHD roller presses is much higher than any solution of vertical roller mills. This results in lower maintenance costs than known from VRM.
- In case of raw material grinding, better product quality resulting in easy burnability of the kiln feed.

In total this leads to lowest OPEX costs for roller press finish grinding. The typical process flow sheet of finish mode raw material grinding plant is shown as per Fig-8.

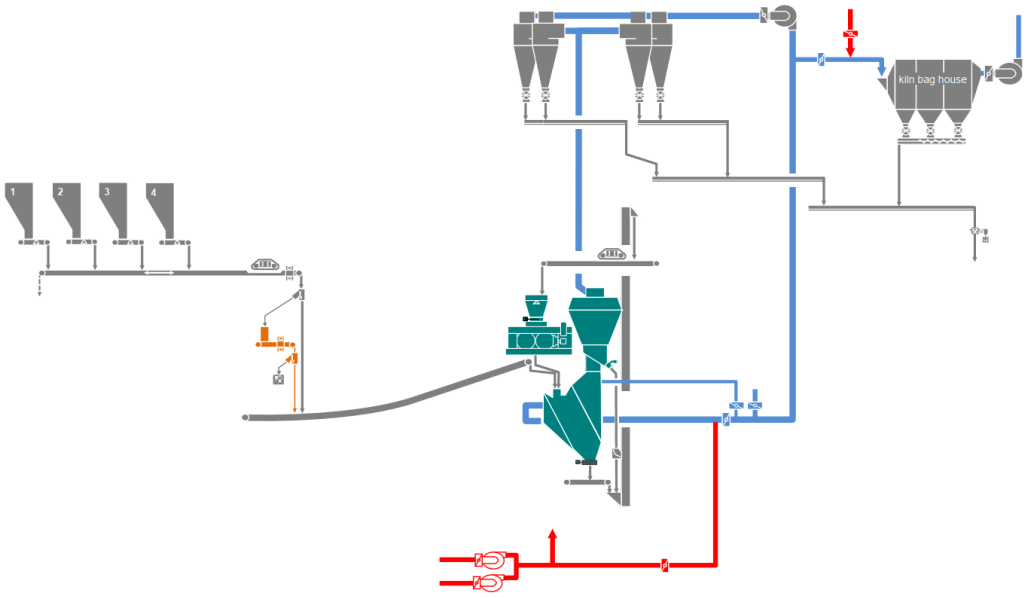


Fig-8: Process flow sheet of finish mode raw material grinding plant

4.0 New raw material grinding plants with RP in finish mode: Case studies

Since its inception in Dec 2000, KHD Humboldt Wedag India (HWI) secured and executed 36 Roller Press finish mode contracts in India for raw material grinding application. Size of the executed Roller Press ranges from 1.7 m dia to 2.2 m dia and with grinding force from 7 MN to 20 MN. Among these references, it is noteworthy to highlight two case studies which become benchmark plants for Indian Cement Industry in terms of lowest sp. power consumption. These two best operating plants are located in Telangan state, India.

4.1 New RM-4 at My Home Industries, Mellacheruvu Cement Works

M/s My Home Industries is a leading cement manufacturer in South India. My home Industries presently operates 4 kiln lines at Mellacheruvu, Telangana. When the group decided to expand the plant capacity with addition of fourth clinkerisation plant in year 2021, it was decided to install an 8400 tpd clinkerisation line with a potential upto 9200 tpd. By that time, group was operating three kilns of 2000 tpd (line-I), 3100 tpd (Line-II) and 3500 tpd (Line-III) with Vertical Roller Mill (VRM) technology for raw material grinding application. My Home group selected KHD Humboldt Wedag for supply of the complete plant including raw mill, pyro line and cement mill. Group entrusted KHD Roller Press finish mode technology for Line-IV raw material and clinker grinding plants because of the sp. power advantage compared to VRMs. Design of single Roller Press circuit for a requiremet of 700 tph raw meal @ 15% R90 was itself a challenge as there was no ready reference of single roller press for such high capacity. With the confidence shown by customer, biggest RP was selected with an increased roller speed for 700 tph raw meal.

Ciruit is designed for a raw mix grindability of 5.5 kWh/t @ 15% R90 at VRM shaft and 3% max. feed moisture. The design data of major machinery (Table-1) installed for this job is as under:

Table-1: My Home, Mellacheruvu RM-4: Design data of RP circuit in finish mode

Equipment	Specifications
Roller Press	**RP20-220/180** roller surface: Complete Hard facing (CHF) roller diameter: 2200 mm roller width: 1800 mm roller speed: 2.3 m/s max. (20.0 rpm max.) connected motors: 2x 2400 kW
Static separator	**VS 112/26** height (feed point to discharge): 11200 mm width: 2600 mm
Dynamic separator	**SKS-LC 4750** rotor diameter: 4750 mm rotor height: 3040 mm connected motor: 140 kW
Separator fan	volume: 10,25,000 m^3/hr, 70 mbar
RP recirculation elevator	conveying capacity: 2500 tph

The process flow sheet of the complete circuit is shown as per the below Fig-9.

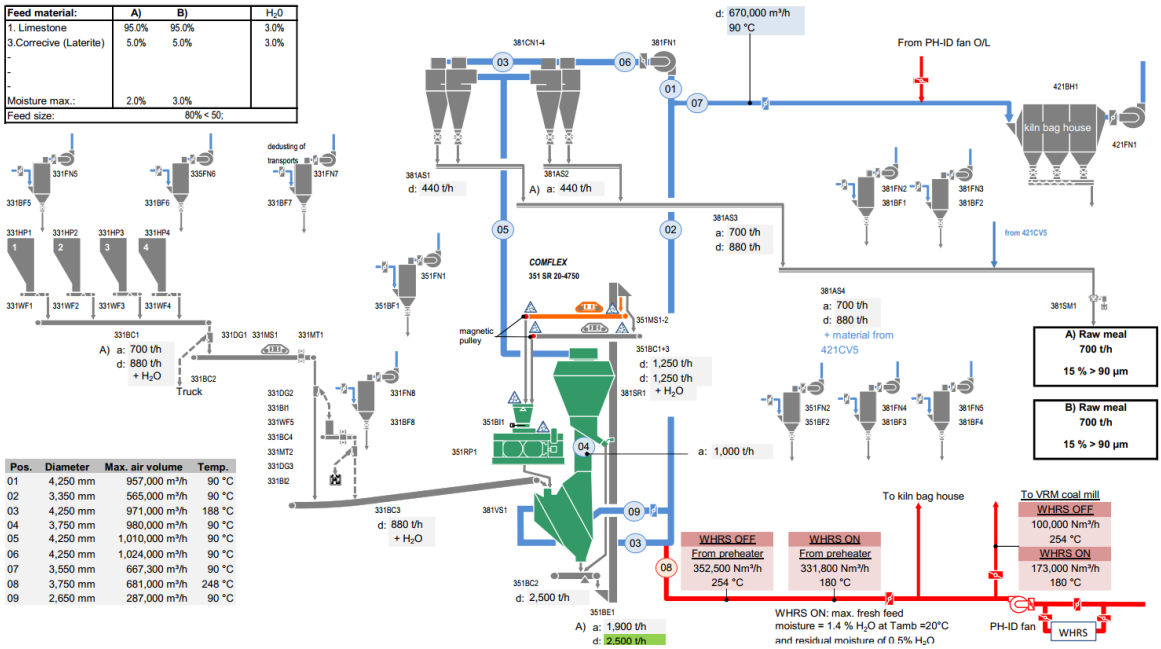


Fig-9: My Home, Mellacheruvu RM-4: Process flow sheet

The execution of the contract went well within the agreed timelines and the plant was commissioned under the supervison of KHD engineers in December 2023. And the plant operated meeting all the performance parameters with in a short period. Performance guarantee test was conducted in October 2024 and the results are tabulated as per below Table-2.

Table-2: My Home, Mellacheruvu RM-4: Performance figures as per PG test

S. No.	Parameter	As per contract	Achieved during PG test
1	Feed mix	95% limestone 5% laterite	95% limestone 5% laterite
3	Production	700 tph	734 tph
4	Product fineness	15% R90	14.65% R90
5	Sp. power consumption at meters (for main equipment i.e., Roller Press, Dynamic separator, Separator fan and RP recirculation elevator)	9.0 kWh/t	9.02 kWh/t

Based on the above achieved results the performance guarantee figures as per the contract are met in all respects of production, product fineness ad sp. power consumption.

Major highlights / takeaways from this contract:

- Success of single and biggest Roller Press (RP20-220/180) with 2.2 m dia roller and speed upto 2.3 m/s for achieving huge production i.e., 700 tph raw meal.
- Achieving lowest sp. power consumption of the complete circuit (from weigh feeders discharge to blending silo feeding elevator) i.e., below 10.0 kWh/t at meters. The adjacent raw mills (VRM) of Line-I, II and III are consuming about 3.0 kWh/t material more than raw mill (RP) of Line-IV.
- Highest availability of the machine and lowest wear of the roller surface as there was no welding of the roller surface till 14000 running hours.
- Sp. power consumption upto clinkerisation is recored below 40.0 kWh/t clinker. This was possible only due to the efficient raw material grinding and pyroprocessing plants supplied by KHD Humboldt Wedag.
- Establishment of more WHRS potential as there is no need of water spray in the RP circuit for raw material grinding application.

4.2 New RM-3 at Deccan Cements Ltd., Bhavanipuram Cement Works

M/s Deccan Cements Limited is also a leading cement manufacturer in South India. Deccan Cements presently operates 3 kiln lines at Bhavanipuram, Janpahad, Telangana. When the group decided to expand the plant capacity with addition of third clinkerisation plant in year 2021, it was decided to install an 3500 tpd clinkerisation line with a potential upto 4000 tpd. By that time, group was operating two kilns of 1500 tpd (line-I) and 3500 tpd (Line-II) with ball mills and Vertical Roller Mill (VRM) technology for raw material grinding application. Deccan group selected KHD Humboldt Wedag for supply of the complete clinkerisation unit including raw mill and pyro line. Group entrusted KHD Roller Press finish mode technology for Line-III raw material grinding plant because of the sp. power advantage compared to VRM.

Ciruit is designed for a raw mix grindability of 6.7 kWh/t @ 15% R90 at VRM shaft and 3% max. feed moisture. The design data of major machinery (Table-3) installed for this job is as under:

Table-3: Deccan Cements, Bhavanipuram RM-3: Design data of RP circuit in finish mode

Equipment	Specifications
Roller Press	**RP13-170/140** roller surface: Complete Hard facing (CHF) roller diameter: 1700 mm roller width: 1400 mm roller speed: 2.0 m/s (22.5 rpm) connected motors: 2x 1200 kW
Static separator	**VS 80/20** height (feed point to discharge): 8000 mm width: 2000 mm
Dynamic separator	**SKS-LC 3500** rotor diameter: 3500 mm rotor height: 2100 mm connected motor: 80 kW
Separator fan	volume: 5,32,500 m^3/hr, 70 mbar
RP recirculation elevator	conveying capacity: 1300 tph

The process flow sheet of the complete circuit is shown as per the below Fig-10.

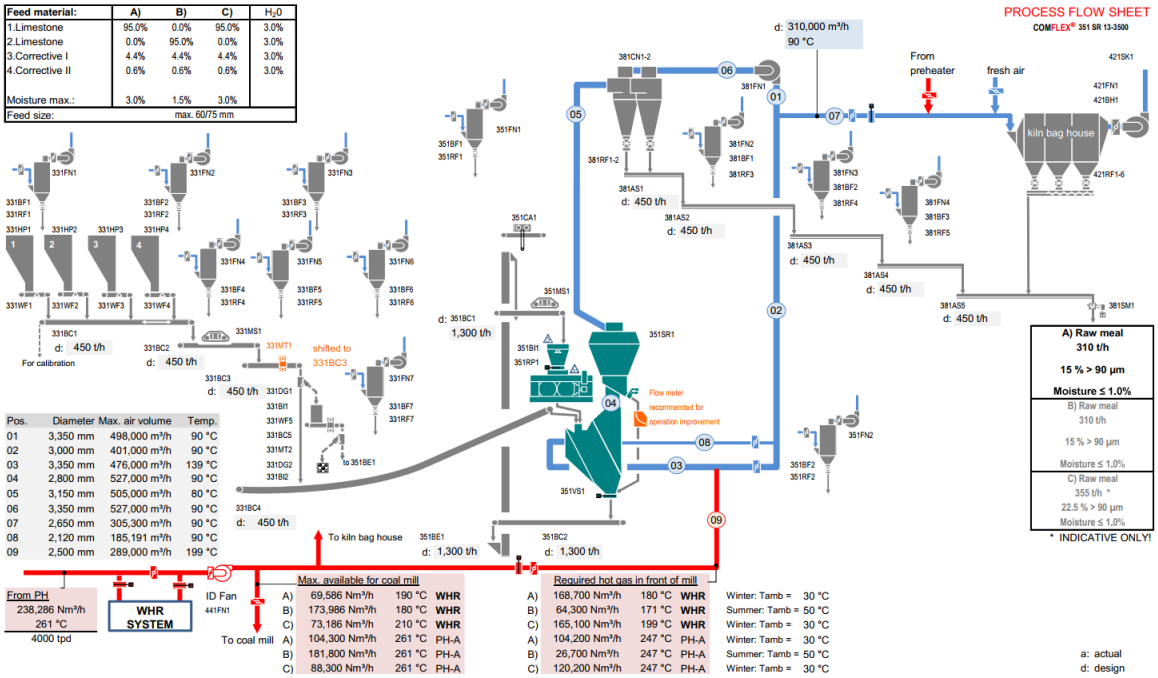


Fig-10: Deccan Cements, Bhavanipuram RM-3: Process flow sheet

The execution of the contract went well within the agreed timelines and the plant was commissioned under the supervison of KHD engineers in August 2024. And the plant operated meeting all the performance parameters with in a short period. Performance guarantee test was conducted in February 2026 and the results are tabulated as per below Table-4.

Table-4: Deccan Cements, Bhavanipuram RM-3: Performance figures as per PG test

S. No.	Parameter	As per contract	Achieved during PG test
1	Feed mix	95% limestone 4.4% iron ore 0.6% laterite	95% limestone 4.4% iron ore 0.6% laterite
3	Production	310 tph	339.6 tph
4	Product fineness	15% R90	10.65% R90
5	Sp. power consumption at meters (for main equipment i.e., Roller Press, Dynamic separator, Separator fan and RP recirculation elevator)	11.0 kwh/t	7.9 kwh/t

Based on the above achieved results the performance guarantee figures as per the contract are met in all respects of production, product fineness ad sp. power consumption.

Major highlights / takeaways from this contract:

- Achieving lowest sp. power consumption of the complete circuit (from weigh feeders discharge to blending silo feeding elevator) i.e., below 9.0 kWh/t at meters. The adjacent raw mill (VRM) of Line-II is consuming about 3.0 kWh/t material more than raw mill (RP) of Line-III.
- Highest availability of the machine and lowest wear of the roller surface as there was no welding of the roller surface till 6000 running hours.
- Sp. power consumption upto clinkerisation is recored below 38.0 kWh/t clinker. This was possible only due to the efficient raw material grinding and pyroprocessing plants supplied by KHD Humboldt Wedag.
- Establishment of more WHRS potential as there is no need of water spray in the RP circuit for raw material grinding application.

5.0 The New Roller Press from KHD Humboldt Wedag: "RPE"

KHD Humboldt Wedag always follows the principle of continuous development and change with the time. At the end of year 2025, big announcement was made with the launch of new Roller Press "RPE" (Fig-11), where E stands for Enhanced, Economical and Efficient. Our new RPE is built with the following new features:

1. Evolved frame

   Replaced almost 200 pre-stressed expansion bolts with just eight bolts assembled (radial spherical plain bearings). The bolts also takeover the function of rubber thrust bearings which became obsolete. The bolts allow the bearing houses to tilt and to move uniformly together with the moveable roller.

2. Efficient feeding device

New material feeding device consists of a standardized RP deflector and brand-new skewing dosing gate minimizing the roll skewing and helps to run rollers at optimal grinding pressure over the entire roller width.

3. Extreme resistance Hi-Chrome surface

   Expected overall surface wear lifetime of up to 50000 operating hours (depends on the material being ground) with no welding work, no risk of resulting damage to the bandages due to heat input.

4. Enhanced ROLCOX 3.0

   With modern HMI (with local and remote access) and advanced PLC hardware upgrade (Siemens S1500).

5. Easy maintenance

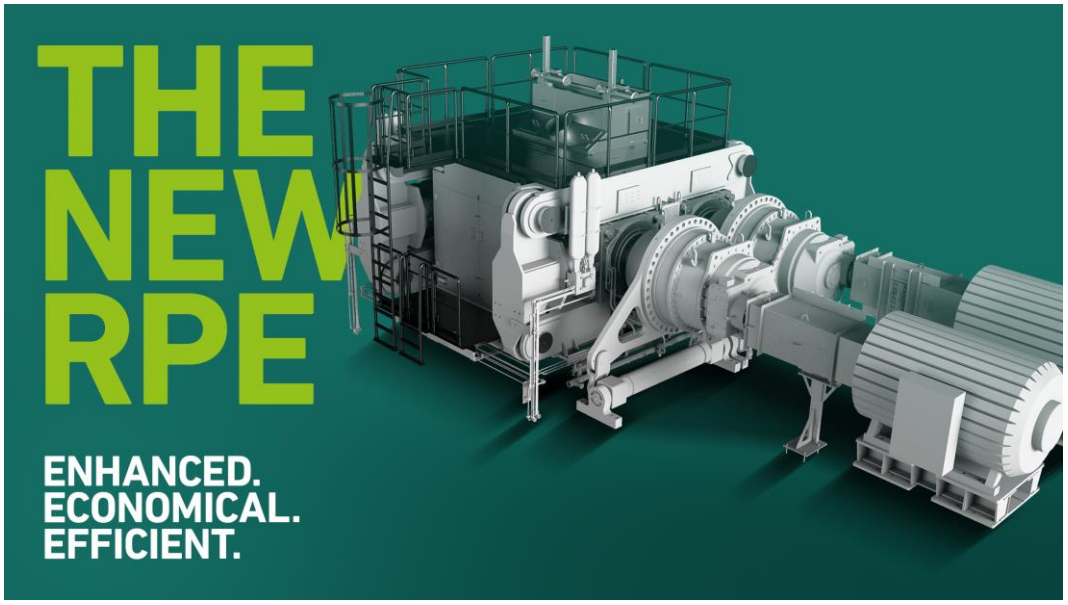


Fig-11: The new Roller Press "RPE"

6.0 Conclusion

KHD Humboldt Wedag has an unprecedented history of grinding expertise in the cement industry. This knowledge and its technology were successfully installed in hundreds of cement plants all over the world. KHD follows a meticulous approach when it comes to process and project definitions, layout and design, engineering and execution.

Any kind of materials, with the sole exception of coal, can be ground in KHD roller presses with minimal wear and maintenance efforts. Incorporated in a Comflex® system, KHD roller presses represent the benchmark of modern grinding application and are always designed to meet the individual needs of its clients.

The latest developments of KHD high-pressure comminution and classification technology offer a vast opportunity to reduce energy consumption in grinding plants and by that also helps our customers to

reduce costs, increase productivity, and to contribute to a more sustainable and CO2 neutral future.

References

1. York Reichardt, Ashok Kumar Dembla and Venkatesh Vanam (2019). "KHD Roller Press circuits: latest developments and stepping into large capacity plants". *16th NCB International conference & exhibition on Cement, Concrete and building materials.*

2. Venkatesh Vanam, Prakash Patil and Ashok Kumar Dembla (2024). "Roller Press technology: A KHD's boon for existing plants to transform into efficient and greener". *18th NCB International conference & exhibition on Cement, Concrete and building materials, Vol. 2, pp. 432-442.*

Data-Driven Clinker Cooler Services: Integrating A Comprehensive Framework for Service Support, Condition Monitoring, and Inventory Optimization Through the Customer Care Service Program (CCSP)

Soundararaj N*, Amit Varu, Praveena K

IKN Engineering India Pvt. Ltd., Chennai, India

ABSTRACT

Clinker coolers operate under severe thermal, mechanical, and abrasive conditions, making effective maintenance essential for ensuring reliable operation, high availability, and sustained performance. Conventional maintenance practices based on periodic inspections and corrective actions often provide limited visibility into developing equipment issues, leading to unexpected failures, increased maintenance costs, and production losses.

To address these challenges, IKN developed the Customer Care Service Program (CCSP), a comprehensive framework that integrates periodic service visits, technical audits, condition assessments, spare parts optimization, remote diagnostics, and digital monitoring technologies. By combining field expertise with data-driven analysis, CCSP enables proactive identification of equipment deterioration, operational issues, and maintenance requirements.

A key component of CCSP is the Cooler Condition Monitoring (CCM) platform, which provides continuous monitoring of critical process and equipment parameters through IIoT-based technologies. The platform supports real-time visualization, automated alerts, trend analysis, and remote technical support, enabling informed maintenance and operational decisions.

This paper presents the structure and implementation of CCSP and demonstrates its effectiveness through industrial case studies involving grate plate temperature management, hydraulic grate drive diagnostics, and root cause analysis of a hydraulic grate drive trip. The studies highlight how the integration of service expertise, condition monitoring, and data analytics facilitated early fault detection, root cause identification, and targeted corrective actions.

The results show that CCSP improves clinker cooler reliability, maintenance effectiveness, spare parts optimization, and operational resilience. The combination of periodic service support and digital monitoring provides a practical approach for enhancing clinker cooler performance and supporting sustainable cement plant operation.

Keywords: Cooler Condition Monitoring (CCM), Industrial Internet of Things (IIoT), cloud computing, Artificial Intelligence-Assisted Diagnostics, Asset Integrity Management, Data-Driven Decision Support.

2.0 Introduction

The cement industry continuously seeks to improve equipment reliability, operational efficiency, and maintenance effectiveness to maximize plant performance and minimize unplanned downtime. Traditional maintenance practices based on periodic inspections and corrective actions often provide limited visibility into developing equipment issues, leading to increased maintenance costs and production losses.

Recent advancements in Industrial Internet of Things (IIoT), cloud computing, and digital monitoring technologies have enabled more proactive and data-driven maintenance strategies. These technologies facilitate continuous equipment monitoring, condition assessment, and early identification of operational issues, supporting improved reliability and maintenance planning.

To address the need for systematic clinker cooler maintenance and performance optimization, IKN developed the Customer Care Service Program (CCSP). The program integrates periodic service visits, technical audits, condition assessments, spare parts and inventory optimization, remote diagnostics, and digital monitoring technologies to provide continuous lifecycle support for clinker cooler systems.

2.0. Customer Care Service Program (CCSP)

The Customer Care Service Program (CCSP) is a structured service framework developed by IKN to support the reliable and efficient operation of clinker cooler systems throughout their lifecycle. The program combines periodic service visits, technical audits, condition assessments, maintenance support, spare parts optimization, remote diagnostics, and digital monitoring to continuously evaluate cooler performance and equipment condition.

By integrating field service expertise with operational data analysis, CCSP enables early identification of process deviations and maintenance requirements. The program provides actionable recommendations for performance improvement, maintenance planning, and inventory management, helping plants improve equipment availability, reduce unplanned downtime, and optimize maintenance costs.

Key Elements of CCSP

- Cooler Condition Monitoring (CCM)
- Periodic Service Visits and Technical Audits
- Equipment Condition Assessment
- Maintenance Planning and Reliability Improvement
- Spare Parts and Inventory Optimization
- Remote Technical Support
- Performance Evaluation and Continuous Improvement

3.0. Cooler Condition Monitoring (CCM)

The rapid advancement of the Industrial Internet of Things (IIoT), cloud computing, and Artificial Intelligence (AI) has enabled the development of intelligent condition monitoring systems capable of continuously assessing equipment health and process performance. These technologies facilitate the collection, transmission, and analysis of large volumes of operational data, transforming conventional maintenance strategies into predictive and data-driven maintenance frameworks.

Beyond fault detection, CCM contributes to Asset Integrity Management by enabling continuous assessment of component health and operating conditions throughout the equipment lifecycle. The system also enhances Operational Resilience by supporting timely maintenance interventions, reducing unplanned downtime, and improving process stability. Through Data-Driven Decision Support, maintenance and operations teams can prioritize corrective actions based on actual equipment condition

rather than fixed maintenance intervals.

3.1. System Components & Architecture

The Cooler Condition Monitoring (CCM) system comprises several integrated hardware and software components that work together to acquire, store, analyze, visualize, and communicate operational data from the clinker cooler. These components collectively enable continuous equipment condition assessment and support proactive maintenance activities.

Programmable Logic Controller (PLC)

The PLC serves as the primary source of process and equipment data within the CCM architecture. Operational parameters such as temperatures, pressures, hydraulic system variables, equipment positions, motor currents, fan operating conditions, and other critical process measurements are continuously collected from the plant control system. The PLC provides reliable and real-time data required for condition monitoring and performance assessment.

Industrial PC

The Industrial PC functions as the local data acquisition and processing gateway. It establishes communication with the PLC, collects operational data, performs preliminary data validation, and manages data transfer to downstream applications. The Industrial PC also hosts the CCM software environment and acts as the interface between the plant network and remote monitoring infrastructure.

Time-Series Database

A time-series database is utilized for high-frequency storage of process and equipment data. The database efficiently manages large volumes of continuously generated operational information while maintaining data integrity and retrieval performance. Historical data stored within the database supports trend analysis, condition assessment, performance evaluation, and long-term equipment health monitoring.

Data Analytics and Diagnostic Engine

The analytical layer continuously evaluates process and equipment behavior using predefined monitoring rules, condition assessment logic, event correlation techniques, and trend analysis algorithms. The system identifies abnormal operating patterns, detects deviations from normal operating conditions, and assists in root cause identification. This analytical capability enables early detection of developing equipment issues and supports predictive maintenance strategies.

Dashboard and Visualization Platform

The CCM dashboard provides operators, maintenance personnel, and plant management with real-time access to equipment condition and process performance information. Interactive dashboards display current operating parameters, historical trends, equipment status, alarm history, and performance indicators. The visualization platform facilitates rapid interpretation of operating conditions and supports informed decision-making

Notification and Alert System

The alert management system continuously monitors critical operating parameters against predefined thresholds and operating criteria. When abnormal conditions are detected, automated notifications are

generated and delivered through email, mobile devices, or the CCM dashboard. This functionality ensures timely awareness of developing issues and enables prompt corrective action.

Secure Remote Connectivity

Secure communication between the plant site and the IKN Service Portal is established through a Virtual Private Network (VPN). Data exchange is facilitated using MQTT protocols, enabling reliable and secure transmission of monitoring data. Remote connectivity allows IKN specialists to access operational information, perform diagnostics, review historical trends, and provide technical support without requiring site visits.

IKN Service Portal

The IKN Service Portal serves as the centralized platform for remote monitoring, diagnostics, reporting, and technical support. Authorized users can securely access equipment performance information, review historical operating data, investigate abnormal events, and obtain expert recommendations. The portal also provides a framework for deploying future software enhancements and monitoring functionalities.

Together, these system components form a comprehensive condition monitoring system that enables continuous equipment surveillance, improves maintenance effectiveness, enhances equipment reliability, and supports data-driven operational decision-making.

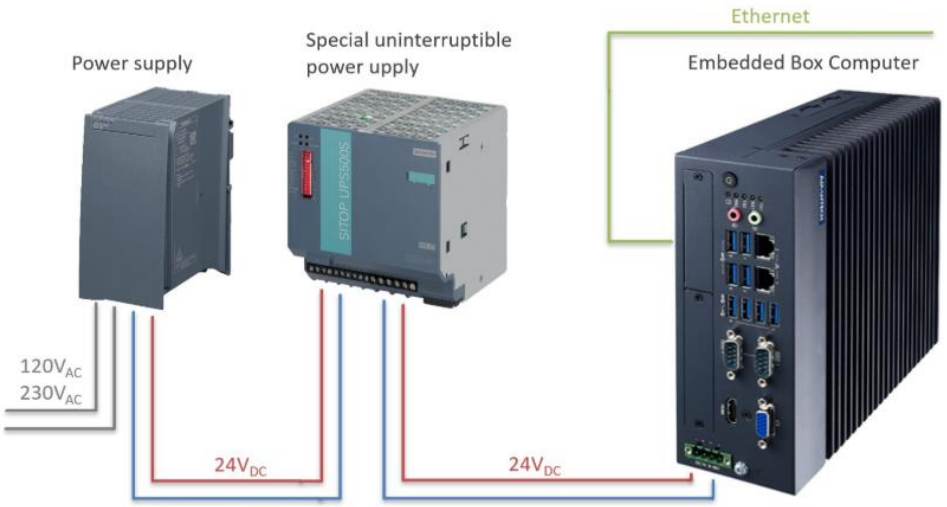


Fig-1: Hardware Components

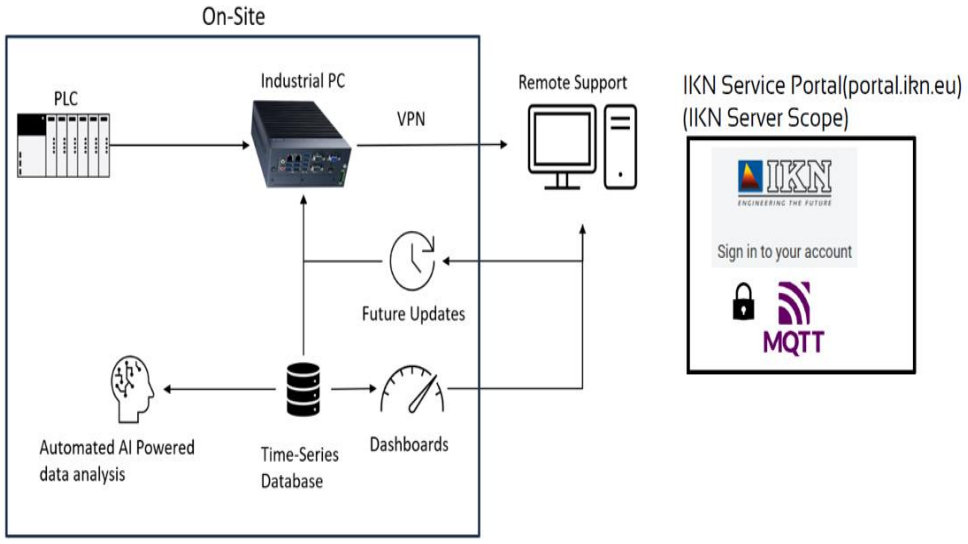


Fig-2: Cooler Condition Monitoring Architecture

To facilitate secure remote access, the Industrial PC communicates with the IKN Service Portal through a Virtual Private Network (VPN) connection using MQTT-based data exchange. This secure communication infrastructure enables remote support by IKN specialists without interfering with the plant control system. Through the service portal, experts can access operating data, review historical trends, perform detailed diagnostics, and provide recommendations for corrective actions.

3.2. Data Analytics and Future AI Diagnostics

The platform utilizes real-time and historical data to identify abnormal operating conditions, detect developing equipment issues, and evaluate performance trends. Through trend analysis and event correlation, CCM supports early fault detection, root cause identification, and proactive maintenance planning.

Automated condition assessment is performed using predefined engineering rules and operating criteria. The platform also supports long-term trend analysis, allowing maintenance teams to identify recurring issues, evaluate equipment performance, and optimize maintenance strategies based on actual operating conditions.

Future developments will focus on integrating Artificial Intelligence (AI) and Machine Learning (ML) technologies to enhance diagnostic capabilities. Potential applications include anomaly detection, fault classification, predictive maintenance recommendations, Remaining Useful Life (RUL) prediction, and intelligent root cause analysis. These advancements will further strengthen the role of CCM in supporting reliability improvement and data-driven decision-making for clinker cooler operation and maintenance.

4.0. Service Visits and Technical Audits

Periodic service visits are a fundamental component of the Customer Care Service Program (CCSP), providing on-site evaluation of clinker cooler operation, equipment condition, and maintenance

practices. These visits are conducted by experienced electrical, process and mechanical specialists to assess cooler performance under actual operating conditions.

During service visits, critical process parameters, mechanical components, hydraulic systems, grate operation, cooling efficiency, and wear patterns are systematically evaluated. Historical operating data, maintenance records, and CCM observations are reviewed to identify performance deviations, recurring issues, and opportunities for improvement.

Based on the findings, detailed recommendations are provided covering operational optimization, maintenance planning, component replacement, and reliability improvement measures. The observations and corrective actions are documented and tracked to ensure effective implementation and continuous performance improvement.

By combining field expertise with operational data analysis, service visits help identify developing issues at an early stage, improve maintenance effectiveness, and support long-term clinker cooler reliability and availability.

Key Activities During Service Visits

- Mechanical Inspections During Planned Shutdowns
- Process Audits & Optimization
- Maintenance and Reliability Evaluation
- Hydraulic and electrical system performance evaluation
- Identification of Improvement Opportunities
- Corrective Action Recommendations
- Operator and Maintenance Training

5.0. Spare Parts Optimization and Inventory Management

The program includes periodic review of inventory levels, spare parts consumption trends, equipment operating conditions, and maintenance history to ensure that critical components are available when required. Special emphasis is placed on wear-intensive components such as grate plates, hydraulic system components and other critical components that directly impact cooler availability and performance.

CCSP supports inventory planning through continuous assessment of component condition, expected service life, historical consumption rates, and operational requirements. This enables plants to maintain optimum inventory levels, reduce emergency procurement requirements, and minimize the risk of extended downtime due to spare part shortages.

In addition, key performance indicators (KPIs) related to spare parts consumption, inventory availability, and maintenance activities are periodically reviewed throughout the contract period. By integrating field observations, maintenance records, and condition monitoring data from the CCM platform, CCSP enables a proactive and data-driven approach to spare parts management. This contributes to improved equipment availability, optimized inventory investment, reduced maintenance delays, and enhanced lifecycle performance of clinker cooler systems. Inventory planning under CCSP is based on original equipment manufacturer components, since the aeration geometry and dimensional

tolerances of clinker-contact parts directly determine air distribution, thermal loading, and consequently the wear life of the surrounding grate structure

6.0. Case Study 1 – Grate Plate Temperature

Background

Excessive grate plate temperatures can lead to accelerated wear, surface damage, reduced component life, and increased maintenance requirements. Through the Cooler Condition Monitoring (CCM), recurring high grate plate temperature events were identified in one of the clinker cooler installations. The elevated temperatures persisted despite normal cooler operating conditions, necessitating a detailed investigation.

Investigation and Analysis

Historical process data obtained through CCM was analyzed to identify the root cause of the temperature excursions. The investigation included evaluation of grate plate temperatures, kiln operating conditions, fuel feeding trends, alternative fuel feeding rates, and pre-calciner performance parameters.

Trend analysis revealed significant fluctuations in pre-calciner outlet temperatures and unstable fuel feeding patterns in calciner. These process disturbances resulted in non-uniform clinker burning conditions and intermittent hot clinker zones entering the cooler. Correlation of process and cooler data confirmed that the grate plate temperature excursions were closely associated with these upstream process instabilities.

The continuous monitoring capability of CCM enabled the identification of these recurring patterns, which were not readily visible through conventional periodic observations.

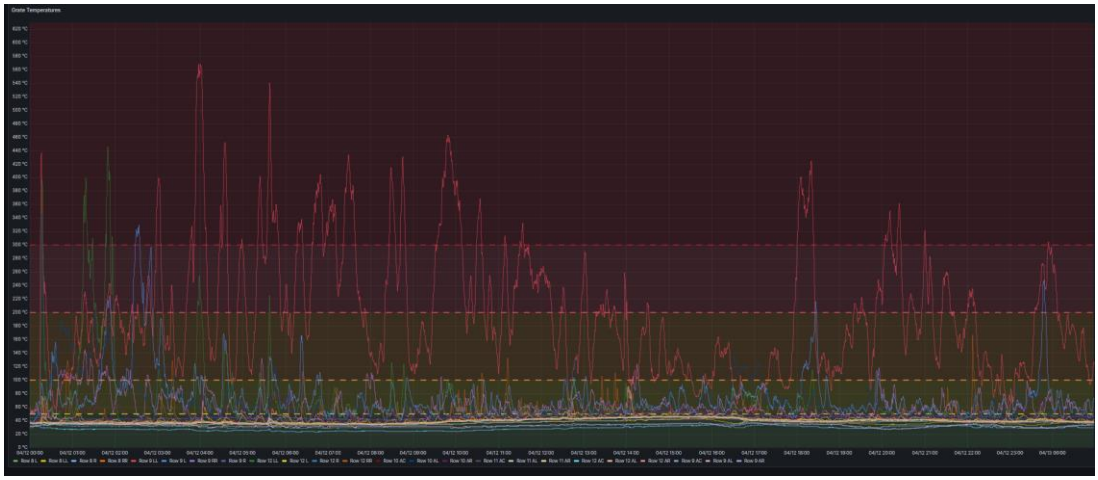


Fig-3: CCM trend showing grate plate temperature spikes

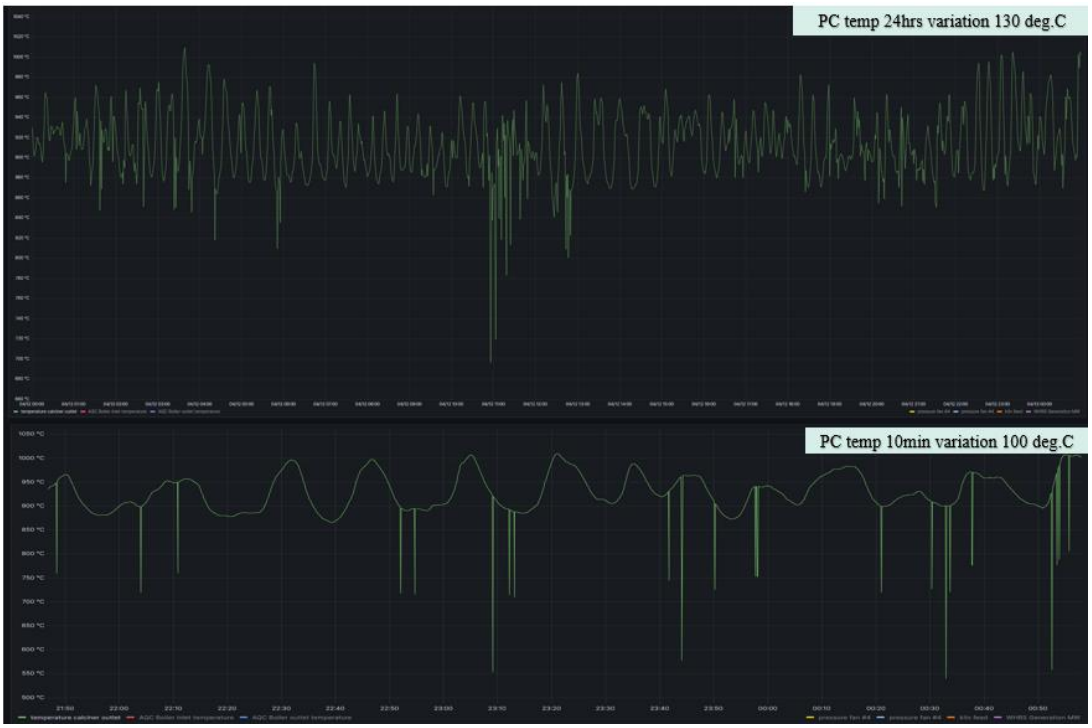


Fig-4: CCM trend showing PC temperature variation

Corrective Actions

Based on the analysis, the following actions were recommended:

- Stabilization of fuel feeding to the calciner and kiln.
- Optimization of combustion conditions in the pre-calciner.
- Improved monitoring of process temperature fluctuations.
- Enhanced coordination between kiln and cooler operation teams.

Results

Following implementation of the recommended actions, process stability improved significantly, resulting in reduced grate plate temperature excursions. Consequently, thermal loading on the grate surface was reduced, lowering the risk of premature component deterioration and extending grate plate service life. The corrective measures enhanced clinker cooler reliability and contributed to more stable cooler operation. This case study demonstrates how the integration of CCM data with process analysis can facilitate root cause identification and support timely corrective actions before equipment performance is adversely affected.

7.0. Case Study 2 – Hydraulic Grate Drive Diagnostics

Background

During normal plant operation, the hydraulic grate drive system began exhibiting irregular operating behavior. Pressure spikes were observed in Cylinder #2, and the position difference between the hydraulic cylinders increased significantly, occasionally exceeding 2 mm during periods of high grate

load. As a result, grate speed control became unstable, causing noticeable deviations from the setpoint and affecting process stability.

Based on the observed pressure behavior, the maintenance team initially suspected Cylinder #2 and planned seal replacement during the next maintenance opportunity. However, before shutdown activities were initiated, a detailed analysis of the hydraulic system data was performed to verify the root cause and identify the affected component.

Investigation and Analysis

As part of the Customer Care Service Program (CCSP), historical hydraulic pressure and cylinder position data were analyzed using the Cooler Condition Monitoring (CCM) platform. Detailed evaluation of the cylinder pressure profiles revealed that the pressure signal (pB1) associated with Cylinder #1 became unstable during the retraction cycle, exhibiting a rapid pressure drop and abnormal fluctuations. Although, the initial symptoms appeared to indicate a problem with Cylinder #2, correlation of pressure and position data identified deterioration of the internal piston seal in Cylinder #1 as the actual root cause. The analysis enabled the affected cylinder to be accurately identified prior to shut down, allowing maintenance activities to be planned with confidence.

Corrective Actions

Based on the findings from the CCM analysis, replacement of the internal seal of Cylinder #1 was recommended during the maintenance. The recommendation was communicated to the plant maintenance team, allowing the required spare parts and maintenance activities to be planned. During the scheduled shutdown, the internal piston seal of Cylinder #1 was inspected and replaced. The maintenance findings confirmed the diagnosis obtained through the CCM analysis, validating the identified root cause.



Fig-5: CCM trend showing pressure profile before incident

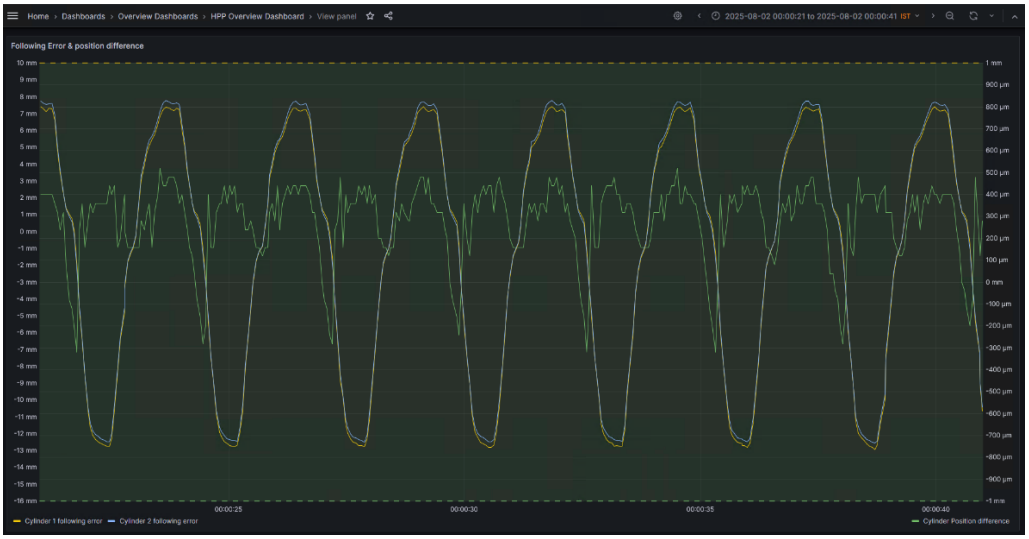


Fig-6: CCM trend showing position difference before incident

Results

Following replacement of the Cylinder #1 piston seal, the hydraulic pressure profile stabilized and cylinder operation returned to normal operating conditions. The position difference between cylinders was eliminated, resulting in improved grate movement synchronization and more stable grate speed control.

A significant benefit of the CCM analysis was the elimination of maintenance guesswork during troubleshooting. Based on the initial symptoms, the maintenance team suspected Cylinder #2 and planned to replace its seal. However, detailed analysis of the hydraulic pressure and position data identified Cylinder #1 as the actual source of the problem. Subsequent inspection during the shutdown confirmed deterioration of the Cylinder #1 piston seal, validating the CCM diagnosis. By accurately identifying the root cause before maintenance intervention, CCM enabled targeted corrective action during a single planned shutdown. This avoided unnecessary replacement of the Cylinder #2 seal, eliminated rework and additional troubleshooting efforts, and prevented a potential second plant stoppage that would have been required to address the actual faulty cylinder.

This case study demonstrates how data-driven diagnostics can improve maintenance efficiency, reduce downtime, and support effective decision-making by ensuring that corrective actions are focused on the actual root cause of the problem.

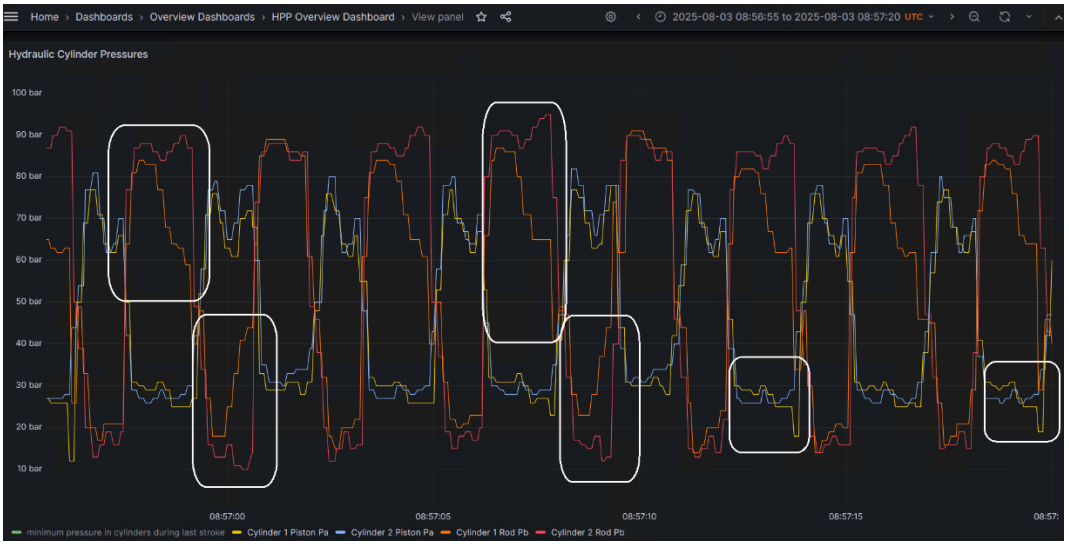


Fig-7: CCM trend showing cylinder-1 and cylinder-2 pressure after incident



Fig-8: CCM trend showing position difference after incident

Key Benefits

- Root cause identified before shutdown.
- Maintenance guesswork eliminated through data-driven analysis.

Table 1

Comparison of Maintenance Outcomes with and Without CCM-Based Diagnostics

Without CCM	With CCM
Cylinder #2 would likely have been replaced first.	CCM correctly identified Cylinder #1.
Incorrect maintenance action.	Targeted maintenance.
Additional troubleshooting required.	Root cause identified before shutdown.
Potential second shutdown to replace the correct cylinder.	Avoided unnecessary maintenance activity.

8.0. Case Study 3 – Root Cause Analysis of Hydraulic Grate Drive Trip Problem

Problem:

Unexpected hydraulic grate drive trip accompanied by multiple alarms, including a communication-related alarm and simultaneous 120 VAC and 24 VDC circuit-breaker trips.

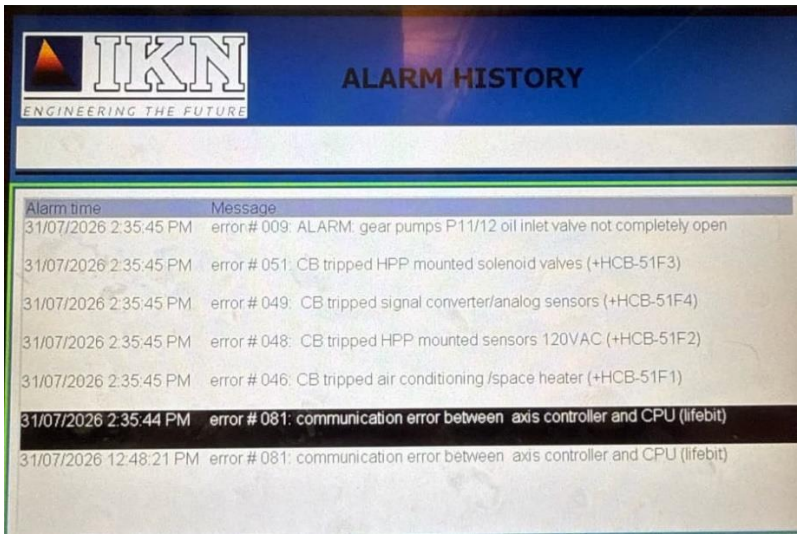


Fig-9: List of alarms

Root Cause Analysis:

Although a communication alarm was recorded during the trip, CCM trend analysis showed that the abnormal event had already started before the communication alarm occurred. The cylinder was operating normally until an abnormal change in the proportional valve command was observed approximately 7 seconds before the main alarms. Subsequent analysis showed that GD-Y1 attempted to build hydraulic pressure, followed by a sudden pressure drop to zero. Correlation of these signals indicated that the +HCB power supply/control circuit was the more probable initiating cause, with the communication and other alarms occurring as consequential indications.

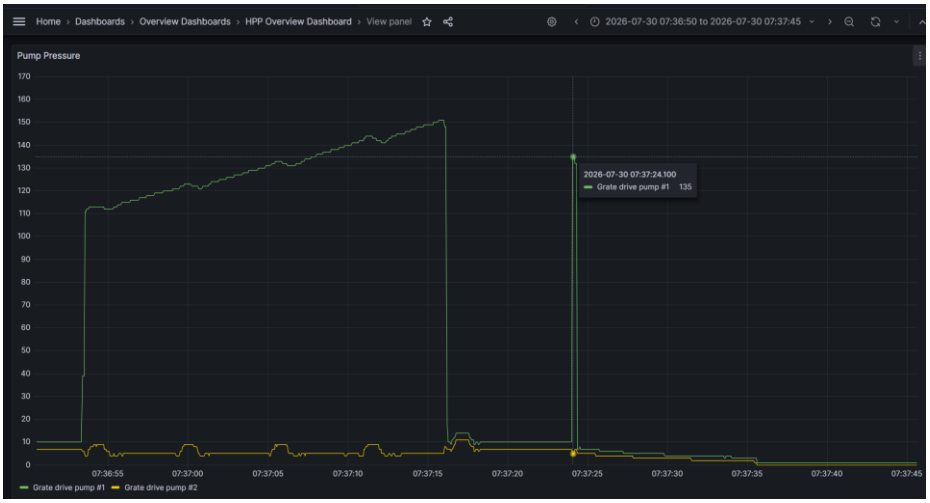


Fig-10: GD-Y1 (pressure relief valve) behaviour during incident

Solution:
Based on the CCM-based root cause analysis, the troubleshooting focus was shifted from the communication alarm to the power supply feeding the +HCB circuit. Investigation identified the circuit breaker in +CGS supplying power to +HCB as the component requiring attention. The circuit breaker was replaced, following which the hydraulic grate drive returned to normal operation and the tripping issue was resolved.

9.0. Conclusion

The Customer Care Service Program (CCSP) provides a comprehensive framework for improving clinker cooler reliability, maintenance effectiveness, and long-term equipment performance through the integration of service expertise, condition monitoring, and data-driven analysis. By combining periodic service visits, technical audits, spare parts optimization, remote diagnostics, and the Cooler Condition Monitoring (CCM) platform, the program enables proactive identification of operational and maintenance-related issues before they impact plant performance.

The case studies presented in this paper demonstrate the practical benefits of the CCSP approach. In the grate plate temperature case, analysis of CCM data helped identify process-related factors contributing to excessive thermal loading, enabling corrective actions that reduced the risk of grate surface damage. In the hydraulic grate drive case, CCM facilitated accurate root cause identification of a deteriorated cylinder seal, eliminating maintenance guesswork, avoiding unnecessary maintenance activities, and preventing a potential additional plant stoppage. In the hydraulic grate drive trip case, trend correlation established that the initiating cause lay in the power supply circuit rather than in the communication alarm that was first recorded, directing troubleshooting to the correct component and restoring normal operation.

The integration of continuous monitoring with engineering expertise allows maintenance decisions to be based on actual equipment condition rather than assumptions, resulting in improved maintenance planning, optimized spare parts utilization, reduced downtime, and enhanced operational reliability.

As digital technologies continue to evolve, the incorporation of advanced analytics, artificial intelligence, and predictive maintenance capabilities will further strengthen the effectiveness of CCSP. The results demonstrate that a structured service framework supported by condition monitoring and data-driven diagnostics can significantly contribute to operational resilience, asset lifecycle optimization, and sustainable clinker cooler operation.

10.0. Acknowledgement

The authors express their sincere gratitude to IKN Engineering India Pvt. Ltd. and IKN GmbH for their support in the development and implementation of the Customer Care Service Program (CCSP) and Cooler Condition Monitoring (CCM) platform.

The authors also acknowledge the valuable cooperation of the participating cement plants for providing operational data, maintenance feedback, and field support that contributed to the case studies presented in this paper.

Special thanks are extended to the service, process, and engineering teams whose technical expertise and continuous efforts in clinker cooler optimization, diagnostics, and maintenance support made this study possible.

References

3. ISO 17359:2018, *Condition Monitoring and Diagnostics of Machines – General Guidelines*, International Organization for Standardization (ISO), Geneva, Switzerland, 2018.

4. ISO 55000:2014, *Asset Management – Overview, Principles and Terminology*, International Organization for Standardization (ISO), Geneva, Switzerland, 2014.

5. Mobley, R. K., *An Introduction to Predictive Maintenance*, 2nd Edition, Butterworth-Heinemann, 2002.

6. Lee, J., Bagheri, B., & Kao, H. A., *A Cyber-Physical Systems Architecture for Industry 4.0-Based Manufacturing Systems*, Manufacturing Letters, Vol. 3, pp. 18–23, 2015

7. IKN GmbH, *Clinker Cooler Technology and Service Documentation*, Internal Technical Publications.

8. Zheng, *H., Paiva, A. R., & Gurciullo, C. S., Advancing from Predictive Maintenance to Intelligent Maintenance with AI and IIoT, arXiv, 2020.*

Prepol STEP COMBUSTOR: A UNIQUE SOLUTION TO COMBUST MOST FLEXIBLE ALTERNATE FUELS

Samuel Zühlsdorf*, Anup Das# Ali Asgar# and Abhinandan B. Jadhav#
**thyssenkrupp Polysius GmbH, Beckum, Germany*

#TKIL Industries Private Ltd., Pune

ABSTRACT

The cement industry with the increased focus on consuming natural resources is now renewed. The focus now is on reducing fuel costs, improving energy efficiency, and lowering carbon emissions through the utilization of alternative fuels (AFs). The pre-calciner is a key area for alternative fuel substitution, as it generates approximately 60% of the heat required in the pyroprocessing line and at the same time accommodates a wider range of fuel qualities than the main burner.

However, conventional calciners face limitations in burning low-quality, coarse, and irregularly shaped waste-derived fuels. These limitations can be related to insufficient particle residence time, incomplete combustion, and reduced process stability.

To address these challenges, thyssenkrupp Polysius has developed the prepol Step Combustor (prepol SC), a specialized combustion chamber equipped with a static grate system that enables the efficient utilization of a wide range of alternative fuels including coarse and low-quality waste materials. The system provides a longer residence time, controlled combustion conditions, and improved fuel flexibility.

This paper presents the working principle, design features, advantages and industrial applications of the prepol SC, along with operational results from cement plants. The findings demonstrate the system's potential to achieve higher thermal substitution rates while maintaining stable kiln operation and controlled emissions.

1.0 Introduction

The cement manufacturing process requires a significant amount of thermal energy, traditionally supplied by fossil fuels such as coal. The use of alternative fuels including refuse-derived fuel (RDF), biomass, and waste materials provides an opportunity to reduce fossil fuel consumption and improve the sustainability of cement production.

The pre-calciner is an important part of the pyroprocessing system as it generates approximately 60% of the heat required in the pyroline. At the same time it is also less sensitive to variations in the alternative fuel quality compared to the main burner.

Modern cement plants can achieve thermal substitution rates (TSR) of up to 100% in the pre-calciner under suitable conditions. However, achieving high substitution rates requires improvements in fuel sourcing, storage, feeding, combustion technology and process control.

1.1 Challenges in Using Alternative Fuels in Conventional Calciners

Conventional calciners have several limitations while handling low-quality and waste-

derived alternative fuels.

- *Residence time*: Lightweight, two-dimensional particles require long residence time, often exceeding five seconds, for complete combustion.
- *Particle size*: Coarse and three-dimensional particles may fall directly into the kiln inlet instead of burning completely in the calciner.
- *Fuel quality*: High moisture content, low calorific value and irregular particle sizes make combustion difficult.
- *Process stability*: Variations in fuel quality and feeding rates can affect combustion conditions and kiln operation.
- *Infrastructure limitations*: Extending or retrofitting conventional calciners to improve combustion performance can be expensive and time consuming.

These challenges limit the use of low-quality alternative fuels and can increase operational costs.

1.1.1 Comparative data – Conventional firing in Calciner vs Prepol SC

Description	Conventional System	Prepol SC (Step Combustor)
1. Residence Time	Avg. ~5 sec	~1000 sec
2. AF Particle size	<50 mm	Upto 300 mm
3. AF Moisture	Limited	Upto 40%
4. Quality of fuel	Requires high & consistent quality AF	Can handle low-quality AF
5. TSR	Avg.15-20%	Upto 80%
6. Disturbance in operation	Sensitive to changes in AF / operating condition	NA

2.0 Working Principle of the prepol® Step Combustor

The prepol Step Combustor is a specialized waste incineration static grate system developed for cement plants. It is designed to burn coarse, moist, and low-quality alternative fuels that are otherwise difficult to combust in conventional calciners.

Its working principle involves the following stages:

1. Fuel feeding: Alternative fuel is fed to the combustion chamber using screw conveyors and a distribution chute.
2. Fuel retention: Coarse particles remain on the combustion grate, while fine particles are lifted into the combustion air.
3. Air blast conveying: A patented air blast system transports and agitates the fuel without requiring any moving mechanical parts in the hot combustion zone.
4. Combustion: Hot tertiary air from the cooler supports drying and incineration of the fuel.
5. Temperature control: Provision for hot meal introduction to regulate combustion temperature.
6. Gas integration: The combustion gases are directed into the pre-calciner system, where the heat is utilized in the clinker production process.

The grate provides a fuel residence time of approximately upto 1000 seconds.

3.0 Key Design Features

The main design features of the prepol® SC include:

- Combustion grate for retaining coarse fuel particles.
- Patented air blast conveying system without moving parts in the hot zone.
- Hot tertiary air supply for drying and combustion.
- Hot meal injection for temperature control.
- High excess air levels to support safe combustion.
- Effective sealing to reduce false air entry.
- Modular design for integration into existing preheater towers.
- Air cannons for continuous fuel agitation.

These features are designed to improve combustion efficiency, operational reliability, and fuel flexibility.

4.0 Advantages of the prepol Step Combustor

The major advantages of the prepol® SC are:

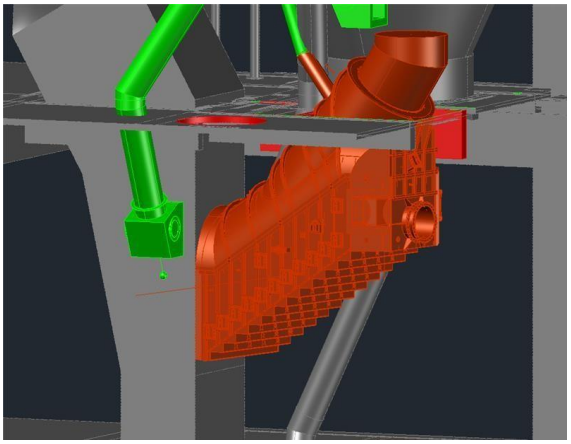
- Fuel flexibility: It can handle a wide variety of alternative fuels, including low-quality and coarse waste materials.
- Longer residence time: The grate allows fuels to remain in the combustion chamber for an extended period.
- Stable operation: Controlled combustion conditions and fuel agitation supports stable kiln operation.
- Low maintenance requirements: The static combustion system has no moving mechanical parts in the hot zone.
- Easy integration: Its modular design allows installation in existing preheater towers with relatively low additional structural loads.
- Emission control: High excess air and better temperature control supports safe combustion with controlled emissions.
- Improved reliability: Design improvements aimed to increase system reliability and reduce operating expenditure.

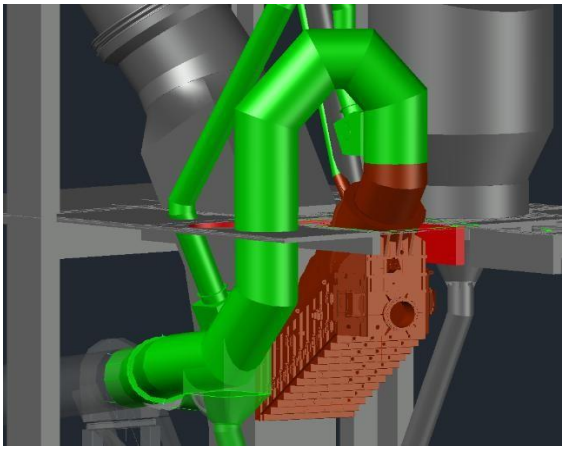
5.0 Reference

5.1 *References in Indian Subcontinent – M/s TCI Max - Trumboo Industries, Srinagar (Under execution….)*

Basic engineering of the project has already been completed and detail engineering for Prepol SC has commenced with following specification -

Alternate Fuel	:	MSW, RDF, Shredded Plastics and Wood chips
% TSR	:	40% (Total)
Thermal rating	:	32 MW
Model	:	4-11





Basic design of accommodating the prepol SC in existing Preheater building and TAD re-routing is complete

5.2 *References outside India - Industrial Applications and Case Studies*

5.2.1 Thailand: TPI Polene Cement Plant

The TPI Polene project in Saraburi, Thailand, is classic case of a large-scale alternative fuel substitution project. The project involves four existing kiln lines with a combined annual clinker production capacity of approximately 12 million tonnes.

Key project details:

- Four independent fuel substitution systems.
- Four prepol® SC installations.
- Alternative fuel handling capacity of up to 4,000 tonnes per day.
- Use of very low-quality alternative fuels.

The operational results include:

- Alternative fuels with average moisture content exceeding 50%.
- Very low heating values.
- Fuel particles fed to Prepol SC : 300 × 300 × 30 mm.
- Up to 20% higher mass flow and up to 50% higher volume flow.
- Stable kiln operation with unchanged clinker production capacity and emission levels.

This project demonstrates the application of the prepol® SC in large cement plants handling difficult alternative fuel qualities.

5.2.2 South Korea: Sungshin Cement Plant

The first prepol SC installation in South Korea was commissioned at Sungshin Cement's Danyang plant in July 2024.

Key project details:

- Location: Danyang, South Korea.
- Production capacity: Approximately 5,800 tonnes per day.
- Thermal substitution rate: 85%.
- Alternative fuel input: Approximately 31 tonnes per hour.
- Prepol SC capacity: 110 MW.

The fuel used was refuse-derived fuel with the following characteristics:

- Particle size: 120–150 mm.
- Predominantly two-dimensional particles.
- Moisture content: Approximately 15%.
- Net calorific value: Approximately 4,500 kcal/kg.

The performance test results reported in the webinar were:

Parameter	Warranty	Achieved
Thermal substitution rate	At least 85%	85.7%
NOx emissions	Maximum 190 ppm	137 ppm
THC emissions	Maximum 20 ppm	19 ppm
Clinker production	5,800 t/h	5,962 t/h

All performance warranty parameters were achieved and the customer signed the performance guarantee test acceptance within one week of the test.

5.2.3 China: Tiannan Hongshi Cement Plant

The Tiannan Hongshi cement plant in Yichun, Jiangxi Province, China, is another example of the application of the prepol SC.

Key project details:

- Location: Yichun, Jiangxi Province, China.
- Customer: Tiannan Hongshi Cement, Hongshi Group.
- Preheater type: TDI/KHD.
- Prepol® SC size: 6-17.
- Design capacity: 78 MW.

- Operating capacity: 22–25 tonnes per hour of RDF.
- Fuel moisture: Less than 15%.
- Lower calorific value: Less than 4,500 kcal/kg.

This project illustrates the system's compatibility for integration in an existing cement production line that uses non Polysius equipment.

5.2.4 Global Installations and Industrial Experience:

At the time of this print there are more than 50 prepol SC installations (including operating projects and projects scheduled for commissioning) demonstrating different system capacities, fuel types, kiln capacities, and operating conditions covering several countries, including Germany, Mexico, Uruguay, Thailand, China, Turkey, Slovakia, South Korea, The United States and India to name of few.

The installations in the Asia-Pacific region, particularly China and Thailand, highlight the system's application in large-scale cement plants with high alternative fuel substitution targets.

6.0 Operational Excellence of Prepol SC:

The industrial references indicate that the prepol SC can process a vide range of alternative fuels under different operating conditions.

The major findings include:

- High thermal substitution rates can be achieved in the pre-calciner.
- Coarse, moist, and low-calorific-value fuels can be utilized.
- Long fuel residence time supports effective combustion.
- Stable kiln operation can be maintained at high alternative fuel usage.
- The system can be integrated into existing cement plants, including third-party installations.
- Performance tests at various installation demonstrated compliance with the reported performance guarantees.

7.0 *Conclusion*

The prepol Step Combustor developed by thyssenkrupp Polysius provides a specialized solution for increasing alternative fuel utilization in cement manufacturing. Conventional calciners face limitations while processing coarse, moist and low-quality waste-derived fuels. The prepol SC addresses these limitations through a static grate-based combustion system, provides longer fuel residence time, controlled temperature, and an air blast conveying mechanism.

The industrial case studies from various plants demonstrate its application across different plant capacities, fuel qualities, and installation conditions. The reported results include high thermal substitution rates, stable kiln operation, and controlled emissions.

The system's modular design, fuel flexibility, and adaptability to existing cement plants make it applicable to a wide range of alternative fuel projects. Continued optimization of the air blast



conveying system is expected to further improve its operational reliability and efficiency.

Overall, the prepol SC represents a technological approach to increasing the thermal utilization of alternative fuels in cement production while reducing dependence on conventional fossil fuels.

8.0 ***Keywords***

Alternative fuels, prepol Step Combustor, cement industry, thermal substitution rate, refuse-derived fuel, pre-calciner, fuel flexibility, combustion efficiency.

"PROCESS OPTIMIZATION AND PLANT ENGINEERING" COST REDUCTION, DUST-FREE OPERATION AND POWER SAVING IN CEMENT MILL BAG HOUSES THROUGH FLOATING SHOE ROTARY AIRLOCK VALVES

Corresponding author: Sreedhar Sukumaran Managing Director

Anval International Pvt Ltd.

Email: info@anval.net; Web: www.anval.net

ABSTRACT

Process optimization and plant engineering in cement plants depend on the auxiliary equipment around the mills as much as on the mills themselves. A cement mill bag house is a clear example: its discharge points need a large quantity of valves, because every hopper or silo needs an airlock. Conventional rotary valves rely on a running clearance that abrasive cement dust widens with time, so the plant gets air leakage, dust spillage, tripping and frequent replacement, and the bag house fan has to work against false air.

This paper examines how a floating shoe rotary airlock, in which a hardened shoe slides on ceramic embedded rotor vanes in place of a running clearance, changes cost, dust control, auxiliary equipment efficiency and power consumption. The method is a review of three cement plant installations: two cement mill bag houses with 12 silos each, and the raw meal feed of a vertical roller mill. For each plant the quantity of valves and motors, connected drive power, annual energy, replacement interval, reported performance and cost savings are compared before and after, and the energy arithmetic is recomputed from the stated motor ratings.

In one 12 silo bag house, 24 conventional valves (double-decker installations) with 3.7 kW motors each (88.8 kW) were replaced by 12 floating shoe valves (1 per silo) with 1.1 kW motors (13.2 kW), a reduction of 85 % in connected power. Reported annual electrical savings are 662,256 kWh per bag house, with a fourfold improvement in bag house performance owing to lower air leakage, an annual saving of INR 59 lakh (at an avg. unit cost of INR 9) at the first plant with a payback of less than a year, and no spillage or tripping. At the vertical roller mill feed, liner/adjustable tips replacements of conventional rotary airlock valves every 3 to 6 months were eliminated and ID fan efficiency was restored.

In addition to the aforesaid cost savings, the combined energy savings corresponds to an indicative 645 tCO2 per year of avoided indirect emissions. The same airlock duty arises in carbon capture plants, where leakage dilutes or loses captured CO2, and a first-order balance is given for that case. The results are based on Anval's internal research and subsequently verified by the plant.

1.0 Introduction

Cement plants spend a large part of their effort on auxiliary equipment: bag houses, fans, conveyors and the valves that discharge dust and meal from them. These items do not make cement, yet they set the cost of dust control, the power drawn per tonne and the maintenance load. The cement mill bag house shows the issue well. Each hopper or silo under the filter needs an airlock to discharge dust without letting air in, so the quantity of valves is large, and every valve brings a motor, a gearbox and a maintenance task.

Conventional rotary valves seal through a running clearance between rotor tips and body. Abrasive cement dust wears the clearance open, and the plant then sees air leakage, spillage and tripping. The

leakage air also reaches the bag house and the ID fan, which must move extra false air, so fan efficiency falls and the filter performs poorly. This paper:

(i) explains why bag house applications need many valves,

(ii) describes a **floating shoe airlock** that removes the running clearance,

(iii) compares valve quantity, power, cost and maintenance at three cement plants, and

(iv) shows that the same duty arises in carbon capture applications, where leakage has a direct cost in CO2.

2.0 Valve Quantity in Cement Mill Bag Houses

A cement mill bag house collects fine, abrasive dust from the mill circuit at 80 to 140 °C and under suction of 5 to 10 kPa, and the dust is discharged through airlocks to the conveying system. The number of discharge points follows the number of hoppers or silos, and a conventional arrangement often puts two valves in series at each point, so that one maintains the seal when the other leaks. **At Ramco Cements' Ariyalur, RR Nagar, Jayanthipuram and at Sarbottam Cement Nepal, 12 silos therefore carry 24 rotary valves with 24 gear motors. At Chettinad Cement Ariyalur, 12 silos therefore carry 12 rotary valves coupled with 12 dump valves and 12 gear motors**. Compared with a single mill feed, the quantity of equipment to buy, power, maintain and replace is ***several times larger.***

This quantity multiplies every weakness of a single valve. If each valve leaks a little, 24 leak paths feed false air into the bag house. If each valve needs replacement every one to two years and refurbishments at every 6 months interval, as at the Ramco and Chettinad plants, 24 valves are replaced in each cycle. If each valve has a 3.7 kW motor, the connected load is 88.8 kW before any process work is done. A valve that seals without a second valve in series cuts all of these together.

3.0 Floating Shoe Rotary Airlock

The **floating shoe valve** replaces the running clearance with a sliding contact. A **hardened SG iron shoe**, **seated on the top port of the body and sealed to it by a double O-ring, is held by gravity against ceramic alumina embedded rotor vane ends, and adjustment screws set the contact** (Fig-1). Because the seal is a contact, wear does not open a leakage path: the shoe follows the rotor [5]. A single valve therefore ensures multi-fold sealing performance, compared to two conventional valves in series.

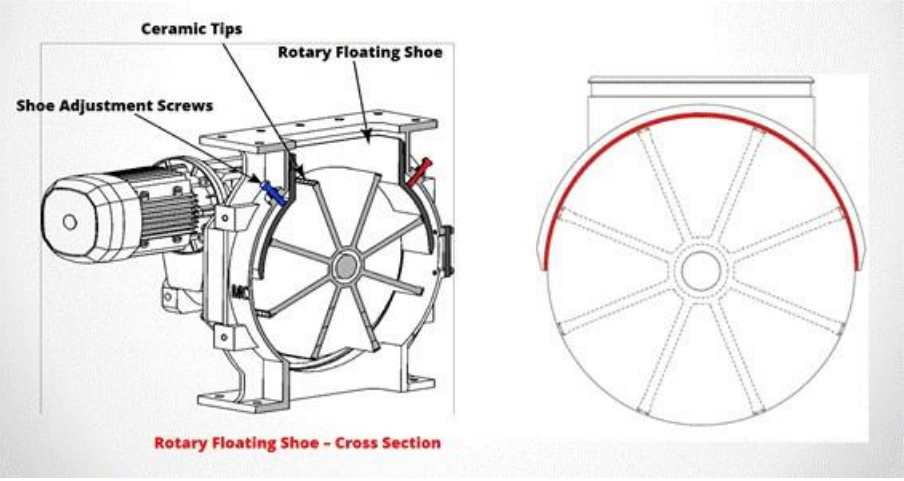


Fig-1: Schematic cross section of the floating shoe rotary airlock showing the gravity-loaded shoe, ceramic embedded rotor ends and shoe adjustment screws.

Laboratory testing at the University of Western Australia concluded that the ceramic embedded rotor ends in contact with the hardened SG iron shoe, handles high abrasive materials with minimum wear [5]. The graphite nodules of the iron are smeared along the sliding direction and form a continuous graphite film that acts as a solid lubricant, so friction is low enough for a small drive: a 1.1 kW motor is used where a conventional valve of the same duty uses 3.7 kW. Anval demonstrates that the floating shoe valves are in operation handling temperatures up to 1050 °C and in pneumatic conveying duties up to 30 bar.

4.0 *Plant Experience*

4.1 Power saving and fewer valves

Table 1 compares the quantity of valves and the power at the three plants. At the Ramco Cements plant, 12 silos had two conventional valves each, with 3.7 kW motors, and the 24 motors consumed 777,888 kWh per year. One **floating shoe valve** with a 1.1 kW motor per silo reduced connected power from 88.8 kW to 13.2 kW (Fig-2), and the reported saving is 662,256 kWh per year. At the Chettinad Cement plant the arrangement was a gravity operated dump valve and a rotary valve per silo, and the reported saving is 2,73,312 kWh per year.

Table 1 Valve quantity and drive power before and after the change

Item	Ramco Cements	Chettinad Cement
Silos or feed points	12 silos	12 silos
Conventional Rotary Valves (Before)	24 (2 per silo)	24 (dump valve and rotary valve per silo)
Rotary Floating Shoe Valve (RFS) (After)	12 (1 per silo)	12 (1 per silo)
Drive motors, (Before)	24 × 3.7 kW = 88.8 kW	12 × 3.7 kW = 44.4 kW
Drive motors (After)	12 × 1.1 kW = 13.2 kW	12 × 1.1 kW = 13.2 kW
Connected power reduction	85 %	70 %
Annual energy consumed (Before)	777,888 kWh	388,944 kWh
Annual energy savings (After)	662,256 kWh	273,312 kWh

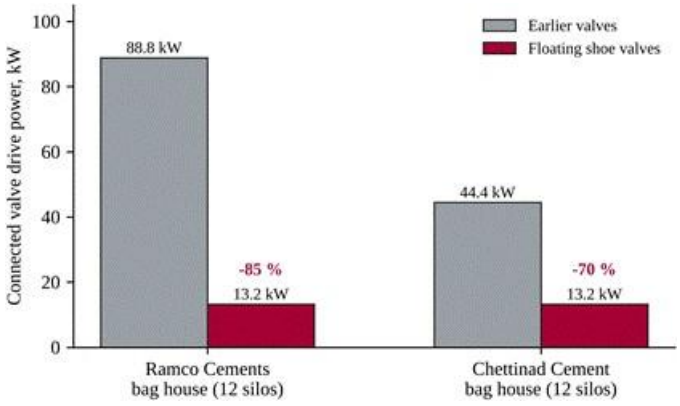


Fig-2: Connected valve drive power of the two cement mill bag houses before and after the change.

4.2 Cost reduction, dust control and fan efficiency

Table 2 lists the reported benefits. Air leakage, spillage and tripping at the Ramco and Chettinad plants were removed, which keeps the area around the bag house free of dust and the filter on line. Because less false air is drawn in, bag house performance improved fourfold at both plants, and at the Shree Cement plant the improvement is in the vertical roller mill and in ID fan efficiency, which had been reduced by leakage at the conventional lined valve. The cost effect has three parts: lower electricity (INR 59 lakh per year at the Ramco Cements plant with a payback of less than a year), fewer replacements (valves earlier replaced every 1 to 2 years, refurbishment of liners/tips every 3 to 6 months), and the labour and downtime that go with them. The reported annual savings are INR 24 lakh at the Chettinad Cement plant.

Table 2 Reported problems, performance and cost effect at three cement plants

Item	Ramco Cements	Chettinad Cement	Shree Cement
Duty and conditions	Cement mill bag house discharge, dP 5 to 10 kPa, 80 to 140 °C	Cement mill bag house discharge, dP 5 to 10 kPa, 80 to 140 °C	Limestone feed to a vertical roller mill, -15 kPa, 80 to 140 °C
Problems (Before)	Abnormal wear, Air leakage, spillage and tripping; valves replaced every 1-2 years & refurbishments every 3-6 months	Abnormal wear, Air leakage, spillage and tripping; valves replaced every 1-2 years & refurbishments every 3-6 months	Abnormal wear, Air leakage, reduced ID fan efficiency; liners replaced every 6 months
Performance (After **RFS**)	Fourfold improvement in bag house performance	Fourfold improvement in bag house performance	Fourfold improvement in mill performance
Maintenance (After **RFS**)	Minimal maintenance	Minimal maintenance	Minimal maintenance
Reported annual saving *(approximate)*	INR 59 lakh (recurring)	INR 24 lakh (recurring)	INR 20 lakh (recurring)
Payback	< year	< year	< year

The bag house energy savings amounts to 662,256 kWh per year, with a grid emission factor of 0.727 tCO2/MWh [6], this is an indicative 645 tCO2 per year of avoided indirect emissions.

Fig-3 shows the effect over six years as an illustration.

Two conventional valves carry repairs of 10% to 50% and a 100% replacement every second year, with productivity loss, and the cumulative operating expenditure reaches 630% with 70% more power cost. One **floating shoe valve (RFS)** draws 70% less power with a productivity gain, needs only a 15% **shoe** replacement in the year 6 to extend the valve life by at least another 5 years, and the cumulative operating expenditure is 15%.

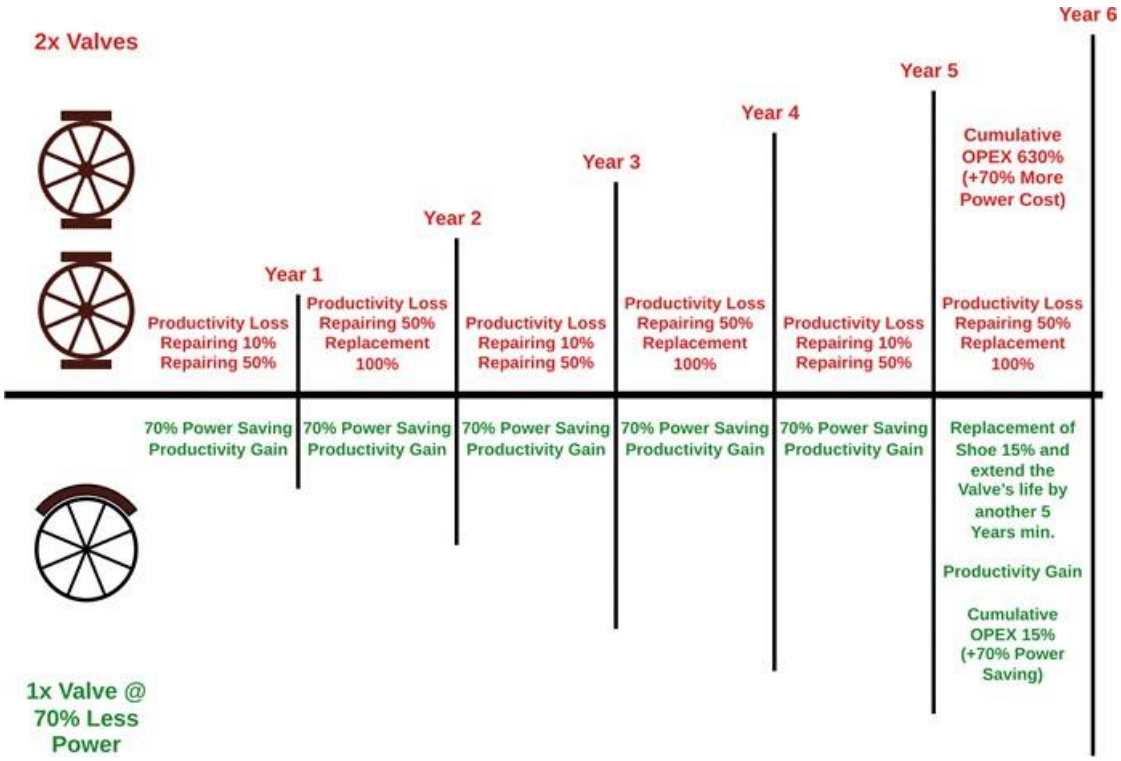


Fig-3: Conventional 2-valve arrangement versus one floating shoe (RFS) valve over 6 years.



(a) Before **(b) After**

Fig-4: Plant area before (a) and after (b) installing the floating shoe valve.

5.0 Other Duties and Scale

The same valve operates in other abrasive and hot duties (Table 3), which shows that the result is not confined to bag houses. Valves with rotor diameters from 950 mm to 2000 mm have also been supplied or are in progress for raw mill, cement mill and coal mill feed duties (16 valves in total), so the design applies to large transfer rates.

Table 3 Other documented duties of the floating shoe valve

Duty	Conditions	Result reported
Boiler ash discharge	350 °C, below 1 mm, very abrasive	**Floating shoe valves** in service over 12 years with minimal consumables
Antimony feed	1000 °C, -100 kPa, 10 mm	**Floating shoe valve** in service over 3 years without spare replacement
Dry sorbent injection (hydrated lime, sodium bicarbonate)	Below 100 µm, hygroscopic	**Floating shoe valves** in service over **5 years &** line stoppage reduced to **zero,** due to clogging
Coal feeding	80 kPa	**Floating shoe valve with Self-clean arrangement** in service over 3 years without spare replacement, Leakage reduced by **70 %**

A rotary valve feed was also developed for the **National Institute of Ocean Technology** for their continuous subsea transport of polymetallic nodules with a 30 bar pressure, at 6000m under the sea [7]. Anval's Rotary Floating Shoe (RFS) valve was named a finalist for the Innovative Technology Award in the Australian Bulk Handling Awards, and Anval exhibited at Bulk Expo 2026, Melbourne [8]. Anval also received an award for excellence in reliability and maintenance, announced officially by the organizers [9].

6.0 Extension to Carbon Capture Plants

Carbon capture is central to the net zero pathway of the Indian cement sector, which assigns about 25% of the total reduction to carbon capture, utilization and storage [1]. Capture plants that circulate solids, such as calcium loop Direct Air Capture (DAC) designs with a calciner, hydrator and carbonation [2,3] need airlocks at each transfer at oxygen free environment and the duty resembles that of hot, abrasive and hygroscopic calcium solids and a gas stream that must not be diluted. Anval's Rotary Floating Shoe Valves (**RFS)** are in service globally. Many carbon capture applications at NTPC plants across India, BEIS direct air capture & greenhouse gas removal program - phase 2 and SZC direct air capture project in the UK are the testimony for **RFS** valves in carbon capture applications.

The floating shoe valve helps in four ways at the solids transfer points of a calcium loop (carbonate feed to the calciner, hot calcium oxide discharge, hydrated lime return and filter dust return). First, purity and yield: the sliding contact stays closed as the rotor tips wear, so air ingress into the CO2-rich calciner gas and CO2 outflow stay at their commissioning level instead of rising with time, which protects the purity and yield.

7.0 Limitations

The performance and cost figures are based on Anval's own case studies at various cement plants mostly acknowledged by the end users. Energy figures assume continuous operation except where stated, and each comparison is against the specific earlier valve arrangement at that plant, so savings at other plants will differ. Independent measurement of leakage, fan current and wear would strengthen the results. For carbon capture, operation in CO2-rich gas, leakage at operating pressure and compatibility with hot lime fines are validated by Anval's clients.

8.0 Conclusions

1. Cement mill bag houses need a large quantity of valves, and in a conventional arrangement each silo carries two, so 12 silos mean 24 valves and 24 motors.
2. One **floating shoe valve** per silo reduced connected power from 88.8 kW to 13.2 kW at the Ramco Cements plants (85% reduction) and from 44.4 kW to 13.2 kW at the Chettinad Cement plant (70% reduction), with reported savings of 662,256 kWh and 273,312 kWh per year.
3. Less wear, minimal air leakage, no spillage and non-tripping gave a dust-free area, a fourfold improvement in bag house performance and better ID fan efficiency, and the reported recurring cost savings of more than INR 59 lakh at the Ramco Cements plants, of more than INR 24 lakh at Chettinad Cement plant and more than INR 20 lakh at the Shree Cement plant.
4. Fewer valves, lower motor ratings and longer replacement intervals reduce capital, power and maintenance together.
5. The same airlock duty arises in carbon capture plants, where leakage should be specified as a design requirement, and validation in that service is still needed.

9.0 *Acknowledgement*

The author thanks the engineering and application teams and the plant teams whose operating experience is reported here.

References

1. GCCA India and TERI (2025). "Decarbonisation Roadmap for the Indian Cement Sector: Net Zero CO2 by 2070". *Executive summary, Global Cement and Concrete Association India and The Energy and Resources Institute, New Delhi.*
2. International Energy Agency (2022). "Direct Air Capture 2022". *IEA, Paris, April 2022.*
3. Keith D.W., Holmes G., St. Angelo D. and Heidel K. (2018). "A Process for Capturing CO2 from the Atmosphere". *Joule, Vol. 2, No. 8, pp. 1573-1594.*
4. Heirloom Carbon Technologies (2026). "Technology". *Company web page, www.heirloomcarbon.com/technology, accessed October 2026.*
5. Sukumaran S. (2017). Study of leak and wear in floating shoe airlocks with the University of Western Australia. *Proc. 15th NCB International Seminar on Cement, Concrete and Building Materials, New Delhi, 5-8 December 2017.*
6. Central Electricity Authority, Government of India. "CO2 Baseline Database for the Indian Power Sector: User Guide" (2023-24 data). *Central Electricity Authority, New Delhi.*
7. Amudha K., Sundaramoorthi V., Umapathy A., Jayanthi K., Gopkumar K. and Ramadass G.A. (2022). "Development of a Subsea Continuous Feed Rotary System for Local Transport of Polymetallic Nodules to the Intermediate Pump System". *IEEE OCEANS 2022, Chennai; National Institute of Ocean Technology, Ministry of Earth Sciences. Available at: https://www.scribd.com/document/1066537657/Development-of-a-Subsea-Continuou s-Feed-Rotary-System-for-Local-Transport-of-Polymetallic-Nodules-to-the-Intermedi ate-Pump-System*
8. Bulk Expo Australia (2026). "Anval International to showcase award-finalist technology and industry-leading bulk handling solutions at Bulk Expo", 24 July 2026. *Bulk Expo 2026, Melbourne. Available at: https://bulkhandlingexpo.com.au/2026/07/24/anval-international-to-showcase-award -finalist-technology-and-industry-leading-bulk-handling-solutions-at-bulk-expo/*
9. Award for excellence in reliability and maintenance to Anval International, official announcement by the organizers. *Available at: https://lnkd.in/p/gnZ4UShR*



PIONEERING TECHNOLOGY: POLYSIUS – CLINKER COOLER WITH REMARKABLE EFFICIENCY POLYTRACK® ECO – CLINKER COOLER WITH OUTSTANDING OPERATING CHARACTERISTICS

Mr. Benski Bert, Mr. Ali Asgar# & Mr. Debajyoti Chatterjee#*

**thyssenkrupp Polysius GmbH, Beckum, Germany #TKIL Industries Pvt. Ltd., Pimpri, Pune*

ABSTRACT

thyssenkrupp Polysius GmbH is one of the few full-range technology suppliers for the cement industry – from individual machines, all the way up to complete cement plants, since decades. For the Indian sub-continent, TKIL Industries has the exclusive rights to propagate and market thyssenkrupp Polysius GmbH technology.

The new polytrack® eco is a significant departure from the previous design philosophy of the Polysius clinker cooler and incorporates new features meant to address the current challenges faced by cement manufacturers worldwide together with tested and proven elements from the established design.

The geometry of the static grate was adapted to improve the lateral distribution of the clinker and the penetration of cooling air into the clinker layer. By narrowing the horseshoe and extending the grate length, the new design helps to distribute the material more evenly over the grate width. The increased length of the new design also ensures that the residence time is sufficient to allow for vigorous heat exchange between the solids and air. This design enormously enhances the heat recuperation resulting in higher secondary and tertiary air temperature.

The polytrack® eco cooler combines efficient operational benefits and its maintenance friendly design concept. The new aeration floor design without tracks and with minimal dead layer maintains the autogenous wear protection of the grate. For increased robustness, all components coming in contact with clinker, are manufactured out of wear and heat resistant steel. Below the grate, the number of hydraulic cylinders and bearing positions has been reduced to minimize maintenance efforts. The new roller bearings being temperature resistant, have a significantly longer operating lifetime. To boost WHRS power generation, Chambers can be connected with hot air recirculation upto 130 deg C to enhance mid air temperature. Due to standardization of the hydraulic unit, the variety of mechanical equipment and quantity of electrical equipment is reduced to the minimum. This results in the huge benefit of shorter delivery time and reduced spare part stock handling.

The new aeration element design enhance and uniform the air distribution area, these optimization in designs significantly reduce the installed pressure drop of up to 10 mbar. These benefits reduce the overall electric power consumption of the cooler fans, cooler hydraulic and crusher to < 4.5 kWh/t. Due to the moving floor principle the cooler efficiency can reach up to 76% and is therefore the most efficient clinker cooler on the market.

SUMMARY

thyssenkrupp Polysius GmbH is one of the few full-range suppliers for the cement industry – from individual machines, all the way up to complete cement plants, since decades. Today the cement market demands efficient, highly flexible and high-capacity kiln plants for cement production of 12,000 tons per day and more. The new polytrack® eco is a significant departure from the previous design philosophy of the Polysius clinker cooler and incorporates new features meant to address the current challenges faced by cement manufacturers worldwide together with tested and proven elements from the established design. The polytrack® eco approves on the aspects of reliability, availability and

accessibility. The simple design focuses on mechanical and process benefits. Depending on the application, the cooler is modularized and can be easily adapted to customer requirement for a plant capacity from 1,000 tpd up to 12,000 tpd. Standard cooler components such as static grate, movable grate and clinker crusher can be aligned to reach the best technical solution with regards to highest cooler efficiency and lowest energy efficiency. The moving floor technology reduce the overall electric power consumption of the cooler fans, cooler hydraulic and crusher to < 4.5 kWh/t. Due to the moving floor principle, the cooler efficiency can reach up to 76% and is therefore the most efficient clinker cooler on the market.

1.0 INTRODUCTION

The polytrack® belongs to the fourth generation of modern clinker coolers. It was introduced to the market in 2001 and, till today, has been installed over hundred and forty times worldwide. Ever since the first installation it has built and maintained, the feedback was: "highly reliable and robust" as well as "state of the art in clinker cooling". Based on the rich experience collected over almost 20 years of successful product placement, thyssenkrupp Polysius GmbH devised and carried out a design upgrade program to align the cooler to the dynamic and more stringent market demands for energy efficiency and lower maintenance efforts. Incorporation of new key design aspects were targeted in order to maximize the performance of the cooler under more complicated operating conditions.

In 2022, the latest clinker cooler model was introduced to the market. The polytrack® eco has been developed with an innovative moving floor concept which has maximum benefits during operation. The new cooler generation combines more efficient operational benefits and its maintenance friendly design concept.

This paper will demonstrate the latest cooler development and its design features. Additionally mechanical and process related benefit will be illustrated.

2.0 New polytrack® eco

The polytrack® eco cooler combines design as well process related benefits and its maintenance friendly concept. This target matches with the tendency in the cement industry towards simplified, fast and predictable maintenance of the key equipment. While the number of positions requiring maintenance in a polytrack® is fairly low, the ambition was there to maximize maintenance friendliness. The benefits to the customers go beyond the issue of maintenance. Figure 1 illustrates a general design of a one-grate cooler in combination with end-roller crusher. The cooler starts with the inclined static grate and will be fed with hot clinker from the rotary kiln. Next to the static grate are the modular chambers which can be either 2.4 m or 4.8 m long, it is possible to design coolers to suit any plant capacity and fit into pre-existing housings, thus enabling fast and uncomplicated conversion projects. With this modularity, it is very easy to preciesly adapt the cooler to customer needs. Every chamber will be provided with cooling air by a separate fan. The chambers are divided with partition walls to maintain the descending pressure level. To support the moving carriage, which is responsible to transport and cool the hot clinker, bearing and drive blocks are installed. The movement will be realized by standardized hydraulic cylinders which are similar in size, to reduce the spare part variety. At the end of the cooling area, the material will be fed to the roller crusher to crush big clinker lumps and homogenize the material to 90 % < 30 mm. The efficient polytrack® roll crusher can be either installed at the cooler discharge as an end crusher or as an intermediate crusher, which serves to increase the temperature of the midair tapping for more efficient waste heat recovery, as well as to minimize the clinker end temperature to meet the demands of the downstream milling equipment.

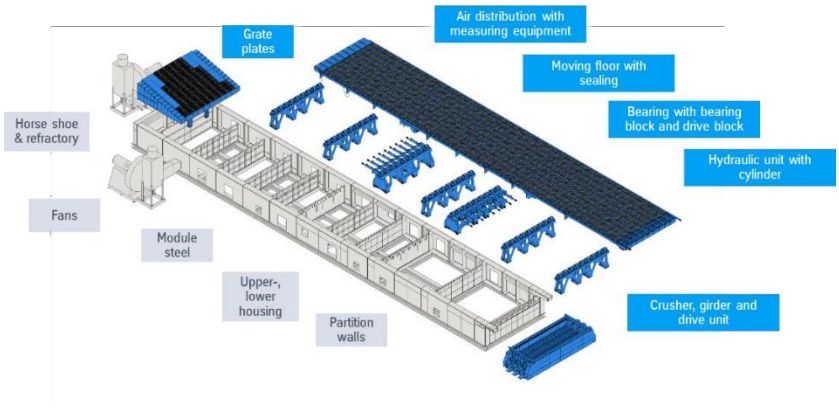


Figure 1: Basic design polytrack® eco

2.1 Static grate

The working principle of the static grate is to handle hot clinker discharged from the kiln. The inclination of the static grate reduces the overall height of the clinker layer. In order to protect the aeration plates from heat damage and extend their operating life, a certain so-called "dead layer" of cold, stationary clinker is necessary. If the dead layer is too thick, it can cause unnecessary flow resistance reducing the effective aeration to the incoming hot clinker. This aeration is crucial to stop phenomena like forming of red river. Practically, these advantages leads to increased recuperation efficiency, better heat exchange, lower heat consumption and increased service life.

The static grate fulfills following key functions:

- Quick initial cooling in order to "freeze" the clinker phases and stabilize the alite content (C3S), therefore ensuring high product quality.
- Enhancing the heat recovery to the kiln and calciner and reducing the fuel consumption of the kiln line.
- Uniformly spreading the material falling from the kiln over the width of the cooler grate to allow a homogeneous cooling result.

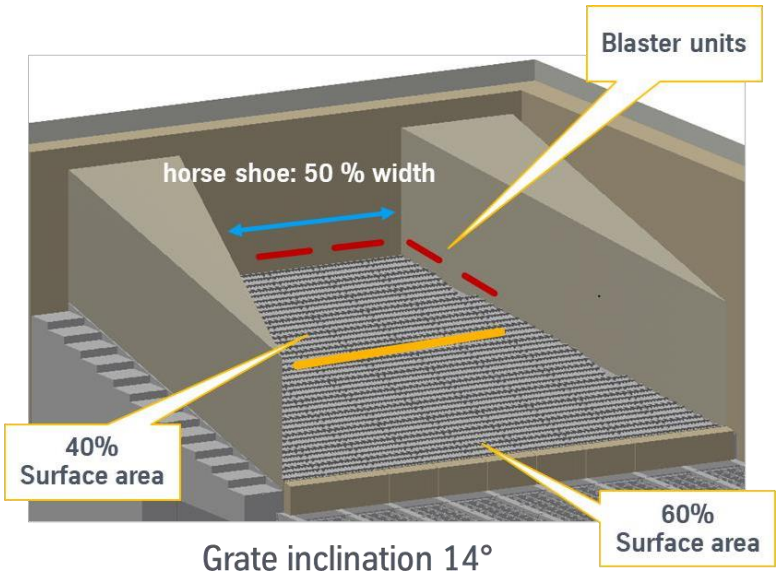


Figure 2: Static grate

2.2 polytrack® eco technology

The new polytrack® eco technology is a significant departure from the previous design philosophy of the Polysius clinker cooler and incorporates new features meant to address the current challenges faced by cement manufacturers worldwide together with tested and proven elements from the old design. Figure 3 show the first installation executed in Germany as a cooler upgrade project where the complete cooler where exchange by the new polytrack® eco with moving floor concept. The main mechanical and process related advantages are:

- High cooling efficiency up to 76 %
- Low clinker outlet temperature 65°C + ambient
- Low power consumption cooler, fans and crusher < 4.5 kWh/t
- High conveying efficiency > 86 %
- To boost WHRS power generation, Chambers can be connected with hot air recirculation upto 130 deg C to enhance mid air temperature
- Superior air distribution due to optimized aeration plates
- No clinker spillage due to superior double sealing concept
- Standardized hydraulic unit leading to reduction of mechanical equipment and reduced spare part stock
- Oxy-fuel ready



Figure 3: New polytrack® eco

2.2.1 Aeration element

The new aeration floor design without tracks and with minimal dead layer maintains the autogenous wear protection of the grate but significantly reduces pressure drops and resulting in lower electric power consumption of the cooler fans. The overall power consumption for cooler, fans and crusher reaches less than < 4.5 kWh/t which is a remarkable value.

Figure 4 show the improved aeration element design which leads to a significant pressure drop reduction

of up to 10 mbar. Additionally, this design enhancement increases the aerated area which brings huge benefits in cooling efficiency and results in a lower clinker temperature. For increased robustness, all components coming in contact with clinker are manufactured out of wear and heat resistant steel. The expected lifetime of aeration elements can reach up to 5 years.

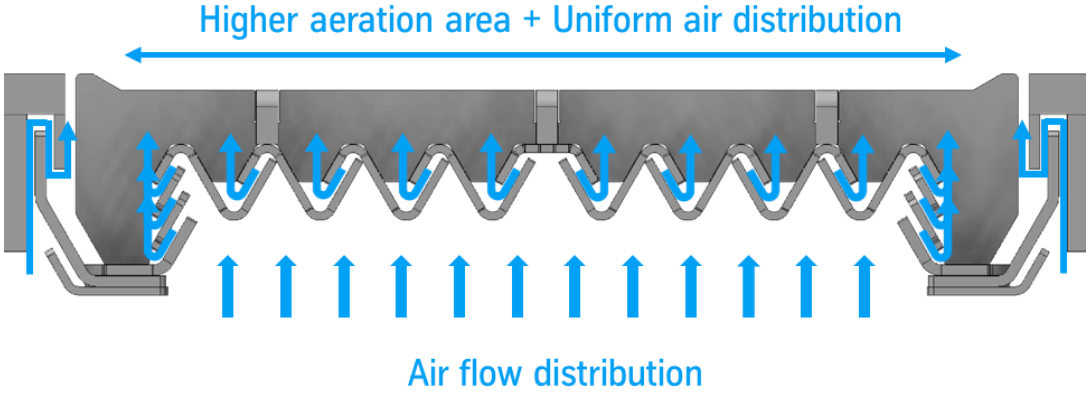


Figure 4: New aeration element

2.2.2 Double labyrinth sealing

The new patented sealing system is a double sealing consisting of **"M"**-shape part and "U"-shape part. Both are thermal and wear resistant containing cast material to reduce significantly wear and tear. Additionally, the clinker grain can´t pass the sealing system and enter the chamber below the cooler. The M and U sealing parts are 400 mm long and connected via bolts to the conveying carriage. This enables a simple and easy exchange of every single sealing element from the top of the cooler during maintenance. Based on the experiences gained from running references, the sealing lifetime can reach up to 3 years.



Figure 5: Double labyrinth sealing

2.2.3 Bearing Unit

The new roller bearings have a significantly longer operating lifetime than the linear bearings used in the past and have the added advantage of being temperature resistant.

The sealed spherical roller bearing unit is a well-tried, tested, very robust and reliable equipment. The bearing will be protected by heat resistant and tight housing and avoid dust entry into the bearing. It's a temperature resistant roller bearing designed to handle up to 150°C with long service lifetime. Scheduled

maintenance can be done during the annual kiln stoppage by using grease which can be injected via a grease pump to enhance the lifetime. As all the bearings are interchangeable, this standardized equipment reduces the amount of spare part. The eco cooler is designed with a minimum of mechanical equipment to reduce the inspection effort.

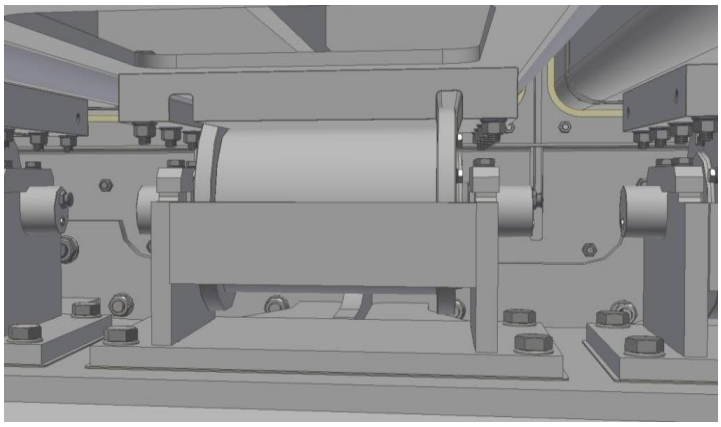


Figure 6: Sealed spherical roller bearing unit

2.2.4 Hydraulic System

The hydraulic system is of modular design and fully pre-tested before shipping to the plant site. A complete final acceptance test will be performed in the workshop of our sub-supplier. A complete check of mechanical and electrical equipment will be done from our specialists. The software simulates operating condition to ensure a trouble-free commissioning. The hydraulic system is an open loop system with optimized hydraulic piping. The modular design brings the added benefits of standard core parts such as pumps, valves, cylinder and electronic equipment. These standard units lead to short delivery times and reduction of cost during execution. The innovative mechanical solution of pressure control called "load sensing" leads to reduction of electrical equipment. The hydraulic pumps are designed for maximum 250 bar to handle unexpected operation condition e.g., flash condition, however, during normal condition the working pressures is around 100 bar. Below the grate structure, the hydraulic cylinders are positioned and their quantity has been reduced to minimize maintenance efforts.

Irrespective of the moving grate length, there are two nos. of hydraulic cylinders for every plank, one to move forward and the second to move the carriage backwards. All hydraulic cylinders have the same size with a diameter of 100 mm. As all the hydraulic cylinders are interchangeable, this equipment standardization, reduces the spare part stock. The operating stroke length is normally in the range of

~150 to 450 mm.

- Open loop hydraulic system
- 3 Standard hydraulic units
- Pumps are designed for 250 bar pressure
- Extremely precise track movement control
- Final Acceptance Test of every unit and tested before being shipped to site



Figure 7: Hydraulic unit

2.3 polytrack® eco Roll Crusher

The roll crusher serves to grind coarse cement clinker. It is used in association with grate coolers, and can be positioned either between the two grates or at the end of cooler. To increase the surface area of the clinker particles and thereby improve the cooling efficiency, roller crusher can be installed between the grates of the clinker cooler. At the front of the crusher the rolls have a screening function, while those in the rear zone work as counter-rotating crushing rolls. These rolls are highly wear-resistant and have air cooled shafts. Due to the low rotating speed of the roller (4 rpm), the wear rate of the roller is essential lower than the one experienced with Hammer crusher. Since the roller units are built as independent modules, each roller unit can be dismantled easily by a simple dismantling device.

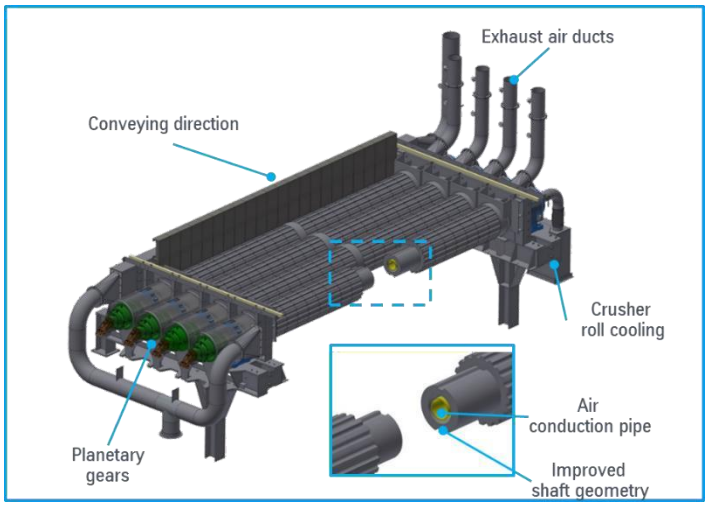


Figure 8: Roll crusher

3.0 Conclusion

The development of the polytrack® eco clinker cooler has formed a successful supplement to the Polysius product range. Now that it has been in operation for five years the cooler design has also proved its

success in practice. Designs in the performance range from 1,350 tpd to 11,500 tpd are currently in operation or are about to be commissioned in the near future. These advantages not only have a beneficial effect on the capital cost of new plants but are often all that make cooler conversions from planetary coolers and reciprocating grates possible, ensuring drastically reduced stoppage times.

The clinker cooler is a key component of any clinker production plant line, and its performance weighs heavily on the final economic performance of a cement plant. The extensive improvement programs carried out on the polytrack® eco tackled those components signaled by the customers to have optimization potential, while keeping the core features that make the polytrack® eco a reliable, high performance, future proof part of any clinker production line.



SUSTAINABLE AND INNOVATIVE REFRACTORY SOLUTIONS FOR ENHANCED AFR UTILIZATION IN CEMENT MANUFACTURING

Working technical paper for NCCBM Hyderabad Seminar, 202C

Sourav Duttagupta, Rajesh Kumar, Purushottam Bedare, Jitnesh Jain and Phil Edwards

Vesuvius India Ltd. and Vesuvius plc

Abstract

Increasing use of alternative fuel resources (AFR) in cement manufacturing is changing the chemical and thermal conditions experienced by refractory linings. Refuse-derived fuel, plastics, biomass and industrial wastes introduce variable concentrations of alkalis, sulphates, chlorides and volatile metals. These species circulate through the kiln system, condense on cooler surfaces and penetrate refractory matrices, where repeated chemical and thermal cycling promotes cracking, spalling and accelerated lining loss. Conventional selection has emphasized abrasion resistance, alkali resistance and build-up control; however, field experience in plastic-rich AFR environments shows that high silicon-carbide content alone may not provide optimum resistance when chloride-bearing species are present.

This paper reviews the principal refractory degradation mechanisms associated with AFR use and describes a zircon-enhanced low-cement refractory containing approximately 10% silicon carbide and 10% zircon-bearing addition in an alumina-silicate matrix. Laboratory evaluation covered initial, dried and fired properties; thermal-spalling and abrasion resistance; hot modulus of rupture; combined alkali-sulphate-chloride cup testing; polished cross-sections; and elemental analysis. Mechanical, abrasion and spalling performance remained broadly comparable with the established formulation, while corrosion testing showed lower potassium and chlorine diffusion and reduced penetration under representative combined-contaminant exposure.

The results support a balanced design approach rather than maximum silicon-carbide loading. Industrial validation at a 4,600 TPD cement plant operating with RDF and municipal waste further demonstrated more than 18 months of service with minimal coating build-up in the kiln inlet, tongue plate and smoke chamber.

Keywords: alternative fuels; AFR; cement refractory; alkali attack; chloride attack; silicon carbide; zircon; corrosion resistance

1. Introduction

The cement industry is increasing its use of alternative fuels to reduce fossil-fuel consumption, support decarbonization objectives and recover energy from non-recyclable waste streams. The resulting fuels are chemically diverse and can include refuse-derived fuel, waste plastics, biomass, tyres, sewage-derived materials and industrial residues.

The sustainability benefit is substantial, but the associated refractory environment is more complex than that created by conventional fuel systems. Variations in chlorine, sulphur, alkalis and volatile metals alter the circulation and condensation behavior within the preheater, calciner, riser duct, kiln inlet and smoke chamber. The refractory lining is therefore exposed not only to temperature and abrasion, but also to recurring chemical penetration and phase formation.

Historically, refractory selection in these areas focused on abrasion resistance, alkali resistance and control of material build-up. Field experience with plastic-rich AFR streams has shown that this approach can be incomplete. In particular, a product designed with a high silicon-carbide content may resist alkali-related build-up yet remain vulnerable to a combined chloride-bearing environment. The

present work evaluates a more balanced silicon-carbide and zircon-bearing matrix intended to restrict the transport of aggressive species without compromising mechanical performance.

2. AFR Utilization and Refractory Challenges

2.1 Evolution of cement fuel systems

Modern precalciner kilns permit a substantial proportion of the total fuel input to be introduced outside the main burner. This flexibility enables the use of multiple waste-derived fuels, but it also shifts part of the chemical load into the calciner and lower preheater. Consequently, refractory selection must reflect the chemistry of the fuel and process circulation, not only the nominal service temperature.

The contaminant profile varies with local fuel availability and preparation. Plastic-rich RDF can contribute chlorine and volatile metals; tyre-derived fuel can contribute sulphur and zinc; sludge and industrial residues may introduce chlorine, alkalis and other metallic species. These inputs combine with the raw meal and recirculating kiln species to establish the actual service atmosphere.

2.2 **Volatilization and condensation**

Alkali, sulphate and chloride species volatilize in hotter parts of the kiln system and condense as the gas stream reaches cooler surfaces. The lower preheater and feed-end regions are therefore exposed to repeated deposition. Potassium chloride is particularly volatile and may become strongly concentrated within the internal circulation.

The supply of condensable species is continuous during operation. A lining may therefore experience repeated filling of open porosity, reaction at the penetration front, thermal cycling and renewed chemical exposure. A single short-duration exposure cannot fully reproduce this mechanism, which is one reason that cement-specific corrosion testing is required.

\Refractory Degradation Mechanisms in AFR Operation

2.3 Alkali penetration and expansive reactions

Condensed alkali salts penetrate the refractory through connected porosity and react with alumina- and silica-bearing phases. Newly formed reaction products may exhibit substantial volume change. The resulting internal stresses create cracks, weaken the matrix and promote spalling during subsequent heating and cooling cycles.

This degradation is governed by both chemistry and transport. A material may possess adequate cold strength yet fail if aggressive species penetrate deeply enough to create a broad reaction zone. Limiting diffusion and penetration is therefore as important as maximizing initial strength.

2.4 Chloride-bearing environments and high-SiC refractories

Silicon carbide is widely used in cement refractories because it can improve resistance to build-up and alkali-related attack and can contribute to thermal-shock performance. However, higher silicon-carbide content is not automatically beneficial in every AFR atmosphere. Chloride-bearing species can influence the stability and protective behaviour of SiC-containing systems, particularly when reactions are repeatedly renewed by volatile circulation.

This distinction is important because a high-SiC benchmark may appear well matched to a high-alkali application while not addressing the complete alkali-sulphate-chloride environment generated by plastic-derived AFR. In this paper, moisture-related acceleration is treated as a possible field hypothesis rather than a demonstrated mechanism, because the available development work directly measures chemical penetration but does not isolate water vapour as an independent variable.

2.5 Secondary acid and anchor corrosion

Sulphate- and chloride-bearing species can penetrate through the working lining and affect insulating layers. Loss of insulation integrity increases heat transfer and permits corrosive species to reach the shell and anchoring system. In susceptible conditions, acid-forming species and hot-gas corrosion may reduce anchor section and compromise lining stability.

3. *Material Design Requirements for AFR Service*

The combined operating environment indicates that an AFR-resistant refractory should be selected against a balanced set of requirements:

- Low connected permeability and restricted chemical transport
- Resistance to alkali, sulphate and chloride attack
- Stable mechanical properties after firing
- Adequate abrasion resistance for entrained solids
- Resistance to repeated heating, cooling and chemically induced expansion
- Installation characteristics suited to the selected application method

The design objective is not to maximize a single constituent. It is to create a matrix in which the chemical-protection mechanisms remain effective while mechanical, thermal and installation properties remain fit for purpose.

4. *Development of the ZX Refractory Concept*

4.1 Design philosophy

The ZX concept combines silicon carbide and zircon-bearing material in a low-cement alumina-silicate matrix. The evaluated formulation contains approximately 10% silicon carbide and 10% zircon-bearing addition.

Constituent	SURCAST FLO 620ZX (%)
Al2O3	51.0
SiO2	26.0
Fe2O3	< 1.2
CaO	< 2.0
SiC	10
Zr	10

4.2 Functional contribution of silicon carbide

At the selected loading, silicon carbide contributes to build-up control, alkali resistance, abrasion performance and thermal-shock behaviour. The selected content is intentionally below the 30% SiC level used in the field benchmark discussed later, because the objective is balanced resistance rather than maximum SiC loading.

4.3 Functional contribution of zircon

The zircon-bearing component is intended to complement SiC through two related mechanisms. First, partial reaction can contribute silica-rich material at the reaction interface, supporting microstructural sealing and reduced permeability. Second, zirconia-bearing phases may assist in fixing calcium and alkali species as more stable zirconate-containing reaction products. These mechanisms are used as the design rationale; the present experimental evidence directly demonstrates reduced potassium and chlorine transport rather than complete identification of every reaction phase.

5. *Laboratory Evaluation*

5.1 Spalling and abrasion resistance

Thermal-shock and abrasion resistance were evaluated using standard test methods. Thermal cycling measured the reduction in modulus of rupture (MOR) after five cycles between 1200°C and room temperature. Abrasion loss was determined after firing at 1000°C for three hours using the ASTM C704 test method.

Property	SURCAST FLO 620ZX
Drop in MOR after 5 cycles at 1200°C	27%
Abrasion loss after 1000°C / 3 h	4.1 cc

5.2 Combined alkali-sulphate-chloride corrosion testing

Cup testing was conducted at 1100°C for five hours. Separate reagent systems were used for carbonates, sulphates and chlorides, followed by a combined exposure containing potassium carbonate, potassium sulphate and potassium chloride. The combined test was applied to both the SURCAST FLO 620ZX and the historical DURAFLO ZX formulations.

Test	Reagent system	Mass
1	Na2CO3 + K2CO3	25 g + 25 g
2	Na2SO4 + K2SO4	25 g + 25 g
3	NaCl + KCl	25 g + 25 g
4	K2CO3 + K2SO4 + KCl	25 g each

Assessment included visible colour change, crack formation, polished cross-section examination and penetration measurement. Visual comparison indicated lower combined-reagent damage in the revised formulation.

5.3 Microscopy, elemental analysis and penetration

EDS measurements at the reaction zone, sidewall penetration region and bulk material indicated lower potassium and chlorine diffusion in VZX 086 than in the standard formulation. Elemental mapping showed potassium and chlorine concentrated in the reaction zone, with no detected presence away from that zone in the reported VZX 086 sample. This supports the conclusion that the revised matrix restricts transport of the principal aggressive species.

Testing with cement raw mix also showed lower measured penetration for VZX 086. Bottom penetration decreased from 10.57 mm to 7.8 mm, while sidewall penetration decreased from 6.68 mm to 3.9 mm.

Measured penetration	SURCAST FLO 620ZX	Duraflo ZX	Reduction
Bottom	7.80 mm	10.57 mm	26%
Sidewall	3.90 mm	6.68 mm	42%

6. *Industrial Validation*

6.1 Plant and operating conditions

A field trial was conducted at a 4,600 TPD cement plant in North India. The material was installed in the kiln inlet, tongue plate and smoke chamber—areas particularly exposed to alternative-fuel-derived contaminants and coating instability. The plant uses refuse-derived fuel (RDF) and municipal solid waste.

Before the trial, the customer reported persistent coating build-up and related maintenance problems in these areas. The trial therefore provided an opportunity to assess the ZX concept under industrial AFR conditions.

6.2 Benchmark operating issues

Under RDF and municipal-waste firing, excessive coating build-up increased maintenance requirements and reduced operating stability.

The trial assessed whether the zircon-enhanced ZX refractory could limit coating formation while resisting the combined alkali-, sulphate- and chloride-bearing environment associated with AFR combustion.

6.3 ZX installation and performance

A total of 30 tonnes of DURAFLO ZX-II was installed between 5 and 11 February 2025 in the kiln inlet, tongue plate and smoke chamber.

The lining comprised 140 mm of calcium-silicate insulation and a 115 mm DURAFLO ZX-II working lining.

At the time of reporting, the lining had operated for more than 18 months. Site observations recorded minimal coating build-up throughout this period, representing a significant improvement over the previous condition.

This performance indicates that the ZX formulation can withstand the aggressive AFR environment while supporting stable operation in areas historically affected by deposition and chemical attack.

6.4 Industrial performance summary

The field results are consistent with the laboratory findings: controlled corrosion testing showed reduced transport of potassium- and chlorine-bearing species, while industrial operation demonstrated sustained lining durability and limited coating formation.

More than 18 months of service with minimal coating build-up in the kiln inlet and smoke chamber indicates that a balanced silicon-carbide/zircon system can improve operational reliability compared with material-selection strategies focused mainly on alkali resistance and build-up control.

7. *Discussion*

The ZX concept improved resistance to combined alkali-, sulphate- and chloride-bearing environments while retaining mechanical, abrasion and thermal-shock performance comparable with the established formulation. Corrosion testing, polished cross-sections and EDS analysis consistently showed lower potassium and chlorine transport. Penetration was reduced by approximately 26% at the specimen bottom and 42% at the sidewall, supporting the design objective of controlling chemical transport rather than maximizing a single constituent.

Industrial observations aligned with the laboratory results. DURAFLO ZX-II was installed in the kiln inlet, tongue plate and smoke chamber of a 4,600 TPD North Indian cement plant using RDF and municipal waste. After more than 18 months, the lining remained in operation with minimal coating

build-up.

This result is operationally important because coating accumulation is a major constraint on AFR use. The field trial indicates that the reduced chemical transport observed in the laboratory can translate into cleaner operating surfaces, lower maintenance exposure and improved stability in critical process areas.

The findings also challenge the assumption that higher silicon-carbide content invariably improves AFR performance. A balanced matrix containing silicon carbide and zircon-bearing additives restricted potassium and chlorine transport and performed successfully under RDF and municipal-waste firing. Refractory selection should therefore address the complete alkali-sulphate-chloride environment rather than alkali resistance alone.

Together, the laboratory and field evidence indicate that controlling chemical transport within the refractory matrix is central to improving lining durability and operating stability in AFR service.

8. *Conclusions*

- AFR use exposes refractory linings to combined alkali, sulphate and chloride attack, repeated condensation and thermal cycling, accelerating penetration, reaction and spalling.
- High silicon-carbide content alone does not guarantee optimum performance in chloride-bearing AFR service; selection must reflect the complete chemical environment.
- The ZX formulation combines silicon carbide and zircon-bearing additions in a low-cement alumina-silicate matrix to balance chemical resistance, transport control and physical performance.
- Laboratory testing showed comparable abrasion, thermal-shock and mechanical performance to the established formulation, together with improved resistance to combined contaminants.
- EDS analysis and penetration measurements showed lower potassium and chlorine transport, with penetration reduced by approximately 26% at the specimen bottom and 42% at the sidewall.
- At a 4,600 TPD North Indian cement plant using RDF and municipal-waste-derived fuels, the field installation delivered more than 18 months of service with minimal coating build-up.
- The agreement between laboratory and field results indicates that zircon-enhanced ZX refractories can improve durability, operating stability and maintenance performance while supporting increased AFR use.



Technical Session-VA

REDUCING CEMENT CONSUMPTION AND EMBODIED CARBON THROUGH RCC-TO-STRUCTURAL STEEL SYSTEM OPTIMIZATION A CASE STUDY OF AN HVDC VALVE HALL

Sh.T. Surya Chandra Rao.| Sh.Paningipalli NVM Prakash**
*Power Grid Corp. of India Ltd., India**

Abstract

The transition towards a low-carbon economy requires not only the decarbonisation of energy generation but also a planning required for reduction in the embodied carbon associated with infrastructure development. Transmission infrastructure, particularly High Voltage Direct Current (HVDC) converter stations, involves substantial quantities of cement, reinforcement steel, and structural steel. Among these materials, cement represents a major source of process and energy-related carbon emissions. Consequently, structural design optimisation offers an additional opportunity to reduce carbon emissions by lowering the quantity of cement-intensive materials required for construction.

This paper presents a conceptual comparative study of a 90 m × 40 m × 30 m HVDC valve hall designed using two alternative structural systems: (i) a conventional reinforced cement concrete (RCC) structural system and (ii) an optimised structural steel framing system with RCC foundations and other functionally necessary concrete components. The functional requirements, geometry, and assumed loading conditions are maintained identical for both alternatives so that the influence of the structural system can be isolated.

As per this case study, it is observed that the conventional RCC system requires approximately 10,460 m^3 of concrete, 3,975 tons of cement, and 1,995 tons of reinforcement steel. Conversely, the optimised steel alternative requires 540 m^3 of concrete, 206 tons of cement, 55 tons of reinforcement steel, and 854 tons of structural steel. The resulting cement reduction is approximately 3,769 tons, corresponding to a 94.8% decrease. Using illustrative material emission factors, the calculated material-related embodied carbon reduces from approximately 7,169 tCO_2e for the RCC alternative to 1,902 tCO_2e for the steel alternative, representing a 73.5% reduction.

The study demonstrates a critical lifecycle engineering principle: a significant reduction in cement consumption does not automatically yield an equivalent linear reduction in total embodied carbon, because the replacement structural steel introduces its own distinct embodied carbon footprint. Therefore, structural system selection must be predicated on a holistic assessment of material quantities, embodied carbon, structural efficiency, construction duration, foundation demands, and total lifecycle costs.

Keywords: *Embodied carbon; cement consumption; RCC; structural steel; HVDC; valve hall; structural Optimisation; sustainable construction; POWERGRID; carbon reduction.*

1. Introduction

The global transition towards renewable energy and low-carbon electricity systems is driving a rapid expansion of transmission infrastructure. Large-scale renewable energy resources are frequently located far from major load centres, necessitating high-capacity transmission systems capable of

transferring massive quantities of electrical power over long distances.

Power Grid Corporation of India Limited (POWERGRID), India's central transmission utility, plays a pioneering role in the development, operation, and maintenance of the country's interstate transmission network. The organisation's infrastructure portfolio encompasses Extra High Voltage AC systems, HVDC transmission systems, substations, converter stations, and extensive civil engineering assets.

However, the expansion of transmission infrastructure creates an indirect environmental challenge. While transmission systems enable the grid-level decarbonisation of the electricity sector, their physical construction consumes substantial quantities of carbon-intensive materials such as cement, concrete, reinforcement steel, and structural steel.

Among these, cement is particularly critical because clinker manufacturing involves both energy-related emissions and significant process emissions arising from limestone calcination. The International Energy Agency (IEA) explicitly identifies material efficiency and cement-sector decarbonisation as vital pathways for mitigating global industrial emissions.

Carbon dioxide emissions from the manufacture of cement in India from 1960 to 2023 *(in million metric tons)*

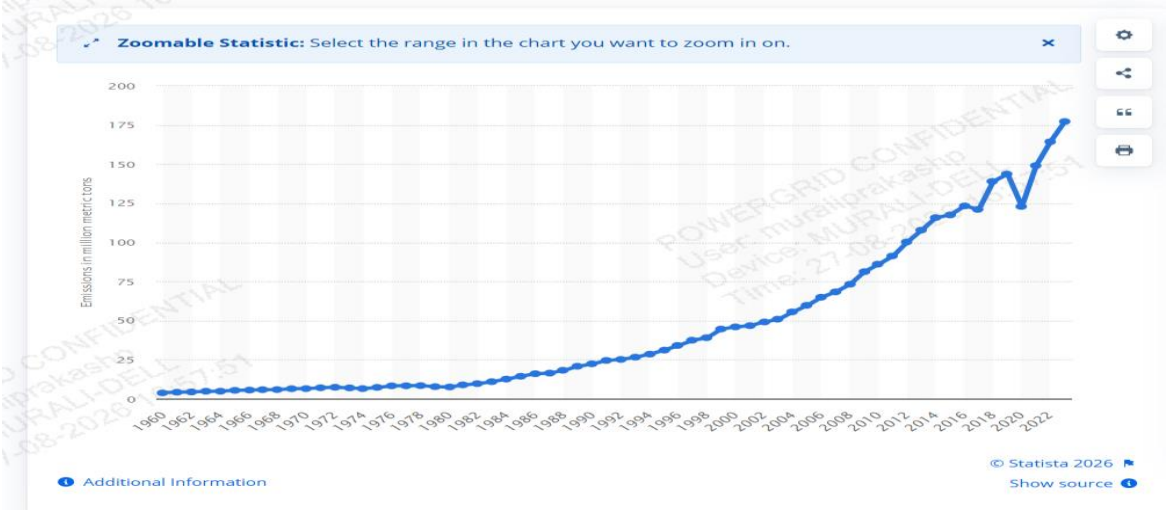


Fig:1 (from Statista Public Domain)

Carbon dioxide emissions from cement manufacturing in India have risen almost fourfold since the turn of the century, reaching 177 $MtCO_2$ in 2023. This accounted for around six percent of India's total fossil and industrial CO_2 emissions that year, and roughly 11 percent of global cement manufacturing emissions.

The rise in India's cement-related emissions has coincided with the increased production of cement to meet growing demand for construction purposes. India is now the second-largest cement producing country worldwide behind only China, having produced more than 400 million tons of this substance in 2023.

India is aiming to become a developed nation by 2047, which will likely see a further increase in cement

production for infrastructure and housing. As such, the country will need to address emissions from this hard-to-abate sector if it is to achieve its ambitious climate commitments. This will require a range of mitigation measures, such as improving energy efficiency, substituting carbon-intensive cement clinker, and using carbon capture technologies, the latter of which are projected to play a key role in reducing global cement industry emissions.

This paper investigates whether altering the structural system configuration can provide a meaningful reduction in cement consumption and total embodied carbon. An HVDC valve hall has been selected as the case study because it is a large-span, high-volume structure with stringent functional, environmental, and structural performance tolerances. Can an optimized structural steel system reduce cement consumption and overall embodied carbon compared with a conventional RCC valve hall structural system without compromising functional performance?

2. Technical Context & System Requirements

2.1 HVDC Transmission Systems

High Voltage Direct Current (HVDC) technology is the industry standard for the long-distance transmission of bulk electrical power. In an HVDC system, electrical power is converted from alternating current (AC) to direct current (DC) at a sending terminal and inverted back from DC to AC at the receiving terminal.The structural and electrical workflow of a simplified HVDC transmission system can be mapped linearly:

AC Grid -> Converter Transformer -> Converter Valves -> DC T/L -> Converter Valves->Converter Transformer->AC Grid

HVDC systems provide unmatched control over power transfer and minimize transmission losses over large-capacity corridors, making the technology highly relevant to India's unique geography where generation zones are highly isolated from load centres.

2.2 The HVDC Valve Hall

An HVDC converter station is a complex industrial campus comprising an AC switchyard, converter transformers, converter valves, a valve hall, a DC yard, smoothing reactors, AC/DC filters, auxiliary cooling systems, and control structures. Among these civil structures, the valve hall is the most critical. It houses delicate converter valves and maintains a strictly controlled interior environment. The structure must satisfy complex engineering demands simultaneously:

- Electrical insulation and strict radio frequency interference (RFI) shielding clearances.
- Mechanical stability, dynamic equipment support, and structural load-bearing capacity.
- Advanced fire safety, blast separation, and environmental isolation.
- High performance under wind loading and extreme seismic events.

2.3 The Need for Structural System Optimisation

Conventional structural solutions for large valve halls typically utilize heavy RCC structural grids. While an RCC system offers high stiffness, built-in fire resistance, and long-term durability, it comes with a massive penalty. It requires high concrete and cement volumes, heavy reinforcement layouts, extensive on-site formwork, extended construction schedules, and a massive deadload that compounds

down into the foundations.

The engineering principle investigated in this study aims to drastically reduce the structural self-weight and concrete volume of the superstructure. This is achieved by utilizing structural steel, which features a significantly higher strength-to-weight ratio.

Because steel production itself has a heavy embodied carbon footprint, the goal of this study is to perform a comparative structural assessment to evaluate if an optimised steel configuration results in a lower net carbon expenditure.

3. Case Study Configuration

The comparative methodology is applied to a conceptual model of an HVDC valve hall with the following envelope dimensions:

- Length: 90 m
- Width: 40 m
- Height: 30 m
- Total Floor Area: 3,600 m^2
- Total Enclosed Volume: 108,000 m^3
- Clear Span Target: Approx. 40 m

3.1 Structural System A: Conventional RCC Alternative

This baseline configuration consists entirely of heavy RCC columns, RCC tie-beams, an integrated RCC roof slab system, concrete shear/fire walls, and deep concrete foundations. The structural load path follows a rigid downstream sequence:

Roof Slab -> RCC Primary Beams -> RCC Main Columns -> RCC Foundations -> Subgrade Soil

The massive self-weight of the RCC superstructure scales exponentially, generating immense foundation reactions that increase subgrade concrete requirements.

3.2 Structural System B: Optimized Steel Alternative

The proposed alternative transitions the superstructure to a lightweight configuration. It utilizes structural steel columns, long-span steel roof trusses or portal frames, secondary steel framing girts, an engineered steel deck sheet system, and targeted RCC fire/separation walls only where functionally mandatory. The structural load path shifts to:

Steel Deck & Roof System -> Steel Trusses/Portals -> Steel Columns -> Base Plates -> RCC Foundations -> Subgrade Soil

This system minimizes the superstructure dead weight, drastically compressing foundation volumes. Furthermore, it permits off-site modular fabrication and rapid on-site erection, minimizing construction timelines and formwork demands.

4. Material Quantities & Methodology

The material quantification is based on a structural design comparison for an equivalent M25 concrete grade baseline, specifying a cement content of 380 kg/m^3.

Structural System A (RCC) Bill of Quantities:

- Roof Slab Concrete Volume: 900 m³
- Support Superstructure Concrete Volume: 9,560 m³
- Total Concrete Volume: 10,460 m³
- Total Cement Mass: 3,975 metric tons (MT)
- Total Reinforcement Steel Mass: 1,995 MT
- Total Structural Steel Mass: 0 M

Structural System B (Steel Alternative) Bill of Quantities:

- Roof Slab Concrete Volume: 540 m³
- Support Superstructure Built-up Framing: 850 MT
- Roof Deck Sheet Framing: 4 MT
- Total Concrete Volume: 540 m
- Total Cement Mass: 206 M
- Total Reinforcement Steel Mass: 55 MT
- Total Structural Steel Mass: 854 MT

5. Comparative Material Analysis

When transitioning from the conventional RCC configuration to the optimized steel alternative, the direct material variances are calculated below:

• Concrete Volume Reduction: 10,460 m³ - 540 m³ = 9,920 m³ (94.8% Reduction)
• Cement Mass Reduction: 3,975 MT - 206 MT = 3,769 MT (94.8% Reduction)
• Reinforcement Steel Reduction: 1,995 MT - 55 MT = 1,940 MT (97.2% Reduction)
• Structural Steel Addition: 0 MT -> 854 MT Added

Table 1: Comprehensive Material Metric Comparison

Structural Parameter	*System A: Conventional RCC*	*System B: Optimised Steel*	*Net Absolute Variance*	*Percentage Variance (%)*
Valve Hall Length	*90 m*	*90 m*	*0 m*	*0.0%*
Valve Hall Width	*40 m*	*40 m*	*0 m*	*0.0%*
Valve Hall Height	*30 m*	*30 m*	*0 m*	*0.0%*
Total Floor Area	*3,600 m²*	*3,600 m²*	*0 m²*	*0.0%*
Total Concrete Volume	*10,460 m³*	*540 m³*	*-9,920 m³*	*-94.8%*
Total Cement Mass	*3,975 MT*	*206 MT*	*-3,769 MT*	*-94.8%*

Reinforcement Steel Mass	*1,995 MT*	*55 MT*	*-1,940 MT*	*-97.2%*
Structural Steel Mass	*0 MT*	*854 MT*	*+854 MT*	*New Demand*

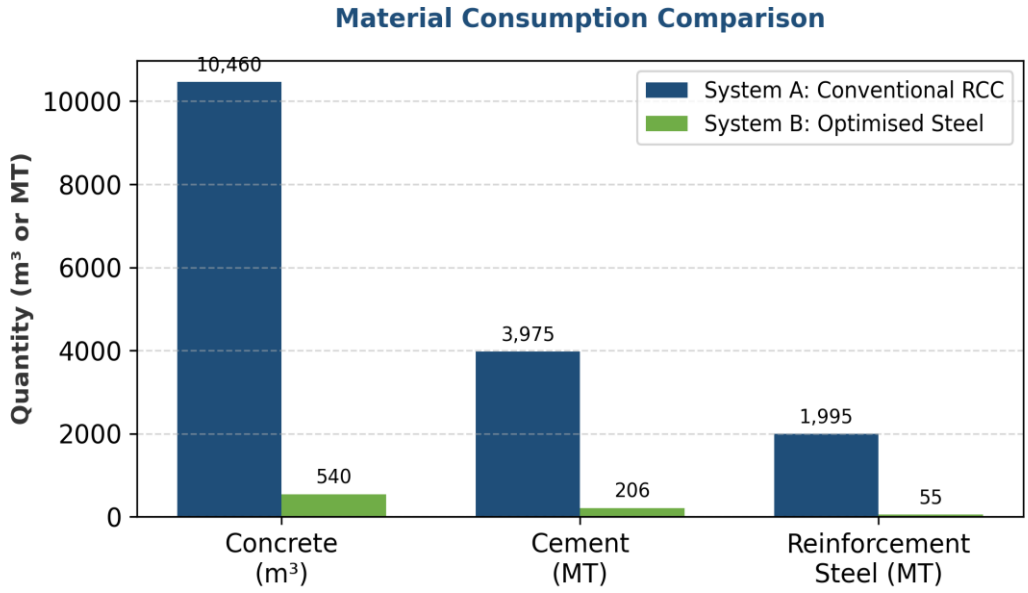


Figure 2: Volumetric and Mass Demand Reduction for Main Structural Materials

6. Embodied Carbon Assessment

To conduct the preliminary carbon inventory, the study adopts the following standard illustrative material emission factors (EF):

- Cement Emission Factor: 0.85 tCO_2e/t
- Reinforcement Steel Emission Factor: 1.90 tCO_2e/t
- Structural Steel Emission Factor: 1.90 tCO_2e/t

6.1 System A (RCC Alternative) Embodied Carbon Calculations

EC_cement = 3,975 MT × 0.85 tCO_2e/t = 3,378.75 tCO_2e
EC_rebar = 1,995 MT × 1.90 tCO_2e/t = 3,790.50 tCO_2e
EC_Total RCC = 3,378.75 + 3,790.50 = 7,169.25 tCO_2e

6.2 System B (Steel Alternative) Embodied Carbon Calculations

EC_cement = 206 MT × 0.85 tCO_2e/t = 175.10 tCO_2e
EC_rebar = 55 MT × 1.90 tCO_2e/t = 104.50 tCO_2e
EC_structural = 854 MT × 1.90 tCO_2e/t = 1,622.60 tCO_2e
EC_Total Steel = 175.10 + 104.50 + 1,622.60 = 1,902.20 tCO_2e

6.3 Carbon and Material Intensity Benchmarks

- Net Carbon Footprint Reduction:

ΔEC = 7,169.25 - 1,902.20 = 5,267.05 tCO_2e (73.5% Net Carbon Savings)

• Floor Area Carbon Intensity (RCC):

7,169.25 tCO_2e / 3,600 m^2 × 1,000 = 1,991.46 $kgCO_2e/m^2$

• Floor Area Carbon Intensity (Steel):

1,902.20 tCO_2e / 3,600 m^2 × 1,000 = 528.39 $kgCO_2e/m^2$

• Cement Avoidance Efficiency (CAE) Index:

CAE = 3,769,000 kg / 3,600 m^2 = 1,046.94 kg Cement/m^2 Avoided

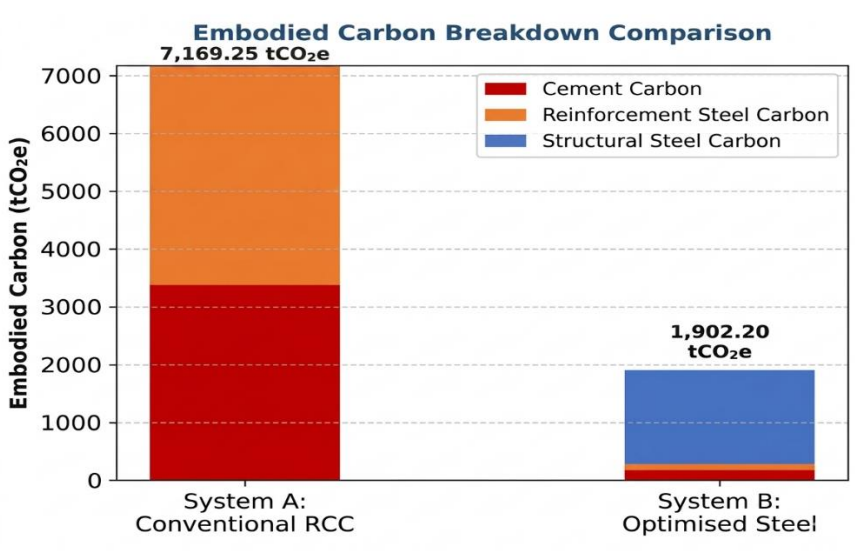


Figure 3: Stacked Embodied Carbon Contributions (tCO_2e)

7. Discussion & Strategic Frameworks

The core engineering takeaway of this study is that a massive 94.8% reduction in total cement consumption does not map linearly to a 94.8% reduction in carbon emissions. Because structural steel possesses its own high initial carbon density, the net carbon mitigation stabilizes at approximately 73.5%.

This underscores the necessity of a holistic, multi-variable structural systems approach.

7.1 Proposed Three-Stage Carbon Minimisation Protocol

To scale this success across utility infrastructure networks, structural engineers should adopt a tiered optimization sequence:

1. Stage 1 –

Structural Optimization: Deploy high-efficiency framing geometries, clear member profiling, direct load-path tracking, and maximized foundation optimization.

2. Stage 2 –

Low-Carbon Material Integration: Utilize supplementary cementitious materials (such as fly-ash and GGBS) to lower concrete intensity.

3. Stage 3 –

Whole-Life Cycle Asset Optimisation: Plan structural connectivity configurations to facilitate adaptive reuse, modular expansions, or simplified end-of-life recycling workflows.

7.2 Multi-Objective Project Performance Matrix

Modern infrastructure design can no longer prioritize capital expenditure (CapEx) in isolation. Future engineering selections must balance four distinct pillars of performance: Optimal Design Selection =

f (Structural Safety) +

f (Economic Efficiency) +

f (Construction Velocity) +

f (Carbon Performance)

8. Conclusions & Future Research Directions

8.1 Final Summary

This conceptual case study demonstrates that replacing a conventional heavy RCC structural configuration with an optimized structural steel frame for a standard 90 m × 40 m × 30 m HVDC valve hall yields substantial environmental dividends. By reducing the superstructure dead load, concrete demand drops by 9,920 m^3 and reinforcement steel drops by 1,940 tons. This avoids 3,769 tons of raw cement, translating to an outstanding 1,046.94 kg of cement saved per square meter of floor area. Accounting for the introduction of 854 tons of structural steel, net material-related embodied carbon drops by over 5,267 tCO_2e, a 73.5% net structural carbon reduction.

8.2 Boundary Limitations & Future Research Scope

As a conceptual study, these findings serve as a preliminary material carbon calculation and are subject to the following system boundaries:

- Exclusions: The current boundary does not include sand, aggregate extraction, finish cladding, protective intumescent coatings, site transport emissions, or assembly energy demands.
- Foundation Cascades: The structural reductions calculated here focus on the superstructure. Because the steel framework radically minimizes global column base reactions, future detailed designs will likely yield significant secondary carbon savings within the foundation concrete and subgrade excavation volume.
- To mature this framework for industrial application at POWERGRID, future research should target:
  - Full 3D finite element structural modeling and site-specific seismic/wind validation.
  - Comparative analysis of composite steel-concrete structural configurations.
  - Transitioning the carbon model to localized, verified Indian Environmental Product Declaration (EPD) lifecycle data.
  - Formulating a formalized Carbon-to-Cost Optimization Index across all modular sub-station asset designs.



References

1. *International Energy Agency (IEA), Cement-sector decarbonisation and material-efficiency resources.*
2. *POWERGRID Corporation of India Limited, HVDC project design and procurement technical data specs.*
3. *Bureau of Indian Standards (BIS): IS 456 (Plain and Reinforced Concrete), IS 800 (General Construction in Steel), and IS 1893 (Criteria for Earthquake Resistant Design of Structures).*

COMPARATIVE BOND BEHAVIOUR OF STEEL AND GFRP REINFORCEMENT IN GEOPOLYMER AND OPC CONCRETE

[1]Dr.G. Mallikarjuna Rao, [2]Sri.M.Kalyan, [3]Jagandas Sabavath, [4]N.Karthikeya, [4]P.Varun Kumar, [4]M.Pavan Kumar [1,2] Assistant Professor, Chaitanya Bharathi Institute of Technology, Hyderabad, Telangana, India, [3]PhD Scholar, National Institute of Technology, Tiruchirappalli, Tiruchirappalli, India, [4]UG Student, Chaitanya Bharathi Institute of Technology, Hyderabad, Telangana, India
Corresponding author: mallikarjunaraog_civil@cbit.ac.in

Abstract:

The growing demand for durable and sustainable reinforced concrete has increased interest in combining geopolymer concrete (GPC) with corrosion-resistant glass fibre reinforced polymer (GFRP) bars. However, the bond-slip behaviour of GFRP bars in GPC remains less understood than that of steel. This paper presents a comparative experimental study of steel and GFRP bars embedded in M20 and M40 grade GPC and ordinary Portland cement (OPC) concrete. Bars of 12 mm and 16 mm diameter were tested with embedment lengths of 100 mm and 150 mm, using fresh-property, strength and pull-out tests in accordance with Indian Standards. Average compressive strengths of M20 and M40 GPC were 21 and 41 MPa, against 20 and 40 MPa for OPC. Average bond strengths were 13.60 MPa for GPC with steel and 11.42 MPa for GPC with GFRP, compared with 11.05 MPa and 12.08 MPa for OPC with steel and GFRP, respectively. Bond strength increased with concrete grade, whereas longer embedment reduced the average bond stress. Steel bars showed less slip owing to higher stiffness and mechanical interlock, while GFRP bars exhibited greater slip and gradual interfacial debonding. Despite lower bond stiffness, GFRP bars remain a promising corrosion-resistant reinforcement when used with GPC.

Keywords: Geopolymer concrete; GFRP bars; Steel reinforcement; Bond-slip behaviour; Pull-out bond strength; Embedded length

1. Introduction:

Reinforced concrete made with ordinary Portland cement (OPC) and steel bars is vulnerable to reinforcement corrosion, particularly in marine, coastal and chemically aggressive environments. Corrosion causes cracking, spalling and loss of bond, and it raises maintenance and rehabilitation costs **[1,2].** This has encouraged the search for lower-impact cementitious matrices and corrosion-resistant reinforcement. Geopolymer concrete (GPC), made from alumino-silicate precursors such as fly ash and ground granulated blast-furnace slag (GGBS), is a promising alternative to OPC concrete. It uses industrial by-products, reduces Portland cement consumption and can match or exceed the mechanical and durability performance of conventional concrete **[3–5].** Its environmental benefit, however, depends on the precursor, activator, curing regime and mix design, and cannot be assumed **[5].** Glass fibre reinforced polymer (GFRP) bars offer corrosion resistance, low density and a high strength-to-weight ratio **[6–8].** Unlike steel, however, GFRP is an anisotropic, non-metallic composite with a low elastic modulus, and its bond depends on surface configuration and the resinfibre system **[7,9].** Reliable bond is essential for stress transfer, anchorage and crack control. Bond in reinforced concrete arises from chemical adhesion, friction and mechanical interlock. In deformed steel bars, rib interlock dominates once adhesion is overcome, whereas in GFRP bars the contribution of each mechanism depends on the surface treatment **[7,9,10].** The lower stiffness of GFRP also produces greater slip at comparable load

levels **[7,10].** Bond models and development-length equations for steel therefore cannot be applied directly to GFRP **[6,8].** Early pull-out studies showed that FRP bond differs from that of steel and is governed by bar type, diameter, surface characteristics, embedded length and concrete strength **[11–13].** Embedded length is especially influential: a longer embedded length raises the pull -out capacity but lowers the average bond stress, because stress transfer along the bar is non-uniform **[11,14].** Bond in GPC has been studied mainly for steel. Sarker **[16]** and Castel and Foster **[17]** found that bond in fly ash and fly ash/slag GPC can be favourable, but that it is sensitive to precursor composition and curing. Studies of GFRP in GPC are limited. Maranan et al. **[18]** reported that bar diameter and bond length significantly affect the bond of sand-coated GFRP bars in GPC, and that anchor heads can substantially raise pull-out capacity **[19].** A recent comparison of steel and sand-coated GFRP bars in GPC found lower bond capacity for GFRP and a different effect of bond length for each bar type **[20].** This reflects the different stress-transfer mechanisms: rib bearing and interlock for steel, and adhesion and friction for GFRP. Reviews confirm that GFRP bond depends on diameter, surface characteristics, concrete strength, embedded length and confinement, and that no universal bond–slip model exists **[6,8,15].** Existing work has mostly examined GFRP in conventional concrete, steel in GPC, or GFRP in a single geopolymer matrix **[21–23].** Direct comparisons of steel and GFRP bars in both GPC and OPC under identical conditions are scarce **[24,25],** and the combined effects of concrete grade, bar diameter and embedded length on their bond–slip response remain insufficiently established **[26–30].** This study therefore compares the bond behaviour of steel and GFRP bars in GPC and OPC of M20 and M40 grades, using 12 and 16 mm bars with embedded lengths of 100 and 150 mm. Pull-out tests were carried out together with compressive, flexural and split tensile strength tests. The aim is to quantify the effects of concrete type, grade, reinforcement type, bar diameter and embedded length on bond strength, slip and failure mode, and so to evaluate GFRP as a corrosion-resistant reinforcement for GPC.

2. Research Significance

The corrosion of steel reinforcement is a major cause of deterioration in reinforced concrete, and the use of Portland cement carries a high environmental cost. Combining GPC with GFRP bars could address both problems, but this depends on reliable bond between the two materials. Bond-slip data for GFRP bars in GPC are limited, and few studies compare steel and GFRP bars in GPC and OPC under identical conditions. This study provides such a comparison, covering two concrete grades (M20 and M40), two bar diameters (12 and 16 mm) and two embedded lengths (100 and 150 mm). The results give an experimental basis for assessing the anchorage and serviceability of GFRP-reinforced GPC. They can also guide the development of bond models and design provisions for sustainable, corrosion-resistant structures in aggressive environments.

3. Experimental Programme

3.1 Materials

OPC 53-grade cement (IS 12269) was used for the conventional concrete, with a 28-day strength of 53.5 MPa, a standard consistency of 30% and initial and final setting times of 35-and 600 min. Fly ash and GGBS, with specific gravities of 2.2 and 2.9, served as the aluminosilicate precursors for GPC. The alkaline activator was a sodium hydroxide and sodium silicate solution in a mass ratio of 2.5:1. Natural fine aggregate (IS 383:2016, Zone II, fineness modulus 2.59) and coarse aggregate had specific gravities of 2.65 and 2.68, respectively. Deformed Fe500 steel bars (yield strength 500 MPa) and GFRP bars (tensile strength 800-1000

MPa, elastic modulus 45-60 GPa) were used as reinforcement, (Figure 1). The GFRP bars had ribbed surface to develop bond through adhesion, friction and mechanical interlock. Bars of 12 and 16 mm diameter were tested in M20 and M40 OPC concrete and GPC with embedded lengths of 100 and 150 mm.



Figure 1. GFRP bars

3.2 Specimens and mix proportions.

OPC concrete and GPC of grades M20 and M40 were prepared in a mechanical mixer, using the mix proportions in Table 1. The GPC used fly ash and GGBS as binders, activated with sodium hydroxide and sodium silicate (1:2.5 by mass), and a superplasticizer at 3% of the binder. The concrete was placed in moulds in layers and compacted thoroughly. After 24 h, the specimens were water-cured until testing. Pull-out specimens were cured for 28 days.

Table 1. Mix proportions (kg/m³)

Material	GPC M20	GPC M40	OPC M20	OPC M40
Fly ash	252	240	-	-
GGBS	108	160	-	-
Cement	-	-	350	480
Total binder	360	400	350	480
Fine aggregate	720	773	710	660
Coarse aggregate	1080	1042	1148	1098
NaOH	64.3	68.57	-	-
Na_2SiO_3	160.7	171.43	-	-
Water	-	-	192	192

3.3 **Fresh and hardened concrete tests.** Workability was measured by the slump and compaction factor tests (IS 1199). Compressive strength was determined on 150 mm cubes (IS 516), split tensile strength on 150 × 300 mm cylinders (IS 5816), and flexural strength on beams (IS 516).

3.4 **Pull-out bond test:** Pull-out tests followed IS 2770 on 150 mm cubes with a centrally placed steel or GFRP bar (12 or 16 mm diameter). The bar was embedded for 100 or 150 mm, and the remaining length was isolated with a pipe or tape to prevent bonding. After 28 days of curing, load was applied gradually until pull-out failure. The load at the onset of slip and the maximum load were recorded. The average bond stress was calculated as

$\tau_b = P / (\pi\ db\ Lb)$

where P is the pull-out load, db the nominal bar diameter and Lb the embedded length. Bondslip curves were obtained by plotting bond stress against measured slip for each combination of concrete type, grade, bar type, diameter and embedded length.

1.1 Fresh Concrete Properties

1.1.1 Slump Test

The workability of the conventional concrete and geopolymer concrete mixtures was evaluated using the slump test. The measured slump values were 75 mm and 60 mm for M20 and M40 OPC concrete, respectively, whereas the corresponding GPC mixtures exhibited slump values of 90 mm and 80 mm shown in Table . The results indicate that the GPC mixtures generally exhibited higher workability than the corresponding OPC mixtures. The higher slump observed for GPC can be attributed to the presence of the alkaline activating solution and the characteristics of the fine binder materials. For M20 concrete, the slump increased from 75 mm for OPC to 90 mm for GPC, representing an increase of approximately 20%. Similarly, for M40 concrete, the slump increased from 60 mm for OPC to 80 mm for GPC. These results indicate that the geopolymer mixtures developed satisfactory fresh-state workability for casting and compaction. The reported slump values and workability classifications are presented in **Table 2.**

Table 2: Slump comparison for OPC concrete and GPC

Concrete Type	**Grade**	**Slump (mm)**	**Workability**
OPC	M20	75 mm	Medium
OPC	M40	60 mm	Medium-Low
GPC	M20	90 mm	Medium-High
GPC	M40	80 mm	Medium

1.1.2 Compaction Factor

The compaction factor results further confirmed the improved workability of the GPC mixtures. The compaction factor was 0.92 for M20 OPC and 0.89 for M40 OPC, while values of 0.95 and 0.93 were obtained for M20 and M40 GPC, respectively shown in Tabl. Thus, GPC exhibited higher compaction factors than the corresponding OPC mixtures. The higher compaction factor suggests that the geopolymer mixtures required comparatively less effort to achieve adequate compaction. The results are consistent with the slump-test observations and demonstrate that the fresh GPC mixtures possessed satisfactory workability characteristics.

Table 3: Workability comparison for OPC concrete and GPC by compaction factor test

Concrete Type	Grade	Compaction Factor	Workability
OPC	M20	0.92	Medium
OPC	M40	0.89	Medium-Low
GPC	M20	0.95	High
GPC	M40	0.93	Medium-High

1.2 Mechanical Properties of Hardened Concrete

The hardened concrete properties were evaluated in terms of compressive strength, flexural strength, splitting tensile strength and reinforcement–concrete bond strength. The experimental program included M20 and M40 grades of both OPC and GPC, reinforced with steel and GFRP bars of 12- and 16-mm diameter and embedment lengths of 100 and 150 mm.

1.2.1 Compressive Strength

The average compressive strength of M20 OPC concrete was 20 MPa, whereas M20 GPC achieved 21 MPa. For M40 concrete, the compressive strength increased from 40 MPa for OPC to 41 MPa for GPC. Thus, the GPC mixtures achieved slightly higher compressive strength than their corresponding OPC mixtures. The increase in compressive strength of GPC may be associated with the development of a comparatively dense geopolymeric binder matrix. The results demonstrate that the investigated geopolymer concrete was capable of achieving compressive strengths comparable to those of conventional OPC concrete at both M20 and M40 grades.

1.2.2 Flexural Strength

The flexural strength of the M20 OPC concrete was found to be an average of 2.9 MPa, whereas that of the M20 GPC concrete was 3.1 MPa. For the M40 concrete, the flexural strength was found to range from 4.2 MPa (OPC) to 4.4 MPa (GPC). The improvement in flexural strength indicates that the geopolymer matrix provided adequate resistance to tensile stresses generated during flexural loading. The slightly higher flexural strength of GPC compared with OPC is consistent with its higher compressive strength.

1.2.3 Splitting Tensile Strength

The average splitting tensile strength of M20 OPC concrete was 2.3 MPa, while M20 GPC exhibited a value of 2.46 MPa. For M40 concrete, the corresponding values were 3.4 MPa and

3.55 MPa for OPC and GPC, respectively. The results indicate that GPC developed slightly higher tensile resistance than OPC at both strength grades. This improvement can be related to the relatively dense binder matrix and improved adhesion within the geopolymeric concrete system.

Table 4: Bond strength comparison for steel and GFRP

Dia	Embed	Grade	Concrete	Reinforcement	Bond (MPa)	Flexural (MPa)	Split (MPa)	Compressive (MPa)
12	100	M20	OPC	Steel	10.5	2.9	2.3	20
12	100	M20	OPC	GFRP	12.46	2.9	2.3	20

12	100	M20	GPC	Steel	13.5	3.1	2.5	22
12	100	M20	GPC	GFRP	12	3	2.4	21
12	150	M20	OPC	Steel	8.17	2.9	2.3	20
12	150	M20	OPC	GFRP	8.66	2.9	2.3	20
12	150	M20	GPC	Steel	10.8	3.1	2.5	22
12	150	M20	GPC	GFRP	7.43	3	2.4	21
16	100	M20	OPC	Steel	10.14	2.9	2.3	20
16	100	M20	OPC	GFRP	10.35	2.9	2.3	20
16	100	M20	GPC	Steel	12.79	3	2.4	21
16	100	M20	GPC	GFRP	9.57	3	2.4	21
16	150	M20	OPC	Steel	7.82	2.9	2.3	20
16	150	M20	OPC	GFRP	8.1	2.9	2.3	20
16	150	M20	GPC	Steel	10.5	3	2.4	21
16	150	M20	GPC	GFRP	10.59	3	2.4	21
12	100	M40	OPC	Steel	14.72	4.2	3.4	40
12	100	M40	OPC	GFRP	17.64	4.2	3.4	40
12	100	M40	GPC	Steel	17.5	4.4	3.6	42
12	100	M40	GPC	GFRP	15.34	4.3	3.5	41
12	150	M40	OPC	Steel	11.49	4.2	3.4	40
12	150	M40	OPC	GFRP	13.34	4.2	3.4	40
12	150	M40	GPC	Steel	14.2	4.4	3.6	42
12	150	M40	GPC	GFRP	10.73	4.3	3.5	41
16	100	M40	OPC	Steel	14.4	4.2	3.4	40
16	100	M40	OPC	GFRP	14.6	4.2	3.4	40
16	100	M40	GPC	Steel	16.34	4.3	3.5	41
16	100	M40	GPC	GFRP	15.1	4.3	3.5	41
16	150	M40	OPC	Steel	11.14	4.2	3.4	40
16	150	M40	OPC	GFRP	11.5	4.2	3.4	40
16	150	M40	GPC	Steel	13.13	4.3	3.5	41
16	150	M40	GPC	GFRP	10.6	4.3	3.5	41

1.3 Bond Strength of Steel and GFRP Reinforcement

Bond behaviour was evaluated through pull-out tests (Fig. 2, Table 4). The test variables were concrete type, reinforcement type, bar diameter and embedded length. The results show that bond strength depends on both the reinforcement type and the surrounding concrete matrix. For M20 concrete with 12 mm bars and a 100 mm embedded length, the bond strengths in GPC were 13.5 MPa for steel and 12.0 MPa for GFRP. The corresponding OPC values were 10.5 MPa and 12.46 MPa. For M40 concrete with the same bar diameter and embedded length, the bond strengths in GPC were 17.5 MPa for steel and 15.34 MPa for GFRP. The OPC values were 14.72 MPa and 17.64 MPa, respectively. Bond strength increased with concrete grade from M20 to M40 for all combinations. This is attributed to the higher strength of the matrix, which offers greater resistance to splitting and interfacial failure. Across all test series, the average bond strength in GPC was 13.60 MPa for steel and 11.42 MPa for GFRP. In OPC, the averages were 11.05 MPa for steel and 12.08 MPa for GFRP. The higher bond strength of steel in GPC is attributed to the mechanical interlocking of its deformed ribs and its high stiffness. GFRP has high tensile strength and corrosion resistance, but its elastic modulus is much lower than that of steel. This leads to greater deformation and slip during pull-out loading. response.

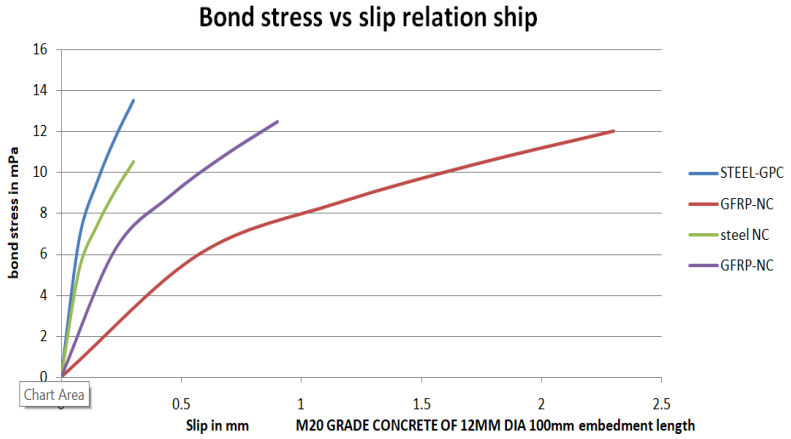
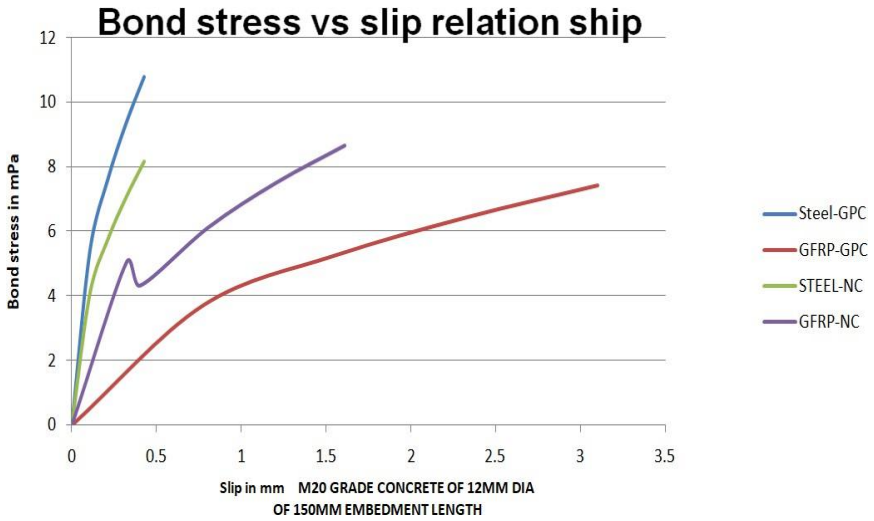


Figure 2: Graph showing bond stress vs slip relationship of m20 grade concrete of 12mm Dia 100mm embedment length

1.4 Bond Stress–Slip Behaviour



The bond stress–slip response was investigated for M20 and M40 concrete using 12 mm and 16 mm diameter bars with embedded lengths of 100 mm and 150 mm. For M20 GPC with 12 mm bars and a 100 mm embedded length, the steel bar reached a maximum bond stress of 13.5 MPa at a slip of about 0.30 mm. The GFRP bar reached 12.0 MPa at a slip of about 2.30 mm. For the 150 mm embedded length, the maximum bond stresses in GPC were 10.8 MPa for steel and 8.665 MPa for GFRP (Fig. 4). In both cases, GFRP bars developed considerably more slip than steel bars before reaching peak bond stress.

Figure 3. Graph showing bond stress vs slip relationship of M20 grade concrete of 12mm dia 150mm embedment length

A similar trend was observed for M40 GPC. For 12 mm bars with a 100 mm embedded length, the maximum bond stresses were 17.5 MPa for steel and 15.34 MPa for GFRP. These values are higher than those obtained for M20 GPC, which shows the beneficial influence of concrete strength on bond resistance (Fig. 5). For 16 mm bars with a 100 mm embedded length in M40 GPC, the maximum bond stresses were 16.34 MPa for steel and 15.10 MPa for GFRP. With a 150 mm embedded length, the

corresponding values were 13.13 MPa and 11.498 MPa, respectively.

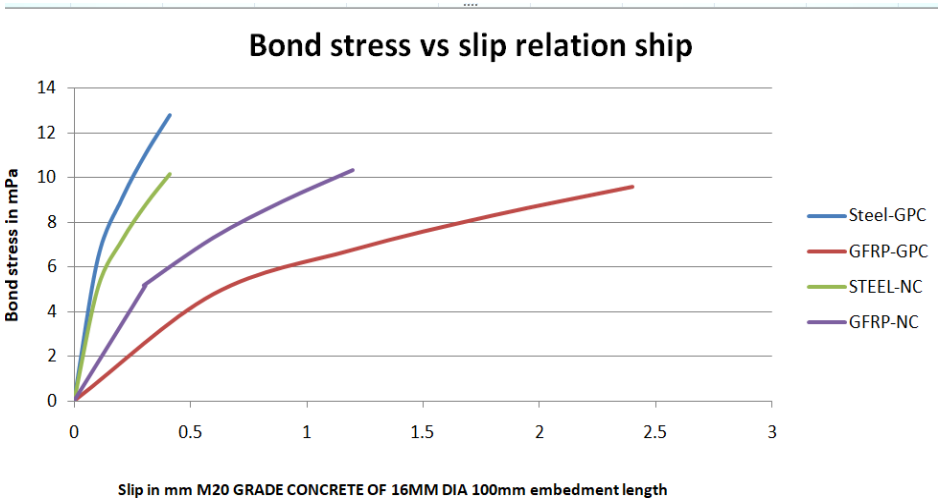


Figure 4. Graph showing bond stress vs slip relationship of M20 grade concrete of 16mm dia 100mm embedment length

The bond stress–slip response shows that steel bars generally developed a higher peak bond stress and lower slip than GFRP bars. This is attributed to the higher stiffness and mechanical interlocking of deformed steel bars. The lower elastic modulus of GFRP allows greater deformation, which results in larger slip at or near the peak bond stress.

1.5 Effect of Embedment Length

Figure 5: shows that embedded length has a significant influence on the measured bond strength. In general, increasing the embedded length from 100 mm to 150 mm reduced the average bond stress. For example, in M40 GPC with 12 mm steel bars, the maximum bond stress decreased from 17.5 MPa at 100 mm to 14.2 MPa at 150 mm. For GFRP bars, it decreased from 15.34 MPa to 11.494 MPa.

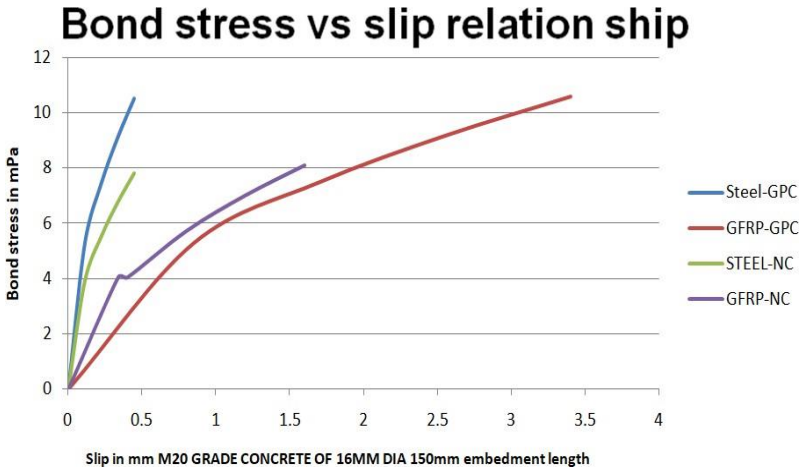


Figure 5: Graph showing bond stress vs slip relationship of m20 grade concrete of 16mm dia 150mm embedment length

This behaviour is explained by the non-uniform distribution of bond stress along the embedded length. As the embedded length increases, the additional bonded surface does not contribute proportionally to

the bond resistance, because the stress is concentrated near the loaded end of the bar (Fig. 7).

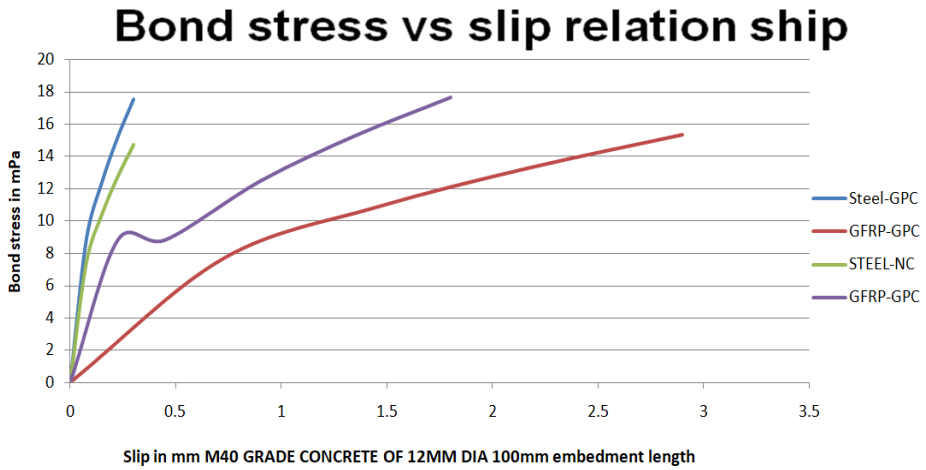


Figure 2. Graph showing bond stress vs slip relationship of m40 grade concrete of 12mm dia 100mm embedment length

The experimental results show that geopolymer concrete can achieve mechanical properties comparable to, and in some cases slightly higher than, those of conventional OPC concrete. The M20 and M40 GPC mixtures had compressive strengths of 21 MPa and 41 MPa, compared with 20 MPa and 40 MPa for OPC. Similar trends were observed for flexural and splitting tensile strength in both grades. The bond results show that concrete grade, reinforcement type, bar diameter and embedded length all influence the reinforcement-concrete interaction. Increasing the concrete grade from M20 to M40 generally increased bond resistance, while increasing the embedded length reduced the average bond stress. Steel bars generally showed higher bond strength and lower slip than GFRP bars, owing to their higher stiffness and the mechanical interlocking provided by the deformed surface. Although GFRP showed lower bond strength and greater slip in several test configurations, its corrosion resistance and low weight are significant advantages in aggressive environments. GFRP can therefore be considered a viable alternative reinforcement for geopolymer concrete where durability and corrosion resistance are priorities, while steel remains preferable where maximum bond strength and stiffness are required.

Conclusions

Based on the experimental investigation of M20 and M40 OPC and geopolymer concrete reinforced with steel and GFRP bars, the following conclusions are drawn:

1. Geopolymer concrete showed higher workability than OPC, with slump values of 90 mm and 80 mm for M20 and M40 GPC, compared with 75 mm and 60 mm for OPC. The compressive strengths of M20 and M40 GPC (21 and 41 MPa) were comparable to those of OPC (20 and 40 MPa).

2. Geopolymer concrete showed slightly higher flexural strength (3.1 and 4.4 MPa) and splitting tensile strength (2.46 and 3.55 MPa) than OPC (2.9 and 4.2 MPa; 2.3 and 3.4 MPa) for M20 and M40, respectively.

3. Steel bars generally showed higher bond strength than GFRP bars in GPC. For M40 GPC with 12 mm bars and a 100 mm embedded length, the maximum bond strengths were 17.50 MPa for steel and 15.34 MPa for GFRP. Bond strength increased with concrete grade from M20 to M40 for both bar types, owing to the greater strength of the surrounding concrete matrix.

4. Increasing the embedded length from 100 mm to 150 mm generally reduced the average bond stress. In M40 GPC, the bond strength of steel decreased from 17.50 MPa to 14.20 MPa, and that of GFRP from 15.34 MPa to 11.49 MPa.

5. Steel bars developed high bond strength with small slip and failed mainly by pull-out with crushing of concrete near the ribs. GFRP bars showed greater slip before and around the peak bond stress and failed mainly by debonding. No brittle failure was observed in the GPC specimens.

6. Geopolymer concrete achieved mechanical and bond properties comparable to OPC. Steel is preferable where maximum bond capacity and stiffness are required, while GFRP is a viable reinforcement for GPC where corrosion resistance and durability are priorities.

References

1. Neville, A. (1999). The confused world of sulfate attack on concrete. *Cement and Concrete Research, 29*(5), 673–675.

2. Tuutti, K. (1982). *Corrosion of steel in concrete*. Swedish Cement and Concrete Research Institute, Stockholm.

3. Davidovits, J. (1991). Geopolymers: Inorganic polymeric new materials. *Journal of Thermal Analysis, 37*, 1633–1656.

4. Provis, J. L., & van Deventer, J. S. J. (Eds.). (2009). *Geopolymers: Structures, processing, properties and industrial applications*. Woodhead Publishing.

5. Habert, G., d'Espinose de Lacaillerie, J. B., & Roussel, N. (2011). An environmental evaluation of geopolymer based concrete production: Reviewing current research trends. *Journal of Cleaner Production, 19*(11), 1229–1238. https://doi.org/10.1016/j.jclepro.2011.03.012

6. Benmokrane, B., Tighiouart, B., & Chaallal, O. (1996). Bond strength and load distribution of composite GFRP reinforcing bars in concrete. *ACI Materials Journal, 93*(3), 254–259.

7. Yan, F., Lin, Z., & Yang, M. (2016). Bond mechanism and bond strength of GFRP bars to concrete: A review. *Composites Part B: Engineering, 98*, 56–69. https://doi.org/10.1016/j.compositesb.2016.04.068

8. D'Antino, T., Bertolli, V., Pisani, M. A., & Poggi, C. (2023). Tensile and interlaminar shear behavior of thermoset and thermoplastic GFRP bars exposed to alkaline environment. *Journal of Building Engineering, 72*, 106581. https://doi.org/10.1016/j.jobe.2023.106581

9. Kakhki, S. A. E., & Kheyroddin, A. (2025). Bond behavior of fiber reinforced polymer bars in concrete: A review. *International Journal of Concrete Structures and Materials, 19*, 120. https://doi.org/10.1186/s40069-025-00859-0

10. Saad, S., & Polak, M. A. (2025). Bond behavior of glass fiber-reinforced polymer (GFRP) bars embedded in concrete: A review. *Materials, 18*(14), 3367. https://doi.org/10.3390/ma18143367

11. Achillides, Z., & Pilakoutas, K. (2004). Bond behavior of fiber reinforced polymer bars under direct pullout conditions. *Journal of Composites for Construction, 8*(2), 173–181. https://doi.org/10.1061/(ASCE)1090-0268(2004)8:2(173)

12. Okelo, R., & Yuan, R. L. (2005). Bond strength of fiber reinforced polymer rebars in normal strength concrete. *Journal of Composites for Construction, 9*(3), 203–213. https://doi.org/10.1061/(ASCE)1090-0268(2005)9:3(203)



13. Tastani, S. P., & Pantazopoulou, S. J. (2006). Bond of GFRP bars in concrete: Experimental study and analytical interpretation. *Journal of Composites for Construction*, *10*(5), 381–391. https://doi.org/10.1061/(ASCE)1090- 0268(2006)10:5(381)

14. Wambeke, B. W., & Shield, C. K. (2006). Development length of glass fiber-reinforced polymer bars in concrete. *ACI Structural Journal*, *103*(1), 11–17. https://doi.org/10.14359/15081

15. Baena, M., Torres, L., Turon, A., & Barris, C. (2009). Experimental study of bond behaviour between concrete and FRP bars using a pull-out test. *Composites Part B: Engineering*, *40*(8), 784–797. https://doi.org/10.1016/j.compositesb.2009.07.003

16. Experimental investigations on the bond behavior between concrete and FRP reinforcing bars. (2018). *Construction and Building Materials*, *173*, 136–148. https://doi.org/10.1016/j.conbuildmat.2018.03.169

17. Experimental study on the bond behavior of GFRP bars in normal and self-consolidating concrete. (2018). *Construction and Building Materials*, *189*, 869–881. https://doi.org/10.1016/j.conbuildmat.2018.09.045

18. Rahman, M. M., Cope, C. T., Abavisani, I., D'Antino, T., Focacci, F., & Carloni, C. (2025). Comprehensive study of GFRP bar-concrete bond behavior using pull-out and three-point bending tests. *Journal of Building Engineering*, *108*, 112819. https://doi.org/10.1016/j.jobe.2025.112819

19. Sarker, P. K. (2011). Bond strength of reinforcing steel embedded in fly ash-based geopolymer concrete. *Materials and Structures*, *44*, 1021–1030. https://doi.org/10.1617/s11527-010-9683-8

20. Castel, A., & Foster, S. J. (2015). Bond strength between blended slag and Class F fly ash geopolymer concrete with steel reinforcement. *Cement and Concrete Research*, *72*, 48–53. https://doi.org/10.1016/j.cemconres.2015.02.016

21. Maranan, G. B., Manalo, A. C., Karunasena, W. M., & Benmokrane, B. (2015). Bond stress-slip behavior: Case of GFRP bars in geopolymer concrete. *Journal of Materials in Civil Engineering*, *27*(1), 04014116. https://doi.org/10.1061/(ASCE)MT.1943-5533.0001046

22. Maranan, G. B., Manalo, A. C., Karunasena, W. M., & Benmokrane, B. (2015). Pullout behaviour of GFRP bars with anchor head in geopolymer concrete. *Composite Structures*, *132*, 1113–1121. https://doi.org/10.1016/j.compstruct.2015.07.021

23. Romanazzi, V., Leone, M., Aiello, M. A., & Pecce, M. R. (2022). Bond behavior of geopolymer concrete with steel and GFRP bars. *Composite Structures*, *300*, 116150. https://doi.org/10.1016/j.compstruct.2022.116150

24. Peng, K.-D., Zeng, J.-J., Huang, B.-T., Huang, J.-Q., Zhuge, Y., & Dai, J.-G. (2022). Bond performance of FRP bars in plain and fiber-reinforced geopolymer under pull-out loading. *Journal of BuildingEngineering*, *57*, 104893. https://doi.org/10.1016/j.jobe.2022.104893

25. Rather, S. A., et al. (2024). Experimental investigation on bond behaviour of the GFRP bars with normal and high strength geopolymer concrete. *Construction and Building Materials*, *429*, 136395. https://doi.org/10.1016/j.conbuildmat.2024.136395

26. Guruprasad, T. N., Prashanth, M. H., Mahanthesh, H. S., & Narasimhan, M. C. (2026). Experimental investigation on the bond behavior of the GFRP bars with one-part geopolymer concrete and conventional concrete. *Research on Engineering Structures & Materials*. https://doi.org/10.17515/resm2026-1474me0122rs

EMBODIED CARBON ASSESSMENT OF EXPANDED POLYSTYRENE (EPS) LIGHTWEIGHT CONCRETE: TRADE-OFFS BETWEEN DENSITY REDUCTION AND CARBON NEUTRALITY

Nandika Srinivas Rao[1*], Uma Shankar Biswal[2], N. Sudharsan[2,]

[1]*UltraTech Cement Limited, Hyderabad, Telangana, India*

[2]*Department of Civil Engineering, Vidya Jyothi Institute of Technology, Hyderabad, Telangana, India*

**Corresponding author: Nandika Srinivas Rao (email: nandika.rao@adityabirla.com)*

ABSTRACT

Lightweight concrete incorporating Expanded Polystyrene (EPS) beads as a partial replacement for coarse aggregate is widely promoted as a low-carbon construction material, primarily on the basis of reduced self-weight and lower cement demand per unit volume. This study examines whether that assumption holds when embodied carbon is quantified directly, using experimental data from three EPS lightweight concrete trial mixes incorporating 23% Class C fly ash as a supplementary cementitious material. The trial mixes achieved fresh densities of 726, 1337 and 1440 kg/m³, with corresponding 28-day compressive strengths of 1.03, 7.82 and 10.35 MPa respectively. Embodied CO_2 was estimated for each mix from constituent quantities using established emission factors for cement, fly ash, fine aggregate, EPS beads and chemical admixtures, and benchmarked against a conventional M25 concrete of 2400 kg/m³ density. The results indicate a density-dependent, non-monotonic carbon outcome: the lowest-density mix showed an approximately 24% reduction in embodied CO_2 relative to the conventional control, but at a compressive strength of only 1.03 MPa; the two higher-density, structurally relevant mixes showed embodied CO_2 approximately 9–12% higher than the control, because cement content per cubic metre was not reduced and the embodied carbon of the EPS beads themselves partially offset the mass savings from reduced aggregate volume. These findings indicate that density reduction via EPS substitution does not automatically translate into embodied-carbon savings for structurally usable lightweight concrete, and that genuine decarbonisation in this material class depends on simultaneously reducing cement content — through higher SCM replacement or alternative binders — rather than relying on EPS substitution in isolation.

Keywords: *Lightweight concrete; Expanded Polystyrene (EPS); Embodied carbon; Fly ash; Carbon neutrality; Compressive strength*

1. Introduction

Reducing the carbon footprint of concrete construction is central to India's Net Zero targets and to the themes of this Conference. Cement manufacture alone accounts for a substantial share of India's industrial CO_2 emissions, and any strategy that reduces concrete's material demand or shifts its constituents toward lower-carbon alternatives is, in principle, relevant to decarbonisation of the built environment. Lightweight concrete produced using Expanded Polystyrene (EPS) beads as a partial or full replacement for coarse aggregate is frequently presented in the literature as one such strategy: EPS reduces concrete density by up to 50–70%, lowers structural dead load, improves thermal insulation, and is manufactured from recycled or waste polystyrene in several reported studies.



However, the claim that EPS lightweight concrete (EPS-LWC) is inherently 'low-carbon' or supports carbon-neutral construction is rarely tested by direct quantification of embodied CO_2. Reduced density is not the same as reduced embodied carbon: EPS itself carries a non-trivial manufacturing carbon footprint (it is a petrochemical-derived product), and if cement content per unit volume is not correspondingly reduced, the carbon-reduction narrative built around lightweight concrete may not hold. This is particularly relevant given that EPS is typically used to displace coarse aggregate — a low-embodied-carbon constituent — rather than cement, which is the dominant contributor to concrete's carbon footprint.

This paper re-examines experimental trial-mix data for EPS-LWC incorporating fly ash as a supplementary cementitious material, originally developed to characterise density, workability and compressive strength, and extends that data with a direct embodied-carbon assessment. The objective is not to propose a new mix design, but to test whether the density reduction achieved in these mixes corresponds to a genuine reduction in embodied CO_2, and to identify the conditions under which EPS-LWC does or does not support carbon-neutral construction goals.

2. Literature Review

Mandlik et al. [1] reviewed the use of EPS as a lightweight aggregate and geofoam material, noting unit weight variation from 1200–2000 kg/m³ for EPS waste aggregate in structural concrete and highlighting cost-effectiveness and waste-utilisation benefits, but did not quantify embodied carbon. Ashish et al. [2] compared conventional M25 concrete with EPS-fly ash lightweight concrete at EPS replacement levels of 5–30%, finding that 5% EPS content gave the highest compressive strength (8 N/mm² and 11 N/mm² at 7 and 28 days) among the EPS variants tested, with strength decreasing as EPS content increased — consistent with the strength–density trend observed in the present trial mixes.

Borkar and Singi [7] examined EPS bead size (1.0–6.3 mm) and the addition of silica fume and polypropylene fibres to improve bond strength and shrinkage behaviour in structural lightweight EPS concrete, underscoring that EPS-LWC's mechanical performance depends heavily on mix-specific modifications rather than EPS content alone. Kavinkumar et al. [5] and Karthiga Murugan et al. [6] studied alternative lightweight fillers (cenospheres, pumice, LECA) and reported that fly ash replacement up to 25% improved strength compatibility — supporting the use of 23% fly ash in the present mixes as a reasonable SCM dosage.

None of the reviewed studies quantified embodied CO_2 or life-cycle carbon impact directly; carbon-related claims in this literature are consistently framed qualitatively ("reduced dead load", "sustainable", "environmentally friendly") rather than through material-flow-based emission accounting. This is a recognised gap: reduced density is frequently used as a proxy for reduced environmental impact in lightweight-concrete research, without verifying that binder content — the dominant source of concrete's embodied carbon — is actually reduced. The present study addresses this gap directly for the specific case of fly-ash-blended EPS-LWC.

3. Materials and Methodology

3.1 Materials

The trial mixes used OPC 53-grade cement conforming to IS 12269-1987, Class C fly ash (IS 3812-2003) at a constant 23% replacement of cementitious mass, clean river sand as fine aggregate (sieved through 4.75 mm), and EPS beads of 2–5 mm diameter (density 12 kg/m³) as a partial replacement for

coarse aggregate. Air entraining admixture (0.2% of cement weight) and CAC-Superflow water-reducing admixture (0.9% of cement weight) were used to control workability and air content. No coarse aggregate was used in any trial mix; EPS beads served as the sole lightweight filler.

3.2 Mix Design

Table 1 presents the constituent quantities for the three trial mixes, all normalised to 1 m³ of concrete. The three mixes span a wide density range (726–1440 kg/m³) through variation in cement, fly ash and fine-aggregate content, with EPS content varying inversely with the other solid constituents to achieve the target density.

Table 1: Mix design of trial mixes (per m³)

Materials	Trial Mix 1	Trial Mix 2	Trial Mix 3
Cement (kg)	408	250	420
Fly ash – 23% (kg)	125	75	125
Fine aggregate (kg)	888	553	1199
EPS (kg)	8.9	14.85	7.4
Superflow – 0.9% (kg)	4.82	2.925	4.725
Air PL – 0.2% (kg)	1.04	0.65	1.05
W/B ratio	0.368	0.378	0.40
Fresh density (kg/m³)	**1337**	**726**	**1440**

3.3 Test Methods

Fresh density, slump (IS 1199-1959) and compressive strength at 7, 14 and 28 days (IS 516-1959) were determined for 150 × 150 × 150 mm cubes cured under standard water-curing conditions. Table 2 summarises the measured fresh and hardened properties for each trial mix.

Table 2: Fresh and hardened properties of trial mixes

Property	Trial Mix 1	Trial Mix 2	Trial Mix 3
Density (kg/m³)	1337	726	1440
Slump (mm)	50	0	55
7-day strength (MPa)	4.29	0.663	7.84
14-day strength (MPa)	6.32	0.893	9.22
28-day strength (MPa)	**7.82**	**1.03**	**10.35**

4. Embodied Carbon Estimation Methodology

Embodied CO_2 for each trial mix was estimated using a material-flow (bottom-up) approach: the mass of each constituent per cubic metre (Table 1) was multiplied by a constituent-specific CO_2 emission factor (Table 3) and summed, following the standard cradle-to-gate approach used in concrete life-cycle assessment (LCA) literature. Emission factors were drawn from the Inventory of Carbon and Energy (ICE) database and published cement life-cycle studies representative of Indian OPC production. Class C fly ash was assigned a low allocated burden (0.01 kg CO_2e/kg) consistent with its status as an industrial by-product whose primary emissions are attributed to the parent thermal power generation process. EPS beads, being a petrochemical-derived, closed-cell polystyrene product, were assigned an emission factor of 3.4 kg CO_2e/kg — substantially higher per unit mass than any other constituent, though its contribution to total mix mass is small.

Equation: *Embodied CO_2 (kg CO_2e/m^3) = Σ (mass of constituent, kg/m^3 × emission factor, kg CO_2e/kg)*

Table 3: Emission factors used for embodied-carbon estimation

A conventional M25 concrete mix (400 kg cement, 650 kg sand, 1200 kg coarse aggregate per m^3, density ≈ 2400 kg/m^3, no fly ash or EPS) was used as the reference control, representing typical normal-weight concrete (NWC) practice in India. This benchmark yields an embodied CO_2 of 357.7 kg CO_2e/m^3, against which the three EPS-LWC trial mixes were compared. It should be noted that this analysis covers only the cradle-to-gate embodied carbon of raw materials, and does not include transport, batching, placement energy, or carbonation uptake during service life; these are acknowledged as limitations addressed in Section 7.

Constituent	Emission factor	Basis
OPC 53-grade cement	0.83 kg CO_2e/kg	Indian OPC LCA studies [9]
Class C fly ash	0.01 kg CO_2e/kg	Waste by-product, low allocated burden
Fine aggregate (sand)	0.0139 kg CO_2e/kg	ICE database [8]
EPS beads	3.4 kg CO_2e/kg	ICE database [8], polystyrene production
Chemical admixtures	1.5 kg CO_2e/kg	Approximate factor for polymer-based admixtures

5. Results and Discussion

5.1 Fresh and Hardened Properties

As shown in Table 2 and Fig. 1, compressive strength increased consistently with density across all three curing ages, consistent with the general EPS-LWC literature [1, 2, 7]. Trial Mix 2 (726 kg/m^3) recorded zero slump and 28-day strength of only 1.03 MPa — too low for structural use, but sufficient to float on water, consistent with insulation-grade or void-fill applications. Trial Mixes 1 and 3 (1337 and 1440 kg/m^3) achieved 28-day strengths of 7.82 and 10.35 MPa respectively, positioning them in the range suitable for non-load-bearing or lightly loaded structural elements such as partition walls and precast panels, per the classification of lightweight concrete for masonry units (800–1400 kg/m^3) and structural purposes (1400–1800 kg/m^3).

5.2 Embodied Carbon Analysis

Table 4 and Fig. 2 present the embodied CO_2 results. Contrary to the common assumption that reduced density directly implies reduced embodied carbon, the results show a non-monotonic relationship. Trial Mix 2, the lowest-density mix, achieved a genuine 24.0% reduction in embodied CO_2 relative to the conventional M25 control. However, Trial Mixes 1 and 3 — the two mixes with structurally meaningful compressive strength — showed embodied CO_2 approximately 9.4% and 11.9% higher than the control, despite being 44.3% and 40.0% lighter by density.

This outcome arises because cement content per cubic metre in Trial Mixes 1 and 3 (408 and 420 kg/m³) was not reduced relative to the control (400 kg/m³) — in fact, Trial Mix 3 used marginally more cement. Since cement is by far the dominant source of embodied carbon in concrete (accounting for over 85% of total mix CO_2 in the control), any volume of aggregate displaced by EPS does not translate into a carbon saving unless the binder content is itself reduced. Compounding this, EPS — despite contributing only 7–15 kg/m³ by mass — carries a disproportionately high emission factor (3.4 kg CO_2e/kg against 0.0139 for the sand it partly displaces), so its own embodied carbon (25–50 kg CO_2e/m³ across the three mixes) is not negligible and further erodes any density-driven saving.

5.3 Carbon Intensity per Unit Strength

Fig. 3 presents embodied CO_2 normalised to 28-day compressive strength (kg CO_2e per m³ per MPa), a metric that captures carbon efficiency relative to structural utility. Trial Mix 2 shows a carbon intensity of 263.9 kg CO_2e/m³/MPa — more than five times higher than Trial Mixes 1 and 3 (50.0 and 38.7 kg CO_2e/m³/MPa respectively), despite its lower absolute embodied CO_2. This indicates that while Trial Mix 2 has the lowest total carbon footprint per cubic metre, it is by far the least carbon-efficient option when structural performance is accounted for. Trial Mix 3, despite having the highest absolute embodied CO_2, is the most carbon-efficient per unit of strength delivered. This distinction is important for design decisions: specifying EPS-LWC purely on the basis of density or total CO_2 per m³, without reference to the structural performance actually required, can lead to carbon-inefficient outcomes.

Fig. 1: Compressive strength development of trial mixes

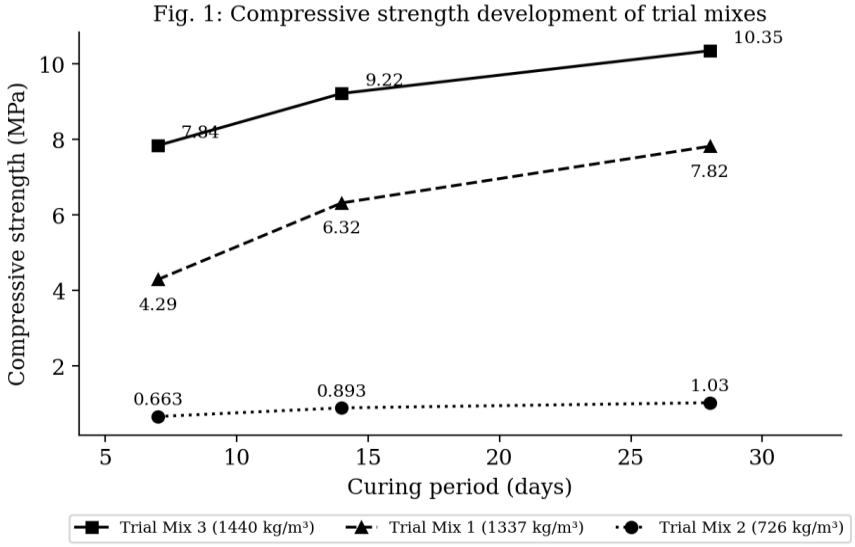


Fig. 1: Compressive strength development of trial mixes

Fig. 2: Embodied CO_2 of trial mixes vs. conventional M25 control

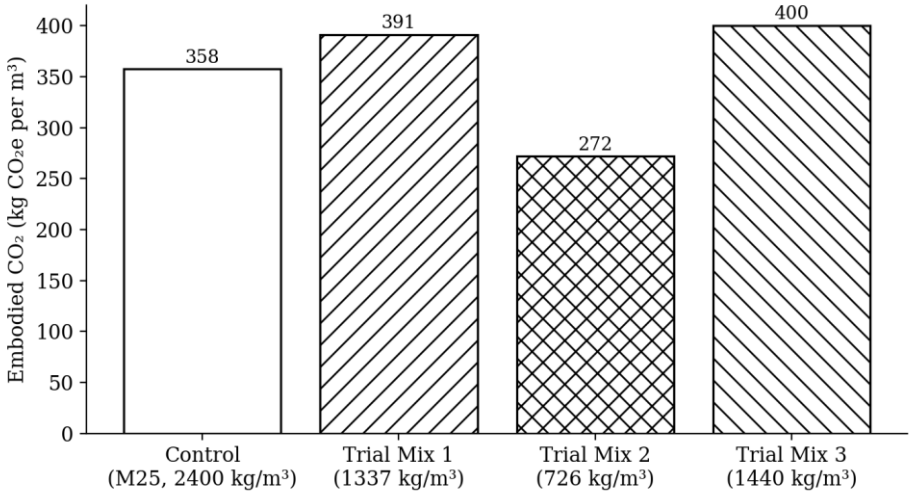


Fig. 2: Embodied CO_2 of trial mixes vs. conventional M25 control

Table 4: Embodied carbon summary

Parameter	Trial Mix 1	Trial Mix 2	Trial Mix 3
Embodied CO_2 (kg CO_2e/m^3)	391.3	271.8	400.3
Change vs. control (%)	+9.4%	−24.0%	+11.9%
CO_2 per MPa (kg CO_2e/m^3/MPa)	50.04	263.87	38.68
Density reduction vs. NWC (%)	44.3%	69.8%	40.0%

Fig. 3: Carbon intensity normalised to 28-day strength

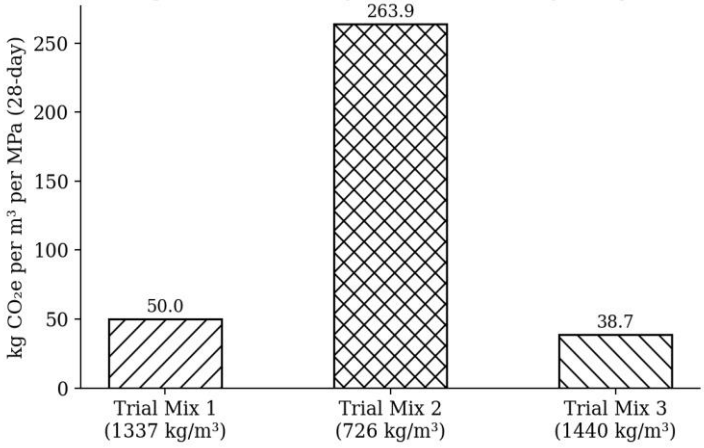


Fig. 3: Carbon intensity normalised to 28-day strength

6. Conclusion

This study quantified the embodied carbon of three EPS lightweight concrete trial mixes incorporating 23% fly ash and compared them against a conventional M25 concrete benchmark. The key findings are:



1. Density reduction via EPS substitution does not automatically reduce embodied carbon. Only the lowest-density, non-structural mix (726 kg/m³) showed a genuine CO_2 reduction (24.0%); the two structurally usable mixes (1337 and 1440 kg/m³) showed 9.4% and 11.9% higher embodied CO_2 than conventional concrete.
2. The primary reason is that cement content per cubic metre was not reduced in the higher-density mixes, and EPS itself carries a non-negligible per-kilogram carbon footprint that offsets the mass reduction achieved by displacing aggregate.
3. Carbon efficiency per unit of strength delivered (kg CO_2e/m^3/MPa) strongly favours the higher-density, higher-strength mixes, indicating that low-density EPS-LWC is carbon-inefficient when actual structural demand is considered.
4. Claims of inherent carbon neutrality or low-carbon performance for EPS-LWC should be substantiated through direct embodied-carbon quantification rather than inferred from density reduction alone.

   For EPS-LWC to genuinely contribute to carbon-neutral construction, cement content must be reduced concurrently with density — through higher SCM replacement, alternative low-carbon binders, or optimisation of the binder-to-filler ratio — rather than relying on EPS substitution of aggregate in isolation.

7. Future Scope

The present embodied-carbon estimate is based on cradle-to-gate material emission factors and does not account for transport distances, batching and mixing energy, curing energy, or end-of-life treatment of EPS (which is not biodegradable). A full life-cycle assessment (LCA) incorporating these stages, together with the in-service thermal-insulation benefit of EPS-LWC (which can offset operational-phase emissions in building envelope applications), would provide a more complete carbon accounting. Future work should also explore mix designs that reduce both density and cement content simultaneously — for example, through higher fly ash or alternative SCM replacement combined with moderate EPS dosage — to identify whether a genuinely lower-carbon, structurally viable EPS-LWC mix is achievable, and should extend the emission-factor basis with region- and supplier-specific Environmental Product Declarations (EPDs) where available.

8. Acknowledgement

The experimental trial-mix data used in this study were generated as part of a B.Tech mini-project, "Development of Light Weight Concrete by using Expanded Polystyrene Beads," undertaken at the Department of Civil Engineering, Vidya Jyothi Institute of Technology, Hyderabad, under the guidance and support from Ultratech Cement.

References

1. Mandlik, A., Sood, T. S., Karade, S., Naik, S., Kulkarni, A., "Light Weight Concrete Using EPS," International Journal of Science and Research (IJSR), Vol. 4, Issue 3, 2015.
2. Moon, A. S., Selokar, L. S., Patle, A. I., Bhoyar, D. S., Kowale, S. D., Quaz, S. S., "Lightweight concrete by using eps beads," International Research Journal of Engineering and Technology (IRJET), Vol. 07, Issue 07, 2020.



3. Karthika, R. B., Vidyapriya, V., Sri, K. V. N., Beaula, M. G. K., Harini, R., Sriram, M., "Experimental Study on Lightweight Concrete Using Pumice Aggregate," Materials Today: Proceedings, https://doi.org/10.1016/j.matpr.2020.09.762.

4. Dhemla, P., Somani, P., Swami, B. L., "Comparative analysis and performance of light weight concrete with varying water cement ratio using plain and blended cement," Materials Today: Proceedings, https://doi.org/10.1016/j.matpr.2023.07.037.

5. Kavinkumar, V., Priya, A. K., Praneeth, R., "Strength of light weight concrete containing fly ash cenosphere," Materials Today: Proceedings, https://doi.org/10.1016/j.matpr.2023.04.094.

6. Murugan, K., Palaniappan, M., Kalappan, K. K., "Experimental studies on light weight concrete using LECA material," Materials Today: Proceedings, https://doi.org/10.1016/j.matpr.2022.11.467.

7. Borkar, Y., Singi, M., "EPS Based Light Weight Concrete Design With Enhancement of Strength," International Journal of Civil and Structural Engineering Research, Vol. 7, Issue 2, 2020.

8. Hammond, G., Jones, C., Inventory of Carbon and Energy (ICE) Database, Version 3.0, University of Bath, United Kingdom.

EXPERIMENTAL INVESTIGATION ON THE MECHANICAL AND DURABILITY PERFORMANCE OF GRAPHENE OXIDE-MODIFIED CONCRETE

V. Bhikshma[1] and Podeti Anil[2]

[1]Senior Professor, Department of Civil Engineering, [2]Research Scholar,

University College of Engineering (Autonomous), Osmania University, Hyderabad - 500 007, Telangana, India

ABSTRACT

Graphene oxide (GO) has emerged as a promising nano-modifier for cementitious composites because of its high specific surface area, two-dimensional sheet structure and oxygen-containing functional groups. However, its effectiveness is strongly dosage-dependent, and a single fixed dosage may not provide optimum performance for different concrete grades. This study experimentally evaluates the mechanical and durability performance of GO-modified M20, M30 and M40 concretes using a grade-specific dosage approach. M20 and M30 concretes were produced with 100% ordinary Portland cement, whereas M40 concrete incorporated 70% cement and 30% ground granulated blast-furnace slag (GGBS). Following preliminary screening, refined GO dosages of 0, 0.020, 0.025, 0.030, 0.035 and 0.040% by weight of cement were investigated. Workability, compressive strength, splitting tensile strength, flexural strength and modulus of elasticity were evaluated, while durability was assessed through water absorption, water permeability and acid-attack resistance. The optimum GO dosages were identified as 0.020% for M20, 0.030% for M30 and 0.040% for M40. At these dosages, 28-day compressive strength improved by 15.93%, 14.08% and 13.26%, respectively; splitting tensile strength improved by 16.23%, 14.60% and 14.52%; and flexural strength improved by 13.09%, 12.71% and 14.93%. The corresponding increases in modulus of elasticity were 10.84%, 10.21% and 9.76%. Water absorption decreased by 18.75%, 17.65% and 16.67%, water permeability decreased by 20.83%, 19.44% and 18.18%, and acid-attack mass loss decreased by 16.67%, 15.38% and 14.81% for M20, M30 and M40, respectively. Workability decreased with increasing GO content, confirming the need for controlled dosage and dispersion. The results demonstrate that grade-specific optimization of GO can enhance mechanical performance and resistance to fluid ingress while avoiding the adverse effects associated with excessive nano-additive content. The findings support the use of low-dose GO as a performance-enhancing nano-modifier in concrete; however, direct carbon-footprint reduction was not quantified in this study.

Keywords: Graphene oxide; mechanical properties; durability; dosage optimization; M20-M40 concrete; GGBS; water absorption; water permeability; acid resistance.

1. INTRODUCTION

Concrete remains the principal construction material for buildings and infrastructure because of its versatility, availability and compressive strength. Its long-term performance, however, is strongly influenced by tensile weakness, microcracking, pore connectivity and the ingress of water or aggressive agents. These limitations have motivated the development of modified cementitious systems capable of improving both mechanical performance and durability.

Nanomaterials can influence cement-based materials at scales below those reached by conventional mineral additions. Graphene oxide (GO) is of particular interest because its two-dimensional nanosheets possess a high specific surface area and oxygen-containing functional groups. In cementitious environments, GO can provide heterogeneous nucleation surfaces, contribute to pore refinement and influence the spatial distribution of hydration products. Previous studies have reported improvements in strength and microstructural compactness when GO is uniformly dispersed at low dosages [1-6].

The beneficial effect of GO is not proportional to dosage. Excessive GO may increase water demand and promote agglomeration, producing non-uniform dispersion and locally weak regions. Consequently, dosage selection is a critical issue. Many studies have examined one concrete grade or a narrow dosage range, whereas practical concrete production requires dosage selection to account for changes in binder composition, water-binder ratio and matrix density.

The present work focuses on M20, M30 and M40 concretes and evaluates GO through a refined, grade-specific dosage range. The study considers workability, compressive strength, splitting tensile strength, flexural strength, modulus of elasticity, water absorption, water permeability and acid-attack resistance. The objective is to identify a practical optimum dosage for each grade based on balanced mechanical and durability performance rather than on compressive strength alone.

2. EXPERIMENTAL PROGRAMME

2.1 Materials

Ordinary Portland cement, fine aggregate, crushed coarse aggregate, potable water, chemical admixture and graphene oxide were used. M20 and M30 concretes contained 100% cement as the binder, while M40 concrete used a blended binder containing 70% cement and 30% GGBS. GO was used as a nano-modifier and its dosage was expressed as a percentage by weight of cement. The principal material properties available from the experimental programme are summarized in Table 1.

Table 1. Selected physical properties of constituent materials.

Material	Property	Value
Cement	Specific gravity	3.12
Cement	Standard consistency	30%
Cement	Initial setting time	33 min
Cement	Final setting time	448 min
Fine aggregate	Specific gravity	2.58
Fine aggregate	Fineness modulus	2.40
Coarse aggregate	Specific gravity	2.60
Coarse aggregate	Water absorption	0.20%
Graphene oxide	Form	Nanosheets in powder form
Graphene oxide	Purity	>= 99%

2.2 Binder system and GO dosage selection

The investigation followed a staged dosage-optimization approach. Preliminary trials were used to identify the response range, after which refined GO dosages of 0, 0.020, 0.025, 0.030, 0.035 and 0.040% were examined for M20, M30 and M40 concretes. The final optimum dosage was selected by considering workability together with mechanical and durability performance.

Table 2. Binder system and refined graphene oxide dosage programme.

Grade	Binder system	Refined GO dosage range (% by wt. of cement)	Optimum GO dosage (%)
M20	100% cement	0, 0.020, 0.025, 0.030, 0.035, 0.040	0.020
M30	100% cement	0, 0.020, 0.025, 0.030, 0.035, 0.040	0.030
M40	70% cement + 30% GGBS	0, 0.020, 0.025, 0.030, 0.035, 0.040	0.040

2.3 GO dispersion, mixing and curing

The required quantity of GO was dispersed in the mixing water before incorporation into the concrete to improve uniformity and limit agglomeration. The dry constituents were mixed first, followed by gradual addition of the GO-water dispersion and chemical admixture. Specimens were cast, compacted, demoulded after the initial setting period and water-cured until the required testing age. Consistent dispersion and mixing sequence were maintained for the control and modified mixes.

2.4 Testing programme

Fresh concrete performance was assessed using slump and compaction factor tests. Mechanical performance was evaluated through compressive strength, splitting tensile strength, flexural strength and modulus of elasticity. Durability performance was assessed using water absorption, water permeability and acid-attack resistance after the prescribed curing period. The test programme was conducted for the control concrete and the GO-modified mixes, with particular emphasis on the final grade-wise optimum dosage.

3. *RESULTS AND DISCUSSION*

3.1 Workability and optimum dosage

Workability decreased as GO dosage increased, primarily because the high specific surface area of GO increases the surface to be wetted and therefore the water demand of the mix. Slump and compaction factor were considered together to assess fresh-state performance. The grade-wise workability trends for the refined GO dosage range are to be presented in Fig. 1(a-b).

The optimum dosage increased from 0.020% for M20 to 0.030% for M30 and 0.040% for M40. The result shows that GO content should not be selected as a single fixed percentage for all concretes. Instead, the optimum level depends on the cementitious matrix and the balance between beneficial nano-scale modification and adverse effects such as increased water demand or agglomeration.

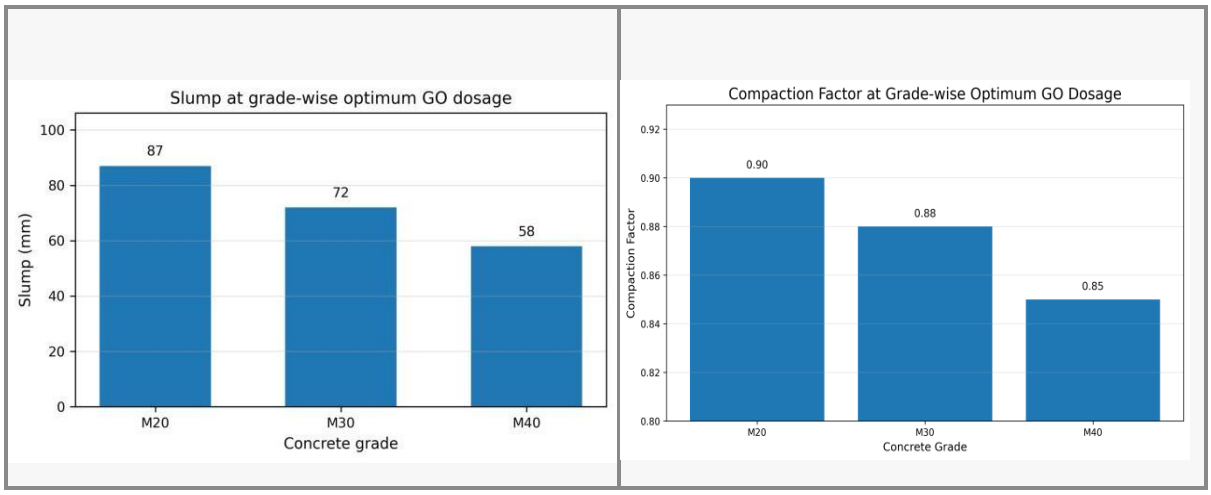


Fig. 1. Workability variation of GO-modified M20, M30 and M40 concrete: (a) slump and (b) compaction factor.

3.2 Mechanical performance

At the respective optimum dosages, all three grades showed improvement in compressive strength, splitting tensile strength, flexural strength and modulus of elasticity relative to the corresponding control mixes. Table 3 summarizes the percentage improvement at the selected optimum dosage, while Fig. 2(a-d) is reserved for the full grade-wise mechanical trends obtained from the refined GO dosage series.

Table 3. Mechanical performance at the grade-wise optimum GO dosage.

Grade	Optimum GO (%)	Slump (mm)	28-d compressive strength improvement (%)	Splitting tensile improvement (%)	Flexural strength improvement (%)	Modulus improvement (%)
M20	0.020	87	15.93	16.23	13.09	10.84
M30	0.030	72	14.08	14.60	12.71	10.21
M40	0.040	58	13.26	14.52	14.93	9.76

The 28-day compressive strength gains were 15.93%, 14.08% and 13.26% for M20, M30 and M40, respectively. The improvement is consistent with a nucleation and pore-refinement mechanism in which well-dispersed GO provides additional surfaces for the development and distribution of cement hydration products. The resulting matrix is expected to exhibit lower pore connectivity and improved local compactness. The slightly lower percentage gain with increasing grade also indicates that the relative benefit depends on the initial characteristics of the control matrix.

Splitting tensile strength increased by 16.23% for M20, 14.60% for M30 and 14.52% for M40. Flexural strength increased by 13.09%, 12.71% and 14.93%, respectively. These results indicate that optimum GO addition is beneficial not only in compression but also under tensile stress states. The improvement is plausibly related to matrix densification, stronger paste-aggregate interaction and restriction of microcrack development; however, these mechanisms should be interpreted as supporting explanations rather than direct measurements within the present mechanical-durability paper.

The modulus of elasticity increased by 10.84%, 10.21% and 9.76% for M20, M30 and M40, respectively. This trend is consistent with the observed enhancement in compressive strength and the development of a more compact cementitious matrix at the optimum GO dosage.

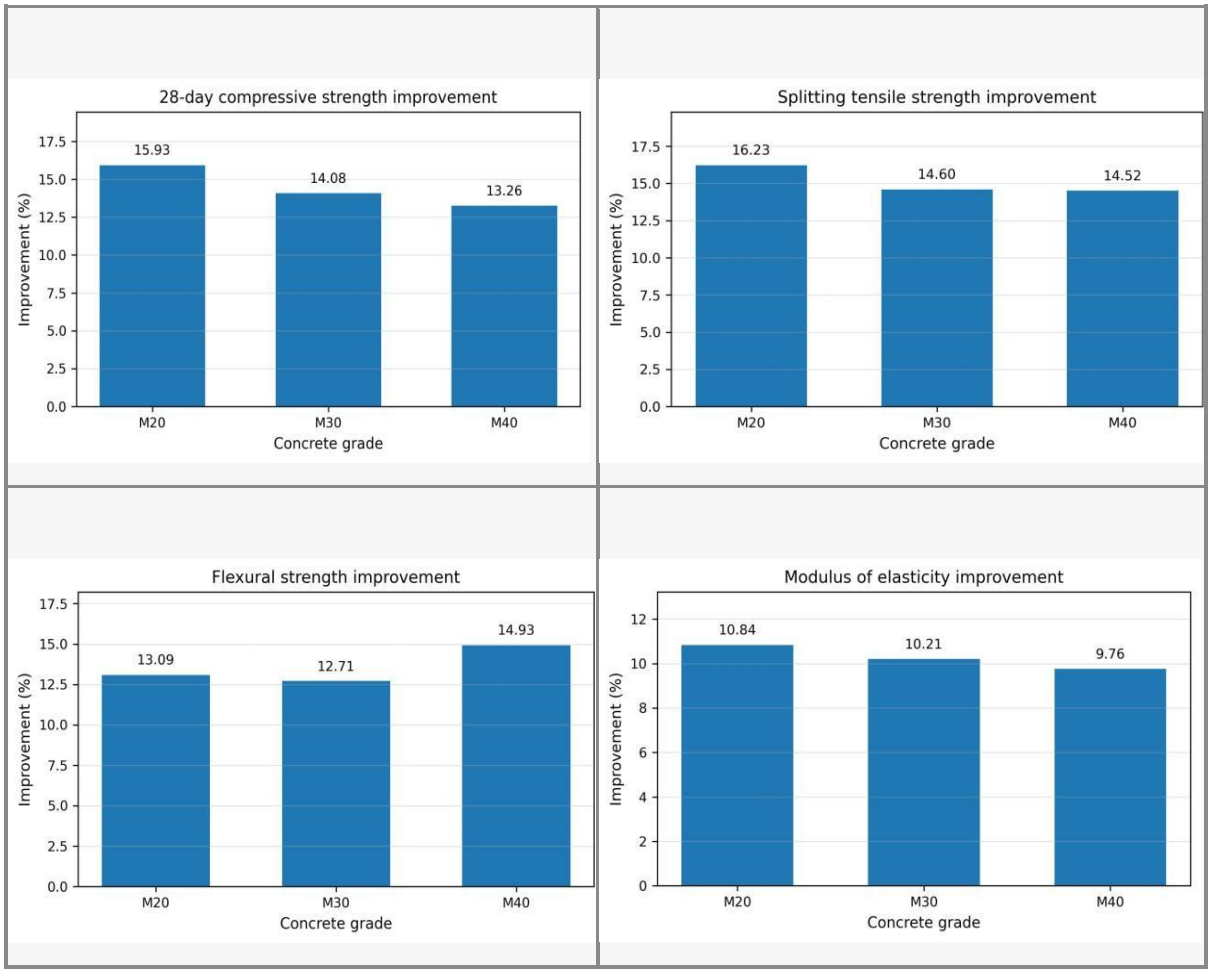


Fig. 2. Mechanical performance of GO-modified M20, M30 and M40 concrete: (a) compressive strength, (b) splitting tensile strength, (c) flexural strength and (d) modulus of elasticity.

3.3 Durability performance

The durability indicators exhibited consistent improvement at the selected optimum GO dosages. Table 4 summarizes the percentage reductions in water absorption, water permeability and acid-attack mass loss. The corresponding control-versus-optimized durability results should be presented graphically in Fig. 3(a-c) using the final approved thesis values.

Table 4. Durability improvement at the grade-wise optimum GO dosage.

Grade	Optimum GO (%)	Water absorption reduction (%)	Water permeability reduction (%)	Acid-attack mass-loss reduction (%)
M20	0.020	18.75	20.83	16.67
M30	0.030	17.65	19.44	15.38
M40	0.040	16.67	18.18	14.81

Water absorption decreased by 18.75%, 17.65% and 16.67% for M20, M30 and M40, respectively. The reduction indicates a less accessible pore system in the optimized GO mixes. Water permeability showed an even larger reduction of 20.83%, 19.44% and 18.18%, demonstrating improved resistance to fluid ingress. Reduced permeability is particularly important for long-term durability because it limits transport pathways through which aggressive agents can enter the concrete.

Acid-attack mass loss decreased by 16.67% for M20, 15.38% for M30 and 14.81% for M40. Although GO does not eliminate chemical deterioration, the improved resistance is consistent with reduced permeability and a denser matrix that slows the ingress of aggressive solution. Across the three grades, the durability gains were highest in M20 and remained substantial in M40.

Taken together, the mechanical and durability results show that the optimum GO dosage should be selected from a multi-parameter assessment. A dosage that maximizes a single strength result may not necessarily provide the best combination of workability, stiffness and resistance to fluid ingress.

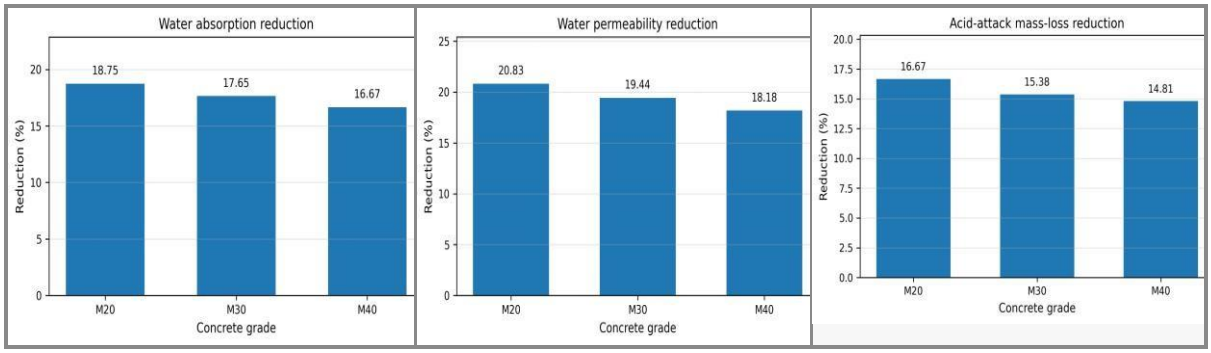


Fig. 3. Durability performance of GO-modified M20, M30 and M40 concrete: (a) water absorption, (b) water permeability and (c) acid-attack mass loss.

3.4 Significance for durable and resource-efficient concrete

The conference theme emphasizes pathways toward more durable and sustainable concrete. Within this context, the present results show that very small GO dosages can improve mechanical performance and reduce transport-related durability indicators. The M40 mix additionally incorporates 30% GGBS as a partial cement replacement, thereby reducing the OPC fraction of the binder. Improved durability may also contribute to longer service life and lower maintenance demand. Nevertheless, this study did not perform a life-cycle assessment or quantify embodied carbon; therefore, no direct claim of carbon neutrality or a specific carbon reduction is made.

4. CONCLUSIONS

1. GO improved the mechanical and durability performance of M20, M30 and M40 concretes when used at a controlled, grade-specific optimum dosage.

2. The optimum dosages were 0.020% for M20, 0.030% for M30 and 0.040% for M40 by weight of cement, confirming that one fixed GO content is not appropriate for all concrete grades.
3. At optimum dosage, 28-day compressive strength increased by 13.26-15.93%, splitting tensile strength by 14.52-16.23%, flexural strength by 12.71-14.93%, and modulus of elasticity by 9.76-10.84%.
4. Water absorption decreased by 16.67-18.75%, water permeability by 18.18-20.83%, and acid-attack mass loss by 14.81-16.67%, indicating improved resistance to fluid ingress and aggressive exposure.
5. Workability decreased with increasing GO dosage; therefore, dispersion quality and dosage control are essential for obtaining consistent performance.
6. The combined results support a grade-specific optimization approach in which GO dosage is selected from the balance of workability, mechanical properties and durability rather than from compressive strength alone.
7. The use of 30% GGBS in the M40 binder and the durability improvements are relevant to more resource-efficient concrete; however, carbon-footprint reduction was not quantified and requires dedicated life-cycle assessment.

ACKNOWLEDGEMENT

The authors acknowledge the support of the Department of Civil Engineering, University College of Engineering (Autonomous), Osmania University, Hyderabad, and the laboratory personnel who assisted during the experimental programme.

REFERENCES

[1] Pan, Z., He, L., Qiu, L., Korayem, A.H., Li, G., Zhu, J.W., Collins, F., Li, D., Duan, W.H. and Wang, M.C. (2015). Mechanical properties and microstructure of a graphene oxide-cement composite. Cement and Concrete Composites, 58, 140-147.

[2] Lv, S., Ma, Y., Qiu, C., Sun, T., Liu, J. and Zhou, Q. (2013). Effect of graphene oxide nanosheets on microstructure and mechanical properties of cement composites. Construction and Building Materials, 49, 121-127.

[3] Lu, Z., Hanif, A., Ning, C., Shao, H., Yin, R. and Li, Z. (2017). Steric stabilization of graphene oxide in alkaline cementitious solutions: Mechanical enhancement of cement composite by GO. Construction and Building Materials, 127, 154-161.

[4] Mohammed, A., Sanjayan, J.G., Duan, W.H. and Nazari, A. (2016). Graphene oxide impact on hardened cement expressed in enhanced freeze-thaw resistance. Journal of Materials in Civil Engineering, 28(9).

[5] Chuah, S., Pan, Z., Sanjayan, J.G., Wang, C.M. and Duan, W.H. (2014). Nano reinforced cement and concrete composites and new perspective from graphene oxide. Construction and Building Materials, 73, 113-124.

[6] Long, W.J., Wei, J.J., Xing, F. and Khayat, K.H. (2018). Enhanced dynamic mechanical properties of cement paste modified with graphene oxide nanosheets and its reinforcing mechanism. Cement



and Concrete Composites, 93, 127-139.

[7] Bureau of Indian Standards. IS 456:2000, Plain and Reinforced Concrete - Code of Practice. New Delhi, India.

[8] Bureau of Indian Standards. IS 10262:2019, Concrete Mix Proportioning - Guidelines. New Delhi, India.

[9] Bureau of Indian Standards. IS 516:1959, Methods of Tests for Strength of Concrete. New Delhi, India.

[10] Bureau of Indian Standards. IS 5816:1999, Splitting Tensile Strength of Concrete - Method of Test. New Delhi, India.

CARBONATION RESISTANCE OF CONCRETE INCORPORATING FLY ASH AND GROUND GRANULATED BLAST FURNACE SLAG UNDER ACCELERATED EXPOSURE

Dr B. Kameswara Rao

Professor, Civil Engineering Department

Koneru Lakshmaiah Education Foundation

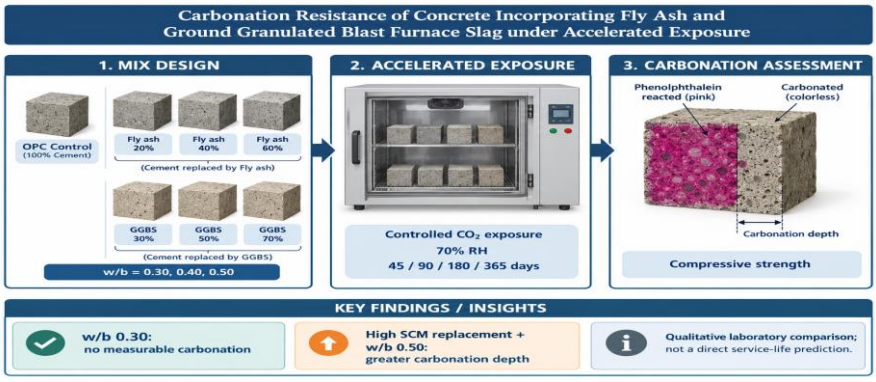
Vijayawada, Andhra Pradesh

1. ABSTRACT

Carbonation of concrete involves the ingress of atmospheric carbon dioxide (CO_2) and its reaction with hydrated cement phases, reducing pore-solution alkalinity and potentially depassivating reinforcement. Supplementary cementitious materials (SCMs) modify both pore Structure and the cementitious matrix's capacity to buffer carbonation. The present experimental investigation compares the accelerated carbonation resistance of ordinary Portland cement (OPC), fly ash, and ground granulated blast-furnace slag (GGBS) concretes.

We investigated 21 mixtures at nominal water-to-binder (w/b) ratios of 0.30, 0.40, and 0.50. Fly ash replaced cement at 20%, 40% and 60%, and GGBS at 30%, 50% and 70%; one OPC control was included at each w/b ratio. Following 28 days of moist curing, 100 mm cubes were exposed in a controlled CO_2 chamber for up to 365 days, with measurements at 45, 90, 180 and 365 days. The reported nominal exposure was 10% CO_2 and 70% relative humidity (RH), subject to final confirmation against laboratory records.

No measurable carbonation depth was reported for the w/b = 0.30 mixtures. At w/b = 0.40, detectable carbonation was limited to the 60% fly ash and 70% GGBS mixtures. At w/b = 0.50, more pronounced carbonation occurred in mixtures with high SCM replacement, including full carbonation of the 60% fly ash mixture by 180 days and of the 70% GGBS mixture by 365 days. Compressive strengths after 365 days of exposure exceeded the respective 28-day values, but the absence of age-matched, unexposed controls prevents attributing these changes to carbonation. The results emphasise the joint influence of w/b ratio and SCM replacement level and should not be directly extrapolated to natural-exposure service life.Keywords: accelerated carbonation; fly ash; GGBS; water-to-binder ratio; phenolphthalein; supplementary cementitious materials; concrete durability.



Graphical abstract. Study design, phenolphthalein-based carbonation assessment and key comparative findings (schematic, not to scale).

2. INTRODUCTION:

Carbonation is an important durability process in reinforced concrete. Carbon dioxide diffuses through partially saturated pores and reacts with portlandite and other hydrate phases, forming carbonates and lowering pore-solution alkalinity. If the carbonation-affected zone reaches reinforcing steel, loss of passivity may permit corrosion where moisture and oxygen are available. Carbonation may locally densify some matrices, but phase assemblage and volume changes depend on binder chemistry and exposure conditions [11,12].

The carbonation of hydrated Portland cement is generally a slow process under natural environmental conditions.[2] The rate of carbonation is governed by several factors, including the concentration of atmospheric CO_2, relative humidity, temperature, concrete permeability, pore Structure, and quality of curing. Carbonation proceeds most rapidly at relative humidity between approximately 50% and 75%, where sufficient moisture is available for the carbonation reaction and the pore system remains accessible to CO_2 diffusion.[3] At relative humidity below approximately 25%, carbonation is negligible due to insufficient moisture for the reaction. Conversely, when relative humidity exceeds about 75%, the pores become saturated with water, restricting carbon dioxide diffusion into the concrete.

High-permeability concrete undergoes carbonation more rapidly than dense, well-compacted, and properly cured concrete. Lower water-to-cement (or water-to-binder) ratios produce a denser microstructure with reduced permeability, thereby limiting CO_2 penetration and improving carbonation resistance. Similarly, adequate compaction and prolonged moist curing significantly reduce the carbonation rate. Reinforced concrete structures in industrial and urban environments are particularly susceptible to carbonation due to relatively high atmospheric CO_2 concentrations.

SCMs affect carbonation through more than calcium hydroxide consumption alone. Fly ash and GGBS change the alkalinity reserve, hydrate assemblage, pore connectivity, moisture state and transport properties. Higher replacement levels can increase measured carbonation depths under some curing and exposure conditions despite beneficial effects on other durability mechanisms [11,12]. The carbonation behaviour of concrete containing SCMs is influenced by several interrelated parameters, including:

- Water-to-binder (w/b) ratio;
- Percentage of cement replacement by SCMs;
- Duration and quality of moist curing;
- Relative humidity and temperature of the surrounding environment;
- Carbon dioxide concentration; and
- Concrete permeability and pore Structure.

The following sections present a comprehensive review of previous investigations on the carbonation behaviour of concrete incorporating fly ash and GGBS.

3. Literature Review:

3.1 Effect of Fly Ash on Carbonation:

A major durability concern with incorporating fly ash in concrete is its influence on carbonation resistance. Although fly ash generally enhances the long-term mechanical properties and resistance to chloride ingress, its effect on carbonation has been reported to be less favourable, particularly at high replacement levels and under inadequate curing conditions.

Long-term investigations conducted in Japan in 1968[4] showed that concrete produced with blended cements exhibited a higher rate of carbonation than concrete prepared with ordinary Portland cement (OPC). The increased carbonation was primarily attributed to reduced calcium hydroxide availability due to the pozzolanic reaction of fly ash.

Subsequently, Tsukayama et al.[5] (1980) reported the results of long-term field exposure studies on fly ash concrete in Japan. Their investigation revealed that carbonation depth was significantly influenced by concrete quality, the water-to-binder ratio, and the duration of moist curing. Lower water-to-binder ratios and prolonged curing substantially improved carbonation resistance.

Ho and Lewis[6] conducted comprehensive investigations on the carbonation behaviour of fly ash concrete and established the following important relationships:

- Carbonation depth decreases with increasing compressive strength.
- Carbonation depth decreases with increasing cement content.
- Carbonation resistance improves significantly with longer periods of moist curing.

These studies clearly indicate that the adverse effect of fly ash on carbonation can be substantially mitigated by producing dense concrete with a low water-to-binder ratio and by providing adequate moist curing.

3.2 Effect of Ground Granulated Blast Furnace Slag (GGBS) on Carbonation:

Ground Granulated Blast Furnace Slag (GGBS) is widely used as a supplementary cementitious material because it significantly improves resistance to chloride penetration, sulfate attack, alkali–silica reaction, and other durability-related deterioration mechanisms. However, numerous studies have reported that slag concrete generally exhibits a higher rate of carbonation than ordinary Portland cement concrete. Higher slag replacement levels reduce the amount of calcium hydroxide available to neutralise carbon dioxide and consequently increase carbonation depth.

Adolf Mayer[7] carried out extensive experimental investigations on the carbonation behaviour of slag concretes. His studies demonstrated that carbonation depth increased with increasing slag content. Concrete containing 50% slag exhibited approximately 1.5 times the carbonation depth of OPC concrete, whereas concrete containing 70% slag showed nearly twice the carbonation depth. He also reported that carbonation resistance was strongly influenced by concrete age, water-to-cementitious materials ratio, and moist-curing duration. Similarly, Osborne[8] of the Building Research Establishment (BRE), United Kingdom, conducted both short-term and long-term investigations on the carbonation of slag concretes. His principal findings were:

1. Higher slag contents considerably increased the adverse effects of inadequate curing, particularly for replacement levels of 70% and 80%.
2. Concretes containing higher percentages of slag generally exhibited slightly higher carbonation rates than OPC concrete.

3. Adequately moist-cured slag concretes attained their design strengths and exhibited little or no measurable carbonation.

These investigations emphasise that proper curing is one of the most effective measures for improving the carbonation resistance of slag concrete.

4. Aim and Scope of the Investigation:

The primary objective of the present investigation was to evaluate the carbonation performance of concrete containing varying proportions of supplementary cementitious materials (SCMs) under accelerated carbonation conditions.

We prepared concrete mixtures using three water-to-binder (w/b) ratios of **0.30, 0.40, and 0.50**. For each water-to-binder ratio, we incorporated fly ash at replacement levels of **20%, 40%, and 60%** by mass of cement. Similarly, we incorporated Ground Granulated Blast Furnace Slag (GGBS) at replacement levels of **30%, 50%, and 70%**. We also cast control concrete specimens using 100% Ordinary Portland Cement (OPC) at each water-to-binder ratio to facilitate comparison with SCM-containing concretes.

After 28 days of moist curing, the specimens were exposed for up to one year to an accelerated carbonation atmosphere described in the source records as 10% CO_2 by volume and nominally 70% RH. The 10% CO_2 value is supported by labels visible in the original specimen photographs and is used consistently in this revision in place of the conflicting 20% value previously printed in Section 6; the original chamber logs should nevertheless be checked. The elevated CO_2 level was intended to accelerate laboratory testing, while approximately 70% RH was selected to retain moisture for carbonation reactions without fully saturating gas-diffusion pathways. Experimental investigations have used elevated CO_2 concentrations and RH levels within this broad range [11–13]; a separate study reported a 10% CO_2/70% RH regime for accelerated carbonation curing [15], although that protocol is not equivalent to the present exposure test. Current common standardised accelerated-carbonation protocols generally specify lower CO_2 concentrations, so 10% should be described as an experimental choice rather than a code-mandated value [12]. NOTE FOR AUTHOR: Some photographed specimen cards state 65% RH; verify whether 70% was the chamber set point and 65% an operating/label value. We examined specimens after 45, 90, 180, and 365 days to determine compressive strength and carbonation depth.

5. Materials:

The investigation used commercially available 53-grade Ordinary Portland Cement (OPC) conforming to the relevant Indian Standards. Class F fly ash was procured from the **NTPC Thermal Power Plant, Dadri**, while Ground Granulated Blast Furnace Slag (GGBS) was obtained from the **Visakhapatnam Steel Plant**.

Natural river sand (Badarpur sand) was used as the fine aggregate, whereas crushed coarse aggregate was obtained from a local quarry. A naphthalene-based high-range water-reducing admixture (superplasticiser) was incorporated to achieve the required workability.

Table 1 presents the physical properties and chemical compositions of the cement, fly ash, and GGBS used in the investigation.

Table 1. Physical Properties and Chemical Composition of Cement, Fly Ash and GGBS

Material	Cement	Fly ash	Slag
Physical Properties:			
Specific gravity	3.14	2.25	2.91
Specific surface area (cm^2/gm)	2546	3980	3300
Standard consistency	28%	-	-
Initial setting time	75 min.	-	-
Final setting time	295 min.	-	-
Chemical Composition (%):			
SiO_2	21.41	57.55	33.20
Al_2O_3	8.95	31.40	18.30
Fe_2O_3	2.80	7.50	0.60
CaO	62.25	1.40	32.60
MgO	1.46	0.29	11.60
SO_3	2.65	0.43	1.00
Na_2O	0.20	0.19	0.21
K_2O	0.22	0.21	0.91
S	0.75	0.12	0.70
Loss on Ignition	0.30%	1.10%	0.91%

6. Experimental Program:

Concrete mixtures were proportioned using the ACI 211.1-22 method, which provides procedures for selecting and adjusting ingredient quantities with attention to consistency, strength, durability, admixtures and SCM use [9]. We adopted this approach as a practical proportioning framework for the prescribed nominal w/b ratios and replacement levels; its selection does not imply that the corresponding Indian method is unsuitable. IS 10262 provides an alternative established procedure [10]. We operated the accelerated carbonation chamber at a reported 10% CO_2 concentration (by volume) and a nominal relative humidity of 65%-70%. We used a saturated calcium nitrate solution to control RH.

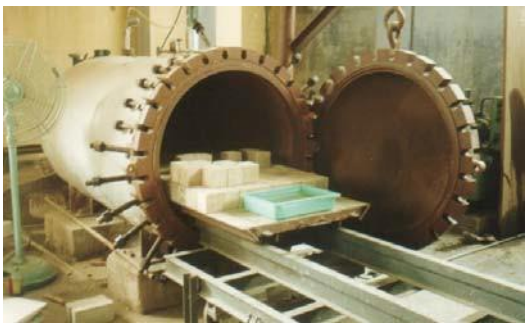
We checked the chamber CO_2 concentration weekly. We removed concrete specimens after 45, 90, 180, and 365 days of exposure, and determined compressive strength and carbonation depth. Table 2 reports the recorded constituent quantities. Table 2. Recorded Concrete Mix Proportions (constituent quantities in kg/m^3 unless otherwise stated)

Table 2. Concrete Mix Proportions

Mix	Water + SP (kg/m^3)	Cement (kg/m^3)	FA (kg/m^3)	CA (kg/m^3)	Fly ash (kg/m^3)	GGBS (kg/m^3)	CF (–)	SP (% binder)
A	160	533	732.26		—	—	0.75	2
B	160	400	843.70		—	—	0.76	2
C	160	360	824.02		—	—	0.79	2
D	160	426.4	698.3	1069	106.6	—	0.78	2
E	160	319.8	665.08		213.2	—	0.82	2
F	160	213.2	631.68		319.8	—	0.81	2
G	160	320	818.62		80	—	0.77	2

Mix	Water + SP (kg/m³)	Cement (kg/m³)	FA (kg/m³)	CA (kg/m³)	Fly ash (kg/m³)	GGBS (kg/m³)	CF (–)	SP (% binder)
H	160	240	793.5		160	—	0.77	2
I	160	160	768.58		240	—	0.81	2
J	160	256	892.6		64	—	0.78	2
K	160	192	870.98		128	—	0.78	2
L	160	128	850.95		192	—	0.79	2
M	160	373.1	720.06		—	159.9	0.76	2
N	160	266.5	712.27		—	266.5	0.75	2
O	165	385	701.4		—	165	0.76	2
P	160	280	835.03		—	120	0.77	2
Q	160	200	829.1		—	200	0.76	2
R	160	120	823.25		—	280	0.79	2
S	190	273	763.49		—	117	0.82	2
T	190	190	766.6		—	190	0.85	2
U	180	108	805.62		—	252	0.85	2

Table 2 note: FA = fine aggregate; CA = coarse aggregate; CF = compaction factor (dimensionless); SP = superplasticiser; GGBS = ground granulated blast-furnace slag.



Photograph 1: Carbonation Chamber



Photograph 2: Arrangement of Specimens

For carbonation-depth assessment, 100 mm concrete cubes were split along their height under a line load in a universal testing machine (UTM). A 2 per cent phenolphthalein indicator solution was sprayed onto freshly split surfaces, and the boundary between colourless (lower pH) and pink/magenta (higher pH) areas was used to estimate the apparent carbonation depth [12,14].

Table 3: The Results of Compressive Strength in MPa

Mix	w/b Ratio	Fly ash	Slag	28 d (MPa)	45 d (MPa)	90 d (MPa)	180 d (MPa)	365 d (MPa)
A	0.3	-	-	44.00	47.04	47.53	60.50	87.67
B	0.4	-	-	30.38	36.75	40.00	46.00	61.00
C	0.5	-	-	37.25	37.24	44.00	46.50	52.67
D	0.3	20	-	45.57	44.50	46.06	65.50	90.00
E	0.3	40	-	40.18	49.98	51.00	59.00	94.00
F	0.3	60	-	23.33	32.34	41.25	48.50	77.17

Mix	w/b Ratio	Fly ash	Slag	28 d (MPa)	45 d (MPa)	90 d (MPa)	180 d (MPa)	365 d (MPa)
G	0.4	20	-	34.83	33.32	45.00	53.50	79.67
H	0.4	40	-	30.33	43.61	49.00	54.50	80.16
I	0.4	60	-	17.33	30.14	34.00	36.00	63.50
J	0.5	20	-	30.17	36.75	41.75	43.00	66.33
K	0.5	40	-	20.83	28.18	40.00	46.00	58.16
L	0.5	60	-	10.78	18.62	22.50	24.00	34.33
M	0.3	-	30	47.67	45.57	51.00	65.50	64.50
N	0.3	-	50	49.00	47.29	50.00	56.50	76.67
O	0.3	-	70	40.67	35.28	49.50	55.00	81.00
P	0.4	-	30	42.14	34.30	44.50	51.00	82.50
Q	0.4	-	50	41.16	31.40	49.00	48.00	60.50
R	0.4	-	70	38.46	40.18	42.50	45.25	74.67
S	0.5	-	30	37.24	33.81	43.00	45.50	53.83
T	0.5	-	50	32.83	39.20	35.50	42.50	50.00
U	0.5	-	70	29.64	32.10	39.50	36.00	44.00

Table 4: Results of Depth of Carbonation

Mix	W/B Ratio	Fly ash (%)	Slag (%)	45 d (mm)	90 d (mm)	180 d (mm)	365 d (mm)
A	0.3	-	-	-	-	-	-
B	0.4	-	-	-	-	-	-
C	0.5	-	-	-	-	-	-
D	0.3	20	-	-	-	-	-
E	0.3	40	-	-	-	-	-
F	0.3	60	-	-	-	-	-
G	0.4	20	-	-	-	-	-
H	0.4	40	-	-	-	-	-
I	0.4	60	-	4.68	13.94	25.00	FC
J	0.5	20	-	-	-	-	-
K	0.5	40	-	1.96	8.22	8.50	8.75
L	0.5	60	-	22.95	38.64	FC	FC
M	0.3	-	30	-	-	-	-
N	0.3	-	50	-	-	-	-
O	0.3	-	70	-	-	-	-
P	0.4	-	30	-	-	-	-
Q	0.4	-	50	-	-	-	-
R	0.4	-	70	2.36	4.81	5.00	5.25
S	0.5	-	30	-	-	-	-
T	0.5	-	50	2.11	4.20	5.25	6.50
U	0.5	-	70	5.83	10.97	26.12	FC

Note: 'FC' means Fully Carbonated.

Some of the photographs of the carbonated specimens can be seen below:

Table 5: Carbonation of Specimens of w/b ratio 0.4 and 60% Fly ash



After 45 Days of Exposure



After 90 Days of Exposure



After 180 Days of Exposure



After 365 Days of Exposure (Fully Carbonated)

Table 6: Carbonation of Specimens of w/b ratio 0.5 and 60% Flyash



After 45 Days of Exposure



After 90 Days of Exposure (Fully Carbonated)



After 180 Days of Exposure (Fully Carbonated)

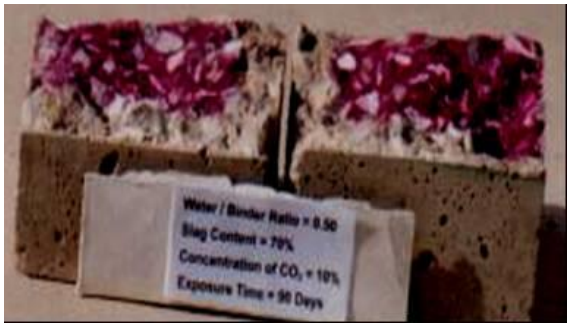


After 365 Days of Exposure (Fully Carbonated)

Table 7: Photographs of Carbonation of Specimens of w/b ratio 0.5 and 70% Slag



After 45 Days of Exposure



After 90 Days of Exposure



After 180 Days of Exposure



After 365 Days of Exposure (Fully Carbonated)

7. Discussion of Experimental Results:

The experimental results obtained from the carbonation and compressive strength investigations are discussed below.

a. Effect of low water-to-binder ratio on carbonation

All mixtures assigned w/b = 0.30 had no visually detectable carbonation in Table 4 through 365 days. A lower w/b ratio typically reduces connected capillary porosity and CO_2 transport when hydration

and curing are otherwise adequate; this provides a plausible explanation, though not direct microstructural proof, since this investigation did not measure pore connectivity [11,12].

b. Effect of high fly ash and slag contents at a water-to-binder ratio of 0.40

At w/b = 0.40, mix I (60% fly ash) showed measurable carbonation (4.68, 13.94, and 25.00 mm at 45, 90, and 180 days, followed by full carbonation at 365 days), and mix R (70% GGBS) showed 2.36 to 5.25 mm between 45 and 365 days. SCM replacement affects both available alkaline buffering phases and pore Structure; those coupled effects, together with the relatively high replacement levels, may account for the behaviour. The original data do not separately quantify portlandite consumption and transport properties [11,12].

c. Effect of higher water-to-binder ratio

At w/b = 0.50, the 60% fly ash mixture L reached 22.95 mm at 45 days, 38.64 mm at 90 days and was recorded as fully carbonated by 180 days. The 70% GGBS mixture U reached 5.83, 10.97 and 26.12 mm at 45, 90 and 180 days, respectively, and was recorded as fully carbonated by 365 days. Mix K (40% fly ash) and mix T (50% GGBS) also exhibited measurable depths. Higher w/b ratios can promote CO_2 transport through a more connected pore network, while SCM replacement changes carbonate-forming phases and buffering capacity. The literature documents these interacting mechanisms, but we did not measure them independently here [11,12].

d. Behaviour of plain concrete

No OPC-only control specimen (mixes A–C) showed a measurable phenolphthalein carbonation front in the recorded observations. Possible explanations include available alkaline buffering phases and differences in permeability/transport behaviour relative to highly replaced SCM mixes. The absence of a visible indicator front should not be interpreted as proof that no carbonation reactions occurred; phenolphthalein marks an apparent pH-defined carbonation boundary rather than total CO_2 uptake [11,12,14].

e. Effect of carbonation on compressive strength

Every mixture had a higher reported compressive strength at 365 days than at the initial 28-day test, although the measured trends are not strictly monotonic at every intermediate date. Therefore, it is accurate to state that no net strength reduction was observed between the reported initial and final measurements. Because the programme provides no age-matched specimens stored outside the CO_2 chamber, it cannot establish whether carbonation increased, decreased or had no effect on strength. Hydration, SCM reactions, and carbonate precipitation may each contribute, depending on conditions [11–13].

f. Strength development with age

The increase in final strength relative to 28 days is compatible with continued binder reaction and maturation, especially for fly ash and slag mixtures, but the available measurements cannot separate continued hydration from carbonation-related effects. The chamber maintained a relatively humid atmosphere, which could facilitate continued reactions, subject to the degree of internal saturation. Mixture-to-mixture variation and the lack of age-matched controls limit attribution of the observed changes [11,12].

8. Conclusions:

Based on the experimental investigation, the following conclusions may be drawn:

1. Under the reported accelerated exposure, the w/b = 0.30 mixtures showed no visible phenolphthalein-defined carbonation front through 365 days, including high fly ash and GGBS replacement levels.
2. The most pronounced carbonation responses occurred among mixtures with higher nominal w/b and high SCM replacement; the response depended on the SCM and its replacement fraction rather than replacement percentage alone.
3. None of the three OPC controls showed a measurable carbonation front by the adopted indicator method, but an undetectable front does not establish the total absence of carbonation reactions.
4. All mixes had greater compressive strength at 365 days than at the 28-day baseline; age-matched non-carbonated controls were unavailable, so carbonation-specific strength effects cannot be isolated.
5. Low w/b ratios and adequate curing are important measures for improving the carbonation performance of high-SCM concrete. The present evidence is laboratory-specific and is not sufficient on its own to directly predict natural-exposure service life [11,12].
6. For reproducibility, the exact CO_2 and RH exposure logs, ACI 211.1 edition, free-water and SP dosages, and phenolphthalein solution formulation should be confirmed before final submission.

REFERENCES

1. ACI Committee 201, "Guide to Durable Concrete," ACI Manual of Concrete Practice, Part 1.
2. LUDWIG, "Durability of Cement Mortars and Concretes," Building Materials and Components Durability, STP-691, ASTM.
3. VERBECK GJ, "Carbonation of Hydrated Portland Cement", Cement and Concrete, STP-205, ASTM.
4. HAMADA M, "Neutralisation (Carbonation) of Concrete and Corrosion of Reinforcing Steel," Proceedings of the 5th International Symposium on the Chemistry of Cements, Tokyo, Japan, October 1968.
5. TSUKAYAMA R, NAGATAKI S, and ABE H, "Long Term Experiments on the Neutralisation of Concrete Mixed with Fly Ash and the Corrosion of Reinforcement," Proceedings of the 7th International Congress on the Chemistry of Cements, Paris, France, 180.
6. HO DWS and LEWIS RK, "Carbonation of Concrete Incorporating Fly Ash or a Chemical Admixture", Proceedings of the 1st International Conference on the Use of Fly Ash, Silica Fume, Slag and Other Mineral By-Products in Concrete, ACI SP-79.
7. ADOLF MEYER, "Investigations on the Carbonating of Concrete," Supplementary Paper III-52, Proceedings of the Fifth International Symposium on Chemistry of Cements, Tokyo, 1968, Part 3, pp. 394-401.



8. OSBORNE GJ, "Carbonation of Blast Furnace Slag Cement Concretes"; Durability of Building Materials; November 1986, Vol. 4, No.1, (Elsevier), pp. 81-96.

9. ACI Committee 211. (1991; reapproved 2009). ACI 211.1-91, Standard Practice for Selecting Proportions for Normal, Heavyweight, and Mass Concrete. American Concrete Institute. https://www.concrete.org/publications/internationalconcreteabstractsportal/m/details/id/5092

10. Bureau of Indian Standards. (2019). IS 10262:2019, Concrete Mix Proportioning—Guidelines (Second Revision). New Delhi: BIS.

11. von Greve-Dierfeld, S., et al. (2020). Understanding the carbonation of concrete with supplementary cementitious materials: a critical review by RILEM TC 281-CCC. Materials and Structures, 53, 136. https://doi.org/10.1617/s11527-020-01558-w

12. Bernal, S. A., et al. (2024). Report of RILEM TC 281-CCC: A critical review of the standardised testing methods to determine carbonation resistance of concrete. Materials and Structures, 57, 173. https://doi.org/10.1617/s11527-024-02424-9

13. Merah, A. (2024). Methods of concrete accelerated carbonation test: a review. Discover Civil Engineering, 1, 53. https://doi.org/10.1007/s44290-024-00057-z

14. Bernal, S. A., Angst, U. M., Provis, J. L., Thiel, C., Gluth, G. J. G., Villagran-Zaccardi, Y., and De Belie, N. (2026). Recommendation of RILEM TC 281-CCC: RILEM CPC-18R1—guideline for measuring the carbonation depth of hardened concrete using a pH indicator solution. Materials and Structures, 59, 137. https://doi.org/10.1617/s11527-026-02966-0

15. Padmalal, A., Kulkarni, K. S., Rawat, P., and Sugandhini, H. K. (2024). Efficacy of Accelerated Carbonation Curing and Its Influence on the Strength Development of Concrete. Buildings, 14(8), 2573. https://doi.org/10.3390/buildings14082573. (Cited as a related example of a 10% CO_2/70% RH regime, not as the identical test protocol.)



Technical Session- VB

IMPORTANCE OF FEASIBILITY STUDY FOR AN ALTERNATE FUEL FEEDING SYSTEM

Sakshi Kadam Amar Patil* Milind Chande* Biswajit Dhar **

** TECHCONS Consulting and Engineering Pvt. Ltd, Navi Mumbai, INDIA*

ABSTRACT

The cement manufacturing industry faces the critical challenge of reducing its reliance on non-renewable coal while maintaining efficient production processes. The process of converting limestone ($CaCO_3$) to cement involves high-temperature heating (around 1400°C), traditionally fueled by coal. With the growing environmental concerns and the finite nature of coal, the industry is increasingly exploring the use of alternative fuels such as municipal waste, food waste, agricultural waste, pharmaceutical waste, wood chips, and tire chips. While many cement plants have successfully integrated alternative fuel-feeding systems, others have faced significant operational and financial setbacks.

The mixed results highlight the necessity for a comprehensive techno-economic feasibility study before investing in alternative fuel feeding systems. This study evaluates critical factors such as the suitability of the cement manufacturing process, consistent availability and cost of alternative fuels, physical and chemical characteristics, plant layout compatibility, and the capital and operational expenditures involved.

A thorough feasibility study helps in identifying the most suitable alternative fuels tailored to the specific needs of each cement plant. It ensures that the selected fuels do not adversely affect the cement production process, offers a reliable supply chain, and proves cost-effective compared to coal. Additionally, it assesses the return on investment, ensuring that the financial implications align with the plant's long-term sustainability goals.

This article underscores the importance of conducting a detailed techno-economic feasibility study by experienced technical consulting firms. Such studies are crucial to making informed investment decisions, mitigating risks, and achieving a successful transition to alternative fuels. By presenting this approach, we aim to emphasize that strategic planning and rigorous evaluation are key to the sustainable future of the cement industry.

1.0 Introduction

Cement is a crucial construction material, essential for global housing and infrastructure. The cement industry is currently grappling with the dual challenge of conserving material and energy resources while reducing CO_2 emissions. To address these issues, cement producers are increasingly focusing on enhancing energy efficiency and incorporating alternative raw materials and fuels. Although the use of alternative fuels has grown significantly, there remains considerable potential for further adoption.

For an alternative fuel to be viable in cement production, it must meet several criteria: it should be easily combustible, cost-effective, safe to use, readily available, and have no adverse effects on clinker quality or ambient air. Additionally, it must be compatible with existing equipment

such as calciners and kilns. Ensuring these factors are favorable is crucial for the productive use of alternative fuels.

Conducting a feasibility study is essential when selecting alternative fuels. Such a study provides a detailed analysis of all critical aspects of a proposed project, determining its likelihood of success. It involves comparing the cost of the proposed project and the cost of the alternative fuel with all direct and indirect costs, against the expected benefits from its usage. This process helps optimize operations and promote sustainable practices in cement plants, ensuring a balance between economic viability, technical feasibility, and environmental sustainability.

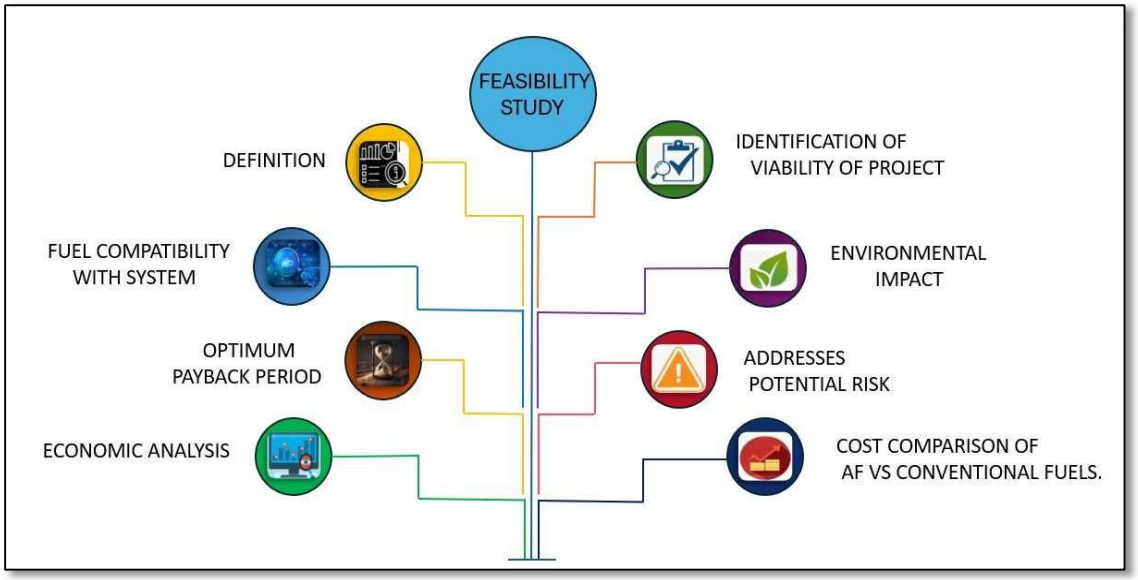
2.0 Feasibility Study

A feasibility study is a methodical approach used to determine the likelihood of success or failure of a proposed project. It involves a comprehensive evaluation of the project's advantages and disadvantages, considering technical, financial, and potential adverse impacts. By systematically analyzing these factors, a feasibility study helps in reaching a logical conclusion about the project's viability, ensuring informed decision-making.

Why feasibility study needs to be done?

Before selecting an alternative fuel for a specific kiln or calciner, it is crucial to conduct a feasibility study. This study assesses the compatibility of the proposed fuel with the existing pyro system, ensuring

it meets all operational requirements. A thorough feasibility study for an alternative fuel will address the following parameters:



➢ ***Fuel Type:***

- **Physical Analysis:** Includes size, bulk density, moisture content, and ease of handling.
- **Chemical Analysis:** Includes calorific value, chemical constituents, and the presence of undesirable elements.

➢ **Cost Effectiveness:** Measured in terms of INR per million kcals.



- **Plant Layout:** Assessment of storage, dosage, and overall manageability.
- **Safety Concerns:** Evaluation of safety during storage, handling, and processing.
- **System Compatibility:** Analysis of whether the existing system can accommodate the fuel, including sufficient calciner residence time for complete combustion and the capability of fans to handle combustion products.
- **Pollution Concerns:** Ensuring there are no undesirable emissions.
- **Economic Viability:** Preference for fuels that offer cost savings in thermal energy per kilogram of clinker produced.
- **Thermal Substitution Rate (TSR):** Determination of the extent of alternative fuel usage.

3.0 Why Alternate Fuels?

The Reserve of fossil fuel is dwindling/depleting with each passing day and hence the call of the day is to conserve these scarce natural resources, to the extent possible Moreover there is progressive quality deterioration, particularly in terms of ash percentage, increasing sulfur and other undesirable elements which goes to promote alternate fuel usage.

Increased logistic cost and more importantly release of greenhouse gas CO2, a major contributor of greenhouse gases thus adding to global warming are other important concerns. At 400- 500 Mts cement / annum, CO2 figures become astronomical.

For e.g. 1 kg bituminous coal will generate about 2.42 kg CO2 avg and each kg clinker requires 0.15 kg coal to 0.2 kg coal.

The Main benefits of alternate fuel usage are:

- Conserving natural fuel.
- Reduction in CO2 emission.
- Conserving limited limestone resources as coal with high ash do require higher lime and hence results in undue strain on our limited quality limestone resources.
- Productive use of agricultural, industrial and municipal waste, which otherwise would have found way to landfills, incineration, or some other unproductive uses.
- Cost benefit vis a vis conventional fuel.

Although Cement Kiln is an established and time-tested avenue for waste disposal because of its high operating temperatures, it must be borne in mind that not all alternate fuel could be tried in cement kilns. Depending on the composition,Y particularly chemical composition, there could be constituents which

could adversely affect the product quality, or disturbance in plant operation and thus affect the heat efficiency of the kiln in question.

In view of the above, it is of utmost importance the need to be selective in choosing the alternate fuels to be used and also the extent of usage and hence the need for a feasibility study.

Typical Example-



Coal/Petcoke (100%)
Total Cost of fuel- Rs 102,64,32,000



Coal/Petcoke (89%) + Alternate Fuel (11%) on TSR basis
Total Cost of fuel- Rs 96,19,66,938

So, the Annual Savings of Fuels using Coal/Petcoke + Alternate fuels is Rs 6,44,65,062

4.0 Way forward from feasibility study

A logical outcome of the above study would be determining the appropriate Thermal Substitution Rate (TSR), which depends on the physical and chemical properties of the fuel and the limitations of the existing pyro system. The selection and sizing of handling equipment also play a critical role in the project's success. Oversized equipment results in higher capital and operating costs and increased air ingress into the preheater, negatively impacting cost efficiency. Conversely, undersized equipment prevents the plant from fully utilizing the potential of alternative fuels. Therefore, the sizing and selection of equipment should be precisely tailored to the specific needs of the system and the availability of the alternative fuel.

5.0 Consequences and Risks of Omitting a Feasibility Study

While the merits of conducting a feasibility study for the selection of alternative fuels have been outlined, it is equally important to consider the potential risks of bypassing this critical step. The primary concerns include:

- **Mismatch Between Pyro-System Capability and Proposed Alternative Fuels:** Without a feasibility study, the selected fuel may not be compatible with the existing pyro system, leading to operational inefficiencies.
- **Cost Considerations:** Inaccurate cost estimations can result in financial losses and reduced economic viability.
- **Selection and Sizing of Equipment:** Improperly sized equipment for storage, handling, and dosage can either inflate capital and operating costs or limit the plant's ability to fully utilize alternative fuels.
- **Operational and Clinker Quality Issues:** Incompatible fuels can adversely affect the clinker quality and overall plant operations.
- **Pollution:** Unsuitable fuels may lead to increased emissions and environmental compliance issues.

Given these risks, it is only logical to conduct a thorough feasibility study before finalizing the use of any alternative fuel. This ensures that the desired benefits are achieved with a high probability of success.

Typical example-

Consider a plant initially designed to operate on tyre chips or carbon black. If this plant is later required to operate on municipal solid waste (MSW) or agricultural waste, it may become highly unviable due to significant differences in physical properties such as bulk density and moisture content, as well as chemical properties like net calorific value (NCV) and the presence of undesirable chemical constituents. Similarly, a plant optimized for tyre chips may be grossly undersized when switched to MSW or rice husk.

This underscores the critical importance of a detailed feasibility study to ensure that the chosen alternative fuel aligns with the plant's capabilities and operational requirements, thereby minimizing risks and maximizing benefits.

6.0 Conclusion

This analysis underscores the critical importance of conducting a comprehensive feasibility study before selecting and shortlisting alternative fuels, determining the possible Thermal Substitution Rate (TSR), and selecting the associated equipment. The potential risks and challenges associated with skipping this vital step far outweigh the efforts and costs involved in conducting the study. A detailed feasibility study ensures that the chosen alternative fuels align with the plant's capabilities and operational requirements, thereby minimizing risks and maximizing benefits for sustainable and cost-effective cement production.

The decision to implement an Alternate Fuel Feeding System in a cement plant should not be based only on CAPEX or estimated cost implications. Its potential impact on the clinker manufacturing process, kiln stability, product quality and overall plant operation should also be carefully assessed. Factors like fuel properties, feeding arrangements, combustion properties and emission control requirements need detailed evaluation. Therefore, a technical feasibility study is essential to assist the plant management to make an informed decision for the implementation of the Alternate Fuel Feeding System.

CERAMIC VORTEX FINDER: A DURABLE ALTERNATIVE TO INCREASE LIFETIME OF DIP TUBES AT THE PREHEATER LOWER STAGES WHEN UTILIZING ALTERNATIVE FUELS

Lars Andersen, Pankaj Gupta, Simon Kofoed-Dam

HASLE Refractories, Denmark

ABSTRACT

Dip tubes are an integral component of the preheater cyclone design in modern cement plants. However, the increasing utilization of alternative fuels (AFs) in combination with a higher maximum operating temperature presents significant challenges to the lifespan of traditional steel dip tubes in the lowest cyclone stages. Accelerated corrosion and the risk of premature failures can lead to process disruptions and emergency shutdowns. But operating without a dip tube negatively impacts the efficiency and performance of the entire preheater tower, resulting in higher fuel and power consumption to compensate for the reduced separation efficiency and heat exchange.

To overcome the drawbacks of standard steel dip tubes at elevated temperatures (deformation due to creep, blockage of cyclone outlet upon failure, Chromium (VI) emissions, etc.), a Ceramic Vortex Finder (CVF) has been developed by HASLE Refractories. The CVF consists of precast and pre-fired ceramic elements, which interlock to form a stable tube suspended from a steel support ring welded to the roof casing.

Recently, a new CVF generation, referred to as GEN3, has been released to address the challenges when utilizing AFs. An extensive development program has been carried out, boasting a re-engineered element design and a newly developed castable material specifically engineered to withstand the harsh conditions prevalent in preheater cyclones operating at elevated temperatures with high levels of AFs. The development program features both advanced simulations' along with intensive laboratory and field tests.

The four-year validation programme demonstrated that GEN3 CVF provides durable, reliable dip tube performance under demanding operating conditions. After successful field trials in selected European cement plants, the system was commercially deployed and is now installed worldwide, including in applications with elevated temperatures and high alternative fuel utilization. This paper presents GEN3 CVF's key features, validation results, and operational experience.

Key Words: Process optimization, energy savings, preheater tower, refractory technology

1.0 Introduction

Cement production is a highly energy-intensive process accounting for about 7% of global industrial energy use [1]. Energy costs make up between 15 and 40% of the total production costs. This share is expected to rise in light of increased competition for alternative fuels (AF) and the introduction of carbon tax mechanisms, necessitating reductions in energy consumption for an economically viable cement production amid the global transition towards greener practices.

More than 85% of the energy utilized in cement production is typically consumed as heat input in the rotary kiln and calciner [2]. While coal and other fossil fuels are still the globally prevalent fuels used in cement production, there is a growing shift towards using AF's such as industrial and municipal



waste materials, biomass, and other low-carbon fuels. Global players such as Heidelberg Materials, Holcim and CRH report thermal substitution rates (TSR) of 34-39% [3][4][5]. In India, this trend is also gaining momentum, with Ultratech Cement and Dalmia Bharat Cement reporting TSRs of 6.6% and 17%, respectively, and individual plants achieving more than 40% TSR [6][7].

However, transitioning to alternative fuel sources, while crucial for reducing the cement industry's carbon footprint, introduces significant operational challenges. Temperature and pressure fluctuations from the unsteady combustion of AFs, along with increased risk of coating formation and build-up in the system, can result in issues maintaining process stability. Additionally, the greater potential for chemical attacks on components and refractory linings can impose higher maintenance costs.

It is no new task for cement plants to prioritize continuous optimization of the entire pyro process to minimize heat and energy consumption, maximize capacity, and ensure minimal downtime. However, the increased use of alternative fuels (AFs) introduces additional layers of complexity to this optimization process.

The design of the cyclones is crucial for achieving high thermal preheater efficiency and maintaining a low pressure drop, which are essential for process stability and proper material flow through the preheater tower. The design of preheater cyclones varies greatly among equipment suppliers. In general, three main design requirements can be identified:

- Low pressure drop
- High separating efficiency
- As structural compact as possible

The objective is to ensure that the calciner preheater facilitates a total heat consumption of ideally no more than 690 kcal/kg clinker for a dry process. Typically, the top cyclones in the preheater tower are designed for high separation efficiency, sacrificing a higher pressure drop to ensure minimal raw meal losses in the pyro process. Conversely, in the lower stages characterized by higher operating temperatures, the focus shifts from separation efficiency to maximizing heat exchange. Final system configuration is usually dictated by several local conditions, raw materials, soil conditions, needed energy recovery, etc. Also construction costs and the desire for minimal tower height and footprint dimensions, play a role.

Within the cyclone, the dip tube (also referred to as a thimble, immersion tube, or vortex finder) plays a key role in defining the flow field and preventing particle short-circuiting. The absence or failure of a dip tube significantly reduces cyclone separation efficiency, resulting in increased recirculation of preheated raw meal to upper cyclone stages and consequently lower heat recovery efficiency.

The overall preheater performance is a function of the single cyclone stages' performance and design. If one or more stages do not operate as intended, the remaining cyclones must compensate, which often leads to higher energy consumption in terms of both heat and power.

New preheater and calcination towers in clinker production lines are dimensioned and designed with a dip tube installed in each stage of the cyclones, whether the system comprises 1, 2, 3, or even 6 stages. The presence of the dip tube is integral to the system's efficiency. Operating without a dip tube in lower stages may be possible, but significantly impairs the system's performance, leading to diminished quality, unstable operation, and inefficient heat exchange—fundamental aspects that the preheater is

designed to optimize. The dip tube ensures that raw meal particles are appropriately separated and preheated before entering the kiln, contributing to the overall thermal efficiency and operational stability of the preheater system.

When operating with a dip tube in all stages, heat economy is optimized, and the flue gas temperature exiting the preheater will be minimized. It should be noted that the recarbonation heat in the second lowest cyclone stage is reduced due to the dip tubes improving the separation rate of the cyclone stage, resulting in lower fuel usage per kg of clinker.

Regarding the impact of dip tubes on the total system pressure drop, two main counteracting contributions must be considered. Running with a dip tube increases the pressure drop throughout the cyclone, which would result in higher ID-fan power consumption if considered in isolation. However, as the mean operating temperature in each stage is reduced when running with dip tubes in every stage, the volume flow is greatly reduced, while the material throughput remains the same. This, in turn, significantly decreases the required work for transporting the raw meal through the preheater tower. In total, the power savings originating from the lower volume flow are greater than the additional power consumption caused by the extra pressure loss induced by the dip tube.

Estimating the exact energy-saving potentials when running with an optimal-designed dip tube is complex due to the numerous factors influencing the total system performance. Hence, only estimates based on communication with customers and internal calculations [8] will be presented in the following. On a general basis, running without a dip tube in the lowest stage of the preheat tower typically increases the heat input by 2-3% and the power draw on draft fan by about 5-7%. The figures presented vary significantly based on the system design and the specific operating conditions.

It is worth noticing that common preheater tower designs stem from a time when coal, pet coke and other standard, homogenous fossil fuels were used. However, the transition towards more sustainable cement production and increasing costs due to carbon taxes, alternative fuels (AFs) are increasingly replacing traditional fuels. In some plants, AFs account for up to 90% of total thermal input. The intensified usage of AFs poses challenges due to more unstable operating conditions (especially temperature and pressure fluctuations due to unsteady combustion characteristics) and increased maximum operating temperatures throughout the preheater cyclones. When running with high AF substitution rates, peak temperatures may occasionally exceed 1150°C.

Utilizing traditional steel dip tubes in these challenging environments presents significant issues. The lowest and second lowest stage cyclones are typically equipped with heat-resistant stainless steel segmented dip tubes made from cast Cr-Ni-alloyed steel. Despite being designed for high-temperature applications, these steel dip tubes face considerable disadvantages with the increased use of alternative fuels (AFs), which can limit their performance and lifespan.

Steel is a ductile material, making it prone to deformation, especially at elevated temperatures. The higher mechanical and thermal loads from AF combustion can accelerate the deformation and creep of commonly used steel dip tubes. Additionally, burning AFs increases the concentration of various corrosive species in the gas phase, such as halides, acids, and alkali salts. To mitigate the intensified corrosion damage, higher alloyed steels are required, resulting in significantly higher investment costs and increased emissions of carcinogenic chromate (Cr(VI)), posing health risks to maintenance personnel.

Typically, cement plants aim to run an 11-month campaign followed by a 4-week maintenance stoppage. Large repairs, such as the replacement of a dip tube, are only possible during this maintenance interval. Hence, the minimum lifespan of a dip tube should be at least one year to cover an entire campaign. However, increased AF utilization may shorten dip tube lifespan to much less than 12 months, with some steel elements falling down after a few months. These detached steel plates can provoke an emergency shutdown, by blocking the cyclone meal outlet or crusher at the end of the clinker cooler, resulting in production loss and economic losses. Given these challenges, many cement plants run without any dip tube in the lowest stage cyclone, despite the associated operational inefficiencies. This trade-off underscores the need for more durable and efficient materials that can withstand the harsh conditions induced by alternative fuel usage.

To overcome the drawbacks of standard steel dip tubes at elevated temperatures, a Ceramic Vortex Finder (CVF) has been developed by HASLE Refractories A/S during the 1980s, referred to as GEN1 in the following. The CVF consists of standardized precast and pre-fired refractory elements, which interlock to form a stable tube suspended from a steel support ring welded to the roof casing.

Recently, a new CVF generation, referred to as GEN3, has been developed to address the increasingly demanding operating conditions in cement plants with high alternative fuel utilization. The GEN3 CVF represents a comprehensive upgrade of the product line, combining a redesigned modular element geometry with a specially developed high-performance refractory material. Following an extended four-year validation and test phase in selected European cement plants, the GEN3 CVF was introduced to global customers in 2023 and has since been installed in a growing number of cement plants worldwide. The present paper summarizes the key development steps leading to the GEN3 CVF and places particular emphasis on recent field experience and installation results.

2.0 Factors influencing the dip tube performance

Before starting a development project, it is crucial to describe and understand the problem that needs to be solved with the new product. For this reason, as a first step, an extensive analysis of the factors influencing the performance of the dip tube in the last stage cyclone of the preheater tower has been conducted. This analysis identified three focus areas, illustrated in Figure 2.

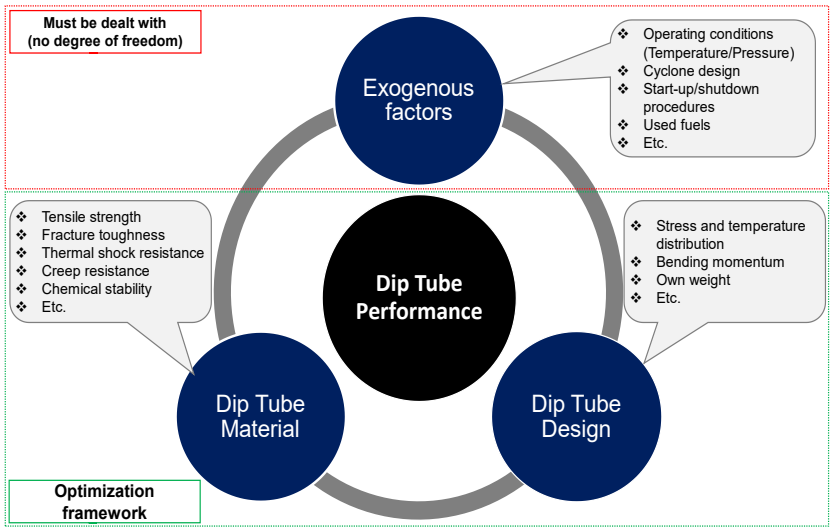


Figure 2: Factors influencing the lifetime/performance of dip tubes in the preheater tower

The exogenous factors are all framework conditions, set by the process design and operating conditions. These factors are usually fixed and must be worked with as they are. It is worth noting that not only the operating temperature and the type of fuels used are important, but also the cyclone design itself, since it sets the pressure distribution and the resulting mechanical loads. The main goal of the development is to create a dip tube design that works well no matter these varying framework conditions.

Given these exogenous factors, the dip tube design and material must be optimized to ensure a good lifetime. The dip tube design has a direct effect on the internal mechanical stresses caused by the external loads acting on it. These loads can be of different kinds, such as tensile loads (tare weight), momentum loads (pressure differences around the dip tube), and shear loads (friction of tangential gas flow on the surface). Finding a good balance between a high section modulus (axial and polar) and low tare weight is key to keeping internal stresses low. In addition, the design should make installation easy, with parts small and light enough to be carried through manholes on-site.

Selecting the proper material for the dip tube is perhaps the most challenging aspect. The material must withstand different thermal, mechanical, and chemical loads, which can vary significantly among cement plants. Since damages can only be repaired during the annual general overhaul, it is crucial to select materials with high resistance towards time-depending degradation mechanisms such as creep, crack propagation, abrasion and all types of corrosion. Ceramic materials are, in general, superior to metals in terms of creep and corrosion resistance, whereas it is vice versa for crack propagation.

Hence the main requirements for both dip tube design and material in the cement industry are summarized as follows:

- No deformation or creep up to a temperature of 1100°C/2000°F
- High strength
- High corrosion resistance toward all common corrosive substances in the gas phase
- High abrasion resistance
- Easy and quick installation

3.0 Features of the Ceramic Vortex Finder (CVF) Generation 3

3.1 Element design

The utilization of large amounts of alternative fuels typically results in more unsteady operating conditions in terms of considerable pressure and temperature fluctuations. This is especially the case if a large variety of inhomogeneous alternative fuels are used, which may lead to small-scale explosions and incomplete burn-off. Volatile operating pressures are of particular importance as they introduce dynamic loads to the dip tube. These dynamic loads induce complex stress states in the dip tube, resulting in a combination of tensile, compressive, and shear stresses that vary in magnitude and direction with time. Such cyclic stresses facilitate fatigue damages, which in turn reduces the dip tube lifetime significantly. Optimizing the CVF element design is the crucial to minimizing internal stresses and thus, the risk of fatigue damage.

The element design of the GEN3 CVF was optimized using advanced FEM software for simulating realistic load cases (Dynamic Simulation environment in Autodesk Inventor) and resulting internal stresses (Autodesk Inventor Nastran). The single work steps are presented in the following.

1) Defining a realistic Load Case

Operating data and cyclone designs from various cement customers were used to define meaningful load cases for the dip tube. The resulting pressure distribution on the inner and outer dip tube surfaces, respectively, is shown in Figure 3.

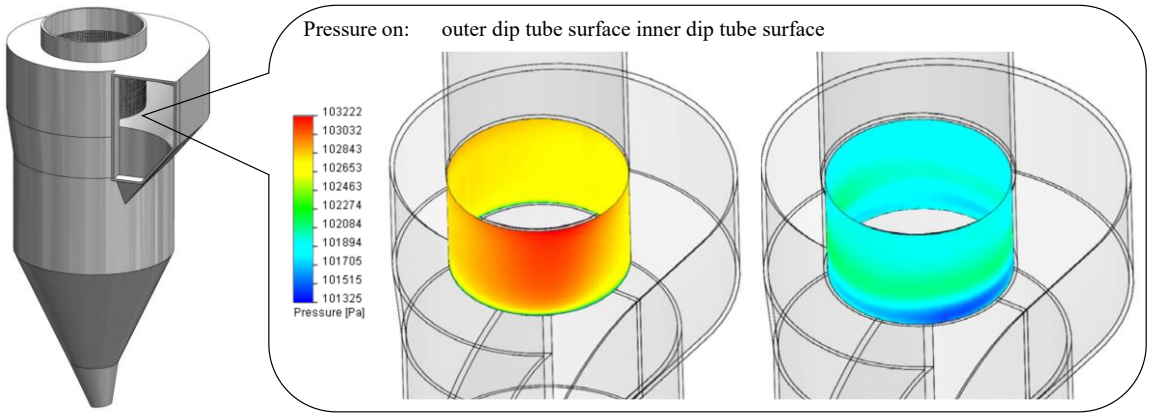


Figure 3: Pressure distribution on the inner and outer surface of the investigated dip tube example. Design parameters are as follows - Dip tube inner/outer diameter: 4710 and 4991 mm, length: 2826 mm, wrap-around inlet (270° scroll) with diameter between 8516 and 7520 mm, inlet velocity/pressure: 910°C/101325 Pa, gas media: idealized air.

2) Optimizing the existing element design

The initial step involved revisiting and analyzing the existing element design using FEM internal stress simulations. Following this analysis, a new X-shaped element design was developed based on the initial GEN1 design to better handle the dynamic and tensile loads. This new design also features advanced tongue-and-groove joints for improved interlocking, while still allowing for easy installation; each element is designed to weigh 15-16 kg.

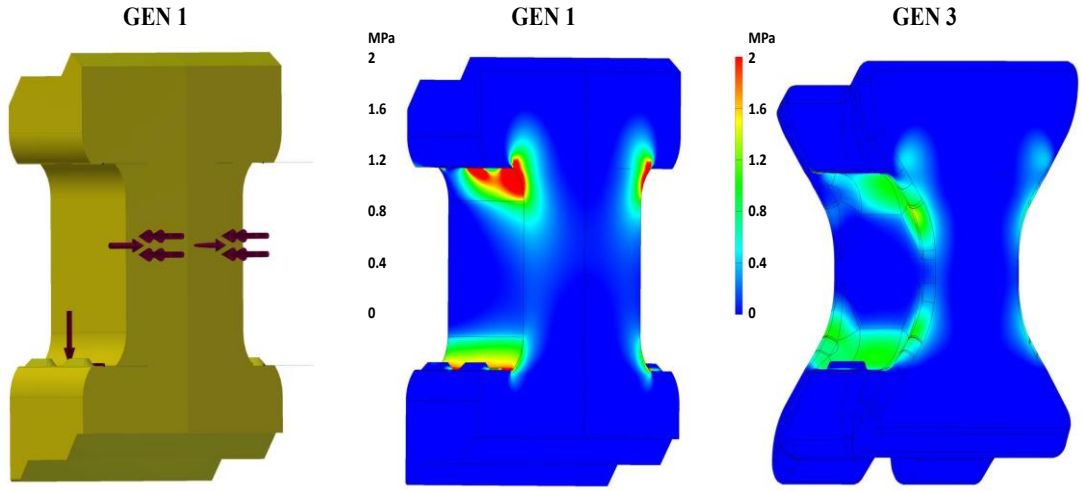


Figure 4: FEM stress analysis of first (GEN1) and new (GEN3) CVF generation. Left: Loads defined on the element, middle: resulting internal stresses in the GEN1 element, right: resulting internal stresses in the newly developed 3 GEN design.

3) Verification of FEM results with physical tests

Finally, physical tests were carried out to verify the FEM optimization, showing an increase in strength of over 35%. In other words, each element can bear a load of more than 5 metric tons before failing.



Figure 5: Physical testing of entire CVF elements. Left: Test setup, right: tested GEN1 and GEN3 elements (the number on the elements represents the breaking load in kN)

3.2 High-performance refractory material

The ceramic elements are made of a newly developed, no-cement refractory castable, called HyPerCast Premium, which contains nanoparticles and has been engineered specifically for this application. As a structural component suspended from the cyclone roof, the CVF distinguishes itself significantly from standard refractory materials. It is imperative for the material to have high tensile and bending strength to handle the loads originating from its own weight force and the pressure differences in the flow field (momentum loads).

To ensure a robust matrix, a thorough particle size distribution optimization has been carried out to create a dense material capable of handling these loads, where nanoparticles are included for maximizing strength. This optimization also achieves high abrasion resistance, which is essential for withstanding the significant wear caused by the passing raw meal and dust particles.

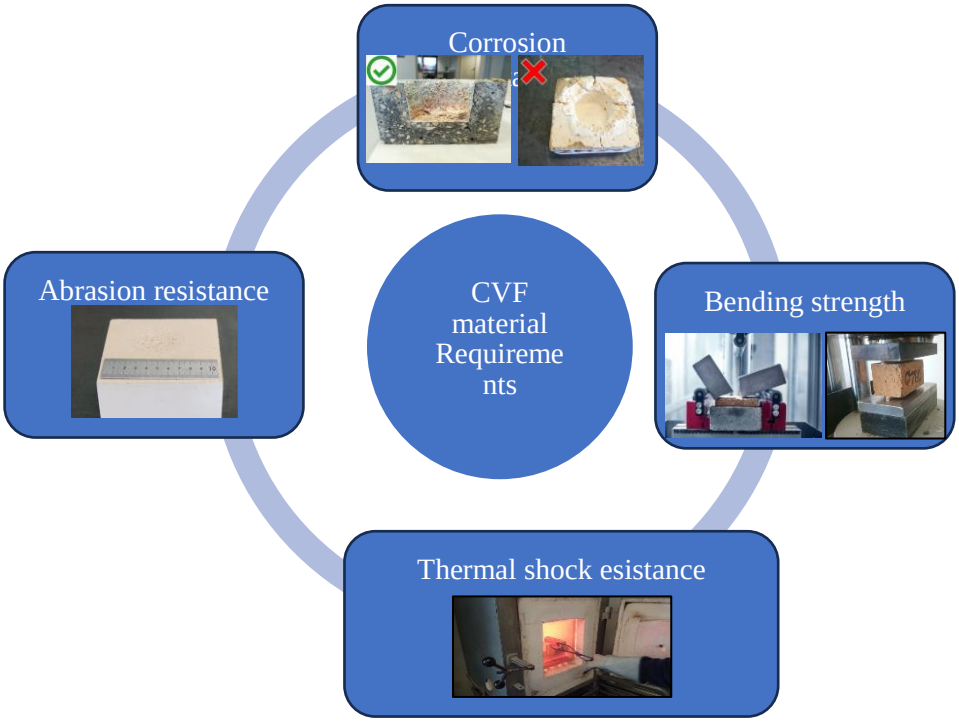


Figure 4: A wide range of lab test were carried out to optimize the material composition

With the addition of silicon carbide, a very high resistance to thermal shock has been achieved, enabling the CVF to withstand the thermal impacts both during shutdown and restart procedures. More importantly, it also enables the CVF to withstand temperature fluctuations during operation, as the more unsteady combustion of alternative fuels (AFs) can cause severe temperature changes within the preheater cyclones.

The CVF elements are cast and prefired under strictly controlled conditions at HASLE's factory in Denmark, ensuring the desired crystalline structure is obtained to maximize strength. During the pre-firing process, the oxidation of silicon carbide additionally forms a protective silica layer on the surface of the precast elements. Despite a fairly low silica (SiO2) content in the material, this layer provides high alkali resistance, mitigating chemical attacks.

Table 1 and 2 summarize the relevant material properties of the newly designed HyPerCast Premium material, highlighting properties crucial for the CVF application in bold.

TABLE 5: CHEMICAL COMPOSITION OF HYPERCAST PREMIUM

Chemical composition (%wt) EN ISO12677	
Al_2O_3	45.0%
SiO_2	7.5%
SiC	43.7%
Fe_2O_3	0.1%

CaO	0.4%
ZrO_2	3.0%

TABLE 6: TECHNICAL DATA OF HYPERCAST PREMIUM

Physical properties (measured at room temperature)					EN ISO 1927-6
After pre-firing to	Bulk Density (g/cm^2)	Open porosity (%)	Permanent linear change (%)	CCS (MPa)	CMOR (MPa)
1350°C	2.87	14.1%	-0.2%	230.5	28.1
Physical properties (measured at elevated temperature)					
	ISO 993-7	ISO 1893	ASTM C704	CEN/TS 15148	ISO993-11
After pre-firing to	HMOR at 900 °C (g/cm^2)	Reversible linear expansion[1] (%)	Abrasion[2] (angle 90°) (cm^3 loss)	Resistance to alkaline attack[3] (mm)	Resistance to thermal shock[4] (%)
1350°C	**47**	1.01%	**1.55**	**1-2 / high**	**66.8% / extra high**

[1] AT MAXIMUM PRE-FIRING TEMPERATURE, [2] TEST TEMPERATURE 500°C FOR SPECIMENS HEATED TO 500°C, OTHERWISE 1000°C, ABRADING MEDIA = SIC, [3] CLASSIFICATION BASED ON PENETRATION DEPTH AT 1100°C: VERY HIGH 0 MM, HIGH 1-2 MM, MEDIUM 3-5 MM, LOW 6-9 MM, VERY LOW >10 MM, [4] CLASSIFICATION BASED ON REMAINING STRENGTH AFTER 5 SHOCK CYCLES: EXTRA HIGH >65%, VERY HIGH 50-65%, HIGH 35-50%, MEDIUM 20-35%, LOW 10-20%, VERY LOW <10%

Overall, the newly developed HyPerCast Premium outperforms the other materials in HASLE's portfolio. Its exceptionally high hot modulus of rupture (HMOR) and abrasion resistance are more than twice those of standard refractories, enabling it to withstand the dynamic momentum loads generated in cyclones during alternative-fuel combustion. Despite its relatively low silica content, the material also provides high resistance to alkali attack, as shown in Figure 5.



Figure 6: Result of the alkaline test according to CEN/TS 15148 using Potassium hydroxide (KOH, 5h at 1100°C)

The high abrasion resistance is attributed to the PSD-optimized matrix incorporating advanced nanoparticles and the protective silica layer originating from the SiC oxidation during preheating.

Another notable advantage of the low silica content is the high refractoriness under load (T_{05}=1690°C) and the related superb creep and deformation resistance at elevated temperatures.

In summary, the new HyPerCast Premium material is expected to withstand the demanding conditions typical of cyclones operating with high levels of alternative fuels (AFs). Verification experiments have demonstrated that the material show no creep or deformation under multidimensional and dynamic tensile loads at elevated temperatures exceeding 1200 ˚C. Consequently, the CVF GEN3 can be used in every preheater tower within the cement industry. Thanks to the very high corrosion resistance against all common corrosive substances in the gas phase as well as the high abrasion resistance of the HyPerCast Premium material, these two degradation mechanisms should not have a limiting effect on the lifetime of the CVF.

4.0 Experiences from the field

Following the lab testing, full-scale field tests at selected customer plants have been completed to evaluate the performance of the GEN3 CVF under varying operating conditions.



Figure 6: installation procedure of the CVF. Left: First, the steel ring is welded to the roof casing, and subsequently ceramic fibre blankets are placed against the steel ring to ensure sufficient space for thermal expansion. Right: Assembling the GEN3-CVF; the top row of ceramic elements is placed on the brackets of the steel support ring, while the remaining elements are suspended from the elements in the top row.

The key validation sites was a 5,000 tpd cement plant in Germany operating with 82-95% refuse-derived fuel. The plant experienced limited-service life of conventional steel dip tubes in the lower stages of its dual-string preheater due to severe corrosion. In the lowest-stage cyclone (~950°C), steel dip tubes typically only lasted 2-3 months before needing replacement, whereas the CVF achieved a service life of one full campaign and the latest installation has now exceeded 15 months in operation. In the second-lowest-stage cyclone (~850°C), the CVF has remained in service for more than four years, compared with approximately three years for steel dip tubes. The successful long-term performance has led to the CVF being adopted as a permanent maintenance solution at the plant, with all four installed CVFs currently remaining in operation.

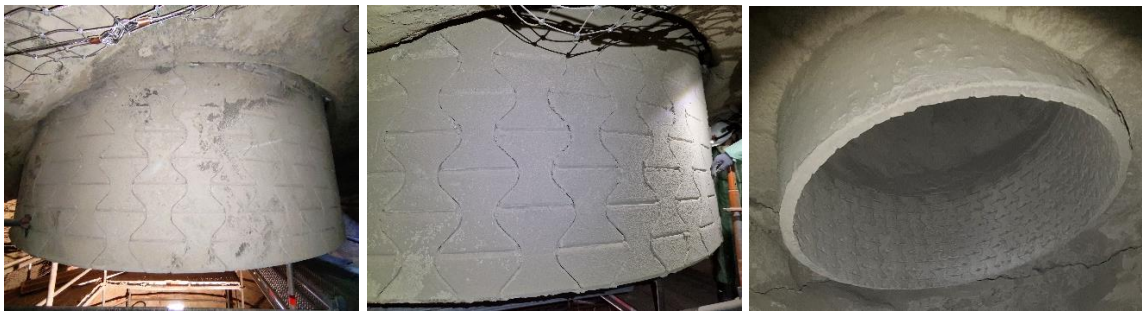


Figure 7: CVF installed at a cement plant in Germany. Left: after 1 year in the second-lowest-stage. Middle: after 2 years in the second-lowest-stage; the achieved service life exceeded 4 years. Right: after 9 months in the lowest-stage; the latest installation remains in operation after more than 15 months.

Following successful completion of the validation and test phase, the GEN3 CVF entered commercial deployment and has since been installed in cement plants across multiple countries and operating environments.

In Australia, a cement plant operating with approximately 40% alternative fuels had previously operated without a dip tube in the lowest-stage cyclone, due to lifetime limitations, where operating temperatures reach 850-900°C. A CVF was installed in January 2023 and achieved a service life of two years and nine months, exceeding the plant's maintenance campaign requirements. The successful performance led to continued implementation of the technology, with a replacement CVF installed in January 2026 that remains in service.



Figure 8: GEN3 CVF installed in the lowest-stage cyclone of an Australian cement plant. The installation achieved a service life of 2 years and 9 months. Left: at installation (January 2023). Middle: after 1 year of operation. Right: after 2 years of operation.

5.0 Concluding development with focus on continues enhancement.

The GEN3 CVF, with its new element design and the HyPerCast Premium castable, has demonstrated its potential to enhance component durability and sustain the efficiency of preheater systems over, an entire campaign – and beyond. Comparably small-sized ceramic elements pose a minimal risk of cyclone blockage if any drop, as they can pass through the feed pipe, allowing operations to continue. Combined with high strength as well as abrasion and corrosion resistance of the HyPerCast Premium material are key factors in this success. These enhancements translate to reduced maintenance costs, increased operational stability, and lower energy consumption, ultimately supporting the cement industry's shift towards sustainable fuel conversion. The GEN3 CVF development project exemplifies the potential of innovative materials and design in overcoming industry challenges, ensuring the

continuous and efficient operation of cement plants in an era of increasing alternative fuel utilization. As the global rollout continues, we continue to build experience from the new generation of CVF in various operating scenarios, further cementing its role in advancing cement production efficiency and sustainability.

6.0 Acknowledgements

We extend our gratitude to our global customers for their invaluable input throughout the project as well as during roll-out installations. Special recognition goes to the dedicated team at Holcim Lägerdorf. Additionally, we appreciate the exceptional efforts of the team at DIFK (Deutsches Institut für Feuerfest und Keramik GmbH) in supporting our work through extensive lab testing.

References

1. International Energy Agency (2020): "Energy Technology Perspectives 2020"
2. Verein Deutscher Zementwerke e.V. (2022): "Environmental Data of the German Cement Industry 2021"
3. Heidelberg Materials (2026): "Annual and Sustainability Report 2023"
4. Holcim (2026): "2025 INTEGRATED ANNUAL REPORT"
5. CRH (2026): "2025 Annual Report"
6. UltraTech Cement Limited (2023), "Integrated and Sustainability Report 2025-26"
7. Dalmia Charat Limited (2023): "Integrated and Sustainability Report 2022-23"
8. Alex C. Hoffmann, Louis E. Stein (2008): "Gas Cyclones and Swirl Tubes"

IMPACT OF USAGE OF HIGH ASH COAL (INDIAN COAL) IN CEMENT INDUSTRY

Anand Singh, Shashikant M Vala, Shyamal Roy & Satyabrata Sharma*

UltraTech Cement, Andheri East, Mumbai-400093, India

ABSTRACT

Indian cement plants frequently utilize high ash domestic coal due to non-availability of good quality fuel because geo political conflicts and economic benefits. High ash coal affects combustion efficiency, calciner performance, kiln heat consumption and clinker quality. Studies on Indian high ash coal indicate that combustion behaviour is controlled by ash content, volatile matter, fixed carbon and fuel ratio rather than GCV alone. Cement industry is facing lot of challenges with Indian coal property like wide ash variation (20-35%), wide variation of calorific value and high inherent moisture. This paper will elaborate regarding the usage of wide quality variation of Indian coal with minimum process disturbance.

Key words: - Combustion efficiency, Clinker quality & Process disturbance.

Introduction

The cement industry is one of the most energy-intensive industries, with fuel contributing a significant portion of the clinker production cost. In recent years, volatility in international fuel markets, geopolitical uncertainties, and the limited availability of good quality fuels have compelled many Indian cement plants to increase the utilization of domestic coal. While domestic coal offers economic advantages, it is generally characterized by higher variation & high ash content & inherent moisture with lower calorific value which can adversely affect combustion efficiency and overall kiln performance. To cope up with this situation many of the Indian cement industry is forced to use domestic coal.

Role of Coal Combustion in Operation

Calciner contributes approximately 60-70% of the total clinker heat requirement, while the kiln main burner contributes the remaining 30-40%. Coal combustion plays a critical role in determining the degree of calcination (DOC), calciner outlet temperature, kiln inlet temperature, fuel efficiency, and clinker quality. The fuel ratio (Fixed Carbon/Volatile Matter) is an important coal quality parameter that influences combustion characteristics. A higher fuel ratio indicates lower volatile matter content, higher ignition temperature, longer burn-out time, and generally a higher fixed carbon content. Indian coals typically have high ash content and variable combustion characteristics, which can adversely affect combustion efficiency and process stability when compared with imported coals.

Coal Combustion characteristics

The composition of coal ash and its calorific value vary significantly with respect to inherent moisture content .

*Corresponding Author: singh.anand@adityabirla.com

The data for some Indian coals are given in **Table 1.0**. Generally, about 90% or more of coal ash consists of silica, alumina, iron oxide and lime. The remaining 10% or less consists mainly of magnesium,

sodium and potassium oxides and titania as basic constituents, and sulphates and phosphates as acidic constituents. Gallium, germanium, nickel, beryllium, boron and chlorine are among the trace elements of coal ash. When heated, coal ash does not melt sharply at any temperature, but begins to soften at a much lower temperature than that at which it becomes molten and flows. For the effective utilization of high-ash coal, maintaining an optimum solid loading ratio, coal conveying velocity, and coal injection velocity is critical. Proper fuel transport and dispersion ensure improved particle distribution, enhanced combustion efficiency, higher burn-out rates, and stable kiln and calciner operation.

High ash coal reduces combustion efficiency by increasing the inert mineral load within the fuel. As a practical guideline, every 1mt ash increase in coal, can increase specific heat consumption by approximately 0.2629 kcal/mt ash, depending on kiln and calciner operating conditions. Therefore, strict control of coal ash, along with optimized volatile matter, fuel ratio, coal fineness, and solid loading ratio, is essential for maintaining stable calciner operation and minimizing thermal energy consumption. Ash Fusion Temperature (AFT) is an important parameter for evaluating the suitability of coal for cement kiln and calciner applications. AFT is strongly influenced by the chemical composition of coal ash. Higher contents of silica (SiO_2) and alumina (Al_2O_3) generally increase the AFT, while iron oxide (Fe_2O_3), alkalis, and sulphur-bearing compounds tend to reduce it. Coal with a low AFT is more susceptible to ash softening, slagging, deposit formation, and build-up within the combustion system, which can adversely affect fuel burn-out, heat transfer, and process stability. Therefore, monitoring AFT along with ash content, volatile matter, fuel ratio, and coal fineness is essential for the efficient utilization of high-ash coal and reliable kiln operation.

AFT (Ash Fusion temp), based on the ash composition having different proportions of oxide, which is mentioned below.

$AFT = 15.15 \times SiO_2 + 19.28 \times Al_2O_3 + 8.03 \times CaO - 0.50 \times Fe_2O_3 - 0.20 \times MgO - 1.00 \times SO_3 - 2.00 \times TAE$

(AFT is the ash fusion temperature in °C and TAE is total alkali equivalent in terms of Na_2O).

Coal field	Analysis of coal ash										Ash fusion range in mildly reducing atmosphere, °C
	SiO	Al_2O_3	Fe_2O_3	TiO_2	CaO	MgO	SO_3	P_2O_5	MnO	K_2O and Na_2O	
Raniganj											
Dishergarh seam, Seetalpur colliery	54.6	21.8	7.4	1.6	5.7	2.8	1.9	1.4	0.1	2.7	1160–1260
Laikdih seam, Laikdih deep colliery	46.0	34.9	6.3	2.4	3.7	2.9	2.4	0.6	trace	0.8	1380–1450
Jharia											
XIV seam, Bararee colliery	45.5	21.8	14.6	2.0	6.2	2.5	2.8	2.7	trace	1.9	1260–1410
XI seam, Sendra Bansjora colliery	57.9	24.0	11.7	1.5	1.1	1.4	1.0	0.4	0.1	0.9	1160–1300
Giridih											
Lower Karharbaree seam, Karharbaree colliery	69.8	18.7	5.6	2.2	1.0	1.0	1.0	0.1	trace	0.6	1260–1420
Kanhan valley											
Damua colliery	55.0	25.8	8.9	1.6	3.7	0.6	0.7	1.6	trace	2.1	1260–1420

Fig-1.0 (Analysis of coal ash)

Effect of ash content on combustion parameters

- Higher ash content reduces combustion efficiency by increasing the inert load in the fuel.
- High ash coal increases specific heat consumption (SHC) due to additional heat absorption by ash.
- Higher ash levels lower flame temperature and slow down combustion.

- High ash coal requires longer residence time for complete fuel burn-out.
- Low Ash Fusion Temperature (AFT) increases the risk of slagging, coating instability, and deposit formation.

Advantages of using of high ash coal

- High ash domestic coal is generally cheaper than imported low ash coal & reduces overall fuel procurement cost and dependence on imported fuels.
- Coal ash contains SiO_2, Al_2O_3, Fe_2O_3, and CaO, which become part of the clinker. It can reduce the requirement of corrective materials such as laterite, bauxite, and iron ore.
- Indian high ash coal often contains lower sulfur compared to petcoke, reducing sulfur cycle-related issues.

Disadvantages of using of high ash coal

- Higher ash content increases thermal energy demand, as additional ash must be heated to process temperature without contributing to clinker formation.
- Increased ash input changes kiln feed chemistry. It may require frequent raw mix corrections to maintain LSF, SM, and AM. It reduces life of mines.
- Lower Flame Temperature:-High ash reduces the combustible fraction of fuel. It may result in poor combustion and lower intensity of flame.
- Higher Free Lime Risk:-Reduced burning efficiency can lead to incomplete clinkerization and elevated free lime.
- Additional gas volume and dust load increase resistance in the system due to high IM (Inherent moisture). It may increase ID fan and process fan power.
- Ash Fusion and Ring Formation Problems:-Low Ash Fusion Temperature (AFT) below 1200^0C can cause calciner build-ups, cyclone blockages, kiln rings & build-up in tertiary air duct.
- Impact on Clinker Quality:-Higher ash variation may cause fluctuations in: Free lime, Liter weight, Clinker nodulization & Cement quality consistency

Key Effects of High Ash Coal

Parameter	Impact
High Ash	Reduced thermal efficiency & increased solid loading ratio while pneumatic transportation
Longer ignition & burnout time	Delayed heat release, lower flame temp and poor calcination
Lower flame temperature	Higher kiln inlet temperature risk leads to increase volatile cyclone in system
Ash contribution	Quality variation, free lime and LSF changes

Optimum Coal Characteristics for Calciner Firing

Parameter	Recommended Range
Ash	20-35 %
Volatile Matter	25-28 %
Fixed Carbon	30-36 %
Fuel Ratio	1.2-1.3

NCV	>4200 kcal/kg

Recommendations

- Maintain SLR (Fuel Solid Loading Ratio must maintain below 4 kg fuel per m^3 & 30-35 m/sec at coal conveying and coal injection) to avoid pulsation of fuel rate.
- Prefer coal NCV above 4200 kcal/kg.
- Maintain optimum coal fineness.
- Monitor DOC, kiln inlet temperature and free lime.
- Account for coal ash contribution in kiln feed chemistry.

Conclusion

High-ash coal can be successfully utilized in cement kilns and calciners when appropriate combustion and process controls are maintained. Achieving stable calcination, controlled heat consumption, and consistent clinker quality requires maintaining the recommended solid loading ratio, optimizing primary air, and selecting coal with a balanced ash content, volatile matter, and fuel ratio.

However, the use of high-ash coal with a low ash fusion temperature can significantly increase the tendency for build-up and ring formation in the kiln system. Therefore, coal ash chemistry should be continuously monitored, particularly for SiO_2, Al_2O_3, Fe_2O_3, CaO, alkalis, and Ash Fusion Temperature (AFT), before increasing the proportion of high-ash coal in the fuel mix.

When multiple fuels are used, effective fuel blending and homogenization are essential to minimize variations in ash composition and maintain process stability. The most effective approach is to prepare a uniform fuel mixture using a stacker-reclaimer system, ensuring consistent fuel quality and a stable ash input to the kiln. This helps reduce fluctuations in kiln operation, clinker chemistry, and overall process performance.

For optimum burner performance and flame stability, a single fuel should preferably be used in the main burner. Mixed fuels can be effectively utilized in the calciner, where fuel flexibility is higher and combustion conditions are more suitable for handling variations in fuel characteristics.

Acknowledgements

The authors are grateful to Sri E R Raj Narayanan, BH & CMO-mfg. & Projects, UltraTech Cement Ltd for his encouragement & supports to complete the above study and permission to publish this paper.

References

1. Roy Shyamal, Srivastava S. and Rajasekar L., "AFT: Determination & Prediction - Importance of Ash Fusion Temperature (AFT) on Cement Kiln Operation [J]", World Cement, March 2015, pp. 107-110.
2. Behera D., Nandi B.K. and Bhattacharya S., "Chemical properties and combustion behaviour of constituent relative density fraction of a thermal coal [J]", Energy Sources Part A: Recovery, Utilization, and Environmental Effects, vol. 41, pp. 654-664, 2018.

3. Ken B.S., Aich S., Saxena V.K. and Nandi B.K., "Combustion behaviour of KOH desulphurised coals assessed by TGA-DTG [J]", Energy Sources Part A: Recovery, Utilization, and Environmental Effects, vol. 40, pp. 2458-2466, 2018.
4. Qi X., Qi Li, Zhang H. and Xin H., "Thermodynamic characteristics of coal reaction under low oxygen concentration conditions [J]", Journal of the Energy Institute, vol. 90, pp. 544-555, 2017.
5. Zhang K., Zhang K., Cao Y. and Pan W.P., "Co-combustion characteristics and blending optimization of tobacco stem and high-sulfur bituminous coal based on thermogravimetric and mass spectrometry analyses [J]", Bioresource Technology, vol. 131, pp. 325-332, 2013.
6. Coal, The Wealth of India: A Dictionary of Indian Raw Materials and Industrial Products, Vol. 2, Council of Scientific and Industrial Research (CSIR), New Delhi, 1950.
7. Bureau of Indian Standards (BIS), New Delhi, IS: 437 (1979), Size Analysis of Coal and Coke for Marketing.
    a. Bureau of Indian Standards (BIS), New Delhi, IS: 439 (1976), Industrial Coke.
    b. Bureau of Indian Standards (BIS), New Delhi, IS: 770 (1977), Classification and Codification of Indian Coals and Lignite.
    c. Bureau of Indian Standards (BIS), New Delhi, IS: 1350 (Part I: 1969), Methods of Test for Coal and Coke - Proximate Analysis.
    d. Bureau of Indian Standards (BIS), New Delhi, IS: 1350 (Part II: 1970), Methods of Test for Coal and Coke - Determination of Calorific Value.
    e. Bureau of Indian Standards (BIS), New Delhi, IS: 1350 (Part III: 1969), Methods of Test for Coal and Coke - Determination of Sulphur.
    f. Bureau of Indian Standards (BIS), New Delhi, IS: 1350 (Part IV, Sec. 1: 1974), Methods of Test for Coal and Coke - Ultimate Analysis - Determination of Carbon and Hydrogen.
    g. Bureau of Indian Standards (BIS), New Delhi, IS: 1350 (Part IV, Sec. 2: 1975), Methods of Test for Coal and Coke - Ultimate Analysis - Determination of Nitrogen.
    h. Bureau of Indian Standards (BIS), New Delhi, IS: 1350 (Part V: 1979), Methods of Test for Coal and Coke - Determination of Special Impurities.
    i. Bureau of Indian Standards (BIS), New Delhi, IS: 1353 (1959), Methods of Test for Coal Carbonisation, Caking Index, Properties and Gray-King Assay (LT) Coke Types.
    j. Bureau of Indian Standards (BIS), New Delhi, IS: 1354 (1992), Methods of Test for Coke - Special Tests.
    k. Bureau of Indian Standards (BIS), New Delhi, IS: 1355 (1959), Methods of Test for Ash of Coal and Coke.
    l. Bureau of Indian Standards (BIS), New Delhi, IS: 4286 (1976), Specification for Domestic Coke

MINERALOGY–PSD DECOUPLING IN OPC 53 CEMENT: EXPLAINING THE WEAK CORRELATION BETWEEN CEMENT ALITE CONTENT AND 28-DAY STRENGTH THROUGH INDUSTRIAL XRD AND PARTICLE SIZE DISTRIBUTION ANALYSIS

Suresh Palla, Vipul Mishra, Lalit Patodi, Mukesh Kakde, Suresh K and Sandeep Deshmukh

Abstract

Ordinary Portland Cement (OPC) strength development is traditionally linked to clinker mineralogy, particularly alite (C_3S) content. However, analysis of a large industrial dataset comprising clinker mineralogy, cement chemistry, particle size distribution (PSD), fineness and strength development demonstrated that 28-day compressive strength is more strongly governed by grinding-induced PSD characteristics than by measured cement alite content. A systematic discrepancy was observed between clinker mineralogy and cement mineralogy determined by X-ray diffraction (XRD)-Rietveld analysis, where cement C_3S values frequently exceeded clinker C_3S values despite dilution by gypsum and addition of performance improver . The study investigates the relationships between clinker mineralogy, PSD, Blaine fineness and strength development. Results indicate that apparent cement C_3S enrichment originates from selective grinding and sample preparation effects rather than actual clinker phase abundance. The highest influence on 28-day strength was associated with the 3-32 µm particle fraction, Blaine fineness and coarse particle reduction. A new concept termed Mineralogy–PSD Decoupling Effect is proposed to explain the divergence between clinker mineralogy and cement mineralogy in industrial grinding systems. The findings suggest that optimization of PSD can yield greater improvements in OPC 53 performance than further increasing kiln alite content.

Keywords: OPC 53, Alite, Belite, XRD-Rietveld, Particle Size Distribution, Cement Strength, Grinding Optimization, Clinker Mineralogy

1. Introduction

Portland cement performance is influenced by multiple interdependent factors including clinker mineralogy, cement fineness, particle size distribution (PSD), sulphate balance, grinding efficiency and hydration kinetics. Traditionally, alite (C_3S) has been regarded as the dominant contributor to strength development, especially at early ages, due to its high hydration rate and rapid formation of calcium silicate hydrate (C-S-H) [1,2].

With increasing adoption of XRD-Rietveld analysis for routine process control, cement manufacturers frequently use measured phase composition of both clinker and cement to predict strength behaviour. Nevertheless, industrial observations often reveal inconsistencies between cement mineralogy and strength development that cannot be adequately explained by clinker phase composition alone.

The present work examines several months of industrial clinker and OPC 53 production data and demonstrates that PSD exerts a significantly greater influence on 28-day strength than measured cement C_3S content. The study further identifies a systematic divergence between clinker and cement mineralogy that can lead to misinterpretation of XRD data during process control.

2. Experimental Methodology

The dataset evaluated in this study comprised both clinker and cement parameters, alongside a comparative analysis of clinker versus cement mineralogy. The clinker parameters measured include tricalcium silicate (C_3S), dicalcium silicate (C_2S), tricalcium aluminate (C_3A), tetracalcium aluminoferrite (C_4AF), free calcium oxide (Free CaO), and magnesium oxide (MgO). The cement parameters were obtained from Ordinary Portland Cement (OPC) 53 grinding and dispatch samples, tracking physical and chemical characteristics such as Blaine fineness, 45µ residue, and 90µm residue. Furthermore, particle size distribution (PSD) fractions were categorised into specific ranges consisting of particles below 3µm, below 5µm, between 3–32µm, and between 5–30µm. Finally, the dataset factored in final cement proportions for C_3S% and C_2S%, concluding with structural performance evaluations based on compressive strength testing at 1, 3, 7, and 28 days. The schematic diagram of clinker mineralogy, sample preparation and mineralogy shown in Figure 1.

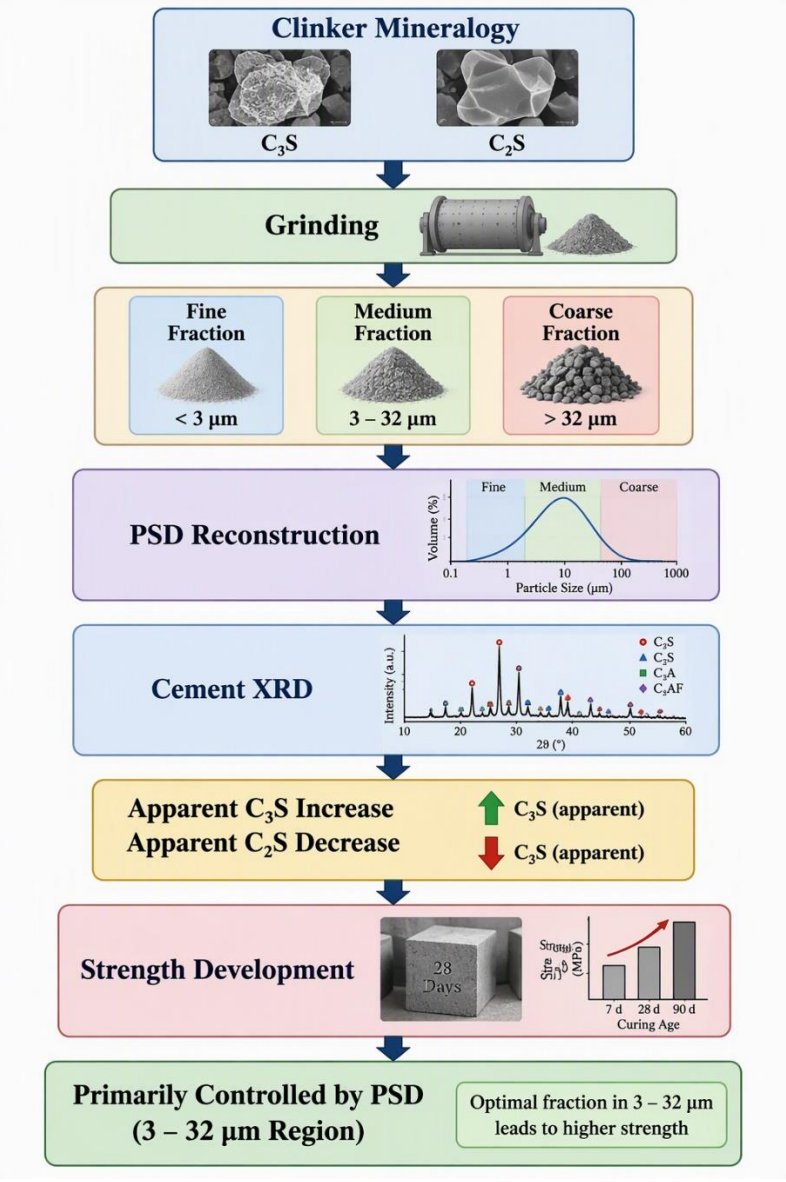


Figure 1. Proposed Mineralogy–PSD Decoupling Model

3. Clinker vs Cement Mineralogy

3.1 Unexpected Mineralogical Difference

A consistent observation was that clinker mineralogy and cement mineralogy did not align resulting in unexpected mineralogical difference.

Typical clinker values:

- C_3S: 45-55%
- C_2S: 25-35%

Typical cement values:

- C_3S: 60-75%
- C_2S: 5-12%

From a mass balance perspective, cement should contain less C_3S than clinker because approximately 7% of the final cement consists of gypsum and performance improver additions. Therefore:

C_3S (cement, theoretical)~C_3S (clinker) x Clinker factor

Yet measured cement C_3S was frequently higher than clinker C_3S. This observation demanded further investigation.

4. Mineralogy–PSD Decoupling Effect

4.1 Selective Grinding of Clinker Phases

Alite and belite exhibit different grinding behaviour. Alite is more brittle, possesses higher fracture propagation and undergoes faster size reduction. Conversely, belite is more compact, displaying higher grinding resistance and slower breakage rate. Due to these distinct properties during grinding, alite preferentially enters finer fractions whereas belite preferentially remains in coarser fractions. As a result, XRD samples prepared from finely ground cement become artificially enriched in alite-bearing particles. This selective enrichment consequently leads to an increase in the measured apparent cement C_3S and a decrease in the apparent cement C_2S without causing any change in the underlying clinker chemistry.

4.2 Contribution of Sample Preparation

Fine grinding during laboratory XRD sample preparation further enhances crystal liberation, alite peak intensity, Rietveld sensitivity towards fine alite-rich fractions. Thus, measured cement C_3S should not be considered equivalent to clinker C_3S (Table 1).

Table 1: Relative Influence of Parameters on 28-Day Strength

Variable Group	Parameter	Relative Influence	Primary Mechanism
PSD	3-32µm Fraction	Very High	Maximum Hydration Efficiency
PSD	5-30µm Fraction	High	Reactive particle population
Grinding	Blaine	Very High	Surface area generation
Grinding	45µm Residue	High (Negative)	Coarse particle dilution
Grinding	90µm Residue	Moderate	Circuit efficiency
Mineralogy	Clinker C_2S	Moderate-High	Later age hydration
Mineralogy	Clinker C_3S	Moderate	Early age hydrate formation
Mineralogy	Cement C_3S	Low-Moderate	PSD-dependant measurement
Burning Quality	Free CaO	Low	Kiln stability indicator

5. Strength Correlation Analysis

Correlation of strength at different ages established based on C3S % for early strength and C2S for latter strength. Actual data reflects shows that residue on 45 and 90 microns shows significant correlation at 1 day and 28 days strength (Table 2).

Table 2: Optimum Mineralogical Balance for OPC 53

Parameter	Recommended Range	Primary Benefit
Clinker C_3S	48-52%	Early Strength
Clinker C_2S	27-31%	Later-age Strength
Free CaO	0.8-1.5%	Stable burning
Blaine	340-355m²/kg	Strength optimisation
3-32µm Fraction	68-72%	Maximum hydration efficiency
45µm Residue	Low	Reduced coarse particles

6. Correlation Between Blaine and 28-Day Strength

The data shows that strength consistently improved with increasing Blaine up to approximately 340-355m²/kg (Figure 2). Beyond this range, strength gains diminished despite additional grinding energy. Similar observations have been reported by Jankovic et al. [8].

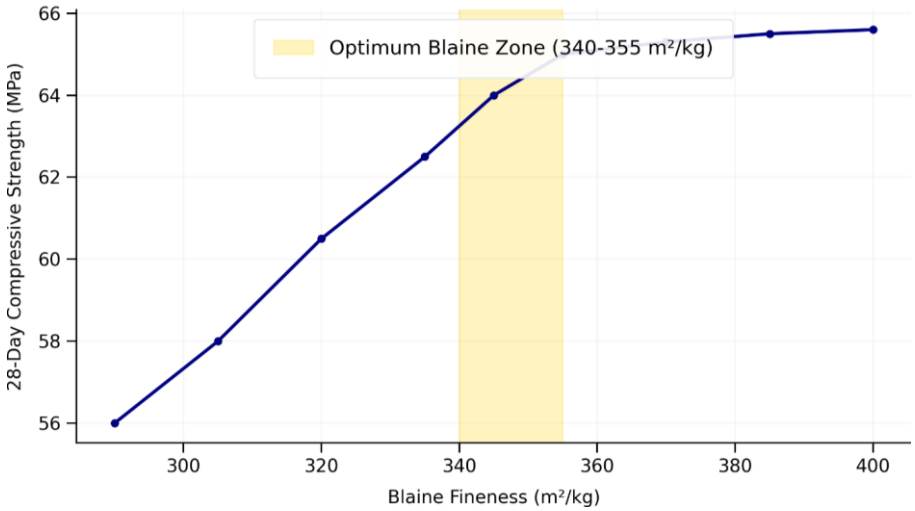
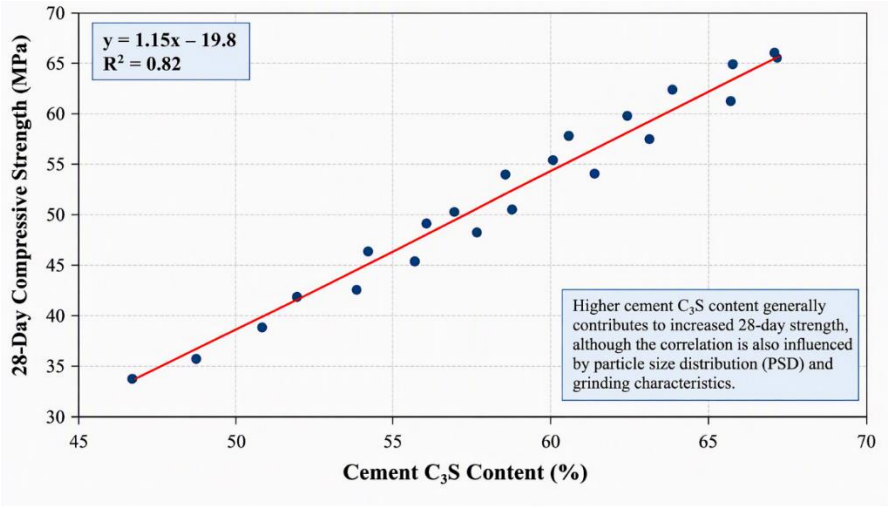


Figure 2: Blaine vs 28-Day Strength

7. Correlation Between Cement C_3S and 28-Day Strength

The data is considerable scatter indicates that increases in cement C_3S alone do not translate directly into strength improvement (Figure 3).

Figure 3. Cement C_3S (AQ) Versus 28-Day Strength



8. Dominant Role of Particle Size Distribution

The strongest relationship with strength occurred within the 3-32 µm particle fraction. This fraction represents the most efficient

particle size range because it offers optimal hydration rate, effective particle packing and high degree of cement utilization. Several periods exhibiting similar cement C_3S values displayed markedly different strengths solely because of PSD differences. This confirms previous findings that PSD often exerts greater influence on strength than total surface area alone [3,4].



9. Clinker C_3S and Clinker C_2S Balance

Contrary to the common assumption that maximum alite is always desirable, the data suggest that balanced clinker mineralogy provides superior overall performance. This C_3S-C_2S balance permits adequate early hydration, sustained later-age strength gain and improved grinding efficiency.

10. Conclusions

- Cement XRD consistently reported higher C_3S and lower C_2S than clinker XRD despite clinker dilution.
- The discrepancy results primarily from selective grinding and sample preparation effects.
- Cement C_3S measured by XRD should not be used as a direct surrogate for clinker C_3S.
- The highest influence on 28-day strength was associated with:
- 3-32 µm particle fraction
- Blaine fineness
- 45 µm residue
- Clinker C_3S remains important for early strength but has lower influence on 28-day strength than PSD optimization.
- Balanced clinker mineralogy (48-52% C_3S and 27-31% C_2S) provides the optimum compromise between early and later-age performance.
- Grinding optimization offers greater opportunity for OPC 53 strength enhancement than further increasing clinker alite content.
- A novel **Mineralogy–PSD Decoupling Effect** is proposed to explain the divergence between clinker mineralogy and cement mineralogy observed in industrial grinding systems.

Références

1. Hewlett, P. C., & Liska, M. (2019). *Lea's Chemistry of Cement and Concrete, 5th Edition*. Butterworth-Heinemann.
2. Taylor, H. F. W. (1997). *Cement Chemistry, 2nd Edition*. Thomas Telford Publishing.
3. Stamm, W. (1983). The Influence of Particle Size Distribution on Cement Properties. *Zement Kalk Gips International*, 36, 539-544.
4. Bensted, J., & Barnes, P. (2002). *Structure and Performance of Cements*. Taylor & Francis. [5] Scrivener, K. L., Snellings, R., & Lothenbach, B. (2016). *A Practical Guide to Microstructural Analysis of Cementitious Materials*. CRC Press.
5. Stutzman, P. E. (2004). Scanning Electron Microscopy Imaging of Hydraulic Cement Microstructure. *Cement and Concrete Composites*, 26, 957-966.



6. Odler, I. (2000). *Special Inorganic Cements*. CRC Press. \[8] Jankovic, A., Valery, W., & Davis, E. (2004). Cement Grinding Optimisation. *Minerals Engineering*, 17(11-12), 1075-1081.
7. ASTM C204. *Standard Test Method for Fineness of Hydraulic Cement by Air-Permeability Apparatus.*
8. EN 196-6. *Methods of Testing Cement: Determination of Fineness.* *** ### Suggested Final Conference Submission Title **Mineralogy–PSD Decoupling in OPC 53 Cement: Explaining the Weak Correlation Between Cement Alite Content and 28-Day Strength Through Industrial XRD and Particle Size Distribution Analysis







National Council for Cement and Building Materials

(Under the Administrative Control of Ministry of Commerce & Industry, Govt of India)

34 KM Stone, Delhi-Mathura Road (NH-2), Ballabgarh-121004, Haryana

https://conference.ncbindia.com

NCB HYDERABAD

NCB Bhawan, Old Bombay Road,
(Gachibowli-Mehdipatnam Road),
Hyderabad-500104
Telangana, India

NCB AHMEDABAD

Smeet Bungalow, Behind Planet House-2 (PH-2) Opp. Shukan Shubh-Labh Apt, Off. Judges Bungalows Road
Bodakdev, Ahmedabad-380054,
Gujarat, India

NCB BHUBANESWAR

Plot 145, Zone B, Shed No. 4, IDCO Central Store, Mancheswar Industrial Estate
Bhubaneswar-751010
Odisha, India